NUREG/CR-5194
EGG-2531

RELAP5/MOD2 Models and Correlations

Prepared by R.A. Dimenna, J.R. Larson, R.W. Johnson, T.K. Larson,
C.S. Miller, J.E. Streit, R G. Hanson, D.M. Kiser

Idaho National Engineering Laboratory
EG&G Idaho, Inc.

Prepared for
U.S. Nuclear Regulatory
Commission

NUREG/CR-5194
EGG-2531
R4

RELAP5/MOD2 Models and Correlations

Manuscript Completed: July 1988
Date Published: August 1988

Prepared by
R.A. Dimenna, J.R. Larson, R.W. Johnson, T.K. Larson,
C.S. Miller, J.E. Streit, R.G. Hanson, D.M. Kiser

Idaho National Engineering Laboratory
Managed by the U.S. Department of Energy

EG&G Idaho, Inc.
P.O. Box 1625
Idaho Falls, ID 83415

Prepared for
Division of Reactor and Plant Systems
Office of Nuclear Regulatory Research
U.S. Nuclear Regulatory Commission
Washington, DC 20555
NRC FIN A6868
Under DOE Contract No. DE-AC07-76ID01570

ABSTRACT

A review of the RELAP5/MOD2 computer code has been performed to assess the basis for the models and correlations comprising the code. The review has included verification of the original data base, including thermodynamic, thermal-hydraulic, and geometric conditions; simplifying assumptions in implementation or application; and accuracy of implementation compared to documented descriptions of each of the models. An effort has been made to provide the reader with an understanding of what is in the code and why it is there and to provide enough information that an analyst can assess the impact of the correlation or model on the ability of the code to represent the physics of a reactor transient. Where assessment of the implemented versions of the models or correlations has been accomplished and published, the assessment results have been included.

FIN No. A6868--Quantification of LBLOCA
Code Uncertainty for TRAC PF-1/MOD1

SUMMARY

The basis for the models and correlations comprising RELAP5/MOD2 has been determined and assessed. Included was both a literature review, to identify the original data base upon which the correlations are founded, and a coding review, to determine how the models and correlations were implemented. Because of the magnitude of the task of reviewing such a large code as RELAP5/MOD2, some sections of the code were covered in more detail than others.

The document forms a basis for an overall conclusion concerning the adequacy of RELAP5/MOD2 for a particular user of the code, since the different strengths and weaknesses will have a greater or lesser impact depending on the application. It is the conclusion of the authors of this document that RELAP5/MOD2 is a powerful calculational tool capable of representing most of the physical phenomena thought to be important for a wide range of reactor operating conditions covering normal, off-normal, and accident situations. Within this general framework, the code still has deficiencies; and this review has attempted to identify those deficiencies for the purpose of interpreting calculational results.

The following summarizes each of the sections of this document individually.

2. FIELD EQUATIONS

The fluid field equations are one-dimensional by design and should not be expected to explicitly represent three-dimensional phenomena. They are shown to have an identifiable path from accepted and documented forms of the conservation equations in standard references. The terms requiring constitutive models for closure are identified and used as the basis for the rest of this document. Approximations made in simplifying the general equations to the area averaged, one-dimensional form are identified. In

general, the fluid field equations represent an adequate approximation to incorporate the effects of the phenomena expected in reactor accident transient analysis, as well as in normal and off-normal transient analysis.

3. FLOW REGIME MAPS

The basis for the flow regime map is discussed in terms of the references cited in the RELAP5/MOD2 code manual. The work described in the cited references is reviewed, as is the comparison of those references to the flow regimes actually modeled in the code. The coded version of the flow regime maps, and the associated models described in Sections 4 and 6, are found to be considerably more complex than indicated in the code manual. The overall conclusions observed that the neither the science of flow regime mapping nor the representation of that science in RELAP5/MOD2 is complete. Specific characteristics of the flow regime maps, such as transition points between regimes, are found to be subject to some uncertainty, although the approximations made are considered to be reasonable engineering assumptions.

4. CLOSURE RELATIONS FOR THE FLUID ENERGY EQUATIONS

This section represents the largest single section of the document. It describes the closure relations upon which most of the code calculations depend, the interfacial and wall energy transfer. The interfacial closure relations are found to be subject to much of the same criticism found in the flow regime mapping technology; i.e., the science is still an active area of research, and the code models are an approximate representation of the current understanding. Many of the interfacial models are considered ad hoc, largely because better information is either not available or is difficult to implement in the code. The current models are generally considered reasonable, if incomplete, engineering approximations to the interfacial heat transfer.

Wall heat transfer closure relations are provided to represent all heat transfer processes anticipated during the course of a reactor accident transient. The correlations are generally of conventional form, but they are applied to reactor situations without detailed justification. Most of the heat transfer relations correlate well with the data on which they were based, but those data may not be fully applicable to reactor conditions or geometries. The implementation of the correlations also require engineering approximations to ensure numerical smoothness in the calculation. The documentation supporting the approximations is generally not available. The implemented heat transfer correlations need a better demonstration of applicability by comparisons with appropriate data.

5. CLOSURE RELATIONS REQUIRED BY THE FLUID MASS CONSERVATION EQUATIONS

No specific conclusions are drawn, as there are no specific mass closure relations. The interphase mass transport is related directly to the interphase and wall heat transfer through the phasic and saturation enthalpies, as described in Section 4.

6. MOMENTUM EQUATION CLOSURE RELATIONS

The wall and interfacial drag models are reviewed in both the code manual and the coding itself. As with the the interfacial heat transfer models, they are found to be considerably more complex than implied by the description in the code manual. The drag correlations are found to be subject to the fact that the science of interfacial transport is incomplete. The models used in the code are largely ad hoc engineering representations of the current understanding of interfacial behavior. They are considered to be reasonable approximations to the physics.

An entrainment model used to partition heat transfer to an estimated liquid droplet field is noted for the annular mist flow regime. Although

the model has no impact on the flow calculation, it is found to be a reasonable representation of the basis correlation for partitioning the heat transfer.

7. FLOW PROCESS MODELS

The abrupt area change model is reviewed based on the discussion in the code manual.

The critical flow model was reviewed in detail, both in the code manual and in the coding. The model is one-dimensional and requires a user-specified discharge coefficient to represent two-dimensional effects at the choke plane and employs an empirical correlation to represent liquid superheating at the choke plane. The development of the critical flow model is based on an assumption of equilibrium. It has received wide assessment, indicating that a careful choice of the discharge coefficient is needed to give good predictions of tabulated data. The model generally calculates too high a choked mass flowrate without the use of a (reducing) discharge coefficient.

8. SPECIAL COMPONENT MODELS

The RELAP5/MOD2 pump model is reviewed in this section. In general, it is found to be an adequate representation of a reactor coolant pump, though a recommendation in the use of the model was made. The internally supplied pump characteristic curves are recommended only in a situation that the user's application is specifically for the internally modeled pump. Otherwise, it is recommended that the user provide pump curves appropriate to the actual pump being modeled.

9. HEAT STRUCTURE PROCESS MODELS

Several heat structure process models are reviewed from an applications point of view. All of the models are engineering representations of heat structure behavior based on analytical models, and

not on correlations. Heat conduction, reactor kinetics, gap conductance, and reflood axial heat structure rezoning are reviewed. The heat conduction and reactor kinetics models are assessed by comparing test calculations performed with the code to published solutions found in journal articles or textbooks. The code is found to give a good representation of all test problems.

10. CLOSURE RELATIONS REQUIRED BY EXTRA MASS CONSERVATION FIELDS

No significant review of either noncondensible gas or liquid solute capabilities in the code was completed. A stated capability of the code to incorporate the effects of noncondensible gases was noted in the discussion of the field equations (Section 2) and in the discussion of critical flow (Section 7).

11. STEADY STATE

The RELAP5/MOD2 steady-state model is reviewed. It is found to be a usable tool to assist the user in achieving a numerically satisfactory steady-state condition prior to beginning a transient calculation. Some recommendations are made in the application of the model.

ACKNOWLEDGMENTS

The process of documenting the history of RELAP5/MOD2 to learn the reasoning used in developing the models and correlations was accomplished only with the help of several of the developers. Discussions with R. A. Riemke were invaluable. Without Dr. Riemke's help, this document would have taken considerably more time and would have been considerably less detailed. The willingness of J. C. Lin, H. Chow, and C. C. Tsai to answer questions concerning heat transfer and flow regime modeling was greatly appreciated and added considerable insight to those sections of the code. The careful review and comments from V. H. Ransom, J. A. Trapp, C. Noble, K. E. Carlson, and E. D. Hughes added to the accuracy of the final document. Finally, the enormous and careful typing effort by S. Martin and D. Miller was instrumental in completing the document and is greatly appreciated.

CONTENTS

FIGURES

TABLES

NOMENCLATURE (with SI units)

A	-	area (m^2)
AJUN	-	area of junction
AVOL	-	cross-sectional area of volume
B	-	body force
C	-	virtual mass coefficient
C_D	-	drag coefficient
CHF	-	critical heat flux (W/m^2)
C_p	-	specific heat capacity at constant pressure (J/kg-K)
D	-	diameter (m)
De,h	-	equivalent or hydraulic diameter (m)
DISS	-	pump dissipation energy term (J/m^3)
d	-	portion of stress tensor, diameter (m)
E	-	nonuniformity term
F	-	force, multiplicative factors
FIG, FIF	-	interfacial drag, vapor or liquid space
FIVOL	-	interphase friction term from volume
FWG, FWF	-	wall drag, vapor or liquid space
G	-	mass velocity (kg/s)
Gr	-	Grashof number
g	-	acceleration of gravity (9.8 m/s^2)
H	-	heat transfer coefficient, pump head
HLOSSF, HLOSSG	-	form or frictional losses (m/s)
h	-	heat transfer coefficient (W/m^2-K), specific enthalpy (J/kg)
I	-	specific internal energy (J/kg)
k	-	thermal conductivity (W/m-K), wave number
k_B	-	Boltzmann constant

L	-	length (m)
m	-	mass transfer rate
Nu	-	Nusselt number
n	-	unit vector
P	-	pressure (Pa)
P_f	-	immediate fission power
Pr	-	Prandtl number
Q	-	heat transfer rate (W/m^3), volumetric flow
Q_f	-	immediate fission energy per fission
q	-	heat flux (W/m^2)
Re	-	Reynolds number
r	-	bubble radius (m), tube radius (m)
S	-	area, entropy (critical flow), internal heat source (reactor kinetics)
St	-	Stanton number
T	-	temperature (K), stress tensor
T_{sat}	-	saturation temperature (K)
$T_{sat}(P)$	-	saturation temperature based on total pressure (K)
$T_{sat}(P_s)$	-	saturation temperature based on partial pressure of steam (K)
t	-	time (s)
U	-	specific internal energy (J/kg)
V	-	volume (m^3), specific volume (m^3/kg)
VISF, VISG	-	numerical viscosity terms (m^2/s^2)
v	-	velocity (m/s)
We	-	Weber number
X_n	-	noncondensible gas quality
X_{tt}^{-1}	-	Martinelli flow parameter
x	-	spatial length dimension (m)

Greek symbols

α	-	void fraction
β	-	thermal coefficient of expansion (1/K), effective delayed neutron fraction
ψ	-	general parameter, fission rate
ϕ	-	neutron flux
Φ	-	angle of inclination
ϵ	-	porosity of a porous medium, area ratio
λ	-	decay constant
ω	-	angular velocity (s^{-1})
μ	-	viscosity (kg/m-s)
ν	-	kinematic viscosity (m^2/s)
ρ	-	density (kg/m^3), reactivity in reactor kinetics (dollars)
Γ	-	volumetric mass exchange rate (kg/m^3-s)
σ	-	surface tension (N/m), Stefan-Boltzmann constant = 5.67×10^{-8} W/m^2-K^4
τ	-	shear stress (N), pump torque
ξ	-	interface normal unit vector
δ	-	annular liquid film thickness
Λ	-	prompt neutron generation time
Σ_f	-	fission cross section

Subscripts

a,b	-	phase designator
ann	-	annular, annulus
bub	-	bubble
CHF	-	critical heat flux

con	-	condensation
cyl	-	cylinder
drp	-	droplet
f	-	liquid
g	-	vapor
HE	-	homogeneous equilibrium
i	-	interfacial parameter
K	-	upstream volume indicator
L	-	downstream volume indicator
onb	-	onset of nucleate boiling
nvg	-	net vapor generation
SCL, SCG	-	subcooled liquid, gas
SHL, SHG	-	superheated liquid, gas
s	-	superficial, steam property
sat	-	saturation
T, t	-	throat value
TB	-	Taylor bubble
up	-	upstream
w	-	wall
x	-	local position characterized by the length from starting point

Symbols

~	-	area average, intermediate time value
^	-	interfacial value
′	-	deviation parameter
·	-	time derivative, donored parameter

RELAP5/MOD2 MODELS AND CORRELATIONS

1. INTRODUCTION

The RELAP5/MOD2 models and correlations document is intended to fill a gap between the code manual,[1-1] which provides a detailed explanation of the code contents and its structure, and the interpretation of the code output, which requires an understanding of not only the information in the code manual but also an understanding of its history, limitations, strengths, and weaknesses. With a detailed understanding of the underlying assumptions and simplifications used to generate and implement the basis equations and models into a computer code, the user can make an intelligent assessment of the applicability and accuracy of the calculations resulting from that code. Depending on the purpose for which the calculations are being performed, the adequacy of the code can then be determined. The purpose of this document is to provide the user with quantitative information addressing the physical basis for the RELAP5/MOD2 computer code, not only as documented in the code manual but also as actually implemented in the FORTRAN coding. The specific version of the code assessed in this project is RELAP5/MOD2, Cycle 36.05, as implemented on the Cyber 176 computer at the Idaho National Engineering Laboratory.

The fundamental reason for writing this models and correlations document is two-fold. First, the Code Scaling, Applicability, and Uncertainty (CSAU) Evaluation methodology[1-2,p.4-102] requires a knowledge of the basis for a computer code calculation to determine each of the pieces of the methodology, scaling capability, code applicability, and code uncertainty. Second, documentation of the actual development of the RELAP5/MOD2 code was not readily available such that the information to satisfy the CSAU needs could be obtained by most users. Completion of this document satisfies both needs and provides a valuable reference for future code applications. In addition, the review of the actual coding required to complete this task has ensured that the code is an accurate reflection of the basis described in the code manual (and vice-versa). In some instances, the review has resulted in identifying bona fide code errors, though by and large these occurrences have been relatively rare.

The level and tone of this document are such that the reader must have a relatively detailed knowledge of thermal-hydraulics. Though that knowledge need not pertain specifically to nuclear reactors, an understanding of code applications to reactor transients will necessarily require an understanding of reactor thermal-hydraulics. The document also requires that the reader have a reasonable understanding of thermal-hydraulic code applications to reactor analyses. This document is neither an input manual nor a general code manual. The existing documentation addressing both of those needs is complete and adequate. Neither is this document a user guideline, though much of the information included herein is important to the knowledgeable user in making modeling decisions and interpreting calculational output. Indeed, the information in this document allows the user to determine whether RELAP5/MOD2 is capable of modeling his or her particular application, whether the calculated result will be directly comparable to measurements or whether they must be interpreted in an average sense, and whether the results can be used to make quantitative decisions. Wherever possible, the code manual has been used to provide necessary information. The code manual has not been repeated where the authors felt the discussion was adequate, but it has been referenced. Material from the code manual has been included in this document only where needed for completeness.

This introduction will give a brief description of RELAP5/MOD2 to acquaint the reader with the code being addressed. The description will provide some of the history of RELAP development leading to the current code capabilities and structure. The code structure will then be discussed. This structure is significant, for it affects the simulated time at which each of the calculated parameters is determined and gives the reader an understanding of the order in which a calculation proceeds and the manner in which transient parameters are passed from one portion of the calculational scheme to the next. The next portion of the introduction will define the scope of this document, as governed by the requirements of the CSAU[1-2] methodology. That will be followed by a description of the document structure, which is closely related to the code structure. Lastly, a short discussion of topics specifically excluded from this document will be given, including an assessment of whether those topics should be included at a later date.

1.1 RELAP5/MOD2

RELAP5/MOD2 is a pressurized water reactor (PWR) system transient analysis code that can be used for simulation of a wide variety of PWR system transients of interest in light water reactor (LWR) safety. The primary system, secondary system, feedwater train, system controls, and core neutronics can be simulated. The code models have been designed to permit simulation of postulated accidents ranging from large break loss-of-coolant accidents to accidents involving the plant controls and fuel system. Transient conditions can be modeled up to the point of fuel damage.

1.1.1 Development of RELAP5/MOD2

RELAP5/MOD2 was produced by improving and extending the modeling base that was established with the release of RELAP5/MOD1[1-3] in December 1980. The modeling approach and instructions for application of the code are documented in a two-volume users manual.[1-1]

The principal design objective of the RELAP5 project is to provide the U.S. Nuclear Regulatory Commission (NRC) with a fast-running and user-convenient LWR system transient analysis code for use in rule-making, licensing audit calculations, evaluation of operator guidelines, and as a basis for a nuclear plant analyzer. A secondary objective is to provide advanced analysis capability to other nuclear power organizations for use in design, safety analysis, and licensing application work.

From the outset of the RELAP5 project, the goal has been to establish a reliable analysis capability for use in the nuclear power industry. The approach has been to rely on first-principles modeling where possible and thus reduce empiricism. The numerical simulation of transient two-phase flow has been a most challenging task. The RELAP5/MOD2 two-phase flow model provides a significantly improved capability over RELAP5/MOD1 and represents an enhanced understanding of the underlying physics of two-phase flow.

An additional goal of the project has been to provide a more comprehensive and generic modeling of the complete nuclear steam supply

system, including turbines, generators, condensers, feed systems, and plant controls. The highly generic modeling capability for the code also permits it to be used in many nonnuclear applications of steam-water systems.

1.1.2 Relationship to Previous Code Versions

The series of RELAP codes began with RELAPSE (REactor Leak And Power Safety Excursion), which was released in 1966. Subsequent versions of this code are RELAP2,[1-4] RELAP3,[1-5] and RELAP4,[1-6] in which the original name was shortened to Reactor Excursion and Leak Analysis Program (RELAP). All of these codes were based on a homogeneous equilibrium model (HEM) of the two-phase flow process. The last code version of this series is RELAP4/MOD7,[1-7] which was released to the National Energy Software Center (NESC) in 1980.

In 1976, the development of a nonhomogeneous, nonequilibrium model was undertaken for RELAP4. It soon became apparent that a total rewrite of the code was required to efficiently accomplish this goal. The result of this effort was the beginning of the RELAP5 project. As the name implies, this is the fifth in the series of computer codes that was designed to simulate the transient behavior of LWR systems under a wide variety of postulated accident conditions. RELAP5 follows the naming tradition of previous RELAP codes, i.e., the odd numbered series are complete rewrites of the program while the even numbered versions had extensive model changes, but used the architecture of the previous code. Each version of the code reflects the increased knowledge and new simulation requirements from both large- and small-scale experiments, theoretical research in two-phase flow, numerical solution methods, computer programming advances, and the increased size and speed of computers.

The principal new feature of the RELAP5 series is the use of a two-fluid, nonequilibrium nonhomogeneous, hydrodynamic model for transient simulation of the two-phase system behavior. RELAP5/MOD2 employs a full nonequilibrium, six-equation, two-fluid model. The use of the two-fluid model eliminates the need for the RELAP4 submodels, such as the bubble rise and enthalpy transport models, which were necessary to overcome the limitations of the single-fluid model.

1.1.3 Code Organization

RELAP5 is coded in a modular fashion using top-down structuring. The various models and procedures are isolated in separate subroutines. The top level structure is shown in Figure 1-1 and consists of input, steady state, transient, plotting, and stripping blocks.

The input block processes input, checks input data, and prepares required data blocks for all program options.

Input processing has three phases. The first phase reads all input data, checks for punctuation and typing errors (such as multiple decimal points and letters in numerical fields), and stores the data keyed by card number such that the data are easily retrieved. A listing of the input data is provided, and punctuation errors are noted.

During the second phase, restart data from a previous simulation is read if the problem is a RESTART type, and all the input data are processed. Some processed input is stored in fixed common blocks, but the majority of the data is stored in dynamic data blocks that are created only if needed by a problem and sized to the particular problem. Extensive input checking is done, but at this level checking is limited to new data from the cards being processed. Relationships with other data cannot be checked because the latter may not yet be processed.

The third phase of processing begins after all input data have been processed. Since all data have been placed in common or dynamic data blocks during the second phase, complete checking of interrelationships can proceed. Examples of cross-checking are: existence of hydrodynamic volumes referenced in junctions and heat structure boundary conditions; entry or existence of material property data specified in heat structures; and validity of variables selected for minor edits, plotting, or used in trips and control systems. As the cross-checking proceeds, cross-linking of the data blocks is done so that it need not be repeated at every time step. The initialization required to prepare the model for start of transient advancement is done at this level.

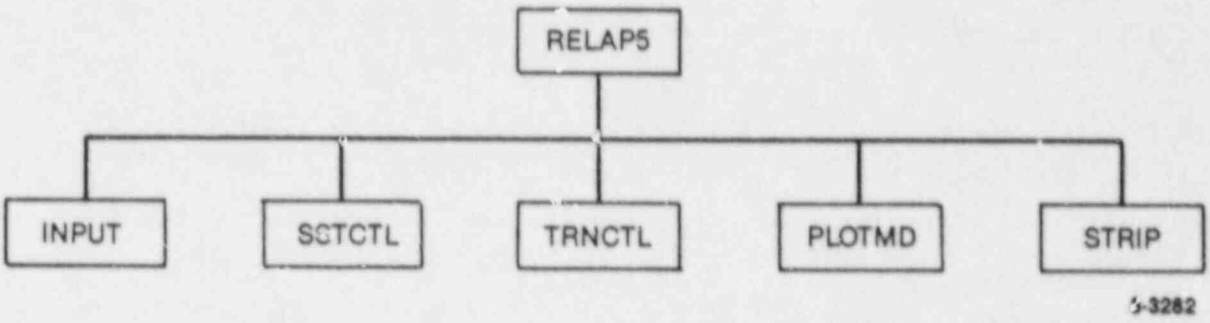

Figure 1-1. RELAP5/MOD2 top level structure.

The steady-state block determines the steady-state conditions if a properly posed steady-state problem is presented. Steady state is obtained by running an accelerated transient until the time derivatives approach zero. The steady-state block is very similar to the transient block but contains convergence-testing algorithms to determine satisfactory steady state, divergence from steady state, or cyclic operation. With this technique, approach to steady state from an initial condition would be identical to a plant transient from the initial condition. Pressures, densities, and flow distributions would adjust quickly; but thermal effects would occur more slowly. To reduce the transient time required to reach steady state, the steady-state option artificially accelerates the heat conduction solution by reducing the heat capacity of the conductors.

The transient block advances the transient solution. Figure 1-2 shows the second-level structures for the transient and steady-state blocks or subroutines. Since these blocks are nearly identical, the transient blocks are discussed with equivalent steady-state block names shown in parentheses.

The subroutine TRNCTL (SSTCTL) consists only of the logic to call the next lower level routines. Subroutine TRNSET (SSTSET) brings dynamic blocks required for transient execution from disk into small core memory (SCM) or large core memory (LCM), performs final cross-linking of information between data blocks, sets up arrays to control the sparse matrix solution, establishes scratch work space, and returns unneeded SCM and LCM. Subroutine TRAN (SSTAT) controls the transient advancement of the solution. Nearly all the execution time is spent in this block, and this block is the most demanding of memory. The subroutine TRNFIN (SSTFIN) releases space for the dynamic data blocks that are no longer needed and prints the transient timing summary.

Figure 1-2 also shows the structure of the TRAN (SSTAT) block. DTSTEP (STSTEP) determines the time-step size and whether transient advancement should be terminated. TSTATE applies hydrodynamic boundary conditions by computing thermodynamic conditions for time-dependent volumes and velocities for time-dependent junctions. The remaining blocks perform or control the calculations for major models within RELAP5: trip logic (TRIP), heat structure advancement (HTADV), hydrodynamic advancement (HYDRO), reactor

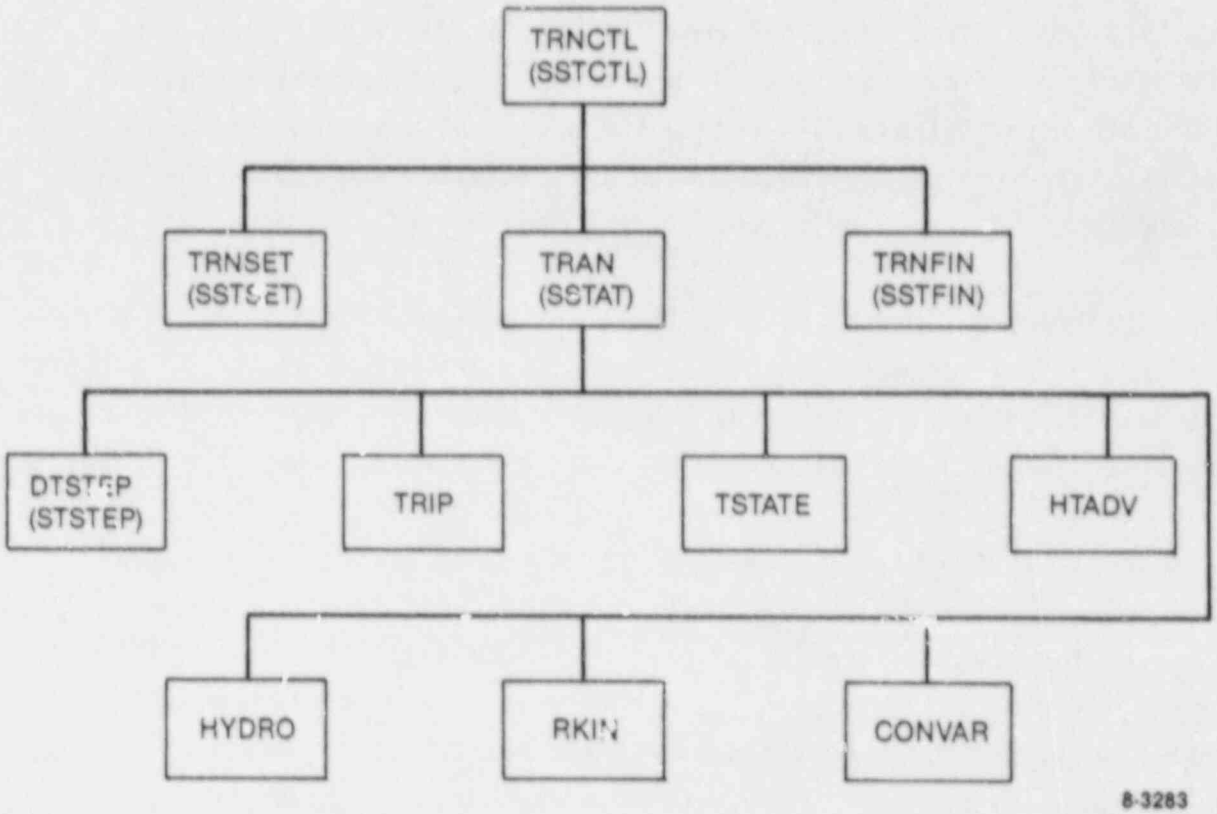

Figure 1-2. RELAP5/MOD2 transient (steady-state) structure.

kinetics advancement (RKIN), and control system advancement (CONVAR). The blocks are executed in the order shown in the figure from left to right, top to bottom. Although implicit techniques are used within some of the blocks (HTADV and HYDRO), data exchange between blocks is explicit; and the order of block execution dictates the time levels of feedback data between models. Thus, HTADV advances heat conduction/convection solutions using only old-time reactor kinetics power and old-time hydrodynamic conditions. HYDRO, since it follows HTADV, can use both new- and old-time heat transfer rates to compute heat transferred into a hydrodynamic volume.

1.2 Document Scope

The ECCS compendium[1-2], Section 4.4.3.1 lists three objectives for a code quality assurance (QA) document:

1. "To provide detailed information on (the quality of) closure equations, that is, on correlation models and/or criteria used in the code."

2. "To describe how these closure relations are coded in the program and assure that what is listed in the code manual is indeed what the code uses."

3. "To provide a technical rationale and justification for using these closure relations (as coded in the program) in the range of interest to [nuclear power plant] NPP safety evaluations."

The requirements the QA document must satisfy to meet these objectives are also listed in the compendium. Specifically, for each model or correlation, the QA document must:

1. Provide information on:

   a. The [illegible]nal source
   b. Its data base
   c. Its accuracy
   d. Its applicability to NPP conditions

2. Provide an assessment of effects, if the correlation is used outside its data base.

3. Describe how it is implemented in the code, that is, how it is coded.

4. Describe any modifications required to overcome computational difficulties.

5. Provide an assessment of effects due to implementation and/or modifications on code overall applicability and accuracy.

These requirements provided the focus for writing this models and correlations document, but the scope of work associated with accomplishing all of them proved to be too great to complete in the allotted time. The principal focus became, then, to provide a sound basis upon which further work could be established, if that were deemed necessary. Items 1, 3, and 4 in the list of document requirements can be seen to address the current status or definition of any model or correlation as implemented in the code. Therefore, these three items must be the first ones addressed. With this in mind, the work documented in this report concentrated on defining the current status of the models and correlations in RELAP5/MOD2, including a line-by-line review of the coding to ensure that it was an accurate reflection of the model descriptions in the code manual and the references cited in the manual. In addition, the data bases upon which individual correlations were based were reviewed and compared to typical reactor conditions. (Generally, these were chosen to be nominal operating conditions, since accident conditions vary depending on the particular accident transient being analyzed). Assessment was limited to a review of existing assessment calculations that appeared to be applicable. No specific assessment calculations were performed for this report, although some quantitative comparisons between certain correlations or models and published data were made for the purpose of demonstrating the accuracy of the implemented models.

A further accomplishment has been a qualitative assessment of the applicability of most of the correlations and models to nominal reactor operating conditions. This assessment is difficult to make in a global sense, because the importance of a model depends on its application, and a given accuracy may be adequate in one transient application but not in another. This emphasizes the significance of another aspect of the CSAU methodology, that of determining the important parameters for the transient of interest. Nonetheless, the evaluation of model or correlation adequacy must ultimately rest with the user. This document provides the information the user needs, in conjunction with a careful transient evaluation, to make that assessment.

1.3 Document Structure

This document is structured about the field equations used as the basis of RELAP5/MOD2. The field equations were chosen as the underlying thread because they provide the structure of the code itself; and using a common structure for the code and the description facilitates the use of this document in understanding the code. Section 2 describes the six basic field equations used in the two-fluid calculation. The equations as implemented in the code are related to published references showing how they are developed from local differential forms of the conservation equations, although the development itself is not included in this document. Each of the terms in the field equations is identified and related to a specific section of this document, so the reader can find the discussion of any item of interest quickly. The numerical form of the equations is included, for it is this numerical representation of the differential equations that actually forms the code. A detailed description of the geometric model used to discretize the equations is provided in code manual.

With the field equations identified, the next most pervasive aspect of the code calculation is probably the determination of the flow regime. Therefore, the flow regime map, or calculation, is discussed in Section 3, with a detailed table of all the flow regimes and the related parameters provided as an appendix to that section. Sections 4, 5, and 6 then provide, in order, a discussion of the models and correlations used to provide closure for the energy, mass, and momentum balance equations. The closure

models for the mass balance equations are closely related to those for the energy equations, so they were included before moving to the discussion of the models related to the momentum equations.

Section 7 describes the flow process models, such as the abrupt area change and the critical flow models. Section 8 describes specific component models, such as the pump model. Section 9 describes the heat structure process models, including the solution of the heat conduction equations and the energy source term model as represented by the reactor kinetics equations. Section 10 describes closure relations required by extra mass conservation fields (incomplete), and Section 11 describes the steady-state model.

1.4 Topics Not Included

Certain significant topics were omitted from the current task because of time limitations. For completeness, we recommend that these topics be addressed in a continuing code review in approximately the order given in the following list:

1. Reflood phenomena, including heat transfer specifically related to reflood.

2. Effects of noncondensibles, except in specific cases where it was convenient to include a brief discussion.

3. Effects of the numerical solution techniques on the representation of physical system response.

4. Effects of liquid solute (boron), or the models used to track liquid solute.

5. Certain component models, including the separator, accumulator, jet pumps, and secondary side components.

6. RELAP5/MOD2 control system, which is largely an algebraic system under the complete control of the user.

7. Nearly-implicit solution technique. This document addresses only the more widely used semi-implicit solution models.

8. Input and output processing routines.

9. State relationships.

10. Horizontal stratification pull-through and entrainment model.

1.5 References

1-1. V. H. Ransom, et al., RELAP5/MOD2 Code Manual, Volumes 1 and 2, NUREG/CR-4312, EGG-2396, August 1985 and December 1985.

1-2. U.S. Nuclear Regulatory Commission, Compendium of ECCS Research for Realistic LOCA Analysis, NUREG-1230 (draft), Section 4.4, May 1987.

1-3. V. H. Ransom, et al., RELAP5/MOD1 Code Manual, Volumes 1 and 2, NUREG/CR-1826, EGG-2070, March 1982.

1-4. K. V. Moore and W. H. Rettig, RELAP2 - A Digital Program for Reactor Blowdown and Power Excursion Analysis, IDO-17263, March 19t

1-5. W. H. Rettig, et al., RELAP3 - A Computer Program for Reactor Blowdown Analysis, IN-1445, February 1971.

1-6. K. V. Moore and W. H. Rettig. RELAP4 - A Computer Program for Transient Thermal-Hydraulic Analysis, ANCR-1127, March 1975.

1-7. S. R. Behling, et al., RELAP4/MOD7 - A Best Estimate Computer Program to Calculate Thermal and Hydraulic Phenomena in a Nuclear Reactor or Related System, NUREG/CR-1988, EGG-2089, August 1981.

2. FIELD EQUATIONS

The RELAP5/MOD2 code[2-1] solves six basic field equations for six dependent variables--pressure (P), specific internal energies (U_g and U_f), void fraction (α_g), and velocities (v_g and v_f). If a noncondensible gas is present, another dependent variable, X_n, the ratio of noncondensible gas mass to total gas mass, is included. An additional eight secondary dependent variables--phasic densities (ρ_g and ρ_f), interphase heat transfer rates per unit volume (Q_{ig} and Q_{if}), phasic temperature (T_g and T_f), saturation temperature (T^s), and vapor generation per unit volume (Γ_g)--are found through the use of closure or constitutive relations.

The field equations are presented to show where the constitutive models and correlations apply to the overall RELAP5/MOD2 solution. The discussion of the field equations will also explain the relative time levels at which the various variables are evaluated.

The basic two-fluid differential equations that form the basis for the hydrodynamic model are presented first, along with a modification to a more convenient form for solution.

2.1 Differential Equations

The differential form of the one-dimensional transient field equations is presented first for a one-component, vapor/liquid system. Modifications necessary to consider noncondensibles as a component in the vapor phase and boron as a nonvolatile solute component of the liquid phase are discussed in a following section.

2.1.1 Vapor/Liquid System

The basic field equations for the two-fluid model consist of two phasic continuity equations, two phasic momentum equations and two phasic energy equations. The equations are recorded in differential streamtube form, with time and one space dimension as independent variables and in terms of time and volume average dependent variables.

The continuity equations in RELAP5/MOD2 can be developed from the differential equation of continuity integrated over a system, in this case a control volume. For a system with a volume V(s), Slattery[2-2,p.217] states

$$\int_{V(s)} \frac{\partial \rho}{\partial t}\, dv + \int_{V(s)} \text{div}\,(\rho \vec{v})\, dv = 0 \quad . \tag{2-1}$$

A similar starting point is used by Hughes, et al.,[2-3] in determining a volume averaged mass conservation equation,

$$\frac{1}{V}\int_{V_a} \frac{\partial}{\partial t}\,\rho_a\, dV + \frac{1}{V}\int_{V_a} \frac{\partial}{\partial x_k}\,(\rho_a v_k^a)\, dV = 0 \quad . \tag{2-2}$$

Hughes, et al., developed Equation (2-2) by applying a generalized Reynolds transport theorem[2-3,p.13] and a volume-averaging relationship[2-2,p.199] to obtain an integrated form of the continuity equation over all the volumes and surfaces in the system. They reduced the integrated expression to obtain the form[2-3,p.18]

$$\frac{\partial}{\partial t}\left(\epsilon \alpha_a \bar{\rho}_a\right) + \frac{\partial}{\partial y_k}\left(\epsilon \alpha_a \widetilde{\rho_a v_k^a}\right) = \dot{m}_{ab} \quad . \tag{2-3}$$

ϵ is the porosity of a porous medium and may be taken as 1 for comparison with RELAP5/MOD2.

Changing the spatial derivative notation to x results in

$$\frac{\partial}{\partial t}\left(\alpha_a \rho_a\right) + \frac{\partial}{\partial x}\left(\alpha_a \rho_a v^a\right) = \dot{m}_{ab} \, . \tag{2-4}$$

The average notation has been dropped consistent with two assumptions:

1. The properties of the control volume are uniform, and

2. Terms representing the deviation from average properties are small compared to terms containing the average properties.

The general volume averaging procedure is more appropriately treated as an area average for the one-dimensional RELAP5 code. The general form of the area average of a parameter ψ_a is given by[2-3,p.47]

$$\overline{\psi_a}^A = \frac{1}{A} \int_{A_a} \psi_a (\vec{k},t)\, dA \ . \tag{2-5}$$

Hughes, et al.,[2-3,p.57] apply this averaging process to the local form of the continuity equation to find a one-dimensional area averaged continuity equation of the form

$$\frac{\partial}{\partial t}\left(A\alpha_a\rho_a\right) + \frac{\partial}{\partial x}\left(A\alpha_a\rho_a v_a\right) = \dot{m}_{ab} \ , \tag{2-6}$$

where notation explicitly denoting the area averages has been dropped in this report. If the area, A, is treated as independent of time, it can be extracted from the time derivative and the entire equation can be divided by A, resulting in

$$\frac{\partial}{\partial t}\left(\alpha_a\rho_a\right) + \frac{1}{A}\frac{\partial}{\partial x}\left(\alpha_a\rho_a v_a A\right) = \frac{1}{A}\dot{m}_{ab} \ . \tag{2-7}$$

If Γ is interpreted as a volumetric rate of mass transfer, then

$$\frac{\partial}{\partial t}\left(\alpha_a\rho_a\right) + \frac{1}{A}\frac{\partial}{\partial x}\left(\alpha_a\rho_a v_a A\right) = \Gamma \ . \tag{2-8}$$

In RELAP5/MOD2, Γ is positive for mass addition to the vapor phase, denoted g. The jump mass balance from Hughes, et al.,[2-3,p.20] can be written

$$\Gamma_g + \Gamma_f = 0, \tag{2-9}$$

so the two phasic continuity equations representing a vapor-liquid system can be written

$$\frac{\partial}{\partial t}(\alpha_g \rho_g) + \frac{1}{A}\frac{\partial}{\partial x}(\alpha_g \rho_g v_g A) = \Gamma_g \tag{2-10}$$

$$\frac{\partial}{\partial t}(\alpha_f \rho_f) + \frac{1}{A}\frac{\partial}{\partial x}(\alpha_f \rho_f v_f A) = -\Gamma_g \quad . \tag{2-11}$$

A similar procedure is used by Hughes, et al.,[2-3,p.59] to determine one-dimensional area averaged momentum equations. The general form of the momentum equation for phase "a" is stated as[2-3,p.43]

$$\frac{\partial}{\partial t}\left(\epsilon\alpha_a \bar{\rho}_a \bar{v}_i^a\right) + \frac{\partial}{\partial x_k}\left(\epsilon\alpha_a \bar{\rho}_a \bar{v}_i^a \bar{v}_k^a\right) = -\epsilon\alpha_a \frac{\partial \bar{p}^a}{\partial x_i} + \epsilon\alpha_a \frac{\partial}{\partial x_k}\bar{\sigma}_{ik}^a$$

$$- \bar{A}_{ab} B_{ab}^{ik}(\bar{v}_i^a - \bar{v}_i^b) - \bar{A}_{\epsilon a} B_{\epsilon a}^{ik} \bar{v}_i^a + \dot{m}_{ab}\hat{v}_i^a - \frac{\partial}{\partial x_k}\left(\epsilon\alpha_a \bar{\rho}_a v_i^{a'} v_k^{a'}\right)$$

$$+ \epsilon\alpha_a \bar{\rho}_a g_i^a \quad , \tag{2-12}$$

where

$$\bar{\sigma}_{ik}^a = -\frac{2}{3}\mu_a \bar{d}_{ii}^a \delta_{ik} + 2\mu_a \bar{d}_{ik}^a$$

$$\bar{d}_{ik}^a = \frac{1}{2}\left(\frac{\partial \bar{v}_i^a}{\partial x_k} + \frac{\partial \bar{v}_k^a}{\partial x_i}\right) \quad ,$$

$$\bar{A}_{ab} B_{ab}^{ik}(\bar{v}_i^a - \bar{v}_i^b) = \frac{1}{V}\int_{S_{ab}(\underline{y},t)} \left[\overline{-p_a' n_i^a + \sigma_{ik}^{a'} n_k^a}\right] dS \quad ,$$

$$\bar{A}_{\epsilon a} B_{\epsilon a}^{ik} \bar{v}_i^a = \frac{1}{V}\int_{S_{\epsilon a}(\underline{y},t)} \left[\overline{-p_a' n_k^a + \sigma_{ik}^{a'} n_k^a}\right] dS \quad ,$$

and

$$\dot{m}_{ab}\hat{v}_i^a = \frac{1}{V}\int_{S_{ab}(\underline{x},t)} \rho_a v_i^a \,({}_s v_k^a - v_k^a)\, n_k^a \, dS \quad .$$

The general form of Equation (2-12) is based on an initial differential form[2-3,p.20][2-2,p.37]

$$\frac{\partial}{\partial t}\left(\rho_a v_i^a\right) + \frac{\partial}{\partial x_k}\left(\rho_a v_i^a v_k^a\right) = -\frac{\partial p_a}{\partial x_i} + \frac{\partial}{\partial x_k}\sigma_{ik}^a + \rho_a g_i^a \quad , \tag{2-13}$$

and an interface jump momentum condition of[2-3,p.21]

$$\rho_a v_i^a \,({}_s\underline{v}^a - \underline{v}^a)\cdot\underline{n}^a + \sigma_{ik}^a n_k^a - p_a n_i^a = \rho_b v_i^b \,({}_s\underline{v}^b - \underline{v}^b)\cdot\underline{n}^b + \sigma_{ik}^b n_k^b - p_b n_i^b \tag{2-14}$$

This is equivalent to the jump momentum condition given by Slattery[2-2,p.227] for a general multiphase system,

$$\left[\vec{\rho v}\cdot(\vec{v}\cdot\vec{\xi} - u_{(\xi)}) - \overline{\overline{T}}\cdot\vec{\xi}\right] = 0 \quad . \tag{2-15}$$

Equation (2-12) can be simplified for application to RELAP5/MOD2 in the same manner as the continuity equation. Area averaging results in[2-3,p.60]

$$\frac{\partial}{\partial t}\left(A\epsilon\bar{\alpha}_a^A \bar{\rho}_a^A \bar{v}_x^a\right) + \frac{\partial}{\partial x}\left(A\epsilon\bar{\alpha}_a^A \bar{\rho}_a^A \bar{v}_x^a \bar{v}_x^a\right) = -A\epsilon\bar{\alpha}_a^A \frac{\partial}{\partial x}\bar{p}_a^A + A\epsilon\bar{\alpha}_a^A \frac{\partial}{\partial x}\bar{\sigma}_{xx}^a \tag{2-16}$$

$$+ A\epsilon\bar{\alpha}_a^A \bar{\rho}_a^A g_x^a + F_{ab}^x + F_{\epsilon a}^x + F_{wa}^x + \overline{\dot{m}_{ab}}^A \hat{v}_x^a - \overline{M_x^a}^A \quad .$$

Setting $\epsilon = 1$ and dropping the F_{ea}^x term and the last term representing a contribution from spatial nonuniformity gives

$$\frac{\partial}{\partial t}\left(A\alpha_a\rho_a v_a\right) + \frac{\partial}{\partial x}\left(A\alpha_a\rho_a v_a^2\right) = -A\alpha_a \frac{\partial}{\partial x} p_a + A\alpha_a \frac{\partial}{\partial x} \sigma_{xx}^a + A\alpha_a\rho_a g \qquad (2\text{-}17)$$

$$+ F_{ab} + F_{wa} + \dot{m}_{ab} \hat{v} .$$

Note the use of constitutive models through F_{ab}, interfacial drag, F_{wa}, wall drag, and $\hat{v}$, an interfacial speed. In addition, RELAP5/MOD2 does not include the viscous stress term, σ_{xx}. Therefore, removing A from the time derivative gives

$$A\frac{\partial}{\partial t}\left(\alpha_a\rho_a v_a\right) + \frac{\partial}{\partial x}\left(A\alpha_a\rho_a v_a^2\right) = -A\alpha_a \frac{\partial}{\partial x} p_a + A\alpha_a\rho_a g + F_{ab} + F_{wa} + \dot{m}_{ab} \hat{v}. \qquad (2\text{-}18)$$

The continuity equation, Equation (2-7), can be applied to the left hand side of Equation (2-18) by expanding the derivatives:

$$A\frac{\partial}{\partial t}\left(\alpha_a\rho_a v_a\right) + \frac{\partial}{\partial x}\left(A\alpha_a\rho_a v_a^2\right)$$

$$= A\alpha_a\rho_a \frac{\partial v_a}{\partial t} + Av_a \frac{\partial(\alpha_a\rho_a)}{\partial t} + v_a \frac{\partial}{\partial x}\left(\alpha_a\rho_a v_a A\right) + A\alpha_a\rho_a v_a \frac{\partial(v_a)}{\partial x}$$

$$= A\alpha_a\rho_a \left[\frac{\partial v_a}{\partial t} + v_a \frac{\partial v_a}{\partial x}\right] + Av_a \left[\frac{\partial(\alpha_a\rho_a)}{\partial t} + \frac{1}{A}\frac{\partial}{\partial x}\left(\alpha_a\rho_a v_a A\right)\right]$$

$$= A\alpha_a\rho_a \left[\frac{\partial v_a}{\partial t} + \frac{1}{2}\frac{\partial(v_a^2)}{\partial x}\right] + Av_a \left[\frac{1}{A}\dot{m}_{ab}\right] . \qquad (2\text{-}19)$$

The right-hand side of Equation (2-19) is often referred to as the nonconservative form. Substituting Equation (2-19) into Equation (2-18), and combining the last term of Equation (2-19) with the m_{ab} term in Equation (2-18) results in

$$A\alpha_a\rho_a \frac{\partial v_a}{\partial t} + \frac{1}{2} A\alpha_a\rho_a \frac{\partial(v_a^2)}{\partial x} =$$

$$- A\alpha_a \frac{\partial}{\partial x} p_a + A\alpha_a \rho_a g + F_{ab} + F_{wa} + \dot{m}_{ab} (\hat{v} - v_a) . \qquad (2\text{-}20)$$

Writing this equation for the vapor phase, g, modifying the form of the constitutive relations F_{ab} and F_{wa}, using one pressure P for both phases, and using $\Gamma_g A$ for $\dot{m}_{ab}$ gives

$$A\alpha_g \rho_g \frac{\partial v_g}{\partial t} + \frac{1}{2} A\alpha_g \rho_g \frac{\partial (v_g^2)}{\partial x} = -A\alpha_g \frac{\partial P}{\partial x} + A\alpha_g \rho_g g - A\alpha_g \rho_g FWG\ (v_g) \qquad (2\text{-}21)$$

$$- A\alpha_g \rho_g FIG\ (v_f - v_g) + A\Gamma_g (\hat{v} - v_g) - C\alpha_g \alpha_f \rho A \left[\frac{\partial}{\partial t} (v_g - v_f) \right.$$

$$\left. + v_f \frac{\partial v_g}{\partial x} - v_g \frac{\partial v_f}{\partial x} \right].$$

A similar equation can be written for the liquid phase:

$$A\alpha_f \rho_f \frac{\partial v_f}{\partial t} + \frac{1}{2} A\alpha_f \rho_f \frac{\partial (v_f^2)}{\partial x} = -A\alpha_f \frac{\partial P}{\partial x} + A\alpha_f \rho_f g - A\alpha_f \rho_f FWF\ (v_f) \qquad (2\text{-}22)$$

$$- A\alpha_f \rho_f FIF\ (v_f - v_g) - A\Gamma_g (\hat{v} - v_f) - C\alpha_g \alpha_f \rho A \left[\frac{\partial}{\partial t} (v_f - v_g) \right.$$

$$\left. + v_g \frac{\partial v_f}{\partial x} - v_f \frac{\partial v_g}{\partial x} \right].$$

Equations (2-21) and (2-22) are the RELAP5/MOD2 form of the phasic momentum equations. The coefficients of the constitutive terms have been modified to agree with the form of the constitutive relations discussed later in this report.

The last term in the RELAP5/MOD2 equations is a virtual mass term, representing a contribution to the interfacial interaction between the phases in somewhat the same manner as FIF or FIG.

The phasic energy equations are found in a manner similar to the other field equations. The local differential form is given by Hughes et al.[2-3,p.62] as

$$\frac{\partial}{\partial t}\left(\rho_a I_a\right) + \frac{\partial}{\partial y_k}\left(\rho_a I_a v_k^a\right) = -\frac{\partial}{\partial y_k} q_k^a - p_a d_{ii}^a + \sigma_{ij}^a d_{ij}^a + \rho_a Q_g^a \quad , \tag{2-23}$$

and an interface jump condition,

$$\rho_a I_a \left({}_s v_i^a - v_i^a\right) n_i^a - q_i^a n_i^a = \rho_b I_b \left({}_s v_i^b - v_i^b\right) n_i^b - q_i^b n_i^b \tag{2-24}$$

Equation (2-23) can be shown to be the same form as the internal energy form of the differential energy balance given in Slattery.[2-2,p.291] Equation (2-24) is a modified form of the jump energy balance shown by Slattery[2-2,p.292] for a total energy balance. The terms representing relative changes in kinetic energy and viscous stress normal to the interface have been dropped in this internal energy representation. In addition, PV work terms implicitly included in an enthalpy form of this jump condition appear to be missing from Equation (2-24).

Hughes, et al.,[2-3,p.63] develop the area-averaged energy equations in the same manner as the other field equations, resulting in a phasic energy equation

$$\frac{\partial}{\partial t}\left(A\epsilon\bar{\alpha}_a^A \bar{\rho}_a^A \bar{I}_a^A\right) + \frac{\partial}{\partial x}\left(A\epsilon\bar{\alpha}_a^A \bar{\rho}_a^A \bar{I}_a^A \bar{v}_x^A\right) = -A\epsilon\bar{\alpha}_a^A \frac{\partial}{\partial x}\bar{q}_x^A \tag{2-25}$$

$$- \bar{p}_a^A \frac{\partial}{\partial x}\left(A\epsilon\bar{\alpha}_a^A \bar{v}_x^A\right) + \bar{p}_a^A \frac{\partial}{\partial t}\left(A\epsilon\bar{\alpha}_a^A\right) + \hat{E}_{ab} + q_{ab} + q_{\epsilon a} + q_{wa}$$

$$+ A\epsilon\bar{\alpha}_a^A \bar{\rho}_a^A Q_g^a - E_a'$$

Treating the area, A, as being independent of time, dividing by A, setting $\epsilon = 1$, removing terms dealing explicitly with the solid phase, dropping the area average notation, and changing the notation for internal energy from I to U results in

$$\frac{\partial}{\partial t}(\alpha_a \rho_a U_a) + \frac{1}{A}(\alpha_a \rho_a U_a v_a A) = -\alpha_a \frac{\partial}{\partial x} q_x^a - \frac{p_a}{A}\frac{\partial}{\partial x}\left(A\alpha_a v\right) - \frac{p_a}{A}\frac{\partial}{\partial t}\left(A\alpha_a\right) + \frac{\hat{E}_{ab}}{A} + \frac{q_{ab}}{A}$$

$$+ \frac{q_{wa}}{A} + \alpha_a \rho_a Q_g^a \qquad (2\text{-}26)$$

The E_a' term is dropped by an assumption that nonuniformity terms are small by comparison with the average terms. The term in q_x^a on the right side of Equation (2-26) represents conduction heat transfer in the fluid and is not included in the RELAP5 field equations. The last term on the right, Q_g^a, is a volumetric energy source term. By dropping the fluid conduction term and modifying Equation (2-26) only to change the form of implementing the energy exchange terms, the RELAP5/MOD2 energy equation is written

$$\frac{\partial}{\partial t}(\alpha_g \rho_g U_g) + \frac{1}{A}\frac{\partial}{\partial x}(\alpha_g \rho_g U_g v_g A) = -P\frac{\partial \alpha_g}{\partial t} - \frac{P}{A}\frac{\partial}{\partial x}(\alpha_g v_g A)$$

$$+ Q_{wg} + Q_{ig} + \Gamma_{ig} h_g^* + \Gamma_w h_g^s + DISS_g \quad , \qquad (2\text{-}27)$$

where only the equation for the vapor phase has been shown. The first four terms show a direct correspondence to Equation (2-26), where a single pressure P was used for both phases. The exchange terms include the same information as Equation (2-26), where Q_{wg} and Q_{ig} account for heat transfer with the walls and through the interface, respectively; Γ_{ig} and Γ_w represent mass transfer; and $DISS_g$ represents a volumetric energy source term, particularly from pump effects and wall friction. The enthalpies h_g^* and h_g^s are chosen to give a total energy balance when the vapor and liquid energy equations are added and accommodate the PV terms missing from Equation (2-24). These will be discussed in more detail later.

A summary of the field differential equations for RELAP5/MOD2 follows with terms noted that will be explained in the discussion of constitutive models. The bracketed letter terms deal with specific constitutive models; Table 2.1 denotes a model for each letter and the section in which an explanation may be found.

TABLE 2-1. CONSTITUTIVE TERMS

A	Mass transfer	Section 5
B	Mass transfer in bulk fluid	Section 5
C	Mass transfer at wall	Section 5
D	Body force - gravity	Section 6
E	Wall friction	Section 6
F	Interphase momentum transfer	Section 5
G	Interphase friction drag	Section 6
H	Virtual mass force	Section 6
I	Wall heat transfer	Section 4
J	Interphase heat transfer	Section 4
K	Interphase latent heat	Section 4
L	Wall latent heat	Section 4
M	Wall friction and pump friction dissipation	Section 6

The phasic continuity equations are

$$\frac{\partial}{\partial t}(\alpha_g \rho_g) + \frac{1}{A}\frac{\partial}{\partial x}(\alpha_g \rho_g v_g A) = \Gamma_g \qquad (2\text{-}28)$$

$$\frac{\partial}{\partial t}(\alpha_f \rho_f) + \frac{1}{A}\frac{\partial}{\partial x}(\alpha_f \rho_f v_f A) = -\Gamma_g \ . \qquad (2\text{-}29)$$

where

$$\Gamma_f = -\Gamma_g \ . \qquad (2\text{-}30)$$

The interfacial mass transfer model assumes that total mass transfer consists of mass transfer in the bulk fluid and mass transfer at the wall,

$$\Gamma_g = \Gamma_{ig} + \Gamma_w \,. \tag{2-31}$$

[A] [B] [C]

The phasic conservation of momentum equations are used in a nonconservative form. For the vapor phase

$$\alpha_g \rho_g A \frac{\partial v_g}{\partial t} + \frac{1}{2}\alpha_g \rho_g A \frac{\partial v_g^2}{\partial x} = -\alpha_g A \frac{\partial P}{\partial x} + \alpha_g \rho_g B_x A - (\alpha_g \rho_g A) FWG(v_g) \tag{2-32}$$

[D] [E]

$$+ \Gamma_g A(v_{gI} - v_g) - (\alpha_g \rho_g A) FIG(v_g - v_f)$$

[F] [G]

$$- C\alpha_g \alpha_f \rho A \left[\frac{\partial (v_g - v_f)}{\partial t} + v_f \frac{\partial v_g}{\partial x} - v_g \frac{\partial v_f}{\partial x} \right],$$

[H]

and for the liquid phase

$$\alpha_f \rho_f A \frac{\partial v_f}{\partial t} + \frac{1}{2}\alpha_f \rho_f A \frac{\partial v_f^2}{\partial x} = -\alpha_f A \frac{\partial P}{\partial x} + \alpha_f \rho_f B_x A - (\alpha_f \rho_f A) FWF(v_f) \tag{2-33}$$

$$- \Gamma_g A(v_{fI} - v_f) - (\alpha_f \rho_f A) FIF(v_f - v_g)$$

$$- C\alpha_f \alpha_g \rho A \left[\frac{\partial (v_f - v_g)}{\partial t} + v_g \frac{\partial v_f}{\partial x} - v_f \frac{\partial v_g}{\partial x} \right].$$

The phasic energy equations are

$$\frac{\partial}{\partial t}(\alpha_g \rho_g U_g) + \frac{1}{A}\frac{\partial}{\partial x}(\alpha_g \rho_g U_g v_g A) = P\frac{\partial \alpha_g}{\partial t} - \frac{P}{A}\frac{\partial}{\partial x}(\alpha_g v_g A) \tag{2-34}$$

$$+ Q_{wg} + Q_{ig} + \Gamma_{ig} h_g^* + \Gamma_w h_g^s + DISS_g$$

[I] [J] [K] [L] [M]

$$\frac{\partial}{\partial t}(\alpha_f \rho_f U_f) + \frac{1}{A}\frac{\partial}{\partial x}(\alpha_f \rho_f U_f v_f A) = -P\frac{\partial \alpha_f}{\partial t} - \frac{P}{A}\frac{\partial}{\partial x}(\alpha_f v_f A) \qquad (2\text{-}35)$$

$$+ Q_{wf} + Q_{if} - \Gamma_{ig} h_f^* - \Gamma_w h_f^s + DISS_f \ .$$

2.1.1.1 Noncondensibles in the Gas Phase. The two-phase, single-component model is extended to account for the presence of a noncondensible component in the gas phase. The noncondensible component is assumed to be in mechanical and thermal equilibrium with the vapor phase and, if the subscript n represents the noncondensible phase,

$$v_n = v_g \qquad (2\text{-}36)$$

and

$$T_n = T_g \ . \qquad (2\text{-}37)$$

The noncondensible gas model assumes that all properties of the gas phase, subscript g, are Gibbs-Dalton mixture properties of the steam/noncondensible mixture. The quality, X, is likewise defined as the mass fraction of the entire gas phase. Thus the two basic continuity equations are unchanged. It is necessary to add an additional mass conservation equation for the noncondensible component

$$\frac{\partial}{\partial t}(\alpha_g \rho_g X_n) + \frac{1}{A}\frac{\partial}{\partial x}(\alpha_g \rho_g X_n v_g A) = 0 \qquad (2\text{-}38)$$

where X_n is the mass fraction of noncondensible component based on the gaseous phase mass.

The phasic momentum and energy equations are unchanged, but the vapor field properties are evaluated for the steam/noncondensible mixture.

2.1.1.2 Boron Component in the Liquid Field. The boron tracking model simulates the transport of a dissolved component in the liquid phase. The solution is assumed to be sufficiently dilute that the following assumptions are valid:

1. Liquid properties are not altered by the presence of the solute.

2. Solute is transported only in the liquid phase and only at the velocity of the liquid phase.

3. The energy transported by the solute is negligible.

4. The inertia of the solute is negligible.

5. The solute is transported at the velocity of the vapor phase if no liquid is present.

Under these assumptions, only an additional field equation for the conservation of the solute is required.

$$\frac{\partial \rho_B}{\partial t} + \frac{1}{A} \frac{\partial (C_B \alpha_f \rho_f v_f A)}{\partial x} = 0 \qquad (2\text{-}39)$$

where the concentration paremeter, C_B, is defined as the concentration of dissolved solid in mass units per mass unit of liquid phase,

$$C_B = \frac{\rho_B}{\rho(1 - X)} \, . \qquad (2\text{-}40)$$

2.1.2 Differential Equation Modified Form

A more convenient set of differential equations upon which to base the numerical solution scheme is obtained by expanding the time derivatives,

replacing the phasic continuity and momentum equations with sum and differences of the continuity and momentum equations and replacing certain terms in the equations with relations as will be explained.

2.1.2.1 Mass Continuity Equations. The sum mass continuity equation is obtained by expanding the time derivatives in Equations (2-28) and (2-29), adding the equations together and using the relation

$$\frac{\partial \alpha_f}{\partial t} = - \frac{\partial \alpha_g}{\partial t} . \tag{2-41}$$

This yields

$$\alpha_g \frac{\partial \rho_g}{\partial t} + \alpha_f \frac{\partial \rho_f}{\partial t} + (\rho_g - \rho_f)\frac{\partial \alpha_g}{\partial t} + \frac{1}{A}\frac{\partial}{\partial x}(\alpha_g \rho_g v_g A + \alpha_f \rho_f v_f A) = 0 . \tag{2-42}$$

The difference mass continuity equation is obtained by expanding the time derivatives in Equations (2-28) and (2-29), subtracting these equations, using Equation (2-31), and substituting Γ_g in the form,

$$\Gamma_g = - \frac{H_{ig}(T^s - T_g) + H_{if}(T^s - T_f)}{h_g^* - h_f^*} + \Gamma_w . \tag{2-43}$$

This yields

$$\alpha_g \frac{\partial \rho_g}{\partial t} - \alpha_f \frac{\partial \rho_f}{\partial t} + (\rho_g + \rho_f)\frac{\partial \alpha_g}{\partial t} + \frac{1}{A}\frac{\partial}{\partial x}(\alpha_g \rho_g v_g A - \alpha_f \rho_f v_f A)$$

$$= - \frac{2[H_{ig}(T^s - T_g) + H_{if}(T^s - T_f)]}{h_g^* - h_f^*} + 2\Gamma_w . \tag{2-44}$$

For the case of noncondensible density, the time derivative in Equation (2-38) is expanded to yield

$$\rho_g X_n \frac{\partial \alpha_g}{\partial t} + \alpha_g X_n \frac{\partial \rho_g}{\partial t} + \alpha_g \rho_g \frac{\partial X_n}{\partial t} + \frac{1}{A}\frac{\partial}{\partial x}(\alpha_g \rho_g X_n v_g A) = 0 . \tag{2-45}$$

2.1.2.2 Momentum Equations. The momentum equations are also written in sum and difference form. The sum momentum equation is obtained by the direct summation of Equations (2-32) and (2-33) with interface conditions [Equations (2-46) and (2-47)] substituted where appropriate and the cross-sectional area canceled throughout. The interface conditions are

$$v_{gI} = v_{fI} = v_I \tag{2-46}$$

and

$$\alpha_g\rho_g FIG = \alpha_f\rho_f FIF = \alpha_g\alpha_f\rho_g\rho_f FI \tag{2-47}$$

The spatial derivatives in the virtual mass term are neglected because of the inaccuracy in approximating them with the coarse nodalization used in system calculations. These operations yield the sum momentum equation

$$\alpha_g\rho_g \frac{\partial v_g}{\partial t} + \alpha_f\rho_f \frac{\partial v_f}{\partial t} + \frac{1}{2}\alpha_g\rho_g \frac{\partial v_g^2}{\partial x} + \frac{1}{2}\alpha_f\rho_f \frac{\partial v_f^2}{\partial x} = -\frac{\partial P}{\partial x} + \rho B_x \tag{2-48}$$

$$- \alpha_g\rho_g v_g FWG - \alpha_f\rho_f v_f FWF - \Gamma_g(v_g - v_f) .$$

The difference of the phasic momentum equations is obtained by dividing the vapor and liquid phasic momentum Equations (2-32) and (2-33) by $\alpha_g\rho_g$ and $\alpha_f\rho_f$ respectively and then subtracting. The interface conditions, Equations (2-46) and (2-47), are again used, and the common cross-sectional area is divided out. Again, the spatial derivatives in the virtual mass term are neglected. The resulting difference momentum differential equation is

$$\frac{\partial v_g}{\partial t} - \frac{\partial v_f}{\partial t} + \frac{1}{2}\frac{\partial v_g^2}{\partial x} - \frac{1}{2}\frac{\partial v_f^2}{\partial x} = -\left(\frac{1}{\rho_g} - \frac{1}{\rho_f}\right)\frac{\partial P}{\partial x} - v_g FWG + v_f FWF \tag{2-49}$$

$$+ \Gamma_g[\rho v_I - (\alpha_f\rho_f v_g + \alpha_g\rho_g v_f)]/(\alpha_g\rho_g\alpha_f\rho_f) - \rho FI(v_g - v_f)$$

$$- C[\rho^2/(\rho_g\rho_f)] \frac{\partial(v_g - v_f)}{\partial t}$$

where the interfacial velocity, v_I, is defined as

$$v_I = \lambda v_g + (1 - \lambda)v_f \tag{2-50}$$

and λ is chosen to be 0 for positive values of Γ_g and 1 for negative values of Γ_g. This ensures that the mass exchange process is dissipative.

2.1.2.3 Energy Equations. The energy equations are not summed or differenced but are left as phasic equations. The time derivative terms are expanded, the interfacial relations are replaced by appropriate terms, and various terms are reduced using the phasic mass conservation equations.

For the vapor energy equation, the Q_{ig} and Γ_{ig} are replaced by the following

$$Q_{ig} = H_{ig}(T^s - T_g) - \left(\frac{1 - \epsilon}{2}\right) \Gamma_w(h_g^s - h_f^s) \tag{2-51}$$

$$\Gamma_{ig} = - \frac{H_{ig}(T^s - T_g) + H_{if}(T^s - T_f)}{h_g^* - h_f^*} , \tag{2-52}$$

where $\epsilon = 1$ for $\Gamma_w > 0$ and $\epsilon = -1$ for $\Gamma_w < 0$.

The H_{ig}, H_{if}, $\partial\alpha_g/\partial t$ and the convective terms are collected giving the following form of the vapor energy equation,

$$(\rho_g U_g + P) \frac{\partial \alpha_g}{\partial t} + \alpha_g U_g \frac{\partial \rho_g}{\partial t} + \alpha_g \rho_g \frac{\partial U_g}{\partial t} + \frac{1}{A} \left[\frac{\partial}{\partial x}(\alpha_g \rho_g U_g v_g A)\right. \tag{2-53}$$

$$\left. + P \frac{\partial}{\partial x}(\alpha_g v_g A)\right] = - \left(\frac{h_f^*}{h_g^* - h_f^*}\right) H_{ig}(T^s - T_g) - \left(\frac{h_g^*}{h_g^* - h_f^*}\right) H_{if}(T^s - T_f)$$

$$+ \left[\left(\frac{1+\epsilon}{2}\right)h_g^s + \left(\frac{1-\epsilon}{2}\right)h_f^s\right]\Gamma_w + Q_{wg} + DISS_g \ .$$

For the liquid energy equation, the Q_{if}, Γ_{ig}, and $\partial\alpha_f/\partial t$ terms are replaced by

$$Q_{if} = H_{if}(T^s - T_f) - \left(\frac{1+\epsilon}{2}\right)\Gamma_w(h_g^s - h_f^s) \qquad (2\text{-}54)$$

and by Equations (2-52) and (2-41). The H_{ig}, H_{if}, $\partial\alpha_g/\partial t$ and the convective terms are collected, yielding the following for the liquid energy equation

$$-(\rho_f U_f + P)\frac{\partial\alpha_g}{\partial t} + \alpha_f U_f \frac{\partial\rho_f}{\partial t} + \alpha_f\rho_f\frac{\partial U_f}{\partial t} + \frac{1}{A}\left[\frac{\partial}{\partial x}(\alpha_f\rho_f U_f v_f A)\right. \qquad (2\text{-}55)$$

$$\left. + P\frac{\partial}{\partial x}(\alpha_f v_f A)\right] = \left(\frac{h_f^*}{h_g^* - h_f^*}\right)H_{ig}(T^s - T_g) + \left(\frac{h_g^*}{h_g^* - h_f^*}\right)H_{if}(T^s - T_f)$$

$$- \left[\left(\frac{1+\epsilon}{2}\right)h_g^s + \left(\frac{1-\epsilon}{2}\right)h_f^s\right]\Gamma_w + Q_{wf} + DISS_f \ .$$

The nonexpanded time derivative form of the mass and energy equations is also used, particularly to improve energy inaccuracies in the phase with the smaller volume fraction.

2.2 Difference Equations

The difference equations are obtained by integrating the differential equations with respect to the spatial variable, dividing out common area terms, and integrating over time. The mass and energy equations are spatially integrated across the cells from junction to junction, while the momentum equations are integrated across the junctions from cell center to cell center.

Several guidelines were followed in developing the difference equations representing the field differential equations. These are summarized from the RELAP5/MOD2 manual.

1. RELAP5 seeks to be consistent and conservative in mass and energy inventories. A greater degree of approximation is allowed for momentum effects. Both mass and energy are convected from the same cell, and each is evaluated at the same time levels (i.e., mass density is evaluated at the old-time level so energy is also evaluated at old time).

2. To achieve fast execution speed, implicit evaluation is used only for those terms responsible for the sonic wave propagation time step limit and those phenomena known to have small time constants. Thus, implicit evaluation is used for the velocity in mass and energy transport terms, the pressure gradient in the momentum equations, and the interphase mass and momentum exchange terms.

3. To further increase computing speed, time-level evaluations are selected so the resulting implicit terms are linear in the new time variables. Where it is necessary to retain nonlinearities, Taylor series expansions about old-time values are used to obtain a formulation linear in the new time variables (higher-order terms are neglected). Linearity results in high computing speed by eliminating the need to iteratively solve systems of nonlinear equations.

4. To allow easy degeneration to homogeneous, or single-phase, formulations, the momentum equations are used as a sum and a difference equation. The particular difference equation used is obtained by first dividing each of the phasic momentum equations by $\alpha_g\rho_g$ and $\alpha_f\rho_f$ for the vapor and liquid phase equations, respectively, and then subtracting.

2.2.1 Field Difference Equations

Using the above guidelines, the finite-difference equations for the mass, energy, and momentum are listed below. Some of the terms are intermediate time variables, which are written with a tilde (~).

The sum density equation is

$$V_L[\alpha^n_{g,L}(\tilde{\rho}^{n+1}_{g,L} - \rho^n_{g,L}) + \alpha^n_{f,L}(\tilde{\rho}^{n+1}_{f,L} - \rho^n_{f,L}) + (\rho^n_{g,L} - \rho^n_{f,L})(\tilde{\alpha}^{n+1}_{g,L} - \alpha^n_{g,L})]$$

$$+ (\dot{\alpha}^n_{g,j+1}\dot{\rho}^n_{g,j+1}v^{n+1}_{g,j+1}A_{j+1} - \dot{\alpha}^n_{g,j}\dot{\rho}^n_{g,j}v^{n+1}_{g,j}A_j)\Delta t$$

$$+ (\dot{\alpha}^n_{f,j+1}\dot{\rho}^n_{f,j+1}v^{n+1}_{f,j+1}A_{j+1} - \dot{\alpha}^n_{f,j}\dot{\rho}^n_{f,j}v^{n+1}_{f,j}A_j)\Delta t = 0 \quad . \tag{2-56}$$

The difference density equation is

$$V_L[\alpha^n_{g,L}(\tilde{\rho}^{n+1}_{g+L} - \rho^n_{g,L}) - \alpha^n_{f,L}(\tilde{\rho}^{n+1}_{f,L} - \rho^n_{f,L}) + (\rho^n_{g,L} + \rho^n_{f,L})(\tilde{\alpha}^{n+1}_{g,L} - \alpha^n_{g,L})]$$

$$+ (\dot{\alpha}^n_{g,j+1}\dot{\rho}^n_{g,j+1}v^{n+1}_{g,j+1}A_{j+1} - \dot{\alpha}^n_{g,j}\dot{\rho}^n_{g,j}v^{n+1}_{g,j}A_j)\Delta t$$

$$- (\dot{\alpha}^n_{f,j+1}\dot{\rho}^n_{f,j+1}v^{n+1}_{f,j+1}A_{j+1} - \dot{\alpha}^n_{f,j}\dot{\rho}^n_{f,j}v^{n+1}_{f,j}A_j)\Delta t$$

$$= -\left(\frac{2}{h^*_g - h^*_f}\right)^n_L V_L\Delta t[H^n_{ig,L}(\tilde{T}^{s,n+1}_L - \tilde{T}^{n+1}_{g,L})$$

$$+ H^n_{if,L}(\tilde{T}^{s,n+1}_L - \tilde{T}^{n+1}_{f,L})] + 2V_L\Delta t\,\Gamma^n_{w,L} \quad . \tag{2-57}$$

The noncondensible density equation is

$$V_L[\rho^n_{g,L}X^n_{n,L}(\tilde{\alpha}^{n+1}_{g,L} - \alpha^n_{g,L}) + \alpha^n_{g,L}X^n_{n,L}(\tilde{\rho}^{n+1}_{g,L} - \rho^n_{g,L})$$

$$+ \alpha^n_{g,L}\rho^n_{g,L}(\tilde{X}^{n+1}_{n,L} - X^n_{n,L})] + (\dot{\alpha}^n_{g,j+1}\dot{\rho}^n_{g,j+1}\dot{X}^n_{n,j+1}v^{n+1}_{g,j+1}A_{j+1}$$

$$- \dot{\alpha}^n_{g,j}\dot{\rho}^n_{g,j}\dot{X}^n_{n,j}v^{n+1}_{g,j}A_j)\Delta t = 0 \quad . \tag{2-58}$$

The vapor energy equation is

$$V_L\,[(\rho^n_{g,L}U^n_{g,L} + P^n_L)(\tilde{\alpha}^{n+1}_{g,L} - \alpha^n_{g,L}) + \alpha^n_{g,L}U^n_{g,L}(\tilde{\rho}^{n+1}_{g,L} - \rho^n_{g,L})$$

$$+ \alpha^n_{g,L}\rho^n_{g,L}(\tilde{U}^{n+1}_{g,L} - U^n_{g,L})] + [\dot{\alpha}^n_{g,j+1}(\dot{\rho}^n_{g,j+1}\dot{U}^n_{g,j+1} + P^n_L)v^{n+1}_{g,j+1}A_{j+1}$$

$$- \dot{\alpha}^n_{g,j}(\dot{\rho}^n_{g,j}\dot{U}^n_{g,j} + P^n_L)v^{n+1}_{g,j}A_j]\Delta t = \Bigg\{ - \left(\frac{h^*_f}{h^*_g - h^*_f}\right)^n_L H^n_{ig,L}(\tilde{T}^{s,n+1}_L - \tilde{T}^{n+1}_{g,L})$$

$$- \left(\frac{h^*_g}{h^*_g - h^*_f}\right)^n_L H^n_{if,L}(\tilde{T}^{s,n+1}_L - \tilde{T}^{n+1}_{f,L}) + [(\tfrac{1+\epsilon}{2})h^{s,n}_{g,L} + (\tfrac{1-\epsilon}{2})h^{s,n}_{f,L}]\Gamma^n_{w,L}$$

$$+ Q^n_{wg,L} + DISS^n_{g,L}\Bigg\}V_L\Delta t \quad . \tag{2-59}$$

The liquid energy equation is

$$V_L[-(\rho^n_{f,L}U^n_{f,L} + P^n_L)(\tilde{\alpha}^{n+1}_{g,L} - \alpha^n_{g,L}) + \alpha^n_{f,L}U^n_{f,L}(\tilde{\rho}^{n+1}_{f,L} - \rho^n_{f,L})$$

$$+ \alpha^n_{f,L}\rho^n_{f,L}(\tilde{U}^{n+1}_{f,L} - U^n_{f,L})] + [\dot{\alpha}^n_{f,j+1}(\dot{\rho}^n_{f,j+1}\dot{U}^n_{f,j+1} + P^n_L)v^{n+1}_{f,j+1}A_{j+1}$$

$$- \dot{\alpha}^n_{f,j}(\dot{\rho}^n_{f,j}\dot{U}^n_{f,j} + P^n_L)v^{n+1}_{f,j}A_j]\Delta t = \Bigg\{\left(\frac{h^*_f}{h^*_g - h^*_f}\right)^n_L H^n_{ig,L}(\tilde{T}^{s,n+1}_L - \tilde{T}^{n+1}_{g,L})$$

$$+ \left(\frac{h^*_g}{h^*_g - h^*_f}\right)^n_L H^n_{if,L}(\tilde{T}^{s,n+1}_L - \tilde{T}^{n+1}_{f,L}) - [(\tfrac{1+\epsilon}{2})h^{s,n}_{g,L} + (\tfrac{1-\epsilon}{2})h^{s,n}_{f,L}]\Gamma^n_{w,L}$$

$$+ Q^n_{wf,L} + DISS^n_{f,L}\Bigg\}V_L\Delta t \quad . \tag{2-60}$$

The difference equation for the sum momentum is

$$(\alpha_g\rho_g)^n_j\,(v^{n+1}_g - v^n_g)_j\Delta x_j + (\alpha_f\rho_f)^n_j\,(v^{n+1}_f - v^n_f)_j\Delta x_j$$

$$+ \tfrac{1}{2}(\dot{\alpha}_g\dot{\rho}_g)_j^n \left[(v_g^2)_L^n - (v_g^2)_K^n\right] \Delta t + \tfrac{1}{2}(\dot{\alpha}_f\dot{\rho}_f)_j^n \left[(v_f^2)_L^n - (v_f^2)_K^n\right]\Delta t$$

$$- \tfrac{1}{2}\left[(\dot{\alpha}_g\dot{\rho}_g)_j^n VISG_j^n + (\dot{\alpha}_f\dot{\rho}_f)_j^n VISF_j^n\right]\Delta t$$

$$= - (P_L - P_K)^{n+1} \Delta t + \left[\rho_j^n B_x - (\alpha_g\rho_g)_j^n (v_g)_j^{n+1} FWG_j^n\right.$$

$$\left. - (\alpha_f\rho_f)_j^n (v_f)_j^{n+1} FWF_j^n - (\Gamma_g)_j^n (v_g - v_f)_j^{n+1}\right] \Delta x_j \Delta t$$

$$- [(\dot{\alpha}_g\dot{\rho}_g)_j^n HLOSSG_j^n v_{g,j}^{n+1} + (\dot{\alpha}_f\dot{\rho}_f)_j^n HLOSSF_j^n v_{f,j}^{n+1}] \Delta t \qquad (2\text{-}61)$$

and the difference momentum equation,

$$\left[1 + C\rho^2/(\rho_g\rho_f)\right]_j^n \left[(v_g^{n+1} - v_g^n) - (v_f^{n+1} - v_f^n)\right]_j \Delta x_j$$

$$+ \tfrac{1}{2}\left[(\dot{\alpha}_g\dot{\rho}_g)/(\alpha_g\rho_g)\right]_j^n \left[(v_g^2)_L^n - (v_g^2)_K^n\right]\Delta t - \tfrac{1}{2}\left[(\dot{\alpha}_g\dot{\rho}_g)/(\alpha_g\rho_g)\right]_j^n VISG_j^n \Delta t$$

$$- \tfrac{1}{2}\left[(\dot{\alpha}_f\dot{\rho}_f)/(\alpha_f\rho_f)\right]_j^n \left[(v_f^2)_L^n - (v_f^2)_K^n\right]\Delta t + \tfrac{1}{2}\left[(\dot{\alpha}_f\dot{\rho}_f)/(\alpha_f\rho_f)\right]_j^n VISF_j^n \Delta t$$

$$= - [(\rho_f - \rho_g)/(\rho_g\rho_f)]_j^n (P_L - P_K)^{n+1} \Delta t - \left\{FWG_j^n (v_g)_j^{n+1} - FWF_j^n (v_-)_j^{n+1}\right.$$

$$- \left[\Gamma_g^n (\rho^n v_I^{n+1} - \alpha_f^n \rho_f^n v_g^{n+1} - \alpha_g^n \rho_g^n v_f^{n+1}) / (\alpha_g\rho_g\alpha_f\rho_f)^n\right]_j$$

$$\left. + (\rho FI)_j^n (v_g - v_f)_j^{n+1}\right\} \Delta x_j \Delta t - \left\{\left[(\dot{\alpha}_g\dot{\rho}_g)/(\alpha_g\rho_g)\right]_j^n HLOSSG_j^n v_{g,j}^{n+1}\right.$$

$$\left. - \left[(\dot{\alpha}_f\dot{\rho}_f)/(\alpha_f\rho_f)\right]_j^n HLOSSF_j^n v_{f,j}^{n+1}\right\} \Delta t \quad . \qquad (2\text{-}62)$$

2.2.2 Donored Terms

The quantities having a dot overscore are donored quantities based on the junction velocities, v_g and v_f. The donored quantities are volume average scalar quantities defined analytically as

$$\dot{\phi} = \frac{1}{2}(\phi_K + \phi_L) + \frac{1}{2}\frac{|v|}{v}(\phi_K - \phi_L),\ v \neq 0 \qquad (2\text{-}63)$$

where ϕ is any of the donored properties and v is the appropriate velocity (that is, vapor or liquid). For the degenerate case of $v = 0$, a density-weighted average formulation is used

$$\dot{\phi} = \frac{\rho_K\phi_K + \rho_L\phi_L}{\rho_K + \rho_L},\ v = 0 \qquad (2\text{-}64)$$

for all donored properties except for the densities. (A simple average is used for the donored densities.) In this equation, ρ_K and ρ_L are the appropriate density (that is, vapor or liquid). Where donored values are not used at junctions, linear interpolations between neighboring cell values are used.

2.2.3 Intermediate-Time Terms for Mass and Energy Equations

The intermediate-time phasic densities used in the mass and energy equations are obtained by linearizing the phasic state relations about the old-time values.

$$\bar{\rho}^{n+1}_{g,L} = \rho^n_{g,L} + \left(\frac{\partial\rho_g}{\partial P}\right)^n_L (P^{n+1}_L - P^n_L) + \left(\frac{\partial\rho_g}{\partial X_n}\right)^n_L (\bar{X}^{n+1}_{n,L} - X^n_{n,L})$$

$$+ \left(\frac{\partial\rho_g}{\partial U_g}\right)^n_L (\bar{U}^{n+1}_{g,L} - U^n_{g,L}),\ \text{and} \qquad (2\text{-}65)$$

$$\bar{\rho}^{n+1}_{f,L} = \rho^n_{f,L} + \left(\frac{\partial\rho_f}{\partial P}\right)^n_L (P^{n+1}_L - P^n_L) + \left(\frac{\partial\rho_f}{\partial U_f}\right)^n_L (\bar{U}^{n+1}_{f,L} - U^n_{f,L}) \quad . \qquad (2\text{-}66)$$

The state derivatives used in Equations (2-65) and (2-66) are obtained from the state relationships.

Intermediate-time interphase heat transfer rates are written in the finite difference form

$$\bar{Q}^{n+1}_{ig,L} = H^{n}_{ig,L}(\bar{T}^{s,n+1}_{L} - \bar{T}^{n+1}_{g,L}) - (\frac{1 - \epsilon}{2})\Gamma^{n}_{w,L}(h^{s,n}_{g,L} - h^{s,n}_{f,L}) \tag{2-67}$$

$$\bar{Q}^{n+1}_{if,L} = H^{n}_{if,L}(\bar{T}^{s,n+1}_{L} - \bar{T}^{n+1}_{f,L}) - (\frac{1 + \epsilon}{2})\Gamma^{n}_{w,L}(h^{s,n}_{g,L} - h^{s,n}_{f,L}) \ . \tag{2-68}$$

The intermediate-time temperatures are obtained by linearizing the temperature relations about the old time values.

$$\bar{T}^{s,n+1}_{L} = T^{s,n}_{L} + \left(\frac{\partial T^{s}}{\partial P}\right)^{n}_{L}(P^{n+1}_{L} - P^{n}_{L}) + \left(\frac{\partial T^{s}}{\partial X_{n}}\right)^{n}_{L}(\bar{X}^{n+1}_{n,L} - X^{n}_{n,L})$$

$$+ \left(\frac{\partial T^{s}}{\partial U_{g}}\right)^{n}_{L}(\bar{U}^{n+1}_{g,L} - U^{n}_{g,L}) \tag{2-69}$$

$$\bar{T}^{n+1}_{g,L} = T^{n}_{g,L} + \left(\frac{\partial T_{g}}{\partial P}\right)^{n}_{L}(P^{n+1}_{L} - P^{n}_{L}) + \left(\frac{\partial T_{g}}{\partial X_{n}}\right)^{n}_{L}(\bar{X}^{n+1}_{n,L} - X^{n}_{n,L})$$

$$+ \left(\frac{\partial T_{g}}{\partial U_{g}}\right)^{n}_{L}(\bar{U}^{n+1}_{g,L} - U^{n}_{g,L}) \tag{2-70}$$

$$\bar{T}^{n+1}_{f,L} = T^{n}_{f,L} + \left(\frac{\partial T_{f}}{\partial P}\right)^{n}_{L}(P^{n+1}_{L} - P^{n}_{L}) + \left(\frac{\partial T_{f}}{\partial U_{f}}\right)^{n}_{L}(\bar{U}^{n+1}_{f,L} - U^{n}_{f,L}) \ . \tag{2-71}$$

The temperature derivatives used in Equations (2-69) through (2-71) are obtained from the state relationships.

2.2.4 Terms for Momentum Equations

A similar approach is used to obtain the finite-difference form for the phasic momentum equations. In this case, volume-average properties for the momentum control volume are taken as junction properties (that is, linear interpolations between mass and energy control volume centers). The momentum flux terms are approximated using a donor-like formulation that results in a centered velocity gradient term and a viscous-like term.

The viscous terms are defined as

$$VISG_j^n = \frac{1}{2}\left\{\left|v_{g,L}^n\right|\left[(v_g^n)_{j+1}(A_{j+1}/A_j) - (v_g^n)_j\right]\right.$$

$$\left. - \left|v_{g,K}^n\right|\left[(v_g^n)_j - (v_g^n)_{j-1}(A_{j-1}/A_j)\right]\right\} \qquad (2\text{-}72)$$

and

$$VISF_j^n = \frac{1}{2}\left\{\left|v_{f,L}^n\right|\left[(v_f^n)_{j+1}(A_{j+1}/A_j) - (v_f^n)_j\right]\right.$$

$$\left. - \left|v_{f,K}^n\right|\left[(v_f^n)_j - (v_f^n)_{j-1}(A_{j-1}/A_j)\right]\right\} \qquad (2\text{-}73)$$

In the momentum Equations (2-61) and (2-62), the scalar or thermodynamic variables needed at the junctions are either linear interpolations between the neighboring cell values or donored quantities. The $HLOSSG_j$ and $HLOSSF_j$ terms contain both code-calculated abrupt area change loss terms and user-specified loss terms.

2.2.5 Nonexpanded Mass and Energy Equations

Using the same averaging techniques, the nonexpanded form of the mass and energy Equations (2-28), (2-29), (2-38), (2-34), and (2-35) are next presented in their final finite difference form.

The nonexpanded vapor density Equation (2-28) becomes

$$V_L[(\alpha_g\rho_g)_L^{n+1} - (\alpha_g\rho_g)_L^n] + (\dot{\alpha}_{g,j+1}^n\dot{\rho}_{g,j+1}^n v_{g,j+1}^{n+1}A_{j+1} - \dot{\alpha}_{g,j}^n\dot{\rho}_{g,j}^n v_{g,j}^{n+1}A_j)\Delta t$$

$$= \bar{\Gamma}_{g,L}^{n+1} V_L\Delta t \quad . \tag{2-74}$$

The intermediate time variable, $\bar{\Gamma}_{g,L}^{n+1}$, is obtained using the finite difference form of Equation (2-43), and is written

$$\bar{\Gamma}_{g,L}^{n+1} = -\frac{H_{ig,L}^n(\bar{T}_L^{s,n+1} - \bar{T}_{g,L}^{n+1}) + H_{if,L}^n(\bar{T}_L^{s,n+1} - \bar{T}_{f,L}^{n+1})}{h_{g,L}^{*,n} - h_{f,L}^{*,n}} + \Gamma_{w,L}^n \quad . \tag{2-75}$$

The nonexpanded liquid density Equation (2-29) becomes

$$V_L[(\alpha_f\rho_f)_L^{n+1} - (\alpha_f\rho_f)_L^n] + (\dot{\alpha}_{f,j+1}^n\dot{\rho}_{f,j+1}^n v_{f,j+1}^{n+1}A_{j+1} - \dot{\alpha}_{f,j}^n\dot{\rho}_{f,j}^n v_{f,j}^{n+1}A_j)\Delta t$$

$$= -\bar{\Gamma}_{g,L}^{n+1}V_L\Delta t \quad . \tag{2-76}$$

The nonexpanded noncondensible density Equation (2-38) becomes

$$V_L[(\alpha_g\rho_g X_n)_L^{n+1} - (\alpha_g\rho_g X_n)_L^n] + (\dot{\alpha}_{g,j+1}^n\dot{\rho}_{g,j+1}^n\dot{X}_{n,j+1}^n v_{g,j+1}^{n+1}A_{j+1}$$

$$- \dot{\alpha}_{g,j}^n\dot{\rho}_{g,j}^n\dot{X}_{n,j}^n v_{g,j}^{n+1}A_j)\Delta t = 0 \quad . \tag{2-77}$$

The nonexpanded vapor energy Equation (2-34) becomes

$$V_L[(\alpha_g\rho_g U_g)_L^{n+1} - (\alpha_g\rho_g U_g)_L^n] + [\dot{\alpha}_{g,j+1}^n(\dot{\rho}_{g,j+1}^n\dot{U}_{g,j+1}^n + P_L^n)v_{g,j+1}^{n+1}A_{j+1}$$

$$- \dot{\alpha}_{g,j}^n(\dot{\rho}_{g,j}^n\dot{U}_{g,j}^n + P_L^n)v_{g,j}^{n+1}A_j]\Delta t = -V_L P_L^n(\bar{\alpha}_{g,L}^{n+1} - \alpha_{g,L}^n)$$

$$+\left\{-\left(\frac{h_f^*}{h_g^* - h_f^*}\right)_L^n H_{ig,L}^n(\bar{T}_L^{s,n+1} - \bar{T}_{g,L}^{n+1}) - \left(\frac{h_g^*}{h_g^* - h_f^*}\right)_L^n H_{if,L}^n(\bar{T}_L^{s,n+1} - \bar{T}_{f,L}^{n+1}) + [(\frac{1+\epsilon}{2})h_{g,L}^{s,n} + (\frac{1-\epsilon}{2})h_{f,L}^{s,n}]\Gamma_{w,L}^n + Q_{wg,L}^n + DISS_{g,L}^n\right\}V_L\Delta t \quad . \tag{2-78}$$

The variables $\bar{\alpha}_{g,L}^{n+1}$, $\bar{T}_L^{s,n+1}$, $\bar{T}_{g,L}^{n+1}$, and $\bar{T}_{f,L}^{n+1}$ are written with a tilde (~) to indicate they are intermediate-time variables. The nonexpanded liquid energy Equation (2-35) becomes

$$V_L[(\alpha_f\rho_f U_f)_L^{n+1} - (\alpha_f\rho_f U_f)_L^n] + [\dot{\alpha}_{f,j+1}^n(\dot{\rho}_{f,j+1}^n\dot{U}_{f,j+1}^n + P_L^n)v_{f,j+1}^{n+1}A_{j+1} - \dot{\alpha}_{f,j}^n(\dot{\rho}_{f,j}^n\dot{U}_{f,j}^n + P_L^n)v_{f,j}^{n+1}A_j]\Delta t = V_L P_L^n(\bar{\alpha}_{g,L}^{n+1} - \alpha_{g,L}^n)$$

$$+\left\{\left(\frac{h_f^*}{h_g^* - h_f^*}\right)_L^n H_{ig,L}^n(\bar{T}_L^{s,n+1} - \bar{T}_{g,L}^{n+1}) + \left(\frac{h_g^*}{h_g^* - h_f^*}\right)_L^n H_{if,L}^n(\bar{T}_L^{s,n+1} - \bar{T}_{f,L}^{n+1}) - [(\frac{1+\epsilon}{2})h_{g,L}^{s,n} + (\frac{1-\epsilon}{2})h_{f,L}^{s,n}]\Gamma_{w,L}^n + Q_{wf,L}^n + DISS_{f,L}^n\right\}V_L\Delta t \quad . \tag{2-79}$$

2.2.6 Volume-Average Velocities

Volume-average velocities are required for the momentum flux calculation, evaluation of the frictional forces, and the Courant time step limit. In a simple constant area passage, the arithmetic average between the inlet and outlet is a satisfactory approximation. However, at branch volumes with multiple inlets and/or outlets, or for volumes with abrupt area changes, use of the arithmetic average results in nonphysical behavior.

The RELAP5 volume-average velocity formulas have the form

$$(v_f)_L^n = \frac{\left\{\Sigma_j \left(\dot{\alpha}_f \dot{\rho}_f v_f\right)_j^n A_j \cdot \Sigma_j A_j\right\}_{\text{inlets}}}{\left\{\Sigma_j \left(\dot{\alpha}_f \dot{\rho}_f\right)_j^n A_j \cdot A_L\right\}_{\substack{\text{inlets and} \\ \text{outlets}}}}$$

$$+ \frac{\left\{\Sigma_j \left(\dot{\alpha}_f \dot{\rho}_f v_f\right)_j^n A_j \cdot \Sigma_j A_j\right\}_{\text{outlets}}}{\left\{\Sigma_j \left(\dot{\alpha}_f \dot{\rho}_f\right)_j^n A_j \cdot A_L\right\}_{\substack{\text{inlets and} \\ \text{outlets}}}} \qquad (2\text{-}80)$$

and

$$(v_g)_L^n = \frac{\left\{\Sigma_j \left(\dot{\alpha}_g \dot{\rho}_g v_g\right)_j^n A_j \cdot \Sigma_j A_j\right\}_{\text{inlets}}}{\left\{\Sigma_j \left(\dot{\alpha}_g \dot{\rho}_g\right)_j^n A_j \cdot A_L\right\}_{\substack{\text{inlets and} \\ \text{outlets}}}}$$

$$+ \frac{\left\{\Sigma_j \left(\dot{\alpha}_g \dot{\rho}_g v_g\right)_j^n A_j \cdot \Sigma_j A_j\right\}_{\text{outlets}}}{\left\{\Sigma_j \left(\dot{\alpha}_g \dot{\rho}_g\right)_j^n A_j \cdot A_L\right\}_{\substack{\text{inlets and} \\ \text{outlets}}}} \qquad (2\text{-}81)$$

2.3 References

2-1. V. H. Ransom, et al., RELAP5/MOD2 Code Manual, NUREG/CR-4312, INEL, EG&G Idaho, Inc., 1985.

2-2. J. C. Slattery, Momentum, Energy, and Mass Transfer in Continua, New York: McGraw-Hill, 1972.

2-3. E. D. Hughes, et al, An Evaluation of State-of-the-Art Two-Velocity Two-Phase Flow Models and Their Applicability to Nuclear Reactor Transient Analysis, Volume 2, EPRI NP-143, EPRI, 1976.

3. FLOW REGIME MAPS

Three flow regime maps for two-phase flow are used in the RELAP5/MOD2 code: (a) a horizontal map ($\pm 15^{0}$ from exact horizontal); (b) a vertical map (for all angles greater than 15^{0} from the horizontal); and (c) a high mixing map for flow through pumps. The flow regime calculations for interfacial heat and mass transfer, interfacial drag, and wall drag are found in subroutine PHAINT. Wall heat transfer depends on the flow regime maps in a less direct way. Generally, void fraction and mass flux are used to incorporate the effects of the flow regime. Because the wall heat transfer is calculated before the hydrodynamics, the flow information is taken from the previous time step.

3.1 Horizontal Flow Regime Map

3.1.1 Map as Coded

A schematic of the horizontal flow regime map as coded in RELAP5/MOD2 is illustrated in Figure 3-1. The map consists of bubbly, slug, annular mist, dispersed (droplets or mist), and horizontally stratified regimes. Transition regions used in the code are indicated. Such transitions are included in the map primarily to preclude discontinuities when going from one correlation to another in drag and heat and mass transfer. Details of the interpolating functions employed between correlations are given in those sections that describe the various correlations. Figure 3-2 illustrates the geometry for horizontal stratification.

Values for the parameters governing the flow regime transitions are shown in Figure 3-3 or listed below. G is the average mixture mass flux given by

$$G = \left| \alpha_g \rho_g v_g + \alpha_f \rho_f v_f \right| \quad . \tag{3-1}$$

$\alpha_{DE} = 0.75$,

$\alpha_{AC} = 0.8$,

$\alpha_{AD} = 10^{-7}$,

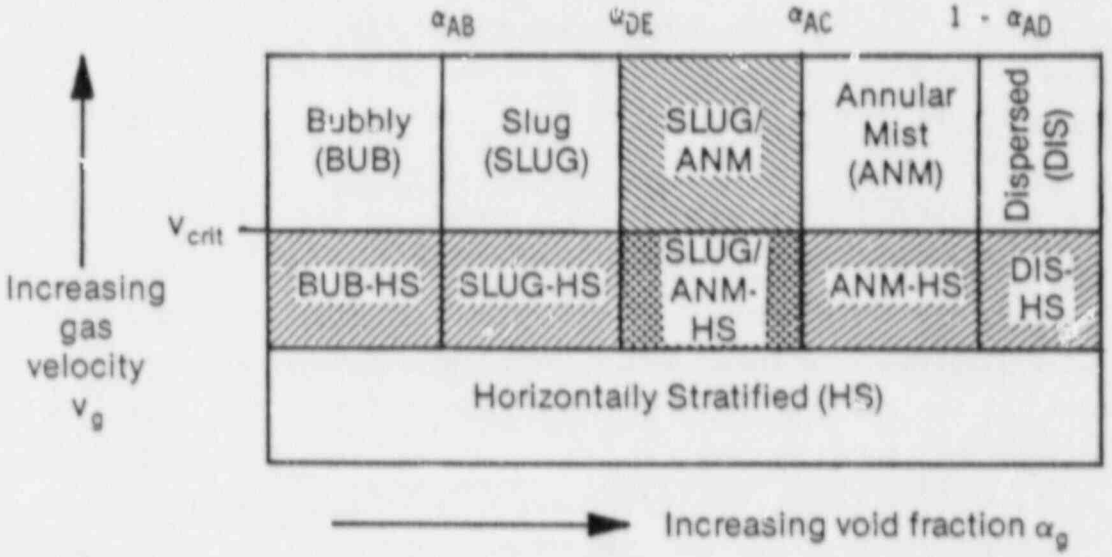

Figure 3-1. Schematic of horizontal flow regime map with hatchings, indicating transition regions.

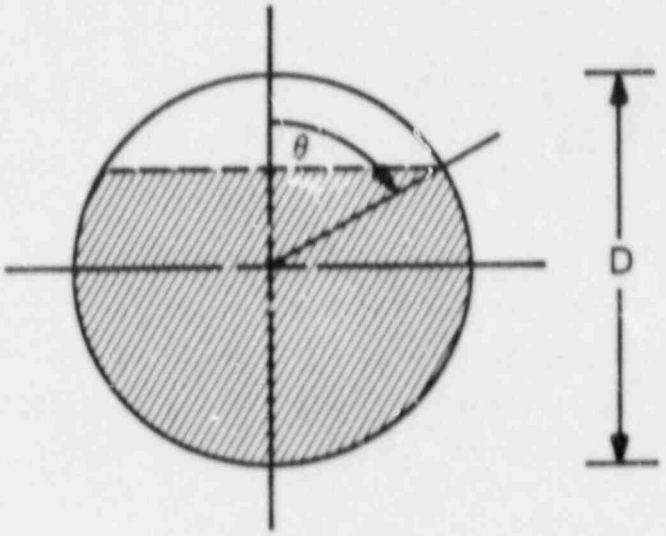

Figure 3-2. Schematic of horizontally stratified flow in a pipe.

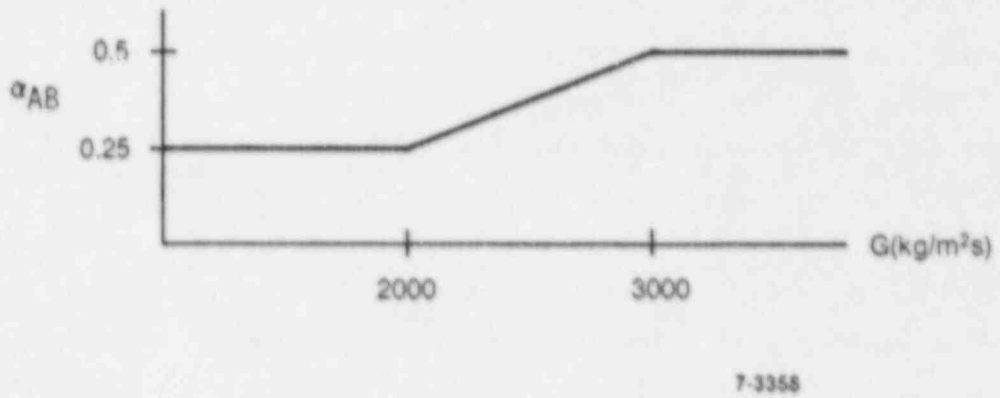

Figure 3-3. Horizontal bubbly-to-slug void fraction transition in RELAP5/MOD2.

and

$$v_{crit} = \frac{1}{2}\left[\frac{(\rho_f - \rho_g)\, g\, \alpha_g\, A}{\rho_g\, D \sin\theta}\right]^{1/2} (1 - \cos\theta) \ . \qquad (3\text{-}2)$$

where D is the pipe diameter or equivalent diameter (hydraulic diameter) and A is the cross-sectional area of the pipe, $A = \pi D^2/4$. θ is the angle between the vertical and the stratified liquid level, as shown in Figure 3-2. The subscripts of the transition void fractions (α_{AB}, α_{DE}, etc.) are mnemonically related to the coded variables representing them.

3.1.2 Map Basis and Assessment

The geometrical configuration of a two-phase flow regime is characterized by a combination of void fraction and interfacial area concentration and arrangement.[3-1] Traditionally, however, flow regime maps have been constructed using superficial velocities[3-2, 3-3] which, strictly, do not uniquely define the flow regime. Ishii and Mishima[3-1] contend that while superficial velocities may provide for suitable flow regime mapping for steady, developed flow, the same is not true for transient or developing conditions such as arise frequently for nuclear reactor thermal-hydraulics. They recommend a direct geometric parameter, such as void fraction, for flow regime determination for unsteady and entrance flows where a two-fluid model (such as is used in RELAP5/MOD2) is more appropriate than a more traditional mixture model. RELAP5/MOD2 uses the void fraction, α_g, to characterize the two-phase flow regimes. Taitel and Dukler[3-4] have devised a horizontal map from analytical considerations, albeit sometimes involving uncorroborated assumptions, that uses at least the void fraction for all regime transitions. Furthermore, in a later paper, they use the same flow transition criteria to characterize transient two-phase horizontal flow.[3-5] Therefore, while void fraction does not uniquely determine the flow regime geometry, it appears to be a reasonable parameter for mapping the flow regimes expected in RELAP5/MOD2 applications and is consistent with the current state of the technology.

3.1.2.1 Transition from Bubbly Flow to Slug Flow. The RELAP5/MOD2 horizontal flow map is a simplification of the vertical map used in the code, which in turn is based on the work of Taitel, Bornea, and Dukler[3-6] (TBD). The bubbly-to-slug transition void fraction used in the code varies from 0.25 to 0.5 depending on the mass flux (see Section 3.1.1). The lower limit of 0.25 is based on a postulate of TBD that coalescence increases sharply when bubble spacing decreases to about half the bubble radius corresponding to about 25% void. TBD then cite three references as supporting this approximate level. The first citation, Griffith and Wallis,[3-7] however, actually cites an unpublished source (Reference 6 in 3-7), indicating that for $\alpha_g < 0.18$ no tendency for slugs to develop was apparent. Griffith and Wallis were measuring the Taylor bubble rise velocity (air slugs) in a vertical pipe and admitted uncertainty about where the bubbly-slug transition should be. (Only two of their own data points fell into the region labeled bubbly flow on their flow regime map.) TBD also cite Griffith and Snyder,[3-8] suggesting that the bubbly-to-slug transition takes place between 0.25 and 0.30. Actually, Griffith and Snyder were studying slug flow using a novel technique. They formed a plastic "bubble" to simulate a Taylor bubble through which they injected air. Their setup allowed the bubble to remain stationary while the flow moved past it. While void fractions as low as 0.08 and no higher than 0.35 were obtained for "slug flow," it seems inappropriate to use such information to calibrate the bubbly-to-slug transition. The third reference cited by TBD uses a semi-theoretical analysis involving bubble collision frequency, which appears to indicate a transition in the range $\alpha_g \sim 0.2$ to 0.3.[3-9] A discussion by Hewitt,[3-10] however, points out some uncertainties and qualifications to the approach of Reference 3-9. Thus, the designation of $\alpha_g = 0.25$ for a transition void fraction from bubbly to slug flow is subject to question, although it does fall within the range suggested by the cited references.

TBD further argue that the void fraction for bubbly flow could be at most 0.52 where adjacent bubbles in a cubic lattice would just touch. They then postulate that 0.52 represents the maximum attainable void fraction for bubbly flow, assuming the presence of viscous turbulent diffusion. RELAP5/MOD2 uses a void fraction of 0.5 as an approximate representation of this condition for high mass flux.

The interpolation in RELAP5 between α_g = 0.25 and 0.5 for the bubbly-to-slug transition is an attempt to account for an increase in maximum bubbly void fraction due to turbulence. The decision to base the transition on an average mixture mass flux increasing from 2000 to 3000 kg/m^{2}s (Section 3.1.1) does not appear to be based on firm ground. If, however, one plots the average mass fluxes on Figure 2 from TBD, the RELAP5 transition for this special case (air-water at 25^{o}C, 0.1 MPa in a vertical 5.0 cm dia. tube) appears reasonable (Figure 3-4). Nevertheless, while the transition criterion based on G looks reasonable for the conditions of Figure 3-4, it is inappropriate to assume that it works well for all flow conditions found in reactor applications. A potentially better criterion for the variation of the bubbly-to-slug transition α_g would be based on dimensionless parameters.

3.1.2.2 Transition from Slug Flow to Annular Mist Flow. The coded transition from slug to annular mist flow takes place between void fractions of 0.75 and 0.80. None of the references given in the code manual as basis for flow regime maps appears to support this transition. Taitel and Dukler[3-4] argue that the transition should take place at the equivalent of α_g = 0.50. Their argument is that the transition from stratified wavy to annular flow will occur if α_g > 0.5 in a pipe, since a sinusoidal wave will be able to reach the top of the pipe, whereas for α_g < 0.5 it will not (but will lead to intermittent or slug/plug flow). They further assume that α_g = 0.5 defines the transition directly from annular to intermittent flow. Weisman et al.,[3-3] however, cast doubt on Taitel and Dukler's simple model for slug-to-annular transition, indicating that the transition void fraction is not a constant, but instead a function of Froude and Kutateladze numbers. (See Section 3.2.2.2 for further discussion of the slug-to-annular mist transition.)

3.1.2.3 Transition from Annular Mist Flow to Dispersed Flow. The void fraction upon which this transition is coded to take place simply corresponds to a very low liquid fraction, $\alpha_f = 10^{-7}$. This liquid fraction was chosen to allow a smooth transition to single-phase vapor flow.

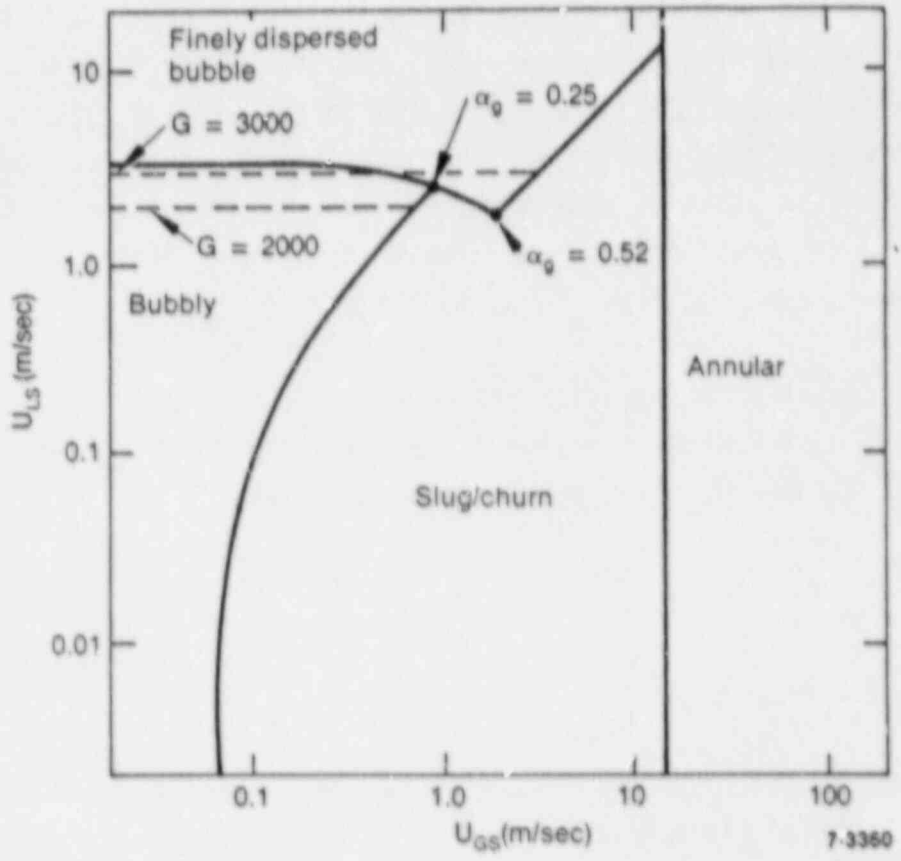

Figure 3-4. Flow pattern map for air/water at 25°C, 0.1 MPa, in a vertical 5.0-cm-diameter tube showing G = 2000, 3000 kg/m^{2}s.

3.1.2.4 Transition to Horizontal Stratification. The transition criterion from horizontally stratified to non-stratified flow, Equation (3-2), is derived directly from Equations (23-24) of Taitel and Dukler[3-4] (TD), which are a statement of a Kelvin-Helmholtz instability. If v_g is greater than v_{crit}, the flow is not stratified; if it is less, then a region of transition takes place (Figure 3-1) before the flow is considered to be completely stratified. The criterion holds that infinitesimal waves on the liquid surface will grow in amplitude if $v_g \geq v_{crit}$, transitioning from stratified flow as the waves bridge the gap to the top of the pipe. The criterion coded corresponds to exactly horizontal flow and does not include any departure from the horizontal, which is present in Equation (23) of Reference 3-4. For a 15^0 tilt, the error would be $1 - (\cos 15^0)^{0.5} < 2\%$, a small error considering the approximate nature of the flow regime modeling.

The horizontal stratification criterion of TD deserves further discussion. The criterion, Equation (3-2), is derived from Equations (23-24) of TD, which are based on Equation (17) of TD given as:

$$v_g > \left[\frac{g(\rho_f - \rho_g)\, h_g}{\rho_g} \right]^{1/2} \qquad (3\text{-}3)$$

Equation (3-3) is supposed to represent the stability limit for waves on a sheet of liquid flowing between parallel plates, h_g being the distance between the upper plate and the equilibrium interface level. This equation appears to come from Section 15.44 of Reference 3-11, which is actually a flow of two fluids with a free surface above the upper fluid. Also, the U in Section 15.44 of Reference 3-11 is the interfacial wave velocity, not the gas phase velocity.

The classical Helmholtz instability is described by Chandrasekhar[3-12] Section 100. The flow geometry is two infinite fluids having densities of ρ and ρ' (with ρ' representing the upper, less dense fluid) moving with

velocities parallel to their equilibrium interfaces of U and U', respectively. A sinusoidal wave propagating parallel to the interface is imposed. It is shown[3-12] that the wave speed takes on complex values if

$$(U - U')^2 > \frac{g}{k} \frac{\rho^2 - \rho'^2}{\rho\rho'} , \qquad (3\text{-}4)$$

which is therefore unstable. k is the wave number given by $k = 2\pi/\lambda$, where λ is the imposed wavelength. For $\rho = \rho_{water}$, and $\rho' = \rho_{air,steam}$, it is obvious that

$$\frac{g}{k} \frac{\rho^2 - \rho'^2}{\rho\rho'} = \frac{g}{k} \frac{(\rho + \rho')(\rho - \rho')}{\rho\rho'} = \frac{g}{k} \rho' \frac{(\rho - \rho')}{\rho\rho'}$$

$$= \frac{g}{k} \frac{(\rho - \rho')}{\rho} = \frac{gg}{2\pi} \frac{(\rho - \rho')}{\rho} .$$

If, now, the imposed wavelength is considered to be $\lambda = h_g/2\pi$ and the liquid velocity $U' = 0$, Eq. (3-3) is obtained. For the case of flow of two liquids between parallel plates, the expression for the wave velocity is given by Milne-Thompson,[3-11] Section 15.42. It is considerably more complex than for the unbounded case of Eq. (3-4).

The classical Helmholtz instability is based on potential flow theory and is derived from a linearized equation. Furthermore, the interfacial wave is assumed to be sinusoidal. Therefore, the following limitations apply to the stability theory compared to real flow:

1. Surface tension effects are neglected. Lamb[3-13] indicates that Eq. (3-4) predicts that the slightest breeze with a high wave number k (or short λ) would cause the surface of a liquid to become unstable. This, of course, is disallowed by surface tension effects.

2. Viscous effects are neglected. Viscosity will also serve to disallow growth of small wavelength disturbances since it will damp them out.

3. A term neglected in the surface displacement equation to simplify the problem is admittedly important if the wave amplitude is not small compared to its wavelength. This condition is clearly not meant for waves of sufficient amplitude to bridge the gas phase in most instances.

4. The imposition of a sinusoidal wave may be reasonable for the low-amplitude waves envisioned for Helmholtz instability, but clearly does not describe real, turbulent, or peaked waves that can actually occur.

5. Turbulent effects are ignored. Turbulence may play a significant role in the transition phenomenon from stratified flow.

Considering the above limitations, it is clear that the horizontal stratification criterion of TD requires some comparison with experiment to assess its validity. TD compare their transition criteria with the published map of Mandhane et al [3-2] The comparison is quite favorable for the conditions of air-water at 25°C and 1 atm in a 2.5-cm-diameter pipe. Choe et al.[3-14] show that the TD criterion works fairly well between intermittent and separated flow for liquids of low or moderate viscosity. When applied to liquids of high viscosity (glycerine solutions), large discrepancies are evident. Weisman et al.[3-3] devise their own stratification versus intermittent criterion which does not account for variations in liquid density, viscosity, or surface tension. They claim that the effects of liquid properties were insignificant for their tests, although inspection of their plotted data shows that predicted values of $v_{sg}/gD^{1/2}$ (v_{sg} = superficial gas velocity) vary from experimental data by as much as a factor of about five.

In summary, there is evidence that the TD horizontal stratification criterion works for low- and moderate-viscosity liquids, including water, at least in small-diameter pipes (up to 5 cm), but fails for high-viscosity liquids.

3.1.3 Effects of Scale

Recent experimental evidence reported by Kukita et al.[3-15] obtained at the JAERI, ROSA-IV, TPTF separate-effects facility for horizontal flow of steam and water in an 18-cm-diameter pipe at high pressure (3-9 MPa) indicates that horizontally stratified flow exists for conditions for which RELAP5/MOD2 predicts unseparated flows. This failure of the stratification criterion [Equations (3-2, 3-3)] is attributed by Reference 3-15 largely to the fact that the code uses the absolute vapor velocity rather than relative velocity ($v_g - v_f$) to test for a stratification condition. Upon substituting relative velocity for vapor velocity, it is shown that predictions for void fraction are significantly improved.[3-15]

3.2 Vertical Flow Regime Map

3.2.1 Map as Coded

A schematic of the vertical flow regime map as coded in RELAP5/MOD2 is shown in Figure 3-5. The schematic is three-dimensional to illustrate flow regime transitions as functions of void fraction α_g, increasing average mixture velocity G/ρ, and boiling regime [pre-critical heat flux (CHF), transition, and post dryout]. G is given by Eq. (3-1), and the average density is given by

$$\rho = \alpha_f \rho_f + \alpha_g \rho_g \ . \qquad (3\text{-}5)$$

The map consists of bubbly, slug, annular mist, and dispersed (droplet or mist) flows in the pre-CHF regime; inverted annular, inverted slug and dispersed (droplet or mist) flows in post dryout; and vertically stratified for sufficiently low mixture velocity G/ρ. Transition regions provided in the code are shown. Details of the interpolating functions employed for the transition regions are given in the sections dealing with the actual heat/mass transfer and drag correlations. Values for the parameters governing the flow regime transitions are listed below and shown in Figure 3-6.

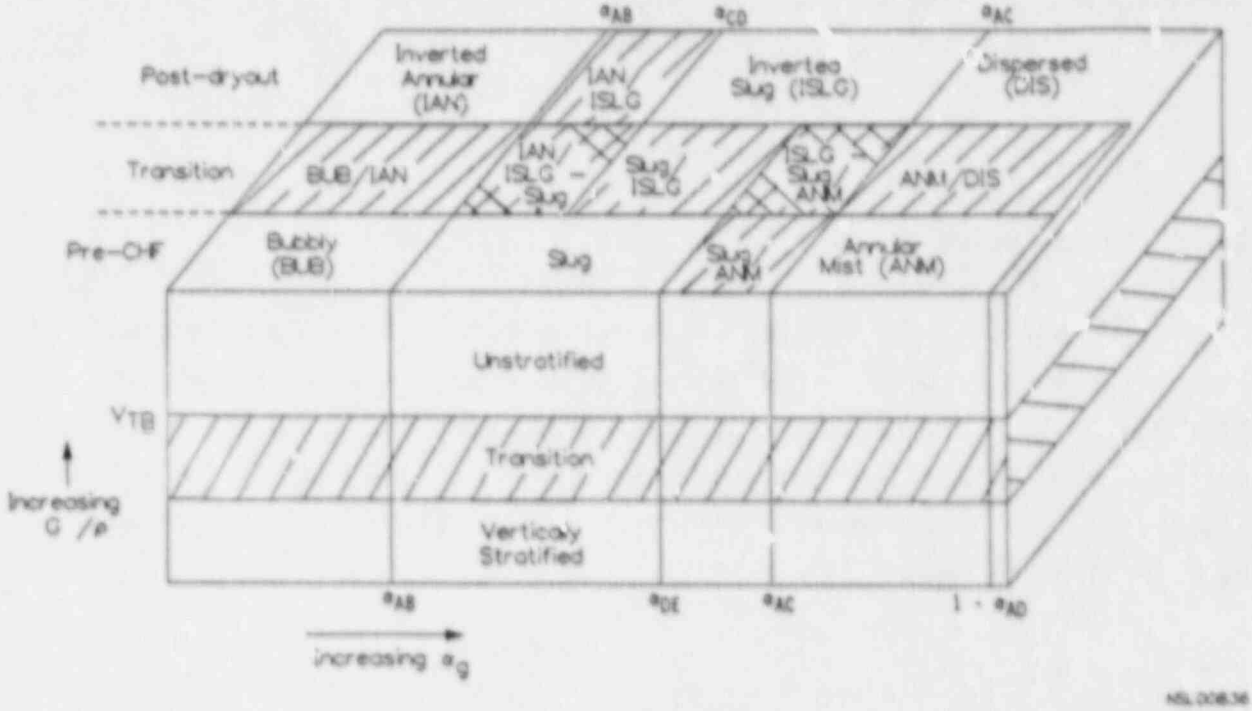

Figure 3-5. Schematic of vertical flow regime map with hatchings indicating transitions.

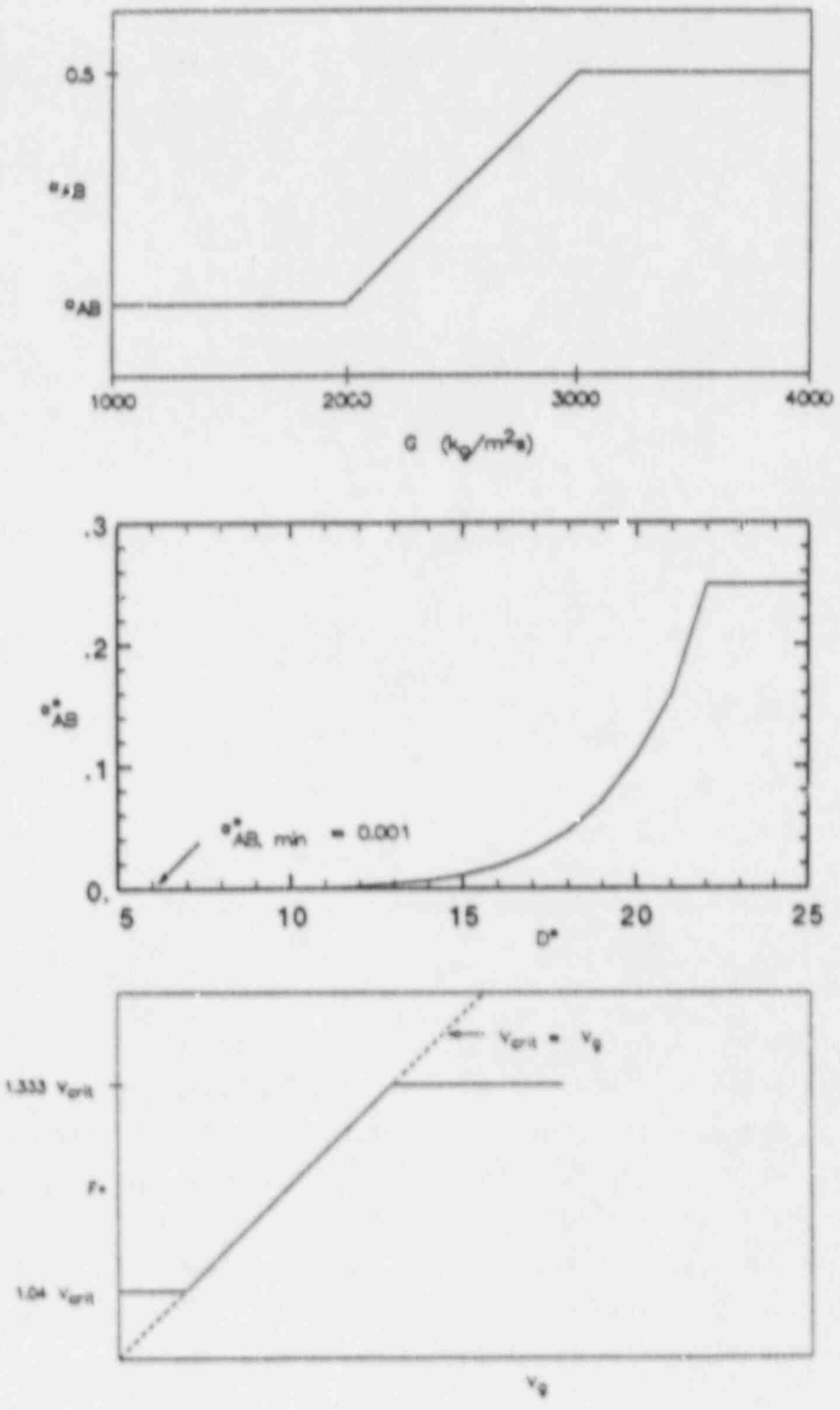

Figure 3-6. Vertical flow regime transition parameters in RELAP5/MOD2.

$$\alpha_{AB} = \begin{cases} \alpha^*_{AB} & \text{for } G \le 2000 \text{ kg/m}^2\text{-s} \\ \alpha^*_{AB} + \dfrac{(0.5 - \alpha^*_{AB})}{1000}(G - 2000) & \text{for } 2000 < G < 3000 \text{ kg/m}^2\text{-s} \\ 0.5 & \text{for } G \ge 3000 \text{ kg/m}^2\text{-s} \end{cases}$$

$$\alpha^*_{AB} = \text{Max}\ (0.25\ \text{Min}\ [1,\ (0.045D^*)^8],\ 10^{-3})$$

where $D^* = D\ [g\ (\rho_f - \rho_g)/\sigma]$.

$$\alpha_{CD} = \alpha_{AB} + 0.2 ,$$

$$\alpha_{AC} = \frac{v_{crit}}{F^*} ,$$

$$F^* = \text{Min}\ [\text{Max}\ (1.04v_{crit},\ |v_g|),\ 1.333v_{crit}] , \text{ and}$$

$$v_{crit} = 1.41\ [\sigma g\ (\rho_f - \rho_g)]^{1/4} / \rho_g^{1/2} . \qquad (3\text{-}6)$$

Thus, $0.75 \le \alpha_{AC} \le 0.96$

$$\alpha_{DE} = \alpha_{AC} - 0.05$$

$$\alpha_{AD} = 10^{-7}$$

$$v_{TB} = 0.35\ [gD\ (\rho_f - \rho_g)/\rho_f]^{1/2} \qquad (3\text{-}7)$$

A further condition must be satisfied for the flow to be considered vertically stratified. In the case of control volumes having only one inlet and one outlet, the void fraction of the volume above is compared to that for the one below. If their difference is less than 0.5, the central volume cannot be vertically stratified. If there are multiple junctions above and below the volume in question, the upper volume having the smallest α_g is compared to the lower volume having the largest. Only connecting volumes that are vertically oriented are considered.

3.2.2 Map Basis and Assessment

The vertical flow regime map is mapped according to void fraction for non-stratified, wetted-wall regimes. This conforms to the recommendation of Ishii and Mishima[3-1] as discussed for the horizontal map in Section 3.1.2. The dry-wall flow regimes (particularly inverted annular and inverted slug) are included[3-16] to account for post-dryout heat transfer regimes where a wetted wall is physically unrealistic. Heat and mass transfer and drag relations for the transition boiling region between pre-CHF and dryout are found by interpolating the correlations on either side (Figure 3-5). This means that for certain void fractions in the transition boiling region, two and sometimes three adjacent correlations are combined to obtain the necessary relations for heat/mass transfer and drag. The exact nature of these transition relations are found in the appropriate sections describing the correlations in question. The further configuration of vertical stratification includes a transition region, Section 3.2.1, wherein up to four correlations are combined to obtain the required constitutive relations.

3.2.2.1 Bubbly-to-Slug Transition. The transition from bubbly flow to slug flow is based on Taitel, Bornea and Dukler[3-6] (TBD). The transition is the same as in the horizontal flow map, Section 3.1.2.1, except for the additional provision of the effect of small tube diameter.

When the rise velocity of bubbles in the bubbly regime, given by TBD as

$$U_o = 1.53 \left[\frac{g\,(\rho_f - \rho_g)\,\sigma}{\rho_f^{\,2}} \right]^{1/4} , \qquad (3\text{-}8)$$

exceeds the Taylor bubble rise velocity, Equation (3-7), it is assumed that bubbly flow cannot exist, since the bubbles will approach the trailing edges of Taylor bubbles and coalesce. As shown in Equation (3-7), the rise

velocity of Taylor bubbles is limited by the pipe diameter such that for sufficiently small D, $v_{TB} < U_o$, thereby precluding bubbly flow. Equating v_{TB} and U_o yields the critical pipe diameter,

$$D_{crit} = 19.11 \left[\sigma/g \left(\rho_f - \rho_g\right)\right]^{1/2} , \tag{3-9}$$

below which bubbly flow is theorized not to exist. In RELAP5, the coefficient in Equation (3-9) has been modified to 1/0.045 = 22.22, precluding bubbly flow for a pipe diameter up to 16% greater than given by Equation (3-9). This criterion is observed down to a void fraction of 0.001 (Figure 3-6b). The designation of $\alpha_{AB,min} = 0.001$ as the minimum void fraction at which slug flow may exist seems arbitrary and possibly too low. In a recent report,[3-17] the degree of subcooling in a RELAP5/MOD2 prediction for a reactor core was significantly improved by redefining $\alpha_{AB,min} = 0.1$ and reverting to Unal's original interphase heat transfer correlation,[3-18] which has been modified in RELAP5/MOD2 (see Section 4.1).

3.2.2.2 Slug-to-Annular Mist Transition. The RELAP5/MOD2 vertical flow regime map combines slug and churn flow regimes into a single regime called slug flow. Also, the annular flow regime is combined with the annular mist regime. The transition from slug flow to annular mist flow is derived from the churn to annular flow transition of TBD.[3-6] The TBD criterion is based on the postulate that annular flow will occur in a vertical pipe when the upward drag forces are sufficient to overcome gravity and can lift the liquid droplets in the core flow region as well as those which may be created by shattering wave crests on the wall-adjacent liquid film. The gas velocity required to effect such a transition is derived in TBD as

$$v_g \geq 3.1 \frac{\left[\sigma g \left(\rho_f - \rho_g\right)\right]^{1/4}}{\rho_g^{1/2}} \tag{3-10}$$

TBD assumes that this transition will occur at high void fraction and that v_g can therefore be replaced by the superficial velocity v_{gs}. If the

right-hand side of Equation (3-10) is denoted v_{crit}, the transition criterion according to TBD can be written

$$v_{gs} \geq v_{crit} \quad . \tag{3-11}$$

Substituting the definition of superficial velocity $v_{gs} = \alpha_g v_g$, one obtains

$$\alpha_g \geq \frac{v_{crit}}{v_g} \tag{3-12}$$

for the transition criterion. This transition criterion, which is conveniently given in terms of the void fraction, is consistent with Equation (32) of TBD or Equation (3-11) herein. However, the net effect of Equation (3-12) is to cause the transition to occur for the assumed high α_g and not necessarily for $v_g \geq v_{crit}$, Equation (3-10). The restriction of transition α_g between 0.75 and 0.96 (Section 3.2.1) in the code is, in fact, consistent with TBD's assumption that the transition α_g be high. The further effect of the coded transition to decrease from $\alpha_g = 0.96$ to 0.75 with increasing gas velocity v_g does not appear to have a documented basis. The purpose of the modification was to improve the performance of the code in the developmental assessment analysis.[3-19]

The postulated transition criterion of TBD, Equation (3-11), as applied by TBD is, in fact, inconsistent with the assumption of high void fraction. For a given set of operating conditions, v_{crit} is a constant (Figure 3-4). However, as the liquid superficial velocity increases, the void fraction decreases and can go as low as 0.3.[3-20]

The constant used in the code in Equation (3-10) is 1.4 instead of 3.1, which is consistent with Wallis.[3-21] Its use in RELAP5 affects only the value of α_g (between 0.75 and 0.96) at which the transition take place, which may or may not be directly related to the balance between drag and gravitational forces. Data shown by Wallis in his Figure 11.18 for air-water in a 1-in.-diameter pipe does show slug flow existing up to a void fraction of .87 and annular flow down to 0.75. Constitutive equations for

void fraction for slug and annular flows coincide at $\alpha_g = 0.8$. The slug and annular flow data of Wallis' Figure 11.18, however, do not appear to support the trend of the coded transition void fraction being a function of the gas velocity.

The size of the transition region between slug and annular mist regimes ($\Delta\alpha = 0.05$) appears to be based on engineering judgment.

3.2.2.3 Post-Dryout Flow Regimes (Inverted Annular, Inverted Slug, Dispersed Droplet). When surface temperatures and wall heat fluxes in confined boiling heat transfer situations are too high to allow surface wetting, inverted flow regimes occur. Inverted regimes are characterized by some form of liquid core surrounded by an annular vapor blanket.[3-16]

A series of studies have begun an investigation into the nature and the controlling parameters of inverted flow regimes including that of De Jarlais and Ishii[3-16] (DI). They report that upon reaching CHF, bubbly flow transitions to inverted annular, slug/plug flow becomes inverted slug, and annular/annular mist flow loses its annular liquid film and becomes dispersed droplet flow (Figure 3-7).

De Jarlais and Ishii[3-16] recommend that initially inverted annular/initially inverted slug and initially inverted slug/initially dispersed droplet transitions be based on the same criteria as their pre-CHF counterparts (bubbly-slug and slug-annular, respectively). While the RELAP5 flow map is not based on the same criteria as those recommended by DI, the correspondence between pre- and post-CHF transitions is observed, as shown in Figure 3-5. Inverted flow regimes are very complex and unstable, transitioning from inverted annular to inverted slug to dispersed droplet as the flow moves up the duct.[3-16] Thus, DI describe the transition to a given post-CHF (inverted) regime in terms of those conditions that initially occur as CHF is reached. The mechanisms for transition under post-dryout conditions are different than for pre-CHF; hence, the transition criteria

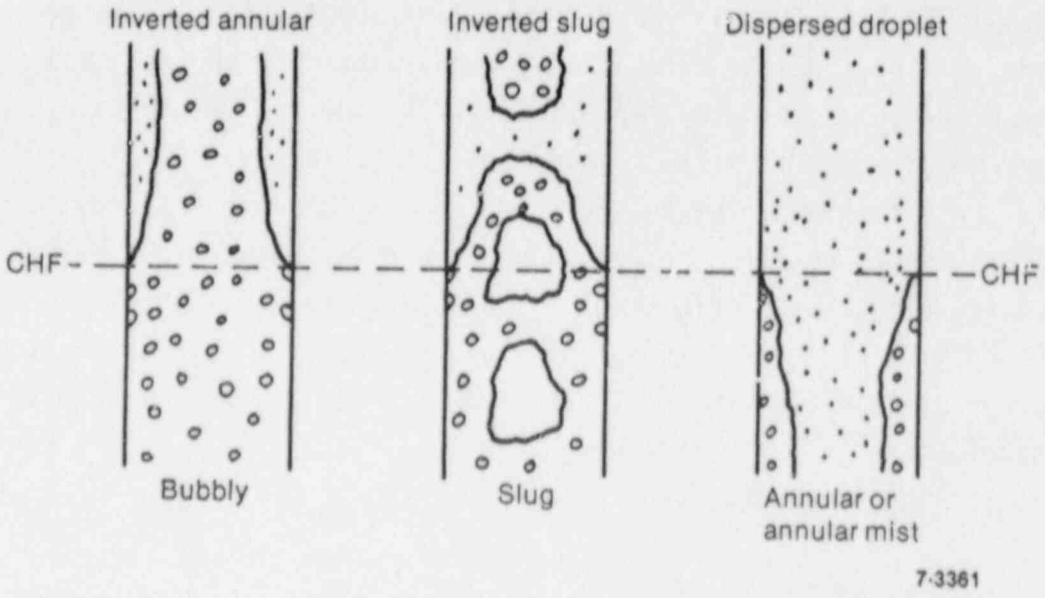

Figure 3-7. Flow regimes before and after the critical heat flux (CHF) transition.

for the latter do not necessarily hold for the former. Nevertheless, since post-dryout transitions are not well understood, it seems reasonable to borrow pre-CHF criteria, as is done in RELAP5.

A further transition region between pre-CHF and dryout where the surface is neither fully wet nor fully dry (analogous to transitional pool boiling) is present in the vertical flow regime map. While boiling under flowing conditions is not the same as pool boiling, such a transitional regime seems appropriate.

3.2.2.4 Vertically Stratified Flow. The vertically stratified flow regime is designed to apply to situations where the flow in a vertical conduit is so slow that an identifiable gas/liquid interface is present. The restriction that the average mixture velocity G/ρ be less than the Taylor-bubble rise velocity represents this condition, since any large bubbles would have risen to the gas/liquid interface maintaining the stratified situation. The further requirement that the void fraction in the volume above the one in question be greater than that for the volume below by 0.5 represents a plausible search to locate the gas/liquid interface. This condition effectively precludes an essentially single-phase flow from inappropriately being labeled stratified when its average mixture velocity falls below the Taylor bubble rise velocity. (The Taylor bubble rise velocity is documented by TBD, Reference 3-6).

3.2.3 Effects of Scale

It has been postulated that a maximum diameter exists for vertical flow of individual dispersed phase drops/bubbles in a continuous phase, precluding the existence of slug flow as it is usually defined. Kocamustafaogullari, Chen, and Ishii[3-22] have derived a unified theory for the prediction of maximum fluid particle size for drops and bubbles. They developed a simple model based on the hypothesis that fluid particle breakup will occur if the rate of growth of a disturbance at the dispersed phase/continuous phase interface is faster than the rate at which it propagates around the interface. They show that the same theory is

applicable to liquid in liquid, droplets in gas, and bubbles in liquid, and show a broad range of experimental data compared to their theoretical predictions with reasonably good results. This theory suggests that there will exist ranges where bubbles cannot coalesce to form slugs that are as large as the pipe diameter, thus preventing transition from bubbly to slug flow.

Some experimental evidence for large pipes also appears to support the above theory. Air-water flow experiments conducted by Science Applications Incorporated (SAI) indicated that slug flow was unable to form in a 30.5-cm vertical pipe; rather, a transition from bubbly to bubbly/churn-type flow with strong local recirculation patterns took place.[3-23] Therefore, there is reasonable evidence to suggest that the slug flow regime modeled in RELAP5/MOD2 is not appropriate to reactor scale pipes. The effect of using the slug flow regime calculations in large pipes is not known.

3.3 High Mixing Flow Regime Map

3.3.1 Map as Coded

The high mixing flow regime map is included in RELAP5/MOD2 to account for flow through pumps. Figure 3-8 illustrates the map, which consists of bubbly and dispersed flow with a transition between them. The transition consists of weighted combinations of bubbly and dispersed correlations, which are described in detail in the sections above. The map is based purely on void fraction, with bubbly flow occurring below 0.5 and dispersed flow above 0.95.

3.3.2 Map Basis and Assessment

Although no references are given in the code manual as a basis for this flow map, it is apparent that the upper limit for bubbly flow of $\alpha_g = 0.5$ is based on Taitel, Bornea and Dukler's[3-6] postulate discussed in Section 3.1.2.1. In the absence of definitive data, this is a reasonable postulate, since vigorous mixing takes place in the pumps. The transition to dispersed flow is consistent with Wallis,[3-21] who presents data

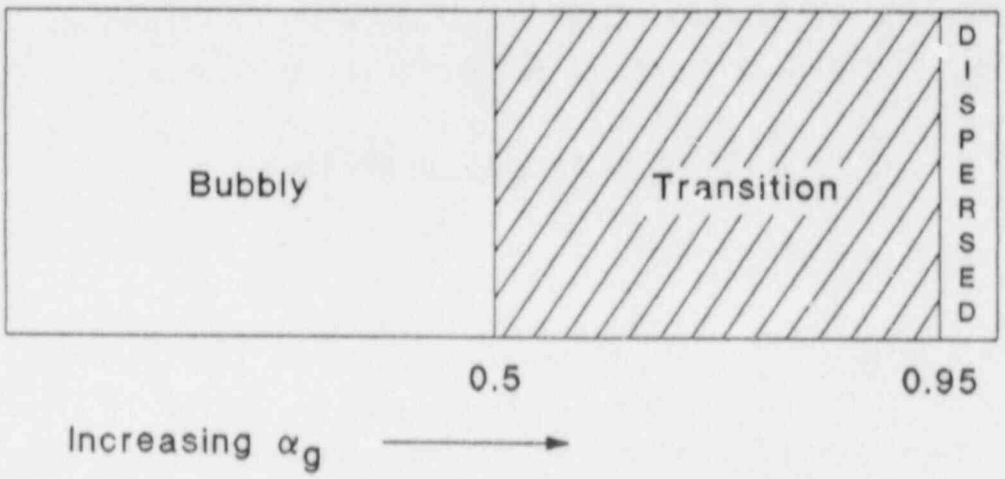

NSL00832

Figure 3-8. Schematic of high mixing flow regime map.

indicating that only dispersed flow exists above $\alpha_g \approx 0.96$. (See Section 3.2.2.2 for further discussion.) The use of a transitional region between bubbly and dispersed flow rather than including a slug flow regime is appropriate, since the highly mixed nature of flow in the pump would disallow large gas bubbles from forming.

3.4 Conclusions

A statement regarding the overall validity of the flow regime maps coded into RELAP5/MOD2 must depend upon the perspective taken. From a scientific viewpoint, the science of two-phase flow is far from complete. Much disagreement still prevails regarding not only the best criteria for flow regime characterization, transition, and pertinent parameters involved, but even on what the full catalog of regimes should include. This situation is complicated by the fact that more than one major area of application exists (nuclear reactor safety, oil pipeline flow, etc.), each of which involves a different set of operating ranges.

In view of the above, a statement based on an engineering perspective seems more appropriate; that is, how well do the coded flow regime maps compare with what is known or how well do they compare with recorded data? Even based on this view, some flow regimes and transitions appear to be supported by the literature, while others are less clear. Even some based on published criteria are probably unsatisfactory when scaled to reactor dimensions. It is clear that considerable room for improvement exists both in the science of flow regimes and in the application of the known science to the code.

3.5 References

3-1 M. Ishii and K. Mishima, Study of Two-Fluid Model and Interfacial Area, NUREG/CR-1873, ANL-80-111, December 1980.

3-2 J. M. Mandhane, G. A. Gregory and K. Aziz, "A Flow Pattern Map for Gas-Liquid Flow in Horizontal Pipes," International Journal of Multiphase Flow, 1, 1974, pp. 537-553.

3-3 J. Weisman, D. Duncan, J. Gibson and T. Crawford, "Effects of Fluid Properties and Pipe Diameter on Two-Phase Flow Patterns in Horizontal Lines," International Journal of Multiphase Flow, 5, 1979, pp. 437-462.

3-4 Y. Taitel and A. E. Dukler, "A Model for Predicting Flow Regime Transitions in Horizontal and Near Horizontal Gas-Liquid Flow," AIChE Journal, 22, 1, 1976, pp. 47-55.

3-5 Y. Taitel, N. Lee, and A. E. Dukler, "Transient Gas-Liquid Flow in Horizontal Pipes: Modeling Flow Pattern Transitions," AIChE Journal, 24, 5, 1978, pp. 920-934.

3-6 Y. Taitel, D. Bornea and A. E. Dukler, "Modeling Flow Pattern Transitions for Steady Upward Gas-Liquid Flow in Vertical Tubes," AIChE Journal, 26, 3, 1980, pp. 345-354.

3-7 P. Griffith and G. B. Wallis, "Two-Phase Slug Flow," Journal of Heat Transfer, ASME, 83, 1961, pp. 307-318.

3-8 P. Griffith and G. A. Snyder, The Bubbly-Slug Transition in a High Velocity Two-Phase Flow, MIT Report 5003-29 (TID-20947), July 1964.

3-9 N. A. Radovcich and R. Moissis, The Transition from Two-Phase Bubble Flow to Slug Flow, MIT Report 7-7673-22, June 1962.

3-10 G. F. Hewitt, "Two-Phase Flow Patterns and Their Relationship to Two-Phase Heat Transfer," in S. Kakac and F. Mayinger (eds.), Two-Phase Flows and Heat Transfer, 1, Washington: Hemisphere Publishing Corp., 1977, pp. 11-35.

3-11 L. M. Milne-Thomson, Theoretical Hydrodynamics, 5th edition, New York: The MacMillan Co., 1968, pp. 445-446.

3-12 S. Chandrasekhar, Hydrodynamic and Hydromagnetic Stability, New York Dover Publications, Inc., 1981, p. 481ff.

3-13 H. Lamb, Hydrodynamics, 6th edition, New York, Dover Publications, Inc., 1945, pp. 373-375.

3-14 W. G. Choe, L. Weinberg and J. Weisman, "Observation and Correlation of Flow Pattern Transition in Horizontal, Co-Current Gas-Liquid Flow," in T. N. Veziroglu and S. Kakac (eds.), Two-Phase Transport and Reactor Safety, Washington: Hemisphere Publishing Corp., 1978.

3-15 Y. Kukita, Y. Anoda, H. Nakamura and K. Tasaka, Assessment and Improvement of RELAP5/MOD2 Code's Interphase Drag Models, Japan Atomic Energy Research Institute, 1986.

3-16 G. DeJarlais and M. Ishii, Inverted Annular Flow Experimental Study, NUREG/CR-4277, ANL-85-31, April 1985.

3-17 H. Stadtke, W. Kolar, "JRC ISPRA Results from Assessment of RELAP5/MOD2 on the Basis of LOBI Test Data," Fifteenth Water Reactor Safety Information Meeting, Gaithersburg, Maryland, October 26-29, 1987.

3-18 H. C. Unal, "Maximum Bubble Diameter, Maximum Bubble-Growth Time and Bubble Growth Rate During the Subcooled Nucleate Flow Boiling of Water Up to 17.7 MN/m^2," International Journal of Heat and Mass Transfer, 198, 1976, pp. 643-649.

3-19 V. H. Ransom, et al., RELAP5/MOD2 Code Manual Vol. 3: Developmental Assessment Problems, INEL Report EGG-TFM-7952, December 1987.

3-20 K. Mishima and M. Ishii, Flow Regime Transition Criteria Consistent with Two-Fluid Model for Vertical Two-Phase Flow, NUREG/CR-3338, ANL-83-42, April 1983.

3-21 G. B. Wallis, One-Dimensional Two-Phase Flow, New York, McGraw-Hill Book Company, 1969.

3-22 G. Kocamustafaogullari, I. Y. Chen and M. Ishii, Unified Theory for Predicting Maximum Fluid Particle Size for Drops and Bubbles, NUREG/CR-4028, ANL-84-67, October 1984.

3-23 T. K. Larson, An Investigation of Integral Facility Scaling and Data Relation Methods (Integral System Test Program), NUREG/CR-4531, EGG-2440, February 1987, p. 43.

4. CLOSURE RELATIONS FOR THE FLUID ENERGY EQUATIONS

The one-dimensional nature of the field equations for the two-fluid model found in RELAP5/MOD2 precludes direct simulation of effects that depend upon transverse gradients of any physical parameter, such as velocity or energy. Consequently, such effects must be accounted for through algebraic terms added to the conservation equations. These terms should be based on correlations deduced from experimental data for their representation, or on models developed from sound physical principles. Some of the correlations used in RELAP5, however, are based on engineering judgment, due partly to the incompleteness of the science and partly to numerical stability requirements. A significant effort has gone into providing smooth transitions from correlation to correlation as conditions evolve to prevent physical as well as numerical instability.

The assessment of the heat transfer correlations used to provide closure for the energy equations is complicated by the detailed nature of the correlations themselves. In general, each correlation is designed to represent energy transfer under a specific set of thermal-hydraulic and thermodynamic conditions, and each is typically measured for a fairly limited range of those conditions. A determination of accuracy may be available for the developmental range of parameters, but an extension of the accuracy estimate outside that range is difficult at best, and perhaps impossible mathematically. This situation is especially evident in Section 4.2, which addresses the wall heat transfer correlations. By treating each correlational model individually, a critical reviewer might generally conclude that the data base over which the model was developed does not apply directly to reactor geometries or thermal-hydraulic conditions. If left at this stage, a conclusion of inadequacy could be reached. Yet the correlations have, in general, enjoyed a fairly widespread utilization and have shown at least a qualitative applicability outside the documented data range for which they were developed. The use of ary given heat transfer correlation, either directly or in a modified form, then becomes an engineering judgement, and the application to reactor conditions becomes an approximation to the expected reactor behavior. When viewed in this context, the use of integral assessments, which inherently measure a global response rather than a local response, becomes more meaningful.

The assessment documented in this section addresses both aspects of the review process, local and global. The heat transfer correlations are assessed on a local basis, with the developmental data base compared to the desired range of application. Generally, an estimate of accuracy or applicability is difficult to make at that level, and this is reflected in the conclusions for each subsection. Additionally, a few integral assessments are discussed for some of the more significant heat transfer packages. These were limited by the time available to search the literature, but they add the perspective of engineering judgment and application to temper the conclusions from the local assessment.

4.1 Interfacial Heat Transfer

In RELAP5/MOD2, the interfacial heat transfer between the gas and liquid phases actually involves both heat and mass transfer. Temperature-gradient-driven interfacial heat transfer is computed between each phase and the interface. The temperature of the interface is assigned the saturation value for the local pressure. Heat transfer correlations for each side of the interface are provided in the code. Since both superheated and subcooled temperatures for each phase are allowed, the heat transfer may be either into or away from the interface for each phase. All of the thermal energy transferred to the interface from either side contributes to vaporization as it is used to compute the mass transfer Γ_g to the gas phase. Conversely, all of the heat transfer away from the interface contributes to condensation, since it is used to compute the mass transferred to the liquid phase ($-\Gamma_g$). In other words, the cases of superheated liquid and superheated gas contribute to vaporization, while both subcooled liquid and subcooled gas contribute to condensation. The net rate of mass transfer is determined by summing the contributions, positive and negative, from each side of the interface.

The form used in defining the heat transfer correlations for superheated liquid (SHL), subcooled liquid (SCL), superheated gas (SHG), and

subcooled gas (SCG) is that for a volumetric heat transfer coefficient (W/m^3K). Since heat transfer coefficients are often given in the form of a dimensionless parameter (usually Nusselt number, Nu), the volumetric heat transfer coefficients are coded as follows

$$H_{ip} = \frac{k_p}{L} Nu\ a_{gf} \qquad (4\text{-}1)$$

where

H_{ip} = volumetric interfacial heat transfer coefficient for phase p (W/m^3K)

k_p = thermal conductivity for phase p (W/m K)

L = characteristic length (m)

a_{gf} = interfacial area per unit volume (m^2/m^3)

Individual correlations for heat/mass transfer are fully detailed in Appendix 4A. Expressions for the cases of SHL, SCL, SHG, and SCG are given for each flow regime recognized by the code. The flow regimes are those cataloged in Section 3. The following section discusses the relationship between the coded correlations and the literature, the stabilizing and smoothing features built into the code, and assessments (when possible) of the validity of the expressions for operating conditions typical to nuclear reactors. The methods employed to smooth transitions amongst flow regimes are given in Appendix 4A and are discussed herein. Furthermore, the techniques used to incorporate effects due to noncondensible gases are presented and discussed. Reference should be made to the flow regime maps in Section 3 to help clarify Appendix 4A and the discussion to follow hereafter.

4.1.1 Flow Regime Correlations

Flow regime correlations are shared amongst the three flow regime maps (horizontal, vertical, and high mixing) for flow regimes identified by the same names.

4.1.1.1 Bubbly Flow.

4.1.1.1.1 Superheated Liquid (SHL, $T_f > T^s$)

Model as Coded

$$H_{if} = \left[\text{Max} \left\{ \begin{array}{l} \frac{k_f}{d_b} \frac{12}{\pi} \Delta T_{sf} \frac{\rho_f C_{pf}}{\rho_g h_{fg}} \beta \\ \frac{k_f}{d_b} (2.0 + 0.74\ Re_b^{0.5}) \end{array} \right\} + 0.4\ |v_f| \rho_f\ C_{pf}\ F_1 \right] a_{gf}\ F_2\ F_3$$

where

$\Delta T_{sf} \equiv T^s - T_f$

$Re_b = \frac{We\ \sigma\ (1 - \alpha_{bub})}{\mu_f\ (v_{fg}^2)^{1/2}}$, $We\ \sigma = \text{Max}\ (We\ \sigma,\ 10^{-10})$

$We = \left(\rho_f d_b\ v_{fg}^2 / \sigma\right) = 5,$

d_b = average bubble diameter (= 1/2 d_{max})

β = 1.0 for bubbly flow

a_{gf} = interfacial area per unit volume

= $3.6\ \alpha_{bub} / d_b$

$\alpha_{bub} = \text{Max}\ (\alpha_g,\ 10^{-5})$

v_{fg} = relative velocity = $\begin{cases} v_g - v_f & \alpha_g \geq 10^{-5} \\ (v_g - v_f)\ \alpha_g 10^5 & \alpha_g < 10^{-5} \end{cases}$

$$v_{fg}^2 = \text{Max}\left[v_{fg}^2, \frac{We\,\sigma}{\rho_f \text{ Min } (D'\alpha_{bub}^{1/3}, D)}\right]$$

D = hydraulic diameter

D' = 0.005 for bubbly flow

F_1 = Min $(0.001, \alpha_{bub}) / \alpha_{bub}$

F_2 = Min $(0.25, \alpha_{bub}) / \alpha_{bub}$

$$F_3 = \begin{cases} 1 & \Delta T_{sf} \le -1 \\ \text{Max } [0.0, F_4 (1 + \Delta T_{sf}) - \Delta T_{sf}] & -1 < \Delta T_{sf} < 0 \\ \text{Max } (0.0, F_4) & \Delta T_{sf} \ge 0 \end{cases}$$

F_4 = Min $[10^{-5}, \alpha_g (1 - Q)] (10^5)$

Q = noncondensible quality (fraction of α_g that is noncondensible)

H_{if} = 0.0 if $\alpha_g = 0.0$ and $\Delta T_{sf} \le 0$

Model Basis and Assessment

The Nusselt number upon which the volumetric heat transfer coefficient H_{if} is based for SHL bubbly flow is coded to be the maximum value produced by one of two correlations. The first correlation is derived from an equation determined analytically by Plesset and Zwick,[4-1] which represents the growth rate of a bubble radius, e.g.,

$$\dot{r}_b = \Delta T_{sat}\, k_f\, [\pi \alpha_f t/3]^{-1/2} / (h_{fg} \rho_g) , \qquad (4\text{-}1)$$

where

$\dot{r}_b$ = time rate of change of bubble radius (m/s)

ΔT_{sat} = liquid phase superheat (K) (= $T_f - T^s$)

α_f = thermal diffusivity of liquid (m^2/s)

k_f = thermal conductivity of liquid (W/m K)

h_{fg} = latent heat of vaporization (J/kg)

ρ_g = gas density (kg/m^3)

C_{pf} = specific heat of liquid (J/kg K) .

According to Collier,[4-2] the solution to Equation (4-1) is

$$r_b = 2\Delta T_{sat} k_f [3t/(\pi\alpha_f)]^{1/2} / (h_{fg}\rho_g) . \quad (4-2)$$

Upon replacing the thermal diffusivity by its definition, substituting Equation (4-2) in Equation (4-1), and rearranging, one obtains

$$r_b = 6k_f\rho_f C_{pf} [\Delta T_{sat}/(h_{fg}\rho_g)]^2 / (\pi r_b) . \quad (4-3)$$

As the bubble grows, there is positive mass transfer Γ_g to the gas phase given by

$$\Gamma_g = \rho_g 4\pi r_b^2 r_b \quad (4-4)$$

Γ_g can also be given in terms of a heat transfer coefficient as

$$\Gamma_g = h_b \Delta T_{sat} (4\pi r_b^2) / h_{fg} , \quad (4-5)$$

where h_b is the heat transfer coefficient (W/m^2K). Defining a Nusselt number for heat transfer to the growing bubble,

$$Nu_b = 2r_b h_b / k_f , \quad (4-6)$$

and combining Equations (4-3) through (4-5), one obtains

$$Nu_b = \frac{12}{\pi} \rho_f C_{pf} \Delta T_{sat} / (\rho_g h_{fg}) \qquad (4\text{-}7)$$

The original bubble growth rate equation of Plesset and Zwick, Equation (4-1), and hence Equation (4-7) (which is used for $H_{if,bubbly}$) is based on several assumptions. These are:

1. The bubble remains spherical throughout its growth.

2. Radial acceleration and velocity of the interface are small.

3. Transitional velocity of the bubble is negligible.

4. Compressibility and viscous effects are negligible.

5. The vapor within the bubble has a uniform temperature and pressure equal to those of the interface.

The authors, Plesset and Zwick,[4-1] indicate that for a superheat of $10^{o}C$ for bubble growth in water, negligible error in their theoretical estimate of bubble growth results from translational bubble velocity (due to buoyancy) for bubble radii up to 1 mm. They further indicate that the heat transfer coefficient to the bubble will increase for non-negligible bubble velocity. Since the study of Plesset and Zwick is apparently for pool boiling, it seems appropriate to use relative velocity (as RELAP5/MOD2 does) rather than absolute bubble velocity.

To account for the increase in Nu_b due to a significant bubble relative velocity, RELAP5/MOD2 employs a second correlation deduced by Lee and Ryley[4-3] (but modified in RELAP5/MOD2); the original correlation from Reference 4-3 is:

$$Nu_b = 2.0 + 0.74 \, Re_b^{0.5} \, Pr^{1/3} \qquad (4\text{-}8)$$

The Prandtl number dependence has been dropped in RELAP5/MOD2. At typical operating conditions (Appendix 4B), the Prandtl number is Pr = 0.98, which represents less than a 1% error for Equation (4-8).

Lee and Ryley derived their correlation, Equation (4-8), by observing the evaporation rate of a water droplet suspended from a glass fiber into a superheated steam flow. The ranges of variables for which the correlation is fitted are: (a) droplet Reynolds number 64-250, (b) superheated steam pressure 14.7-29 psia, (c) superheat 5-61^{o}F, and (d) steam velocity 9-39 ft/s. The data, as plotted by Reference 4-3, fall within $\pm$ 20% of the correlation. The form of Equation (4-8) is not original with Lee and Ryley; Frossling[4-4] and Ranz and Marshall[4-5] each fitted similar equations to their respective data, obtaining coefficients of 0.552 and 0.6, respectively (as compared to 0.74). Kreith[4-6] compiles data from several sources for forced convective heat transfer to spheres ranging from 0.033 to 15 cm in diameter for droplet Reynolds numbers ranging from 20 to 10^5. For the range of Re above that employed by Lee and Ryley (250-10^5) Equation (4-8) is in excellent agreement with the data plotted in Reference 4-6. All of the data plotted by Kreith are for atmospheric or near-atmospheric pressures.

There are several additional limitations of the data upon which Lee and Ryley based their correlating equation. The most obvious is that they measured droplet evaporation and not bubble growth. Since their correlation also holds for forced convective heat transfer over a sphere,[4-6] however, it seems that it should apply to a spherical bubble. Bubbles in bubbly flow, of course, deform significantly, especially as they get bigger, raising questions as to the overall validity of Equation (4-8) for bubbly flow. A further significant complication is the presence of turbulence in the flow. This is not the case for the range of Re plotted in Kreith,[4-6] since laminar flow prevails below droplet Reynolds numbers of 10^5 and since, presumably, care was taken to minimize free stream turbulence from those flows. Finally, the pressures at which the aforementioned data were taken are far below typical reactor operating pressures, bringing additional doubt to the viability of Equation (4-8) for typical operating conditions.

Additional smoothing functions have been added to H_{if} for SHL bubbly, as indicated in Appendix 4A. The additive term $0.4|v_f|\rho C_{pf}F_1$ is included to represent surface nucleation effects at low void fraction. Function F_2 serves to diminish H_{if} for a void fraction between 0.25 and 0.5, although the opposite would seem to be in order since it is assumed (see Section 3.1.2.1) that bubbly flow can exist above $\alpha_g = 0.25$ only if vigorous turbulent diffusion is present. Such diffusion should act to enhance the heat transfer. Functions F_3 and F_4 relate to effects of noncondensibles at low void fraction. It is noted that no minimum bubble diameter is specified in the code, although a max d_b one is ($d_{b\ max}$ = hydraulic diameter).

Interfacial Area and Assessment

Specification of the volumetric heat transfer coefficients H_{if} and H_{ig} requires an estimate of the interfacial area per unit volume a_{gf}. Wallis[4-7] gives a detailed description of how the interfacial area per unit volume for a spray of droplets can be found. An adapted version of Wallis's discussion is given below, since RELAP5/MOD2 also uses it for bubbly flow.

A distribution for droplet diameter for a spray in the form of a probability density function and based on a model deduced by Nukiyama and Tanasawa[4-8] is given as

$$p^*(d^*) = 4d^{*2}\, e^{-2d^*} \qquad (4\text{-}9)$$

where

p^* = $p(d)d'$ is the dimensionless probability function,

d^* = dimensionless droplet diameter = d/d',

d' = most probable droplet diameter (m), and

d = droplet diameter (m).

The Sauter-mean diameter, d_{sm}, can be computed from p*(d). A droplet having the Sauter-mean diameter has the same area-to-volume ratio as the entire spray (that is, total surface area of the droplets vs. the total volume of the droplets). One can write[4-7]

$$d_{sm} = \frac{\int_0^\infty d^3 p(d) dd}{\int_0^\infty d^2 p(d) dd} . \tag{4-10}$$

Incorporating Equation (4-9) and writing in dimensionless form, one has

$$d^*_{sm} = \frac{\int_0^\infty d^{*5} e^{-2d^*} dd^*}{\int_0^\infty d^{*4} e^{-2d^*} dd^*} . \tag{4-11}$$

The improper integrals in Equation (4-11) can be evaluated in terms of the gamma function giving

$$d^*_{sm} = \frac{\Gamma(6)/2^6}{\Gamma(5)/2^5} = \frac{5!2^5}{4!2^6} = \frac{5}{2} . \tag{4-12}$$

The area-to-volume ratio for a droplet having a Sauter-mean diameter is

$$\left| \frac{A_{sm}}{V_{sm}} \right|_{drop} = \frac{\pi d_{sm}^2}{\frac{\pi}{6} d_{sm}^3} = \frac{6}{d_{sm}} . \tag{4-13}$$

Now a_{gf} can be written

$$a_{gf} = \frac{A_{interfacial}}{\text{unit volume}} = \frac{A_{interfacial}}{V_{drops}/\alpha_f} , \tag{4-14}$$

but

$$\left| \frac{A_{sm}}{V_{sm}} \right|_{drop} = \frac{A_{interfacial}}{V_{drops}}$$

from the definition of Sauter-mean diameter. Hence, one can rewrite Equation (4-14) as

$$a_{gf} = \frac{6\alpha_f}{d_{sm}} = \frac{6\alpha_f}{d'} \left(\frac{2}{5}\right) = \frac{2.4\alpha_f}{d'} \quad , \tag{4-15}$$

where Equation (4-12) has been used.

The dimensionless mean droplet diameter $d_o^* = d_o/d'$ can be found from[4-9]

$$d_o^* = \int_{-\infty}^{\infty} d^* p^*(d^*) dd^* \quad . \tag{4-16}$$

The lower limit of the integral in Equation (4-16) can be set to zero since a negative diameter is meaningless. Substituting $p^*(d^*)$ from Equation (4-9) into Equation (4-16) and integrating, one obtains

$$d_o^* = 4\Gamma(4)\ /2^4 = \frac{3}{2} \quad . \tag{4-17}$$

Combining Equations (4-15) and (4-17), one obtains

$$a_{gf} = \frac{3.6\alpha_f}{d_o} \quad . \tag{4-18}$$

It remains to specify the mean droplet diameter, d_o, in order to find a_{gf}. This is done by assuming that $d_o = 1/2\ d_{max}$ and using the critical Weber defined by

$$We_{crit} = \rho_c\ (v_g - v_f)^2\ d_{max}/\sigma \quad , \tag{4-19}$$

where ρ_c is the density of the continuous phase.

Before a value for d_{max} can be calculated from Equation (4-19), the value for critical We for droplet break-up must be specified. A similar We_{crit} for maximum bubble size in bubbly flow can also be specified.[4-7]

The values used in RELAP5/MOD2 for We_{crit} for droplets and bubbles are 3 and 10, respectively. (In the code itself, We_{crit} is given in terms of d_o rather than d_{max}, with values for droplets and bubbles given as 1.5 and 5.0, respectively.)

Although Equation (4-18) for interfacial area has been derived for droplet flow, it is used in RELAP5/MOD2 for bubbly flow as well.

In assessing the determination of the volumetric interfacial area, a_{gf}, it must be remembered that the final result depends upon the fluid properties and three intermediate results: (a) the particle diameter distribution function used to compute the Sauter-mean diameter, (b) the relationship between d_{sm} and d_{max}, and (c) the values used for We_{crit}, which determine the maximum particle size. While the particle diameter distribution is based on Nukiyama and Tanasawa,[4-8] the choice of $d_o = d_{max}/2$ is an assumption. Also, while the critical droplet We is assumed to be 3, Wallis[4-7] and Ishii and Chawla[4-10] recommend a value of 12 (for non-viscous liquids such as water). For maximum bubble diameter, Reference 4-10 uses $We_{crit} = 8$. Furthermore, TRAC[4-11] uses values of 4 and 7.5 for droplets and bubbles, respectively. While there appears to be considerable variation in the parameters used to compute a_{gf}, their combination gives, for RELAP5/MOD2,

$$a_{gf} = \frac{3.6\alpha_d}{d_o} = \begin{cases} 0.72\ \dfrac{\alpha_g \rho_f\ (v_g - v_f)^2}{\sigma}, & \text{bubbles} \\ 2.4\ \dfrac{\alpha_f \rho_g\ (v_g - v_f)^2}{\sigma}, & \text{droplets} \end{cases} \qquad (4\text{-}20)$$

and for TRAC,

$$a_{gf} = \frac{6\rho_c \alpha_d (v_g - v_f)^2}{We\ \sigma} = \begin{cases} 0.8\ \dfrac{\alpha_g \rho_f (v_g - v_f)^2}{\sigma}, & \text{bubbles} \\ 1.5\ \dfrac{\alpha_f \rho_g (v_g - v_f)^2}{\sigma}, & \text{droplets} \end{cases} \qquad (4\text{-}21)$$

where subscript d refers to the dispersed phase.

In arriving at the combination of parameters that produces Equation (4-20), RELAP5/MOD2 developers tuned the critical Weber number such that reasonable drag forces (which depend on drag coefficients and a_{gf}) would be predicted in order to simulate data from several separate effects tests.[4-12] Further discussion regarding these development efforts is given in the section on interfacial drag, Section 6.1.

In summary, the determination of volumetric interfacial area a_{gf} for RELAP5/MOD2 is based partly on published theory/experiment and partly on tuning related parameters to fit RELAP5/MOD2 simulations of separate-effects test data. Comparisons of data and calculations for pressure and void fraction in the Edwards pipe blowdown experiments are shown in Reference 4-12.

4.1.1.1.2 Bubbly Subcooled Liquid (SCL, $T_f < T^s$)

Model as Coded

$$H_{if} = \frac{F_3 F_5 h_{fg} \rho_g \rho_f \alpha_{bub}}{\rho_f - \rho_g},$$

where

$$\rho_f - \rho_g = \text{Max}\ (\rho_f - \rho_g,\ 10^{-7})$$

F_3, α_{bub} as for bubbly SHL

$$F_5 = \begin{cases} 0.075 & \alpha_{bub} \geq 0.25 \\ 1.8\phi C \exp\ (-45\alpha_{bub}) + 0.075 & \alpha_{bub} < 0.25 \end{cases}$$

$$C = \begin{cases} 61.0 - 6.489 \times 10^{-5} (P - 1.7 \times 10^5) & P \le 10^6 \text{ Pa} \\ 2.3 \times 10^9 & P > 10^6 \text{ Pa} \end{cases}$$

P = Pressure (Pa)

$$\phi = \begin{cases} 1 & |v_f| < 0.61 \\ [1.639344|v_f|]^{0.47} & |v_f| \ge 0.61 \end{cases}$$

Model Basis and Assessment

The heat transfer coefficient used in this code for subcooled liquid is based on Unal[4-13] but has been modified significantly. Unal gives the heat transfer coefficient for condensation at a bubble interface for subcooled nucleate flow boiling as

$$h = \frac{C \phi h_{fg} d}{2 \left(\frac{1}{\rho_g} - \frac{1}{\rho_f}\right)}, \qquad (4\text{-}22)$$

where

$$\phi = \begin{cases} \left|\frac{v_f}{0.61}\right|^{0.47} & v_f > 0.61 \text{ m/s} \\ 1 & v_f \le 0.61 \text{ m/s} \end{cases}$$

$$C = \begin{cases} 0.25 \times 10^{10} P^{-1.418} & 10^6 < P \le 17.7 \times 10^6 \text{ Pa} \\ 65 - 5.69 \times 10^5 (P - 10^5) & 10^5 \le P \le 10^6 \text{ Pa} \end{cases}$$

and d is the bubble diameter. The volumetric heat transfer coefficient H_{if} is found by multiplying h by the volumetric interfacial area, a_{gf}, Equation (4-18). At the same time, Equation (4-18) provides an expression for the average bubble diameter that can be used for d in Equation (4-22).

Hence, one can write

$$H_{if} = h\, a_{gf} = \frac{C\phi h_{fg}\, d\, a_{gf}}{2\left(\frac{1}{\rho_g} - \frac{1}{\rho_f}\right)} = \frac{3.6\alpha_f C\phi h_{fg}}{2\left(\frac{1}{\rho_g} - \frac{1}{\rho_f}\right)} = \frac{1.8\alpha_g C\phi h_{fg}\, \rho_f\, \rho_g}{\rho_f - \rho_g} \qquad (4\text{-}23)$$

Unal provides the ranges for which his correlation fits the experimental data: (a) pressure, 0.1-17.7 MPa, (b) heat flux, 0.47-10.64 MW/m^2, (c) bulk liquid velocity, 0.80-9.15 m/s, (d) subcooling, 3-86 K, (e) maximum bubble diameter, 0.08-1.24 mm, and (e) maximum bubble growth time, 0.175-5 ms. The assumptions made by Unal appear to be quite reasonable and supportable.

Comparison of Equation (4-23) with the coded version, Appendix 4A, indicates that modifications have been made. The constants found in the coefficient C of Equation (4-22) have been altered somewhat. The primary modification, however, is that the product 1.8 Cϕ is exponentially decreased from its original value at $\alpha_g = 0.0$ and summed with a constant 0.075 up to $\alpha_g = 0.25$; beyond $\alpha_g = 0.25$ it is simply replaced by 0.075. The value 0.075 was considered to be more appropriate for higher void fractions.[a]

The above modifications were made to improve predictions for various separate-effects tests, but present work has indicated they may have been inappropriate. The net effect of the coded modifications to Unal's correlation is to change the value of the heat transfer coefficient h by an order of magnitude. If one computes a value for H_{if} based on typical conditions, Appendix 4B, for $\alpha_g = 0.1$ and liquid velocity $v_f = 2$ m/s, there results for Equation (4-23) and the coded version,

$$H_{if} = \begin{cases} 7.19 \times 10^6 \text{ W/m}^3\text{K} & \text{Equation (4-23)} \\ 6.43 \times 10^5 \text{ W/m}^3\text{K} & \text{RELAP5/MOD2} \end{cases} \qquad (4\text{-}24)$$

---

a. Personal communication, J. C. Lin to R. A. Riemke, May 24, 1988. The value 0.075 was determined from work by R. T. Lahey, Jr., reference unknown.

Stadke and Kolar[4-14] arrive at a similar conclusion in their assessment report on RELAP5/MOD2 for some Joint Research Centre (JRC, Ispra, Italy) test results. They found, as mentioned in Section 3.2.2.1, that subcooling was reduced by about 50% for the LOBI-MOD2 test A2-90 (simulation of a loss of normal onsite and offsite power with additional failure to SCRAM) by using Unal's original correlation vs. the coded version. This further led to significantly improved predictions for the primary system pressure.

In summary, the RELAP5/MOD2 correlation is not the same one proposed by Unal[4-13]. It has been modified somewhat and combined with a correlation more appropriate to higher void fractions. Further assessment is required to determined its accuracy and resolve criticism of the model.

4.1.1.1.3 Bubbly Superheated Gas (SHG, $T_g > T^s$)

Model as Coded

$$H_{ig} = Nu_{ib} F_6 F_7 a_{gf}$$

where

$Nu_{ib} = 10^4$

a_{gf} as for bubbly SHL

$F_6 = [1 + \eta (100 + 25\eta)]$, $\eta = |Max (-2, \Delta T_{sg})|$

$$F_7 = \frac{Max (\alpha_g, 10^{-5})}{Max (\alpha_g, 10^{-9})} .$$

Model Basis and Assessment

The volumetric heat transfer coefficient, H_{ig}, for Bubbly SHG is not based on a theoretical or empirical correlation. The Nusselt number, $Nu_{ib} = 10^4$, is chosen to be large in order to bring the gas temperature

rapidly toward the saturation temperature. Function F_6, Appendix 4A, clearly enhances this tendency, especially as ΔT_{sg} increases in magnitude. Function F_7 apparently improves numerical stability for low void fractions. The determination of volumetric interfacial area, a_{gf}, is discussed in Section 4.1.1.1.1. Clearly, there is room for improving the determination of H_{ig} for this case, although to the best of our knowledge, this might require further experimental work.

4.1.1.1.4 Bubbly Subcooled Gas (SCG, $T_g < T^s$)

Model as Coded

H_{ig} as for bubbly SHG

(Note that F_6 has a different form for $\Delta T_{sg} > 0$).

Model Basis and Assessment

The expression used for bubbly SCG is the same as for bubbly SHG, Appendix 4A, except that the Nu enhancing function F_6 increases H_{ig} dramatically for large subcooled levels, pushing T_g more quickly toward saturation temperature. The fact that Nu for subcooled gas is much greater than for superheated gas, especially as the subcooling increases, seems appropriate in view of the unstable nature of the subcooled state. Nevertheless, a better basis for the correlation for bubbly SCG is needed.

4.1.1.2 Slug Flow. In slug flow, interfacial heat transfer can be divided into two distinct parts: (a) the heat transfer between the large Taylor bubbles and the liquid surrounding them and (b) the heat transfer between the small bubbles in the liquid slug and their host liquid. The heat transfer for each part is summed to obtain the total. For the total heat transfer per unit volume, $Q_{ip}(W/m^3)$, between a given plane and the interface, one has

$$Q_{ip} = \frac{h_{TB} A_{TB} \Delta T}{V_{tot}} + \frac{h_{bub} A_{bub} \Delta T}{V_{tot}} , \qquad (4\text{-}25)$$

where

h_{TB} = heat transfer coefficient for Taylor bubble (W/m^2K)

A_{TB} = interfacial area of Taylor bubble (m^2)

h_{bub} = heat transfer coefficient for small bubbles (W/m^2K)

A_{bub} = interfacial area of small bubbles (m^2)

V_{tot} = total volume of cell (m^3)

ΔT = temperature difference between the phase in question and the saturation temperature.

Equation (4-25) can be rewritten

$$Q_{ip} = h_{TB} \frac{A_{TB}}{V_{TB}} \frac{V_{TB}}{V_{tot}} \Delta T + h_{bub} \frac{A_{bub}}{V_{bub}} \frac{V_{bub}}{V_{tot}} \Delta T \qquad (4\text{-}26)$$

or finally

$$Q_{ip} = H_{ip,TB} \Delta T + H_{ip,bub} \Delta T \quad . \qquad (4\text{-}27)$$

Hence, the volumetric interfacial area for each part can be computed either based on the volume of that part (Taylor bubble or slug volume) or based on the total volume. The final volumetric interfacial area, a_{gf}, must be based on the total cell volume as implied by Equation (4-25). One can write

$$a_{gf,TB} = \frac{A_{TB}}{V_{TB}} \frac{V_{TB}}{V_{tot}} = a^*_{gf,TB} f_{TB} \qquad (4\text{-}28)$$

and

$$a_{gf,bub} = \frac{A_{bub}}{V_{bub}} \frac{V_{bub}}{V_{tot}} = a^{*}_{gf,bub} f_{bub} , \qquad (4\text{-}29)$$

where f_{TB} and f_{bub} represent volumetric fractions as defined by Equations (4-28) and (4-29).

RELAP5/MOD2 recognizes the contributions from the two distinct divisions of slug flow toward the total heat transfer. The correlations for the contributions for the bubbles in the liquid slug are based on those computed for bubbly flow, but are exponentially diminished as α_g increases. The details of the coded correlations for slug flow heat/mass transfer appear in Appendix 4A.

4.1.1.2.1 Slug-Superheated Liquid (SHL)

Model as Coded

$$H_{if} = H_{if,TB} + H_{if,bub}$$

where

$H_{if,TB}$ = $3.0 \times 10^{6} a^{*}_{gf,TB} \alpha_{TB} F_{8}$

$a^{*}_{gf,TB}$ = volumetric interfacial area = [4.5/D](2)

F_{8} = Min (1, $- \Delta T_{sf}$)

α_{TB} = Taylor bubble void fraction = $(\alpha_g - \alpha_{gs})/(1 - \alpha_{gs})$

= Taylor bubble volume/total volume

α_{gs} = the average void fraction in the liquid film and slug region

= $\alpha_{AB} F_g$

$$F_g = \exp\left[-8\left(\frac{\alpha_g - \alpha_{AB}}{\alpha_{AC} - \alpha_{AB}}\right)\right]$$

α_{AB} = α_g for bubbly-to-slug transition

α_{AC} = α_g for slug-to-annular mist transition

and

$H_{if,bub}$ is as for H_{if} for bubbly SHL with the following modifications:

α_{bub} = $\alpha_{AB} F_g$

v_{fg} = $(v_g - v_f) F_g^2$

$a_{gf,bub}$ = $(a_{gf})_{bub} (1 - \alpha_{TB}) F_g$

β = F_g

Model Basis and Assessment

The coded two-part correlation for slug SHL is presented in detail in Appendix 4A. The contribution for the large Taylor bubbles, $H_{if,TB}$, is an ad hoc correlation. It is given a large value to promote a rapid return of T_f toward the saturation temperature, since SHL is a metastable state.

The Taylor bubble void fraction α_{TB} is used to determine the fraction f_{TB}, Equation (4-28), that comes from interfacial heat/mass transfer across the Taylor bubble boundary; f_{bub}, Equation (4-29), is set equal to $(1 - \alpha_{TB})$. α_{TB} is computed from simple geometric considerations and can be given in terms of α_g and the average void fraction in the portion of the

flow where the liquid is the continuous phase, α_{gs}.[4-15] The expression used for α_{gs} causes it to drop exponentially from the bubbly-slug transition α_g to near zero as α_g approaches the slug-annular mist transition. Function F_8 is used to smooth the calculation for small values of $|\Delta T_{sf}|$.

The part of H_{if} that is used to account for the heat transfer in the continuous liquid portion of the flow is based directly on H_{if} for bubbly flow, SHL, Section 4.1.1.1.1, but with some modifications (see Appendix 4A). These additional modifications to $H_{if,bub}$ serve to further reduce the contribution of $H_{if,bub}$ to the total volumetric coefficient.

In summary, the primary purpose of H_{if} for slug SHL is to drive the liquid temperature to the saturation value.

Interfacial Area

The expression used for the interfacial area for the Taylor bubble portion of slug flow, $a^*_{gf} = [4.5/D](2)$, is based on an argument of Ishii and Mishima.[4-15] If one computes the surface area per unit volume of a cylinder, one obtains

$$\frac{A_{cyl}}{V_{cyl}} = \frac{\pi D_{cyl}}{\frac{\pi}{4}} \frac{L_{cyl} + 2\,\frac{\pi}{4} D^2_{cyl}}{D^2_{cyl}\, L_{cyl}} . \qquad (4\text{-}30)$$

... the length of the cylinder L_{cyl} increases, the surface area of the ends of the cylinder becomes negligible and the area-to-volume ratio becomes

$$\lim_{L_{cyl} \to \infty} \frac{A_{cyl}}{V_{cyl}} = \frac{4}{D_{cyl}} . \qquad (4\text{-}31)$$

Assuming that a Taylor bubble can be approximated by a cylinder and employing the relation[4-15] $D_{TB} = 0.88\, D_{pipe}$, one has

$$\frac{4}{D_{cyl}} = \frac{4}{0.88D} = \frac{4.55}{D} \simeq \frac{4.5}{D} , \qquad (4\text{-}32)$$

where D is the hydraulic diameter. Except for the factor of two, Equation (4-32) is the same result given by Ishii and Mishima for volumetric interfacial area. It is noted that it is appropriate to use the cylinder/bubble volume in Equation (4-30) for RELAP5/MOD2, since the fraction of the computational cell used for $H_{if,TB}$ is the ratio of the Taylor bubble volume to the cell volume (see Model Basis and Assessment above). Ishii and Mishima[4-15] insert a coefficient into the expression for a^*_{gf} to account for rippling of the Taylor bubble surface. A value of two is used in RELAP5/MOD2 for this coefficient.

4.1.1.2.2 Slug Subcooled Liquid (SCL)

Model as Coded

$$H_{if} = H_{if,TB} + H_{if,bub}$$

where

$$H_{if,TB} = 1.18942\ Re_f^{0.5} Pr_f^{0.5} \frac{k_f}{D}\ a^*_{gf,TB}\ \alpha_{TB}$$

where

α_{TB} and $a^*_{gf,TB}$ are as for slug SHL

$Pr_f = C_{pf}\ \mu_f / k_f$

$Re_f = \rho_f\ D\ Min\ (|v_f - v_g|, 0.8) / \mu_f$

and

$H_{if,bub}$ is as for bubbly SCL .

Model Basis and Assessment

The volumetric heat transfer coefficient for the interfacial heat transfer for the Taylor bubble portion for slug SCL is based on a dependence of the Reynolds and Prandtl numbers.[a] The Nusselt number upon which $H_{if,TB}$ is based varies as $Re^{0.5}$, Appendix 4A. This dependence lies between that for laminar flow, $Re^{0.3}$, and that for turbulent flow, $Re^{0.8}$, as reported by Kreith.[4-6] Also, the coefficient 1.18942 lies between the laminar Seider-Tate correlation coefficient, 1.86, and the turbulent Dittus-Boelter coefficient, 0.023.[4-6] [The Seider-Tate correlation is also a function of $(D/L)^{0.33}$.] Since the liquid flow past a Taylor bubble does not exhibit the full effects of turbulence but is probably not purely laminar, the correlation used in the code should give a result that is plausible, although it may still be significantly in error.

The expression used for the bubbly part of the volumetric coefficient $H_{if,bub}$, is the same as that used for slug SHL, Section 4.1.1.1.2. The apportionment of the two contributions to H_{if} is effected the same as for slug SHL, as is the determination of a_{gf}.

4.1.1.2.3 Slug Superheated Gas (SHG)

Model as Coded

$$H_{ig} = H_{ig,TB} + H_{ig,bub}$$

where

$$H_{ig,TB} = (2.2 + 0.82\ Re_g^{0.5})\ \frac{k_g}{D}\ a^*_{gf,TB}\ \alpha_{TB}$$

where

$a^*_{gf,TB}$ and α_{TB} are as for slug SHL

$$Re_g = \rho_g\ |v_f - v_g|\ D\ /\ \mu_g$$

---

a. The literature reference for this correlation is unknown as of this writing, and it is in the process of being researched.

and

$$H_{ig,bub} = Nu_{ib} F_6 (1 - \alpha_{TB}) a_{gf,bub}$$

where

α_{TB}, $a_{gf,bub}$ and F_g are as for slug SHL

and

Nu_{ib} and F_6 are as for bubbly SHG .

Model Basis and Assessment

The contribution to the volumetric heat transfer coefficient from the Taylor bubble interfacial heat transfer, Appendix 4A, is based on a modified form of the Lee-Ryley[4-3] correlation derived for laminar flow heat transfer to a sphere (Section 4.1.1.1.1). The coefficients have been augmented from the original, and the Prandtl number dependence has been dropped as is the case for interfacial heat transfer for bubbly flow. While the bullet-shaped cap on the Taylor bubble may approximate a sphere, it seems inappropriate to use the Lee-Ryley correlation for this case.

The heat transfer coefficient for the bubbly flow contribution is ad hoc and simply provides a large value for $H_{if,bub}$. Since slug SHG is a stable thermodynamic state, it would seem that the ad hoc correlation is inappropriate. The apportionment of H_{if} between the two contributions is based on the same α_{TB} as for slug SHL, Section 4.1.1.2.1.

4.1.1.2.4 Slug Subcooled Gas (SCG)

Model as Coded

$$H_{ig} = H_{ig,TB} + H_{ig,bub}$$

where

$$H_{ig,TB} = Nu_{ib} F_6 \alpha_{TB} a^*_{gf,TB}$$

where α_{TB} and $a^*_{gf,TB}$ are as for slug SHL,

$H_{ig,bub}$ is as for slug SHG,

and

Nu_{ib} and F_6 are as for bubbly SHG.

Model Basis and Assessment

Both contributions to H_{if} for slug SCG ($H_{if,TB}$ and $H_{if,bub}$) are ad hoc correlations that simply employ large values for Nu. Although the two parts look similar, the interfacial area is different for each. The large values for Nu used for slug SCG are apparently designed to drive the gas temperature toward the saturation value. This seems reasonable in view of the fact that subcooled gas is an unstable state.

4.1.1.3 Annular Mist Flow. For annular mist flow, the interfacial heat transfer results from two contributory sources: (a) the heat transfer between the annular liquid film and gas core, and (b) the heat transfer between the gas core and entrained liquid droplets. The correlations that are used to represent the overall volumetric heat transfer are constructed from the two contributing sources, as in the case for slug flow. Equations (4-25 through 4-29) for slug flow apply to annular mist flow as well except for the identities of the two sources. One can write [see Equation 4-27)]

$$Q_{ip} = H_{ip,ann} \Delta T + H_{ip,drp} \Delta T , \qquad (4\text{-}33)$$

where subscript ann refers to the annular film-gas core contribution and subscript drp refers to the droplet-gas core contribution. The details of the correlations coded in RELAP5/MOD2 are recorded in Appendix 4A.

4.1.1.3.1 Annular Mist Superheated Liquid (SHL)

Model as Coded

$$H_{if} = H_{if,ann} + H_{if,drp}$$

where

$$H_{if,ann} = 3.0 \times 10^{6}\ a_{gf,ann}\ F_{10}$$

$$a_{gf,ann} = (4C_{ann}/D)(1 - \alpha_{ff})^{1/2}$$

$$C_{ann} = (30\alpha_{ff})^{1/8}\ (2.5)$$

$$\alpha_{ff} = \text{Max}\ (0.0,\ \alpha_f F_{11})$$

$$F_{11} = \gamma^{*}\ \text{Max}\ [0.0,\ (1-G^{*})]\ \exp\ (-C_e \times 10^{-5} \lambda^{6})$$

$$C_e = \begin{cases} 4.0 & \text{horizontal} \\ 7.5 & \text{vertical} \end{cases}$$

$$\lambda = \begin{cases} v_g^{*}/v_{crit} & \text{horizontal flow} \\ \alpha_g v_g / v_{crit} & \text{vertical flow} \end{cases}$$

$$v_g^{*} = \text{Max}\ (v_g,\ 10^{-15})$$

$$v_{crit}\ (\text{horizontal}) = 0.5 \left[\frac{(\rho_f - \rho_g)\ g \alpha_g A_{pipe}}{\rho_g\ D \sin \theta}\right]^{1/2} (1 - \cos \theta)$$

[see Equation (3-2)]

$$v_{crit}\ (\text{vertical}) = 1.4\ [\sigma^{*} g\ (\rho_f - \mu_g)]^{1/4} / \rho_g^{1/2}$$ [see Equation (3-6)]

$$\sigma^{*} = \text{Max}\ (\sigma,\ 10^{-7})$$

$$G^{*} = 10^{-4}\ Re_f^{0.25}$$

$$Re_f = \rho_f \alpha_f |v_f| D/\mu_f$$

$$\gamma^* = \begin{cases} \gamma & \alpha_g > \alpha_{AC} \text{ and } \alpha_f < \alpha_{EF} \\ 1 & \text{otherwise} \end{cases}$$

$$\gamma = \frac{\alpha_f - \alpha_{AD}}{\alpha_{EF} - \alpha_{AD}}$$

$$a_{AD} = 10^{-7}$$

$$\alpha_{EF} = \text{Max}\left[2\,\alpha_{AD},\ \text{Min}\left(2 - 3\,\frac{\rho_g}{\rho_f},\ 2 \times 10^{-4}\right)\right]$$

$$F_{10} = \text{Min}\,(1.0 + \lambda^{1/2} + 0.05\,\lambda,\ 6)$$

$$H_{if,drp} = \frac{k_f}{d_d} F_{12}\,(2)\,a_{gf,drp}$$

d_d = characteristic droplet diameter

$$= \frac{We\,\sigma}{\rho_g\, v_{fg}^{**2}},\quad We = 1.5,\quad We\,\sigma = \text{Max}\,(We\,\sigma,\ 10^{-10})$$

$$v_{fg}^{**2} = \begin{cases} v_{fg}^{*2}\,\alpha_f 10^6 & \alpha_f < 10^{-6} \\ v_{fg}^{*2} & \alpha_f \geq 10^{-6} \end{cases}$$

$$v_{fg}^{*2} = \begin{cases} v_{fg}^2\,F_{11}\gamma & \alpha_g > \alpha_{AC} \text{ or } \alpha_f < \alpha_{EF} \\ v_{fg}^2\,F_{11} & \text{otherwise} \end{cases}$$

v_{fg}^2 is as for bubbly SHL except

$$\alpha_{bub} = \alpha_{fd}$$

$$D' = 0.0025$$

$$\alpha_{fd} = \text{Max}\left[\frac{\alpha_f - \alpha_{ff}}{1 - \alpha_{ff}},\ \alpha^*_{AD}\right]$$

$$\alpha^*_{AD} = \begin{cases} \alpha_{AD}\gamma + 10^{-5}(1 - \gamma) & \alpha_g > \alpha_{AC} \text{ or } \alpha_f < \alpha_{EF} \\ \alpha_{AD} & \text{otherwise} \end{cases}$$

$$F_{12} = [1 + \xi\,(250 + 50\xi)]$$

$$\xi = \text{Max}\,(0, -\Delta T_{sf})$$

$$a_{gf,drp} = \frac{3.6\,\alpha_{fd}}{d_d}(1 - \alpha_{ff})\ .$$

Model Basis and Assessment

The Nusselt number, upon which the annular film portion of the volumetric heat transfer coefficient is based, is simply a large number, apparently designed to push T_f toward the saturation temperature. Function F_{10}, Appendix 4A, is a smoothing function that greatly decreases $H_{if,ann}$ as the velocity ratios parameter λ approaches zero.

The Nusselt number for the droplet to gas core is represented by a function, F_{12}, which grows quadratically as the magnitude of ΔT_{sf} increases. It also helps drive T_f toward T^s.

Interfacial Area

The interfacial areas per unit volume for the annular film-gas core interface contribution as well as that for the droplet-gas core are based on

simple geometric considerations as given by Ishii and Mishima.[4-15] It is appropriate to give the derivation leading to the results of Reference 4-15 and then show how these results are transformed into the coded version.

The volumetric interfacial area of the liquid annular film in a pipe is

$$a_{gf,ann} = \frac{\pi D' L}{\frac{\pi}{4} D^2 L} = \frac{4D'}{D^2} \tag{4-34}$$

where

D' = diamcter of liquid annulus

D = diameter of pipe

L = unit pipe length.

An expression for the ratio D'/D can be found in terms of void fractions. First, one can write

$$\frac{V_{core}}{V_{tot}} = \frac{(\pi/4)D'^2 L}{(\pi/4D)^2 L} = \frac{D'^2}{D^2}$$

where

V_{core} = idealized volume of the gas core

V_{tot} = volume of control volume .

Also, one can write

$$\frac{V_{core}}{V_{tot}} = \frac{V_g/V_{tot}}{V_g/V_{core}} = \frac{\alpha_g}{\alpha_{gd}} = \frac{\alpha_g}{1 - \alpha_{fd}} . \tag{4-35}$$

Hence,

$$a_{gf,ann} = \frac{4}{D}\left(\frac{D'}{D}\right) = \frac{4}{D}\left(\frac{\alpha_g}{1 - \alpha_{fd}}\right)^{1/2}, \qquad (4\text{-}36)$$

which is the expression given by Reference 4-15.

In these expressions,

V_g = volume of gas (all of which is assumed to be in the core)

α_{gd} = void fraction in the core [defined in Equation (4-35)]

α_{fd} = liquid fraction in the core [defined in Equation (4-35)].

The coded expression for volumetric interfacial area is given in terms of α_{ff}, the liquid fraction of the annular film, or

$$\alpha_{ff} = \frac{V_{f,\ film}}{V_{tot}} = 1 - \frac{V_{core}}{V_{tot}} = 1 - \frac{\alpha_g}{1 - \alpha_{fd}}$$

Rewriting, one obtains

$$\frac{\alpha_g}{1 - \alpha_{fd}} = 1 - \alpha_{ff} \qquad (4\text{-}37)$$

Applying this result to Equation (4-35) yields

$$a_{gf,ann} = \frac{4}{D}\left(1 - \alpha_{ff}\right)^{1/2} \qquad (4\text{-}38)$$

This is the same as the coded version shown above, with the exception of the C_{ann} factor. C_{ann} contains a multiplier of 2.5 as a roughness factor to increase the surface area for mass transfer, and a term $(30\ \alpha_{ff})^{1/8}$ that gives a value near unity for α_{ff} between 0.01 and 0.1, yet ensures $\alpha_{gf,ann} \rightarrow 0$ as $\alpha_{ff} \rightarrow 0$.

The volumetric interfacial area for the droplets in the gas core is derived as detailed in Section 4.1.1.1.1 and is given by Equation (4-18):

$$a^{*}_{gf,drp} = \frac{3.6\ \alpha_{fd}}{d_d} \quad ,$$

where d_d denotes a droplet diameter and α_{fd} is the liquid fraction in the gas core. In order to normalize $a^{*}_{gf,drp}$ to the total cell volume, it must be multiplied by the fraction of the total cell volume occupied by the core, Equation (4-35). Using Equation (4-37) one has

$$a_{gf,drp} = \frac{3.6\ \alpha_{fd}}{d_d} (1 - \alpha_{ff}) \quad , \qquad (4\text{-}39)$$

which is the coded version as indicated in Appendix 4A. The liquid fraction of the annular film, α_{ff}, depends upon the amount of liquid entrained in the gas core.

Liquid Droplet Entrainment Model and Assessment

This model is discussed in Section 6.3.

4.1.1.3.2 Annular Mist Subcooled Liquid (SCL)

Model as Coded

$$H_{if} = H_{if,ann} + H_{if,drp}$$

where

$$H_{if,ann} = 10^{-3}\ \rho_f C_{pf} \left|v_f\right| a_{gf,ann} F_{10}$$

$a_{gf,ann}$ and F_{10} are as for annular mist SHL

and

$$H_{if,drp} = \frac{k_f}{d_d} F_{13} a_{gf,drp} ;$$

where

$a_{gf,drp}$ and d_d are as for annular mist SHL

and

$$F_{13} = 2.0 + 7.0 \text{ Min } (1.0 + \frac{C_{pf} \Delta T_{sf}}{h_{fg}}, 8.0)$$

Model Basis and Assessment

The volumetric heat transfer coefficient for annular mist SCL is comprised of two parts (Appendix 4A). The contribution from the interface between the liquid annular film and the gas core is based on a model given by Theofanous.[4-16] Theofanous makes reference to an earlier work (Brumfield, Houze, Theofanous[4-17]) wherein models are obtained for the mass transfer coefficient for gas absorption by a turbulent, thin, falling liquid film. The mass transfer models are compared with data for water at 25°C absorbing various gases for turbulent Reynolds number $Re_t << 500$. (Re_t is defined below.) The agreement with the data is very good. Theofanous[4-16] then writes the heat transfer analogues of the mass transfer correlations, using the same numerical coefficients and exponents. These are:

$$Nu_t = \begin{cases} 0.25 \, Re_t^{3/4} \, Pr^{1/2} & Re_t > 500 \\ 0.70 \, Re_t^{1/2} \, Pr^{1/2} & Re_t < 500 \end{cases} \qquad (4\text{-}40)$$

where

$Nu_t = \frac{h\lambda}{k}$, λ = integral scale of turbulence ,

$$Re_t = \frac{u\lambda}{\nu}, \quad u = \text{turbulence intensity},$$

and where a fully developed residence time is assumed. Introducing the Stanton number St = Nu/Re·Pr and approximating[4-16] $u \simeq 5 \times 10^{-2} v$, where v is bulk liquid velocity, Equation (4-40) can be rewritten as

$$St = \frac{h}{\rho_f C_{pf} v_f} = \begin{cases} 5.0\ Re_t^{-1/4}\ Pr^{-1/2} & Re_t > 500 \\ 14.0\ Re_t^{-1/2}\ Pr^{-1/2} & Re_t < 500 \end{cases} . \qquad (4\text{-}41)$$

Theofanous[4-16] then declares that the usual range for Re_t is 10^2 - 10^3 and chooses Pr = 3. Finally, he indicates that for either Re_t >500 or Re_t <500, one obtains for St, using the numbers indicated

$$St = 1 \times 10^{-3} \text{ to } 3 \times 10^{-3} . \qquad (4\text{-}42)$$

Theofanous[4-16] goes on to develop an expression for the decay of St for a liquid jet flow where the turbulence decays with increasing distance from the initial orifice. He finally arrives at a correlation which compares favorably with experimental data[4-16] and is written as

$$St = 2 \times 10^{-2} \left(\frac{l}{d}\right)^{-1/2} . \qquad (4\text{-}43)$$

Comparing Equation (4-43) to Equation (4-42) for a value of l = d (d = orifice diameter, l = streamwise distance), Theofanous[4-16] notes a difference in St of an order of magnitude for which he can only partly account.

The coded version for the heat transfer coefficient is (Appendix 4A).

$$h = 10^{-3} \rho_f C_{pf} |v_f|\ F_{10} , \qquad (4\text{-}44)$$

where it has been assumed that St = 10^{-3} as given in Equation (4-42).

Several weaknesses in the coded correlations as it relates to the original mass transfer model of Brumfield et al.,[4-17] can be identified:

1. The original correlation is based on a falling liquid film probably surrounded by quiescent air, whereas annular mist flow involves a flowing, possibly turbulent, possibly laminar vapor core.

2. The original correlation is based on the liquid velocity against quiescent air; the liquid velocity in the code is a single bulk value representing both the liquid annular film and the liquid droplets in the core. As such, it is possible for the liquid velocity to be zero when the mass flow of droplets in one direction is balanced by an annular film flow in the opposite direction. In such a case, the code would incorrectly predict zero for $H_{if,ann}$.

3. The original correlation is based on turbulent flow for the liquid film. In an actual reactor flow, the liquid film may be in laminar flow, or it may be stationary, as in vertical flow when just enough drag is imparted by the core flow to prevent downflow of the annular film.

4. The original mass transfer correlation is based on isothermal flow; the code attempts to simulate flows with boiling heat transfer where bubbles may form at the pipe wall and push their way toward the annular film/vapor core interface, thereby dynamically enhancing the mass/heat transfer.

5. The original correlation for mass transfer[4-16] is valid for high values of Schmidt number, Sc, whereas the heat transfer analogue of Sc, the Prandtl number, is of order unity for most flows of thermal-hydraulic interest. This means that the heat transfer analogue of the original mass transfer correlation is not valid for small Re_t.[4-16]

6. Finally, there is the problem discussed above, that an order-of-magnitude difference exists between Equation (4-42) and Equation (4-43) for $l/d \sim 1$.

In summary, the weaknesses described above make the applicability of the correlation for $H_{if,ann}$ to reactor conditions unclear. It must be assessed against experiment to determine its validity.

The volumetric heat transfer coefficient for the vapor core interface to liquid droplets is based on a paper by Brown.[4-18] Brown solves a classical transient heat conduction problem for a sphere immersed suddenly in a uniform temperature bath. The boundary condition at the surface is simply that the surface temperature remains constant at the bath temperature, implying a very large heat transfer coefficient from the bath to the sphere. Brown then forms an internal energy balance in which he defines an internal heat transfer coefficient between the surface and internal mean temperature. He sets this heat transfer equal to the increase in the thermal energy of the sphere. He has thus linearized an unsteady, one-dimensional heat conduction problem. He produces a graph showing the variation of $Nu = hd/k$ versus T_m/T_s, or the ratio of mean to surface temperature, Figure 4-1. The mean temperature is, of course, a function of time. The coded version of $H_{if,drp}$ is based on the curve in Figure 4-1. The fact that Nu drops as T_m/T_s increases follows from Fourier's law of conduction, which indicates that the heat transfer will decrease if the temperature gradient (related to T_s-T_m) decreases. The coded version of Nu for this case (Appendix 4A) is represented by Function F_{13}, which is

$$F_{13} = 2.0 + 7.0 \text{ Min } \left(1.0 + \frac{C_{pf}\,\Delta T_{sf}}{h_{fg}},\ 8.0\right) \quad . \tag{4-45}$$

F_{13} gives Nu = 9, compared to Nu = 10 in Figure 4-1, for $T_m/T_s = 1$ ($\Delta T_{sf} = 0$). It also gives the correct trend of Nu increasing as T_m/T_s decreases (ΔT_{sf} increasing). It is not clear, however, how Brown arrived at the curve for Nu in Figure 4-1, since Nu is a complicated function of T_m/T_s and involves specification of droplet diameter and length of time since initiation of heat transfer. Brown does not specify either of the above in arriving at his functional relationship, Figure 4-1.

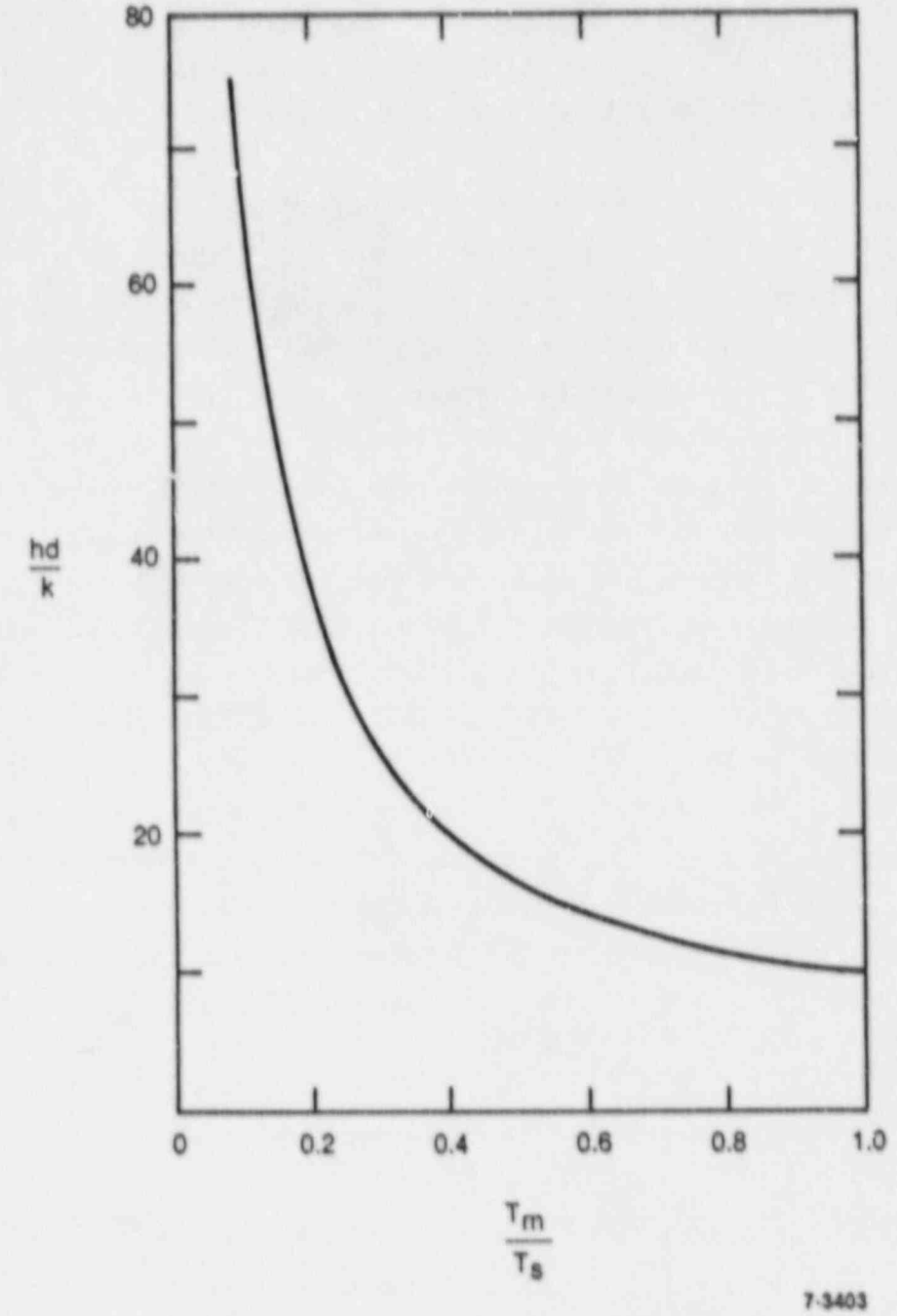

Figure 4-1. Nusselt number as a function of mean-to-surface-temperature ratio for heat conduction in a sphere.

In evaluating the validity of the model for Nu provided by Brown,[4-18] the following points are noted:

1. Brown's heat transfer problem does not address increasing droplet size due to condensation except in a correction applied to the mean temperature, T_m. It is not clear if his correction is incorporated in obtaining the curve in Figure 4-1. Furthermore, it appears that his correction is wrong, since it does not account for the relative masses of the original drop and the additional condensate. His correction is given as[4-18]

$$T_m = \frac{T_f}{1 + C_{pf}\Delta T_{sf}/h_{fg}} \tag{4-46}$$

where T_m is the mean temperature of the original drop and T_f that for the drop plus new condensate.

2. Brown assumes that the surface temperature of the drop remains constant; this same condition is assumed in RELAP5/MOD2 wherein the interface is assumed equal to the saturation temperature. Thus, the 'convective' heat transfer between the interface and mean droplet temperature is actually based on conduction. True convection in the droplet is neglected. On the whole, this seems an appropriate simplification.

3. It is stated by Brown that his curve, Figure 4-1, is based on $k = 0.38$ Btu/hr ft^{o}F, the thermal conductivity of water at about 150^{o}F.

In summary, it seems that the correlation for $H_{if,drp}$ could be based on firmer ground by including the effects of condensation and comparing such with experimental data. An evaluation of this correlation requires assessment against experiment.

4.1.1.3.3 Annular Mist Superheated Gas (SHG)

Model as Coded

$$H_{ig} = H_{ig,ann} + H_{ig,drp}$$

where

$$H_{ig,ann} = \frac{k_g}{D}\, 0.023\, Re_g^{0.3}\, a_{gf,ann}\, F_{10}$$

$$Re_g = \rho_g \left| v_g - v_f \right| D\alpha_g / \mu_g$$

F_{10} and $a_{gf,ann}$ are as for annular mist SHL

and

$$H_{ig,drp} = \frac{k_g}{d_d} (2.0 + 0.5\, Re_d^{0.5})\, a'_{gf,drp}$$

where

d_d is as for annular mist SHL

$$Re_d = \frac{We\, \sigma\, (1 - \alpha_{drp})^3}{\mu_g \left[v_{fg}^{**2} (1 - \alpha_{drp}) \right]^{1/2}}, \qquad \begin{array}{l} We \equiv 1.5, \\ We\, \sigma = Max\, (We\, \sigma,\ 10^{-10}) \end{array}$$

$$a'_{gf,drp} = \begin{cases} a_{gf,drp} & \alpha_f \geq \alpha^*_{AD} \\ a_{gf,drp} \left[\dfrac{\alpha_f F_{14}}{\alpha^*_{AD}} + (1 - F_{14}) \right] & \alpha_f < \alpha^*_{AD} \end{cases}$$

$a_{gf,drp}$, α_{drp}, v_{fg}^{**2}, and α^*_{AD} are as for annular mist SHL

and

$$F_{14} = 1.0 - 5.0\, Min\, [0.2,\ Max\, (0,\ \Delta T_{sg})] .$$

Model Basis and Assessment

The coded correlation for the heat transfer between the vapor and the liquid-vapor interface for annular mist SHG consists of two parts (Appendix 4A).

The contribution to H_{ig} from the heat transfer from the gas to the liquid annular film is represented by a correlation obviously based on the Dittus-Boelter relation. While the Dittus-Boelter correlation is valid for turbulent flow, there is no test for turbulent flow in the code. An evaluation of this model requires an assessment against experiment.

The expression used to represent heat transfer from the vapor core to the entrained liquid droplets is based on the correlation of Lee and Ryley,[4-3] except that the coefficient of the Reynolds number is changed from 0.74 to 0.5. A discussion of the Lee-Ryley model is given in Section 4.1.1.1.1.

The Reynolds number used for the modified Lee-Ryley correlation[4-3] employs a mixture viscosity defined as

$$\mu_m = \mu_c (1 - \alpha_d)^{-.5} , \qquad (4\text{-}47)$$

where c and d represent continuous and dispersed phases, respectively. This relationship is given by Ishii and Chawla[4-10] for use in a drag correlation for dispersed droplet flow. The Lee-Ryley correlation, however, employs Re based on the continuous phase ($Re = U_\infty d/\nu$), where U_∞ is the free-stream velocity and d is the droplet diameter. It seems inappropriate, therefore, to use a mixture viscosity.

Another significant limitation of the coded correlation appears to be that the liquid velocity, v_f, used in the Reynolds number is some average of the annular film and entrained droplets, rather than just the velocity of the droplets. The relative velocity computed, then, is not a true relative velocity for the droplets flowing in the vapor core.

In summary, significant doubts remain about the validity of H_{ig} for annular mist SHG.

4.1.1.3.4 Annular Mist Subcooled Gas (SCG)

Model as Coded

$$H_{ig} = H_{ig,ann} + H_{ig,drp}$$

where

$$H_{ig,ann} = Nu_{ib} a_{gf,ann} F_{10} F_6$$

where Nu_{ib} and F_6 are as for bubbly SHG, and $a_{gf,ann}$ and F_{10} are as for annular mist SHL

and

$$H_{ig,drp} = Nu_{ib} a'_{gf,drp} F_6$$

where

$a'_{gf,drp}$ is as for annular mist SHG .

Model Basis and Assessment

Both parts of the volumetric heat transfer coefficient H_{ig} for annular mist SCG are based on large values which increase quadratically as ΔT_{sg} increases (Function F_6, Appendix 4A). This practice is clearly intended to push T_g toward the saturation temperature from its metastable subcooled state.

4.1.1.4 Inverted Annular Flow. The volumetric heat transfer coefficients for inverted annular flow, H_{if} and H_{ig}, are each based on the contributions from two sources: (a) the interfacial heat transfer between the bubbles and liquid in the liquid slugs (see Figure 3-7) and (b) the interfacial heat transfer between the core-located liquid slugs and the annular vapor film surrounding them. Equations (4-25 through 4-29) for

slug flow apply to inverted annular flow with the annular contribution replacing that for the Taylor bubble (TB). Hence, one can write for the total heat transfer:

$$Q_{ip} = H_{ip,bub}\,\Delta T + H_{ip,ann}\,\Delta T \quad . \tag{4-48}$$

Details of the various expressions used to represent H_{if} and H_{ig} for inverted annular flow are found in Appendix 4A.

4.1.1.4.1 Inverted Annular Superheated Liquid (SHL)

Model as Coded

$$H_{if} = H_{if,bub} + H_{if,ann}$$

$H_{if,bub}$ is as for H_{if} for bubbly with the following modifications:

$$v_{fg} = (v_g - v_f)\,F_{16}^2$$

where

$$F_{16} = 1 - F_{17}$$

$$F_{17} = \exp\left[\frac{-8\,(\alpha_{AB} - \alpha_{IAN})}{\alpha_{AB}}\right] F_{18}$$

$$\alpha_{IAN} = \begin{cases} \alpha_g & \text{Inverted annular} \\ \alpha_{AB} & \text{IAN/ISLG transition (see Figure 3-5)} \end{cases}$$

$$F_{18} = \text{Min}\,(\alpha_g/0.05,\ 1)$$

$$\beta = F_{16}$$

$$\alpha_g = \alpha_{bub}$$

$$\alpha_{bub} = \text{Max}\left[\frac{(\alpha_{IAN} - \alpha_B)}{(1 - \alpha_B)},\ 10^{-7}\right]$$

$$\alpha_B = F_{17}\,\alpha_{IAN}$$

$$a_{gf,bub} = \frac{3.6\,\alpha_{bub}}{d_b}\,(1 - \alpha_B)\,F_{16}$$

and

$$H_{if,ann} = 3 \times 10^6\, a_{gf,ann}$$

where

$$a_{gf,ann} = \frac{4}{D}\,F_{15}\,(2.5)$$

$$F_{15} = (1 - \alpha_B)^{1/2}$$

Model Basis and Assessment

The volumetric coefficient, $H_{if,bub}$, for inverted annular SHL is based on that for pure bubbly flow SHL, Section 4.1.1.1.1, with some modifications to account for the fact that it only represents one part of the interfacial heat transfer. Function F_{16} (Appendix 4A) is an ad hoc function that accounts for the decrease in that portion of the void fraction related to the bubbles as α_g increases. Conversely, F_{17} (= 1 - F_{16}) represents the increasing portion of α_g due to the annular gas blanket. As such, the interfacial area, $a_{gf,bub}$, is correctly apportioned (see Section 4.1.1.3.1), as are α_B, the average gas volume of the annular vapor blanket (analogous to α_{ff}), and α_{bub}, the void fraction of the bubbles in the liquid slugs.

The selection of the correlation to be used for $H_{if,bub}$, either Plesset-Zwick[4-1] or Lee-Ryley,[4-3] (Section 4.1.1.1.1), is affected, however, by diminishing the first (via parameter β) and increasing the second [via $v_{fg}(F_{16})^2$]. In forcing the selection of the Lee-Ryley correlation for larger α_g, which is appropriate, this logic also increases the magnitude of the Lee-Ryley correlation, which seems inappropriate.

The value used for $H_{if,ann}$ is simply a large number to drive i_f toward the saturation temperature, since this is a metastable state. The combination of the two parts of H_{if} amounts to an ad hoc correlation which must be assessed against experiment.

4.1.1.4.2 Inverted Annular Subcooled Liquid (SCL)

Model as Coded

$$H_{if} = H_{if,bub} + H_{if,ann}$$

where

$H_{if,bub}$ is as for bubbly SCL

and

$$H_{if,ann} = \frac{k_f}{D} 0.023 \, Re_{IAN}^{0.9} \, a_{gf,ann} \, F_3$$

where

$$Re_{IAN} = \rho_f \left| v_f - v_g \right| (1 - \alpha_{IAN})/\mu_f$$

$a_{gf,ann}$ and α_{IAN} are as for inverted annular SHL and F_3 is as for bubbly SHL.

Model Basis and Assessment

The same expression is used to compute $H_{if,bub}$ for SCL as for bubbly SCL, Section 4.1.1.1.2. The expression used for $H_{if,ann}$ is obviously based on the Dittus-Boelter correlation for turbulent flow in a duct. While the relative velocity is appropriately used in computing the Reynolds number for the Dittus-Boelter correlation, the correctness of the values it gives is unknown and must be assessed against experiment.

4.1.1.4.3 Inverted Annular Superheated Gas (SHG)

Model as Coded

$$H_{ig} = H_{ig,bub} + H_{ig,ann}$$

where

$$H_{ig,bub} = Nu_{ib}\ F_6\ a_{gf,bub}$$

where

Nu_{ib} and F_6 are as for bubbly SHG and $a_{gf,bub}$ is as for inverted annular SHL

and

$$H_{ig,ann} = \frac{k_g}{D}\ F_{19}\ a'_{gf,ann}$$

where

$$F_{19} = [2.5 - \Delta T_{sg}\ (0.20 - 0.10\ \Delta T_{sg})]$$

$$a'_{gf,ann} = a_{gf,ann}/F_{20}$$

$$F_{20} = 0.5\ \text{Max}\ (1.0 - F_{15},\ 0.04)$$

F_{15} and $a_{gf,ann}$ are as for inverted annular SHL .

Model Basis and Assessment

Both contributions to H_{ig} for inverted annular SHG are clearly ad hoc correlations and must be compared to experiment for evaluation purposes.

4.1.1.4.4 Inverted Annular Subcooled Gas (SCG)

Model as Coded

H_{ig} is as for inverted annular SHG

Note that $\Delta T_{sg} > 0$ for this case (Function F_{19}).

Model Basis and Assessment

The same expression is used for this case as for inverted annular SHG with the minor variation of F_{19} for $\Delta T_{sg}>0$ versus $\Delta T_{sg}<0$, as noted in Appendix 4A. Since the expression used gives increasingly large values for Nu as $|\Delta T_{sg}|$ increases, the treatment is consistent with those for metastable SCG for other flow regimes.

4.1.1.5 Inverted Slug Flow. The inverted slug flow regime as envisioned by DeJarlais and Ishii[4-19] consists of bubble impregnated liquid slugs flowing in a pipe core surrounded by a vapor blanket containing liquid droplets, (see Figure 3-7). The coded volumetric heat transfer coefficients recognize the liquid droplets, vapor blanket and liquid slugs, but not the presence of bubbles in the slugs. Contributions to the interfacial heat/mass transfer in the bulk are recognized, then, as coming from two sources: (a) the liquid droplet interfaces in the vapor annulus and (b) the liquid slug/annulus interface. It is assumed, apparently, that the liquid slugs are so long that any contributions to interfacial heat transfer at their ends are negligible. One can write for the heat transfer as coded

$$Q_{ip} = H_{ip,ann}\,\Delta T + H_{ip,drp}\,\Delta T \qquad (4\text{-}49)$$

Details of the expressions for H_{if} and H_{ig} are given in Appendix 4A.

4.1.1.5.1 Inverted Slug Superheated Liquid (SHL)

Model as Coded

$$H_{if} = H_{if,ann} + H_{if,drp}$$

where

$$H_{if,ann} = \frac{k_f}{D} F_{12} (9) a_{gf,ann}$$

where

$$a_{gf,ann} = \frac{4.5}{D} \alpha_B (2.5)$$

$$\alpha_B = (\alpha_f - \alpha_{drp})/(1 - \alpha_{drp})$$

$$\alpha_{drp} = (1 - \alpha_{AC}) F_{21}$$

$$F_{21} = \exp\left[-8\frac{(\alpha_{AC} - \alpha_g)}{(\alpha_{AC} - \alpha_{AB})}\right]$$

F_{12} is as for annular mist SHL

and

$$H_{if,drp} = \frac{k_f}{d_d} F_{12} (9) a_{gf,drp}$$

where

$$a_{gf,drp} = (3.6\, \alpha_{drp}/d_d)(1 - \alpha_B)$$

d_d = characteristic droplet diameter

$$= \frac{We\ \sigma}{\rho_g v_{fg}^2},\ We \equiv 1.5,\ We\ \sigma = Max\ (We\ \sigma,\ 10^{-10})$$

v_{fg}^2 is as for bubbly SHL except that

$v_{fg} = (v_g - v_f) F_{21}^2$, We = 1.5,

$D' = 0.0025$, $\alpha_g = \alpha_{drp}$.

Model Basis and Assessment

The expressions for $H_{if,ann}$ and $H_{if,drp}$ are both based on large values for the Nusselt number as provided by function F_{12} (Appendix 4A). This tends to drive T_f toward the saturation temperature and is consistent with other treatments in the code for metastable states.

Interfacial Area

The interfacial areas for the annulus/droplet portion and the slug/annulus portion are derived analogously to those for slug flow, Section 4.1.1.2. The void fraction of the liquid slug, α_B, is analogous to that for a Taylor bubble, α_{TB}, and the average droplet void in the vapor blanket, α_{drp}, is analogous to the average void, α_{gs}, in the liquid annulus for slug flow (Appendix 4A). That is, the interfacial areas are computed for inverted slug flow by simply reversing the liquid and vapor phases from slug flow. The droplet void, α_{drp}, in the vapor annulus is based on an ad hoc expression which exponentially increases the portion of α_f due to droplets as α_g increases until the transition void, α_{AC}, is reached, at which point all of the liquid is appropriately assumed to be in droplet form (see function F_{21}, Appendix 4A).

4.1.1.5.2 Inverted Slug Subcooled Liquid (SCL)

Model as Coded

$$H_{if} = H_{if,ann} + H_{if,drp}$$

where

$$H_{if,ann} = \frac{k_f}{D} F_{13} a_{gf,ann}$$

F_{13} is as for annular mist SCL

$a_{gf,ann}$ is as for inverted slug SHL

and

$$H_{if,drp} = \frac{k_f}{d_d} F_{13} a_{gf,drp}$$

where

$a_{gf,drp}$ is as for inverted slug SHL .

Model Basis and Assessment

The expressions for $H_{if,ann}$ and $H_{if,drp}$ for inverted slug SCL are both based on Brown's[4-18] model for droplets condensing in vapor. The weaknesses of this model are discussed in Section 4.1.1.3.2. While Brown's model may be appropriate for $H_{if,drp}$, it clearly is not appropriate for the heat transfer between the liquid slug and vapor interface. An evaluation of the expressions for inverted slug SCL for H_{if} requires assessment against experiment.

4.1.1.5.3 Inverted Slug Superheated Gas (SHG)

Model as Coded

$$H_{ig} = H_{ig,ann} + H_{ig,drp}$$

where

$$H_{ig,ann} = \frac{k_g}{D} \frac{F_{19}}{F_{22}} a_{gf,ann}$$

F_{19} is as for inverted annular SHG

$a_{gf,ann}$ is as for inverted slug SHL

$$F_{--} = \text{Max}\left\{0.02, \text{Min}\left[\frac{\alpha_g}{4}\left(1 - \frac{\alpha_g}{4}\right), 0.2\right]\right\}$$

and

$$H_{ig,drp} = \frac{k_g}{d_d}\left(2.0 + 0.5\, Re_{drp}^{0.5}\right) a_{gf,drp}$$

where

d_d and $a_{gf,drp}$ are as for inverted slug SHL

and

$$Re_{drp} = \frac{We\ \sigma\ (1 - \alpha_{drp})^{2.5}}{\mu_g\ (v_{fg}^2)^{0.5}}$$

where We = 1.5, We σ = Max (We σ, 10^{-10}), and v_{fg}^2 is as for inverted slug SHL.

Model Basis and Assessment

The Nusselt number upon which $H_{ig,ann}$ for inverted slug SHG is based (F_{19}/F_{22}, Appendix 4A) is ad hoc and requires comparison with experiment for evaluation.

The correlation used in the code for Nu for $H_{ig,drp}$ is a modified version of the Lee-Ryley[4-3] model for heat transfer to a droplet (see Section 4.1.1.1.1) in the process of evaporation. While the coded version of the Lee-Ryley correlation is within experimental uncertainty for Pr = 1, Section 4.1.1.1.1, the complications of turbulence in the vapor blanket combined with the fact that liquid velocity is some average of the droplet and slug fields must be considered. Thus, a complete validation for H_{ig} for this case must include comparison with experiment.

4.1.1.5.4 Inverted Slug Subcooled Gas (SCG)

Model as Coded

H_{ig} is as for inverted slug SHG.

Model Basis and Assessment

The same expressions are used for inverted slug SCG as for SHG for H_{ig}, Section 4.1.1.5.3. This is not consistent with the practice used for similar metastable states for other flow regimes, wherein Nu is set to a large value to push T_f toward T^s. The reason for the difference is that no impact is expected on the calculational results, since subcooled gas does not exist for the post-CHF flow regimes. Comparison with experiment is required for an assessment of the validity of the model used here.

4.1.1.6 Dispersed (Droplet) Flow.

4.1.1.6.1 Dispersed Superheated Liquid (SHL)

Model as Coded

$$H_{it} = \frac{k_f}{d_d} F_{12} F_{23} a_{gf}$$

where

F_{12} is as for annular mist SHL

$$F_{23} = \frac{\text{Max } (\alpha_f, 10^{-5})}{\text{Max } (\alpha_f, 10^{-10})}$$

except for horizontal, post-CHF flow

where $F_{23} = \alpha_f / \text{Max } (\alpha_f, 10^{-10})$

$$a_{gf} = 3.6 \alpha_{drp}/d_d$$

$$\alpha_{drp} = \text{Max } (\alpha_f, 10^{-5})$$

$$d_d = \frac{We\ \sigma}{\rho_g v_{fg}^2}, \quad We = 1.5, \quad We\ \sigma = \text{Max } (We\ \sigma, 10^{-10})$$

v_{fg}^2 is as for bubbly SHL except that

$$v_{fg} = \begin{cases} v_g - v_f & \alpha_f < 10^{-6} \\ (v_g - v_f)\,\alpha_f\,10^6 & \alpha_f \geq 10^{-6} \end{cases}$$

We = 1.5, D′ = 0.0025 .

Model Basis and Assessment

The volumetric heat transfer coefficient, H_{if}, for dispersed SHL is based on an ad hoc expression for Nusselt number which increases quadratically as $|\Delta T_{sf}|$ increases (function F_{12}, Appendix 4A), thus driving T_f toward T^s. Another function, F_{23}, is incorporated to drive the flow to single-phase vapor for very low values of α_f. This practice is used to smooth the transition to single phase.

The volumetric interfacial area is based on the same derivation as that for bubbly flow (which is, in fact, based on the interfacial area of a droplet spray, see Section 4.1.1.1.1.).

4.1.1.6.2 Dispersed Subcooled Liquid (SCL)

Model as Coded

$$H_{if} = \frac{k_f}{d_d} F_{13} F_{23} a_{gf}$$

where

F_{13} is as for annular mist SCL

F_{23} and a_{gf} are as for dispersed SHL.

Model Basis and Assessment

The volumetric heat transfer coefficient for dispersed SCL is based on the model of Brown,[4-18] which is discussed in detail in Section 4.1.1.3.2 for annular mist SCL. The same conclusions apply here.

4.1.1.6.3 Dispersed Superheated Gas (SHG)

Model as Coded

$$H_{ig} = \frac{k_g}{d_d} (2.0 + 0.5\, Re_{drp}^{0.5})\, F_{24}\, a_{gf}$$

where d_d and a_{gf} are as for dispersed SHL

$$Re_{drp} = \frac{We\ \sigma\ (1 - \alpha_{drp})^3}{\mu_g \left[v_{fg}^2\ (1 - \alpha_{drp})\right]^{1/2}}\ ,\ We\ \sigma = Max\ (We\ \sigma,\ 10^{-10})$$

where We, σ, α_{drp}, and v_{fg}^2 are as for dispersed SHL

$$F_{24} = Max\ [0.0,\ F_{26}\ (F_{25} - 1) + 1]$$

$$F_{25} = 10^5\ Min\ (\alpha_f,\ 10^{-5})$$

$$F_{26} = 1.0 - 5.0\ Min\ [0.2,\ Max\ (0.,\ \Delta T_{sg})]\ .$$

Model Basis and Assessment

The Nusselt number correlation upon which H_{ig} for dispersed SHG is based is a modified form of the Lee-Ryley[4-3] model, where 0.5 has replaced 0.74 as the coefficient of $Re^{0.5}$ and the Prandlt number dependence has been dropped. A detailed discussion of the Lee-Ryley correlation is given in Section 4.1.1.1.1.

The viscosity upon whi h the Reynolds number of the coded version of this correlation is based is a mixture viscosity. Use of the mixture viscosity is appropriate for the drag correlations of Ishii and Chawla,[4-10] from whence the expression for mixture viscosity is taken (see Section 4.1.1.3.3). Since Lee and Ryley[4-3] based their Reynolds number on the viscosity of the continuous phase, use of the mixture viscosity appears to be inappropriate. At α_f = .2, the Reynolds number computed using mixture viscosity is 43% lower than that based on continuous-phase viscosity. This leads to an error of about 6.5%, since $Nu \propto Re^{0.5}$.

In summary, while it may appear that the coded correlation is based on a published source, there are enough variations (including scaling, Section 4.1.1.1.1) to require comparison with experiment for complete evaluation.

4.1.1.6.4 Dispersed Subcooled Gas (SCG)

Model as Coded

$$H_{ig} = Nu_{ib} F_6 F_{24} a_{gf}$$

where

Nu_{ib} and F_6 are as for bubbly SHG

F_{24} and a_{gf} are as for dispersed SHG.

Model Basis and Assessment

The volumetric heat transfer coefficient as coded for dispersed droplet SCG is simply based on a large value for Nu (= $10^4 F_6$, Appendix 4A) which will push T_g toward the saturation temperature.

4.1.1.7 Horizontally Stratified Flow

4.1.1.7.1 Horizontally Stratified Superheated Liquid (SHL)

Model as Coded

$$H_{if} = \frac{k_f}{D_{hf}} \left[0.023 \, Re_f^{0.8} \, F_{12} - 3.81972 \, \frac{v T_{sf} \rho_f C_{pf}}{\rho_g h_{fg} \, Max \, (4\alpha_g, 1)} \right] a_{gf}$$

where

D_{hf} = liquid phase hydraulic diameter

$$= \pi\alpha_f D / (\pi - \theta + \sin\theta) \text{ (see Figure 3-2 for definition of } \theta)$$

$$Re_f = \rho_f \alpha_f D \left| v_f - v_g \right| / \mu_f$$

$$a_{gf} = (4 \sin\theta / \pi D) F_{27}$$

$$F_{27} = 1 + \left| \frac{v_g}{v_{crit}} \right|^{1/2}$$

Model Basis and Assessment

The expression used for the Nusselt number for H_{if} for horizontally stratified flow, while giving the appearance of modeling two processes (main interface plus entrained droplet interface), is effectively an ad hoc relation which gives a large value. This is due to the presence of function F_{12}. This practice promotes the return of T_f toward T^s, which is generally used in the code for metastable states. The Nusselt number is converted to a heat transfer coefficient by use of a hydraulic diameter defined in the usual way,

$$\text{hydraulic diameter} = \frac{4 \times \text{phasic cross-sectional area}}{\text{phasic wetted parameter}}$$

The expression for hydraulic diameter in Appendix 4A incorporates the expression

$$\pi\alpha_f = (\pi - \theta + \sin\theta \cos\theta) \quad , \tag{4-51}$$

which can be derived from simple geometric considerations. (See Figure 3-2 for the definition of angle θ).

Interfacial Area

The volumetric interfacial area is based on simple geometric considerations. It is easily shown that

$$a_{gf} = \frac{4\sin\theta}{\pi D} \tag{4-52}$$

for a smooth interface. A multiplicative parameter is applied to a_{gf} in the code to attempt to account for an increase in a_{gf} due to a wavy surface. This parameter is represented by function F_{27}, which appropriately increases as v_g/v_{crit} increases. An evaluation of the validity of function F_{27} requires comparison with experiment.

4.1.1.7.2 Horizontally Stratified Subcooled Liquid (SCL)

Model as Coded

$$H_{if} = \frac{k_f}{D_{hf}} (0.023\ Re_f^{0.8})\ a_{gf}$$

where

D_{hf}, Re_f, and a_{gf} are as for horizontally stratified SHL.

Model Basis and Assessment

The expression for Nusselt number for horizontally stratified SCL is obviously based on the Dittus-Boelter correlation. The Reynolds number used for the correlation does not employ the phasic hydraulic diameter, as is the widely accepted practice for this correlation. Furthermore, the Dittus-Boelter correlation is valid for single-phase flow in solid-boundary ducts and not necessarily for a fluid-fluid boundary. Developmental assessment against Bankoff's stratified flow condensation experiments[4-12,20] provided an indication of model acceptability. Comparison with further experiments is required for complete evaluation.

4.1.1.7.3 Horizontally Stratified Superheated Gas (SHG)

Model as Coded

$$H_{ig} = \frac{k_g}{D_{hg}} [0.023\ Re_g^{0.8} + Nu_{ib}\ F_6\ (4)\ Max\ (0.0,\ 0.25 - \alpha_g)]\ a_{gf}$$

where

D_{hg} = vapor phase hydraulic diameter

= $\pi\alpha_g D/(\theta + \sin\theta)$

Re_g = $\alpha_g \rho_g D \left|v_f - v_g\right| / \mu_g$

Nu_{ib} and F_6 are as for Bubbly SHG

and a_{gf} is as for horizontally stratified SHL .

Model Basis and Assessment

The Nusselt number upon which the expression for H_{ig} for horizontally stratified SHG is based has two parts, the first of which is the Dittus-Boelter correlation. The same criticisms pertaining to horizontally stratified SCL apply, including the fact that Re_g is not based on the phasic hydraulic diameter. The other part upon which Nu is based is simply a large number (Nu_{ib} F_6). Thus, H_{ig} is basically ad hoc for this thermodynamically stable state.

4.1.1.7.4 Horizontally Stratified Subcooled Gas (SCG)

Model as Coded

$H_{ig} = Nu_{ib} F_6 a_{gf}$

where

a_{gf} is as for horizontally stratified SHL.

Model Basis and Assessment

The expression for H_{ig} for this case is the same as for horizontally stratified SHG (except for the difference in F_6 for a SCG, Appendix 4A). The use of a large Nu to drive T_g toward T^s is consistent with the treatment of other metastable states.

4.1.1.8 Vertically Stratified Flow and Transition--The two-phase flow in vertical control volumes can become vertically stratified for low mass fluxes. If the volume average mixture mass flux is less than the Taylor bubble rise velocity, or

$$\frac{G/\rho}{v_{TB}} < 1 \ , \qquad (4\text{-}53)$$

where G, ρ and v_{TB} are given by Equations (3-1, 3-5, and 3-7), respectively, transition to vertically stratified flow begins. If the criterion in Equation (4-53) is not met, the flow is completely unstratified.

The correlations used for H_{if} and H_{ig} in the transition region (Figure 3-5) are combinations of those already computed for non-stratified flow and the stratified correlations (Appendix 4A). The transition region extends down to $G/(\rho v_{TB}) = 2/3$ for the stable states (SCL, SHG). The exceptions to this transition interval are for $\alpha_f < 0.01$ or $\Delta T_{sf} < 0$ for H_{if}, and $\alpha_g < 0.1$ or $\Delta T_{sg} > 0$ for H_{ig}.

4.1.1.8.1 Vertically Stratified Superheated Liquid (SHL)

Model as Coded

$$H_{if} = H_{if,reg} F_{30} + 14.7 k_f a_{gf} (1 - F_{30}) F_{31}$$

where reg = flow regime of flow below the stratified vapor/liquid interface, which can be BUB, SLUG, SLUG/ANM, ANM, IAN, IAN/ISLG, ISLG, DIS, IAN/ISLG - SLUG, ISLG - SLUG/ANM. ANM/DIS, BUB/IAN, SLUG/ISLG (see flow regime maps, Figures 3-1, 3-5).

F_{30} = Max (F_{32}, F_{33}, F_{34})

F_{32} = [1.0 - Min (1.0, $100\alpha_f$)]

F_{33} = Max [0.0, 3 Min (1.0, $G/\rho v_{TB}$) - 2]

v_{TB} = Taylor bubble rise velocity, Equation (3-7)

$$G = \left|\alpha_g \rho_g v_g + \alpha_f \rho_f v_f\right|$$

$$\rho = \alpha_g \rho_g + \alpha_f \rho_f$$

$$F_{34} = \text{Min}\ (1.0,\ -0.5\ \Delta T_{sf})$$

$$F_{31} = \text{Min}\ (1.0,\ 10\alpha_g)$$

$$a_{gf} = \frac{A_c}{V} = \frac{A_c}{A_c D_L} = \frac{1}{D_L}$$

where D_L = length of volume cell and A_c = cross-section area of cell.

Model Basis and Assessment

Vertical stratification can occur for superheated liquid only in the interval $-2 < \Delta T_{sf} < 0$. Even then, it is considered to be in a transition state, since the partitioning function F_{30} is nonzero (Appendix 4A). The heat transfer coefficient, h_{if} (W/m^2K), is not given in terms of a Nusselt number; rather, it is given such that $h_{if} = 14.7\ k_f$. The expression used for h_{if} was adjusted to give optional performance for MIT, Neptunus, and Semiscale pressurizer experiments.[4-12,21] This basis for the finally implemented value of h_{if} is not documented in the literature. For the typical operating conditions given in Appendix 4B, $h_{if} = 7.6\ W/m^2K$.

Interfacial Area

The interfacial area per unit volume for vertically stratified flow is simply the cross-sectional area of the control volume divided by its volume, which results in the reciprocal of cell-volume length, D_l.

4.1.1.8.2 Vertically Stratified Subcooled Liquid (SCL)

Model as Coded

H_{if} is as for vertically stratified SHL.

Model Basis and Assessment

Fully vertically stratified flow can exist for SCL. The same expression is used for SCL as was used for SHL, except that the partition function allows fully stratified flow; that is, function $F_{34} = 0$ for all $\Delta T_{sf} > 0$, which allows the partition function F_{30} to be zero.

4.1.1.8.3 Vertically Stratified Superheated Gas (SHG)

Model as Coded

$$H_{ig} = H_{ig,reg} F_{35} + 81.4 k_g a_{gf} (1 - F_{35})$$

where

F_{35} = Max (F_{33}, F_{36}, F_{37})

reg, F_{33}, D_L are as for vertically stratified SHL

F_{36} = [1.0 - Min (1.0, $10\alpha_g$)]

F_{37} = Min (1.0, 0.5 ΔT_{sg})

a_{gf} is as for vertically stratified SHL.

Model Basis and Assessment

The volumetric heat transfer coefficient for vertically stratified flow for SHG is based on an ad hoc expression for $h_{ig}(W/m^2K)$; h_{ig} is set equal to 81.4 k_g. This value was chosen to give optional performance for MIT, Neptunus, and Semiscale pressurizer experiments.[4-12,4-21] The basis for the finally implemented value of h_{ig} is not documented in the literature. For the typical operating conditions of Appendix 4B, the heat transfer coefficient is $h_{ig} = 6.5$ W/m^{2}K.

The transition H_{ig} is analogous to that for H_{if} with the function F_{35} linearly partitioning the contributions between stratified and unstratified models (Appendix 4A). The interfacial area is the same as for SHL. Comparison with experimental data is required to evaluate the model for H_{ig} for vertically stratified flow.

4.1.1.8.4 Vertically Stratified Subcooled Gas (SCG)

Model as Coded

H_{ig} is as for vertically stratified SHG.

Model Basis and Assessment

Fully stratified flow for SCG is not recognized, only a transition between stratified and unstratified flow (Appendix 4A). Otherwise, the model used for vertically stratified SCG is the same as for SHG.

4.1.2 Flow Regime Transitions

A number of transitions between flow regimes are incorporated into RELAP5/MOD2 for purposes of interfacial heat and mass transfer. These transitions are illustrated schematically in Figures 3-1, 3-5, and 3-8 (horizontal, vertical and high mixing maps, respectively). Included are:

Horizontal

1. Slug - annular mist

2. Horizontally stratified - nonstratified

Vertical

1. Slug - annular mist

2. Vertically stratified - nonstratified

3. Inverted annular - inverted slug

4. Transition boiling regime (post-CHF, pre-dryout)

   a. Bubbly - inverted annular

   b. (Inverted annular - inverted slug) - slug

   c. Slug - inverted slug

   d. Inverted slug - (slug - annular mist)

   e. Annular mist - dispersed (droplet).

High Mixing Map

Bubbly - dispersed (droplet)

These transitions are included in the code to prevent the numerical instability which can arise when abruptly switching from one flow regime to another. In most cases, the correlation from one regime is exponentially reduced, while that for the other is exponentially increased from a negligible amount to full value. The only exception is the transition from bubbly to dispersed flow for the high mixing map, which uses linear interpolation. In some cases, three and even four correlations/models are combined to obtain the volumetric heat transfer coefficients. For instance, the transitional boiling region between slug and the transition between inverted annular and inverted slug (IAN/ISLG-SLUG) can undergo transition to vertical stratification, combining four models to obtain H_{if} and H_{ig}.

The full details of the transition/combination logic used in the code are found in Appendix 4A.

4.1.3 Modifications to Correlations - Noncondensible Gas

The presence of a noncondensible gas is represented by the fraction Q of void fraction α_g which is attributable to the noncondensible gas. The effects of a noncondensible gas are represented by multipliers that modify the volumetric heat transfer coefficients, H_{if} and H_{ig}. Function F_4, which is embedded in function F_3, is an ad hoc modifier for H_{if} for bubbly SHL (Appendix 4A). Its influence is felt whenever H_{if} for bubbly flow is used to help define the overall H_{if} for a flow regime. Further ad hoc modifications are applied to H_{if} and H_{ig} for all flow regimes or transition regimes depending on the thermodynamic state (SHL, SCL, SHG, SCG) as detailed in Appendix 4A, Modifications for Noncondensible Gas.

4.2 Wall-to-Fluid Heat Transfer

A boiling curve is used in RELAP5/MOD2 to govern the selection of heat transfer correlations. In particular, the heat transfer regimes modeled are classified as pre-CHF and post-CHF regimes. Condensation heat transfer is also modeled, and the effects of noncondensible gases are modeled.

The pre-CHF regime consists of models for single-phase liquid convection, subcooled nucleate boiling, and saturated nucleate boiling. The model assumes that the wall is totally wetted by liquid and that the wall is not wetted by vapor. Therefore, the heat transfer rate per unit volume from the wall to the vapor, Q_{wg}, is equal to zero. The heat transfer rate per unit volume from the wall to the liquid, Q_{wf}, is given by the expression

$$Q_{wf} = h_f A_w (T_w - T_f)/V \ , \qquad (4\text{-}54)$$

where h_f is the heat transfer coefficient, A_w is the total wall heat transfer area, and T_w and T_f are the wall and liquid temperatures, respectively. V is the volume of the fluid cell adjacent to the heat slab.

The post-CHF regime consists of models for transition film boiling, film boiling, and single-phase vapor convection. A mechanistic model developed is adapted so that

$$Q_{wf} = h_f A_w F_f (T_w - T_f)/V \quad (4\text{-}55)$$

$$Q_{wg} = h_g A_w (1 - F_f) (T_w - T_g)/V \quad (4\text{-}56)$$

where A_w is the total wall heat transfer area and F_f is the fraction of wall surface contacted by the liquid. For single-phase vapor convective heat transfer, the wall is assumed to be dry and the heat transfer area between the wall and the liquid is negligible. Therefore, the heat transfer rate per unit volume from the wall to the liquid, Q_{wf}, is negligible. The heat transfer rate per unit volume from the wall to the vapor, Q_{wg}, is given by the expression

$$Q_{wg} = h_g A_w (T_w - T_g)/V \ . \quad (4\text{-}57)$$

In the condensation regime, heat transfer to the wall from liquid and vapor is dependent on the flow regime. Heat transfer from liquid to the wall is modeled by convection in the low-void regime, and heat transfer from vapor to the wall is modeled by condensation in the high-void regime. The heat transfer rate per unit volume from liquid to the wall is given by the expression

$$Q_{wf} = [(1 - \alpha_g) h_f (T_w - T_f)] A_w/V \ , \quad (4\text{-}58)$$

where h_f is the convective heat transfer coefficient. The heat transfer rate per unit volume from the vapor to the wall is modeled by condensation and expressed as

$$Q_{wg} = [\alpha_g h_{con} (T_w - T_g)]A_w/V \ ,$$

where h_{con} is the condensation heat transfer coefficient.

The heat transfer package in RELAP5/MOD2 uses heat transfer correlations that are based on fully developed flow, where entrance length effects are not considered. The approach of using these correlations in a transient code such as RELAP5 is often referred to as the quasi-steady approached. Some of the correlations use a length variable, and the code

uses the cell length for this variable. This was felt to be reasonable, since coarse nodalizations are used in system calculations. Some of the correlations were modified, and this was done in order to provide better agreement of code calculations compared to data during the developmental assessment.[4-12]

4.2.1 Logic for Selection of Heat Transfer Modes

The following list gives the modes by which heat is transferred between heat structure surfaces and the circulating fluid contained in the reactor primary and secondary systems.

Mode 0 Convection to noncondensible-water mixture

Mode 1 Single-phase liquid convection at critical and supercritical pressure

Mode 2 Single-phase liquid convection at subcritical pressure

Mode 3 Subcooled nucleate boiling

Mode 4 Saturated nucleate boiling

Mode 5 Subcooled transition film boiling

Mode 6 Saturated transition film boiling

Mode 7 Subcooled film boiling

Mode 8 Saturated film boiling

Mode 9 Single-phase vapor convection

Mode 10 Condensation when void equals one

Mode 11 Condensation when void is less than one.

If the noncondensible quality is greater than 0.0001, then 20 is added to the mode number. Thus, the mode number can be 20 to 31. Figure 4-2 is a schematic diagram showing the logic built into the code to select the appropriate heat transfer mode.

The following discussion presents the correlations used to calculate the heat transfer for a specific mode. For each mode, the text provides the code model or correlation basis, the model as coded, an assessment of the model or correlation, scaling considerations, and a summary and conclusion.

4.2.2 Correlations for Single-Phase Liquid At Subcritical and Supercritical Pressure (Modes 1 and 2), Single-Phase Vapor (Mode 9)

The single-phase routines include correlations for forced turbulent and laminar convection for liquid and vapor, free laminar and turbulent convection for liquid, and free turbulent convection for vapor. The liquid flow correlations are used for supercritical water.

4.2.2.1 Dittus-Boelter Correlation for Forced Turbulent Liquid and Vapor Flow.

4.2.2.1.1 Model Basis--The Dittus-Boelter correlation[4-22] was originally derived for turbulent flow in smooth tubes for application to automobile radiators. It takes the form

$$h = 0.023 \frac{k}{De} Pr^{n} Re^{0.8} \qquad (4\text{-}59)$$

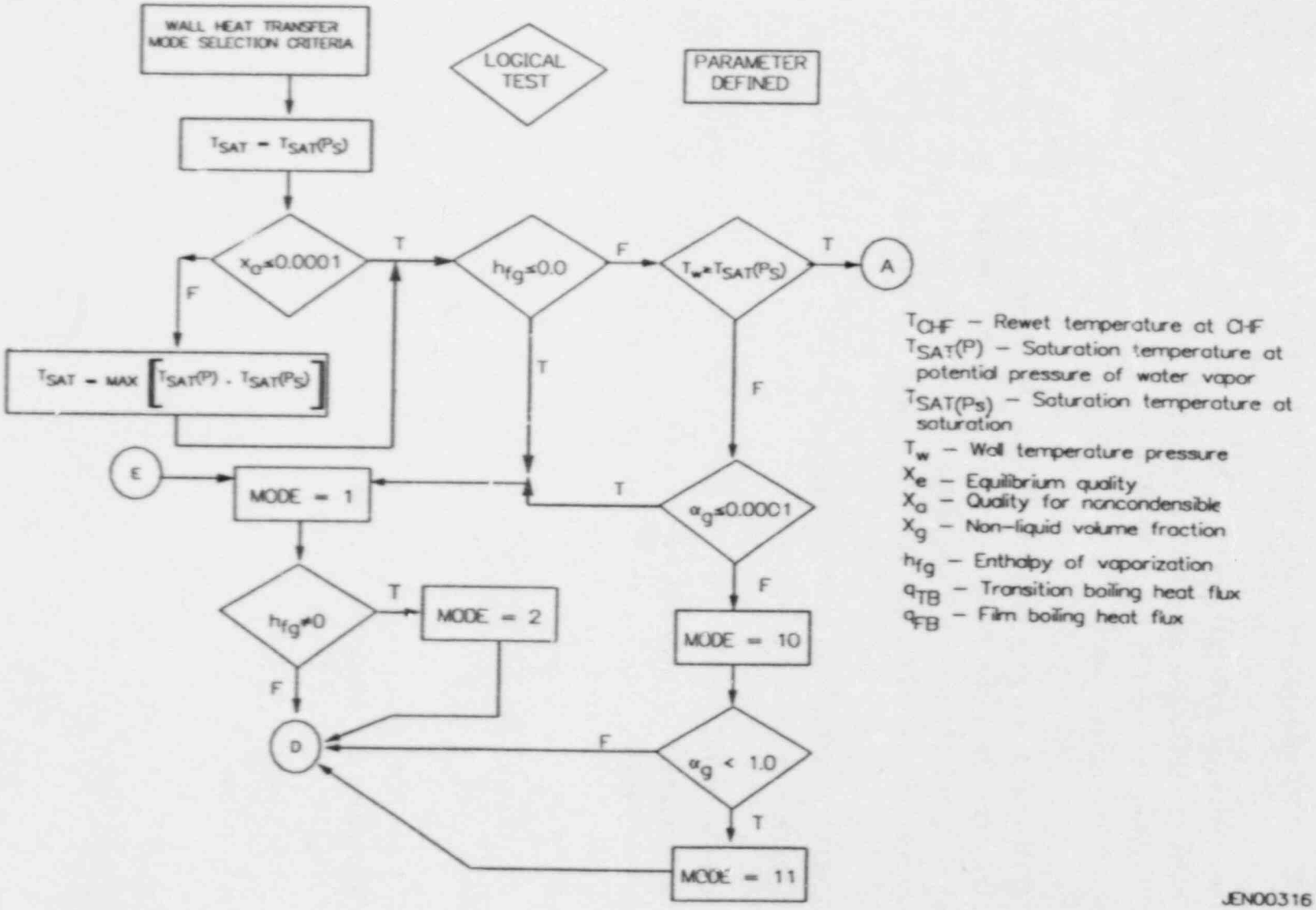

Figure 4-2. Schematic of wall heat transfer logic.

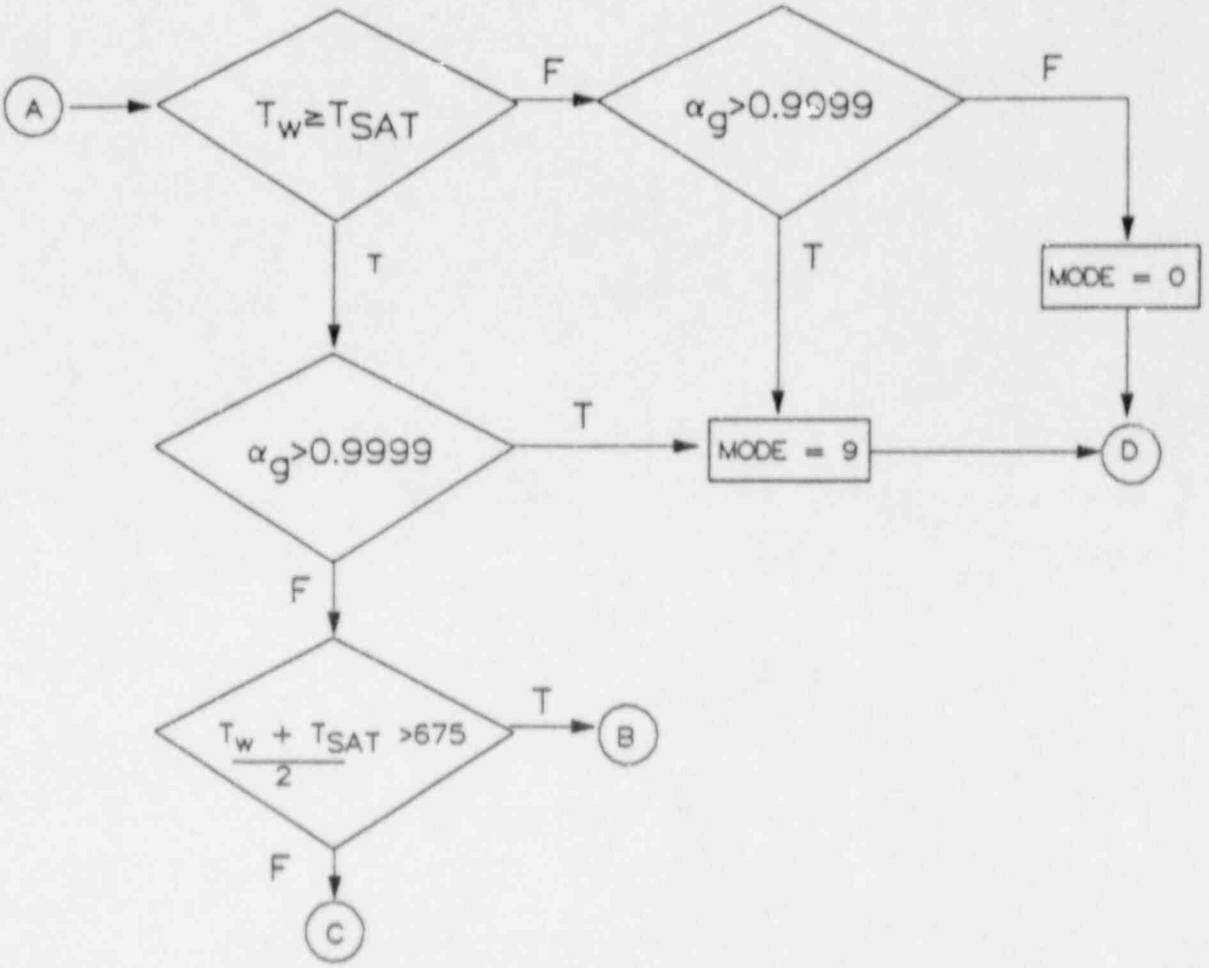

Figure 4-2. (Continued)

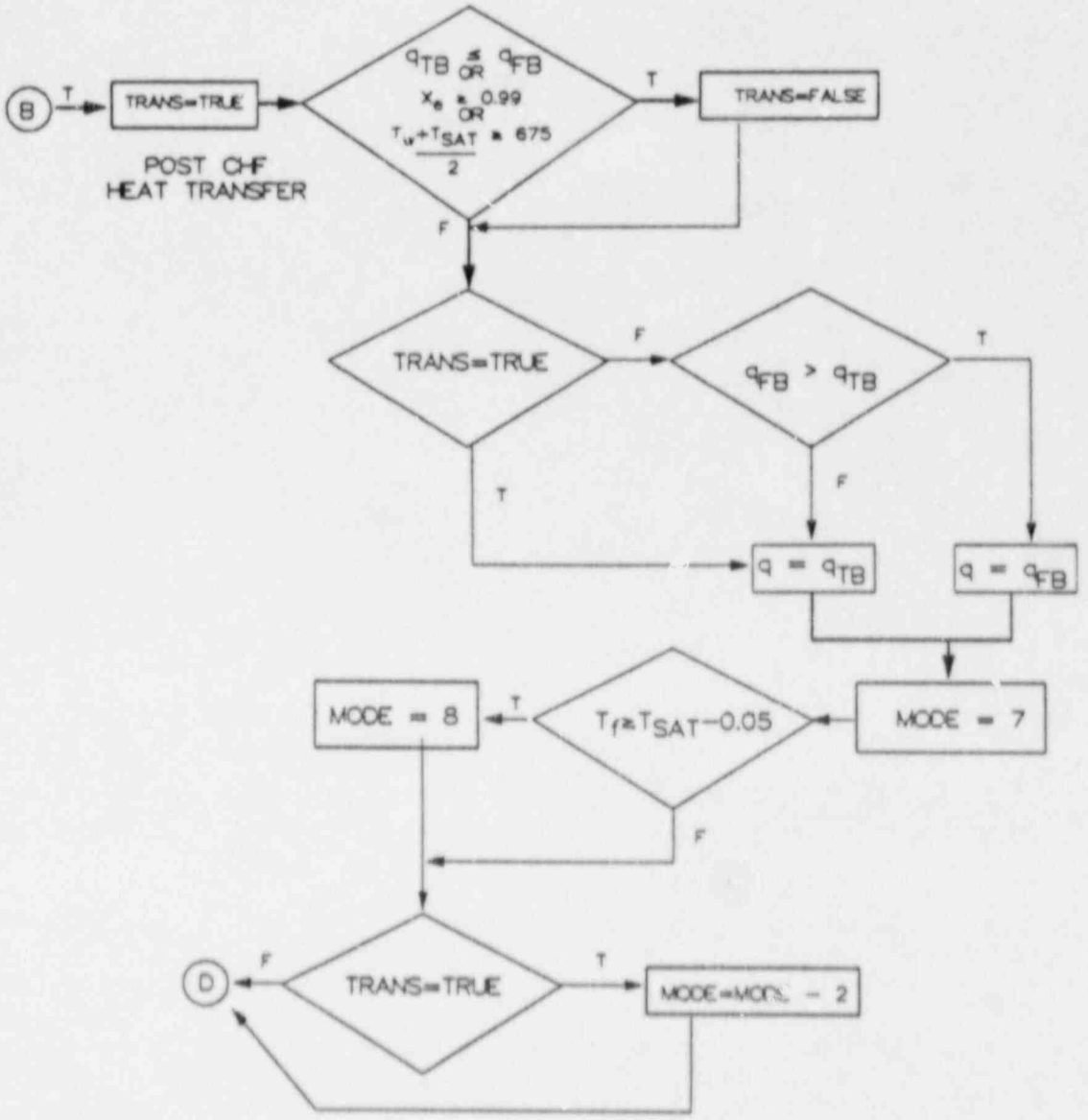

Figure 4-2. (Continued)

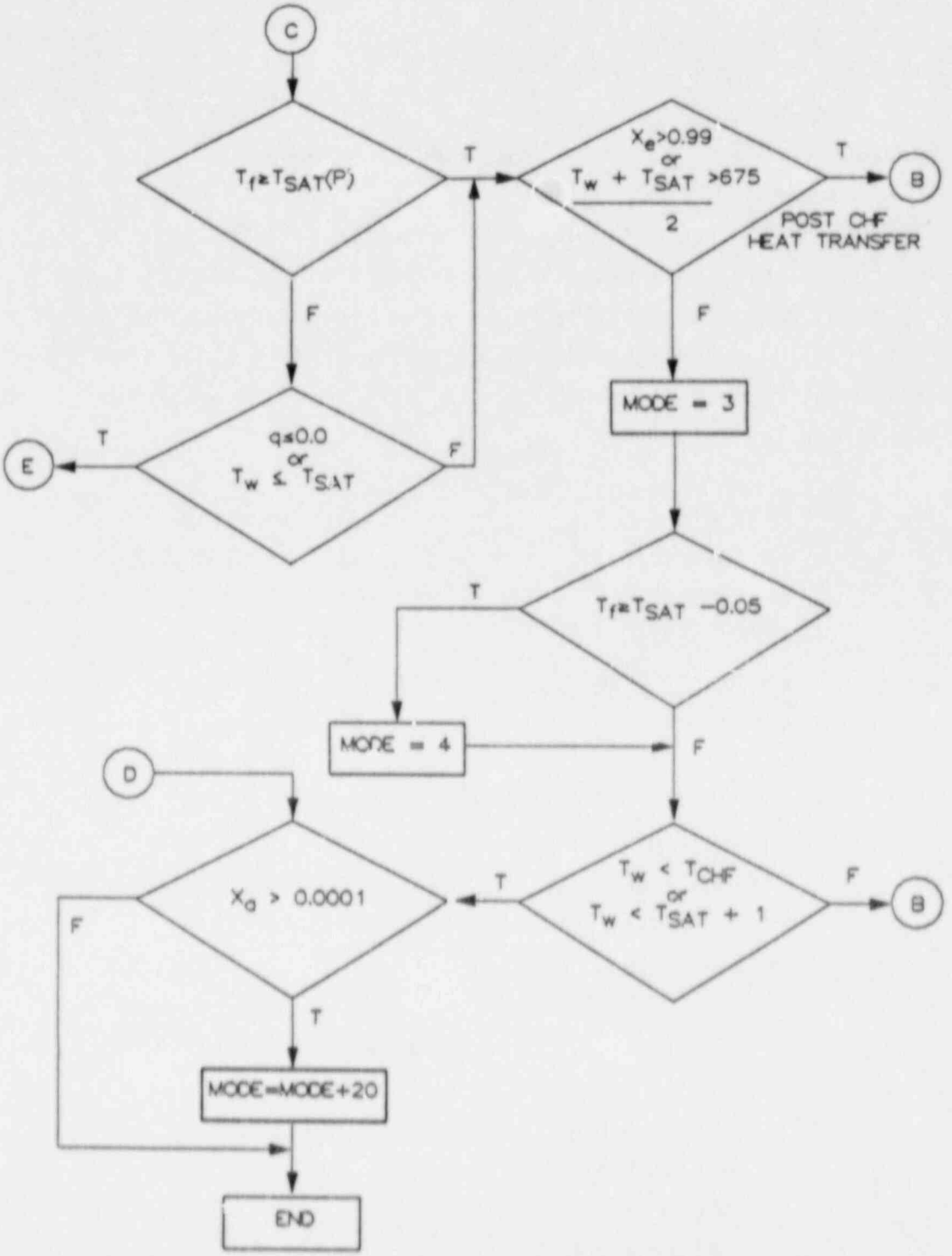

Figure 4-2. (Continued)

where the physical properties are evaluated at the bulk fluid temperature and where

n = 0.4 for heating, 0.3 for cooling.

The constant, 0.023, was recommended later by McAdams.[4-23]

The original correlation was developed from data for heating water,[4-24,4-25] heating and cooling water and oil,[4-26] and heating and cooling gases with [illegible] the literature. The data obtained were for long tubes, with an [illegible] onductance obtained using a log mean temperature diffe[illegible] of the data were reported by Stanton in 1897. The con[illegible]ions [illegible] are

Ref. [illegible]		-	water (heating)
	[illegible]cient	-	850 to 15,300 W/m^2-K
	[illegible]ube ID	-	0.0095, 0.0127, 0.0254 m
	Velocity	-	0.183 to 6.1 m/s
	Data scatter	-	~40%
	Data points	-	~60
Ref. 4-25	Fluid	-	water (heating)
	Tube ID	-	0.0074 to 0.0145 m
	Tube length	-	0.44 to 1.24 m
	Fluid velocity	-	0.065 to 4.9 m/s
	Coefficient	-	840 to 20,700 W/m^2-K
Ref. 4-26	Fluids	-	water, miscellaneous oils
	Tube ID	-	0.0157 m
	Tube length	-	2.74 m
	Heating parameters		
	Velocity	-	0.27 to 5.98 m/s
	Fluid temperature	-	301 to 349 K
	Coefficient	-	227 to 8860 W/m^2-K
	Data points	-	55

Cooling parameters		
V ocity	-	0.34 to 5.15 m/s
Fluid temperature	-	319 to 540 K
Coefficient	-	80 to 3975 W/m^2-K
Data points	-	62
Literature fluids	-	unspecified gases
Pressure range	-	10,342 to 1.31 x 10^6 Pa
Temperature range	-	289 to 1,033 K
Mass velocity range	-	0.98 to 32.2 kg/s-m^2
Tube ID range	-	0.0127 to 0.152 m
Number of data points	-	unspecified.

The correlation was obtained by drawing mean curves through the heating and cooling data of Ref. 4-26. The data of Ref. 4-24, 4-25, and the gas data were plotted against the mean curves to evaluate the applicability of the correlation to other data. Attempts were made to improve the correspondence of Ref. 4-26 data to the correlation based on using the wall, bulk fluid, or average film temperature for property evaluation, but no improvement was noted. Manipulation of the data also did not eliminate the need for separate curves for correlating heating and cooling. No mention was made concerning the deviation between the data and the correlation.

As reported by Kreith,[4-27] Equation (4-59) has been confirmed experimentally for a variety of fluids to within ±25% for uniform wall temperature as well as uniform heat flux conditions with moderate temperature differences between the wall and fluid (constant property conditions) within the following ranges of parameters:

$0.7 < Pr < 160$

$Re > 6000$

$L/D > 60.$

At very small temperature differences (near adiabatic) in air and helium, results[4-28] were well correlated by the form of Equation (4-59) using a constant of 0.021 instead of 0.023. The test conditions were

Tube ID	-	0.00584 m
Tube length	-	0.635 m
Pressure	-	0.689 to 0.965 MPa
Temperature	-	298 K

Other development[4-29] indicates that the correlation likely overpredicts an h [Equation (4-59)] for gases by 10-25% at moderate to high temperature differences.

Reference 4-30 tested Equation (4-53) against water vapor data while being heated for the conditions

Tube ID	-	0.0127 m
Tube length	-	0.914 m
Pressure	-	0.17, 0.34, 0.51 MPa
Inlet temperature	-	422, 644, 867 K
Mass velocity	-	2.3 to 54.2 kg/s-m^2
Re	-	1900 to 35,000
Heat flux	-	7569 to 97,760 W/m^2
Wall temperature	-	478 to 1256 K
Vapor temperature	-	422 to 1089 K
Pr	-	0.7 - 1.1

The data for Re > 6000 fit the analysis within ±5% when a thermal radiation model was included with Equation (4-59).

4.2.2.1.2 Model as Coded--The model is coded as presented with n = 0.4 for all usage.

The model is applied in the transition region between laminar and turbulent forced flow as the Re decreases, until the laminar flow h value,

Equation (4-60), exceeds that for turbulent flow. This procedure simplifies the process connecting the correlations by forcing continuity in the calculated value over the transition.

An alternate lower limit for application of Equation (4-59) for liquid flow is determined when $Gr \geq Re^2$. If this test is met, the free convection correlations for liquid flow apply. The Gr number is calculated using D_h as the characteristic length.

For vapor flow, a turbulent free convection correlation is also evaluated and the largest coefficient determined from the Dittus-Boelter correlation, a laminar forced flow correlation for liquid or vapor Equation (4-60), and the turbulent free convection vapor correlation Equation (4-64) is selected for application.

A small hole exists in the logic if $Re < 10^{-4}$ and $Gr < Re^2$ where no h value would be computed. If this condition were to occur, the value of h from the previous time step would be retained.

4.2.2.1.3 Assessment--The entrance effect (L/D > 60) is neglected. That is, local conditions characterize the flow profiles, and history effects are neglected. The effect of neglecting the entrance length is thought to be small for a highly turbulent flow entering the rod array. Oscillating flow would complicate consideration of the entrance effect.

Application of the correlation for Re < 6000 is questionable. The flow may follow either a laminar or turbulent solution or oscillate between flow types. In some situations, this correlation may be justified; but in other situations, the result is an overprediction of the h. For example, helium flow in a small tube has been characterized by the form of Equation (4-59) with a constant of 0.021 to an accuracy of ±4% at Re > 3000.[4-28] For Re < 2100, only a laminar flow coefficient would be correct. This transition is illustrated for air in Ref. 4-27, p. 289.

The assumption is made that the form of the equation for heating is satisfactory for cooling also. Therefore, the correlation is coded with the exponent on the Prandtl number n = 0.4. The use of n = 0.4 instead of 0.3 for cooling applications would result in a 15% higher prediction for vapor and 10% higher for liquid at 17.24 MPa (2500 psia). For fluid at a lower saturation pressure or at a superheated temperature, the difference caused by n diminishes significantly.

The connecting criterion of selecting the largest h from the forced and laminar flow correlations ensures the application of the turbulent flow correlation to Re < 1000, probably too low a value to be accurate.

The transition between liquid forced and free turbulent convection is simply treated as a switch resulting in a discontinuous value of h as Gr exceeds Re^2. When equality of Gr and Re^2 exists, the buoyancy forces and drag forces affecting the velocity profile are of the same order of magnitude (Ref. 4-31). In reality the transition encompasses a significant range in Gr and Re. Specific transitional values are known for vertical concurrent flow. The effects of combined free and forced convection are different for opposing flow and result in significant changes in the value of h.

The Gr number for determining transition from forced to free convection is miscalculated. The characteristic length is the vertical length for external free convection on a vertical surface. Using D_h for the characteristic length instead of an assumed value of, say 0.3048 m, changes Gr by $\sim 10^4$. Thus, a computed h is likely much too small where the hydraulic diameter is used for the characteristic length.

Analysis and experiment[4-32,4-33] indicate that for turbulent forced convection exterior and parallel to a rod bundle, the h value is a function of the rod spacing to diameter ratio. For spacing/diameter ratios typical of PWRs, Reference 4-33 indicates the increase in h could be ~30%.

Heat transfer from a heated tube wall to superheated steam during turbulent forced convection has been experimentally obtained and correlated.[4-34] The data were taken for the conditions as follows:

Tube ID	-	0.00846 m
Tube length	-	0.3048 m
Pressure	-	2.07 to 10.34 MPa
Temperature	-	255 to 755 K
Superheat	-	296 to 334 K
Wall temperature	-	616 to 972 K
Heat flux	-	0.157 to 0.905 MW/m^2
Mass velocity	-	195 to 1074 $kg/s\text{-}m^2$
Re	-	60,000 to 370,000

The correlation has the same form as Equation (4-59) and fit the data within ±10%. The data were also used to derive better constants for Equation (4-59). With n = 1/3, a constant of 0.0211, and thermodynamic properties evaluated at the film temperature, the resulting modification to Equation (4-59) would apply nearly as well.

Other work[4-29] has resulted in excellent fitting of data of liquids and gases covering wide ranges in parameters. The form is more complex but is solvable directly. However, no superheated water vapor data were tested.

4.2.2.1.4 Scaling Considerations--Scaling effects are handled through the non-dimensional Re number by selection of an equivalent or hydraulic diameter. The selection logic is size-dependent because of the miscalculation of Gr by using the hydraulic diameter as the characteristic length. As the hydraulic diameter increases, the transition from forced to free convection occurs at higher flow rates.

4.2.2.1.5 Summary and Conclusions--Accuracy of ±25% could be expected for high-temperature-and-pressure liquid at Re > 6000. Application of the correlation at Re < 6000 gives questionable results with undetermined

accuracy. A more extensive literature survey is needed to evaluate application to turbulent flows with $2000 < Re < 6000$, and to determine the impact of entrance effects.

Application of the correlation at low Re until a larger h is calculated from a laminar correlation results in misapplication and a loss of accuracy below $Re \simeq 2100$.

No documented basis was found for the switch from forced to free convection flow, and no means is provided for considering changes in h that occur with combined flow inside a vertical tube or fuel rod bundle. Significantly better correlations are available for turbulent forced convection heating and cooling of single-phase liquid and vapor.[4-29,4-34]

4.2.2.2 Laminar Forced Convection Correlation for Liquid and Vapor.

4.2.2.2.1 Model Basis--The model is an exact solution[4-35] for fully developed laminar flow in a tube with a uniform wall heat flux and constant thermal properties. The solution takes the form

$$h = 4.36 \frac{k}{De} , \qquad (4\text{-}60)$$

with k evaluated at the average bulk fluid temperature.

Some data exist to indicate that the solution is correct. For example, Ref. 4-36 provides a comparison for helium flow in a tube. The solution is confirmed to within $\pm 10\%$. More extensive literature review is necessary to provide additional information.

4.2.2.2.2 Model as Coded--The correlation is applied as presented to single-phase liquid and vapor when the calculated value of h exceeds that of the turbulent forced convection correlation, Equation (4-59). This

procedure simplifies the process of connecting the correlations by forcing continuity in h over the transition. The transition occurs at Re between 350 and 700, obtained by equating the Nusselt numbers and solving for Re for the range of Pr likely for water and vapor.

The lower limit of h for liquid application is reached when $Gr \geq Re^2$ for the bulk fluid. If this test is met, the free convection correlations for liquid flow apply. Gr is calculated using the hydraulic diameter.

For vapor application, a lower limit exists when the h value calculated by the turbulent free convection correlation, Equation (4-64) for vapor exceeds that for laminar forced convection.

4.2.2.2.3 Assessment--The practice of using the hydraulic diameter in correlations does not hold for laminar flow.[4-37] Thus, the exact solution for flow in a tube does not necessarily apply to external flow along a rod bundle. No solution was found for the rod bundle.

For laminar flow with small heat transfer coefficients, entrance effects become more important than for turbulent flow. Neglecting the entrance length for a developing parabolic velocity profile has a pronounced effect on the average h over the length. Based on information presented in Kreith[4-27] from the analytical solutions of Kays,[4-38] the h as modeled can be 30% to 75% low, depending on Pr over the several feet of length required to develop the profile. Reference 4-22 also presents a correlation for viscous flow in tubes which includes the effect of the entrance length and with h decreasing along the length.

The wall boundary condition is also important. For comparison, the average h for a constant wall temperature is ~80% of the h for the constant heat flux assumption. Neither ideal condition applies directly to reactor conditions, but the constant heat flux assumption used in this correlation will result in the higher value of h.

The transition between liquid laminar forced convection and free convection is simply treated as a switch, resulting in a discontinuous value of h and a potential for oscillations about the discontinuity. The Gr is miscalculated, as it should be, based on a vertical characteristic length. In reality, the transition between flow occurs over a range of conditions as a function of Re and Gr. The h is also a function of the forced and free convection component directions (same or opposite), entrance length effects, and the geometry (inside of a tube or exterior in a rod bundle with a power distribution). Many studies have been conducted for mixed flow, but the effects have not been quantified.[4-39] Recommendations for vertical flow mixed convection have been made.[4-39]

4.2.2.2.4 Scaling--Scaling effects cannot be handled through the non-dimensional Re number by selection of an equivalent or hydraulic diameter. Therefore, the size of the facility being modeled is of concern, for it can potentially impact the determination of the heat transfer coefficient. The selection logic is size dependent because of the use of the hydraulic diameter.

4.2.2.2.5 Summary and Conclusion--The treatment ignores many known important effects. Its validity can be determined only through comparisons with carefully designed and operated experiments.

4.2.2.3 Laminar Free Convection Correlation for Liquid.

4.2.2.3.1 Model Basis--The correlation recommended by McAdams[4-23] for laminar flow over short vertical plates and cylinders takes the form

$$h = 0.59 \frac{k}{De} (PrGr)^{1/4} , \qquad (4\text{-}61)$$

with all properties evaluated at the film temperature.

The correlation fits air data for flat vertical plates presented by the author within about 5%. The form of the equation has been correlated with data from vertical planes and short horizontal surfaces for water, oils, alcohol, and air, using a value for the initial constant of 0.555.[4-40] The correlation represents liquid water and other fluids with the initial constant differing by -10%[4-39] to +23%.[4-41] The recommended range is $10^4 \leq GrPr \leq 10^9$.[4-23] The form with constant = 0.61 also represented free air convection at the entrance of a vertical tube. As the internal boundary layer developed, however, the constant and exponent changed significantly[4-42] and could not be represented by a single expression.

4.2.2.3.2 Model as Coded--The model is coded as shown above. The model is applied to horizontal or vertical surfaces exposed to liquid flow if $Gr \geq Re^2$ and if $Gr \leq 10^9$. It uses the hydraulic or equivalent diameter of the volume as the characteristic length instead of a vertical length.

4.2.2.3.3 Assessment--The h values are small in comparison to forced convection values. No known basis exists for using the hydraulic or "equivalent" diameter as the characteristic length for application to Equation (4-61).

The correlation was developed for an external flow condition and applies to single cylinders if $D/L \geq 35/Gr^{1/4}$[4-31] with Pr = 1, a condition likely found for turbulent free convection in the core for high-temperature (530-600 K) liquid water with a characteristic length of one foot or larger. No known basis exists for application of the correlation to internal flow conditions, such as a fuel rod bundle, interior or exterior flows through or over steam generator tubes, or interior flows in horizontal or vertical reactor piping.

The transition from laminar to turbulent free convection is generally considered to be a function of the Gr or Gr·Pr product[4-31] with an arbitrary value selected to be ~10^9. The actual transition is known to occur over a range of Gr or Gr·Pr product.[4-27,31] The coefficient varies with the vertical distance, complicating correlation by a simple expression. Length to diameter ratios have been included in correlations developed in the literature.[4-39]

4.2.2.3.4 Scaling--The correlation will scale by using the appropriate characteristic length in appropriate applications. The use of a hydraulic diameter in the selection logic and h calculation brings in a scale dependence.

4.2.2.3.5 Summary and Conclusions--The application of this correlation to reactor conditions and geometries has no documented basis. A more complete study of free convection correlations and reactor applications is reported in Reference 4-39.

4.2.2.4 Turbulent Free Convection Correlation for Liquid When $10^9 < Gr < 10^{13}$.

4.2.2.4.1 Model Basis--The correlation was developed by Eckert and Jackson[4-43] for a flat vertical surface, assuming an analytical velocity profile based on measurements in air for free convection and an analytical temperature profile based on measurements in forced convection for Pr = 1. The solution is shown below in terms of an average heat transfer coefficient over the turbulent surface length,

$$h = 0.0246 \frac{k}{De} Pr^{7/15} Gr^{2/5} (1 + 0.494 Pr^{2/3})^{-2/5}, \quad (4\text{-}62)$$

where the physical properties are evaluated at the bulk fluid temperature. The final form of the correlation was obtained by rearrangement of the terms into the following form and solving for the constant with Pr = 0.72.

$$h = 0.021 \frac{k}{De} (Gr\ Pr)^{2/5} , \qquad (4\text{-}63)$$

The correlation is estimated to be within 10 to 15% agreement with data obtained in the literature by the authors for air, oil and water over $10^9 < Gr < 10^{12}$ (low temperature, atmospheric pressure).

4.2.2.4.2 Model as Coded--The model is coded as presented and applied to horizontal and vertical surfaces exposed to liquid flow if $Gr \geq Re^2$ and if $10^9 < Gr \leq 10^{13}$. The hydraulic diameter of the volume is used as the characteristic length, which eliminates the problem of determining an actual vertical length.

4.2.2.4.3 Assessment--The h values are small compared to forced convection values. A discontinuity exists at the switch point ($Gr = 10^9$) between Equation (4-61) and (4-63). Its magnitude is dependent on Pr. For liquid water in a reactor, the Pr can range from ~0.8 to 4.0. The value of h from Equation (4-63) will be 23% low at Pr = 0.8 but only 2% low at Pr = 4.

The Gr value used to determine applicability and h is miscalculated, because the hydraulic length is assumed to be the characteristic length. No known basis exists for selecting the hydraulic diameter or equivalent diameter as the characteristic length. The correlation can be applied to external flow over vertical cylinders if there is no boundary layer interference and if $D/L \geq 35/Gr^{1/4}$ [4-31] with Pr = 1. No known basis exists for application to internal flow conditions of a fuel rod bundle, the interior or exterior of steam generator tubes, or the interior of horizontal or vertical reactor piping. Little data are available to substantiate

correlations at $Gr > 10^{12}$. Results of turbulent correlations at identical conditions can vary by 100%.[4-39] Not all data can be represented because of discrepancies in experimental systems and measurements.

Mixed free and forced convection have been previously addressed in Section 4.2.2.2.

4.2.2.4.4 Scaling--The correlation will scale by using the appropriate characteristic length in appropriate applications. The use of the hydraulic diameter in the selection logic and h calculation provides a scale dependence.

4.2.2.4.5 Summary and Conclusions--The application of this correlation to reactor conditions and geometries has no documented basis.

4.2.2.5 Turbulent Free Convection Correlation for Liquid When $Gr > 10^{13}$.

4.2.2.5.1 Model Basis--The correlation may be attributed to Bayley.[4-44] The correlation is for a vertical flat plate, and has the form

$$h = 0.10 \frac{k}{De} (Gr\ Pr)^{1/3} \qquad (4\text{-}64)$$

where the properties are evaluated at the bulk fluid temperature.

4.2.2.5.2 Model as Coded--The model is coded as shown above. It is applied to horizontal or vertical surfaces exposed to liquid flow if $Gr \geq Re^2$ and if $Gr > 10^{13}$.

4.2.2.5.3 Assessment--The Gr value used to determine applicability is miscalculated as the hydraulic diameter is used as the characteristic length. No known basis exists for using the hydraulic diameter as the characteristic length, although the correlation form makes the heat transfer coefficient independent of the characteristic length chosen. The correlation was developed for an external flow condition and applies to vertical cylinders for Pr = 1 if there is no boundary layer interference and if $D/L \geq 35/Gr^{1/4}$ [4-31] for Pr = 1.

No known basis exists for application of the correlation to internal flow conditions of a fuel rod bundle, the interior or exterior of steam generator tubes, or the interior of horizontal or vertical reactor piping.

Little data are available to substantiate correlations at $Gr > 10^{12}$. Results of turbulent correlations at identical conditions can vary by 100%.[4-39] Bayley's correlation differs from the recommendations of Jakob[4-40] and McAdams[4-23] by 30%.

The correlation could be used for $Gr > 10^{9}$, eliminating the need for the correlation presented in Section 4.2.2.4.

A discontinuity exists at the switch point ($Gr = 10^{13}$) between Equations (4-63) and (4-64). The magnitude of Equation (4-64) is 30 to 34% low compared to Equation (4-63).

4.2.2.5.4 Scaling--The correlation will scale by using the appropriate characteristic length. Because of its form, use of the hydraulic diameter will not affect the scaling characteristics of the correlation.

4.2.2.5.5 Summary and Conclusions--The application of this correlation to reactor conditions and geometries has no documented basis. A more complete study of free convection correlations and reactor applications is reported in Ref. 4-39.

4.2.2.6 Turbulent Free Convection Flow Correlation for Vapor.

4.2.2.6.1 Model Basis--The correlation may be attributed to Bayley.[4-44] The correlation is for a vertical flat plate, and has the form

$$h = 0.10 \frac{k}{De} (Gr\ Pr)^{1/3} , \qquad (4\text{-}64)$$

where the properties are evaluated at the bulk fluid temperature. The model was developed for $Pr \simeq 1$ and fit air data very closely. It would apply to liquids and gases if $Gr \geq 10^9$. See Section 4.2.2.5 for further comments.

4.2.2.6.2 Model as Coded--The model is coded as follows

$$h = 0.23\ k \left[\frac{\rho_g^2 \left| T_w - T_f \right| Pr}{T_f \mu_g^2} \right]^{1/3} \qquad (4\text{-}65)$$

where the characteristic length has cancelled out and the gravitational constant has been lumped into the initial constant. To simplify the calculation, the thermal coefficient of expansion, β, has been replaced by $1/T_f$, which is exact for a perfect gas.

The model is applied whenever the value for h exceeds that of the forced convection turbulent flow correlation, Equation (4-59), and laminar flow Equation (4-60).

4.2.2.6.3 Assessment--The connecting logic ensures a continuous value for h. The correlation computes h values from 45.4 W/m^2-K upward, generally much lower than forced flow h values.

The correlation form makes the heat transfer coefficient independent of the characteristic length chosen. The correlation was developed for an external flow condition and applies to vertical cylinders if there is no boundary layer interference and $D/L \geq 35/Gr^{1/4}$[4-31] for Pr = 1 as analytically determined. No known basis exists for application of the correlation to internal flow conditions of a fuel rod bundle, the interior or exterior of steam generator tubes, or the interior of horizontal or vertical reactor piping.

Steam behavior does not approximate that of a perfect gas, so replacing β by $\frac{1}{T_f}$ is incorrect. A comparison of β for saturated water vapor at 150 atmospheres pressure with $\frac{1}{T_f}$ shows that $\beta = 13 \times 10^{-3}$ while $\frac{1}{T_f} = 1.6 \times 10^{-3}$,[4-45] a factor of 8 difference.

No known data exist for free convection to steam. Mixed convection effects are not considered, as discussed in Section 4.2.2.2.

4.2.2.6.4 Scaling--The correlation form makes the calculated h independent of scale. The selection logic, however, uses the hydraulic diameter as the characteristic length, which makes the selection scale-dependent.

4.2.2.6.5 Summary and Conclusions--The application of this correlation to reactor conditions and geometries has no documented basis. A more complete study of free convection correlations and reactor applications is reported in Ref. 4-39.

4.2.2.7 Integral Assessment of Heat Transfer (Mode 2), Dittus-Boelter. The Dittus-Boelter correlation was originally developed for the analysis and design of tubular automobile radiators. However the correlation has been widely used for a variety of applications. A demonstration of the use of the Dittus-Boelter correlation in a reactor-type system follows for subcooled liquid forced feed convection in turbulent flow conditions.

The steady-state calculation for the RELAP5/MOD2 calculation of Semiscale Test S-NH-3 is shown below.[4-46] For the steady-state calculation the core power is a given and constant value. If the system pressure (P_{sys}) is constant along with the hot and cold leg temperatures (T_{hot} and T_{cold}), it is implied that $Q_{in} = Q_{out}$ for the system. In this case, the driving mechanism for the heat transfer from the heater rods to the steam generators is forced convection to single-phase liquid via the Dittus-Boelter correlation. (The pumps in the primary coolant loop are on throughout the steady-state calculation.) For the steady-state calculation for Semiscale Test S-NH-3, Figure 4-3 shows that the primary system pressure is constant. The steam generator secondary pressures were also constant, as shown in Figure 4-4. Similarly the $\dot{m}_{in}$ and $\dot{m}_{out}$ of the steam generators are steady, as shown in Figures 4-5 and 4-6. With these conditions, the code calculated the cold leg temperature to be 549 K, which was in agreement with the measured cold leg temperature. The calculated core coolant temperature rise was 39.4 K, compared to a temperature rise of 37.4 K in the experiment. The 2-K difference represents a 5.35% deviation from the measured value, which was due to a slightly lower predicted-than-measured mass flow rate through the core region. This comparison suggests that the Dittus-Boelter correlation is providing accurate transfer of energy throughout the system in the steady-state condition.

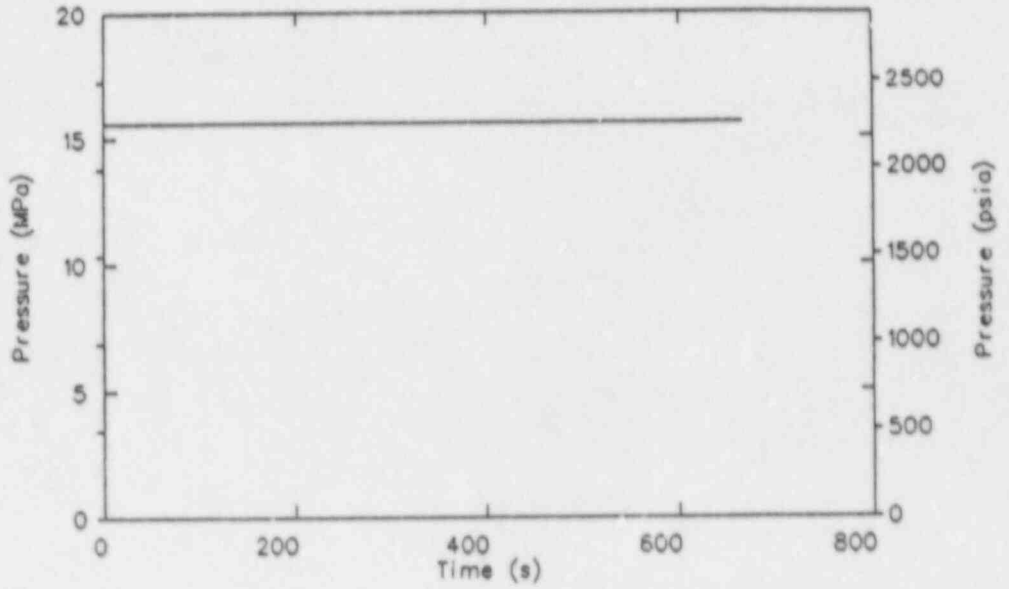

Figure 4-3. Steady-state pressurizer pressure for Semiscale Test S-NH-3.

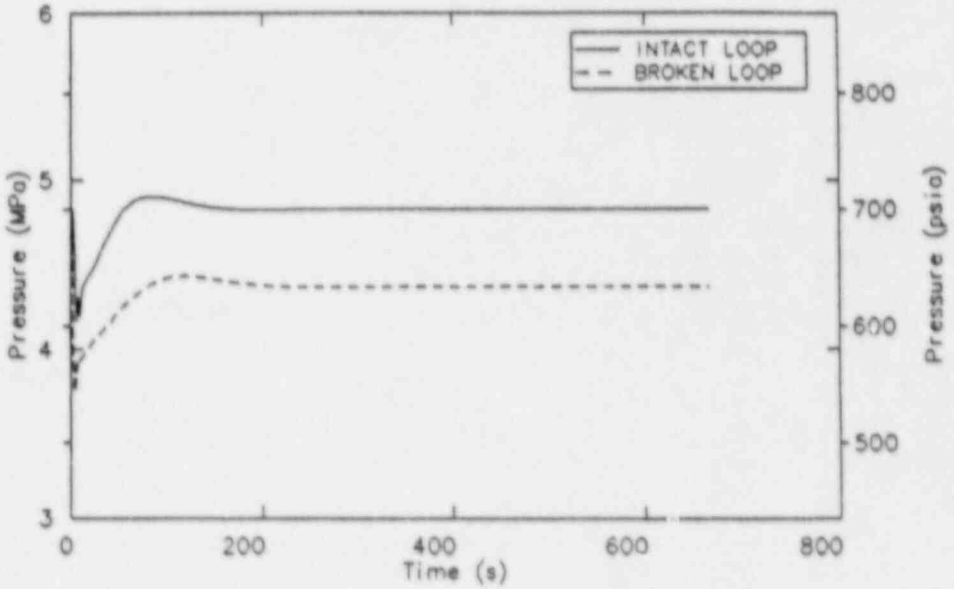

Figure 4-4. Steady-state intact and broken loop steam generator secondary pressures for Semiscale Test S-NH-3.

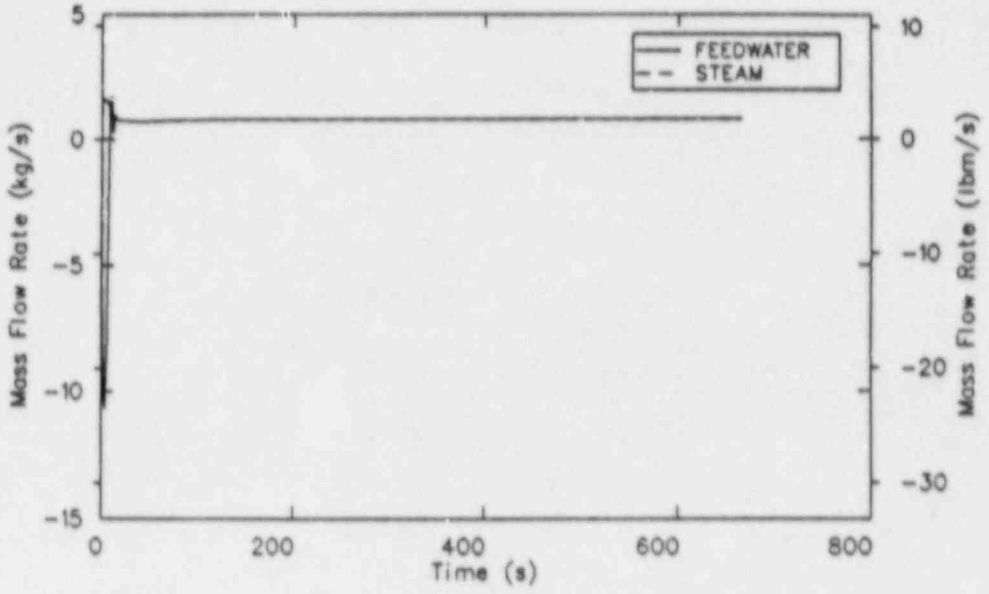

Figure 4-5. Steady-state intact loop steam generator secondary steam and feedwater mass flow rates for Semiscale Test S-NH-3.

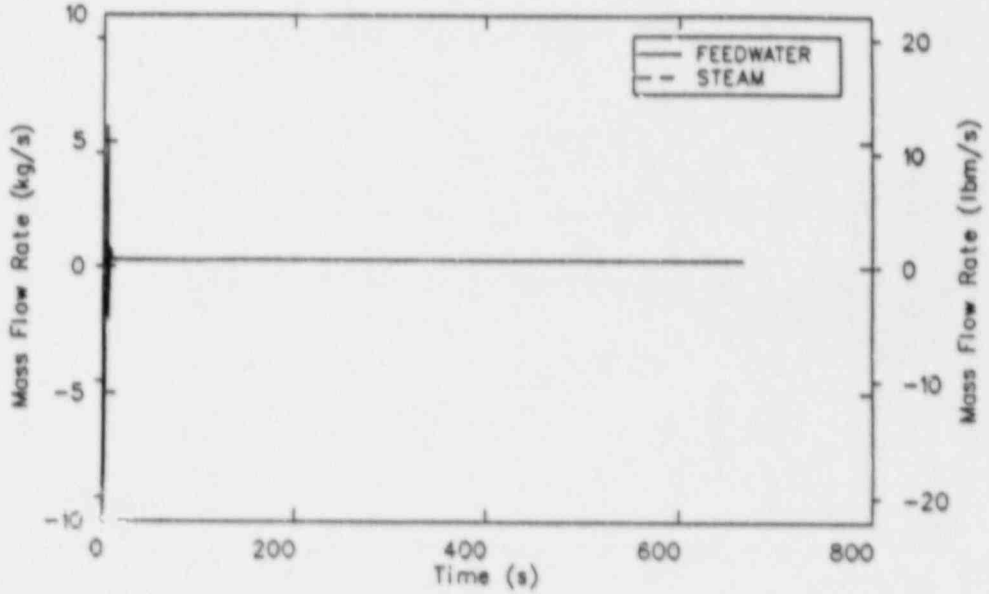

Figure 4-6. Steady-state broken loop steam generator secondary steam and feedwater mass flow rates for Semiscale Test S-NH-3.

Similarly, steady-state results were compared for full-scale facility calculations (Reference 4-47). Steady-state calculations at 92% and 100% power levels in the Davis-Besse facility were evaluated. Table 4-1 summarizes these results.

4.2.3 Correlations for Saturated Nucleate Boiling (Mode 4) and Subcooled Nucleate Boiling (Mode 3)

The Chen correlation[4-48] is used for saturated nucleate boiling. For subcooled nucleate boiling, the Chen correlation is modified. Modifications for vertically stratified flow are also included.

4.2.3.1 Correlation for Saturated Nucleate Boiling.

4.2.3.1.1 Model Basis--The model of Chen[4-48] for tubular internal flow consists of two parts, one for the heat transfer due to nucleate boiling, h_{mic}, and one for the heat transfer due to turbulent liquid forced convective flow, h_{mac}. The correlation is as follows:

$$h = h_{mic} + h_{mac} \cdot \tag{4-66}$$

The components are presented below.

The Dittus-Boelter correlation, Equation (4-59), with the addition of an F factor, is assumed to express the convective heat transfer coefficient, h_{mac}. The F factor accounts for increased convective heat transfer because of the influence of the void generated in the boundary layer by boiling. Thus,

$$h_{mac} = 0.023 \frac{k_g}{D_e} (Pr)_f^{0.4} (Re)_f^{0.8} F \ , \tag{4-67}$$

TABLE 4-1. SUMMARY OF STEADY-STATE RESULTS FOR THE DAVIS-BESSE FACILITY AT 92% AND 100% POWER

	T_{CL} (K)		T_{HL} (K)		Secondary Pressure (MPa)	
Power Level	Measured	Calculated	Measured	Calculated	Measured	Calculated
92%	566.9 K	566.7 K	591.3 K	591.4 K	6.024 MPa	6.043 MPa
100%	565.2 K	565.9 K	592.2 K	592.6 K	6.38 MPa	6.348 MPa

where

Re_f = $\alpha_f \rho_f v_f D_h / \mu_f$

F = Reynolds number factor shown in Figure 4-7.

The F factor has also been expressed as an analytical equation[4-49] as follows:

$$F = \begin{cases} 1.0 & X_{tt}^{-1} \leq 0.10 \\ 2.35\ (X_{tt}^{-1} + 0.213)^{0.736} & X_{tt}^{-1} > 0.10 \end{cases}, \qquad (4\text{-}68)$$

$$X_{tt}^{-1} = \left| \frac{\alpha_g}{(1-\alpha_g)} \frac{\rho_g}{\rho_f} \frac{v_g}{v_f} \right|^{0.9} \left(\frac{\rho_f}{\rho_g}\right)^{0.5} \left(\frac{\mu_g}{\mu_f}\right)^{0.1},$$

where X_{tt}^{-1} is the Martinelli flow parameter. F is defined over the range of X_{tt}^{-1} between 0.1 and 100.

The correlation of Forster and Zuber,[4-50] with the addition of an S_f factor, was assumed to represent the boiling heat transfer coefficient, h_{mic}. Thus,

$$h_{mic} = 0.00122 \frac{k_f^{0.79}\, C_{pf}^{0.45}\, \rho_f^{0.49}}{\sigma^{0.5}\, \mu_f^{0.29}\, h_{fg}^{0.24}\, \rho_g^{0.24}} \Delta T_{sat}^{0.24}\, \Delta P_{sat}^{0.75}\, S_f, \qquad (4\text{-}69)$$

where

S_f = suppression factor shown in Figure 4-8, the ratio of effective to wall superheat. S_f is defined for values between 0.1 and -0.84.

The S_f factor has been expressed analytically[4-49]

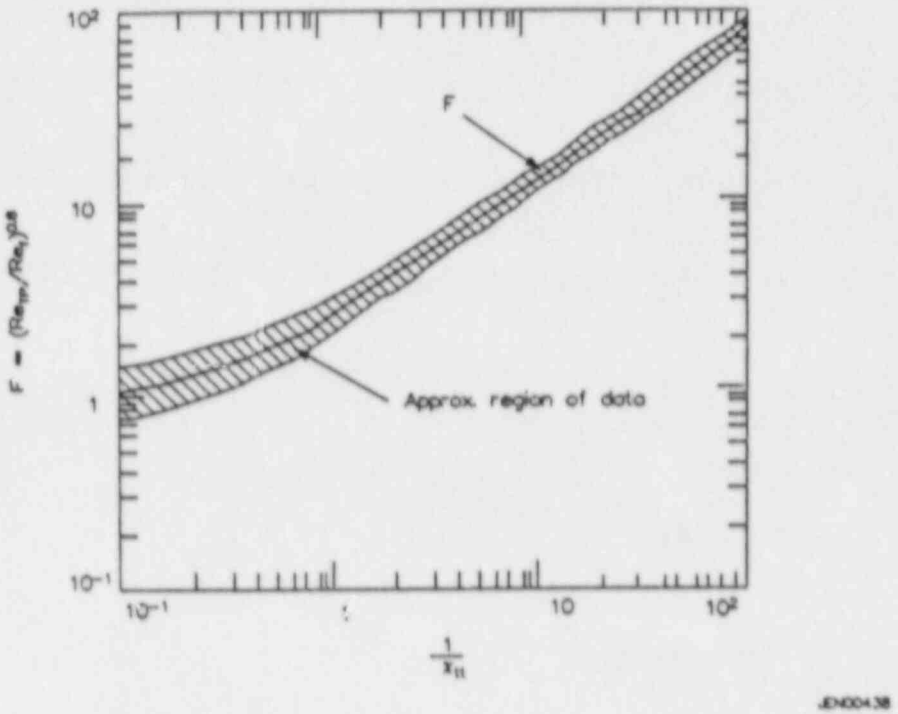

Figure 4-7. Reynolds number factor, F.

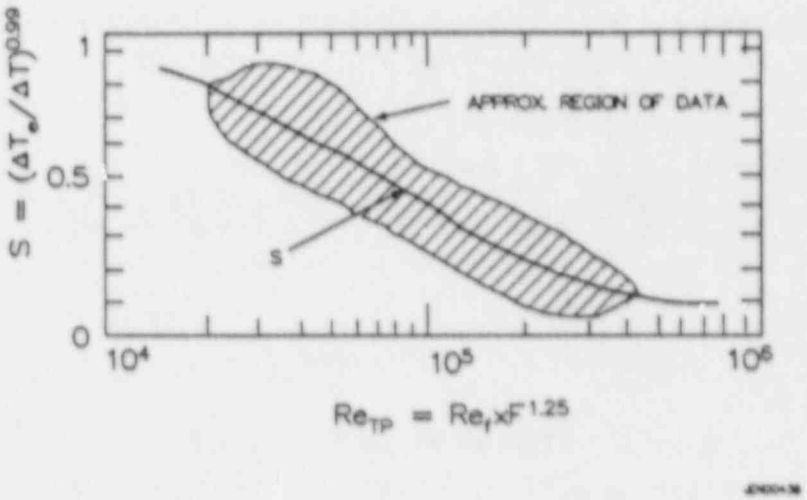

Figure 4-8. Suppression factor, S.

where

$$S_f = \begin{cases} [1 + 0.12\ (Re_{TP})^{1.14}]^{-1} & Re_{TP} < 32.5 \\ [1 + 0.42\ (Re_{TP})^{0.78}]^{-1} & 32.5 \leq Re_{TP} < 70.0 \\ 0.1 & Re_{TP} \geq 70 \end{cases}$$

$$Re_{TP} = \frac{\alpha_f \rho_f v_f D_e}{m_f} F^{1.25} \times 10^{-4} .$$

The S_f factor accounts for decreased boiling heat transfer because the effective superheat across the boundary layer is less than the superheat based on a wall temperature.

The F and S_f factors were determined by an iterative process. First, F was calculated assuming a functional relationship with the Martinelli flow parameter, X_{tt}, and the ratio of the two-phase to liquid Re numbers. With F determined, the convective component was extracted from the total heat transfer, leaving the boiling component. Then, S_f was determined assuming it to be a function of the local two-phase Re. The process was continued for 10 iterations. The solid lines drawn through the data ranges of Figures 4-7 and 4-8 were taken as the values for F and S_f.

Table 4-2 indicates data for water, for which the correlation was developed and tested. The mean percent deviations between the correlation and the data sets are presented in the last column. Table 4-3 presents nonwater data used in development and testing of the Chen correlation. The data ranges indicate that little high-pressure data were used to develop and test the correlation. The mean deviation for all the data considered is stated as 11.6%.

TABLE 4-2. RANGE OF CONDITIONS FOR WATER DATA USED IN TESTING CHEN CORRELATION

Ref.	Geometry	Flow Direction	Pressure (MPa)	Liquid Velocity (m/s)	Quality (%)	Heat Flux x 10^{-4} (W/m^2)	Average Deviation (%)
4-51	Tube	Up	0.05-0.27	0.06-1.5	15-71	8.8-6.3	14.7
4-52	Tube	Up	0.29-3.48	0.24-4.5	3-50	20.5-24.0	15.1
4-53	Tube	Down	0.11-0.21	0.24-0.82	2-14	4.4-15.8	8.5
4-54	Annulus	Up	0.10-0.24	0.06-0.27	1-59	10.1-5.5	10.8
4-55	Tube	Down	0.11-0.47	0.54-3.41	1-19	4.1-27.8	15.4

TABLE 4-3. RANGE OF CONDITIONS[a] FOR NON-WATER DATA USED IN TESTING CHEN CORRELATION[4-56]

Fluid	Pressure (MPa)	Reduced Pressure (MPa)	Liquid Velocity (m/s)	Quality (%)	Heat Flux x 10^{-4} (W/m^2)	Average Deviation (%)
Methanol	0.1	0.013	0.3-0.76	1-4	2.2-5.6	11.3
Cyclohexane	0.1	0.026	0.4-0.85	2-10	0.9-4.1	13.6
Pentane	0.1	0.031	0.27-0.67	2-12	0.9-39.0	6.3
Heptane	0.1	0.038	0.3-0.73	2-10	0.6-3.0	11.0
Benzene	0.1	0.021	0.3-0.73	2-9	1.3-42.6	11.9

a. All data taken in a tube with upflow.

Recent development[4-57] has extended the data base over which the correlation has been exposed. The maximum pressure of the data base was increased to 7.0 MPa for saturated water. The specific effect of this comparison was not noted.

4.2.3.1.2 Model as Coded--The model is coded as expressed in Equation (4-66) and the following components, subject to the modifications as explained below.

A test is made to determine if h calculated by laminar forced convection Equation (4-60) is larger than the h_{mac} from Equation (4-66). [Equation (4-66) is Equation (4-59) times the F factor.] If so, the value from Equation (4-60) is used without including the F factor.

Chen's boiling suppression factor, S_f, is modified as a function of the void fraction and the magnitude of S_f itself. The modified factor, S_F, which replaces and increases the value of the suppression factor S_f, is determined as a function of α_g as follows:

$$\alpha_g \leq 0.3 \qquad S_F = 1.0$$

$$0.3 < \alpha_g \leq 0.8 \qquad S_F = 1 - 2\,(1 - S_f)\,(\alpha_g - 0.3)$$

$$\alpha_g > 0.8 \qquad S_F = S_f \quad . \qquad (4\text{-}70)$$

Figure 4-9 shows the multiplying effects of the functional relationship. S_F is continuous over the range of α_g.

Where the code flow regime model indicates that vertical stratified flow exists (difference in α_g between vertical adjacent cells >0.5 and the product of the average fluid density, ρ, and Taylor bubble rise velocity, v_{TB}, > G), a multiplier, M_f, is applied to h_{mac} and h_{mic} [Equation (4-66)], for the lower cell. M_f is an area fraction to which the coefficient is applied. The functional relationship is as follows:

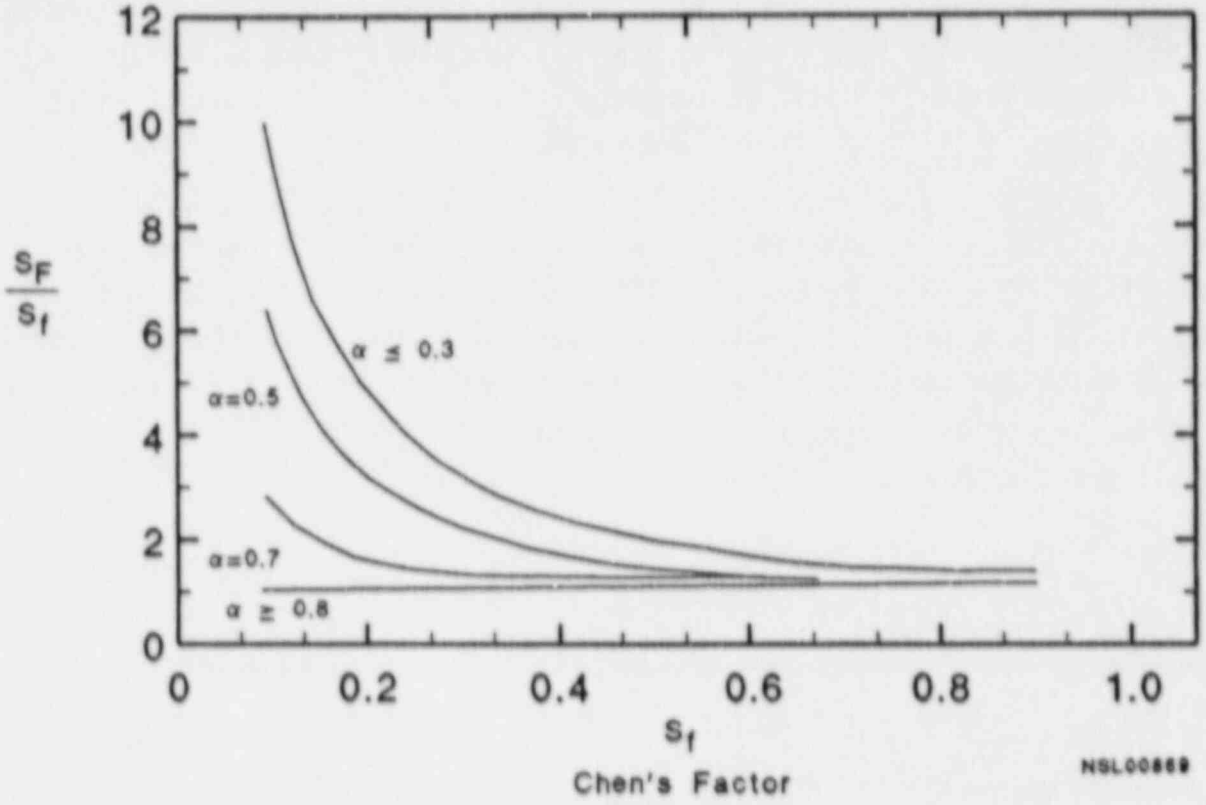

Figure 4-9. Ratio of code's S_F factor to Chen's S_f factor as a function of α_g.

$$\frac{G}{\rho v_{TB}} \leq \frac{2}{3} \qquad M_f = \alpha_f$$

$$\frac{2}{3} < \frac{G}{\rho v_{TB}} \leq 1 \qquad M_f = \alpha_f + (1 - \alpha_f)\left(\frac{G}{\rho v_{TB}} - \frac{2}{3}\right) 3 \; . \qquad (4\text{-}71)$$

The function is shown graphically in Figure 4-10. The function values for abscissa values greater than 2/3 provide smoothing to eliminate a discontinuity from occurring when the abscissa is unity.

Heat transfer to the vapor above the phase interface in the lower cell is calculated by the larger of the h values computed for turbulent forced convection, Equation (4-59), or turbulent free convection, Equation (4-65). A multiplier, $M_g = 1 - M_f$ is applied to the equations.

4.2.3.1.3 Assessment--The suppression factor, S_f (Figure 4-8), fails to go to zero as α_g goes to unity. The modified factor, S_F, does not correct for this. Also, the equations representing the S_f factor do not match the solid line drawn in the plot presented by Chen. For example, for several Re_{TP} values, the S_f factors from the plot and equation are as follows

$Re_{TP} \times 10^{-4}$	S_f plot	S_f equation
70	-0.1	0.0797
10	-0.4	0.58

The equations for S_f are from unpublished work attributed to D. Butterworth.[4-49]

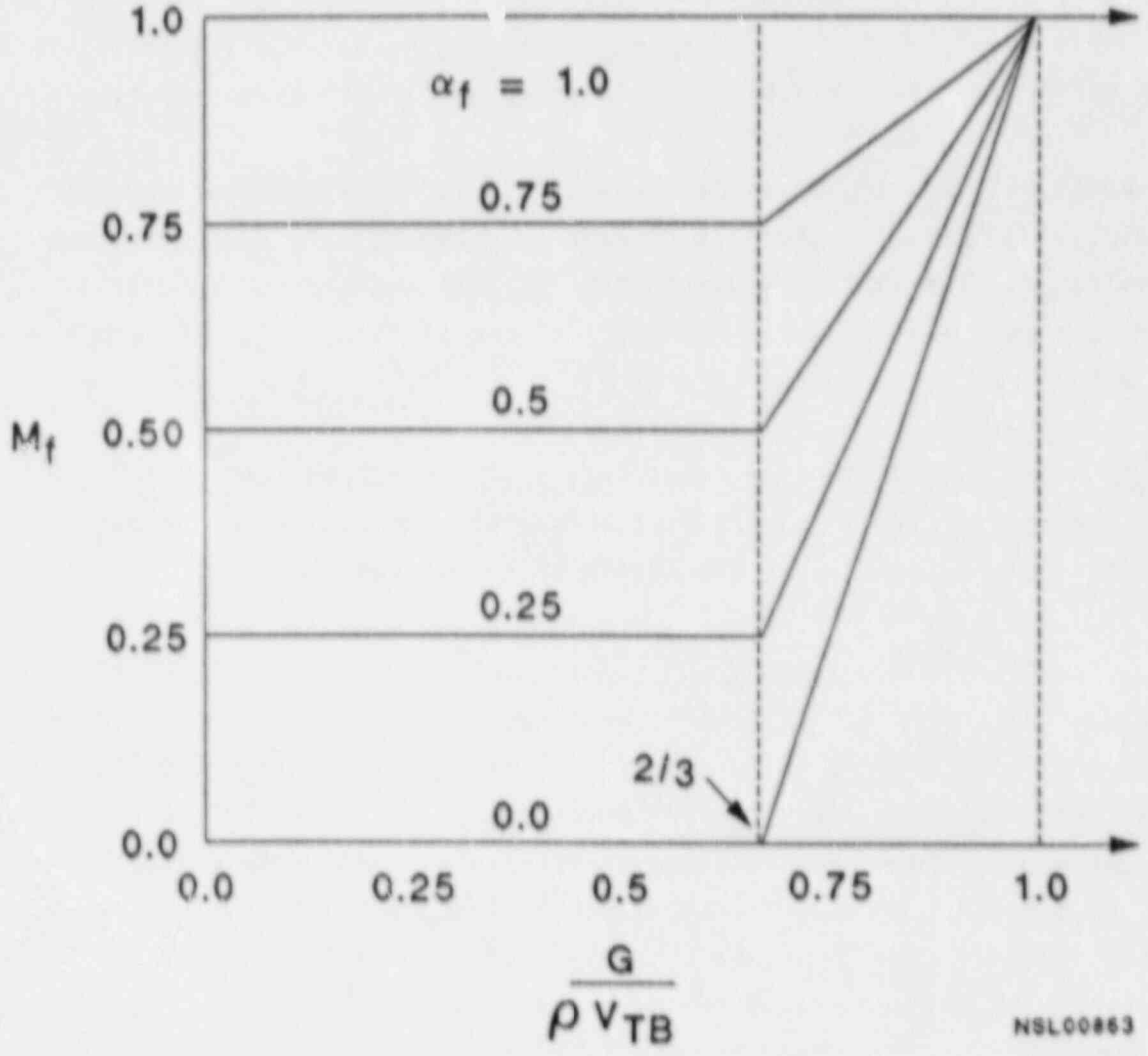

Figure 4-10. Boiling heat transfer multiplier as a function of α_f, volume cell mass flux, and Taylor bubble velocity.

The correlation for the boiling component is based on data for flow inside a tube or annulus. Much larger boiling coefficients have been obtained on the secondary side of tubes in the Semiscale steam generator.[4-58] The reason for this discrepancy is not clear. To increase heat transfer rates, S_f is modified as presented in Figure 4-9. A comparison is shown in Figure 4-11 between the coded model, the unmodified Chen correlation, and the Thom correlations[4-59] for one fluid condition. While this modification may better represent the actual boiling coefficient for a particular fluid state, no basis is known for the coded modification.

Additional boiling model development[4-57] and assessment of various correlations, including Chen's,[4-48] over an extended data base have been accomplished. For 1891 data points from 13 data sources for saturated water, the mean deviation for the authors' correlation was 21.1%, compared to a value for Chen's correlation of 27.6.

4.2.3.1.3 Scaling Considerations--The forced convection component scales with a characteristic length. The boiling component characteristic length is not a function of the system.

4.2.3.1.4. Summary and Conclusions--The original correlation describes the phenomenon reasonably well for the data and geometry for which it was developed. It is being applied in the code to different geometries and different fluid states. Recent development indicates that better correlations for saturated boiling are available. Some data exist that indicate significant differences between boiling coefficients on the inside and outside of a tube. Further evaluation of the application of this correlation to reactor situations is warranted.

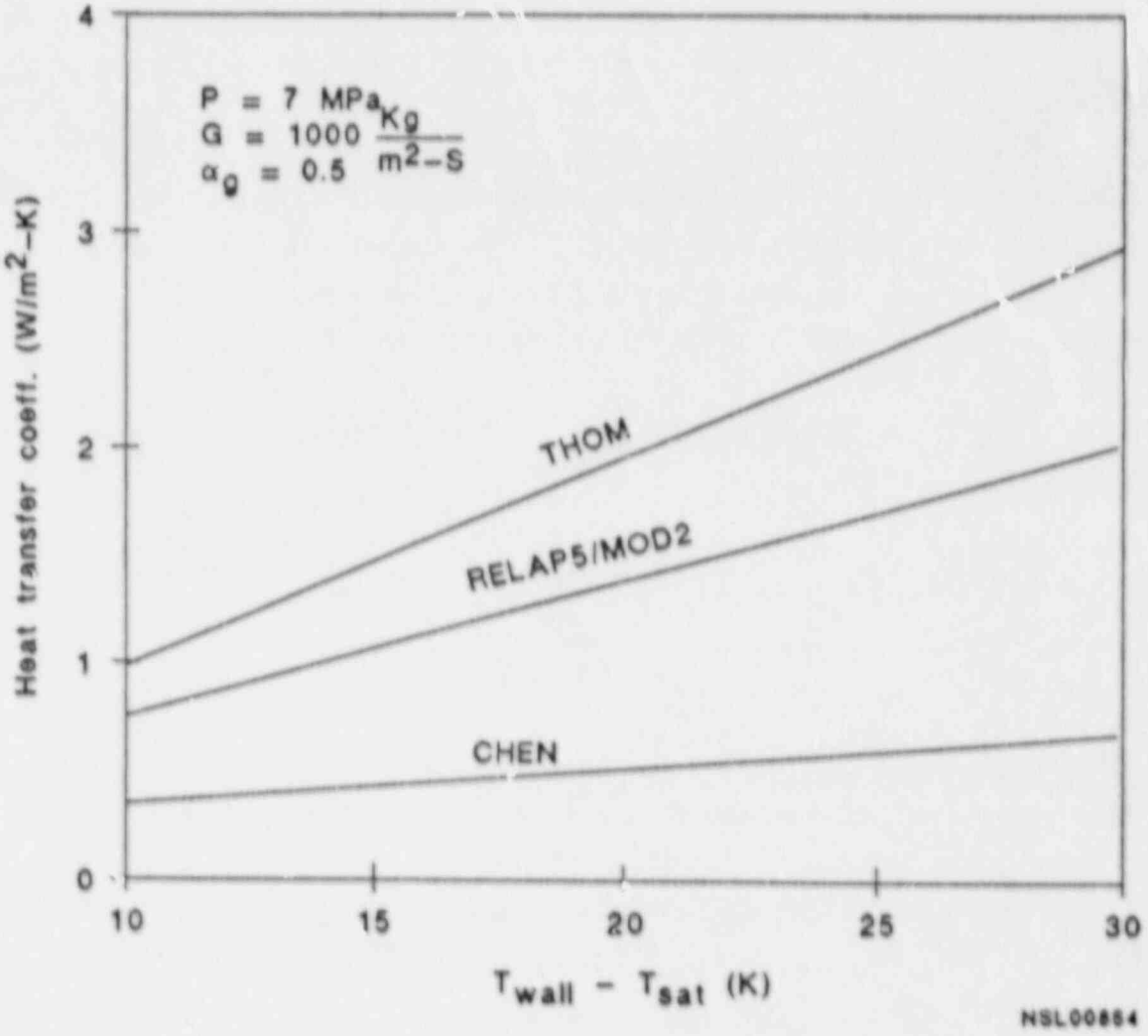

Figure 4-11. Saturated nucleate boiling heat transfer coefficient as computed by Chen correlation, RELAP5/MOD2, and Thom correlation.

4.2.3.2 Correlation for Subcooled Nucleate Boiling.

4.2.3.2.1 Model Basis--The model basis is the same as for saturated nucleate boiling expressed by Equation (4-66), with changes[4-49] as follows:

F

$$R_{eTP} = \frac{GD}{\mu_f} \quad . \tag{4-72}$$

The correlation has been tested with some water, ammonia, and n-butyl alcohol fluid data by Moles and Shaw.[4-60] The data scatter was large (+180 to -60%), with the data generally being underpredicted. The sources of the data or fluid conditions were not specified.

4.2.3.2.2 Model as Coded-- The Chen F factor is modified to F' as follows

$$T_{sat} > T_f \geq (T_{sat} - 5) \qquad F' = F - 0.2\,(T_{sat} - T_f) \quad \text{(F-1)}$$

$$T_f < (T_{sat} - 5) \qquad F' = 1 \quad . \tag{4-73}$$

The functional relationship is shown in Figure 4-12. This procedure provides smoothing of F for the liquid forced convection h if the fluid temperature falls between T_s (at zero subcooling, the F value is applied) and T_{sat} - 5 if the Martinelli parameter, X_{tt}^{-1}, is greater than 0.1. The procedure does not change the F factor value if $X_{tt}^{-1} \leq 0.1$, where F already equals unity.

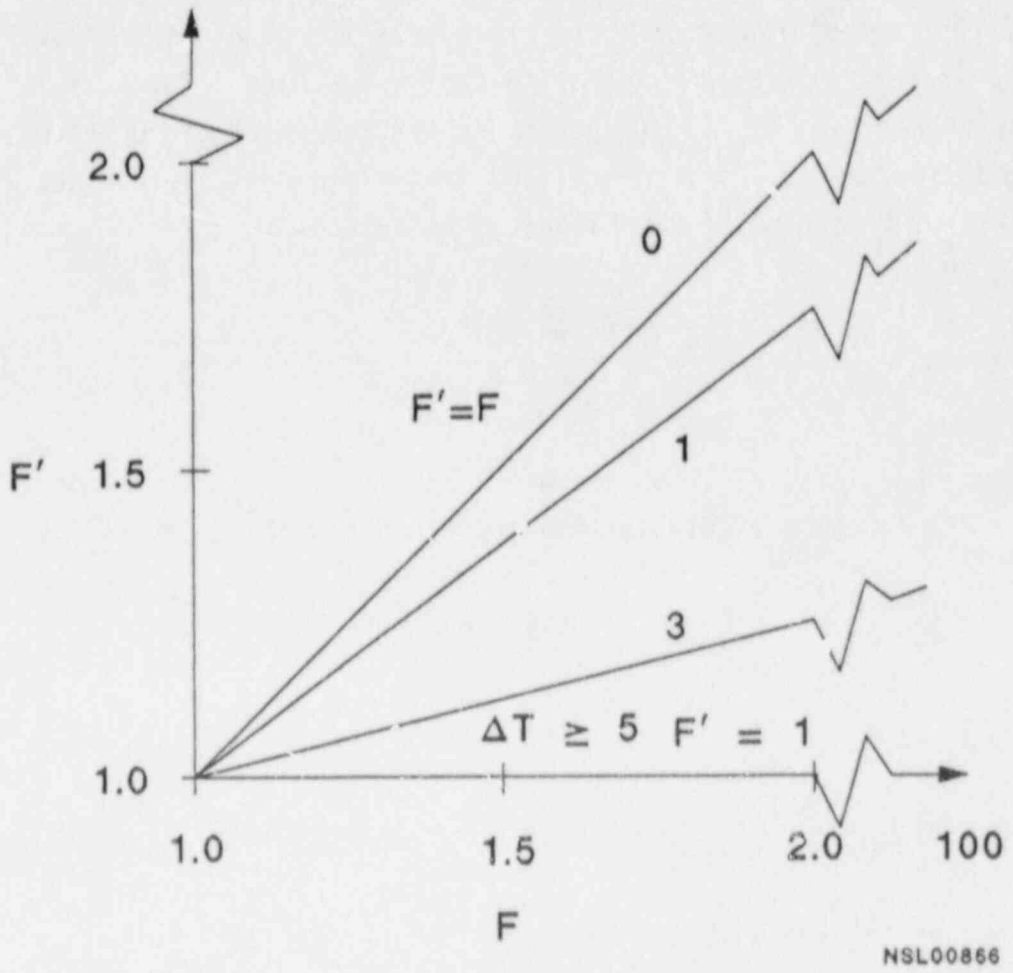

Figure 4-12. Modified F factor (F') as a function of F and subcooling (ΔT_{sat}).

S_F is modeled as follows. If $\alpha_g \leq 0.3$, S_F is set equal to a boiling heat transfer factor, bhtf. This factor provides smoothing for S_F from zero to one as the wall temperature increases. The factor is calculated by two procedures, one using the wall temperature necessary for the onset of nucleate boiling (onb), and the other using the wall temperature necessary for net vapor generation (nvg) as base points. The absolute accuracy of either of these procedures is not of importance, as they only provide an arbitrary point to apply smoothing. The wall temperature superheat ($T_w - T_{sat}$) necessary for the onset of nucleate boiling, defined as ΔT_{onb}, is calculated from the expression derived by Bergles and Rohsenow[4-61] (in SI units) as follows:

$$\Delta T_{onb} = 0.5556 \frac{556.7\, q_{onb}^{0.35355}\, p^{0.0234}}{p^{1.156}} \qquad (4\text{-}74)$$

The expression relates ΔT_{onb} to the wall heat flux, q_{onb}, at the onset of boiling. The functional relationship between bhtf, ΔT_{onb}, and ΔT_{sat} is

$$\begin{aligned} \Delta T_{sat} + 2 \leq \Delta T_{onb} \qquad & \text{bhtf} = 0 \\ -2 \leq (\Delta T_{sat} - \Delta T_{onb}) < 0 \qquad & \text{bhtf} = 1 - \tfrac{1}{2}(\Delta T_{sat} - \Delta T_{onb}) \\ \Delta T_{sat} + 2 \geq \Delta T_{onb} \qquad & \text{bhtf} = 1 \quad . \end{aligned} \qquad (4\text{-}75)$$

The functional relationship is shown graphically in Figure 4-13.

A bhtf factor is also calculated based on the wall temperature at which net vapor generation occurs. The onset of net vapor generation is taken from Saha and Zuber[4-62] as follows:

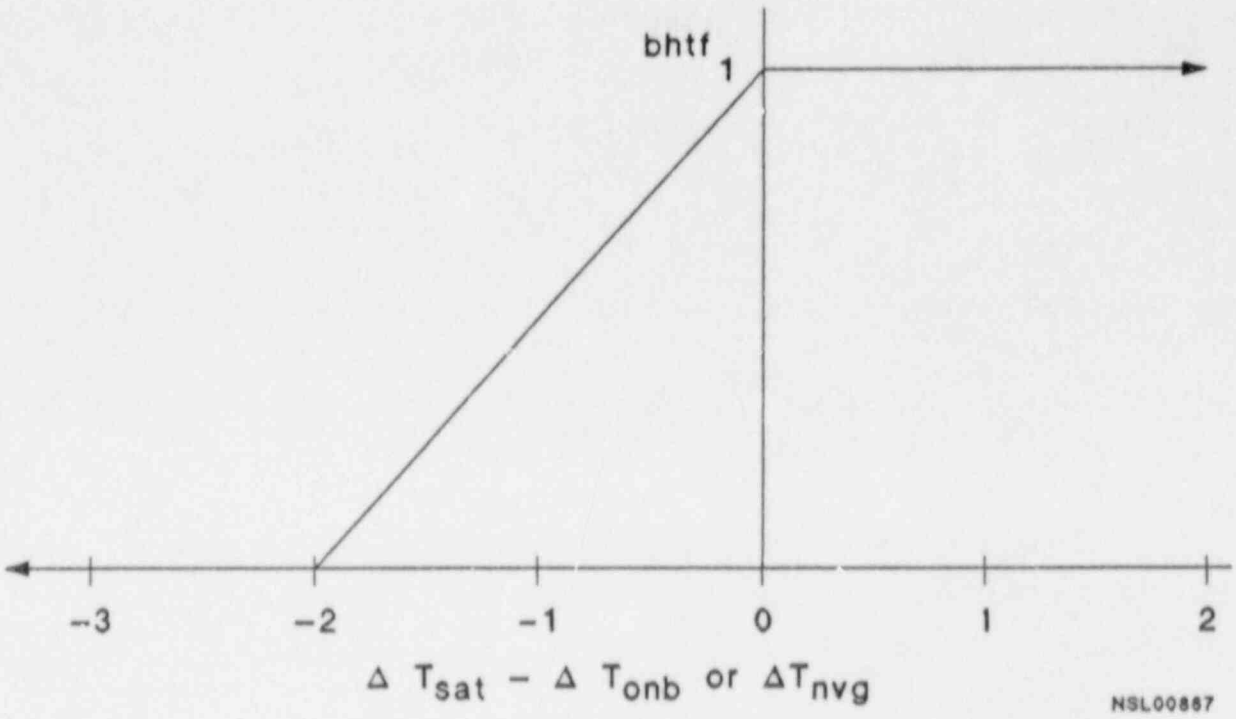

Figure 4-13. Plot of bhtf versus the difference between ΔT_{sat} and ΔT_{onb} or ΔT_{nvg}.

if $Pe \leq 70{,}000$, $$\Delta T_{nvg} = 0.002198\, q_{nvg} \left(\frac{D_h}{k_f}\right)^{a}$$

and if $Pe > 70{,}000$, $$\Delta T_{nvg} = \frac{153.85\, q_{nvg}{}^{a}}{g\, C_{pf}} \quad . \qquad (4\text{-}76)$$

The expression relates ΔT_{nvg}, the wall temperature in excess of the saturation temperature, to the wall heat flux, q_{nvg}, at the onset of net vapor generation. The functional relationship between bhtf ΔT_{nvg}, and ΔT_{sat} is

$$\Delta T_{sat} + 2 \leq \Delta T_{nvg} \qquad bhtf = 0$$

$$-2 < (\Delta T_{sat} - \Delta T_{nvg}) < 0 \qquad bhtf = 1 - \tfrac{1}{2} (\Delta T_{sat} - \Delta T_{nvg})$$

$$\Delta T_{sat} + 2 \geq \Delta T_{nvg} \qquad bhtf = 1 \quad . \qquad (4\text{-}77)$$

The functional relationship is shown graphically in Figure 4-13.

The largest value of bhtf calculated by either procedure is set equal to S_f.

It is expected that α_g for subcooled nucleate boiling would never exceed 0.3. However, if a larger α_g were computed, S_f would be determined as for saturated nucleate boiling as follows:

if $\alpha_g > 0.3$ $$S_f = bhtf\, S_f \qquad (4\text{-}78)$$

Vertical stratification is treated in the same manner described previously for saturated nucleate boiling.

---

a. The constants in the reference are given as 0.0022 and 154.

4.2.3.2.3 Assessment--The modification resulting in the F′ factor can result in a considerably larger multiplying factor than recommended for subcooling between 0 and an arbitrary 5 K. The modification does result in a smooth transition between subcooled and saturated forced convection as the subcooling goes to zero.

The S_f factor is discarded for $\alpha_g \leq 0.3$ and replaced by a new procedure determining S_f. The new procedure is based on the wall and fluid temperature difference, resulting in the onset of boiling or net vapor generation. For heating the fluid, the onset of nucleate boiling is reached before net vapor generation. Thus, the procedure smooths the application of the boiling heat transfer component when T_w falls into an arbitrary 2-K range below T_{onb}.

Subcooled boiling is not expected for $\alpha_g > 0.3$. However, no logic prevents the code from performing a subcooled boiling calculation if $\alpha_g > 0.3$.

Reference 4-59 develops a correlation for subcooled boiling which fits data from a variety of sources with a variety of fluids, mostly for upward flow in a circular tube. The subcoolings of the data range from 3 to 278 K. The correlation fits the bulk of the data by ±40% but fails at zero subcooling. During developmental assessment, the code was compared with Christensen's subcooled boiling experiment and showed good comparisons with the axial void profile.[4-12]

4.2.3.2.4 Scaling Considerations--The forced convection component scales with a characteristics length. The boiling component characteristic length is not a function of the system.

4.2.3.2.5 Summary and Conclusions--Insufficient evidence exists to determine the applicability or range of uncertainty for the correlation to conditions representing subcooled boiling.

The correlation of Reference 4-59 was independently evaluated[4-58] and determined to be the "best" for subcooled water boiling. An analytical comparison of the Reference 4-59 correlation with the correlation used in RELAP5/MOD2 as a function of selected parameters would provide evidence to better evaluate the code.

Table 4-1 demonstrates good agreement between the calculated and the measured results (within the measurement accuracy), suggesting that the transfer of energy from the heater rods to the steam generator is being correctly treated.

The wall-to-fluid heat transfer coefficients are provided by the Dittus-Boelter correlation[4-22] for these steady-state calculations. Although direct measurements of surface and fluid temperatures and heat fluxes are not available to provide direct verification of the accuracy of the heat transfer coefficient calculation, the consistent agreement between primary system measured and calculated parameters implies that the heat transfer coefficient is satisfactory. The demonstrated ability of RELAP5/MOD2 to represent initial, steady-state conditions in a variety of experimental and reactor systems provides an indirect measure of the applicability of the Dittus-Boelter correlation to reactor temperatures and pressures for steady-state conditions and moderate temperature differences.

A review of the calculated response compared to the measured response provides a qualitative indication of the applicability of the Chen correlation[4-48] beyond the range of the developmental data. Figure 4-14 presents a comparison of the measured and calculated collapsed liquid level in the core during Semiscale Test S-NH-3. The collapsed liquid level is indicative of the core liquid inventory even if the void distribution is not accurately calculated. The coolant in the core undergoes a rather simplistic energy increase from the heater rods, which first accounts for the removal of subcooling and then the vaporization of liquid. The process is dominated by the transfer of energy into the fluid by nucleate boiling calculated with the Chen correlation. Figure 4-14 shows that, although the timing of events is different in the calculated and measured responses, the

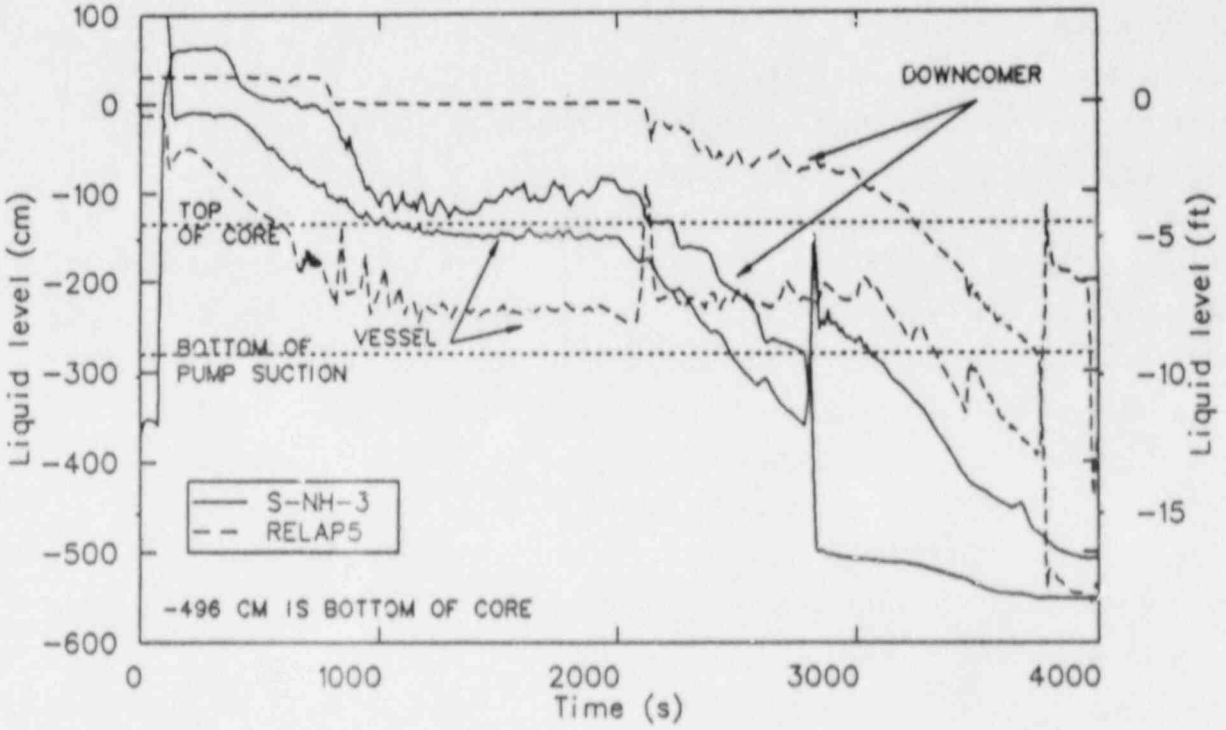

Figure 4-14. Comparison of the calculated and measured collapsed liquid level in the core for Semiscale Test S-NH-3.

calculated rate of coolant inventory decrease is the same as measured. Over these same corresponding time periods, system pressures and break flow rates were similar and essentially contrast in both the experiment and the calculation. Therefore, the core liquid depletion is a reasonable measure of the energy input from the heater rods. RELAP5/MOD2 used the Chen correlation during this phase of the transient, and the results compared favorably with the test. The Chen correlation was used during this period beyond the range of pressures represented in the developmental data set.

Another area of concern relative to the use of the Chen correlation for heat transfer in tube bundles is that the developmental data base was for heat transfer inside tubes. No discussion appeared in the code documentation that addressed the extension of the correlation to heat transfer from external surfaces in tube bundles. Deissler and Taylor[4-63] investigated the phenomena associated with heat transfer and flow over a tube bundle in parallel flow. Their work characterized the effects of tube spacing on the friction factor and on the heat transfer coefficient. The conclusion was that the heat transfer and frictional effects are dominated by fluid flowing close to the surface; and, with close spacing, the bundle values for the heat transfer coefficient and friction factor are less than those for flow inside circular tubes, h_{cir} and f_{cir}. As the spacing ratio increases, the effect of neighboring tubes lessens and the heat transfer and friction factor become dominated by surface effects. Figure 4-15 summarizes Deissler and Taylor results. This figure was deduced from work presented by Kays.[4-64]

4.2.3.3 Integral Assessment of Heat Transfer Modes 3 and 4. Review of the subcooled and saturated boiling heat transfer correlations (both are modified Chen) in the RELAP5/MOD2 code suggests that the correlation is used by the code outside of the range of conditions from which it was originally derived. Specifically, the code uses the Chen correlation for subcooled nucleate boiling conditions at system pressures greater than 13.5 MPa (1972 psia) and for saturated nucleate boiling conditions at system pressures greater than 6.25×10^5 MPa (906 psia). The correlation was developed from data acquired at pressures up to 3.48 MPa (505 psia).

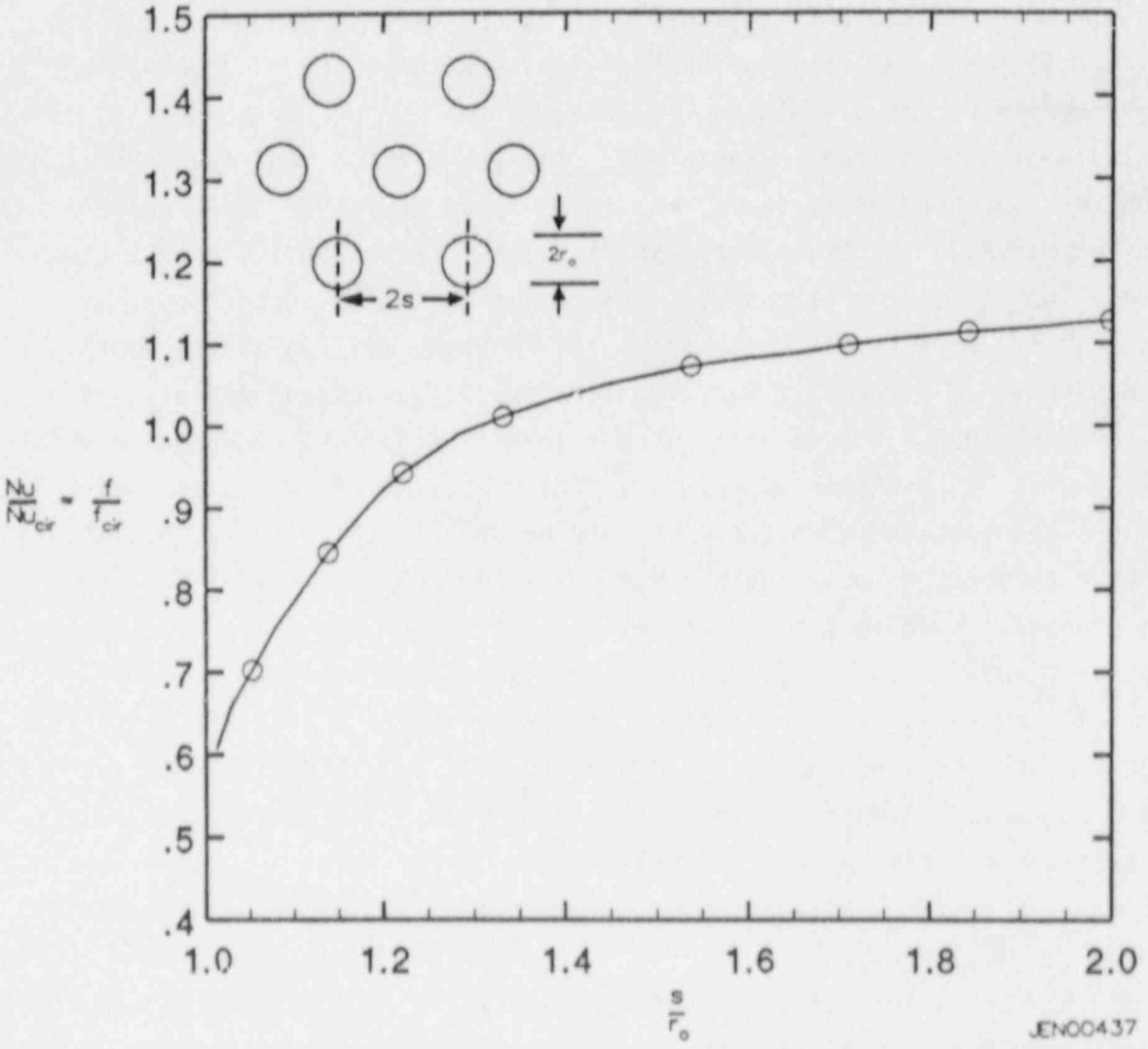

Figure 4-15. Summary of Deissler and Taylor results for flow in circular tubes and tube bundles.

Additionally, the Chen correlation was developed from experimental data taken for flow inside tubes. However, the code uses the correlation for parallel flow in tube bundles and rod bundles. These "out-of-intended-range" applications will be addressed below.

4.2.3.3.1 Chen Correlation Use at High Pressure--A RELAP5/MOD2 calculation of Semiscale Test S-NH-3[4-46] was reviewed to demonstrate the Chen correlation capability in the high-pressure range (P > 3.48 MPa). A cursory review of the calculation relative to the use of the Chen correlation is summarized in Table 4-4. The table shows that the core region saw subcooled nucleate boiling (Mode 3) in the upper core region beginning early in the transient (~50 s), with a corresponding bubbly flow regime. The state of heat transfer progressed to subcooled boiling throughout the core region, with saturated nucleate boiling at the upper core region at about 625 s. The slug flow regime was calculated at this time (and throughout the majority of the transient) in the core region. The table shows that the transient continued to the point of saturated nucleate boiling throughout the core (~4100 s) and eventually to saturated boiling in the lower core region only, with a MIST flow regime calculated. The Chen correlation was used in the heat transfer calculation beginning at a system pressure of about 13.6 MPa (1972 psia) when subcooled nucleate boiling began. Throughout a major portion of the transient (~50 s to ~5200 s), the system pressure remained above the range of data from which the Chen correlation was developed, as shown in Figure 4-16. For a brief period of the calculation (corresponding to the restart of the primary coolant pumps), the Chen correlation was replaced by single-phase liquid forced convection.

The Semiscale core simulator is representative of the geometry expected in reactor systems. For the Semiscale Mod-1 core, rod pitch (2s) was 1.43 cm and rod diameter ($2r_0$) was 1.07 cm; the ratio of s/r is 1.34. Figure 4-15 suggests that for s/r_0 equal to 1.34, the Nu/Nu_{cir} is about 1.08 This indicates that the use of the Chen correlation for nucleate boiling in tube bundles may not be remarkably different from its use inside of tubes based on the physical behavior shown for heat transfer from the tube surface in Figure 4-15. Further work to verify this effect for boiling heat transfer is warranted.

TABLE 4-4. SUMMARY OF THE RELAP5/MOD2 CALCULATION OF SEMISCALE TEST S-NH-3 RELATIVE TO USE OF THE CHEN CORRELATION

Transient Time (s)	Pressure Pa (psia)	Heat Transfer Mode	Heat Flux W/m^2 (Btu/hr ft^2)	Flow Regime	Calculated Heat Transfer Coefficients, W/m^{2}K (Btu/h ft^{2}F)
50	1.36 E7 (1972)	3 (upper core)	1.06 E6 (336000)	Bubbly	-32000 (5636)
150	7.70 E6 (1119)	3 (upper core)	46000 (14500)	Slug	-16000 (2817)
350	6.60 E6 (957)	3 (upper core)	40000 (-12700)	Slug	-18000 (3170)
623	6.25 E6 (906)	3 (lower & mid core)	38000 (-12000)	Slug	17000 (-3000)
		4 (upper core)	38000 (-12000)	Slug	17000 (-3000)
823	6.07 E6 (880)	3 (lower core)	25000 (-7900)	Slug	13000 (-2300)
		4 (upper core)	35000 (11100)	Slug	17000 (-3000)
2127	5.22 E6 (789)	3 (lower core)	32000 (10000)	Slug	-15000 (-2650)
3400	5.87 E6 (851)	3 (lower core)	8000 (-2540)	Slug	-8000 (-1410)
		4 (upper core)	30000 (9500)	Slug	-15000 (-2650)
4100	5.62 E6 (815)	4 (core)	-28000 (-8800)	Slug	-14500 (-2550)
7400	2.12 E6 (307)	4 (lower core)	-8000 (-2540)	Mist	-8000 (1400)

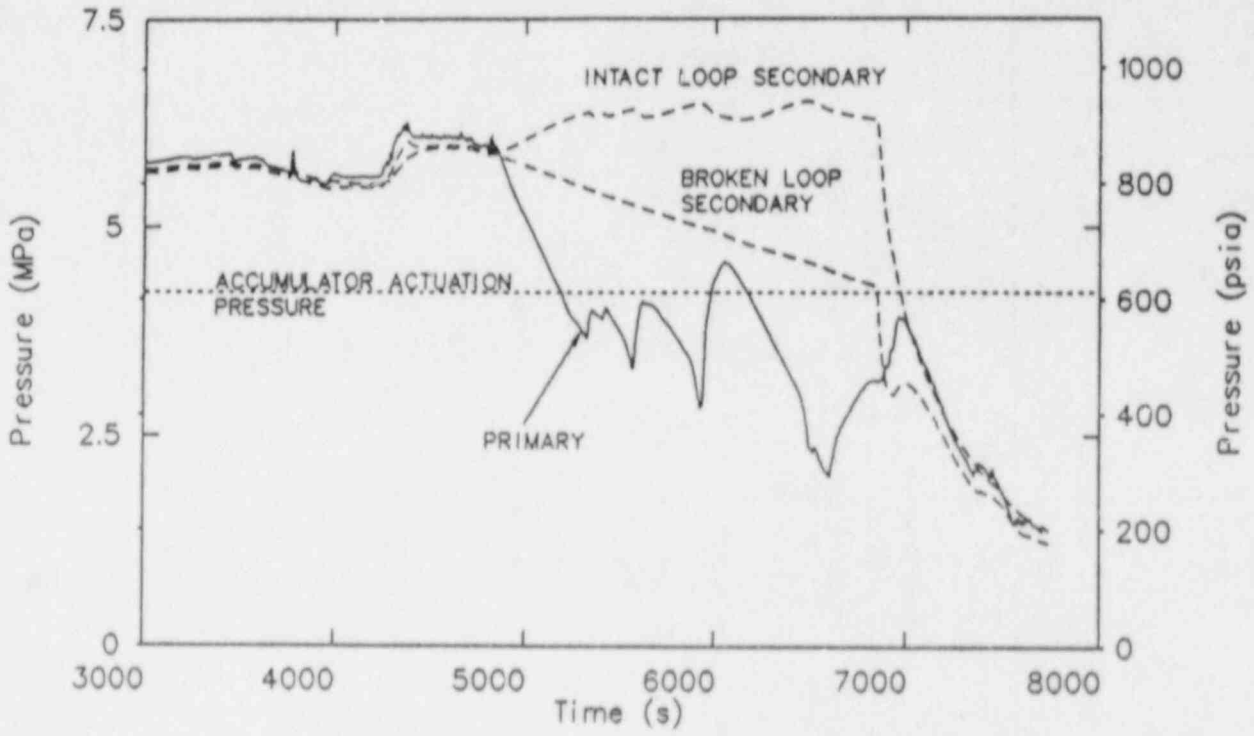

Figure 4-16. Calculated system pressure for Semiscale Test S-NH-3.

4.2.4 Correlations for Saturated Transition Boiling (Mode 6) and Subcooled Transition Boiling (Mode 5).

The same correlation is applied to saturated and subcooled flow.

4.2.4.1 Correlations for Subcooled and Saturated Transition Boiling

4.2.4.1.1 Model Basis--The Chen transition boiling model, Reference 4-65, considers the total transition boiling heat transfer to be the sum of individual components, one describing wall transfer to the liquid and a second describing the wall heat transfer to the vapor. Radiative heat transfer from wall to fluid is not specifically described in the model, as it is estimated to be less than 10% of the total. Whatever radiation effects are present are lumped into the liquid and vapor heat transfer components.

The development is stated to be primarily applicable to a dispersed flow regime, where liquid droplets are suspended in a bulk vapor stream, although it is recognized that an inverse annular flow regime, where a vapor film separates a bulk liquid core from the wall, may be present near the CHF point. Non-equilibrium phase states are treated through the apportioning of heat energy to the individual phases. The model is expressed as:

$$q_t = q_f F_f + h_g (T_w - T_g) (1 - F_f) , \qquad (4\text{-}79)$$

where

q_t = the total heat flux

F_f = the fractional liquid wetted wall area.

The q_f term is a complex mechanistic relationship predicting the average heat flux during the time of contact between the liquid and the wall. The heat removal process is described by a three-step model

considering a prenucleation period, a bubble growth period, and a film evaporation period. This relationship is replaced in the code adaptation. Thus, it is not described further.

F_f is dependent on the amount of liquid present at any instant at a particular section of the heated tube and on the probability of this liquid contacting the hot wall. F_f is empirically correlated as:

$$F_f = e^{-\lambda(T_w - T_s)^{1/2}} , \qquad (4\text{-}80)$$

where

λ = λ_1 or λ_2, whichever is greate.

λ_1 = $C_1 - C_2\, G/10^5$

λ_2 = $C_3\, G/10^5$, (the units of G are $\frac{\text{lbm}}{\text{hr - ft}^2}$)

C_2 = $\frac{0.05}{1 - \alpha_g'^{40}} + 0.075\, \alpha_g'$

C_1 = $2.4\, C_2$

C_3 = $0.2\, C_2$.

The numerical coefficients in C_2 are incorrectly given as 0.005 and 0.075 in the reference paper. Similarly, the constant in C_1 is incorrectly given as 24 in the reference.[a]

The void fraction α_g' is calculated using the homogeneous model with the actual quality.

---

a. Private communication, J. C. Chen to R. W. Shumway, May, 1988.

The h_g term in Equation (4-79) is based on Reynolds analogy for forced turbulent vapor flow in a duct with the Colburn suggested $Pr^{2/3}$ factor multiplying the Stanton number. The analogy takes the form

$$St\ Pr^{2/3} = \frac{f}{2}\ , \tag{4-81}$$

where

f = friction factor.

The model uses an explicit form for f which approximates the work of Beattie,[4-66] who developed friction factors for two-phase post-CHF conditions. The form is $f = 0.037\ Re^{-0.17}$. The coefficient for wall to vapor heat transfer then takes the form

$$h_g = 0.0185\ Re^{0.83}\ Pr^{1/3}. \tag{4-82}$$

This h_g term is replaced in the code adaptation and is not described further.

The model was compared to data (4167 points) from eight sources for water flowing in tubes with a mean deviation[a] of 16.0%. Table 4-5 lists

---

a. The mean deviation is taken to be

$$M = \frac{\sum_1^N \left| \frac{Q_{measured} - Q_{predicted}}{Q_{measured}} \right|}{N}$$

The standard deviation is

$$S = \frac{\sum_1^N \left(\left[\frac{Q_{measured} - Q_{predicted}}{Q_{measured}} \right]^2 \right)^{1/2}}{N - 1}$$

TABLE 4-5. CHEN TRANSITION BOILING CORRELATION

Geometry: Vertical tube
Flow: Upward
Experimental method: Heat flux controlled, uniform heat flux at the wall

Data Source	System Pressure (MPa)	Tube Diameter (m)	Mass Flux 10^3 (kg/s-m^2)	Equilibium Quality	Heat Flux 10^5 (W/m^2)	Data Points
B&W	0.42-10.4	1.27	40.7-678	0.675-1.728	1.00-6.63	904
Bennett	6.89	1.26	380-5235	0.30-0.9	3.47-20.5	1111
Bennett & Kearsey	6.77-7.03	1.26	1112-1871	0.516-1.083	1.29-14.6	73
Bertoletti	6.89	0.488	1085-3946	0.383-0.90	1.36-15.8	65
Bishop	16.6-19.5	0.91-0.25	2034-3377	0.16-0.96	8.92-16.6	43
Era	6.89-7.28	0.60	1098-3024	0.456-1.238	2.09-16.5	576
Jansson	0.64-7.07	1.27	16.3-1024	0.392-1.634	0.34-9.97	836
Herkenreth	14.0-19.5	1.0-2.0	693-3526	0.151-1.270	2.58-16.6	559

the parameter ranges. The model was also compared with some of the same data and additional data (4668 points) from ten sources,[4-67] resulting in a standard deviation of 35.5%. Table 4-6 lists the parameter ranges for the independent evaluation. Using a mean deviation as used by Chen resulted in a 25.6% deviation.

4.2.4.1.2 Model as Coded--Total wall heat flux, q_t, is obtained from components describing the wall-to-liquid heat flux and wall-to-vapor heat flux as follows:

$$q_t = q_{CHF} F_f M_f + h_g (T_w - T_g) \alpha_g (1 - F_f M_f) . \quad (4\text{-}84)$$

The term q_{CHF} corresponds to the boiling heat flux calculated for the local wall temperature and fluid conditions existing when CHF is initially exceeded upon entering the post-CHF heat transfer regimes. This substitution simplifies the computational process. The CHF computational models are described in a later section.

The following modifications were made to the process for calculating F_f. The void fraction, α_g, was calculated using the code fluid model. To limit the possibility of dividing by zero during the evaluation of constant C_2, a limit was placed on α_g as follows:

$0 < \alpha_g \leq 0.999$, $\alpha_g' = \alpha_g$, and for

$\alpha_g > 0.999$, $\alpha_g' = 0.999$. (4-84)

The square root of the saturation temperature difference, $(T_w - T_s)^{1/2}$, was taken to be the minimum of

TABLE 4-6. INDEPENDENT EVALUATION OF CHEN TRANSITION BOILING CORRELATION

Experimenter	No. Points	Wall Temp. (K)	$T_{wall} - T_{sat}$ (K)	Pressure (MPa)	Mass Flux (kg/m^2-s)	Heat Flux ($W/m^2 \times 10^6$)	Quality	Heat Transfer Coefficient (W/m^2-K)
Babcock & Wilcox	904	617 - 1053	112 - 560	0.42 - 104.5	40.1 - 679.5	0.101 - 0.656	0.68 - 1.73	221 - 4384
Bennett	1113	572 - 1113	70 - 555	6.89	379.7 - 5234.2	0.370 - 2.074	0.22 - 1.44	982 - 9511
Bennet	73	576 - 869	18 - 310	6.78 - 7.03	1110.6 - 1871.3	0.129 - 1.460	0.52 - 1.08	3407 - 7836
Bertoletti	65	576 - 727	18 - 169	6.89	1086.2 - 3939.2	0.137 - 1.581	0.38 - 0.90	3929 - 21907
Bishop	78	656 - 883	14 - 259	16.62 - 21.52	1356.0 - 3376.4	0.662 - 1.924	0.07 - 0.96	5593 - 93249
Era	592	571 - 903	13 - 343	6.89 - 7.28	1092.9 - 3023.9	0.203 - 1.652	0.46 - 1.24	1172 - 16740
General Electric	846	646 - 1000	96 - 558	0.64 - 7.07	16.5 - 1023.9	0.034 - 0.997	0.17 - 1.63	85 - 4145
Markenrath	842	692 - 865	12 - 242	14.00 - 20.5	692.9 - 3555.4	0.253 - 1.666	0.12 - 1.32	1732 - 66703
Schmidt	75	665 - 897	21 - 252	20.68 - 21.55	707.8	0.303 - 0.850	0.10 - 0.90	3373 - 14962
Swenson	80	658 - 767	17 - 126	20.68	949.2 - 1356.0	0.297 - 0.574	0.15 - 0.98	4060 - 24990

$$(T_w - T_s)^{1/2} \text{ or } |T_w - T_{CHF}| , \quad (4\text{-}85)$$

where T_{CHF} is the wall temperature permitting rewet at the CHF point. This procedure ensures that the computed wetted wall area fraction, F_f, remains bounded.

If the flow regime has been identified as being vertically stratified then the boiling portion of the heat flux is further multiplied by a factor equal to M_f, as discussed in Section 4.2.3.1.

The effective h_g for the wall-to-vapor heat transfer component is the largest value calculated by one of three correlations previously presented. The correlations are set forth as Equations (4-59), (4-60), and (4-64). In computing the value used for comparison, the α_g term is applied to Equations (4-59) and (4-60), but not to Equation (4-64). The α_g term, an assumed vapor-wall area contact fraction, was applied by Iloeje[4-68] and others with Equation (4-59) (or equivalent) in earlier developments for calculating the vapor wall heat transfer. Chen's vapor-wall contact area fraction, as modified by the stratification factor, is also included.

The calculated heat flux value for transition boiling is applied to post-CHF heat transfer if it is larger than the corresponding value for film boiling.

4.2.4.1.3 Assessment--The application of q_{CHF}, h_g, and F_f is not consistent with their development. The application of the terms is discussed as follows.

Chen's[4-65] model for transition boiling, a complex mechanistic model, was developed to describe heat transfer from the wall to the liquid in contact with the heated wall and from the wall to the vapor in contact with the wall. Chen stated that the heat flux to the liquid should not exceed that value estimated for CHF as determined by an appropriate correlation. He used Zuber's CHF correlation for pool boiling,[4-69] as modified by Griffith et al.[4-70] The RELAP5/MOD2 model discards the model for liquid

heat transfer and replaces it with the limiting code-calculated CHF value. Reference 4-67 evaluated the use of the modified Zuber correlation as a replacement for the liquid heat transfer. The comparison showed improvement at high heat fluxes, but the standard deviation for the data-correlation comparison increased from 34.5% to 48.5%. RELAP5/MOD2 uses the modified Zuber CHF correlation below a mass flux of 100 kg/s-m^2. Above 200 kg/s-m^2, the Biasi[4-71] correlation applies. Linear interpolation occurs between 100 and 200 kg/s-m^2. The range of mass flow parameter values for Chen's data sources exceeds that for which the Zuber correlation is used in the code. Thus, it is very likely that the CHF value used to determine the wall-to-liquid heat flux in the code could be too large when G > 100 kg/s-m^2.

Chen also developed an empirical model, F_f, for computing the wall fraction area in contact with the liquid. The term $(1 - F_f)$ was then the wall fraction area in contact with the vapor. The F_f factor was obtained by fitting data in conjunction with the discarded liquid and vapor models and thus does not directly apply to the replacement models.

The code application of F_f is also inconsistent with the wall area fraction assumed to be in contact with vapor. The code uses α_g as a weighting factor to determine the wall-to-vapor contact area fraction as well as the $(1 - F_f)$ factor. This is a double correction.

The superposition of the wetted and dry wall area fractions for a vertically stratified flow pattern is not compatible with the flow pattern inherent in the Chen correlation for flow transition boiling with the wetted and dry areas internally defined. Thus, there is no basis for application of the M_f factor to weight the wetted and dry wall area fractions.

4.2.4.1.4 Scaling Considerations--The effects of scaling for the CHF calculation are described in a later section. The effects of scaling on the vapor convection heat transfer have been previously addressed. Scaling is not expected to be a factor in the application of heat transfer components in obtaining a total heat flux for subcooled or saturated transition boiling.

4.2.4.1.5 Summary and Conclusions--The use of the original model,[4-65] in view of its complexity and noted deficiencies, seems undesirable. The model in the code is simpler but has not been evaluated. Thus, the accuracy of the code model cannot be assessed without comparing it to data.

4.2.5 Correlations for Saturated Film Boiling (Mode 8) and Subcooled Film Boiling (Mode 7)

Film boiling is described by heat transfer mechanisms that occur during several flow patterns, namely inverted annular flow, slug flow and dispersed flow. The wall-to-fluid heat transfer mechanisms are conduction across a vapor film blanket next to a heated wall, convection to flowing vapor and between the vapor and droplets, and radiation across the film to a continuous liquid blanket or dispersed mixture of liquid droplets and vapor. The liquid does not touch the wall because of a repulsive force generated by the evaporating liquid. The fluid environment may be stagnant or flowing, saturated or subcooled. The analytical models for conduction, convection, and radiation which form the basis for the code models are described below.

4.2.5.1 Model Basis for Conduction. The conductive mechanism can be attributed to the work of several investigators.[4-72,72,74] Bromley[4-72] developed an expression to describe the laminar conductive flow of heat energy from a horizontal tube to a stagnant fluid environment. The expression takes the form

$$h = C \left[\frac{g \rho_g k_g^2 (\rho_f - \rho_g) h'_{fg} C_{pg}}{Pr_g (T_w - T_s) d} \right]^{1/4}, \qquad (4\text{-}86)$$

where h'_{fg} is a correction factor to the heat of vaporization, h_{fg}, to additionally include the approximate energy absorbed by the vapor surrounding the tube. Bromley took this additional energy to be described by the arithmetic average temperature of the vapor. Thus,

$$h'_{fg} = h_{fg} + 0.5\, C_{pg} (T_w - T_s) \quad . \qquad (4\text{-}87)$$

The rod diameter is d. The constant C was determined analytically by the solution process, with values depending on the slip assumption for the vapor-liquid interface. However, a value for C was also determined from fitting data. The value adopted is C = 0.62. Data were taken as described below.[a]

Carbon tube diameter	-	0.63, 0.95, 1.27 cm
Stainless steel tube diameter	-	0.476 cm
Pressure	-	atmospheric
Fluids	-	water, nitrogen, n-pentane, benzene, carbon tetrachloride, and ethyl alcohol.

The water data were somewhat overpredicted.

Essentially all the data were correlated within ±18%. The conductive portion of the total experimental heat flux was obtained by calculating and subtracting a radiation component based on a parallel plate model using an appropriate wall and liquid emissivity (not stated).

Berenson[4-73] performed a hydrodynamic stability analysis for laminar film boiling above a flat plate. A solution was obtained for the most dangerous wave length resulting in instability. The form of the solution was similar to that of Equation (4-86) with the differences

$$d = \left[\frac{\sigma}{g\,(\rho_f - \rho_g)}\right]^{1/2}$$

---

a. Data tables are on file with the American Documentation Institute, Washington, D.C.

and

$C = 0.425$.

The d and the bracketed term were observed to be characteristic lengths for film boiling on a horizontal tube and a horizontal flat plate, respectively.

Breen and Westwater[4-74] compared data to Equation (4-86) and observed film boiling flow patterns. They determined that heat transfer from horizontal tubes in a stagnant fluid pool could be characterized by the ratio of the minimum critical hydrodynamic wave length, λ_{mc}, to the tube diameter.

$$\text{If } \frac{\lambda_{mc}}{d} < 0.8, \text{ where } \lambda_{mc} = 2\pi \left[\frac{\sigma}{g\,(\rho_f - \rho_g)}\right]^{1/2}, \qquad (4\text{-}88)$$

the heat transfer rate exceeded that given by Equation (4-86). This limit marked the departure from viscous vapor flow and a smooth liquid-vapor interface to turbulent vapor flow and a wavy interface. The data considered included that from horizontal tubes with diameters ranging from 0.185 to 1.85 in. and the fluids freon-113 and isopropanol boiling at atmospheric pressure and saturation temperature.

The relationship noted between the hydrodynamic wave length and horizontal tube diameter provides a reasonable rationale for the code correlation described in the next section.

4.2.5.1.1 Conduction Model as Coded--The code model for energy transport to the vapor film is that obtained by replacing the diameter of Equation (4-86) with the minimum critical wave length, λ_{mc}, defined above. The equation is:

$$h = 0.92163 \left[\frac{(\rho_f - \rho_g)}{\sigma}\right]^{1/2} \frac{k_g^{\,3}\, \rho_g\, (\rho_f - \rho_g)\, h'_{fg}}{\mu_g\, (T_w - T_s)}^{1/4} \alpha_f \qquad (4\text{-}89)$$

where

$$h'_{fg} = h_{fg} + 0.5\, C_{pg}\,(T_w - T_s), \text{ and}$$

$$g = 9.8\ \frac{m}{s}\ .$$

Equation (4-89) includes a multiplier, α_f. This factor smooths h over the range of the α_f likely seen from an inverted annular flow pattern (high α_f) to a dispersed flow film boiling (low α_f). The equation is valid for heat transfer calculations from short vertical surfaces where the flow is laminar. The lengths for laminar flow are no more than several inches. The properties ρ_g, h_g, and C_{pg} are evaluated at the gas temperature, T_g, while μ_g and k_g are evaluated at a film temperature

$$T_{film} = (T_w + T_{sat})/2\ . \qquad (4\text{-}90)$$

4.2.5.1.2 Model Basis for Convection--As the liquid core for the inverted annular flow pattern shrinks, convection to the vapor increases and becomes the predominant heat transfer mechanism for significant flow rates. The single-phase vapor correlations previously presented in Section 4.2.2 become the model basis.

4.2.5.1.3 Convection Model as Coded--The coefficient describing the convective portion of film boiling heat transfer to the vapor is taken to be the largest of the following expressions.

h from Equation (4-59) α_g , μ in Re calculated at T_w

h from Equation (4-60) α_g , or (4-91)

h from Equation (4-64) .

To calculate the heat flux, T_g is taken to be the maximum of T_g or T_{sat}. Convection between the vapor and liquid is included in the interfacial heat transfer models.

4.2.5.1.4 Model Basis for Radiation--The radiation mechanism for heat transfer can be attributed to Sun.[4-75] The main purpose of the reference is to develop an engineering method for calculating boiling water reactor (BWR) fuel rod heat transfer to the cooling medium during emergency core cooling (ECC) top spray injection. The report presents a method for estimating the radiation energy transfer between a vapor-liquid-droplet mixture enclosed by a wall. Interchange between metal surfaces is not considered, which implies that all wall surfaces must be at equal temperatures, so no net energy transfer occurs between surfaces. The model considers the vapor-liquid mixture as an optically thin medium, which means the vapor and liquid do not self-absorb emitted radiation. Thus, the vapor and liquid may be treated as simple nodes. The "surface areas" of the liquid and vapor are both taken to be equal to the wall surface area with view factors of unity. The three "surfaces" are isothermal, radiosity is uniform, and the "surfaces" are diffuse emitters and reflectors. The radiation heat fluxes are expressed by Sun as

$$q_{wf} = F_{wf}\sigma(T_w^4 - T_s^4)$$

$$q_{wg} = F_{wg}\sigma(T_w^4 - T_g^4) \qquad (4\text{-}92)$$

$$q_{gf} = F_{gf}\sigma(T_g^4 - T_s^4) \ .$$

The subscripts wf, wg, and gf denote wall-to-liquid, wall-to-vapor, and vapor-to-liquid heat transfer, respectively. The liquid is assumed to be at the saturation temperature corresponding to the total pressure. Also

F = gray-body factor and

σ = Stefan-Boltzman constant, 5.670×10^{-8} W/m^2-K^4

The gray-body factors are defined in turn as

$$F_{wf} = 1/[R_2(1 + R_3/R_1 + R_3/R_2)]$$

$$F_{wg} = 1/[R_1(1 + R_3/R_1 + R_3/R_2)]$$

$$F_{gf} = 1/[R_2(1 + R_1/R_2 + R_1/R_3)] \quad . \qquad (4\text{-}93)$$

The R terms are given as

$$R_1 = (1 - \epsilon_g)/[\epsilon_g(1 - \epsilon_g\ \epsilon_f)]$$

$$R_2 = (1 - \epsilon_f)/[\epsilon_g(1 - \epsilon_g\ \epsilon_f)]$$

$$R_3 = 1/(1 - \epsilon_g\ \epsilon_f) + (1 - \epsilon_w)/\epsilon_w \quad . \qquad (4\text{-}94)$$

The emissivities, ϵ, are given as

$$\epsilon_g = 1 - \exp(-a_g\ L_m)$$

$$\epsilon_f = 1 - \exp(-a_f\ L_m)$$

$$\epsilon_w = 0.7 \quad . \qquad (4\text{-}95)$$

L_m is a mean path length, and a_g and a_f are vapor and liquid absorption coefficients, respectively defined as

$$L_m = D_h$$

$$a_f = X_a\ \frac{\pi\ d^2\ n}{4} \qquad (4\text{-}96)$$

where

X_a = absorption efficiency

n = droplet number density

d = droplet diameter.

The number density is

$$n = \frac{6\ G_f\ A}{\pi d^3\ \rho_f\ A\ v_f} = \frac{6\alpha_f}{\pi d^3} \quad . \tag{4-97}$$

The absorption efficiency, X_a, is 0.74 for drops of size range 0.01 to 0.2 cm diameter, where $\pi d/\lambda >> 1$ when λ is the characteristic wave length emitted by the heated wall ($\lambda = 2.3 \times 10^{-6}$ m for 1255 K).

From the above

$$a_f = \frac{1.11\ \alpha_f}{d} \quad . \tag{4-98}$$

The emissivities of water vapor and zircaloy are taken directly from references for a fixed temperature.

The author states that comparison of model calculations (which include convection from vapor to droplets) with empirical FLECHT data shows the average droplet size in FLECHT is about 0.228 cm. This average drop size corresponds well to data in the literature. Thus, it is concluded that the model predicts the thermal behavior during ECC spray cooling. The drop diameter found also shows that the fluid mixture is optically thin for the assumed conditions. No evaluation of the radiation portion of the model was made.

4.2.5.1.5 Radiation Model as Coded--The coded model applies the equations above with some changes as follows. A liquid droplet size is determined by two expressions and the minimum is selected for application. The first expression calculates an upper limit droplet size that can pass through the tube

$$d_{max} = (\alpha_f)^{1/2} D_h \ . \qquad (4\text{-}99)$$

The second expression calculates the average droplet size based on a Weber number criterion of 7.5

$$d_{ave} = \frac{We\ \sigma}{\rho_g (v_g - v_f)^2} \ , \qquad (4\text{-}100)$$

where $(v_g - v_f)^2$ may not be less than 0.005 to keep from dividing by zero.

The liquid emissivity/absorptivity is calculated using the minimum d calculated and a path length of $L_m = 0.9\ D_h$. The value used is taken to be the smaller of the calculated value or 0.75. The vapor emissivity assumed to be 0.02. The wall emissivity is assumed to be 0.9. The radiative interchange between wall and vapor and vapor to liquid is neglected.

The heat flux from film boiling is applied to post-CHF heat transfer if it is larger than the corresponding value determined from transition boiling.

4.2.5.1.6 Assessment--Equation (4-89) (omitting α_g) is valid only for an inverted annular flow pattern in a stagnant pool. The vapor film is very thin, and h is not a function of α_g. For flow situations, the film thickness grows and the liquid column shrinks, breaks into slugs surrounded by vapor, and eventually is dispersed into droplets carried with the vapor. The effective wall-to-fluid h then varies from magnitudes of ~170 W/m^2-s to values near 2000 as dispersed flow occurs.

The model [Equation (4-89)] is a minimum value. A number of factors can cause significantly higher h values. The conductive h for the inverted annular flow pattern with a thin film is affected by geometry, environmental flow, and subcooling.

Experimental film boiling work[4-76] with short vertical cylinders measuring 0.95 to 1.90 cm in diameter and 6.6 to 16.5 cm in length in stagnant organic fluid pools yielded results with marked deviation from results predicted by Equation (4-86). The heat transfer rates were two to four times larger and exhibited a different trend. An analytical model[4-77] was developed, assuming a viscous vapor flow beginning at the cylinder lower edge, with a transition based on a critical Re to a turbulent vapor flow pattern and a wavy phase interface. The analytical model was compared to data for methanol, benzene, carbon tetrachloride, nitrogen, and argon for the cylinder lengths stated previously. The data scatter was within ±32%.

Investigation[4-78] for the effect of upward crossflow over a horizontal tube determined that the heat transfer coefficients were larger when the ratio of the liquid velocity to the square root of the (diameter · g) product was larger than two. For example, the heat transfer rate would be double for a 1-in. horizontal tube with no crossflow if

$$\frac{v_f}{(gd)^{1/2}} > 4 \, . \qquad (4\text{-}101)$$

Fluids investigated were benzene, carbon tetrachloride, ethyl alcohol, and n-hexane.

The effect of subcooling was also investigated[4-79] for a horizontal tube with upward cross flow. Increases of 20% to 300% were determined as a function of flow velocities (1-4 m/s) as subcooling was increased from zero

to 40 K with the four fluids used in Reference 4-78. Reference 4-80 provides a specific correction factor for the subcooled liquid in inverted annular flow.

Other factors that increase the h of Equation (4-89) include flow direction, grid spacers, and entrance effects.

The application of Equation (4-89) to liquid droplets in a slug flow or dispersed flow regime has no basis. The trend of the magnitude is likely correct, but the magnitude calculated needs testing.

The lack of a vapor-to-liquid heat transfer mechanism ensures non-equilibrium between the phases.

An erroneous value of the Stefan-Boltzman constant, ($\sigma = 1.3 \times 10^{-8}$), is coded. The general reason for modifying the constant was to give better comparisons with data during developmental assessment. Specific reasons were not identified.

The emissivity of zircaloy is a function of the oxide layer thickness. A value of 0.7 is obtained almost instantaneously after exposure to steam.[4-81] The emissivity value for vapor (0.02) is an approximation for pressures during reflood and is far too low for high pressure (with values of ~0.05-0.15). Implementing a correlation for vapor emissivity as used in TRAC-BD1[4-82] would be appropriate.

If the radiative transfer from the wall to the liquid is significant, the components of wall to vapor and vapor to liquid should be included. The magnitudes are only certainly small during reflood.

The basis for the Weber number for liquid droplet size has not been resolved. The hydrodynamic calculations in the code are based on a maximum value of 3 for dispersed flow.

The radiation model does not apply to inverted annular flow likely present at low vapor void fractions.

The effective liquid droplet emissivity in a scattering regime is not limited to a value of 0.75. The 0.75 value would apply to the liquid wall present during inverted annular flow.

Bennett's and Chen's heated tube experiments were used to compare calculated results under post-CHF conditions during developmental assessment. The results are discussed in References 4-12, 4-20, and 4-83.

At intermediate to high mass flow rates and low qualities, the heat transfer to dispersed flow can be represented by a single correlation. This eliminates the need for interfacial heat transfer (vapor to liquid) and radiation heat transfer. The correlation of Delorme and Groeneveld[4-84] has compared well with data based on a wide range of flow rates qualities, heat fluxes, and pressure above 1000 psia. An evaluation[4-85] of many correlations for dispersed flow indicates that they cannot be applied with good accuracy beyond the data range for which they are developed. Other more recent work[4-86] has tested new tubular data against several correlations. The scope of the comparisons was very limited and prevents comparison with Reference 4-85.

4.2.5.1.6 Scaling Considerations--There are no scaling considerations of concern.

4.2.5.1.8 Summary and Conclusions--The low end of h values is correctly represented. However, the effect of many parameters which tend to increase h is not included. The addition of a convection heat transfer contribution provides additional heat transfer, but the effect has not been quantified. At high flow rates and low qualities, a single correlation would be sufficient and would provide a better basis. Radiation to dispersed flow is not needed except for low flow rates and high surface temperatures.

The radiation heat transfer model is valid only for dispersed flow. Another model assuming a cylindrical liquid core is needed for inverted annular flow. The flow regime assumed should be consistent with hydrodynamic calculations. The radiant heat transfer from wall to vapor and vapor to liquid should be added to the solution. Other corrections are needed (Stefan-Boltzman constant, ϵ_{max} limitations, a good emissivity value for a high-temperature liquid surface).

The code model for film boiling does not have sound technical basis.

4.2.6 Correlations for Critical Heat Flux

The CHF routines consist of two correlations, one for a high flow rate and one for a very low flow rate.

4.2.6.1 High-Flow-Rate CHF Correlation

4.2.6.1.1 Model Basis--The correlation was developed by Biasi[4-71] and consists of two equations, one for high quality and one for low quality. The equation that calculates the larger heat flux is selected for application. The equations are

$$q_{CHF-B} = \frac{1.883 \times 10^7}{D_h^n G^{1/6}} \left[\frac{f(P)}{G^{1/6}} - X_e\right] \quad (4\text{-}102)$$

for the low-quality region, and

$$q_{CHF-B} = \frac{3.78 \times 10^7 h(P)}{D_h^n G^{0.6}} [1-X_e] \quad (4\text{-}103)$$

for the high-quality region,

where

$$n = \begin{cases} 0.4, \text{ for } D_h \geq 1 \text{ cm} \\ 0.6, \text{ for } D_h < 1 \text{ cm} \end{cases}$$

$$f(P) = 0.7249 + 0.099\ P\ e^{(-0.032P)}$$

$$h(P) = -1.159 + 0.149\ P\ e^{(-0.019P)} + 8.99P/(10 + P^2)$$

P = pressure (bar).

The equations were developed by fitting data over the following parameter ranges:

Data points	-	4551
Geometry	-	inside circular tubes
Diameter	-	0.3 to 3.75 cm
Length	-	0.20 to 6.00 m
Pressure	-	0.27 to 14.0 MPa
Mass flow rate	-	100 to 6000 $\frac{kg}{m^2\text{-}s}$
Equilibrium quality at CHF	-	$\frac{1}{1 + \frac{\rho_f}{\rho_g}}$ to 1
Axial power distribution	-	uniform .

The accuracy of the correlation is stated to be 0.1% for the average error (algebraically determined) and 7.25% for the standard deviation. 85.5% of all data points were within 10% of the correlation.

The correlation has been compared to additional data banks by several workers. Reference 4-87 compares the predictions of the correlation to some 15,000 data points. The range of data in the bank (Reference 4-87) is seen in Figure 4-17.

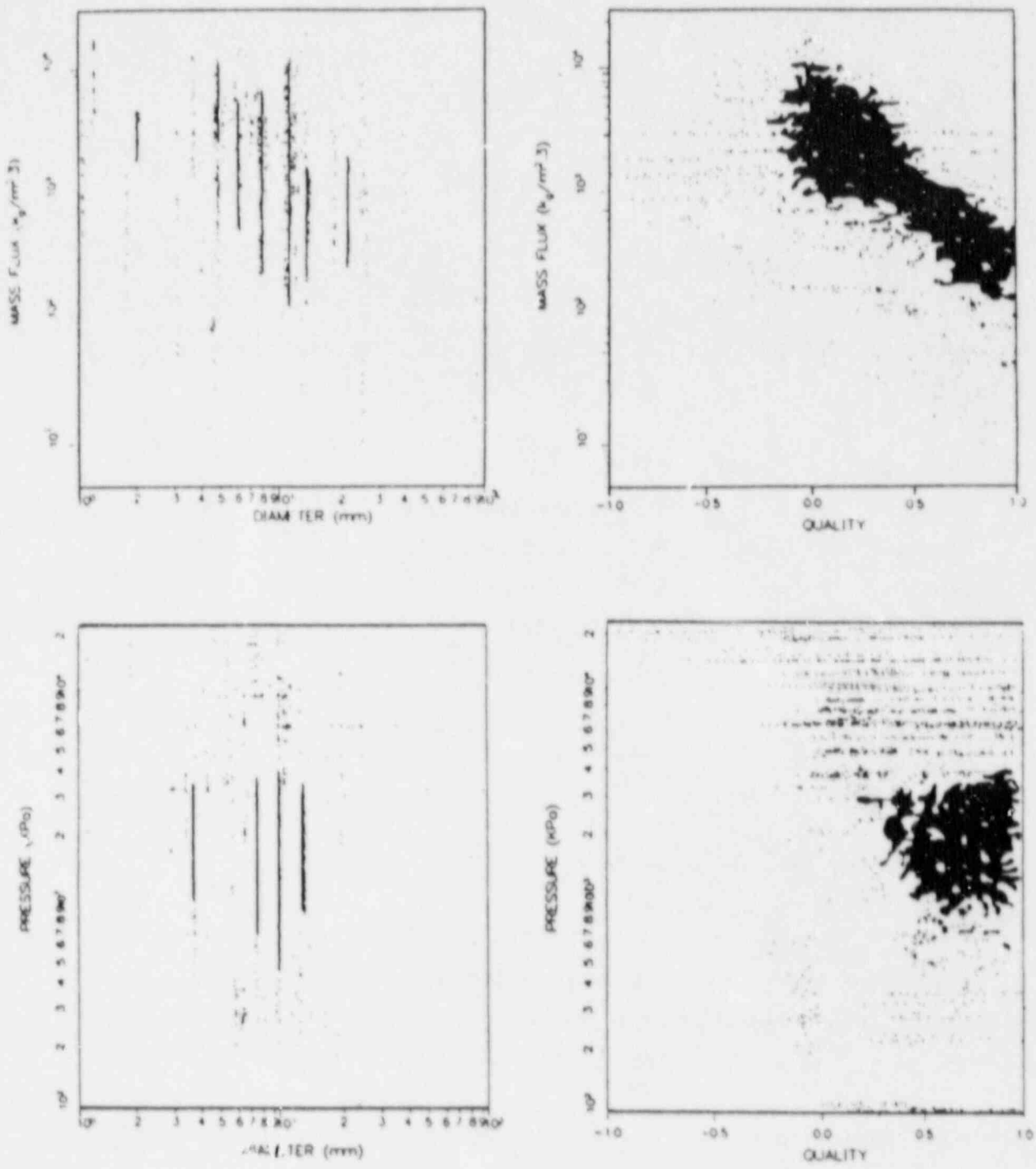

Figure 4-17. Range of CHF tube data.

The comparison is tabulated in Table 4-7. The correlation is compared to two sets of data, (a) all the data bank and (b) data over which the correlation was developed. The data were compared by specifying the quality at CHF or the inlet subcooling for the data point. The comparison indicates that the Biasi correlation[4-71] is reasonably good in calculating CHF where the equilibrium quality is well known at the location of interest, that is by computation for constant inlet conditions and X determined by heat balance. Where the local condition X is specified, the correlation-data comparison indicates considerably more scatter.

The Biasi correlation has also been compared to 1928 round-tube data points from the Harwell data bank.[a] Essentially all the data fell with +40% to -50% of the correlation. The average error was -8% and the standard deviation was 17%.

The correlation has also been compared to data from another source.[4-88] The data are characterized by the following parameter ranges:

Data points	-	177
Geometry	-	inside circular tube
Flow direction	-	vertical upflow
Diameter	-	1.49 cm
Length	-	7.0 m
Inlet subcooling	-	10 ± 3 K
Pressure	-	3.0 to 15.0 MPa
Mass flux	-	500 to 3000 kg/m^2-s
Heat flux	-	1×10^4 to 125×10^4 W/m^2 .

The data are within the parameter range upon which the correlation was based. The mean error between the measurement and the calculation (using

---

a. G. F. Hewitt, "Critical Heat Flux Discussion", NRC Experts Meeting on Thermal-Hydraulic Correlations, Silver Springs, Maryland, (Harwell, unpublished), March 28-29, 1986.

TABLE 4-7. BIASI CORRELATION COMPARED TO CHALK RIVER DATA BANK

	Data Within the Error Bound (%)						
	Constant Dryout Quality			Constant Inlet Subcooling			No. of Data Points
	±10%	±20%	±50%	±10%	±20%	±50%	
All data	19.30	36.64	67.04	71.23	92.38	99.39	14401
Validity only	21.32	41.12	73.04	77.60	96.60	99.91	9936

RELAP5/MOD2) was -60.8%, the negative value indicating that the correlation calculation was higher than the measurement. The reason for the discrepancy was not identified.

4.2.6.1.2 Model as Coded--The model is coded as expressed by Equations (4-102) and (4-103), except as modified and discussed below.

The minimum pressure limit for which the correlation was tested (2.7 bar) is the minimum used in the coding.

The correlation is applied whenever the mass flux is equal to or greater than 200 kg/m^2-s. For G > 300 kg/m^2-s, the maximum of Equation (4-102) or (4-103) is applied. For G < 300 kg/m^2-s, the high quality correlation, Equation (4-102), is applied.

If 100 < G < 200 kg/m^2-s, a linear interpolation with mass flux is performed, with the q_{CHF} value obtained from the low-flow correlation (modified Zuber) described in Section 4.2.4.2. The functional relationship for the interpolation is

$$q_{CHF} = q_{CHF-Z} + \left(\frac{G-100}{100}\right)\left(q_{CHF-B} - q_{CHF-Z}\right) \qquad (4\text{-}104)$$

where

q_{CHF-Z} = CHF evaluated by modified Zuber correlation,

100 < G < 200 kg/m^2-s.

4.2.6.1.3 Assessment--The correlations have been extensively reviewed and evaluated in Reference 4-89. Some of that review is repeated here. The equation is based only on the local conditions at the location of concern. Local condition correlations are not as well-founded as correlations based on history effects; however, appropriate history effects based on length or inlet conditions are difficult to ascertain during transients or flow reversals.

The correlations are stated to be primarily valid for predicting a high quality dryout dispersed flow pattern as opposed to a low quality flow pattern where an intermittent vapor film limits the bulk liquid contact with the wall. The correlation also exhibits an inverted mass flux effect, where the calculated CHF decreases with increasing mass flux.

Comparison[4-87] with other correlations and CHF tables has shown that more accurate methods are available. Factors have also been defined that will correct predictions based on round-tube data for a standard condition for application to rod bundles and other more general conditions.

The potential error in a local condition hypothesis has been illustrated. Differences in q_{CHF} significantly larger than 50% have been noted for cosine axial heat flux distributions as compared to uniform axial distributions in tubes and annuli.

4.2.6.1.4 Scaling Considerations--There are no considerations of size alone.

4.2.6.1.5 Summary and Conclusions--The correlation prediction should be considered an approximation to the CHF. More accurate methods are available but will be difficult to implement. Therefore, the importance of the CHF prediction to the calculational result must be determined to assess the adequacy of the approximation.

4.2.6.2 Low-Flow-Rate CHF Correlation

4.2.6.2.1 Model Basis--The correlation is based on an analytical development of Zuber et al., for horizontal pool boiling of a saturated liquid[4-90] on a flat plate. The correlation is of the form

$$q_{CHF} = 0.131\, h_{fg}\, \rho_g^{1/2}\, [\sigma g(\rho_f - \rho_g)]^{1/4} \quad . \qquad (4\text{-}105)$$

The correlation was compared to data attributed to Borishanski.[4-91] The data consisted of 117 points for water, benzene, ethanol, pentane, heptane, and propane. The accuracy of the data comparison was not evaluated. However, observation of a plot in Ref. 4-90 would indicate an error band of about +55% to -23%.

The analysis for flat plate geometry was extended to the interior of vertical tube geometry.[4-92] A multiplier of 0.9 was added to Equation (4-105).

The correlation was also compared to low-flow-rate freon CHF data inside a tube.[4-70] Upflow, downflow, countercurrent flow and flow reversal data were used. It was found that the data could be correlated by multiplying Equation (4-105) by $(1 - \alpha_g)$. The vapor void fraction was obtained from a drift flux model.

4.2.6.2.2 Model as Coded--The model as coded is Equation (4-105) with the $(1 - \alpha_g)$ multiplier subject to the changes noted below. The 0.9 suggested multiplier is not used.

The correlation is applied to low-flow-rate situations where $G < 200$ kg/m^2-s. For $100 < G < 200$ kg/m^2-s, a linear interpolation with the mass flux, G, is made using the low-flow and high-flow correlations as previously explained in Section 4.2.4.1. When $G < 200$ kg/m^2-s and the flow regime model has determined that vertically stratified flow exists between vertically adjacent cells, a functional relationship is applied to the low-flow CHF correlation in the lower cell. The criteria for stratified flow are met whenever the product of the average fluid density, ρ, and the Taylor bubble rise velocity is larger than the total mass flux, that is, when $\frac{G}{\rho v_{TB}} < 1$. This test is performed in the hydraulic sections of the

code. The functional relationship, M_z, replaces the $(1 - \alpha_g)$ quantity and increases the effective cell area fraction to which the low flow critical heat flux is applied. The functional relationship is expressed as follows:

$$\frac{2}{3} \leq \frac{G}{\rho v_{TB}} \leq 1 \qquad M_z = 1 - 3\left(\frac{G}{\rho v_{TB}} - \frac{2}{3}\right)(1-\alpha_f)$$

$$\frac{G}{\rho v_{TB}} < \frac{2}{3} \qquad M_z = 1 \,. \tag{4-106}$$

The relationship is shown in Figure 4-18.

4.2.6.2.3 Assessment--The application of the Zuber low-flow correlation to a stratified flow pattern does not have a sound physical basis. In particular, the weighting factor, M_z, should be reviewed. Comparison with Harwell tubular low flow rate has been accomplished and is awaiting publication. Results are not currently available. Some assessment with RELAP5/MOD2 calculations is discussed in Section 4.2.6.3.

4.2.6.2.4 Scaling Considerations--Size scaling is not a concern.

4.2.6.2.5 Summary and Conclusions--Limited data are available to assess application to reactor conditions and geometry.

4.2.6.3 Integral Assessment of the Transition Boiling Film Boiling, and CHF Correlations. The post-CHF correlations in the RELAP5/MOD2 code (transition and film boiling wall-to-coolant heat transfer) have received limited assessment. The post-CHF heat transfer correlations are heating derived from uniformly heated tube data obtained for steady-state conditions. Extension of these correlations to tube bundle geometries with non-uniform heating represents application outside the range of the original data base, as noted in the sections addressing the individual correlations.

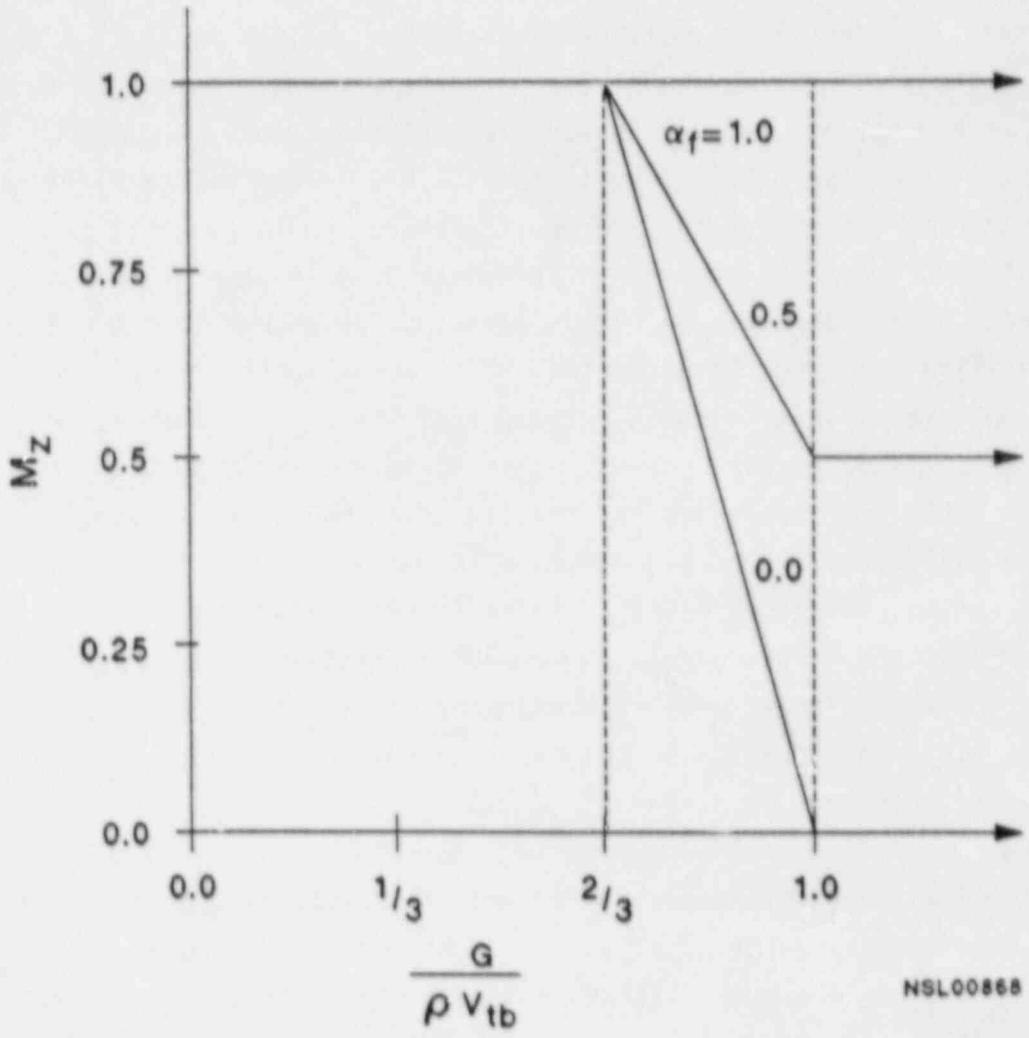

Figure 4-18. Low flow rate CHF multiplier as a function of α_f, volume cell mass flux, and Taylor bubble velocity.

Figure 4-19 presents the results of a steady-state, post-CHF heat transfer experiment, as described in Reference 4-93. The figure demonstrates the progression of the heat transfer processes from nucleate boiling low in the test section to the point of CHF marked by a rapid increase in wall temperature. Following the rapid increase of temperature characteristic of transition boiling (considerably larger wall superheat required to transfer the heat flux input to the wall), the wall temperatures stabilized and actually began to decrease as the required wall superheat is established. The decreasing wall temperature may reflect an increasing heat transfer coefficient regime downstream of the CHF point. Reference 4-94 presents an assessment study by Sjoberg specifically addressing the capability of the RELAP5/MOD2 code to predict CHF in a separate-effects facility and the subsequent post-CHF heat transfer. The range of experimental data for the studies in Reference 4-94 invoked the Biasi correlation in the calculations. Base-case results showed that the Biasi CHF correlation consistently predicted CHF to occur downstream of the observed location These results suggest that the correlation may be nonconservatively predicting CHF at higher fluid quality than that observed. Table 4-8 summarizes the results of calculations of measured data for several CHF correlations and agrees with the stated conclusion of non-conservatism (Reference 4-95). The table also shows that for the specific study, the Biasi correlation produced relatively good results compared to other correlations. Sjoberg provided a code update that fixed CHF at the observed elevation in the facility and proceeded to evaluate the post-CHF heat transfer correlations.

Figure 4-20 shows typical measured and calculated axial temperature profile comparisons for the cases with the CHF location fixed at the observed location. These results suggest that the transition and film boiling correlations are duplicating the phenomena observed. The study points out that the calculated wall-to-coolant heat flux was overpredicted at high-pressure conditions (10 MPa) (note the lower post-CHF wall temperature relative to the measured temperature profile); and, conversely, the heat flux was underpredicted for lower-pressure conditions (7 MPa). This study was for an in-tube flow condition.

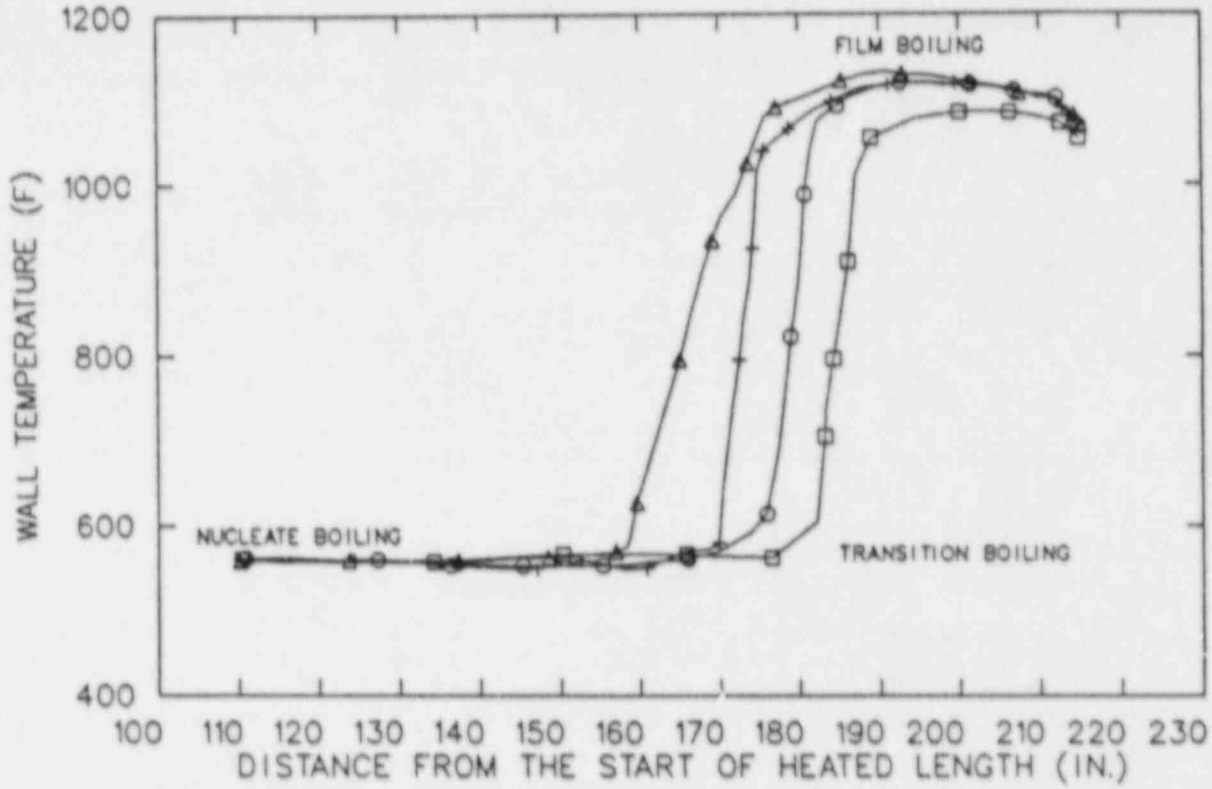

Figure 4-19. Steady-state post-CHF heat transfer experimental results.

TABLE 4-8. COMPARISON OF CRITICAL HEAT FLUX CORRELATIONS

Test	TE Height (cm)	DNB - Time Delay (s)								
		Measurement	Mod. Zuber	W-3	Slifer	Smolin	B-W-2	Macbeth	Biasi	Tong	Thorgerson
DNB-1	135	No DNB	2.6	--	--	--	--	--	--	--	--
	190	No DNB	0.7	0.65	--	--	0.7	1.2	--	0.92	0.4
	259	0.7	0.6	0.45	--	--	0.52	0.8	0.9	0.75	0.4
	327	0.4	0.5	0.2	1.1	1.1	0.4	0.6	0.6	0.8	0.4
	377	0.7	0.5	0.1	1.15	1.15	0.3	0.68	0.6	--	0.4
DNB-3	135	No DNB	0.8	0.7	1.5	1.5	0.7	1.0	1.4	--	0.38
	190	No DNB	0.65	0.5	1.2	1.2	0.65	0.84	1.0	0.64	0.38
	259	0.45	0.5	0.35	1.0	1.0	0.4	0.8	0.7	0.57	0.34
	327	0.2	0.4	0.15	0.85	0.85	0.25	0.55	0.46	0.63	0.34
	377	0.5	0.4	0.1	0.8	0.8	0.2	0.62	0.5	--	0.3
DNB-7	135	No DNB	2.3	--	--	--	--	--	--	--	--
	190	No DNB	0.8	0.65	--	--	0.8	1.4	--	--	0.6
	259	0.7	0.65	0.5	--	--	0.7	0.9	0.9	0.8	0.5
	327	0.5	0.55	0.35	1.5	--	0.4	0.65	0.65	0.8	0.4
	377	0.7	0.6	0.4	1.45	1.45	0.4	0.75	0.65	--	0.4
DNB-8	135	No DNB	1.1	0.65	--	--	--	--	--	--	--
	190	No DNB	0.8	0.6	--	--	0.82	0.93	1.2	0.85	0.8
	259	0.6	0.65	0.45	1.2	1.2	0.6	0.85	0.85	0.7	0.5
	327	0.5	0.55	0.4	0.95	0.95	0.45	0.75	0.7	0.75	0.4
	377	0.6	0.6	0.4	1.0	1.0	0.4	0.8	0.6	--	0.4
DNB-9	135	No DNB	0.9	0.85	--	--	--	--	--	--	--
	190	No DNB	0.75	0.65	1.3	1.3	0.75	0.9	1.2	0.8	0.8
	259	0.7	0.65	0.5	1.1	1.1	0.6	0.8	0.85	0.7	0.5
	327	0.5	0.55	0.4	1.0	1.0	0.5	0.75	0.7	0.78	0.4
	377	0.6	0.6	0.45	1.0	1.0	0.5	0.8	0.65	--	0.4
DNB-11	135	No DNB	2.0	--	--	--	--	--	--	--	--
	190	No DNB	1.5	1.6	3.2	3.2	1.7	1.9	1.8	1.5	1.5
	259	1.2	1.25	1.25	1.45	1.45	1.35	1.5	1.5	1.4	1.5
	327	0.9	1.2	1.2	1.75	1.75	1.3	1.45	1.5	1.5	1.2
	377	1.0	1.2	1.2	1.7	1.7	1.3	1.5	1.4	--	1.2

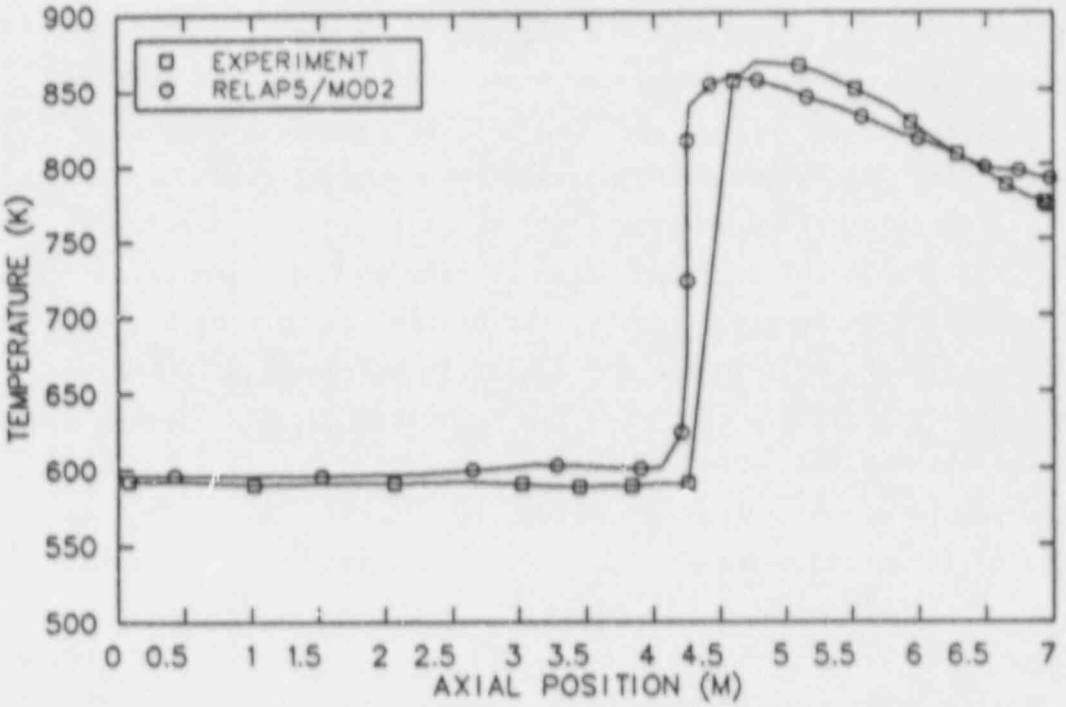

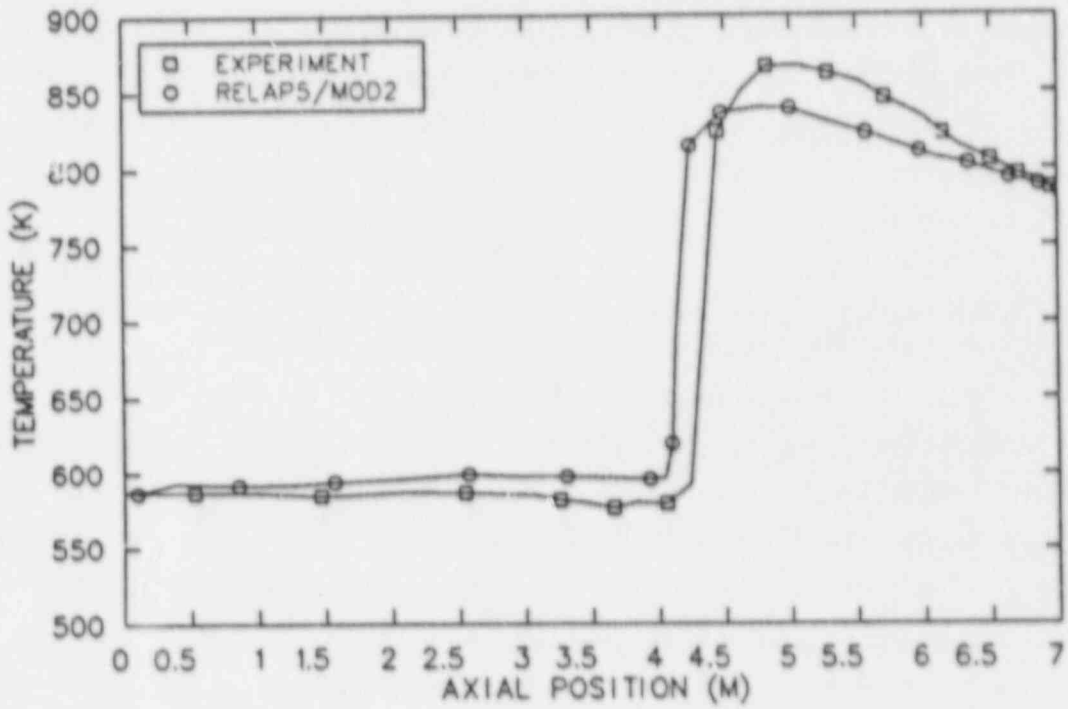

Figure 4-20. Typical measured and calculated axial temperature profiles.

Eriksson[4-96] performed an assessment in the FIX-II facility which contains a rod bundle core simulator. This study addresses the low-flow CHF correlation (Zuber) in RELAP5/MOD2 and the application of the post-CHF correlations to the rod bundle configuration. First, relative to the low-flow CHF correlation in the code, the results show that CHF was calculated to occur at higher fluid quality then was observed. This result is similar to those observed for the Biasi correlation as reported by Sjoberg.[4-94] Although CHF occurred later in time in the calculation (Figure 4-21a), the temperature rise of the heater rod surface suggests that the heat flux from the wall to the coolant is in agreement with that occurring in the experiment. Figure 4-21b indicates (as did Sjoberg's work) that at lower system pressure (3 MPa) the calculated heat flux for the upper core region may be slightly underpredicted, as evidenced by a slightly higher rate of temperature increase in the calculation.

The cited references suggest a capability of RELAP5/MOD2 to accurately predict post-CHF heat transfer phenomena. The observation is also that the CHF correlations for low and high mass flux conditions predict CHF to occur at higher fluid quality than observed in experiments, which indicated the possibility for obtaining nonconservative results. Verification of the analysis leading to the above conclusions is currently being performed and may result in changes to the conclusions drawn.

4.2.7 Correlations for Condensation (Modes 10 for $\alpha_g = 1$ and 11 for $\alpha_g < 1$)

The condensation heat transfer routines consist of three correlations that were analytically derived for specific situations. The correlations are for (a) laminar film condensation on an inclined plane, (b) laminar film condensation inside a horizontal tube with a stratified liquid surface, and c) turbulent film condensation inside a vertical tube. To provide smoothing, the correlations are weighted by void fraction over the potential range of flow conditions; and a void fraction weighted convection component is added to the condensation component to determine the total heat transfer coefficient.

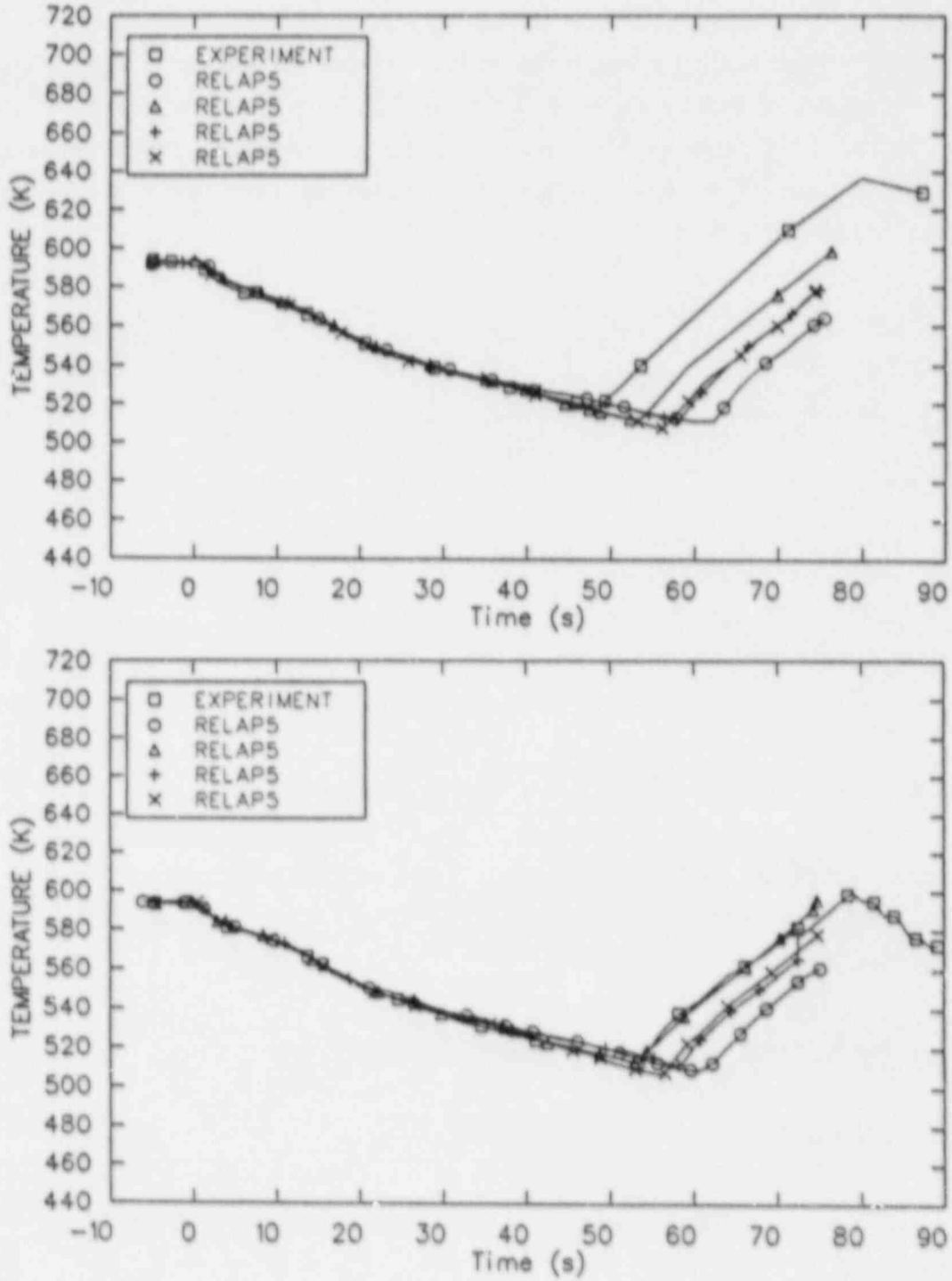

Figure 4-71. Measured and calculated cladding temperature response.

4.2.7.1 Correlation for Laminar Film Condensation for an Inclined Surface.

4.2.7.1.1 Model Basis--The original work was accomplished by Nusselt[4-97] as presented by Collier.[4-98] The correlation for the average laminar film condensation heat transfer coefficient (over the entire length where a laminar film exists) on the top of an inclined flat surface or vertical flat surface is of the form

$$h = 0.943 \left[\frac{\rho_f (\rho_f - \rho_g) g \sin \theta h_{fg} k_f^3}{\mu_f l (T_i - T_w)} \right]^{1/4} \qquad (4\text{-}107)$$

where

l = length of surface

T_i = vapor-liquid interface temperature

$\sin \theta$ = angle of surface from horizontal.

Assumptions in the analysis for the top of an inclined surface include:

1. Constant fluid properties,
2. Vapor exerts no drag on liquid surface,
3. Liquid subcooling is neglected,
4. Momentum changes in the liquid film are negligible, and
5. The heat transfer is by conduction through the liquid film.

The application of the equation may be extended to the exterior/interior of a vertical tube if the film thickness is small compared to the tube exterior/interior diameter.

Further analytical developments in the original work, as summarized by Collier,[4-98] are included. The effect of subcooling and nonlinear temperature distribution was added by modifying the latent heat of vaporization[4-99] as follows:

$$h'_{fg} = h_{fg} + 0.68\, C_{pf}\, (T_i - T_w) \quad . \tag{4-108}$$

Others[4-100,101] have considered the effect of interfacial drag. This effect is small if Pr = 1.0. Variation of the typical properties has been considered and could be treated by using an effective film temperature

$$T_{film} = T_w + F\, (T_i - T_w) \quad , \tag{4-109}$$

where

$$F = 0.25^{(4-94)} \text{ or } 0.31^{(4-95)}.$$

4.2.7.1.2 Model as Coded--No analytical improvements have been incorporated. The model in the code is Equation (4 107) modified as described below. Sin θ is replaced by the fluid volume elevation rise over the length of the horizontal projection. The length of the surface is taken as the cell length. Gravity is taken as 9.80665 m/s^2.

The liquid surface temperature at the vapor interface is taken to be the saturation temperature.

The correlation value is calculated if the cell is inclined. The value for h is applied if the numerical value obtained is larger than the value obtained from Equation (4-113) for interface shear-induced turbulent

condensation. Equation (4-113) is not considered if $v_g < 0.001$. The h value obtained is multiplied by α_g to provide smoothing over the α_g range.

If $\alpha_f > 0$, an h determined from convection heat transfer correlations is added to the condensation h. A liquid convection coefficient is computed for turbulent forced convection [Equation (4-59)], laminar forced convection [Equation (4-60)], and turbulent free convection [Equation (4-63)]. The largest of the three h values is selected and multiplied by α_f before being added to the condensation coefficient to form the total coefficient. This procedure provides smoothing over the α_f range as the fluid state changes from vapor to liquid.

4.2.7.1.3 Assessment--Application to the inside/outside surface of an inclined tube is incorrect. The analytical basis does not include liquid dropping off the top of an inside surface or the bottom of an outside surface.

The total length of the surface exposed to laminar film condensation should be applied. Using the cell length where several cells in series form the surface tends to increase the average h value. This effect is not expected to be large, though, because length affects h only to the -1/4 power.

The correlation form is not strictly valid for superheated vapor. The heat capacity between the actual and saturated temperature must be accounted for, as illustrated by Jakob.[4-102] The solution form including the superheat effect is much more complex and the change may be less than the uncertainty of the basic correlation.

The analytical improvements delineated above would improve the validity for appropriate applications.

Experiments indicate that the value can be 40-50% too low. The increased heat transfer is attributed to vapor velocity and ripples changing the film thickness, or turbulence. Collier[4-98] recommends that the computed value be increased by 20%. Note that the length approximation mentioned above serves to increase the calculated value of h.

The correlation is valid only after a film has been established and is not a function of the vapor void coefficient. The effect of the α_g factor decreases an already too small coefficient. From a strictly heat transfer point of view, this relationship should only be applied for smoothing over the proximity of the entrance section.

The coefficient is not a function of liquid convection mechanisms. However, the addition of a liquid-based forced or free convection provides smoothing over an exit section when the film thickens, thereby reducing conduction. The liquid convection component also increases the magnitude of the total coefficient, which is recognized as being too small. The correlation is valid only for a laminar film. Transition to turbulent film condensation is known to occur, and other correlations are available for a turbulent film.

4.2.7.1.4 Scaling Considerations--No scaling considerations are of concern.

4.2.7.1.5 Summary and Conclusions--The addition of a convection component, the smoothing technique, and correlation selection logic of applicability should be reexamined to determine the appropriateness of the approximations introduced compared to the needs for condensation correlations in typical applications to reactor conditions and geometry.

The application of the cell length instead of the surface length is expected to be a relatively small effect compared to other uncertainties in the condensation model.

4.2.7.2 Correlation for Stratified Flow Inside a Tube.

4.2.7.2.1 Model Basis--The correlation is a modification[4-103] to the development of Nusselt[4-97] for laminar condensation on the outside of a horizontal tube. It is assumed that the liquid film collects on the upper surfaces, drains to the tube bottom, and collects with negligible vapor shear. The condensate drains out one end because of a hydraulic gradient.

The correlation takes the form

$$h = F \left[\frac{\rho_f (\rho_f - \rho_g) g h'_{fg} k_f}{D_h \mu_f (T_g - T_w)} \right]^{1/4} . \qquad (4\text{-}110)$$

The F term corrects for the liquid level in the tube bottom with the form

$$F = (1 - \frac{\phi}{\pi}) F' . \qquad (4\text{-}111)$$

The angle 2ϕ corresponds to the angle subtended from the tube center to the chord forming the liquid level. The values for F' range in magnitude upward from 0.725, where 2ϕ = zero. F corrects for the condensing area fraction as well as the heat transfer coefficient. The development[4-103] indicates that a value of 0.296 for F is an average value appropriate for free flow from a horizontal tube, with the liquid level controlled by the critical depth at the exit.

The angle 2ϕ changes if the tube drains because of inclination or fills up because of a pressure gradient. The angle is determined from

$$\alpha_f = \frac{\phi - \frac{1}{2} \sin 2\phi}{\pi} \qquad (4\text{-}112)$$

The development determined that for the parameter range of concern the bottom liquid layer was in laminar flow. The analytical work indicated that the heat transfer through the bottom layer was less than 2.5% of the total for angles of 2ϕ between 90-170^0 and was therefore neglected in the correlation.

Data were taken for the conditions as follows:

Tube material	-	copper
Tube length	-	0.718 m
Tube ID	-	1.45 cm
Fluid	-	refrigerant 113
Tube inclination		0 to 37^0
Vapor Re	-	to 35,000.

The bulk of data points were within +8 to -16% of the correlation for level flow. The author estimates an accuracy of $\pm$15% for h. The correlation was tested to an inclined angle of about 37^0 with reasonable results. It is not valid for vertical flow. The Re number limit for vapor entering the tube is 35,000.

4.2.7.2.2 Model as Coded--The model in the code is Equation (4-110) with F = 0.296 and without the correction to the latent heat of vaporization. The correlation is used unless the correlation for turbulent flow, Equation (4-113), has a larger value and unless $v_g <$ 0.001. Smoothing based on α_g and α_f and addition of a liquid convection component are applied as described in Section 4.2.7.1.

4.2.7.2.3 Assessment--The correlation completely described the heat transfer mechanism for application over the range tested. Thus, there is no basis for adding a liquid flow convection component.

The F value should be changed appropriately if the chord angle for the liquid level changes beyond the appropriate range.

4.2.7.2.4 Scaling Considerations--No scaling considerations are of concern.

4.2.7.2.5 Summary and Conclusions--The addition of correction components, the smoothing technique, and correlation selection logic should be reexamined. Additional analysis is needed to determine the distortion caused by the smoothing technique, as well as the effects introduced from the liquid convection term.

4.2.7.3 Correlation for Turbulent Film Condensation.

4.2.7.3.1 Model Basis--The primary development[4-104] results in the form

$$h = 0.065 \left[\frac{k_f \rho_f^{1/2}}{\mu_f}\right] \left[\frac{\mu C_p}{k}\right]_f^{1/2} \tau_i \frac{1}{2} , \qquad (4\text{-}113)$$

where τ_i is the interfacial shear stress given by

$$\tau_i = f_i \frac{G_g^2}{2 \rho_g} .$$

The vapor mass flux is an average value over a section of, or over a complete, condensing tube. The apparent friction factor, f_i, is assumed equal to that for a vapor flow in contact with the pipe wall. The Blasius expression[4-98] for f_i is

$$f_i = \frac{0.079}{Re_g^{1/4}} . \qquad (4\text{-}114)$$

The gas mass flux over a length section is given in terms of the entrance and exit mass flux

$$G_g = \left[\frac{G_m^2 + G_{in}\,G_{out} + G_{out}^2}{3}\right]^{1/2} \qquad (4\text{-}115)$$

The correlation referenced is for the average h for a vertical condensing tube with downflow. The condensing tube normally has a short entrance section without a film and an exit section liquid full or nearly so. It was developed based on the observation that high vapor flow rates provided significant shear stress on the condensate film. This shear stress induced significant turbulence in the film and provided significantly enhanced heat transfer compared to correlations for a turbulent film in the presence of a near stagnant vapor. The induced film turbulence was estimated to occur at a film Re = 250 compared to Re = 2000 for films with a quasi-stagnant vapor environment.

The correlation neglects gravitational and momentum effects on the liquid film. The correlation is valid if the vapor shear forces exceed the gravitational forces on the liquid film in a vertical geometry. The correlation is not valid for turbulent film flow with film Re > 2000, in the absence of a vapor shear stress. Another simple correlation developed by Colburn[4-105] would be appropriate for a turbulent film with low Pr numbers and a neglible vapor shear stress.

Data was taken for the conditions as follows:

Geometry	-	vertical downflow
Tube material	-	copper
Tube length	-	2.53 m
Tube ID	-	1.16 cm
Fluids	-	water, methanol, ethanol, toulene, trichloroethylene

No other conditions were specified.

Comparison between data and the correlation was made.[4-104] Heat transfer effects in liquid full exit sections were eliminated in the analysis and data comparisons. Observation of the comparison shown indicates that the correlation shows the correct trend with data scattered (±40%) evenly above and below the calculation. Water data seem to be overpredicted by the correlation by ~0 to 20%. No statement concerning accuracy was made in the reference.

The effect of vapor shear was also examined analytically in Ref. 4-106. The analysis results "agree well" with Ref. 4-104 over Pr = 2 to 5 where data were taken.

4.2.7.3.2 Model as Coded--The model is coded as presented except that the code-calculated volume average gas velocity is used for the calculation.

The correlation results are applied whenever $v_g > 0.001$ m/s and the computed h is bigger than that obtained from Equations (4-106) or (4-110).

Smoothing for α_g and α_f is applied as previously described. If $\alpha_f > 0$, a liquid convective heat transfer coefficient is added to the condensation coefficient, as previously described in Section 4.2.7.1.

4.2.7.3.3 Assessment--The correlation, Equation (4-113), is based on average condensing tube behavior. It is well suited for downflow in the interior of a once-through steam generator tube including an entrance section over which the liquidfilm develops. A liquid-filled exit section should be treated separately. The correlation does not apply to U tubes with upflow, runback, or a liquid filled bend.

Picking and applying the correlation producing the biggest h value simplifies the code selection logic and ensures a continuous h, but this procedure has to be interpreted as an approximation. There is no physical basis to support choosing the largest coefficient when correlations overlap.

Additional analysis[4-107] and comparison with additional data have resulted in an improved model for a local condition h capable of handling upflow, downflow, and horizontal flow. In upflow, the correlation can predict the point of runback where the balance of gravity, momentum change, and shear forces equals zero. The correlation underpredicts (~20%) original water data[4-106] with the h range of 1140 to 5700 W/m^2-K and straddles additional water data (±30%) with the h range of 11400-57000 W/m^2-K

4.2.7.3.4 Scaling Considerations--No scaling considerations are of concern.

4.2.7.3.5 Summary and Conclusions--The basis for application of and selection among the condensation correlations in RELAP5/MOD2 is not well established. Discrepancies between development and application assumptions have been identified which can affect the calculated results from the correlations. Nonetheless, the code logic correctly recognizes when a condensation correlation is needed and implements one of the three available.

A better method[4-107] is available for calculation of local coefficients for horizontal flow, downflow, and upflow including runback. The implementation of a better condensation package should be considered in light of known code difficulties related to condensation during selected reactor transients.

4.3 Wall-to-Wall Radiation

RELAP5/MOD2 has no model that calculates wall-to-wall radiation heat transfer directly. The effects of wall-to-wall radiation are treated indirectly via heat transfer to the fluid and subsequent heat transfer from the fluid to cooler walls, but this indirect handling of the requisite energy transfer cannot be construed as a radiation model. At the present time, no pressing need to include such a model into the code has been identified.

4.4 Energy Source Term

4.4.1 Direct Power to the Fluid

Volumetric heat sources can be placed into any heat structure in RELAP5/MOD2. The power for the heat source can be determined from the reactor kinetics package that calculates the time-dependent power response or from a table or a control system. The internal power source can be partitioned by the use of three factors.

The first factor is applied to indicate the internal heat source generated in the heat structure. The other t[illegible]ctors provide for direct heating of the fluid in the hydrodynamic volume communicating with the heat structure surface. A user-specified multiplicative factor times the internal power in the heat structure is added directly to the energy source term in the associated control volume to provide the direct moderator heating. The energy transferred is partitioned between the liquid and vapor phases by means of the static quality. The sum of all the factors multiplying the source power should be unity to conserve energy in the calculation.

The direct heating model is simply a portioning of energy and is clearly applicable in any situation where the application of direct heating has been justified. No scaling dependence or uncertainties past those associated with the determination of the input are introduced by the model itself.

4.5 Wall and Interfacial Heat Transfer Partitioning

The heat transfer correlations described above are based to determine a heat transfer coefficient which relates an energy transfer rate to a temperature difference. Two distinct cases were discussed: (a) interfacial heat transfer through an assumed interface as a result of differences in the bulk temperature of the liquid and vapor phases and (b) wall heat transfer, providing energy to either the liquid or vapor phase, or both. A special case of wall heat transfer occurs when the wall is communicating with a

two-phase mixture, for then boiling or condensation can occur as a direct result of the wall heat transfer. This heat transfer is similar to the interfacial heat transfer described in (a), but it is treated separately in the code because it is not a result of differences between bulk phase temperatures. The following discussion will address the various heat transfer conditions by identifying those terms in the energy equation used to account for them and by showing the relationship of each term to the overall mass and energy balance. Because the interpretation of each of these terms in the energy equation is nontrivial, they will also be related to the heat transfer output information typically contained in a RELAP5/MOD2 major edit. The discussion to follow will address the boiling model. The condensation model is completely analagous.

4.5.1 Heat Transfer Terms in the Energy Equation

The phasic energy equations stated in Section 2.1.1, Equations (2-34) and (2-35), are

$$\frac{\partial}{\partial t}(\alpha_g \rho_g U_g) + \frac{1}{A}\frac{\partial}{\partial x}(\alpha_g \rho_g U_g v_g A) = -P\frac{\partial \alpha_g}{\partial t} - \frac{P}{A}\frac{\partial}{\partial x}(\alpha_g v_g A) \qquad (4\text{-}116)$$

$$+ Q_{wg} + Q_{ig} + \Gamma_{ig} h_g^* + \Gamma_w h_g^{\nu} + DISS_g$$

$$[I] \quad [J] \quad [K] \quad [L]$$

$$\frac{\partial}{\partial t}(\alpha_f \rho_f U_f) + \frac{1}{A}\frac{\partial}{\partial x}(\alpha_f \rho_f U_f v_f A) = -P\frac{\partial \alpha_f}{\partial t} - \frac{P}{A}\frac{\partial}{\partial x}(\alpha_f v_f A) \qquad (4\text{-}117)$$

$$+ Q_{wf} + Q_{if} - \Gamma_{ig} h_f^* - \Gamma_w h_f^s + DISS_f \, .$$

For consistency, the identification of the terms of interest here is the same as in Section 2.1.1, viz.

I	wall heat transfer
J	interphase heat transfer

K interphase latent heat

L interphase wall heat

These four terms relate the wall heat transfer to the fluid energy, and they relate each of the phases through the interfacial heat transfer. Terms I and L refer to wall heat transfer. Term I is the total wall heat transfer to the given phase, either liquid or vapor, so the sum of Q_{wf} and Q_{wg} is the total wall heat transfer to the fluid space, Q, as shown in Ref. 4-108, Equation (12). Unlike the implication of Equation (4-12) ($Q = Q_{wg} + Q_{wf}$), each term is treated in two parts in the code, one representing a convective heat transfer term to each phase without a corresponding phase change, and one representing an immediate change of phase, such as the energy required to produce subcooled boiling in the liquid phase. The association between heat and mass transfer is given in Equation (4-118) (boiling) and (4-119) (condensing).

$$\Gamma_w = \frac{-Q_{if}^w}{h_g^s - h_f^s}, \quad \Gamma_w > 0 \tag{4-118}$$

$$\Gamma_w = \frac{-Q_{ig}^w}{h_g^s - h_f^s}, \quad \Gamma_w < 0 \; . \tag{4-119}$$

This association relates terms I and L through Γ_w. It will be discussed in more detail shortly.

Terms J, Q_{ig}, and Q_{if} are interfacial heat transfer terms resulting from both bulk energy exchange due to phasic temperature differences and wall heat transfer in the form of boiling or condensing. They relate to both terms K and L, which are Γ_{ig}, the interfacial mass transfer resulting from a difference in phasic temperatures, and Γ_w, the mass transfer resulting from wall heat transfer.

The relationships among these four terms are algebraically complete and correct in the RELAP5/MOD2 code manual,[4-108] so the derivations will not be repeated here. It is useful, however, to summarize the assumptions used to determine those relationships.

1. The phasic enthalpies, h_g^* and h_f^*, associated with interphase mass transfer in Equations (4-116) and (4-117) are defined such that the interface energy jump conditions are satisfied. Specifically, $h_g^* = h_g^s$ and $h_f^* = h_f$ for vaporization, and $h_g^* = h_g$ and $h_f^* = h_f^s$ for condensation. This is tantamount to the bulk fluid being heated or cooled to the saturation condition at the interface and the phase change taking place at saturation conditions.

2. It is assumed that the summation of terms J, K, and L in Equations (4-116) and (4-117) vanishes, i.e., the sum of the interface transfer terms vanishes. Because the interface itself is not a material region, this assumption is consistent with the two-fluid model.

3. Assumption 2 is satisfied by requiring that the wall heat transfer terms associated with interface changes and the bulk exchange terms sum to zero independently.

The ramifications of these assumptions and their implementation in the code will be discussed next.

4.5.1.1 Wall Heat Transfer. Wall heat transfer is obvious in only one term in the energy equation, Q_{wf} or Q_{wg}. The code treats this in two parts, so it may be written

$$Q_{wf} = Q_{conv} + Q_{boil}, \qquad (4\text{-}120)$$

where Q_{conv} is that portion of the wall heat transfer treated as a convective heat flux and Q_{boil} is that portion which results in the subcooled or saturated boiling from the liquid phase. The division of Q_{wf} is accomplished at the time the heat transfer coefficient is calculated. Figure 4-22 shows the structure of the heat transfer calculation in RELAP5/MOD2. The heat transfer correlation calculations are performed in the subroutines CONDEN, DITTUS, PREDNB, PSTDNB, and TPAWHT, discussed in Section 4.2. Where a fraction of the heat transfer causes boiling, for example, that energy is accumulated in the variable GAMW. An example is the Chen correlation described in Section 4.2.3 and implemented in subroutine PREDNB.

Heat transfer from a heat structure to the liquid space in the adjoining control volume is calculated in two parts in subroutine PREDNB as discussed above. The convective part, Q_{conv} (QCONV in the code), is found as a volumetric energy source (energy/volume). The remainder is found as a difference between the total energy to the liquid during the time step and that portion of the total which is Q_{conv}. This difference is converted to a mass of steam (for the boiling case) by dividing by h_{fg}, the latent heat of vaporization taken at saturation conditions. A correction factor is applied to h_{fg} to include differences between code assumptions and experimental measurements as described for the individual correlation in Section 4.2. This equivalent mass of steam is stored as GAMW and eventually passed upward through the logic sequence shown in Figure 4-22 to be stored in variable GAMMAW in subroutine HTADV.

The final partitioning of phase energy takes place in subroutine HTADV and includes three terms:

Q(K) = total power delivered to a control volume K (W)

QWG(K) = power delivered to the vapor space in control volume K via heat transfer from heat structures and direct heating. Direct heating to the control volume is based on a user-input factor and quality weighting through variable QUALS(K) (W)

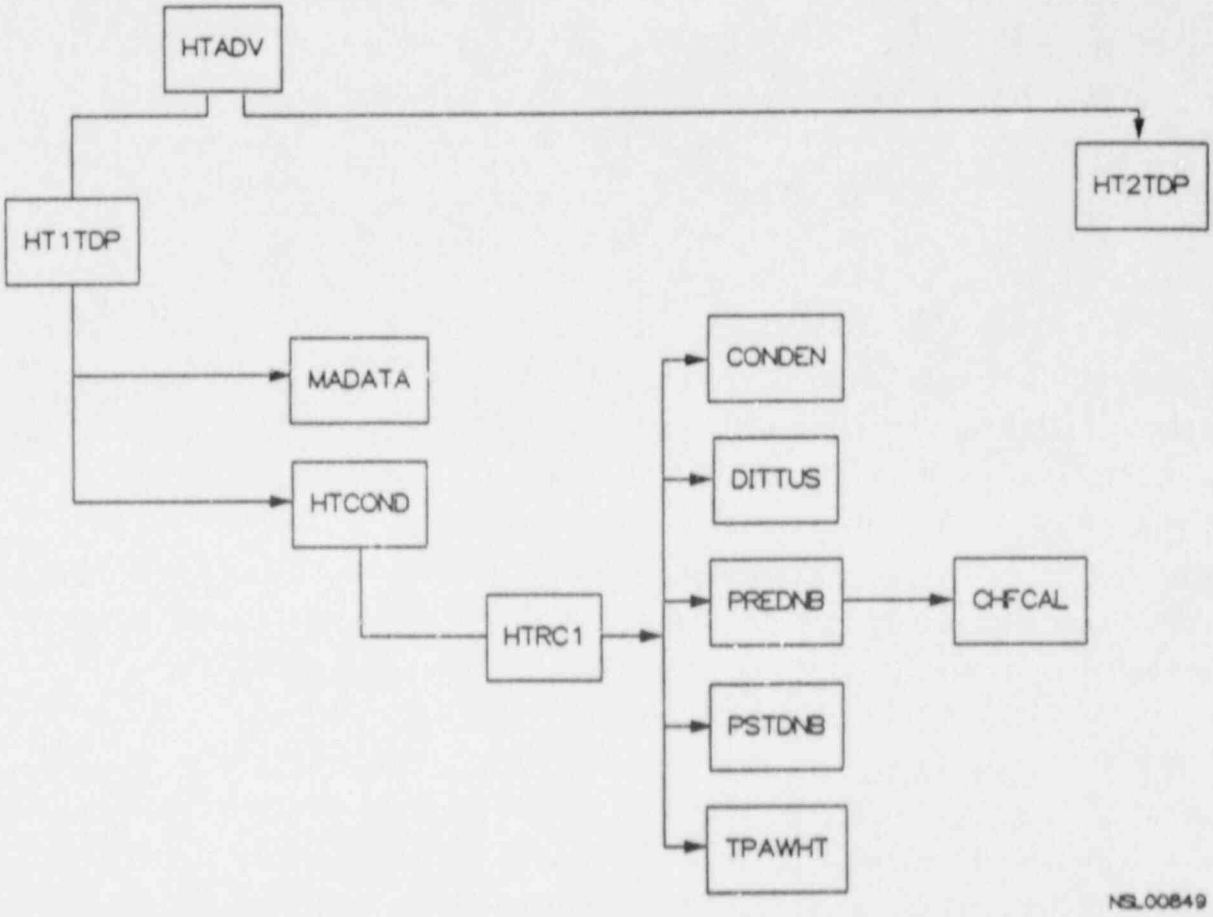

Figure 4-22. Heat transfer structure.

GAMMAW(K) = mass per unit volume transferred between phases as a direct result of wall heat transfer in the form of either boiling or condensation (kg/m^3-s)

The total energy to the vapor space in the case of boiling is the QWG + GAMMAW * conversion factor, where the conversion factor is to change GAMMAW to energy units and to incorporate the volume of the fluid space.

Note also that the calculation of GAMMAW in HTADV is tested to ensure that the phase from which the mass transfer is taken is not overdepleted. For example, a boiling condition is checked to ensure that GAMMAW does not represent a greater mass of liquid than is available to boil in 90% of the current time step. For the boiling situation,

$$\Gamma_w = \text{MIN}\left(\Gamma_w, \frac{.9\alpha_f\rho_f}{\Delta t}\right) . \qquad (4\text{-}121)$$

In the event this test shows Γ_w greater than 90% of the remaining liquid in the control volume, the value of Γ_w is reset to the 90% limiting value. A similar test is performed for a condensation calculation to allow no more than 90% of the available steam in a given control volume to condense in a single time step. This test results in less vaporization (or condensation) for a system calculation when the void fraction in a control volume is close to either zero or unity.

4.5.1.2 Bulk Interphase Heat Transfer. The relationship between interfacial heat and mass transfer is similar in the use of (h_g^* - h_f^*) to determine the mass transfer associated with the interfacial heat transfer. The code includes no specific variable to represent interfacial heat transfer. Instead, it is incorporated into the energy equation in terms of an interfacial heat transfer coefficient, H_{ig} or H_{if}, and a calculated temperature difference, (T^s - T_g) or (T^s - T_f), respectively. There is a test performed during the calculation of H_{if}, though, to estimate the liquid mass available for boiling and to adjust H_{if} downward

if the projected vapor generation (based on old time values) would exceed the available mass. A similar test is performed on the steam mass available for condensation.

4.5.1.3 Interphase Heat and Mass Transfer. The reduction of the energy equation from its basic form in Equation (4-117) (liquid phase) to the following[4-108]

$$\frac{\partial}{\partial t}(\alpha_f \rho_f U_f) + \frac{1}{A}\left[\frac{\partial}{\partial x}(\alpha_f \rho_f U_f v_f A) + P\frac{\partial}{\partial x}(\alpha_f v_f A)\right]$$

$$= P\frac{\partial \alpha_g}{\partial t} + \left(\frac{h_f^*}{h_g^* - h_f^*}\right) H_{ig}(T^s - T_g) + \left(\frac{h_g^*}{h_g^* - h_f^*}\right) H_{if}(T^s - T_f)$$

$$- \left[\left(\frac{1+\epsilon}{2}\right)h_g^s + \left(\frac{1-\epsilon}{2}\right)h_f^s\right]\Gamma_w + Q_{wf} + DISS_f \quad , \qquad (4\text{-}122)$$

from which the numerical form is derived, requires an assumption for the interface transfer terms described above. Combining the phasic energy equations, Equations (4-116) and (4-117), into a mixture form by adding results in the following collection of terms representing the total interface energy transfer:

$$Q_{ig} + Q_{if} + \Gamma_{ig}\,(h_g^* - h_f^*) + \Gamma_w\,(h_g^s - h_f^s) \qquad (4\text{-}123)$$

Assumption 2 above is a requirement that the sum of these terms vanish, i.e.,

$$Q_{ig} + Q_{if} + \Gamma_{ig}\,(h_g^* - h_f^*) + \Gamma_w\,(h_g^s - h_f^s) = 0 \quad . \qquad (4\text{-}124)$$

Assumption 3 goes on to assume further that the wall terms and bulk transfer terms vanish separately, thus,

$$H_{ig}\,(T^s - T_g) + H_{if}\,(T^s - T_f) + \Gamma_{ig}\,(h_g^* - h_f^*) = 0 \qquad (4\text{-}125)$$

and

$$Q_{ig}^{w} + Q_{if}^{w} + \Gamma_w (h_g^s - h_f^s) = 0 \qquad (4\text{-}126)$$

Equation (4-126) is rewritten in the form

$$\Gamma_w = \frac{-Q_{if}^{w}}{h_g^s - h_f^s} \quad , \Gamma_w > 0 \qquad (4\text{-}127)$$

and

$$\Gamma_w = \frac{-Q_{ig}^{w}}{h_g^s - h_f^s} \quad , \Gamma_w < 0 \qquad (4\text{-}128)$$

and is evaluated in the heat transfer correlation when boiling or condensing is calculated. The energy associated with Γ_w is never deposited in the associated fluid space, but rather is carried in the calculational scheme as a mass generation rate. The energy is accounted for in terms of Γ_w and is converted into an energy form in the energy equation itself, as seen in Equation (4-116) or (4-117). Note that the saturation enthalpy multiplying Γ_w in both phasic energy equations properly incorporates the latent heat such that the energy contribution (positive or negative) from Γ_w is correct.

The other mass transfer term arises from bulk exchange between the liquid and vapor spaces. Equation (4-126) is the essential defining equation and is rewritten as

$$\Gamma_{ig} = - \frac{H_{ig} (T^s - T_g) + H_{if} (T^s - T_f)}{h_g^* - h_f^*} \quad . \qquad (4\text{-}129)$$

The actual coding for Γ_{ig} is included in its final form in subroutine EQFINL, where the back substitution following the implicit pressure solution

is completed. Γ_{ig} is not calculated directly, but its contribution to the energy equation is determined exactly as shown above in Equation (4-129). Figure 4-23 provides an overview of the energy partitioning used in RELAP5/MOD2.

There is a significant mismatch in notation that has no impact on code calculated results, but that does cause some difficulty in understanding the results. Γ_{ig} is the mass transfer associated with bulk energy exchange, and specifically does not include any direct effects of mass transfer from wall heat transfer. Q_{if} and Q_{ig}, on the other hand, include the energy associated with both forms of mass transfer, as shown in Equation (4-130) and (4-131):

$$Q_{ig} = H_{ig} (T^s - T_g) + Q^w_{ig} \quad , \text{ and} \tag{4-130}$$

$$Q_{if} = H_{if} (T^s - T_f) + Q^w_{if} \; . \tag{4-131}$$

The sum of Q_{ig} and Q_{if} represents the net energy exchange between the phases.

Although the subroutines containing the coding used to calculate the energy equation have been mentioned in the preceding discussion, the actual coding has not been shown, nor has the logic used been discussed in detail. The reason for this is that the coding and logic are a close representation of the equations described in the RELAP5/MOD2 code manual, so no insight would be gained by a further discussion.

4.5.2 Interpreting RELAP5/MOD2 Output and the Energy Equation

Interpretation of RELAP5/MOD2 output is complicated by the multiple contributions to the various terms in the energy equations as well as the limited output available for analysis. The three variables printed in a major edit are macroscopic terms related to the entire control volume, the total wall heat transfer to the control volume, Q, the total wall heat

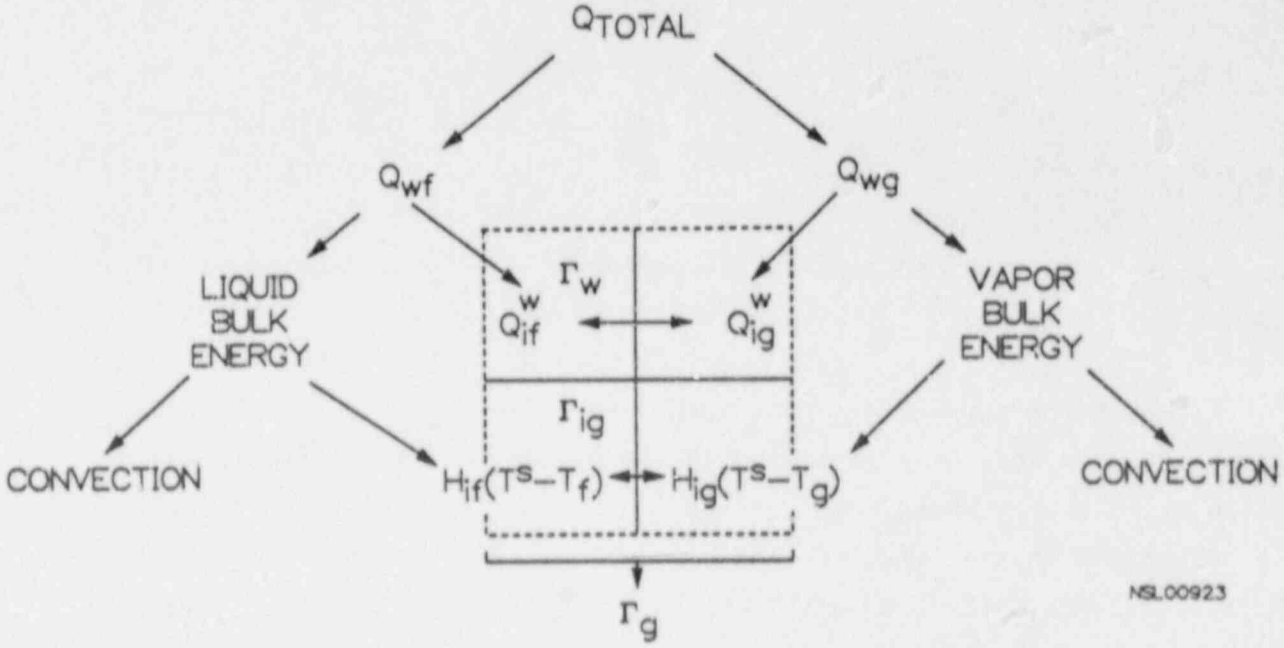

Figure 4-23. Energy partitioning in RELAP5/MOD2.

transfer to the vapor space in the control volume, QWG, and the total vapor generation, DOTM. In terms of variables discussed above, Q is straightforward and includes all wall energy from (or to) the heat structure. Q can be interpreted as consisting of two terms, QWF and QWG, the total wall energy transferred to each of the phases. These two terms include wall energy convected to the particular phase and energy associated with the mass transfer. QWG is printed in the major edits; QWF must be inferred from QWF = Q - QWG. QWF includes the convective term, noted earlier as Q_{conv}, and the Γ_w term associated with boiling. From Equation (4-118), the energy associated with Γ_w is

$$Q_{if}^{w} = -\Gamma_w (h_g^s - h_f^s) \tag{4-132}$$

Note that in this form Q_{if}^{w} is a negative contribution to the liquid phase, for the net result on the phase is a removal of mass and its internal energy. Note also that a test is performed such that a given heat structure will contribute to either Q_{if}^{w} or Q_{ig}^{w}, depending on the thermal-hydraulic conditions of the associated fluid space. but it will not contribute to both in the same time step. Thus, the energy terms for each phase in the control volumes are identified. DOTM, noted as vapor generation in the output, is the total interphase mass transfer and includes both the bulk and wall terms.

4.6 References

4-1. M. S. Plesset and S. A. Zwick, "The Growth of Vapor Bubbles in Superheated Liquids," Journal of Applied Physics, 25, 4, 1954, pp. 493-500.

4-2. J. G. Collier, Convective Boiling and Condensation, New York: McGraw-Hill Book Co., Inc., 1972.

4-3. K. Lee and D. J. Ryley, "The Evaporation of Water Droplets in Superheated Steam," Journal of Heat Transfer, ASME, November 1968, pp. 445-451.

4-4. N. Frossling, Gerlands Beitr. Geophys., 52, 1938, p 170.

4-5. W. E. Ranz and W. R. Marshall, Jr., Chem. Eng. Prog., 48, 1952, pp. 141-146, 173-180.

4-6. F. Kreith, Principles of Heat Transfer, 3rd edition, New York: Intex Educational Publishers, 1973.

4-7. G. B. Wallis, One-dimensional Two-phase Flow, New York: McGraw Hill Book Co., Inc., 1969.

4-8. S. Nukiyama and Y. Tanasawa, Trans. Soc. Mech. Engrs. (Japan), 5, 18, 1969, p. 63.

4-9. E. Kreyszig, Advanced Engineering Mathematics, 5th edition, New York, John Wiley and Sons, 1983, p 918.

4-10. M. Ishii and T. C. Chawla, Local Drag Laws in Dispersed Two-Phase Flow, NUREG/CR-1230, ANL-79-105, 1979.

4-11. D. R. Liles et al., TRAC-PF1/MOD1: An Advanced Best-Estimate Computer Program for Pressurized Water Reactor Thermal-Hydraulic Analyses, NUREG/CR-3858, LA-10157-MS, July 1986.

4-12. V. H. Ransom, et al., RELAP5/MOD2 Code Manual, Vol. 3: Develcpmental Assessment Problems, EGG-TFM-7952, December 1987.

4-13. H. C. Unal, "Maximum Bubble Diameter, Maximum Bubble-Growth Time and Bubble Growth Rate During the Subcooled Nucleate Flow Boiling of Water up to 17.7 MN/m^2," International Journal of Heat and Mass Transfer, 19, 1976, pp. 643-649.

4-14. H. Stadtke, W. Kolar, "JRC ISPRA Results from Assessment of RELAP5/MOD2 on the Basis of LOBI Test Data," Fifteenth Water Reactor Safety Information Meeting, Gaithersburg, Maryland, October 26-29, 1987.

4-15. M. Ishii and K. Mishima, Study of Two-Fluid Model and Interfacial Area, NUREG/CR-1873, ANL-80-111, December 1980.

4-16. T. G. Theofanous, "Modeling of Basic Condensation Processes," The Water Reactor Safety Research Workshop on Condensation, Silver Springs, MD, May 24-25, 1979.

4-17. L. K. Brumfield, R. N. Houze and T. G. Theofanous, "Turbulent Mass Transfer at Free, Gas-Liquid Interfaces, with Applications to Film Flows," International Journal of Heat and Mass Transfer, 18, 1975, pp. 1077-1081.

4-18. G. Brown, "Heat Transmission of Condensation of Steam on a Spray of Water Drops," Proceedings of the General Discussion on Heat Transfer, 11-13 September, 1951, published by the Institution of Mechanical Engineers, pp. 49-52.

4-19. Y. Kukita, Y. Anoda, H. Nakamura and K. Taska, Assessment and Improvement of RELAP5/MOD2 Code's Interphase Drag Models, Japan Atomic Energy Reserach Institute, 1986.

4-20. J. C. Lin et al., "Nonequilibrium Constitutive Models for RELAP5/MOD2", ANS Topical Meeting on Anticipated and Abnormal Plant Transients in Light Water Reactors, Jackson, WY, September 26-29, 1983.

4-21. J. C. Lin et al., "RELAP5/MOD2 Pressurizer Modeling," ASME Winter Meeting, New Orleans, LA, December 9-14, 1984.

4-22. F. W. Dittus and L. M. K. Boelter, "Heat Transfer in Automobile Radiators of the Tubular Type," Publications in Engineering, 2, University of California, Berkeley, 1930, pp. 443-461.

4-23. W. H. McAdams, Heat Transmission, 3rd edition, New York: McGraw-Hill, 1954.

4-24. W. H. McAdams and T. H. Frost, "Heat Transfer by Conduction and Convection," Industrial and Engineering Chemistry, 14, 1922, p. 1101.

4-25. W. H. McAdams and T. H. Frost, "Heat Transfer for Water Flowing Inside Pipes," Refrigerating Engineering, 10, 1924, p. 23.

4-26. F. H. Morris and W. G. Whitman, "Heat Transfer for Oils and Water in Pipes," Industrial and Engineering Chemistry, 20, 1928, p. 234.

4-27. F. Kreith and M. S. Bohn, Principles of Heat Transfer, 4th edition, New York: Harper and Row, 1986.

4-28. H. C. Reynolds, Jr., Internal Low Reynolds Number Turbulent Heat Transfer, University of Arizona, EMMT Lab TR 2, January 1968.

4-29. C. A. Sleicher and M. W. Rouse, "A Convenient Correlation for Heat Transfer to Constant and Variable Property Fluids in Turbulent Pipe Flow," International Journal of Heat Mass Transfer, 18, 1975, pp. 677-683.

4-30. P. S. Larsen and H. A. Lord, Convective and Radiative Heat Transfer to Superheated Steam in Uniformly and Non-Uniformly Heated Tubes, Westinghouse Electric Corporation, Atomic Power Division, 08742-1-F, February 1969.

4-31. B. Gebhart, Heat Transfer, 2nd edition, New York: McGraw-Hill, 1971.

4-32. R. G. Deissler and M. F. Taylor, Reactor Heat Transfer Conference of 1956, TID-7529, November 1957, pp. 416-461.

4-33. J. Weisman, "Heat Transfer to Water Flowing Parallel to Tubes," Nuclear Science and Engineering, 6, 1959, pp. 78-79.

4-34. J. B. Heineman, An Experimental Investigation of Heat Transfer to Superheated Steam in Round and Rectangular Channels, ANL-6213, 1960.

4-35. J. R. Sellars, M. Tribus, and J. S. Klein, "Heat Transfer to Laminar Flows in a Round Tube or Flat Conduit: The Graetz Problem Extended," Transactions, American Society of Mechanical Engineers, 78, 1956, p. 441.

4-36. R. W. Shumway, Variable Properties Laminar Gas Flow Heat Transfer and Pressure Drop in Annuli, University of Arizona EMMT Lab TR 3, August 1969.

4-37. L. C. Burmeister, Convective Heat Transfer, New York: John Wiley & Sons, 1983.

4-38. W. M. Kays, "Numerical Solution for Laminar Flow Heat Transfer in Circular Tubes," Transactions, American Society of Mechanical Engineers, 77, 1955, pp. 1265-1274.

4-39. R. Viskanta and A. K. Mohanty, TMI-2 Accident: Postulated Heat Transfer Mechanisms and Available Data Base, NUREG/CR-2121, ANL-81-26, April 1981.

4-40. M. Jakob, Heat Transfer, I, New York: John Wiley & Sons, 1949.

4-41. Y. S. Touloukian, G. A. Hawkins, and M. Jakob, "Heat Transfer by Free Convection from Heated Vertical Surfaces to Liquids," Transactions, American Society of Mechanical Engineers, 70, January 1948, pp. 13-18.

4-42. L. P. Davis and J. J. Perona, "Development of Free Convection Flow of a Gas in a Heated Vertical Open Tube," International Journal of Heat Mass Transfer, 14, 1971, pp. 889-903.

4-43. E. R. G. Eckert and T. W. Jackson, "Analysis of Turbulent Free Convection Boundary Layer on a Flat Plate," National Advisory Committee for Aeronautics Report, No. 1015, 1951.

4-44. F. J. Bayley, "An Analysis of Turbulent Free Convection Heat Transfer," Proceedings Institute of Mechanical Engineering, 169, 20, 1955, p. 361.

4-45. E. R. G. Eckert and R. M. Drake, Jr., Analysis of Heat Transfer, New York: McGraw-Hill, 1972.

4-46. M. M. Megahed, RELAP5/MOD2 Assessment Simulation of Semiscale MOD-2C Test S-NH-3, NUREG/CR-4799, EGG-2519, October 1987.

4-47. C. B. Davis, Davis-Besse Uncertainty Study, NUREG/CR-4946, EGG-2510, August 1987.

4-48. J. C. Chen, "A Correlation for Boiling Heat Transfer to Saturated Fluids in Convective Flow," Process Design and Development, 5, 1966, pp. 322-327.

4-49. T. A. Bjornard and P. Griffith, "PWR Blowdown Heat Transfer," Thermal and Hydraulic Aspects of Nuclear Reactor Safety, 1, American Society of Mechanical Engineers, New York, 1977, pp. 17-41.

4-50. K. Forster and N. Zuber, American Institute of Chemical Engineering Journal, 4, 1955, p. 531.

4-51. G. E. Dengler, J. N. Addoms, Chemical Engineering Progress Symposium Ser. 52, 18, 1956, pp. 95-103.

4-52. V. E. Schrock and L. M. Grossman, Nuclear Science and Engineering, 12, 1962, pp. 474-81.

4-53. R. L. Sani, Downflow Boiling and Nonboiling Heat Transfer in a Uniformly Heated Tube, UCRL 9023, 1960.

4-54. J. A. R. Bennett, J. G. Collier, H. T. C. Pratt, J. D. Thornton, "Heat Transfer to Two-Phase Gas Liquid Systems," Atomic Energy Research Establishment, AERE-R3159, 1959.

4-55. R. M. Wright, Downflow Forced-Convention Boiling of Water in Uniformly Heated Tubes, UCRL-9744, August 1961.

4-56. S. A. Guerrieri and R. D. Talty, Chemical Engineering Progress Symposium Series 52, 18, 1956, pp. 69-77.

4-57. K. E. Gungor, and R. H. S. Winterton, "A General Correlation for Flow Boiling in Tubes and Annuli," International Journal Heat Mass Transfer, 29, 1986, pp. 351-356.

4-58. T. J. Boucher, "Scale Model Test Results for an Inverted U-Tube Steam Generator with Comparisons to Heat Transfer Correlations," ASME Winter Meeting, Boston, MA, December 1987.

4-59. J. R. S. Thom et. al., "Boiling in Subcooled Water During Flow Up Heated Tubes or Annuli," Proceedings, Institution of Mechanical Engineers, 180 (Part 3C), 1966, pp. 226-246.

4-60. F. D. Moles and J. R. G. Shaw, "Boiling Heat Transfer to Subcooled Liquids Under Conditions of Forced Convection," Transactions, Institution Chemical Engineers, 50, 1972, pp. 76-84.

4-61. A. E. Bergles and W. M. Rohsenow, "The Determination of Forced Convection Surface Boiling Heat Transfer," Paper 63-HT-22, 6th National Heat Transfer Conference, August 11-14, 1963.

4-62. P. Saha and N. Zuber, "Point of Net Vapor Generation and Vapor Void Fraction in Subcooled Boiling," Proc. of the 5th International Heat Transfer Conference, Tokyo, Paper B4.7, 1974.

4-63. Deissler, R. G., and M. F. Taylor, Reactor Heat Transfer Conference of 1956, TID-7529, November 1957.

4-64. Kays, W. M. Convective Heat and Mass Transfer, New York: McGraw-Hill Book Co., 1986.

4-65. J. C. Chen, R. K. Sundaram, F. T. Ozkaynak, A Phenomenological Correlation for Post-CHF Heat Transfer, NUREG-0237, June 1977.

4-66. D. R. H. Beattie and P. B. Whalley, "A Simple Two-Phase Frictional Pressure Drop Calculational Method," International Journal of Multiphase Flow, 8, 1982, pp. 83-87.

4-67. S. L. Richlen, Chen Non-Equilibrium Correlation Evaluation, EG&G Idaho, CDAP-TR-004, January 1978.

4-68. O. C. Iloeje, "A Study of Wall Rewet and Heat Transfer in Dispersed Vertical Flow," PhD. Thesis, MIT Heat Transfer Lab., 1974.

4-69. N. Zuber, M. Tribus and J. W. Westwater, "Hydrodynamic Crisis in Pool Boiling of Saturated and Subcooled Liquid," 2nd International Heat Transfer Conference, Denver, Colorado, 1961

4-70. P. Griffith, C. T. Avedisian, and J. P. Walkush, "Co[illegible]er Flow Critical Heat Flows," American Institute of Chemical [illegible]eers, 15th National Heat Transfer Conference, 1975.

4-71. Biasi, et. al., "Studies on Burnout Part 3 - A New Correlation for Round Ducts and Uniform Heating and Its Comparison with World Data", Energia Nucleare, 14, 1967, pp. 530-536.

4-72. L. A. Bromley, "Heat Transfer in Stable Film Boiling," Chemical Engineering Progress, 46, 1950, pp. 221-227.

4-73. P. J. Berenson, "Film Boiling Heat Transfer form a Horizontal Surface," Journal of Heat Transfer, 1961, pp. 351-358.

4-74. B. P. Breen and J. W. Westwater, "Effect of Diameter of Horizontal Tubes on Film Boiling Heat Transfer," Chemical Engineering Progress, 58, 1962, p. 67.

4-75. K. H. Sun, J. M. Gonzales-Santalo, and C. L. Tien, "Calculations of Combined Radiation and Convection Heat Transfer in Rod Bundles Under Emergency Cooling Conditions," Journal of Heat Transfer, 1976, pp. 414-420.

4-76. Y. Y. Hsu and J. W. Westwater, "Film Boiling from Vertical Tubes," American Institute of Chemical Engineers Journal, 4, 1958, p. 58.

4-77. Y. Y. Hsu and J. W. Westwater, "Approximate Theory for Film Boiling on Vertical Surfaces," Chemical Engineering Progress Symposium Series 30, 56, 1960, p. 15.

4-78. L. A. Bromley, N. R. LeRoy and J. A. Robbers, "Heat Transfer in Forced Convection Film Boiling," Industrial and Engineering Chemistry, 45, 1953, p. 2639.

4-79. E. I. Motte and L. A. Bromley, "Film Boiling of Flowing Subcooled Liquids," Industrial and Engineering Chemistry, 49, 1957, p. 1921.

4-80. D. C. Groeneveld, "Inverted Annular and Low Quality Film Boiling," International Workshop on Fundamental Aspects of Post-Dryout Heat Transfer, Salt Lake City, Utah, 1984.

4-81. D. L. Hagrman, G. A. Reymann, R. E. Mason, MATPRO-Version II (Revision 2), A Handbook of Materials Properties for use in the Analysis of Light Water Reactor Fuel Rod Behavior, NUREG/CR-0479, TREE-1280, Rev. 2, 1981, p. 231.

4-82. D. D. Taylor et al., TRAC-BD1/MOD1: An Advanced Best Estimate Computer Program for Boiling Water Reactor Transient Analysis, Vol. 1, NUREG/CR-3633, EGG-2294, April 1984, p. 65.

4-83. J. C. Lin, et al., "RELAP5/MOD2 Post-CHF Heat and Mass Transfer Models," International Workshop on Fundamental Aspects of Post-Dryout Heat Transfer, Salt Lake City, UT, April 1-4, 1984.

4-84. D. C. Groeneveld and G. G. L. Delorme, "Prediction of Thermal Non-Equilibrium in the Post-Dryout Regime," Nuclear Engineering and Design, 36, 1976, pp. 17-26.

4-85. B. Scruton and B. Chojnowski, Post-Dryout Heat Transfer for Steam/Water Flowing in Vertical Tubes at High Pressure, CEGB Report No. PB-84-23386J, TL-397, 1982.

4-86. R. C. Gottula, et al., Forced Convection, Non-Equilibrium Post-CHF Heat Transfer Experiment Data and Correlation Comparison Report, NUREG/CR-3193, EGG-2245, March 1985.

4-87. D. C. Groeneveld, S. C. Cheng, and T. Doan, "1986 AECL-UO Critical Heat Flux Lookup Table", Heat Transfer Engineering, 7, 1986, pp. 46-62.

4-88. A. Sjoberg and D. Caraher, Assessment of RELAP5/MOD2 Against Twenty Five Dryout Experiments Conducted at the Royal Institute of Technology, NP-86/66, 1986.

4-89. D. R. Liles et al., TRAC-PF1/MOD1 Correlations and Models, NUREG-5069, LA-11208-MS, August 1988.

4-90. N. Zuber, M. Tribus, and J. W. Westwater, "The Hydrodynamic Crisis in Pool Boiling of Saturated and Subcooled Liquids", International Developments in Heat Transfer, 1961, pp. 230-236.

4-91. V. M. Borishanski, "An Equation Generalizing Experimental Data on the Cessation of Bubble Boiling in a Large Volume of Liquid", Zhurnal Tekhnicheski Fiziki, 25, 1956, p. 152.

4-92. J. H. Lienhard, and V. K. Dhir, "Hydrodynamic Predictions of Peak Pool-Boiling Heat Fluxes from Finite Bodies", Journal of Heat Transfer, 95, 1973, pp. 152-158.

4-93. J. C. Chen, "Review of Post-Dryout Heat Transfer in Dispersed Two-Phase Flow," Presentation at the International Workshop on Fundamentals of Post-Dryout Heat Transfer, Salt Lake City, Utah, April 1-4, 1984.

4-94. A. Sjoberg, D. Caraher, Assessment of RELAP5/MOD2, Against Twenty Five Dryout Experiments Conducted at the Royal Institute of Technology, NUREG/IA-0009, October 1986.

4-95. I. Vojtek, Heat Transfer Processes During Intermediate and Large Break Loss-of-Coolant Accidents (LOCAs), NUREG/IA-0002, September 1986.

4-96. J. Eriksson, Assessment of RELAP5/MOD2, Cycle 36, Against FIX-II Split Break Experiment No. 3027, NUREG/IA-0005, September 1986.

4-97. W. Nusselt, "Die Oberflachenkondensation des Wasserdampfes," Ver. deutsch. Ing., 60, 1916, pp. 541 and 569.

4-98. J. G. Collier, Convective Boiling and Condensation, 2nd edition, New York: McGraw-Hill, 1981.

4-99. W. M. Rohsenow, "Heat Transfer and Temperature Distribution in Laminar Film Condensation," Trans. American Society of Mechanical Engineers, 78, 1956, pp. 1645-1648.

4-100. T. B. Drew and W. H. McAdams, Heat Transmission, 3rd edition, New York: McGraw-Hill, 1954.

4-101. E. M. Sparrow, W. J. Minkowycz, and M. Saddy, "Forced Convection Condensation in the Presence of Non-Condensibles and Interfacial Resistance," Int. J. Heat Mass Transfer, 10, 1967, pp. 1829-1845.

4-102. M. Jakob, Heat Transfer, Vol. 1, New York: John Wiley & Sons, Inc., 1949, p. 666.

4-103. J. C. Chato, "Laminar Condensation Inside Horizontal and Inclined Tubes," American Society of Heating, Refrigeration and Air Conditioning Engineering Journal, 4, 1962, pp. 52-60.

4-104. E. F. Carpenter and A. P. Colburn, "The Effect of Vapor Velocity on Condensation Inside Tubes," Proc. of General Discussion on Heat Transfer, Institute Mechanical Engineering/American Society of Mechanical Engineers, 1951, pp. 20-26.

4-105. A. P. Colburn, "The Calculation of Condensation Where a Portion of the Condensate Layer is in Turbulent Motion," Trans. American Institute of Chemical Engineers, 30, 1933-34, p. 187.

4-106. W. M. Rohsenow, J. H. Webber, and A. T. Ling, "Effect of Vapor Velocity on Laminar and Turbulent Film Condensation," Trans. American Society of Mechanical Engineers, 78, 1956, pp. 1637-1643.

4-107. M. Soliman, J. R. Schuster, P. J. Berenson, "A General Heat Transfer Correlation for Annular Flow Condensation," J. of Heat Transfer, 90, May 1968, pp. 267-276.

4-108. V. H. Ransom, et al., RELAP5/MOD2 Code Manual, Volume 1, NUREG/CR-4312, EGG-2396, August 1985.

APPENDIX 4A

CORRELATIONS FOR INTERFACIAL HEAT AND MASS TRANSFER IN THE BULK FLUID FOR RELAP5/MOD2

APPENDIX 4A

CORRELATIONS FOR INTERFACIAL HEAT AND MASS TRANSFER IN THE BULK FLUID FOR RELAP5/MOD2

Bubbly Flow

SHL (superheated liquid, $\Delta T_{sf} < 0$)

$$H_{if} = \left[\text{Max} \left\{ \begin{array}{l} \dfrac{k_f}{d_b} \dfrac{12}{\pi} \Delta T_{sf} \dfrac{\rho_f C_{pf}}{\rho_g h_{fg}} \beta \\ \dfrac{k_f}{d_b} (2.0 + 0.74\ Re_b^{0.5}) \end{array} \right\} + 0.4\ |v_f| \rho_f\ C_{pf}\ F_1 \right] a_{gf}\ F_2\ F_3$$

where

$\Delta T_{sf} \equiv T^s - T_f$

$Re_b = \dfrac{We\ \sigma\ (1 - \alpha_{bub})}{\mu_f\ (v_{fg}^2)^{1/2}}$, $We\ \sigma = \text{Max}\ (We\ \sigma,\ 10^{-10})$

$We = \left(\rho_f d_b\ v_{fg}^2 / \sigma \right) = 5,$

d_b = average bubble diameter ($= 1/2\ d_{max}$)

β = 1.0 for bubbly flow

a_{gf} = interfacial area per unit volume

$= 3.6\ \alpha_{bub} / d_b$

$$\alpha_{bub} = \text{Max } (\alpha_g, 10^{-5})$$

$$v_{fg} = \text{relative velocity} = \begin{cases} v_g - v_f & \alpha_g \geq 10^{-5} \\ (v_g - v_f)\, \alpha_g 10^5 & \alpha_g < 10^{-5} \end{cases}$$

$$v_{fg}^2 = \text{Max} \left[v_{fg}^2, \frac{We\ \sigma}{\rho_f \text{ Min } (D' \alpha_{bub}^{1/3}, D)} \right]$$

D = hydraulic diameter

D' = 0.005 for bubbly flow

$$F_1 = \text{Min } (0.001, \alpha_{bub}) / \alpha_{bub}$$

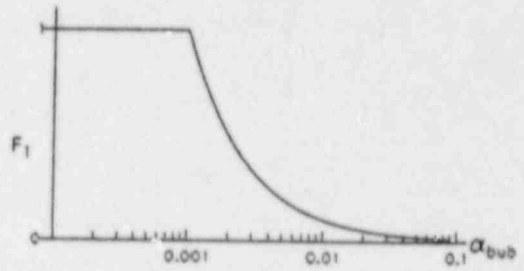

$$F_2 = \text{Min } (0.25, \alpha_{bub}) / \alpha_{bub}$$

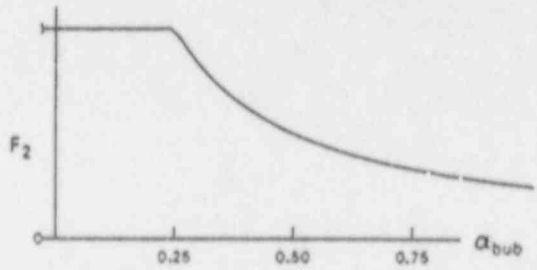

$$F_3 = \begin{cases} 1 & \Delta T_{sf} \leq -1 \\ \text{Max } [0.0,\ F_4\ (1 + \Delta T_{sf}) - \Delta T_{sf}] & -1 < \Delta T_{sf} < 0 \\ \text{Max } (0.0,\ F_4) & \Delta T_{sf} \geq 0 \end{cases}$$

$$F_4 = \text{Min } [10^{-5},\ \alpha_g\ (1 - Q)]\ (10^5)$$

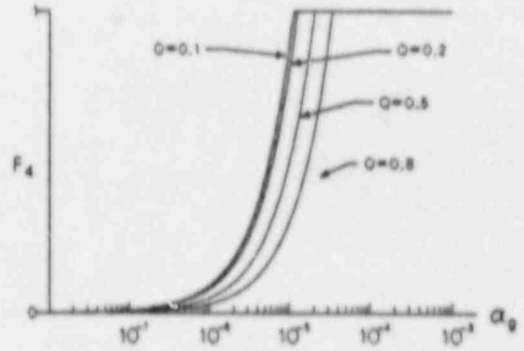

Q = noncondensible quality (fraction of α_g that is noncondensible)

H_{if} = 0.0 if $\alpha_g = 0.0$ and $\Delta T_{sf} \leq 0$

SCL (subcooled liquid, $\Delta T_{sf} > 0$)

$$H_{if} = \frac{F_3 \, F_5 \, h_{fg} \, \rho_g \, \rho_f \, \alpha_{bub}}{\rho_f - \rho_g}$$

where

$\rho_f - \rho_g$ = Max $(\rho_f - \rho_g, 10^{-7})$

F_3, α_{bub} as for bubbly SHL

$$F_5 = \begin{cases} 0.075 & \alpha_{bub} \geq 0.25 \\ 1.8\phi C \exp(-45\alpha_{bub}) + 0.075 & \alpha_{bub} < 0.25 \end{cases}$$

$$C = \begin{cases} 61.0 - 6.489 \times 10^{-5} (P - 1.7 \times 10^5) & P \leq 10^6 \text{ Pa} \\ 2.3 \times 10^9 & P > 10^6 \text{ Pa} \end{cases}$$

P = Pressure (Pa)

$$\phi = \begin{cases} 1 & |v_f| < 0.61 \\ [1.639344 |v_f|]^{0.47} & |v_f| \geq 0.61 \end{cases}$$

SHG (superheated gas, $\Delta T_{sg} \leq 0$)

$H_{ig} = Nu_{ib} \, F_6 \, F_7 \, a_{gf}$

where

$Nu_{ib} = 10^4$

a_{gf} as for bubbly SHL

$F_6 = [1 + \eta\ (100 + 25\eta)]$, $\eta = |\text{Max}\ (-2, \Delta T_{sg})|$

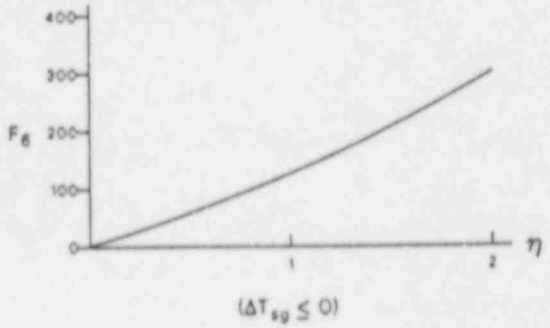

$(\Delta T_{sg} \leq 0)$

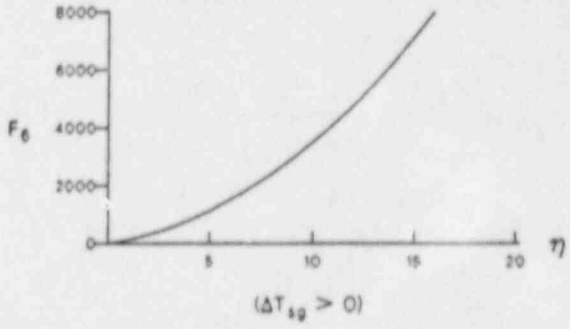

$(\Delta T_{sg} > 0)$

$$F_7 = \frac{\text{Max}\ (\alpha_g,\ 10^{-5})}{\text{Max}\ (\alpha_g,\ 10^{-9})}$$

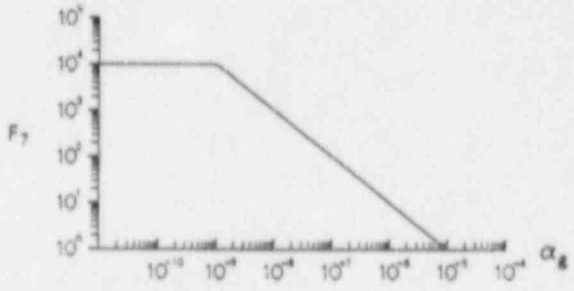

SCG (subcooled gas, $\Delta T_{sg} > 0$)

H_{ig} as for bubbly SHG

(Note that F_6 has a different form for $\Delta T_{sg} > 0$).

Slug Flow

SHL ($\Delta T_{sf} < 0$)

$$H_{if} = H_{if,TB} + H_{if,bub}$$

where

$$H_{if,TB} = 3.0 \times 10^6 \, a^*_{gf,TB} \, \alpha_{TB} \, F_8$$

where

$a^*_{gf,TB}$ = volumetric interfacial area = [4.5/D] (2)

F_8 = Min (1 - ΔT_{sf})

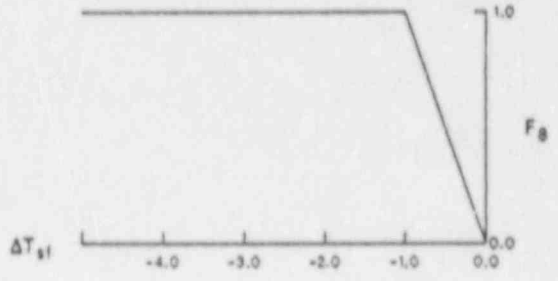

α_{TB} = Taylor bubble void fraction = $(\alpha_g - \alpha_{gs})/(1 - \alpha_{gs})$
= Taylor bubble volume/total volume

α_{gs} = the average void fraction in the liquid film and slug region
= $\alpha_{AB} F_9$

$$F_9 = \exp\left[-8 \left(\frac{\alpha_g - \alpha_{AB}}{\alpha_{AC} - \alpha_{AB}}\right)\right]$$

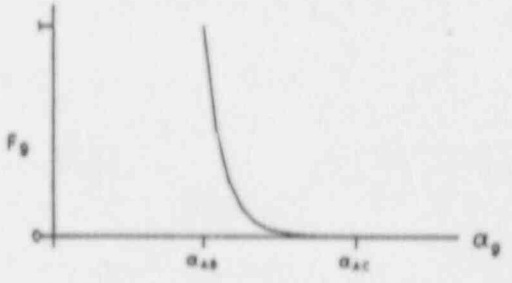

α_{AB} = α_g for bubbly-slug transition

α_{AC} = α_g for slug-annular mist transition

and

$H_{if,bub}$ is as for H_{if} for bubbly SHL with the following modifications:

α_{bub} = $\alpha_{AB} F_g$

v_{fg} = $(v_g - v_f) F_g^2$

$a_{gf,bub}$ = $(a_{gf})_{bub} (1 - \alpha_{TB}) F_g$

β = F_g

SCL ($\Delta T_{sf} > 0$)

H_{if} = $H_{if,TB} + H_{if,bub}$

where

$$H_{if,TB} = 1.18942 \, Re_f^{0.5} Pr_f^{0.5} \frac{k_f}{D} a^*_{gf,TB} \alpha_{TB}$$

where

α_{TB} and $a^*_{gf,TB}$ are as for slug SHL

$Pr_f = C_{pf} \mu_f / k_f$

$Re_f = \rho_f D \, Min (|v_f - v_g|, 0.8) / \mu_f$

and

$H_{if,bub}$ is as for bubbly SCL

SHG ($\Delta T_{sg} < 0$)

$$H_{ig} = H_{ig,TB} + H_{ig,bub}$$

where

$$H_{ig,TB} = (2.2 + 0.82\ Re_g^{0.5})\ \frac{k_g}{D}\ a^*_{gf,TB}\ \alpha_{TB}$$

where

$a^*_{gf,TB}$ and α_{TB} are as for slug SHL

$$Re_g = \rho_g\ |v_f - v_g|\ D\ /\ \mu_g$$

and

$$H_{ig,bub} = Nu_{ib}\ F_6\ (1 - \alpha_{TB})\ a_{gf,bub}$$

where

α_{TB}, $a_{gf,bub}$ and F_g are as for slug SHL

and

Nu_{ib} and F_6 are as for bubbly SHG

SCG ($\Delta T_{sg} > 0$)

$$H_{ig} = H_{ig,TB} + H_{ig,bub}$$

where

$$H_{ig,TB} = Nu_{ib}\ F_6\ \alpha_{TB}\ a^*_{gf,TB}$$

where α_{TB} and $a^*_{gf,TB}$ are as for slug SHL,

$H_{ig,bub}$ is as for slug SHG,

and

Nu_{ib} and F_6 are as for bubbly SHG.

Annular Mist Flow

SHL ($\Delta T_{sf} < 0$)

$$H_{if} = H_{if,ann} + H_{if,drp}$$

where

$$H_{if,ann} = 3.0 \times 10^6 \, a_{gf,ann} \, F_{10}$$

where

$$a_{gf,ann} = (4C_{ann}/D)(1 - \alpha_{ff})^{1/2}$$

$$C_{ann} = (30\alpha_{ff})^{1/8} (2.5)$$

$$\alpha_{ff} = \text{Max} (0.0, \alpha_f F_{11})$$

$$F_{11} = \gamma^* \text{ Max} [0.0, (1-G^*)] \exp (-C_e \times 10^{-5} \lambda^6)$$

$$C_e = \begin{cases} 4.0 & \text{horizontal} \\ 7.5 & \text{vertical} \end{cases}$$

$$\lambda = \begin{cases} v_g^*/v_{crit} & \text{horizontal flow} \\ \alpha_g v_g / v_{crit} & \text{vertical flow} \end{cases}$$

$$v_g^* = \text{Max} (v_g, 10^{-15})$$

$$v_{crit} \text{ (horizontal)} = 0.5 \left[\frac{(\rho_f - \rho_g) \, g \alpha_g A_{pipe}}{\rho_g \, D \sin \vartheta} \right]^{1/2} (1 - \cos \theta) \quad ,$$

[see Equation (3-2)] .

$$v_{crit} \text{ (vertical)} = 1.4 \, [\sigma^* g \, (\rho_f - \rho_g)]^{1/4} / \rho_g^{1/2} \text{ [see Equation (3-6)]}$$

$$\sigma^* = \text{Max}\ (\sigma,\ 10^{-7})$$

$$G^* = 10^{-4}\ Re_f^{0.25}$$

$$Re_f = \rho_f \alpha_f \left| v_f \right| D/\mu_i$$

$$\gamma^* = \begin{cases} \gamma & \alpha_g > \alpha_{AC} \text{ and } \alpha_f < \alpha_{EF} \\ 1 & \text{otherwise} \end{cases}$$

$$\gamma = \frac{\alpha_f - \alpha_{AD}}{\alpha_{EF} - \alpha_{AD}}$$

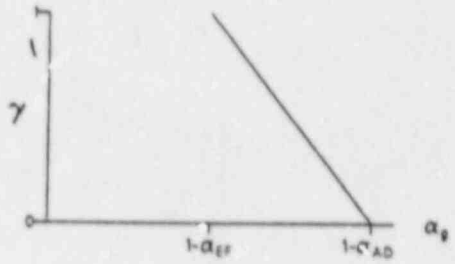

$$a_{AD} = 10^{-7}$$

$$\alpha_{EF} = \text{Max}\left[2\ \alpha_{AD},\ \text{Min}\ (2 - 3\ \frac{\rho_g}{\rho_f},\ 2 \times 10^{-4})\right]$$

$$F_{10} = \text{Min}\ (1.0 + \lambda^{1/2} + 0.05\ \lambda,\ 6)$$

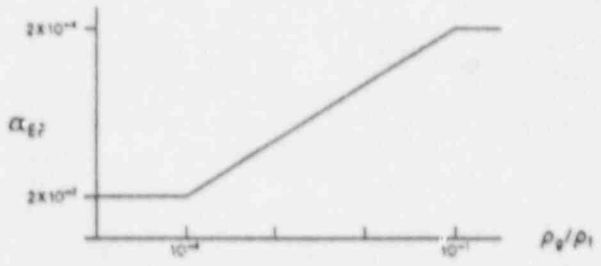

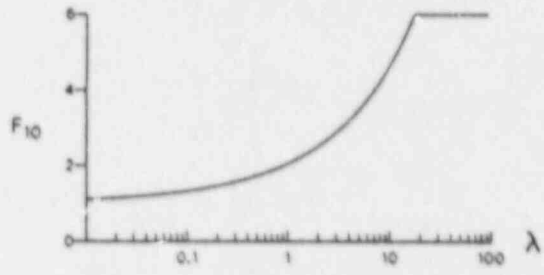

and

$$H_{if,drp} = \frac{k_f}{d_d} F_{12} (2) a_{gf,drp}$$

where d_d = characteristic droplet diameter

$$= \frac{We\ \sigma}{\rho_g v_{fg}^{**2}}, \quad We = 1.5, \quad We\ \sigma = Max\ (We\ \sigma,\ 10^{-10})$$

$$v_{fg}^{**2} = \begin{cases} v_{fg}^{*2}\ \alpha_f 10^6 & \alpha_f < 10^{-6} \\ v_{fg}^{*2} & \alpha_f \geq 10^{-6} \end{cases}$$

$$v_{fg}^{*2} = \begin{cases} v_{fg}^2\ F_{11}^{\gamma} & \alpha_g > \alpha_{AC} \text{ or } \alpha_f < \alpha_{EF} \\ v_{fg}^2\ F_{11} & \text{otherwise} \end{cases}$$

v_{fg}^2 is as for bubbly SHL except

$$\alpha_{bub} = \alpha_{fd}$$

$$D' = 0.0025$$

$$\alpha_{fd} = Max \left[\frac{\alpha_f - \alpha_{ff}}{1 - \alpha_{ff}},\ \alpha_{AD}^* \right]$$

$$\alpha_{AD}^* = \begin{cases} \alpha_{AD}^{\gamma} + 10^{-5} (1 - \gamma) & \alpha_g > \alpha_{AC} \text{ or } \alpha_f < \alpha_{EF} \\ \alpha_{AD} & \text{otherwise} \end{cases}$$

$$F_{12} = [1 + \xi (\not{2}50 + 50\xi)]$$

$$\xi = Max\ (0,\ -\Delta T_{sf})$$

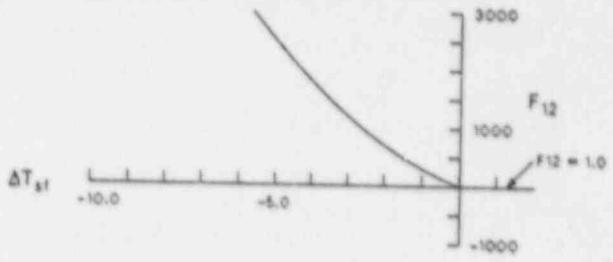

$$a_{gf,drp} = \frac{3.6\ \alpha_{fd}}{d_d}\ (1 - \alpha_{ff})$$

SCL ($\Delta T_{sf} > 0$)

$H_{if} = H_{if,ann} + H_{if,drp}$

where

$$H_{if,ann} = 10^{-3}\ \rho_f C_{pf}\ |v_f|\ a_{gf,ann}\ F_{10}$$

where

$a_{gf,ann}$ and F_{10} are as for annular mist SHL

and

$$H_{if,drp} = \frac{k_f}{d_d}\ F_{13}\ a_{gf,drp}$$

where

$a_{gf,drp}$, d_d are as for annular mist SHL

and

$$F_{13} = 2.0 + 7.0\ \text{Min}\ \left(1.0 + \frac{C_{pf}\ \Delta T_{sf}}{h_{fg}},\ 8.0\right) .$$

SHG ($\Delta T_{sg} < 0$)

$H_{ig} = H_{ig,ann} + H_{ig,drp}$

where

$$H_{ig,ann} = \frac{k_g}{D}\ 0.023\ Re_g^{0.3}\ a_{gf,ann}\ F_{10}$$

where

$$Re_g = \rho_g \left| v_g - v_f \right| D\alpha_g / \mu_g$$

F_{1f} and $a_{gf,ann}$ are as for annular mist SHL

and

$$H_{ig,drp} = \frac{k_g}{d_d} \left(2.0 + 0.5\ Re_d^{0.5}\right) a'_{gf,drp}$$

where

d_d is as for annular mist SHL

$$Re_d = \frac{We\ \sigma\ (1 - \alpha_{drp})^3}{\mu_g \left[v_{fg}^{**2}\ (1 - \alpha_{drp})\right]^{1/2}}, \qquad \begin{array}{l} We = 1.5, \\ We\ \sigma = Max\ (We\ \sigma,\ 10^{-10}) \end{array}$$

$$a'_{gf,drp} = \begin{cases} a_{gf,drp} & \alpha_f \geq \alpha^*_{AD} \\ a_{gf,drp} \left[\dfrac{\alpha_f F_{14}}{\alpha^*_{AD}} + (1 - F_{14})\right] & \alpha_f < \alpha^*_{AD} \end{cases}$$

$a_{gf,drp}$, α_{drp}, v_{fg}^{**2}, and α^*_{AD} are as for annular mist SHL

and

$$F_{14} = 1.0 - 5.0\ Min\ [0.2,\ Max\ (0,\ \Delta T_{sg})]\ .$$

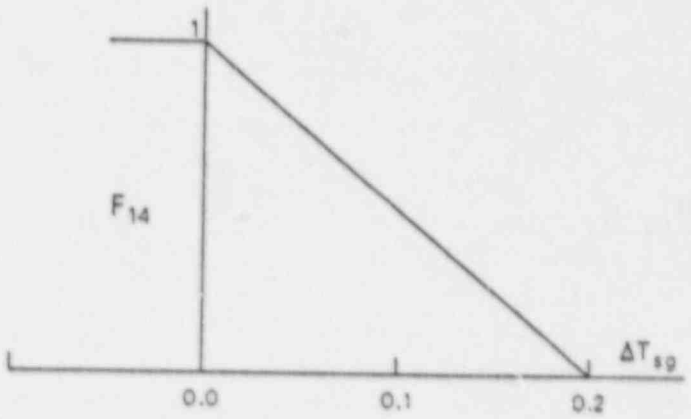

SCG ($\Delta T_{sg} > 0$)

$$H_{ig} = H_{ig,ann} + H_{ig,drp}$$

where

$$H_{ig,ann} = Nu_{ib} a_{gf,ann} F_{10} F_6$$

where Nu_{ib} and F_6 are as for bubbly SHG and $a_{gf,ann}$ and F_{10} are as for annular mist SHL

and

$$H_{ig,drp} = Nu_{ib} a'_{gf,drp} F_6$$

where

$a'_{gf,drp}$ is as for annular mist SHG

Inverted Annular Flow

SHL ($\Delta T_{sf} < 0$)

$$H_{if} = H_{if,bub} + H_{if,ann}$$

where

$H_{if,bub}$ is as for H_{if} for bubbly with the following modifications:

$$v_{fg} = (v_g - v_f) F_{16}^2$$

where

$$F_{16} = 1 - F_{17}$$

$$F_{17} = \exp\left[\frac{-8 (\alpha_{AB} - \alpha_{IAN})}{\alpha_{AB}}\right] F_{18}$$

$$\alpha_{IAN} = \begin{cases} \alpha_g & \text{Inverted annular} \\ \alpha_{AB} & \text{IAN/ISLG transition (see Figure 3-5)} \end{cases}$$

$$F_{18} = \text{Min } (\alpha_g/0.05, 1)$$

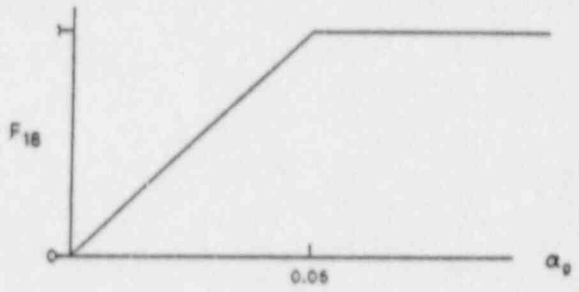

$$\beta = F_{16}$$

$$\alpha_g = \alpha_{bub}$$

$$\alpha_{bub} = \text{Max} \left[\frac{(\alpha_{IAN} - \alpha_B)}{(1 - \alpha_B)}, 10^{-7} \right]$$

$$\alpha_B = F_{17}\, \alpha_{IAN}$$

$$a_{gf,bub} = \frac{3.6\, \alpha_{bub}}{d_b} (1 - \alpha_B)\, F_{16}$$

and

$$H_{if,ann} = 3 \times 10^6\, a_{gf,ann}$$

where

$$a_{gf,ann} = \frac{4}{D} F_{15}\, (2.5)$$

$$F_{15} = (1 - \alpha_B)^{1/2}$$

SCL ($\Delta T_{sf} > 0$)

$$H_{if} = H_{if,bub} + H_{if,ann}$$

where

$H_{if,bub}$ is as for bubbly SCL

and

$$H_{if,ann} = \frac{k_f}{D} 0.023 \, Re_{IAN}^{0.8} \, a_{gf,ann} \, F_3$$

where

$$Re_{IAN} = \rho_f \left| v_f - v_g \right| (1 - \alpha_{IAN})/\mu_f$$

$a_{gf,ann}$ and α_{IAN} are as for inverted annular SHL and F_3 is as for bubbly SHL.

SHG ($\Delta T_{sg} < 0$)

$$H_{ig} = H_{ig,bub} + H_{ig,ann}$$

where

$$H_{ig,bub} = Nu_{ib} \, F_6 \, a_{gf,bub}$$

where

Nu_{ib} and F_6 are as for bubbly SHG and $a_{gf,bub}$ is as for inverted annular SHL

and

$$H_{ig,ann} = \frac{k_g}{D} F_{19} \, a'_{gf,ann}$$

where

$$F_{19} = [2.5 - \Delta T_{sg} (0.20 - 0.10 \Delta T_{sg})]$$

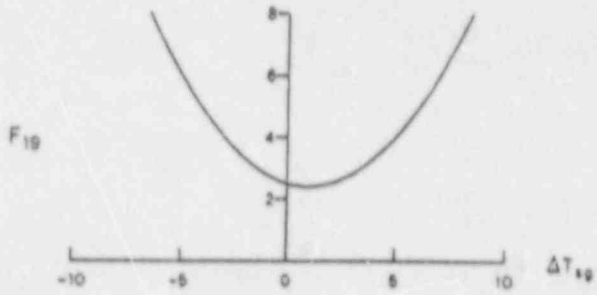

$$a'_{gf,ann} = a_{gf,ann}/F_{20}$$

$$F_{20} = 0.5 \text{ Max } (1.0 - F_{15}, 0.04)$$

F_{15} and $a_{gf,ann}$ are as for inverted annular SHL .

SCG ($\Delta T_{sg} > 0$)

H_{ig} is as for inverted annular SHG

Note that $\Delta T_{sg} > 0$ for this case (Function F_{19}).

Inverted Slug Flow

SHL

$H_{if} = H_{if,ann} + H_{if,drp}$

where

$$H_{if,ann} = \frac{k_f}{D} F_{12} (9) a_{gf,ann}$$

where

$$a_{gf,ann} = \frac{4.5}{D} \alpha_B(2.5)$$

$$\alpha_B = (\alpha_f - \alpha_{drp})/(1 - \alpha_{drp})$$

$$\alpha_{drp} = (1 - \alpha_{AC})\, F_{21}$$

$$F_{21} = \exp\left[-8\frac{(\alpha_{AC} - \alpha_g)}{(\alpha_{AC} - \alpha_{AB})}\right]$$

F_{12} is as for annular mist SHL

and

$$H_{if,drp} = \frac{k_f}{d_d} F_{12}\,(9)\, a_{gf,drp}$$

where

$$a_{gf,drp} = (3.6\, \alpha_{drp}/d_d)(1 - \alpha_B)$$

d_d = characteristic droplet diameter

$$= \frac{We\ \sigma}{\rho_g\, v_{fg}^2},\ We = 1.5,\ We\ \sigma = Max\ (We\ \sigma,\ 10^{-10})$$

v_{fg}^2 is as for bubbly SHL except that

$v_{fg} = (v_g - v_f)\, F_{21}^2$, We = 1.5,

$D' = 0.0025$, $\alpha_g = \alpha_{drp}$

<u>SCL</u> ($\Delta T_{sf} > 0$)

$$H_{if} = H_{if,ann} + H_{if,drp}$$

where

$$H_{if,ann} = \frac{k_f}{D} F_{13} a_{gf,ann}$$

where

F_{13} is as for annular mist SCL

$a_{gf,ann}$ is as for inverted slug SHL .

and

$$H_{if,drp} = \frac{k_f}{d_d} F_{13} a_{gf,drp}$$

where

$a_{gf,drp}$ is as for inverted slug SHL .

SHG ($\Delta T_{sg} < 0$)

$$H_{ig} = H_{ig,ann} + H_{ig,drp}$$

where

$$H_{ig,ann} = \frac{k_g}{D} \frac{F_{19}}{F_{22}} a_{gf,ann}$$

where

F_{19} is as for inverted annular SHG

$a_{gf,ann}$ is as for inverted slug SHL

$$F_{22} = \text{Max}\left(0.02, \text{Min}\left[\frac{\alpha_g}{4}\left(1 - \frac{\alpha_g}{4}\right), 0.2\right]\right)$$

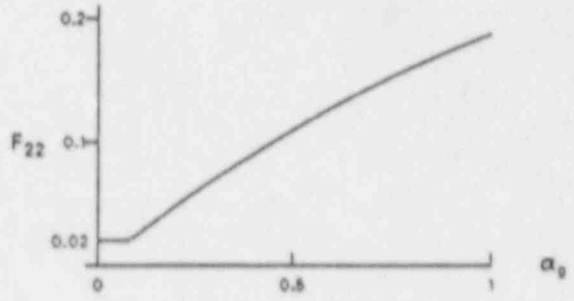

and

$$H_{ig,drp} = \frac{k_g}{d_d} (2.0 + 0.5\ Re_{drp}^{0.5})\ a_{gf,drp}$$

where

d_d and $a_{gf,drp}$ are as for inverted slug SHL

and

$$Re_{drp} = \frac{We\ \sigma\ (1 - \alpha_{drp})^{2.5}}{\mu_g\ (v_{fg}^2)^{0.5}}$$

where We = 1.5, We σ = Max (We σ, 10^{-10}), and v_{fg}^2 is as for inverted slug SHL.

SCG ($\Delta T_{sg} > 0$)

H_{ig} is as for inverted slug SHG .

Dispersed (Droplet) Flow

SHL ($\Delta T_{sf} < 0$)

$$H_{if} = \frac{k_f}{d_d} F_{12}\ F_{23}\ a_{gf}$$

where

F_{12} is as for annular mist SHL

$$F_{23} = \frac{\text{Max}\ (\alpha_f,\ 10^{-5})}{\text{Max}\ (\alpha_f,\ 10^{-10})}$$

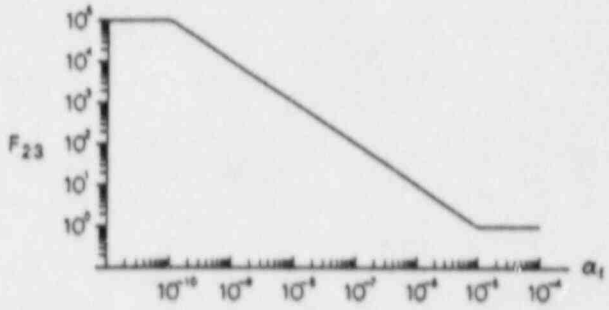

except for horizontal, post-CHF flow

where $F_{23} = \alpha_f / \text{Max}\ (\alpha_f,\ 10^{-10})$

$$a_{gf} = 3.6\ \alpha_{drp}/d_d$$

$$\alpha_{drp} = \text{Max}\ (\alpha_f,\ 10^{-5})$$

$$d_d = \frac{We\ \sigma}{\rho_g v_{fg}^2},\ We = 1.5,\ We\ \sigma = \text{Max}\ (We\ \sigma,\ 10^{-10})$$

v_{fg}^2 is as for bubbly SHL except that

$$v_{fg} = \begin{cases} v_g - v_f & \alpha_f < 10^{-6} \\ (v_g - v_f)\ \alpha_f\ 10^6 & \alpha_f \geq 10^{-6} \end{cases}$$

$We = 1.5,\ D' = 0.0025$

SCL ($\Delta T_{sf} > 0$)

$$H_{if} = \frac{k_f}{d_d} F_{13}\ F_{23}\ a_{gf}$$

where

F_{13} is as for annular mist SCL

F_{23} and a_{gf} are as for dispersed SHL .

SHG ($\Delta T_{sg} < 0$)

$$H_{ig} = \frac{k_g}{d_d} (2.0 + 0.5\ Re_{drp}^{0.5})\ F_{24}\ a_{gf}$$

where d_d and a_{gf} are as for dispersed SHL

$$Re_{drp} = \frac{We\ \sigma\ (1 - \alpha_{drp})^3}{\mu_g \left[v_{fg}^2\ (1 - \alpha_{drp})\right]^{1/2}}\ ,\ We\ \sigma = Max\ (We\ \sigma,\ 10^{-10})$$

where We, σ, α_{drp}, and v_{fg}^2 are as for dispersed SHL

$$F_{24} = Max\ [0.0,\ F_{26}\ (F_{25} - 1) + 1]$$

$$F_{25} = 10^5\ Min\ (\alpha_f,\ 10^{-5})$$

$$F_{26} = 1.0 - 5.0\ Min\ [0.2,\ Max\ (0.,\ \Delta T_{sg})]\ .$$

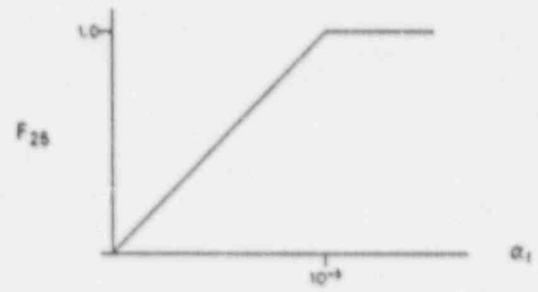

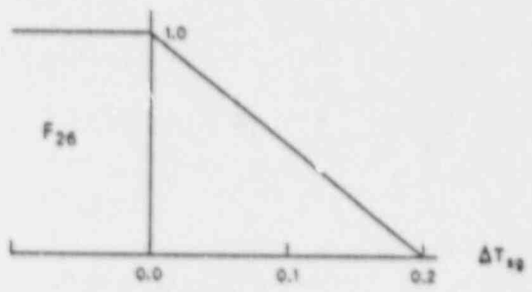

SCG ($\Delta T_{sg} > 0$)

$H_{ig} = Nu_{ib} F_6 F_{24} a_{gf}$

where

Nu_{ib} and F_6 are as for bubbly SHG

F_{24} and a_{gf} are as for dispersed SHG .

Horizontally Stratified Flow

$H_{if} = 0$ unless $\alpha_g > 0$ or $\Delta T_{sf} < -1$

$H_{ig} = 0$ unless $\alpha_f > 0$ or $\Delta T_{sg} > 0.2$

otherwise:

SHL ($\Delta T_{sf} < 0$)

$$H_{if} = \frac{k_f}{D_{hf}} \left[0.023 \, Re_f^{0.8} \, F_{12} - 3.81972 \, \frac{\Delta T_{sf} \rho_f C_{pf}}{\rho_g h_{fg} \, \text{Max} \, (4\alpha_g, 1)} \right] a_{gf}$$

where

D_{hf} = liquid phase hydraulic diameter

= $\pi \alpha_f D / (\pi - \theta + \sin\theta)$ (see Figure 3-2 for definition of θ)

Re_f = $\rho_f \alpha_f D \left| v_f - v_g \right| / \mu_f$

a_{gf} = $(4 \sin \theta / \pi D) \, F_{27}$

$$F_{27} = 1 + \left| \frac{v_g}{v_{crit}} \right|^{1/2}$$

SCL ($\Delta T_{sf} > 0$)

$$H_{if} = \frac{k_f}{D_{hf}} (0.023\ Re_f^{0.8})\ a_{gf}$$

where

D_{hf}, Re_f and a_{gf} are as for horizontally stratified SHL .

SHG ($\Delta T_{sg} < 0$)

$$H_{ig} = \frac{k_g}{D_{hg}} [0.023\ Re_g^{0.8} + Nu_{ib}\ F_6\ (4)\ Max\ (0.0,\ 0.25 - \alpha_g)]\ a_{gf}$$

where

D_{hg} = vapor phase hydraulic diameter

= $\pi\alpha_g D/(\theta + \sin\theta)$

Re_g = $\rho_g \alpha_g D \left|v_f - v_g\right| / \mu_g$

Nu_{ib} and F_6 are as for bubbly SHG

and a_{gf} is as for horizontally stratified SHL .

SCG ($\Delta T_{sg} > 0$)

$$H_{ig} = Nu_{ib}\ F_6\ a_{gf}$$

where

a_{gf} is as for horizontally stratified SHL.

Vertically Stratified Flow

SHL ($\Delta T_{sf} < 0$)

$$H_{if} = H_{if,REG}\, F_{30} + 14.7\, k_f\, a_{gf}\, (1 - F_{30})\, F_{31}$$

where REG = flow regime of flow below the stratified vapor/liquid interface, which can be BUB, SLUG, SLUG/ANM, ANM, IAN, IAN/ISLG, ISLG, DIS, IAN/ISLG - SLUG, ISLG - SLUG/ANM, ANM/DIS, BUB/IAN, SLUG/ISLG (see flow regime maps, Figures 3-1, 3-5).

F_{30} = Max (F_{32}, F_{33}, F_{34})

F_{32} = [1.0 - Min (1.0, $100\alpha_f$)]

F_{33} = Max [0.0, 3 Min (1.0, $G/\rho v_{TB}$) - 2]

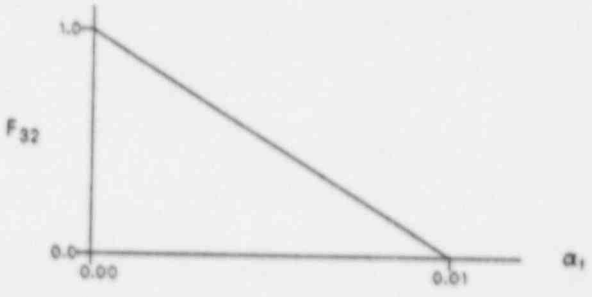

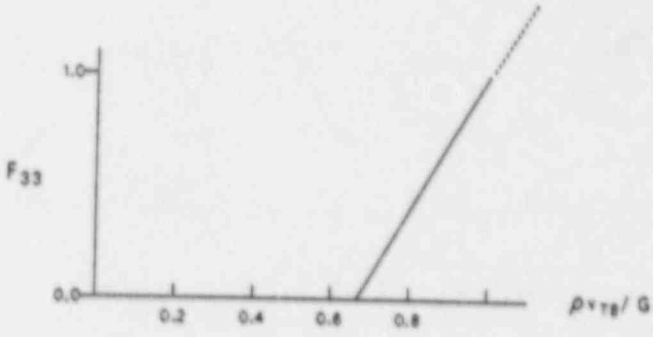

v_{TB} = Taylor bubble rise velocity, Equation (3-7)

$G = \left|\alpha_g \rho_g v_g + \alpha_f \rho_f v_f\right|$

$\rho = \alpha_g \rho_g + \alpha_f \rho_f$

F_{34} = Min (1.0, $-0.5\, \Delta T_{sf}$)

F_{31} = Min (1.0, $10\alpha_g$)

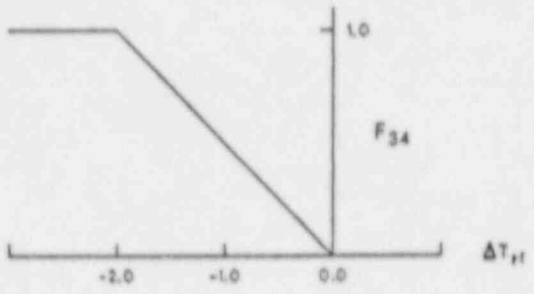

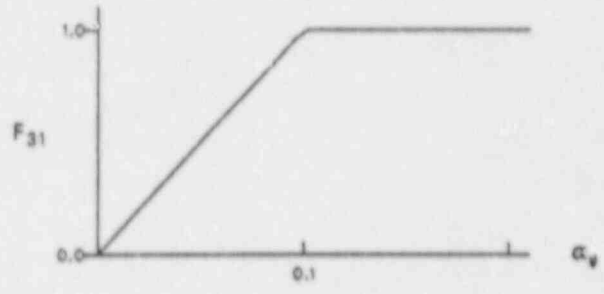

$$a_{gf} = \frac{A_c}{V} = \frac{A_c}{A_c D_L} = \frac{1}{D_L}$$

where D_L = length of volume cell and A_c = cross-section area of cell .

SCL ($\Delta T_{sf} > 0$)

H_{if} is as for vertically stratified SHL .

SHG ($\Delta T_{sg} < 0$)

$H_{ig} = H_{ig,REG} F_{35} + 81.4 k_g a_{gf} (1 - F_{35})$

where

F_{35} = Max (F_{33}, F_{36}, F_{37})

REG, F_{33}, D_L are as for vertically stratified SHL

F_{36} = [1.0 - Min (1.0, $10\alpha_g$)]

F_{37} = Min (1.0, 0.5 ΔT_{sg})

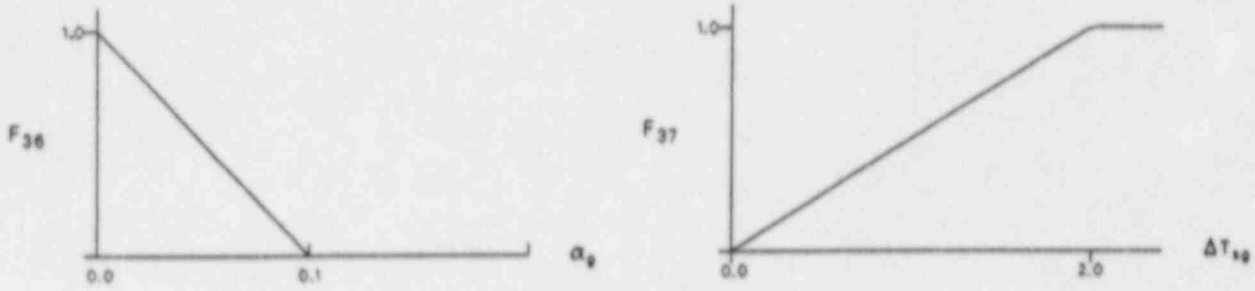

a_{gf} is as for vertically stratified SHL .

SCG ($\Delta T_{sg} > 0$)

H_{ig} is as for vertically stratified SHG .

Transitions

Notes:

1. The abbreviations for flow regimes are defined in Figures 3-1 and 3-5.

2. Subscript 'p' represents both f for liquid and g for gas phases.

3. Transition void fractions are illustrated in Figures 3-1 and 3-5.

Horizontal Flow

Slug-Annular Mist Transition

$$H_{ip_{SLUG-ANM}} = \left[H_{ip_{SLUG}}\right]^{FSLUG} \left[H_{ip_{ANM}}\right]^{FANM}$$

where

$$FANM = Max\ (0.0,\ Min\ [20\ (\alpha_g - \alpha_{DE}),\ 1.])$$

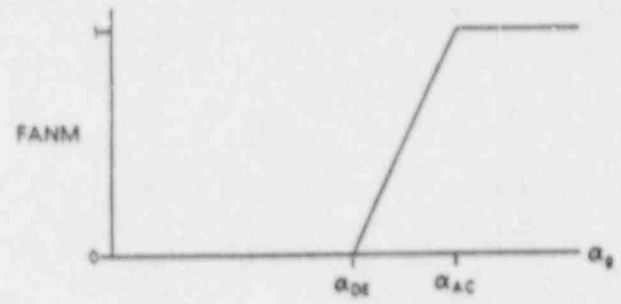

$$FSLUG = 1 - FANM$$

Transition to Horizontally Stratified Flow

$$H_{ip_{REG-HS}} = H_{ip_{REG}} \left[\frac{H_{ip_{HS}}}{H_{ip_{REG}}}\right]^{FSTRAT}$$

where

REG = BUB, SLUG, SLUG/ANM, ANM, or DIS, as appropriate

$FSTRAT = F_{28}\ F_{29}$

$F_{28} = Max\ [0.0,\ 1 - Max\ (2v_g/v_{crit} - 1,\ 0.)]$

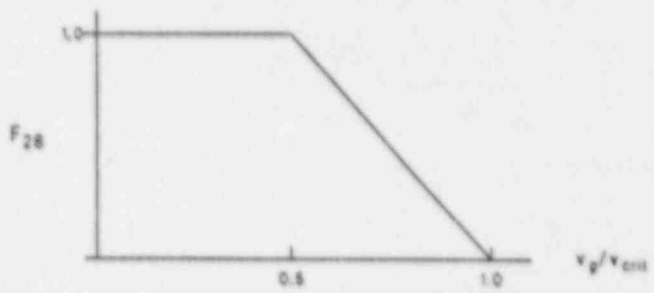

V_{crit} is as for annular mist SHL (horizontal)

$$F_{29} = \text{Min}\,[1.0,\ \alpha_f/\alpha_{EF},\ \text{Max}\,(0.0,\ 10^5\alpha_g - 1)]$$

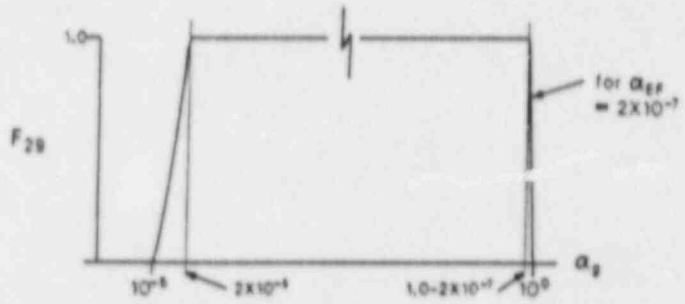

α_{EF} is as for annular mist SHL .

Vertical Flow

Slug-Annular Mist Transition

$H_{ip_{SLUG/ANM}}$ is as for $H_{ip_{SLUG/ANM}}$ for horizontal flow

Transition from Nonstratified to Vertically Stratified

See vertically stratified flow herein .

Inverted Annular-Inverted Slug Transition

$$H_{ip_{IAN\text{-}ISLG}} = \left[H_{ip_{IAN}}\right]^{FIAN} \left[H_{ip_{ISLG}}\right]^{FISLG}$$

where

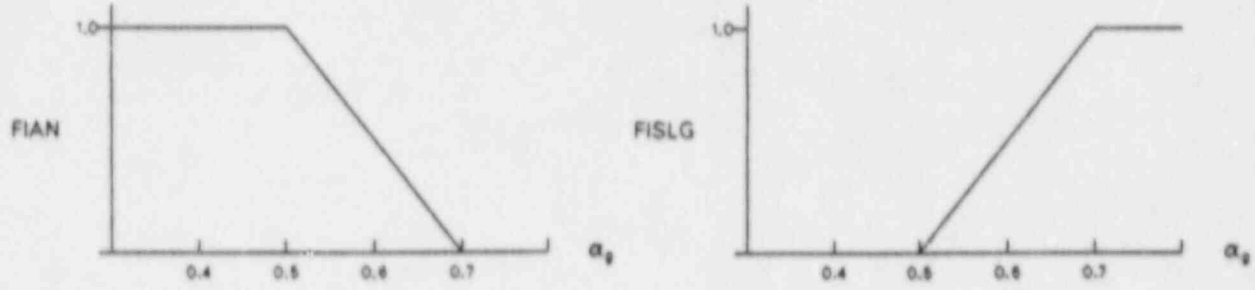

Transitional Boiling Regimes

$$H_{ip_{REG1-REG2}} = H_{ip_{REG1}} \left[\frac{H_{ip_{REG2}}}{H_{ip_{REG1}}}\right]^Z$$

where

REG1 - REG2 can represent BUB-IAN, SLUG-(IAN/ISLG), SLUG-ISLG, (SLUG/ANM)-ISLG or ANM-DIS. (See Figure 3-5)

$$Z = \text{Max}\ (0.0, \text{Min}\ [1.0, 10.000454\ (1.0 - \exp(-0.5T_{gsat}))\ (0.4 - \alpha_{AB})])$$

$$T_{gsat} = T_g - T^S - 1.0$$

<u>High Mixing Map</u>

Bubbly-Dispersed Transition

$$H_{ip_{BUB-DIS}} = FBUB\ H_{ip_{BUB}} + FDIS\ H_{ip_{DIS}}$$

where

$$FDIS = \text{Max}\,(0.0, \text{Min}\,[(\alpha_g - \alpha^*)/(1 - \alpha^* - \alpha^{**}), 1.0])$$

$$\alpha^* = 0.5 \exp\,[-10.0\,(\alpha_g - 0.5)]$$

$$\alpha^{**} = 0.05 \exp\,[-10.0\,(0.95 - \alpha_g)]$$

$$FBUB = 1 - FDIS$$

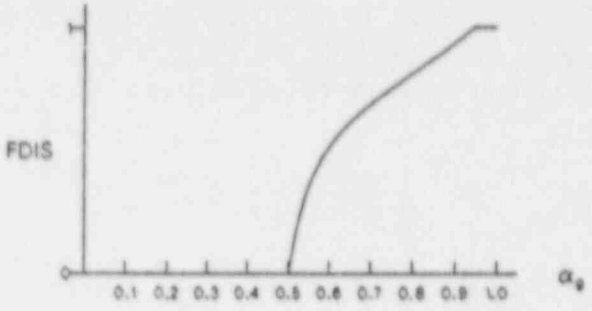

Modifications for Noncondensible Gas

Note: Function F_4 which is part of Function F_3 represents a modification to H_{if} for bubbly SHL based on the noncondensible quality Q (fraction of α_g which is noncondensible). The modifications below are applied to all volumetric heat transfer coefficients H_{if} and H_{ig} as described.

SHL ($\Delta T_{sf} < 0$)

H_{if} remains unchanged (except as noted above)

SCL ($\Delta T_{sf} > 0$)

$$H_{if} = H_{if_{REG}}\,(F_{40}\,[1 + \exp\,(-1000\,F_{38}F_{40})]\,F_{39} + (1 - F_{39}))$$

where

REG = flow regime or transition regime in question

F_{38} = 1.0 - Min (ΔT_{sf}, 80.0)(0.005)

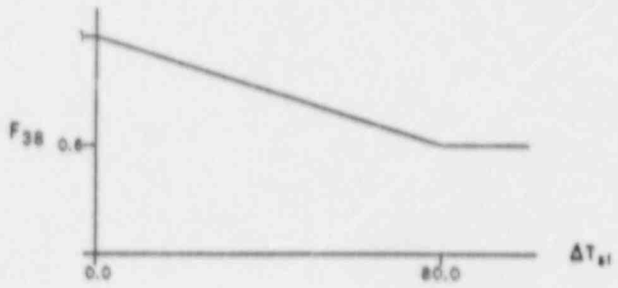

F_{39} = Min (10^{-5}, α_g) 10^5

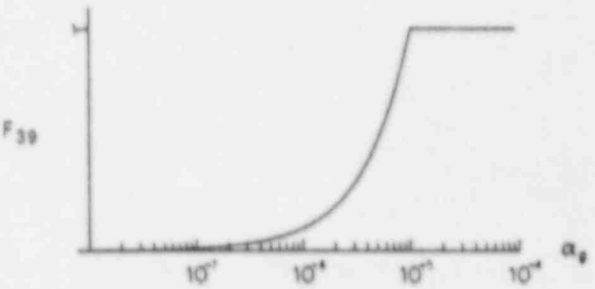

F_{40} = (1 - Q)

SHG ($\Delta T_{sg} < 0$)

H_{ig} remains unchanged

SCG ($\Delta T_{sg} > 0$)

$H_{ig} = H_{ig_{REG}} F_{40}$

F_{40} as for SCL above.

REG = flow regime in question

APPENDIX 4B

FLUID PROPERTIES FOR WATER AND STEAM FOR A TYPICAL REACTOR OPERATIONAL CONDITION

APPENDIX 4B

FLUID PROPERTIES FOR WATER AND STEAM
FOR A TYPICAL REACTOR OPERATIONAL CONDITION

Temperature = 315.56°C (600°F)

Pressure = 10.640 MPa (1543.220 psia)

h_{fg} = 1.280×10^6 J/kg (550.501 Btu/lbm)

Saturation Properties

Water

ρ_f = 677.. kg/m^3 (42.309 lbm/ft^3)

C_{pf} = 6346.1 J/kg-K (1.5157 Btu/lbm-°F)

k_f = 0.5175 W/m-K (0.299 Btu/hr-ft-°F)

μ_f = 7.996×10^{-5} kg/m-s (5.3731×10^{-5} lbm/ft-sec)

σ = 1.086×10^{-2} N/m (0.744×10^{-3} lb_f/ft)

Steam

ρ_g = 59.94 kg/m^3 (3.7417 lbm/ft^3)

C_{pg} = 7209 J/kg-K (1.7219 Btu/lbm-°F)

k_g = 0.0796 W/m-K (4.598×10^{-2} Btu/hr-ft-°F)

μ_g = 2.061×10^{-5} kg/m-sec (1.3848×10^{-5} lbm/ft-s)

5. CLOSURE RELATIONS REQUIRED BY FLUID MASS CONSERVATION EQUATIONS

The fluid mass conservation equations require only the mass transfer rate between the phases, Γ_g, for closure. The code calculation of Γ_g is directly tied to the energy partitioning relationships discussed in Section 4.5. Therefore, there is no new information to be added in this section. The entirety of the mass conservation closure relations was addressed in Section 4.5.

6. MOMENTUM EQUATION CLOSURE RELATIONS

This section discusses the relations necessary for closure in the momentum equation. The relations covered are interphase drag and wall drag.

6.1 Interphase Drag

6.1.1 Basis

The field difference equation for the difference momentum equation, Equation (2-62),

$$\left[1 + C\rho^2/(\rho_g\rho_f)\right]_j^n\left[(v_g^{n+1} - v_g^n) - (v_f^{n+1} - v_f^n)\right]_j\Delta x_j$$

$$+ \tfrac{1}{2}\left[(\dot{\alpha}_g\dot{\rho}_g)/(\alpha_g\rho_g)\right]_j^n\left[(v_g^2)_L^n - (v_g^2)_K^n\right]\Delta t - \tfrac{1}{2}\left[(\dot{\alpha}_g\dot{\rho}_g)/(\alpha_g\rho_g)\right]_j^n VISG_j^n\Delta t$$

$$- \tfrac{1}{2}\left[(\dot{\alpha}_f\dot{\rho}_f)/(\alpha_f\rho_f)\right]_j^n\left[(v_f^2)_L^n - (v_f^2)_K^n\right]\Delta t + \tfrac{1}{2}\left[(\dot{\alpha}_f\dot{\rho}_f)/(\alpha_f\rho_f)\right]_j^n VISF_j^n\Delta t$$

$$= -\left[(\rho_f - \rho_g)/(\rho_g\rho_f)\right]_j^n(P_L - P_K)^{n+1}\Delta t - \Big\{FWG_j^n(v_g)_j^{n+1} - FWF_j^n(v_f)_j^{n+1}$$

$$- \left[\Gamma_g^n\,(\rho^n v_j^{n+1} - \alpha_f^n\rho_f^n v_g^{n+1} - \alpha_g^n\rho_g^n v_f^{n+1})/(\alpha_g\rho_g\alpha_f\rho_f)^n\right]_j$$

$$+ (\rho FI)_j^n(v_g - v_f)_j^{n+1}\Big\}\,\Delta x_j\Delta t - \Big\{\left[(\dot{\alpha}_g\dot{\rho}_g)/(\alpha_g\rho_g)\right]_j^n HLOSSG_j^n v_{g,j}^{n+1} \qquad (6\text{-}1)$$

$$- \left[(\dot{\alpha}_f\dot{\rho}_f)/(\alpha_f\rho_f)\right]_j^n HLOSSF_j^n v_{f,j}^{n+1}\Big\}\Delta t$$

contains the term

$$(\rho FI)_j^n(v_g - v_f)_j^{n+1} \qquad (6\text{-}2)$$

which accounts for interphase drag due to the difference in velocities of the two phases.

The interphase drag per unit volume due to the difference in velocities of the two phases is

$$FI_{gf} = - f_{gf} |v_g - v_f| (v_g - v_f) , \quad (6\text{-}3)$$

with

$$f_{gf} = \frac{1}{8} \rho_c S_F a_{gf} C_D , \quad (6\text{-}4)$$

where

ρ_c = density of the continuous phase

C_D = drag coefficient

a_{gf} = interfacial area per unit volume

S_F = shape factor, assumed to be unity (1.0).

The term FI_{gf} in Equation (6-3) is related to the term FI in Equation (6-2) by the relation $FI_{gf} = \alpha_g \alpha_f \rho_g \rho_f FI(v_g - v_f)$.

To determine the interphase drag per unit volume, either f_{gf} or the combination of C_D and a_{gf} must be used.

6.1.2 Code Implementation

The RELAP5/MOD2 semi-implicit solution scheme for calculating liquid and vapor junction velocities uses the sum and difference momentum equations and is explained in the comments of subroutine VEXPLT as:

The momentum equations are written as a sum and difference equation. The sum equation is of the form

SUMF*(VEL. Liquid at new time) + SUMG*(VEL. Gas at new time) (6-5a)
= all old time terms (SUMOLD) .

The difference equation is of the form

DIFF*(VEL. liquid at new time) + DIFG*(VEL. Gas at new time) (6-5b)
= all old time terms (DIFOLD) .

The terms making up the difference momentum equation are

```
Difference Momentum Equation
DIFR=ETURBN*(RHOGA-RHOFA)/RHOFGA
SCRACH=(1.0+VIRMAS)*DX
DIFF=SCRACH+(FRICFJ+FJFG+VPGNX+HLOSSF)*DT
DIFG=-SCRACH-(FRICGJ+FJFG+VPGNX+HLOSSG)*DT
DIFOLD=(VELFJO(I)-VELGJO(I))*SCRACH-(DIFR*(PO(L)-PO(K))
+(CONVF-CONVG) - DPSTF(IX))*DT                          (6-6)
```

The interphase friction term, FJFG, is shown in the coding as

```
Interphase Drag
FJFG = (FIJ(I)*DX*(ABS(VELGJO(I)-VELFJO(I))+0.01)
+ FIDXUP(IX))*(RAVRF + RAVRG)                           (6-7)
```

The interphase friction term, FJFG, makes use of the term FIJ which is determined in subroutine PHAINT. If the terms in Equations (6-1), (6-4), (6-6), and (6-7) are matched, it can be shown that FIJ is equivalent to f_{gf}. The term FIJ is determined for each junction from different models depending on what flow regimes are calculated for the volumes adjoining the junction.

For a typical junction, the form of FIJ in terms of volume properties is as follows:

$$FIJ(I) = \frac{FIVOL(K)*V(K)+FIVOL(L)*V(L)}{V(K) + V(L)} * AJUN(I)\left[\frac{\frac{DL(K)}{AVOL(K)} + \frac{DL(L)}{AVOL(L)}}{DL(K) + DL(L)}\right] \quad (6\text{-}8)$$

where

FIVOL = interphase friction term, f_{gf}, from volume

V = volume of volume

AVOL = cross sectional area of volume

DL = length of volume

AJUN = area of junction

K = upstream volume indicator

L = downstream volume indicator .

The FIVOL terms are determined either directly from an expression for f_{gf} or from the combination C_D and a_{gf} and the remaining known terms in Equation (6-4).

For each RELAP5/MOD2 flow regime described, the model basis for either f_{gf} or the combination of C_D and a_{gf} and the code implementation will be described.

6.1.3 Individual Interphase Drag Models

The individual models for bubbly, slug, annular mist, inverted annular, inverted slug, and dispersed flow regimes will be discussed. Also models for transition regions between the above regimes are discussed, as well as the model assumptions for stratified flows.

6.1.3.1 Bubbly Flow

6.1.3.1.1 Model--The bubbly and mist flow regimes are both considered dispersed flow. According to Wallis[6-1] and Shapiro,[6-2] the

dispersed bubbles or droplets can be assumed to be spherical particles with a size distribution of the Nukiyama-Tanasawa form. The Nukiyama-Tanasawa distribution function in nondimensional form is

$$p^* = 4d^{*2}\, e^{-2d^*} \quad , \tag{6-9}$$

where $d^* = d/d'$; d' is the most probable particle diameter, and p^* is the probability of particles with nondimensional diameter of d^*. With this distribution, it can be shown that the average particle diameter $d_o = 1.5\, d'$, and the surface area per unit volume is

$$a_{gf} = \frac{6\bar{a}}{d'} \frac{\int d^{*2}\, p^*\, dd^*}{\int d^{*3}\, p^*\, dd^*} = \frac{2.4\bar{\alpha}}{d'} \quad , \tag{6-10}$$

where $\bar{\alpha} = \alpha_g$ for bubbles and $\bar{\alpha} = \alpha_f$ for droplets. In terms of the average diameter, d_o, the interfacial area per unit volume, a_{gf}, is

$$a_{gf} = 3.6\bar{\alpha}/d_o \quad . \tag{6-11}$$

The average diameter d_o is obtained by assuming that $d_o = 1/2\, d_{max}$ The maximum diameter, d_{max}, is related to the critical Weber number, We, by

$$We = d_{max}\, \rho_c\, (v_g - v_f)^2/\sigma \quad . \tag{6-12}$$

The values for We are presently taken as We = 10 for bubbles and We = 3.0 for droplets, these values being based on the maximum diameter, d_{max}.

The drag coefficient is given by Ishii and Chawla[6-3] for the viscous regime as

$$C_D = 24\, (1 + 0.1\, Re_p^{0.75})/Re_p \quad , \tag{6-13}$$

where the particle Reynolds number Re_p is defined as

$$Re_p = \left| v_g - v_f \right| d_o \rho_c / \mu_m \quad . \tag{6-14}$$

The mixture viscosity, μ_m, is $\mu_m = \mu_f / \alpha_f$ for bubbles and $\mu_m = \mu_g / (\alpha_g)^{2.5}$ for droplets.

6.1.3.1.2 Code Implementation--The coefficients for bubbly regime interphase drag as coded in the PHAINT and FIDIS subroutines are tabulated in Appendix 6A. Appendix 6A shows the interphase area per unit volume, a_{gf}, to have the same form and coefficient as Equation (6-11). The relationship for C_D has the same form as Equation (6-13), but with significantly higher coefficients. The manual mentions a critical Weber number of 10 for bubbles, while Appendix 6A shows the code using a value of 5. The difference is based on using an average diameter instead of a maximum diameter.

6.1.3.2 Slug Flow

6.1.3.2.1 Model--Slug flow is modeled as series of Taylor bubbles separated by liquid slugs containing small bubbles. A sketch of a slug flow pattern is shown in Figure 6-1. The Taylor bubble has a diameter nearly equal to the pipe diameter and a length varying from one to one hundred pipe diameters.

Let α_{gs} be the average void fraction in the liquid film and slug region. The void fraction of a single Taylor bubble, α_b, in the total mixture is then

$$\alpha_b = (\alpha_g - \alpha_{gs}) / (1 - \alpha_{gs}) \quad . \tag{6-15}$$

By approximating the ratio of the Taylor bubble diameter to the tube diameter and the diameter-to-length ratio of a Taylor bubble, Ishii and

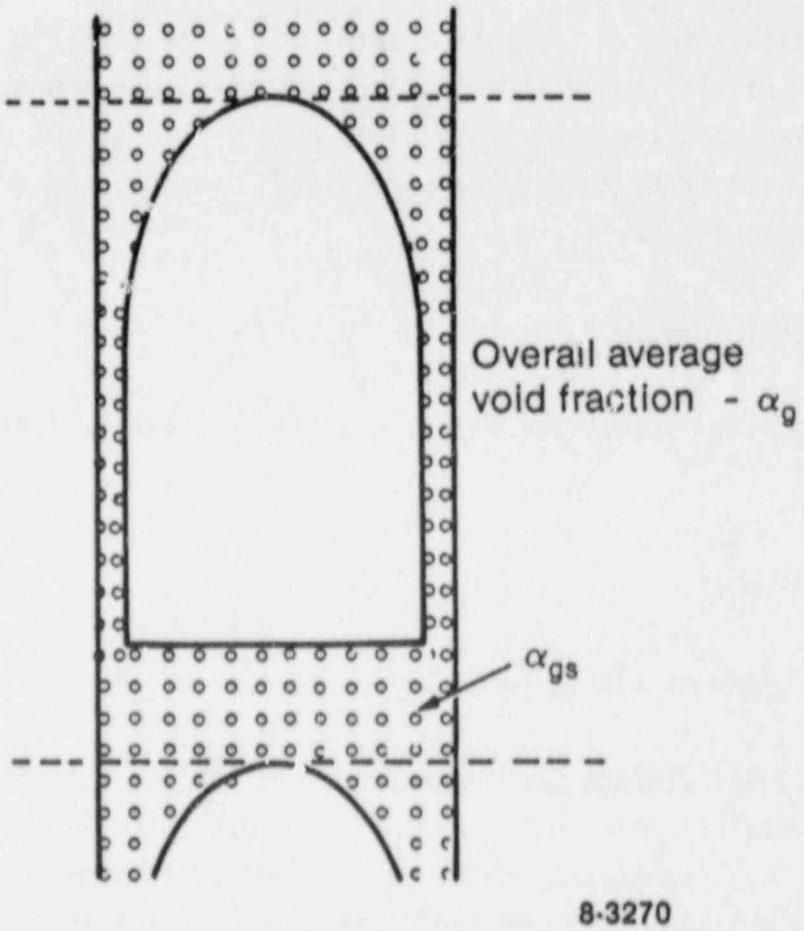

Figure 6-1. Slug flow pattern.

Mishima[6-4] obtained the surface-to-volume ratio of a Taylor bubble as 4.5/D. Consequently, the interfacial area per unit volume, a_{gf}, for slug flow is

$$a_{gf} = (4.5\ C_t/D)\alpha_b + (3.6\ \alpha_{gs}/d_o)(1 - \alpha_b)\ , \qquad (6\text{-}16)$$

where C_t is a roughness parameter that is introduced to account for irregularities in the surface of large Taylor bubbles. C_t is assumed to be unity (1.0) for interphase drag.

To provide a smooth transition into and out of slug flow, α_{gs} [in Equation (6-15)] is considered as a free parameter varying from $\alpha_{B\text{-}S}$ at the bubbly-to-slug flow regime transition to nearly zero at the slug-to-annular mist flow regime transition. The variation is represented by the exponential expression

$$\alpha_{gs} = \alpha_{B\text{-}S} \exp[-\ 8(\alpha_g - \alpha_{B\text{-}S})/\ (\alpha_{S\text{-}A} - \alpha_{B\text{-}S})]\ . \qquad (6\text{-}17)$$

The drag coefficient for Taylor bubbles is given by Ishii and Chawla[6-3] as

$$C_D = 9.8\ (1 - \alpha_b)^3, \qquad (6\text{-}18)$$

where α_b is given by combining Equations (6-15) and (6-17).

6.1.3.2.2 Code Implementation--The coefficients for slug regime interphase drag as coded in the PHAINT and FIDIS subroutines are tabulated in Appendix 6A. Appendix 6A shows the interphase area per unit volume, a_{gf}, to have the same form and coefficient as Equation (6-16). The expression for C_D shown in Appendix 6A has two terms, one of the form of Equation (6-17) but with a different coefficient and based on the α_{TB} rather than on α_B. The second term is of the form of the bubbly C_D in Equation (6-13).

Code results were compared to General Electric level swell experiments[6-5,6] The code was shown to calculate void profiles similar to the experiments. Quantative adequacy will depend on the application.

6.1.3.3 Annular Mist

6.1.3.3.1 Model--Annular mist flow is characterized by a liquid film along the wall and a vapor core containing entrained liquid droplets. Let α_{ff} be the average liquid volume fraction of the liquid film along the wall. Then, from simple geometric considerations, the interfacial area per unit volume can be shown to be

$$a_{gf} = (4C_{an}/D)(1 - \alpha_{ff})^{1/2} + (3.6\alpha_{fd}/d_o)(1 - \alpha_{ff}) \ , \qquad (6\text{-}19)$$

where C_{an} is a roughness parameter introduced to account for waves in the liquid wall film. Its form is

$$C_{an} = (30\ \alpha_{ff})^{1/8} \ .$$

This gives a value near unity for α_{ff} between 0.01 and 0.1, yet ensures that $C_{an} \to 0$ as $\alpha_{ff} \to 0$.

α_{fd} is the average liquid volume fraction in the vapor core, for which

$$\alpha_{fd} = (\alpha_f - \alpha_{ff})/\ (1 - \alpha_{ff}) \ . \qquad (6\text{-}20)$$

A simple relation based on the flow regime transition criterion and liquid Reynolds number is used to correlate the average liquid film volume fraction. For vertical flow regimes, the entrainment relation is

$$\alpha_{ff} = \alpha_f\ C_f\ \exp\left[- 7.5 \times 10^{-5}\ (\alpha_g\ v_g\ /u_c)^6 \right] \ , \qquad (6\text{-}21)$$

where u_c is the entrainment critical velocity given by

$$u_c = 1.4 \left[\sigma g (\rho_f - \rho_g)\right]^{1/4} / \rho_g^{1/2} \quad . \tag{6-22}$$

For horizontal flow regimes, the entrainment relation is

$$\alpha_{ff} = \alpha_f C_f \exp\left[- 4.0 \times 10^{-5} (v_g / v_{gL})^6 \right] , \tag{6-23}$$

where v_{gL} is the horizontal stratification critical velocity given by Equation (3-2). The term C_f is expressed as

$$C_f = 10^{-4} \alpha_f \rho_f v_f \frac{D}{\mu_f} \quad . \tag{6-24}$$

The interfacial friction factor, f_i, for the liquid film takes the place of C_D in Equation (6-4), and is described by a correlation obtained by Bharathan et al.,[6-7] for which

$$f_i = 4[0.005 + A(\delta^*)^B] \tag{6-25}$$

where

$$\log_{10} A = -0.56 + 9.07/D^* \tag{6-26}$$

$$B = 1.63 + 4.74/D^*$$

$$\delta^* = \delta\left[\frac{(\rho_f - \rho_g)g}{\sigma}\right]^{1/2} \quad .$$

The term δ^* is the liquid wall film Deryagin number for which δ is the film thickness, and D^* is the dimensionless diameter given by

$$D^* = D[g(\rho_f - \rho_g)/s]^{1/2} \quad . \tag{6-27}$$

6.1.3.3.2 Code Implementation--The friction factor and interphase area per unit volume for annular mist as coded in subroutine PHAINT are tabulated in Appendix 6A.

6.1.3.4 Inverted Annular, Inverted Slug, Dispersed (Droplet), Horizontally Stratified, Vertically Stratified, and Transition Flow Regimes. The interphase drag coefficient and interphase area per unit volume for these regimes as coded in subroutine PHAINT are tabulated in Appendix 6A.

6.2 Wall Drag

6.2.1 Basis

The field difference equations for the sum momentum equation, Equation (2-61),

$$
\begin{aligned}
&(\alpha_g\rho_g)_j^n\,(v_g^{n+1} - v_g^n)_j\Delta x_j + (\alpha_f\rho_f)_j^n\,(v_f^{n+1} - v_f^n)_j\Delta x_j \\
&\quad + \tfrac{1}{2}(\dot{\alpha}_g\dot{\rho}_g)_j^n\left[(v_g^2)_L^n - (v_g^2)_K^n\right]\Delta t + \tfrac{1}{2}(\dot{\alpha}_f\dot{\rho}_f)_j^n\left[(v_f^2)_L^n - (v_f^2)_K^n\right]\Delta t \\
&\quad - \tfrac{1}{2}\left[(\dot{\alpha}_g\dot{\rho}_g)_j^n VISG_j^n + (\dot{\alpha}_f\dot{\rho}_f)_j^n VISF_j^n\right]\Delta t \\
&= -(P_L - P_K)^{n+1}\,\Delta t + \left[\rho_j^n B_x - (\alpha_g\rho_g)_j^n (v_g)_j^{n+1} FWG_j^n\right. \\
&\quad \left. - (\alpha_f\rho_f)_j^n (v_f)_j^{n+1} FWF_j^n - (\Gamma_g)_j^n (v_g - v_f)_j^{n+1}\right]\Delta x_j\Delta t \\
&\quad - \left[(\dot{\alpha}_g\dot{\rho}_g)_j^n HLOSSG_j^n\, v_{g,j}^{n+1} + (\dot{\alpha}_f\dot{\rho}_f)_j^n HLOSSF_j^n\, v_{f,j}^{n+1}\right]\Delta t
\end{aligned}
\tag{6-28}
$$

and the difference momentum equation, Equation (2-62),

$$
\left[1 + C\rho^2/(\rho_g\rho_f)\right]_j^n\left[(v_g^{n+1} - v_g^n) - (v_f^{n+1} - v_f^n)\right]_j\Delta x_j
$$

$$+ \tfrac{1}{2}\left[(\dot{\alpha}_g\dot{\rho}_g)/(\alpha_g\rho_g)\right]_j^n\left[(v_g^2)_L^n - (v_g^2)_K^n\right]\Delta t - \tfrac{1}{2}\left[(\dot{\alpha}_g\dot{\rho}_g)/(\alpha_g\rho_g)\right]_j^n VISG_j^n\Delta t$$

$$- \tfrac{1}{2}\left[(\dot{\alpha}_f\dot{\rho}_f)/(\alpha_f\rho_f)\right]_j^n\left[(v_f^2)_L^n - (v_f^2)_K^n\right]\Delta t + \tfrac{1}{2}\left[(\dot{\alpha}_f\dot{\rho}_f)/(\alpha_f\rho_f)\right]_j^n VISF_j^n\Delta t$$

$$= - \left[(\rho_f - \rho_g)/(\rho_g\rho_f)\right]_j^n(P_L - P_K)^{n+1}\Delta t - (FWG_j^n(v_g)_j^{n+1} - FWF_j^n(v_f)_j^{n+1}$$

$$- \left[\Gamma_g^n\,(\rho^n v_I^{n+1} - \alpha_f^n\rho_f^n v_g^{n+1} - \alpha_g^n\rho_g^n v_f^{n+1})/(\alpha_g\rho_g\alpha_f\rho_f)^n\right]_j$$

$$+ (\rho FI)_j^n(v_g - v_f)_j^{n+1}\Big)\,\Delta x_j\Delta t - \Big\{\left[(\dot{\alpha}_g\dot{\rho}_g)/(\alpha_g\rho_g)\right]_j^n HLOSSG_j^n v_{g,j}^{n+1}$$

$$- \left[(\dot{\alpha}_f\dot{\rho}_f)/(\alpha_f\rho_f)\right]_j^n HLOSSF_j^n v_{f,j}^{n+1}\Big\}\Delta t \qquad (6\text{-}1)$$

contain the terms

$FWG_j^n(v_g)_j^{n+1}\,\Delta x_j$

and

$FWF_j^n(v_f)_j^{n+1}\,\Delta x_j$.

These terms represent the pressure loss due to wall shear from cell center to cell center of the cell volumes adjoining the particular junction that the momentum equation is considering. There are possibilities of wall shear of single-phase liquid, single-phase vapor, or two-phase mixture. The wall drag or friction is dependent not only on the phase of the fluid but also on the flow regime characteristics.

The wall friction model is based on a two-phase multiplier approach in which the two-phase multiplier is calculated from the heat transfer and fluid flow service (H.T.F.S.) modified Baroczy correlation.[6-8] The individual phasic wall friction components are calculated by apportioning

the two-phase friction between the phases using a technique derived from the Lockhart-Martinelli[6-9] model. The model is based on the assumption that the frictional pressure drop may be calculated using a quasi-steady form of the momentum equation.

The following subsections will describe the two-phase multiplier approach, phase effects, apportioning wall friction, H.T.F.S. two-phase multiplier, flow regime factors, and friction factors.

6.2.1.1 The Two-Phase Friction Multiplier Approach. The overall friction pressure drop can be expressed in terms of the liquid-alone wall friction pressure drop

$$\left(\frac{\partial P}{\partial x}\right)_{2\phi} = \phi_f^2 \left(\frac{\partial P}{\partial x}\right)_f , \tag{6-29}$$

or the vapor-alone wall friction pressure drop

$$\left(\frac{\partial P}{\partial x}\right)_{2\phi} = \phi_g^2 \left(\frac{\partial P}{\partial x}\right)_g , \tag{6-30}$$

where ϕ_f and ϕ_g are the liquid-alone and vapor-alone two-phase friction multipliers, respectively. The phasic wall friction pressure gradients are expressed as

$$\left(\frac{\partial P}{\partial x}\right)_f = \frac{\lambda_f' M_f^2}{2D\rho_f A^2} \tag{6-31}$$

for the liquid-alone, and

$$\left(\frac{\partial P}{\partial x}\right)_g = \frac{\lambda_g' M_g^2}{2D\rho_g A^2} \tag{6-32}$$

for the vapor-alone, where the prime indicates the liquid and vapor-alone friction factors, respectively, calculated at the respective Reynolds numbers

$$Re_f' = \frac{\alpha_f \rho_f |v_f| D}{\mu_f} \tag{6-33}$$

and

$$Re_g' = \frac{\alpha_g \rho_g |v_g| D}{\mu_g} \quad . \tag{6-34}$$

The liquid and vapor mass flow rates, respectively, are defined as

$$M_f = \alpha_f \rho_f v_f A \tag{6-35}$$

and

$$M_g = \alpha_g \rho_g v_g A \quad . \tag{6-36}$$

Throughout the current literature the overall two-phase friction pressure gradient is calculated using two-phase friction multiplier correlations. However, regardless of the correlation used, the multipliers may be interrelated using Equations (6-29) through (6-32) and the Lockhart-Martinelli[6-9] ratio defined as

$$\chi^2 = \frac{(\frac{dP}{dx})_f}{(\frac{dP}{dx})_g} = \frac{\phi_g^2}{\phi_f^2} \quad . \tag{6-37}$$

In RELAP5 these equations are used to apportion the overall wall friction into liquid and vapor wall friction coefficients.

6.2.1.2 Phase Effects. Two-phase friction can be modeled in terms of two-phase friction multipliers and known friction factors using the method developed by Lockhart-Martinelli.[6-9] Chisholm[6-10] also developed a theoretical basis for the Lockhart-Martinelli model that provides a rationale for relating the equations to empirical results.

From the theoretical basis developed by Chisholm, irrespective of flow regime, the quasi-steady phasic momentum equations can be expressed in scalar form as

$$\alpha_f A (\frac{\partial P}{\partial x})_{2\phi} - \tau_f p_f + S_{FI} = 0 \tag{6-38}$$

for the liquid, and

$$\alpha_g A\left(\frac{\partial P}{\partial x}\right)_{2\phi} - \tau_g p_g - S_{FI} = 0 \qquad (6\text{-}39)$$

for the vapor, where τ_f and τ_g are the liquid and vapor wall shear stresses, respectively, p_f and p_g are the liquid and vapor wetted wall perimeters, respectively, and S_{FI} is a stress gradient due to interphase friction. These equations can be expressed in terms of Darcy friction factors and simplified so that

$$\left(\frac{dP}{dx}\right)_{2\phi}\left(1 + S_R \frac{\alpha_g}{\alpha_f}\right) = \frac{\lambda_f \rho_f v_f^2}{2D}\left(\frac{\alpha_{fw}}{\alpha_f}\right) \qquad (6\text{-}40)$$

for the liquid, and

$$\left(\frac{dP}{dx}\right)_{2\phi}(1 - S_R) = \frac{\lambda_g \rho_g v_g^2}{2D}\left(\frac{\alpha_{gw}}{\alpha_g}\right) \qquad (6\text{-}41)$$

for the vapor, where the interphase friction term, S_R, is defined as

$$S_R = \frac{S_{FI}}{\alpha_g A\left(\frac{\partial P}{\partial x}\right)_{2\phi}} \quad . \qquad (6\text{-}42)$$

The terms α_{fw} and α_{gw} are the liquid and vapor volume fractions, respectively, at the wall, and α_f and α_g are the overall liquid and vapor volume fractions, respectively. Taking the ratio of Equation (6-40) to (6-41) gives

$$Z^2 = \frac{\lambda_f \rho_f v_f^2\left(\frac{\alpha_{fw}}{\alpha_f}\right)}{\lambda_g \rho_g v_g^2\left(\frac{\alpha_{gw}}{\alpha_g}\right)} = \frac{1 + S_R \frac{\alpha_g}{\alpha_f}}{(1 - S_R)} \quad . \qquad (6\text{-}43)$$

Consider the pure liquid case where $\alpha_g = 0$ and $\alpha_{fw} = \alpha_f$ and for which Equation (6-40) reduces to

$$\left(\frac{\partial P}{\partial x}\right)_{2\phi} = \left(\frac{\partial P}{\partial x}\right)_f = \frac{\lambda_f \rho_f v_f^2}{2D} \quad . \tag{6-44}$$

For this case, the friction factor, λ_f, can be precisely calculated based on a Reynolds number expressed in terms of D. Similarly, for the two-phase case, liquid and vapor friction factors can be calculated based on the Reynolds numbers of

$$R_f = \frac{\rho_f \left(\frac{\alpha_f}{\alpha_{fw}}\right) D |v_f|}{\mu_f} \quad , \quad R_g = \frac{\rho_g \left(\frac{\alpha_g}{\alpha_{gw}}\right) D |v_g|}{\mu_g} \tag{6-45}$$

for the liquid and vapor, respectively. These terms have the property that as one phase or the other disappears, the friction factors calculated reduce to their single-phase formulations.

Equations (6-40) and (6-41) can be rewritten as

$$\left(\frac{dP}{dx}\right)_{2\phi} \frac{Z^2}{\alpha_g + \alpha_f Z^2} = \frac{\lambda_f \rho_f v_f^2}{2D} \left(\frac{\alpha_{fw}}{\alpha_f}\right) \tag{6-46}$$

$$\left(\frac{dP}{dx}\right)_{2\phi} \frac{1}{\alpha_g + \alpha_f Z^2} = \frac{\lambda_f \rho_f v_g}{2D} \left(\frac{\alpha_{gw}}{\alpha_g}\right) \tag{6-47}$$

for the liquid and vapor, respectively. However, these equations are now flow regime-dependent, since knowledge of the wetted wall and overall void fractions is required in order to calculate the friction factors. The term Z^2 can also be considered as a correlating factor relating the overall two-phase friction pressure gradient to the known phasic friction factors.

The quasi-steady phasic momentum equations similar to Equations (6-46) and (6-47) can also be written in terms of the RELAP5 friction coefficient, where

$$\alpha_f\left(\frac{dP}{dx}\right)_{2\phi}\frac{Z^2}{\alpha_g + \alpha_f Z^2} = FWF(\alpha_f\rho_f v_f) \tag{6-48}$$

for the liquid, and

$$\alpha_g\left(\frac{dP}{dx}\right)_{2\phi}\frac{1}{\alpha_g + \alpha_f Z^2} = FWG(\alpha_g\rho_g v_g) \tag{6-49}$$

for the vapor. Taking the sum of these two equations gives the overall quasi-steady, two-phase pressure gradient as

$$\left(\frac{dP}{dx}\right)_{2\phi} = FWF(\alpha_f\rho_f v_f) + FWG(\alpha_g\rho_g v_g) \tag{6-50}$$

It should be noted that the calculation of the phasic friction factors using the Reynolds numbers given by Equation (6-45) and the assumption that two-phase flows behave similarly to single-phase flows in the laminar, transition, and turbulent regimes provides the rationale relating Equations (6-46) and (6-47) to empirical data. It is this same rationale that allows expressing the correlating term, Z^2, in terms of friction factors that are independent of interphase friction, as given by Equation (6-43). It is this equation that forms the basis for apportioning the overall two-phase wall friction between the phases.

6.2.1.3 Apportioning Wall Friction. Overall two-phase wall friction can be apportioned into phasic components by combining Equations (6-48) and (6-49) with Equations (6-29) through (6-32) and (6-43), (6-46), and (6-47) which results in

$$\phi_f^2\frac{\lambda_f'\rho_f(\alpha_f v_f)^2}{2D}\frac{\alpha_{fw}\lambda_f\rho_f v_f^2}{\alpha_{gw}\lambda_g\rho_g v_g^2 + \alpha_{fw}\lambda_f\rho_f v_f^2} = FWF(\alpha_f\rho_f v_f) \tag{6-51}$$

for the liquid, and

$$\phi_g^2 \frac{\lambda_g' \rho_g (\alpha_g v_g)^2}{2D} \frac{\alpha_{gw} \lambda_g \rho_g v_g^2}{\alpha_{gw} \lambda_g \rho_g v_g^2 + \alpha_{fw} \lambda_f \rho_f v_f^2} = FWG(\alpha_g \rho_g v_g) \quad (6\text{-}52)$$

for the vapor, where the two-phase multiplier terms are calculated using a two-phase friction multiplier correlation. Flow regime effects are also included in the relationships between wetted wall and overall void fractions and their effect in calculating the friction factor terms.

6.2.1.4 The H.T.F.S. Two-Phase Friction Multiplier Correlation. In RELAP5, only the H.T.F.S. correlation[6-8] is used to calculate two-phase friction multipliers. This correlation was chosen because it is correlated to empirical data over very broad ranges of phasic volume fractions, phasic flow rates, and flow regimes. The correlation has also been shown to give good agreement with empirical data.

The H.T.F.S. correlation for the two-phase friction multiplier is expressed as

$$\phi_f^2 = 1 + \frac{C}{\chi} + \frac{1}{\chi^2} \quad (6\text{-}53)$$

for the liquid-alone multiplier, or

$$\phi_g^2 = \chi^2 + C\chi + 1 \quad (6\text{-}54)$$

for the vapor-alone multiplier, where C is the correlation term and χ is the Lockhart-Martinelli ratio given by Equation (6-37). The correlation term is expressed in terms of scalar mass flux, G, and the Baroczy dimensionless property index, A, such that

$$2 \leq C = -2 + f_1(G)\, T_1 \quad (6\text{-}55)$$

where

$$f_1(G) = 28 - 0.3\,(G)^{0.5} \quad (6\text{-}56)$$

$$T_1 = \text{EXP}\left[-\frac{(\log_{10}A + 2.5)^2}{2.4 - G(10^{-4})}\right] \tag{6-57}$$

$$A = \frac{\rho_g}{\rho_f}\left(\frac{\mu_f}{\mu_g}\right)^{0.2} \tag{6-58}$$

$$G = \alpha_f\rho_f v_f + \alpha_g\rho_g v_g \quad . \tag{6-59}$$

The terms ρ, μ, α, and v denote the density, viscosity, volume fraction, and velocity, respectively.

If the H.T.F.S. correlation is combined with the wall friction formulations by combining Equations (6-29) through (6-32), (6-35) through (6-37), (6-63), and (6-54), then

$$\left(\frac{dP}{dx}\right)_{2\phi} = \phi_f^2\left(\frac{dP}{dx}\right)_f = \phi_g^2\left(\frac{dP}{dx}\right)_g$$

$$= \frac{1}{2D}\left[\lambda_f'\rho_f(\alpha_f v_f)^2 + C\sqrt{\lambda_f'\rho_f(\alpha_f v_f)^2\lambda_g'\rho_g(\alpha_g v_g)^2} + \lambda_g'\rho_g(\alpha_g v_g)^2\right] \quad . \tag{6-60}$$

Equation (6-60) can then be combined with Equation (6-51) and (6-52) and simplified such that

$$FWF(\alpha_f\rho_f) = \alpha_{fw}\frac{\rho_f\lambda_f|v_f|}{2D}\left[\lambda_f'\rho_f(\alpha_f v_f)^2 + C\sqrt{\lambda_f'\rho_f(\alpha_f v_f)^2\lambda_g'\rho_g(\alpha_g v_g)^2}\right.$$

$$\left. + \lambda_g'\rho_g(\alpha_g v_g)^2\right] \Big/ \left[\alpha_{gw}\lambda_g\rho_g v_g^2 + \alpha_{fw}\lambda_f\rho_f v_f^2\right] \tag{6-61}$$

for the liquid, and

$$FWG(\alpha_g\rho_g) = \alpha_{gw}\frac{\rho_g\lambda_g|v_g|}{2D}\left[\lambda_f'\rho_f(\alpha_f v_f)^2 + C\sqrt{\lambda_f'\rho_f(\alpha_f v_f)^2\lambda_g'\rho_g(\alpha_g v_g)^2}\right.$$

$$+ \lambda'_g \rho_g (\alpha_g v_g)^2 \Big] \Big/ \Big[\alpha_{gw} \lambda_g \rho_g v_g^2 + \alpha_{fw} \lambda_f \rho_f v_f^2 \Big] \qquad (6\text{-}62)$$

for the vapor.

In RELAP5, the friction factor and velocity terms are calculated in such a manner that as the velocity terms disappear, the equations give the correct limits. For example, the friction factor terms are evaluated such that

$$\lim_{|(\frac{\alpha_f}{\alpha_{fw}})v_f| \to 0} (\lambda_f |(\frac{\alpha_f}{\alpha_{fw}})v_f|) = \frac{64\mu_f}{D\rho_f} = \lim_{|\alpha_f v_f| \to 0} (\lambda'_f |\alpha_f v_f|)$$

$$\lim_{|(\frac{\alpha_g}{\alpha_{gw}})v_g| \to 0} (\lambda_g |(\frac{\alpha_g}{\alpha_{gw}})v_g|) = \frac{64\mu_g}{D\rho_g} = \lim_{|\alpha_g v_g| \to 0} (\lambda'_g |\alpha_g v_g|) \qquad (6\text{-}63)$$

and the velocity terms are evaluated such that

$$\lim_{|v_f| \to 0} |v_f| = \epsilon = \lim_{|v_g| \to 0} |v_g| \qquad (6\text{-}64)$$

Hence, for stagnant flow or single-phase conditions, a positive and finite friction coefficient is always calculated. Thus, the numerical possibility of an infinite or negative friction coefficient is eliminated.

In Equations (6-61) and (6-62), flow regime effects are included in the terms (α_{fw}/α_f) and (α_{gw}/α_g) for the liquid and vapor, respectively. These terms are such that

$$\alpha_{fw} = 1 - \alpha_{gw} \qquad (6\text{-}65)$$

$$\alpha_f = 1 - \alpha_g \quad . \qquad (6\text{-}66)$$

Equations (6-65) and (6-66) are restricted such that as overall phasic volume fraction disappears its corresponding wall film volume fraction disappears so that

$$\lim_{\alpha_f \to 0} \left(\frac{\alpha_{fw}}{\alpha_f}\right) = 1, \quad \lim_{\alpha_f \to 0} \left(\frac{\alpha_{gw}}{\alpha_g}\right) = 1 \tag{6-67}$$

and similarly,

$$\lim_{\alpha_g \to 0} \left(\frac{\alpha_{gw}}{\alpha_g}\right) = 1, \quad \lim_{\alpha_g \to 0} \left(\frac{\alpha_{fw}}{\alpha_f}\right) = 1 \quad . \tag{6-68}$$

6.2.1.5 Flow Regime Factors for Phasic Wall Friction. Phasic wall friction is expressed in terms of wall shear stress, which in turn requires knowledge of the surface area wetted by each phase. From the flow regime model discussed in Section 3, expressions for the wall film phasic volume fractions can be derived. Using these expressions, the phasic wall friction factors that appear in Equations (6-40) and (6-41) may then be computed.

In the flow regime map, seven flow regimes are modeled, which are; for pre-CHF heat transfer, the bubbly, slug, and annular mist; for post-CHF heat transfer, the inverted-annular, inverted-slug, and mist; and for stratified flow, the vertically and horizontally stratified. For the transition regime between pre- and post-CHF heat transfer, an interpolation scheme is also implemented in the code.

To implement flow regime effects in the two-phase wall friction model, first consider the wall liquid and vapor volume fractions. These terms are

$$\frac{p_f}{p} = \alpha_{fw} \, , \tag{6-69}$$

which represents the liquid volume fraction in the wall film and

$$\frac{p_g}{p} = \alpha_{gw} \, , \tag{6-70}$$

which represents the vapor volume fraction in the wall film where the terms p_f, p_g, and p are the perimeters wetted by the liquid, vapor, and mixture, respectively. Then, from the flow regime model, these are formulated for all of the flow regimes in Appendix 6A.

6.2.1.6 The Friction Factor Model. In RELAP5, the friction factor is computed using a high-speed calculational scheme representing an engineering approximation to the Colebrook correlation.[6-11]

The friction factor model is simply an interpolation scheme linking the laminar, laminar-turbulent transition, and turbulent-full turbulent transition regimes. The laminar friction factor is calculated as

$$\lambda_L = \frac{64}{R}, \quad 0 \leq R \leq 2000 , \tag{6-71}$$

where R is the Reynolds number. The laminar-turbulent friction factor is interpolated as

$$\lambda_{L,T} = 5.285 \left[1.189 - \left(\frac{4000}{R}\right)^{0.25}\right] (\lambda_{t,4000} - \lambda_{L,2000}) + \lambda_{L,2000}, \quad 2000 < R < 4000 \tag{6-72}$$

where $\lambda_{L,2000}$ is the laminar factor at a Reynolds number of 2000 and where $\lambda_{t,4000}$ is the turbulent friction factor at a Reynolds number of 4000. The interpolation factor is defined such that

$$0 \leq 5.285 \left[1.189 - \left(\frac{4000}{R}\right)^{0.25} \right] \leq 1 \tag{6-73}$$

The turbulent-full turbulent friction factor is interpolated as

$$\lambda_{t,tt} = \frac{\left[1 - \left(\frac{4000}{R}\right)^{0.25}\right]}{\left[1 - \left(\frac{4000}{R_c}\right)^{0.25}\right]} (\lambda_{tt} - \lambda_{t,4000}) + \lambda_{t,4000}, \quad 4000 \leq R \leq R_c , \tag{6-74}$$

where the interpolation factor is defined such that

$$0 \leq \frac{[1 - (\frac{4000}{R})^{0.25}]}{[1 - (\frac{4000}{R_c})^{0.25}]} \leq 1 \qquad (6\text{-}75)$$

and R_c is the critical Reynolds number at which the Colebrook equation gives a constant friction factor of

$$\lambda_{tt} = [1.74 - 2\text{Log}_{10}(2\epsilon/D)]^{-2} \qquad (6\text{-}76)$$

and where ϵ is the surface roughness.

The critical Reynolds number is given as

$$R_c = \frac{378.3}{\sqrt{\lambda_{tt}}} (\frac{2\epsilon}{D})^{-1} \quad . \qquad (6\text{-}77)$$

If precise values for $\lambda_{t,4000}$ are used, Equations (6-71) and (6-72) are identical to the formulations used in the Colebrook friction factor model for the laminar and transition regimes. Equation (6-76) is also identical to the solution of the Colebrook model for Reynolds numbers greater than the critical Reynolds number. Therefore, the interpolation scheme in the friction factor model lies in the formulation of Equation (6-74), which is linear in $(1/R)^{0.25}$. The maximum deviation between the friction factor calculated using Equation (6-74) and that calculated using the Colebrook correlation is within the third significant figure for a moderate ϵ/D of 0.0003. As ϵ/D increases, the deviation decreases until at an ϵ/D such that $R_c < 4000$ the value given by Equation (6-74) is precisely that of Equation (6-76). In any case, the results calculated using Equation (6-74) are negligibly different from those calculated by the Colebrook equation. This accuracy is achieved using a good estimate for $\lambda_{t,4000}$ given by

$$\lambda_{t,4000} = \lambda_o + K(\lambda_{tt} - \lambda_1) \qquad (6\text{-}78)$$

where λ_o is a constant evaluated from the Blasius smooth pipe formula at a Reynolds number of 4000, such that $\lambda = 0.0398$.

The coefficients have been evaluated as $K = 0.558$, $\lambda_1 = 0.0158$, by the method of least squares.

In calculational schemes, it is desirable to evaluate the friction factor in terms of $\lambda|\psi v|$ so that the limiting terms will be correctly calculated as defined by Equation (6-63). For this case, the Reynolds number must be defined as

$$R = \frac{\rho D}{\mu} |\psi v| \tag{6-79}$$

and Equation (6-74) can be rewritten as

$$\lambda|\psi v| = \lambda_L^* + L[5.285\ (1.189 - R^*)](L[(1 - R^*)/(1 - R_c^*)]$$

$$(\lambda_{tt} - \lambda_{t,4000})\ |\psi v| + \lambda_{t,4000}|\psi v| - \lambda_L^*) \tag{6-80}$$

where $L(y)$ denotes a general limit function such that

$0 \leq L(y) \leq 1$,

$R^* = (4000/R)^{0.25}$, $R_c^* = (4000/R_c)^{0.25}$,

and

$R \geq 2000$, $R_c \geq 4000$,

and where the laminar term is

$$\lambda_L^* = \frac{64\mu}{\rho D} \ . \tag{6-81}$$

The accuracy of the improved friction factor model can be observed in Figure 6-2, which is a plot of results calculated by Equation (6-80) compared to similar results calculated by the Colebrook equation. Four curves are plotted for each model representing roughness-to-diameter ratios of $2\epsilon/D = 0.0$, 0.0006, and 0.02, and 0.1, respectively. Equation (6-80)

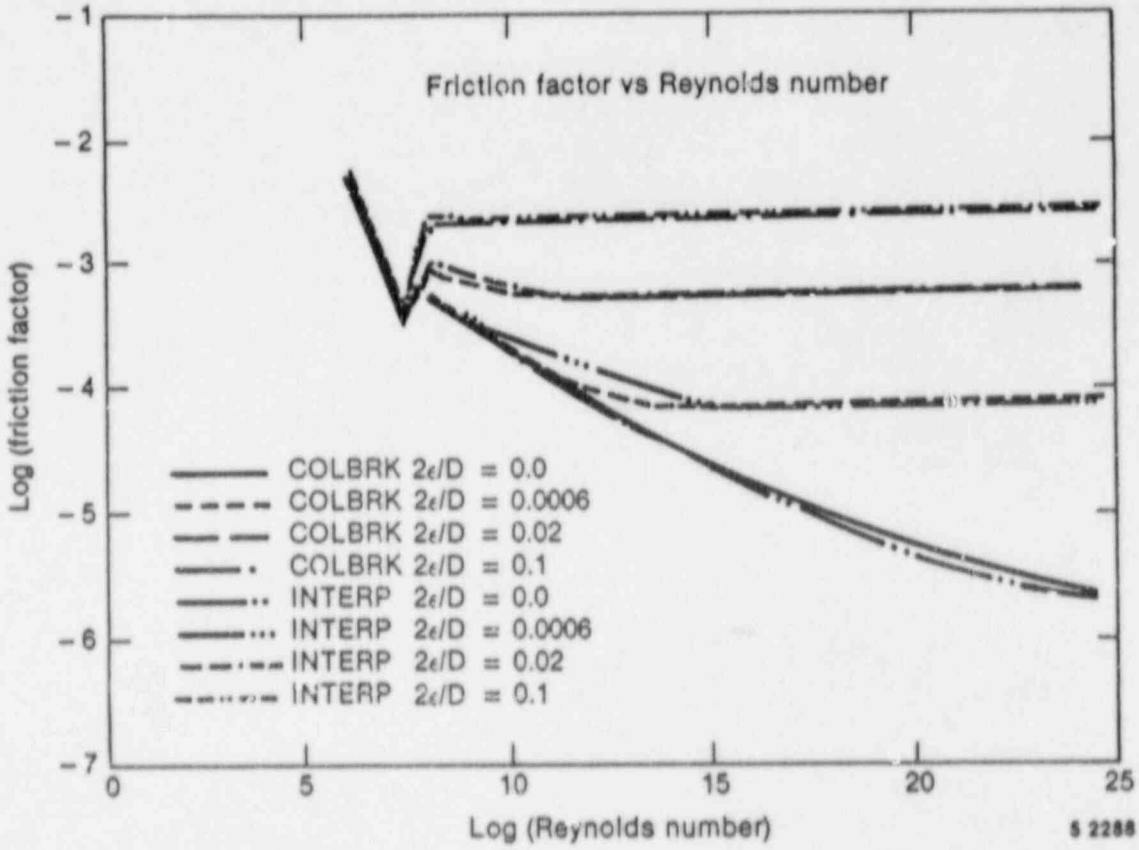

Figure 6-2. Comparison of friction factors for the Colebrook and the improved RELAP5 friction factor models.

results are labeled INTERP in the plot legend. Colebrook equation[6-11] results are labeled COLBRK in the plot legend. The axes of the plot are scaled logarithmically.

6.2.2 General Code Implementation

The wall drag model is used to determine friction terms in the sum and difference momentum equations solved for liquid and vapor velocities as discussed in Section 6.1.2 for the semi-implicit scheme. A short section of listing from VEXPLT show the sum and difference equations and the wall friction terms, FRICFJ and FRICGJ.

```
c
c        loss factors for momentum equations and dissipation
  453 hlossf = (abs(velfjo(i))+scrach)*rfvfj*(formfj(i)+flossf+fjet)
      hlossg = (abs(velgjo(i))+scrach)*rgvgj*(formgj(i)+flossg+fjet)
c
  470 signi=sign(1.0,xjc(i))
      signil=sign(1.0,xjc(i+1))
      delpz = ncrosk*dz(k)*rho(k)*signi + ncrosl*dz(l)*rho(l)*signil
      psmf=(fricfj+hlossf)*avrf
      psmg=(fricgj+hlossg)*avrg
      psld=-(convfs+convgs)-delpz+ph
      vpgnx=vpgen*dx
c

c        sum momentum equation
c        ---------------------
      sumf=avrf*dx+(psmf-vpgnx)*dt
      sumg=avrg*dx+(psmg+vpgnx)*dt
      sumold = (avrf*velfjo(i) + avrg*velgjo(i))*dx
     *       + eturbn*(po(k)-po(l))*dt + psld*dt
c       vapor generation term for difference equation
      scrach = avrg
      if(vpgen.lt.0.0) scrach = -avrf
      vpgnx  = vpgnx/scrach
c
c        virtual mass interaction
      virmas = faaj(i)*avrho**2/rhofga
c
c        difference momentum equation
c        ----------------------------
      difr=eturbn*(rhoga-rhofa)/rhofga
      scrach=(1.0+virmas)*dx
      diff=scrach+(fricfj+fjfg+vpgnx+hlossf)*dt
      difg=-scrach-(fricgj+fjfg+vpgnx+hlossg)*dt
      difold=(velfjo(i)-velgjo(i))*scrach-(difr*(po(l)-po(k))
     1       +(convf-convg)-dpstf(ix))*dt
c
```

The sum momentum equation contains terms PSMF and PSMG that are dependent on FRICFJ and FRICGJ, while the difference momentum equation uses the FRICFJ and FRICGJ themselves. The point of showing the list and noting the terms is to trace the wall drag terms from the solution back to the place where they are determined.

The development of the FRICFJ and FRICGJ terms from an earlier point in subroutine VEXPLT is shown in the listings as

```
c
c ----- liquid friction
      fricfk = ncrosk*dxk*fwalf(k)*ravrf
      fricfl = ncrosl*dxl*fwalf(l)*ravrf
c
c ----- vapor friction
      fricgk = ncrosk*dxk*fwalg(k)*ravrg
      fricgl = ncrosl*dxl*fwalg(l)*ravrg
c
c ----- junction friction
          fricfj     = fricfk + fricfl
          fricgj     = fricgk + fricgl
c
```

The k and l subscripts indicate upstream and downstream volumes relative to the junction of interest.

The FWALF and FWALG terms contain the friction model information and are determined in subroutine FWDRAG with some necessary variables being calculated in earlier subroutines. For instance, flow regime effects are calculated in subroutine PHAINT, and for the wall drag model, the pertinent flow regime effect is the measure of the wetted wall area. In Appendix 6A, the α_{fw} and α_{gw} terms listed represent the fractions of the wall wetted and not wetted respectively.

Also calculated in earlier subroutines and passed to the wall drag model are the critical Reynolds number, old time volume averaged flows, and a factor for interpolation between wet wall and dry wall flow regime friction factors. The critical Reynolds number is the same as shown in Equation (6-77).

The wall drag model in subroutine FWDRAG makes two loops over all volume cells. The first calculates the single-phase friction factors for wet wall and/or dry wall cases and interpolates if both cases are present. The second loop tests to see if the fluid is two-phase and, if so, calculates the H.T.F.S two-phase multiplier and, for either single- or two-phase, makes a final calculation of the FWALF and FWALG. In VEXPLT, the FWALF and FWALG are combined with other terms to form FRICFJ and FRICGJ, as shown on the previous page. The FWF and FWG terms in Equations (6-28) and (6-1) are related to the FRICFJ and FRICGJ terms by the relations FRICFJ = FWF·Δx and FRICGJ = FWG·Δx, where Δx is half the length of the upstream volume plus half the length of the downstream volume.

The single-phase friction relation as programmed in RELAP5 appears to agree with the development of Section 6.2.1.5 and the equivalent portion of the manual, but this area needs further verification in subroutine FWDRAG. It should be noted that the expression for critical Reynolds number is wrong, as printed in the manual.

In an effort to verify the single-phase friction relation, some representative points in Figure 6-1 were checked with both a solution to the Colebrook equation, the friction factor from Equation (6-76) and the critical Reynolds number Equation (6-77). The resulting calculated points were consistant with Figure 6-2.

The H.T.F.S. correlation is programmed as is described in Section 6.2.1.4 with the exception that a maximum value of the scalar mass flux, G, set as 8711.1111 in SI values, is used in subroutine FWDRAG. This value is used to ensure that $f_1(G) \geq 0$ in Equation (6-56). Also the exponent on G in the subroutine and in Equation (6-56) of Section 6.2.1.4 is one half, while the manual evidently has a typo and shows no exponent.

6.3 Entrainment Correlation

In the annular-mist flow regime, the calculation of wall-to-coolant heat transfer requires the proper apportioning of the liquid in the wall region as an annular film and in the vapor region as droplets. The code uses the Ishii and Mishima[6-12,13] correlation for the entrainment fraction as a basis for calculating the liquid volume fraction in the film region and the liquid volume fraction in the vapor region. The correlation determines the fraction of liquid flux flowing as droplets by the following expression:

$$E = \tanh \left(7.25 \times 10^{-7} \, We^{1.25} \, Re_f^{0.25}\right) \tag{6-82}$$

where

We = Weber number for entrainment

Re_f = total liquid Reynolds number.

The Ishii-Mishima entrainment correlation has been compared to air-water data over the ranges 1 atm < P < 4 atm, 0.95 cm < D < 3.2 cm, $370 < Re_f < 6400$, and $j_g < 100$ m/s, with satisfactory results. The correlation has also been developed to account for entrance effects and the development of entrainment.

The code, using the Ishii-Mishima correlation as a basis for determining entrainment, calculates the fraction of the total liquid volume residing in the annular film region (α_{ff}) by:

$$\frac{\alpha_{ff}}{\alpha_f} = \text{Max} \left(0.0, F_{11}\right) \quad , \tag{6-83}$$

where

$$F_{11} = \gamma^* \, \text{Max} \left[0.0, (1 - G^*)\right] \exp \left(-C_e \times 10^{-5} \lambda^6\right)$$

γ^* = factor accounting for entrance effects and ranges from 0.0 to 1.0

$G^* = (10^{-4})(Re_f^{0.25})$

$$C_e = \begin{cases} 4.0 & \text{horizontal} \\ 7.5 & \text{vertical} \end{cases}$$

$$\lambda = \begin{cases} [\text{Max}\ (v_g,\ 10^{-15})]/v_{crit} & \text{horizontal} \\ \alpha_g v_g / v_{crit} & \text{vertical} \end{cases}$$

$$v_{crit} = \begin{cases} 0.5 \left[\dfrac{(\rho_f - \rho_g)\ g\ \alpha_g\ A_{pipe}}{\rho_g\ D \sin\theta}\right]^{1/2} (1 - \cos\theta) & \text{horizontal} \\ 1.4\ [\sigma^* g\ (\rho_f - \rho_g)]^{1/4} / \rho_g^{1/2} & \text{vertical} \end{cases}$$

$\sigma^* = \text{Max}\ (\sigma,\ 10^{-7})$.

From this expression, the fraction of liquid volume that exists as droplets α_{fg} in the vapor phase can be calculated since

$$\alpha_{ff} + \alpha_{fg} = \alpha_f . \qquad (6\text{-}84)$$

Dividing by the total liquid volume fraction (α_f) and substituting Equation (6-83) yields

$$\frac{\alpha_{fg}}{\alpha_f} = (1 - F_{11}) \quad . \qquad (6\text{-}85)$$

This relationship provides the entrainment volume fraction that is comparable to the Ishii-Mishima parameter (E) calculated in Equation (6-82).

To demonstrate that the entrainment correlation in the code calculates the same entrainment fraction that the Ishii-Mishima correlation would

predict, a set of conditions was taken from a small-break calculation for the Semiscale facility (Reference 6-14). The code indicated that the annular mist flow regime existed at the subject location. The conditions of the coolant are summarized as

ρ_g = 28.64 kg/m^3

ρ_f = 765.86 kg/m^3

v_g = 0.90463 m/s

v_f = 0.31068 m/s

D = 0.0127 m

α_g = 0.9980

α_f = 2.0E-3

μ_f = 9.689E-5 N/m

The Ishii-Mishima correlation calculated a liquid volume fraction existing as droplets in the vapor region of E = 0.0004978. The RELAP5/MOD2 code calculated the fraction to be 0.0004633, which suggests that the code representation of the correlation is relatively accurate.

6.4 References

6-1. G. B. Wallis, One-Dimensional Two-Phase Flow, New York: McGraw-Hill Book Company, 1969.

6-2. A. H. Shapiro and A. J. Erickson, Transactions of ASME, 79, 1957, p. 775.

6-3. M. Ishii and T. C. Chawla, Local Drag Laws in Dispersed Two-Phase Flow, NUREG/CR-1230, ANL-79-105, 1979.

6-4. M. Ishii and K. Mishima, Study of Two-Fluid Model and Interfacial Area, NUREG/CR-1873, ANL-80-111, 1980.

6-5. V. H. Ransom et al., RELAP5/MOD2 Code Manual, Volume 3: Developmental Assessment Problems, EGG-TFM-7952, December 1987.

6-6. H. Chow and V. H. Ransom, "A Simple Interphase Drag Model for Numerical Two-Fluid Modeling of Two-Phase Flow Systems", ANS Topical Meeting on Nuclear Thermal Hydraulics, New Orleans, LA, June 1984.

6-7. D. Bharathan, H. T. Richter and G. B. Wallis, Air-Water Counter-Current Annular Flow in Vertical Tubes, EPRI NP-786, 1978.

6-8. K. T. Chaxton, J. G. Collier, J. A. Ward, H.T.F.S., Correlation for Two-Phase Pressure Drop and Void Fraction in Tubes, AERE-R7162, 1972.

6-9. R. W. Lockhart and R. C. Martinelli, "Proposed Correlation of Data for Isothermal Two-Phase, Two Component Flow in Pipes," Chemical Engineering Progress, 45, 1, 1949, pp. 39-48.

6-10. D. Chisholm, "A Theoretical basis for the Lockhart-Martinelli Correlation for Two-Phase Flow," J. Heat-Mass Transfer, 10, 1967, pp. 1767-1778.

6-11. C. F. Colebrook, "Turbulent Flow in Pipes with Particular Reference to the Transition Region Between Smooth and Rough Pipe Laws," J. Institution Civil Engineers, 11, pp. 133-156, 1939.

6-12. I. Kataoka and M. Ishii, "Entrainment and Deposition Rates of Droplets in Annular Two-Phase Flow," CONF-830301-11, ASME-JSME Thermal Engineering Joint Conference; Honolulu, HI, March 20, 1985.

6-13. M. Ishii and K. Mishima, Correlations for Liquid Entrainment in Annular Two-Phase Flow of Low Viscous Fluid, Argonne National Laboratory Report, ANL/RAS/LWR 81-2, 1981.

6-14. M. Megahed, RELAP5/MOD2 Assessment Simulation of Semiscale MOD-2C, Test S-NH-3, NUREG/CR-4799, EGG-2519, October 1987.

APPENDIX 6A

COEFFICIENTS FOR INTERFACIAL AND WALL DRAG MODELS AS CODED FOR VOLUME CELLS FOR RELAP5/MOD2

APPENDIX 6A

COEFFICIENTS FOR INTERFACIAL AND WALL DRAG MODELS AS CODED FOR VOLUME CELLS FOR RELAP5/MOD2

Bubbly Flow

Interfacial Drag

$$f_{gf} = \frac{1}{8} \rho_f \, a_{gf} \, C_D$$

where

$\frac{1}{8} C_D = (5.0 + 0.37 \, Re_b^{0.75})/Re_b$

$a_{gf} = 3.6 \, \alpha_{bub}/d_b$, $\alpha_{bub} = Max(\alpha_g, 10^{-5})$

d_b = average bubble diameter

$= (We \, \sigma)/(\rho_f \, v_{fg}^2)$, $We = 5$, $We \, \sigma = Max(We \, \sigma, 10^{-10})$

v_{fg} is as for bubbly flow SHL, Appendix 4A

$$Re_b = \frac{We \, \sigma \, (1 - \alpha_{bub})}{\mu_f \, (v_{fg}^2)^{0.5}}$$

Wall Drag

$\alpha_{fw} = \alpha_f$

$\alpha_{gw} = \alpha_g$

Slug Flow

Interfacial Drag

$f_{gf} = f_{gf,TB} + f_{gf,bub}$

where

$$f_{gf,TB} = \frac{1}{8} \rho_f \, a_{gf,TB} \, C_{D,TB}$$

where

$$a_{gf,TB} = 4.5 \, \alpha_{TB}/D$$

α_{TB} is as for slug flow SHL, Appendix 4A

$$\frac{1}{8} C_{D,TB} = 1.225 \, (1 - \alpha_{TB})^3$$

and

$$f_{gf,bub} = \frac{1}{8} \rho_f \, a_{gf,bub} \, C_{D,bub}$$

where

$$a_{gf,bub} = (3.6 \, \alpha_{gs}/d_b)(1 - \alpha_{TB})$$

$$\frac{1}{8} C_{D,bub} = (5.0 + 0.37 \, Re_s^{0.75})/Re_s$$

$$Re_s = \frac{We \, \sigma \, (1 - \alpha_{bub})}{\mu_f \, (v_{fg}^2)^{0.5}}, \quad We = 5.0, \quad We \, \sigma = Max \, (We \, \sigma, \, 10^{-10})$$

α_{bub}, α_{gs}, d_b, and v_{fg} are as for slug flow SHL, Appendix 4A.

Wall Drag

$$\alpha_{fw} = (1 - \alpha_{bub})$$

$$\alpha_{gw} = \alpha_{bub}$$

α_{bub} is as above .

Annular Mist Flow

Interfacial Drag

$$f_{gf} = f_{gf,ann} + f_{gf,drp}$$

where

$$f_{gf,ann} = \frac{1}{8} \rho_g \, a_{gf,ann} \, C_{D,ann}$$

where

$$a_{gf,ann} = (4 \, C_{ann}/D)(1 - \alpha_{ff})^{0.5}$$

$$C_{ann} = (30 \, \alpha_{ff})^{1/8}$$

α_{ff} is as for annular mist flow SHL, Appendix 4A

$$\frac{1}{8} C_{D,ann} = 0.0025 + 0.1375 \, (10)^{9.07/D^*} \, (\delta^*)^{1.63 + 4.74/D^*}$$

$$D^* = D[g(\rho_f - \rho_g)/\sigma]^{0.5}, \; 1/D^* = \text{Min} \, (30.0, \; 1/D^*)$$

$$\delta^* = \delta[g(\rho_f \quad \rho_g)/\sigma]^{0.5}, \; \delta^* = \text{Max} \, (10^{-8}, \; \delta^*)$$

where

δ = annular liquid film thickness

$= \frac{1}{2} (D - D')$, D' = diameter of annulus

$= \frac{D}{2} (1 - D'/D) = \frac{D}{2} [1 - (1 - \alpha_{ff})^{1/2}]$

α_{ff} is as for annular mist flow SHL, Appendix 4A

and

$$f_{gf,drp} = \frac{1}{8} \rho_g \, a_{gf,drp} \, C_{D,drp}$$

where

$$a_{gf,drp} = \frac{3.6 \, \alpha_{fd}}{d_d} (1 - \alpha_{ff})$$

α_{fd}, d_d are as for annular mist flow SHL, Appendix 4A

$$\frac{1}{8} C_{D,drp} = (5.0 + 0.37 \, Re_{drp}^{0.75})/Re_{drp}$$

$$Re_{drp} = \frac{We\ \sigma(1 - \alpha_{fd})^{2.5}}{\mu_g\ (v_{fg}^2)^{0.5}},\ We = 1.5,\ We\ \sigma = Max\ (We\ \sigma, 10^{-10})$$

v_{fg} is as for annular mist flow SHL, Appendix 4A

Wall Drag

$$\alpha_{fw} = \alpha_f^{0.25}$$

$$\alpha_{gw} = 1 - \alpha_f^{0.25}$$

Inverted Annular Flow

Interfacial Drag

$$f_{gf} = f_{gf,bub} + f_{gf,ann}$$

where

$$f_{gf,bub} = \frac{1}{8}\ \rho_f\ a_{gf,bub}\ C_{D,bub}$$

where

$$a_{gf,bub} = \frac{3.6\ \alpha_{bub}}{d_b}\ (1 - \alpha_B)$$

α_{bub}, d_b, α_B are as for inverted annular SHL, Appendix 4A

$$\frac{1}{8}\ C_{D,bub} = (5.0 + 0.37\ Re_b^{0.75})/Re_b$$

$$Re_b = \frac{We\ \sigma\ (1 - \alpha_{bub})}{\mu_f\ (v_{fg}^2)^{1/2}},\ We = 5.0,\ We\ \sigma = Max\ (We\ \sigma,\ 10^{-10})$$

v_{fg} as for inverted annular flow SHL, Appendix 4A

and

$$f_{gf,ann} = \frac{1}{8}\ \rho_f\ a_{gf,ann}\ C_{D,ann}$$

where

$$a_{gf,ann} = (4/D)(1 - \alpha_B)^{0.5}$$

$\frac{1}{8} C_{D,ann}$ is as for annular mist interfacial drag above except with α_B replacing α_{ff}

Wall Drag

$\alpha_{fw} = 1 - \alpha_B^{0.25}$

$\alpha_{gw} = \alpha_B^{0.5}$, α_B as for inverted annular interfacial drag.

Inverted Slug Flow

Interfacial Drag

$f_{gf} = f_{gf,ann} + f_{gf,drp}$

where

$$f_{gf,ann} = \frac{1}{8} \rho_f a_{gf,ann} C_{D,ann}$$

where

$$a_{gf,ann} = 4.5 \alpha_B/D$$

α_B is as for inverted slug flow SHL, Appendix 4A

$$\frac{1}{8} C_{D,ann} = 1.225 (1 - \alpha_B)^3$$

and

$$f_{gf,drp} = \frac{1}{8} \rho_g a_{gf,drp} C_{D,drp}$$

where

$$a_{gf,drp} = (3.6 \alpha_{drp}/d_d)(1 - \alpha_B)$$

α_{drp}, d_d are as for inverted slug SHL, Appendix 4A

$$C_{D,drp} = (5.0 + 0.37 Re_{drp}^{0.75})/Re_{drp}$$

$$Re_{drp} = \frac{We\ \sigma\ (1 - \alpha_{drp})^{2.5}}{\mu_g\ (v_{fg}^2)^{0.5}},\ We = 1.5,\ We\ \sigma = Max(We\ \sigma,\ 10^{-10})$$

v_{fg}^2 is as for inverted slug SHL, Appendix 4A

Wall Drag

$\alpha_{fw} = \alpha_{drp}$

$\alpha_{gw} = 1 - \alpha_{drp}$, α_{drp} as for inverted slug interfacial drag

Dispersed (Droplet) Flow

Interfacial Drag

$f_{gf} = \frac{1}{8}\ \rho_g\ a_{gf}\ C_D$

where

$a_{gf} = 3.6\ \alpha_{drp}/d_d$

α_{drp}, d_d are as for dispersed flow SHL, Appendix 4A

$C_D = (\frac{2}{3}.0 + 0.37\ Re_{drp}^{0.75})/Re_{drp}$

$$Re_{drp} = \frac{We\ \sigma\ (1 - \alpha_{drp})^{2.5}}{\mu_g\ (v_{fg}^2)^{0.5}},\ We = 1.5,\ We\ \sigma = Max\ (We\ \sigma,\ 10^{-10})$$

v_{fg} as for dispersed flow SHL, Appendix 4A.

Wall Drag

$\alpha_{fw} = \alpha_f$

$\alpha_{gw} = \alpha_g$

Horizontally Stratified Flow

Interfacial Drag

$$f_{gf} = \frac{1}{8} \rho_g \, a_{gf} \, C_D$$

where

$$a_{gf} = 4 \sin\theta / \pi D$$

$$\frac{1}{8} C_D = \frac{1}{8} \text{Max} \begin{bmatrix} 64/Re_g \\ 0.3164/Re_g^{0.25} \end{bmatrix}$$

$$Re_g = \rho_g \, (|\, v_g - v_f| + 0.01) \, D_{hg}/\mu_g$$

D_{hg} = hydraulic diameter, gas phase

$$= \pi \alpha_g D/(\theta + \sin\theta)$$

Wall Drag

$$\alpha_{fw} = 1 - \alpha_g^*$$

$$\alpha_{gw} = \alpha_g^*$$

$$\alpha_g^* = \theta/\pi$$

Vertically Stratified Flow

Interfacial Drag

The interfacial drag for the junction above a vertically stratified volume is taken as that associated with the control volume immediately above the stratified volume.

Wall Drag

$$\alpha_{fw} = \alpha_f$$

$\alpha_{gw} = \alpha_g$

Transition Flow Regimes

Note: The abbreviations for the flow regimes are defined in Figures 3-1 and 3-5.

Horizontal Flow

Slug-Annular Mist Transition

$$f_{gf_{SLUG/ANM}} = \left[f_{gf_{SLUG}}\right]^{FSLUG} \left[f_{gf_{ANN}}\right]^{FANM}$$

$$FWF_{SLUG/ANM} = (FWF_{SLUG})FSLUG + (FWF_{ANM})\ FANM$$

$$FWG_{SLUG/ANM} = (FWG_{SLUG})FSLUG + (FWG_{ANM})\ FANM$$

where FSLUG and FANM are as for Transitions, Appendix 4A

Transition to Horizontally Stratified Flow

$$f_{gf_{REG-HS}} = f_{gf_{REG}} \left[\frac{f_{gf_{HS}}}{f_{gf_{REG}}}\right]^{FSTRAT}$$

$$FWF_{REG-HS} = (FWF_{HS})\ FSTRAT + (FWF_{REG})(1 - FSTRAT)$$

$$FWG_{REG-HS} = (FWG_{HS})\ FSTRAT + (FWG_{REG})(1 - FSTRAT)$$

where FSTRAT is as for transitions, Appendix 4A, and REG = BUB, SLUG, SLUG/ANM, ANM or DIS as appropriate.

Vertical Flow

Slug-Annular Mist Transition

The same formulas as for horizontal flow apply

Inverted Annular-Inverted Slug Transition

$$f_{gf_{IAN/ISLG}} = \left[f_{gf_{IAN}}\right]^{FIAN} \left[f_{gf_{ISLG}}\right]^{FISLG}$$

$$FWF_{IAN/ISLG} = (FWF_{IAN})FIAN + (FWF_{ISLG})FISLG$$

$$FWG_{IAN/ISLG} = (FWG_{IAN})FIAN + (FWG_{ISLG})FISLG$$

where FIAN and FISLG are as for transitions, Appendix 4A

Transition Boiling Regimes

$$f_{gf_{REG1-REG2}} = f_{gf_{REG1}}\left[\frac{f_{gf_{REG2}}}{f_{gf_{REG1}}}\right]^{Z}$$

where

REG1-REG2 can represent BUB-IAN, SLUG-(IAN/ISLG), SLUG-ISLG, (SLUG/ANM)-ISLG or ANM-DIS. (See Figure 3-5.)

Z = Max (0.0, Min [1.0, 10.000454 (1.0-exp(-0.5T_{gsat}))(0.4-α_{AB})])

α_{AB} = transition from bubbly to slug flow. (See Figures 3-1, 3-4).

$T_{gsat} = T_g - T^s - 1.0$

$$FWF_{REG1-REG2} = (FWF_{REG1})FREG1 + (FWF_{REG2})FREG2$$

$$FWG_{REG1\text{-}REG2} = (FWG_{REG1})FREG1 + (FWG_{REG2})FREG2$$

where FREG1 and FREG2 are given for the various flow regimes in transitions, Appendix 4A.

High Mixing Map

Bubbly-Dispersed Transition

$$f_{gf_{BUB\text{-}DIS}} = (f_{gf_{BUB}})FBUB + (f_{gf_{DIS}})FDIS$$

$$FWF_{BUB\text{-}DIS} = (FWF_{BUB})FBUB + (FWF_{DIS})FDIS$$

$$FWG_{BUB\text{-}DIS} = (FWG_{BUB})FBUB + (FWG_{DIS})FDIS$$

where FBUF and FDIS are as in Transitions, Appendix 4A.

7. FLOW PROCESS MODELS

7.1 Abrupt Expansions and Contractions

In the sum and difference field equations, Equations (2-61) and (2-62), the HLOSSF and HLOSSG terms account for momentum losses due to abrupt expansions or contractions of flow areas. The abrupt area change model used to determine these terms is based on the Bourda-Carnot[7-1,7-2] formulation for a sudden enlargement and standard pipe flow relations, including the vena-contracta effect for a sudden contraction or an orifice or both. Quasi-steady continuity and momentum balances are employed at points of abrupt area change. The numerical implementation of these balances is such that hydrodynamic losses are independent of upstream and downstream nodalization. In effect, the quasi-steady balances are employed as jump conditions that couple fluid components having abrupt changes in cross-sectional area. This coupling process is achieved without change to the basic linear semi-implicit numerical time-advancement scheme.

7.1.1 Basis of Model

The basic assumption used for the transient calculation of two-phase flow in flow passages with points of abrupt area change is: the transient flow process can be approximated as a quasi-steady flow process that is instantaneously satisfied by the upstream and downstream conditions (that is, transient inertia, mass, and energy storage are neglected at abrupt area changes). However, the upstream and downstream flows are treated as fully transient flows.

There are several bases for the above assumption. A primary consideration is that available loss correlations are based on data taken during steady flow processes; however, transient investigations[7-3] have verified the adequacy of the quasi-steady assumption. The volume of fluid and associated mass, energy, and inertia at points of abrupt area change is generally small compared with the volume of upstream and downstream fluid components. The transient mass, energy, and inertia effects are approximated by lumping them into upstream and downstream flow volumes.

Finally, the quasi-steady approach is consistent with modeling of other important phenomena in transient codes (that is, heat transfer, pumps, and valves).

7.1.1.1 Single-Phase Abrupt Area Change Model. The modeling techniques used for dynamic pressure losses associated with abrupt area change in a single-phase flow are reviewed briefly before discussing the extension of these methods to two-phase flows. In a steady, incompressible flow, losses at an area change are modeled by the inclusion of an appropriate dynamic head loss term, h_L, in the one-dimensional modified Bernoulli equation

$$(v^2/2 + P/\rho)_1 = (v^2/2 + P/\rho)_2 + h_L \quad . \tag{7-1}$$

The particular form of the dynamic head loss is obtained by employing the Bourda-Carnot[7-2] assumption for calculating losses associated with the expansion part of the flow process. Losses associated with the contracting part of the flow process are small relative to the expansion losses and are neglected.

The most general case of an abrupt area change is a contraction with an orifice at the point of contraction. Such a configuration is shown in Figure 7-1. Three area ratios are used throughout this development. The first is the contraction area ratio at the vena-contracta relative to the minimum physical area, $\epsilon_c = A_c/A_T$. The second is the ratio of the minimum physical area to the upstream flow area, $\epsilon_T = A_T/A_1$. The third is the ratio of the downstream to upstream area, $\epsilon = A_2/A_1$.

The loss associated with the contracting fluid stream from Station 1 to c (the point of vena-contracta) is neglected [measurements indicate that the contracting flow experiences a loss no larger than $\Delta P_f \cong 0.05\ (\frac{1}{2}\ \rho v_c^2)$ where v_c is the velocity at the vena-contracta], whereas the dynamic pressure loss associated with the expansion from the vena-contracta to the downstream section is given by

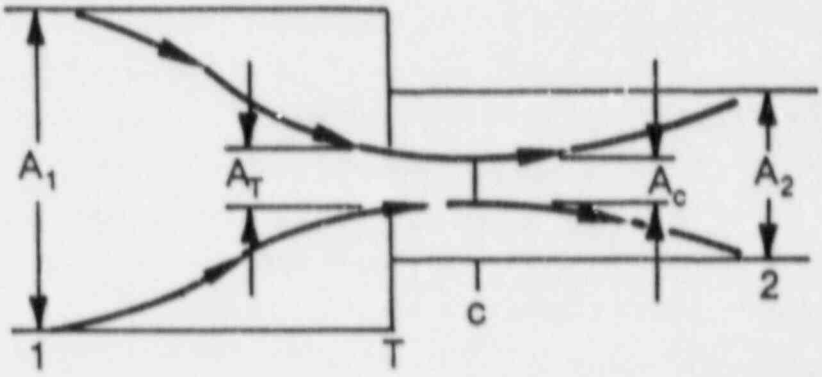

Figure 7-1. Orifice at abrupt area change.

$$\Delta P_f = 1/2\ \rho(1 - A_c/A_2)^2\ v_c^2 \quad . \qquad (7\text{-}2)$$

The contraction ratio, $\epsilon_c = A_c/A_T$, is an empirical function of $\epsilon_T = A_T/A_1$. The function ϵ_c has the form $\epsilon_c = 0.62 + 0.38(\epsilon_T)^3$. Using the continuity equations, $v_c = \frac{A_T v_T}{A_c} = v_T/\epsilon_c$, and $v_T = \frac{A_2 v_2}{A_T} = \frac{\epsilon}{\epsilon_T} v_2$, Equation (7-2) can be written as

$$\Delta P_f = 1/2\ \rho\ (1 - \frac{\epsilon}{\epsilon_c \epsilon_T})^2\ v_2^2 \quad . \qquad (7\text{-}3)$$

Equation (7-3) is applicable to all the cases of interest. For a pure expansion, $\epsilon_T = 1$, $\epsilon_c = 1$,, and $\epsilon > 1$; for a contraction, $\epsilon_T = \epsilon < 1$ and $\epsilon_c < 1$. Each of these is a special case of Equation (7-3). The two-phase dynamic pressure loss model is based on an adaptation of the general single-phase head loss given by Equation (7-3).

7.1.1.2 Two-Phase Abrupt Area Change Model. The two-phase flow through an abrupt area change is modeled in a manner very similar to that for single-phase flow by defining phasic flow areas. The two phases are coupled through the interphase drag, a common pressure gradient, and the requirement that the phases coexist in the flow passage.

The one-dimensional phasic stream-tube momentum equations are given in Section 2. The flow at points of abrupt area change is assumed to be quasi-steady and incompressible. In addition, the terms in the momentum equations due to body force, wall friction, and mass transfer are assumed to be small in the region affected by the area change. The interphase drag terms are retained, since the gradient in relative velocity can be large at points of abrupt area changes.

The momentum equation can be integrated along a streamline approximately for a steady, incompressible, smoothly varying flow to obtain modified Bernoulli-type equations

$$\left(1/2\ \rho_f v_f^2 + P\right)_1 = \left(1/2\ \rho_f v_f^2 + P\right)_2 + \left(\frac{FI'}{\alpha_f}\right)_1 (v_{f1} - v_{g1})\ L_1 + \left(\frac{FI'}{\alpha_f}\right)_2 (v_{f2} - v_{g2})\ L_2 \qquad (7\text{-}4)$$

and

$$\left(1/2\ \rho_g v_g^2 + P\right)_1 = \left(1/2\ \rho_g v_g^2 + P\right)_2 + \left(\frac{FI'}{\alpha_g}\right)_1 (v_{g1} - v_{f1})\ L_1 + \left(\frac{FI'}{\alpha_g}\right)_2 (v_{g2} - v_{f2})\ L_2\ , \qquad (7\text{-}5)$$

where $FI' = \alpha_f\ \alpha_g\ \rho_f\ \rho_g\ FI$ and FI is given by Equation (6-3). The interphase drag is divided into two parts associated with the upstream and downstream parts of the flow affected by the area change.

7.1.1.3 General Model. Consider the application of Equations (7-4) and (7-5) to the flow of a two-phase fluid through a passage having a generalized abrupt area change (the flow passage shown in Figure (7-2).[a] Here, the area A_T is the throat or minimum area associated with an orifice located at the point of the abrupt area change. Since each phase is governed by a modified Bernoulli-type equation, it is reasonable to assume that losses associated with changes in the phasic flow area can be modeled by separate dynamic pressure loss terms for both the liquid and gas phases. Hence, we assume that the liquid sustains a loss as if it alone (except for interphase drag) were experiencing an area change from $\alpha_{f1}\ A_1$ to $\alpha_{fT}\ A_T$ to $\alpha_{f2}\ A_2$, and the gas phase experiences a loss as if it alone were flowing through an area change from $\alpha_{g1}\ A_1$ to $\alpha_{gT}\ A_T$ to $\alpha_{g2}\ A_2$. The area changes for each phase are the phasic area changes (see Figure 7-2). When the losses for these respective area changes [based on the Bourda-Carnot model and given by Equation (7-3)] are added to Equations (7-4) and (7-5), the following phasic momentum equations are obtained:

---

a. In Figure 7-2, the flow is shown as a separated flow for clarity. The models developed are equally applicable to separated and dispersed flow regimes.

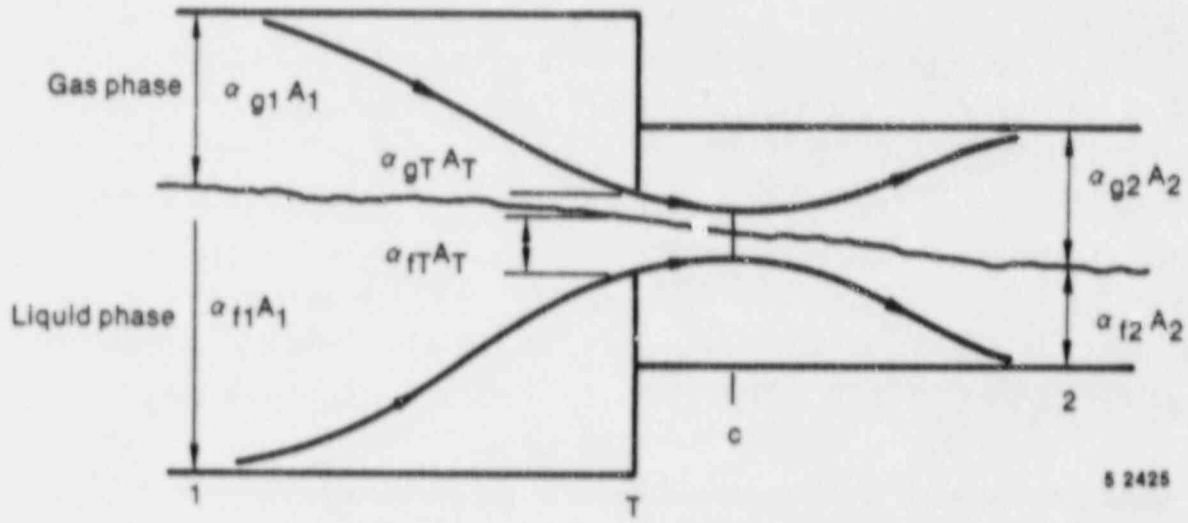

Figure 7-2. Schematic of flow of two-phase mixture at abrupt area change.

$$(1/2\ \rho_f v_f^2 + P)_1 = (1/2\ \rho_f v_f^2 + P)_2 + 1/2\ \rho_f \left(1 - \frac{\alpha_{f2}\ \epsilon}{\alpha_{fT}\ \epsilon_{fc}\ \epsilon_T}\right)^2 (v_{f2})^2$$

$$+ \left(\frac{FI'}{\alpha_f}\right)_1 (v_{f1} - v_{g1})\ L_1 + \left(\frac{FI'}{\alpha_f}\right)_2 (v_{f2} - v_{g2})\ L_2 \qquad (7\text{-}6)$$

and

$$(1/2\ \rho_g v_g^2 + P)_1 = (1/2\ \rho_g v_g^2 + P)_2 + 1/2\ \rho_g \left(1 - \frac{\alpha_{g2}\ \epsilon}{\alpha_{gT}\ \epsilon_{gc}\ \epsilon_T}\right)^2 (v_{g2})^2$$

$$+ \left(\frac{FI'}{\alpha_g}\right)_1 (v_{g1} - v_{f1})\ L_1 + \left(\frac{FI'}{\alpha_g}\right)_2 (v_{g2} - v_{f2})\ L_2 \ . \qquad (7\text{-}7)$$

These phasic momentum equations are used across an abrupt area change. In Equations (7-6) and (7-7), ϵ_{fc} and ϵ_{gc} are the same tabular function of area ratio as in the single-phase case except the area ratios used are the phasic area ratios

$$\epsilon_{fT} = (\alpha_{fT}/\alpha_{f1})\ \epsilon_T \qquad (7\text{-}8)$$

and

$$\epsilon_{gT} = (\alpha_{gT}/\alpha_{g1})\ \epsilon_T \ , \qquad (7\text{-}9)$$

respectively. The area ratios, $\epsilon = A_2/A_1$ and $\epsilon_T = A_T/A_1$, are the same as for single-phase flow.

The interphase drag effects in Equations (7-6) and (7-7) are important. These terms govern the amount of slip induced by an abrupt area change; and, if they are omitted, the model will always predict a slip at the area change appropriate to a completely separated flow situation and give erroneous results for a dispersed flow.

7.1.2 Code Implementation

A few remarks concerning the way Equations (7-6) and (7-7) are applied to expansions and contractions, both with and without an orifice, are necessary. In a single-phase, steady flow situation, given the upstream conditions, v_1 and P_1, using the continuity equation ($v_1A_1 = v_2A_2$) and Equation (7-1) one can solve for v_2 and P_2. Equations (7-6) and (7-7), along with the two phasic continuity equations, can be used in a similar manner except now the downstream void fraction is an additional unknown which must be determined.

7.1.2.1 Expansion. For the purpose of explanation, consider the case of an expansion ($\alpha_{fT} = \alpha_{f1}$, $\epsilon > 0$, $\epsilon_T = 1$, $\epsilon_{fc} = \epsilon_{gc} = 1$, $FI'_1 = 0$, $L_1 = 0$) for which Equations (7-6) and (7-7) reduce to

$$(1/2\ \rho_f v_f^2 + P)_1 = (1/2\ \rho_f v_f^2 + P)_2 + 1/2\ \rho_f \left(1 - \frac{\alpha_{f2}\epsilon}{\alpha_{f1}}\right)^2 (v_{f2})^2 + \left(\frac{FI'}{\alpha_f}\right)_2 (v_{f2} - v_{g2})\ L_2 \qquad (7\text{-}10)$$

and

$$(1/2\ \rho_g v_g^2 + P)_1 = (1/2\ \rho_g v_g^2 + P)_2 + 1/2\ \rho_g \left(1 - \frac{\alpha_{g2}\epsilon}{\alpha_{g1}}\right)^2 (v_{g2})^2 + \left(\frac{FI'}{\alpha_g}\right)_2 (v_{g2} - v_{f2})\ L_2 \ . \qquad (7\text{-}11)$$

These two equations with the incompressible continuity equations

$$\alpha_{f1} v_{f1} A_1 = \alpha_{f2} v_{f2} A_2 \qquad (7\text{-}12)$$

and

$$\alpha_{g1} v_{g1} A_1 = \alpha_{g2} v_{g2} A_2 \qquad (7\text{-}13)$$

are a system of four equations having four unknowns, α_{f2} ($\alpha_{g2} = 1 - \alpha_{f2}$), v_{f2}, v_{g2}, and P_2, in terms of the upstream conditions, α_{f1} ($\alpha_{g1} = 1 - \alpha_{f1}$), v_{f1}, v_{g1}, and P_1. (The interphase drag, FI', is a known function of the flow properties.) It is important to note that the downstream value of the liquid fraction (α_{f2}) is an additional unknown compared with the single-phase case and is determined (with the downstream velocities and pressure) by simultaneous solution of Equations (7-10), (7-11), (7-12), and (7-13) without additional assumptions. It is reassuring that by taking a proper linear combination of Equations (7-6) and (7-7), the usual overall momentum balance obtained using the Bourda-Carnot[7-2] assumption can be obtained.[7-4,7-5]

If, as in the cited literature,[7-4 through 7-7] only the overall momentum balance is used at an expansion, there will be an insufficient number of equations to determine all the downstream flow parameters, α_{f2}, v_{f2}, v_{g2}, and P_2. The indeterminancy has been overcome in cited works by means of several different assumptions concerning the downstream void fraction.[a] In the model developed here [Equations (7-10) and (7-11)], division of the overall loss into liquid and gas parts, respectively, results in sufficient conditions to determine all downstream flow variables, including α_{f2}. In addition, the present model includes force terms due to interphase drag in Equations (7-10) and (7-11) which are necessary to predict the proper amount of slip and void redistribution that occurs at points of area change.

7.1.2.2 Contraction. Consider the application of Equations (7-6) and (7-7) to a contraction. To determine both the downstream conditions and throat conditions from the upstream values of $\alpha_{f1}(\alpha_{g1})$, v_{f1}, v_{g1}, and P_1, an additional consideration needs to be made. To obtain the throat values, apply the momentum equations valid for the contracting section of flow (here, the L_1 portion of the interphase force is associated with the contraction)

---

a. J. G. Collier[7-4] mentions three different assumptions that have been used: (i) $\alpha_{f2} = \alpha_{f1}$, (ii) α_{f2} is given by a homogeneous model, and (iii) α_{f2} is given by the Hughmark void fraction correlation.

$$(1/2\ \rho_f v_f^2 + P)_1 = (1/2\ \rho_f v_f^2 + P)_T + \left(\frac{FI'}{\alpha_f}\right)_1 (v_{f1} - v_{g1})\ L_1 \qquad (7\text{-}14)$$

$$(1/2\ \rho_g v_g^2 + P)_1 = (1/2\ \rho_g v_g^2 + P)_T + \left(\frac{FI'}{\alpha_g}\right)_1 (v_{g1} - v_{f1})\ L_1 \qquad (7\text{-}15)$$

$$\alpha_{f1} v_{f1} A_1 = \alpha_{fT} v_{fT} A_T \qquad (7\text{-}16)$$

$$\alpha_{g1} v_{g1} A_1 = \alpha_{gT} v_{gT} A_T \quad . \qquad (7\text{-}17)$$

These four equations are solved simultaneously for the values of $\alpha_{fT}(\alpha_{gT})$, v_{fT}, v_{gT}, and P_T at the throat section (the minimum physical area). No additional or special assumptions are made concerning the throat conditions, since they follow as a direct consequence of the unique head loss models for each phase. After the throat values have been obtained, the conditions at the point of vena-contracta are established, assuming the void fraction is the same as at the throat. Thus, ϵ_c and ϵ_{gc} are established using the tabular function in Appendix A of Reference 7-1 and the throat area ratios, ϵ_{fT} and ϵ_{gT}, defined by Equations (7-8) and (7-9). To determine the downstream values, Equations (7-6) and (7-7) can be applied directly from Stations 1 to 2 with the throat values known or the expansion loss equations can be used from the throat section to Station 2. Both approaches produce identical downstream solutions. As in the case of an expansion, because the proper upstream and downstream interphase drag is included, this modeling approach establishes the phase slip and resulting void redistribution. An orifice at an abrupt area change is treated exactly as the contraction explained above (that is, with two separate calculations to establish first the throat and then the downstream flow variable).

7.1.2.3 Countercurrent Flow. The preceding development implicitly assumed a cocurrent flow. For countercurrent flow, Equations (7-6) and (7-7) are applied exactly as in cocurrent flow except the upstream sections for the respective phases are located on different sides of the abrupt area change. The difference appears in how the throat and downstream voids are determined. To determine the throat properties, equations similar to Equations (7-14), (7-15), (7-16), and (7-17) are used with the upstream

values appropriate for each phase. These four equations are then solved for $\alpha_{fT}(\alpha_{gT})$, v_{fT}, v_{gT}, and P_T. To determine the downstream values for each phase, only the head loss terms are needed for the downstream voids. (The downstream v_f, v_g, and P do not appear.) For countercurrent flow, these voids are set such that the downstream void of each phase plus the upstream void of the opposite phase adds to one. (Both phases together must fill the flow channel.) With the throat and downstream voids now known, Equations (7-6) and (7-7) can be used directly to determine the total loss for each phase at the abrupt area change.

7.2 Critical Flow Model

In reactor blowdown transients, choked or critical flow will exist at the locale of the break. Furthermore, under certain circumstances, choked flow can exist at a point internal to the system or at multiple locations within the system. A one-dimensional choked flow model developed by Ransom and Trapp[7-8,7-9] is employed in RELAP5/MOD2 to predict the existence of choked flow at a break or internal location and to establish the flow boundary condition if choking is predicted to occur. Since reactor blowdown transients can encompass single-phase and multi-phase flows, the choked flow model is designed to handle subcooled choked flow, two-phase choked flow (one-component and two-component), and single-phase-vapor choked flow.

Choking is a condition where the mass discharge from a system or at an internal point in the system becomes independent of conditions downstream. In other words, for a given set of upstream conditions, the mass flow does not increase as the downstream pressure is decreased. Physically, choking occurs when acoustic signals can no longer propagate upstream. Such a situation exists when the fluid discharge velocity is equal to or exceeds the local propagation velocity. The following sections detail the basis for the choking criteria used in RELAP5 and the implementation of the criteria described above for the various thermodynamic states that can occur during a blowdown transient.

7.2.1 Basis for Choking Models

As described above, various thermodynamic states and flow conditions can prevail during a reactor blowdown transient. The basis for the subcooled choking model and the two-phase choking model used in RELAP5 are described below.

7.2.1.1 Subcooled Choking Model. The subcooled choking model employed in RELAP5 is similar in concept to the model proposed by Burnell[7-10] and has been designed to reflect the physics occurring during the break flow process. Both models assume a Bernoulli expansion to the point of vapor inception at the choke plane. The RELAP5[7-11] subcooled choking model is somewhat different from the model proposed by Moody[7-12] in that the Moody model assumes that an isentropic process occurs up to the choke plane. In the early stage of a blowdown, the fluid approaching the break is a subcooled liquid. Because the downstream pressure (containment) is much lower than the upstream pressure, the fluid will undergo a phase change at the break. The phase change is accompanied by a large change in the fluid bulk modulus and hence sound speed. The sound speed change is most pronounced for the liquid-to-liquid/vapor transition point, although there is also an abrupt change at the liquid/vapor-to-pure-vapor transition. The large change in sound speed mandates that extreme care be used in analyzing the choked flow process when upstream conditions are subcooled.

The physics involved during subcooled choking can be better appreciated by considering flow through a converging-diverging nozzle connected to a stagnation volume containing subcooled high pressure water, as shown in Figure 7-3. When the downstream pressure P_d is slightly less than the upstream pressure P_{up}, subcooled flow exists throughout the nozzle. The throat conditions for an idealized situation can be analyzed using the Bernoulli equation i.e.

$$v_t = \left[\frac{2(P_{up} - P_t)}{\rho}\right]^{1/2} \qquad (7\text{-}18)$$

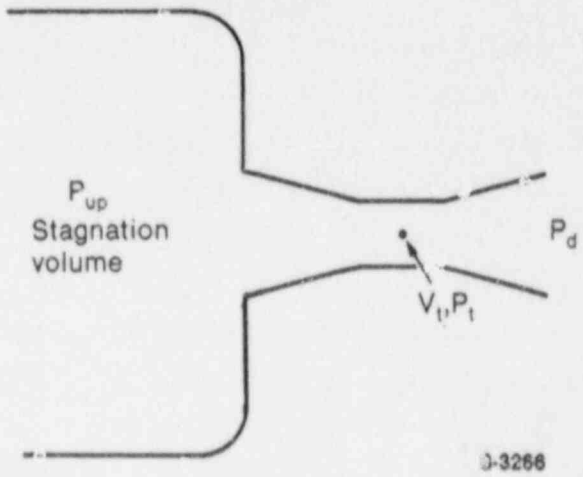

Figure 7-3. Converging - diverging nozzle.

As the downstream pressure is decreased, a point is eventually reached where the pressure at the throat is equal to the local saturation pressure, P_{sat}. Further reduction in the downstream pressure results in vaporization of fluid at the throat if homogeneous equilibrium assumptions are made. As discussed above, a slight amount of vapor at the throat results in a significant reduction of the sound speed. Conservation of mass requires that the velocity of the two-phase mixture at the throat be equal to the velocity of the subcooled fluid just upstream of the throat. At this point, the velocity in the subcooled region is less than the subcooled fluid sound speed; but, in the two-phase region, the throat velocity can be larger than the two-phase sound speed. Under this condition, the flow is choked; since downstream pressure changes cannot be propagated upstream, and the supersonic two-phase flow at the throat must increase in velocity and the pressure drop as the flow expands in the divergent section. In effect, there is no point in the flow stream where the Mach number is unity. This stems from the discontinuous sound speed change at the phase transition, although the fluid properties are continuous through the transition. Figure 7-4a represents this condition schematically, and the flow rate can be established in ideal frictionless flow with Equation (7-18) where P_t is the local saturation pressure.

As the upstream pressure is decreased for the situation above, the throat pressure remains at P_{sat} and the subcooled fluid velocity at the throat decreases. As P_{up} is further decreased, a point is eventually reached where the throat velocity is equal to the homogeneous equilibrium sound speed a_{HE} and the Mach number becomes unity on the two-phase side of the throat while the Mach number in the subcooled side is much less than unity. Schematically, this is shown in Figure 7-4b.

With further decreases in P_{up}, the location where the pressure reaches P_{sat} moves upstream relative to the throat position. Upstream of the saturation point, the subcooled fluid velocity is less than the [illegible]phase sound speed. Between the saturation point and the throat, the two-phase velocity is less than the two-phase sound speed; and, at the

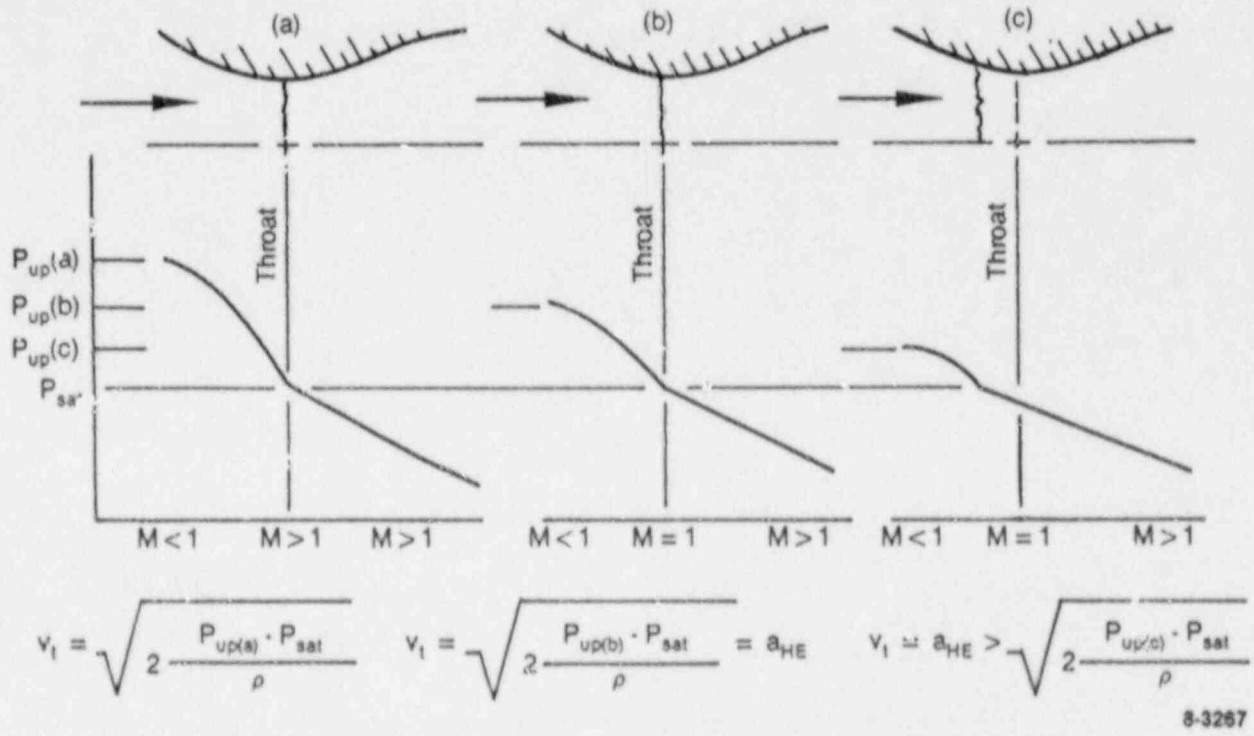

Figure 7-4. Subcooled choking process.

throat, the fluid velocity is equal to the two-phase sound speed, as shown in Figure 7-4c. Ultimately, as P_{up} is decreased further, the saturation point moves further and further upstream until the flow is all two-phase.

The homogeneous process described above, although idealized, is an accurate representation when vapor is first formed. Non-equilibrium effects, however, can result in vapor formation at a pressure considerably less than the local saturation pressure. In other words, the existence of superheated liquid results in the onset of vaporization at P_t ($<P_{sat}$), rather than at local saturation pressure. A model described by Alamgir and Lienhard[7-13] and Jones[7-14,7-15] can be used to calculate the throat pressure at which vaporization first occurs. This model is

$$\Delta P = P_{sat} - P_t =$$

$$0.258 \frac{\sigma^{3/2} T_R^{13.76}}{\sqrt{k_B i_c}} \frac{V_g}{V_g - V_f} \left[1 + 2.078\ E\text{-}8 \left(\rho_f \frac{1}{A_t} \frac{dA_t}{dx} v_c^3 \right)^{0.8} \right]^{1/2}$$

$$- 6.9984\ E\text{-}2 \left(\frac{A_t}{A} \right)^2 \rho_f \frac{v_c^2}{2} \qquad (7\text{-}19)$$

where

σ = surface tension

T_R = temperature ratio, T/T_c

T = fluid temperature

T_c = critical temperature

k_B = Boltzmann constant

V_g = vapor specific volume

V_f = liquid specific volume

ρ_f = liquid density

A = cell area

A_t = throat area

v_c = throat velocity .

In this equation, T, V_g, V_f, ρ_f, and A are upstream volume quantities. In the RELAP5 implementation, $P_{sat} - P_t$ is taken to be the maximum of zero and the value from Equation (7-19), i.e.

$$P_{sat} - P_t = \max (0.0, \Delta P) . \tag{7-20}$$

For the situation shown in Figure 7-4a, then the idealized choking criteria is

$$v_c = \left[v_{up}^2 + 2 \frac{(P_{up} - P_t)}{\rho} \right]^{1/2} , \tag{7-21}$$

where P_t is calculated from Equation (7-20). For the situations in Figure 7-4b and 7-4c, the choking criterion is

$$v_c = a_{HE} ; \tag{7-22}$$

and the two-phase choking criteria to be described in the next section applies. In the implementation of the model, both Equations (7-21) and (7-22) are evaluated; the maximum of the two is used to determine the choking velocity at the throat. This velocity is then imposed numerically at the throat. The implementation is described in Section 7.2.2.2.

7.2.1.2 Two-Phase One-Component Choking Model. The two-phase choking model employed in RELAP5 is based on the model described by Trapp and Ransom[7-8,7-9] for non-homogeneous, non-equilibrium flow. Trapp and Ransom developed an analytic choking criteria using a characteristic analysis of a

two-fluid model that included relative phasic acceleration terms and derivative-dependent mass transfer. During the original development and implementation of this model, both frozen flow and thermal equilibrium assumptions were employed to test the analytic criteria. Comparisons to existing data [7-8] indicated that the thermal equilibrium assumption was the more appropriate and is thus assumed in the following development.

The two-fluid model employed in the development of the RELAP5 two-phase choking criteria includes an overall mass conservation equation, two-phasic momentum equations, and the mixture energy equation written in terms of entropy. The equation set is written without non-differential terms, such as wall drag and heat transfer, since these terms do not enter into the characteristic analysis. The differential equations are

$$\frac{\partial}{\partial t}\left(\alpha_g\rho_g + \alpha_f\rho_f\right) + \frac{\partial}{\partial x}\left(\alpha_g\rho_g v_g + \alpha_f\rho_f v_f\right) = 0 \tag{7-23}$$

$$\alpha_g\rho_g\left[\frac{\partial v_g}{\partial t} + v_g\frac{\partial v_g}{\partial x}\right] + \alpha_g\frac{\partial P}{\partial x} + C\,\alpha_g\alpha_f\rho\left[\frac{\partial v_g}{\partial t} + v_f\frac{\partial v_g}{\partial x} - \frac{\partial v_f}{\partial t} - v_g\frac{\partial v_f}{\partial x}\right] = 0 \tag{7-24}$$

$$\alpha_f\rho_f\left[\frac{\partial v_f}{\partial t} + v_f\frac{\partial v_f}{\partial x}\right] + \alpha_f\frac{\partial P}{\partial x} + C\,\alpha_f\alpha_g\rho\left[\frac{\partial v_f}{\partial t} + v_g\frac{\partial v_f}{\partial x} - \frac{\partial v_g}{\partial t} - v_f\frac{\partial v_g}{\partial x}\right] = 0 \tag{7-25}$$

and

$$\frac{\partial}{\partial t}\left(\alpha_g\rho_g S_g + \alpha_f\rho_f S_f\right) + \frac{\partial}{\partial x}\left(\alpha_g\rho_g S_g v_g + \alpha_f\rho_f S_f v_f\right) = 0 \tag{7-26}$$

where

α_g = vapor fraction

α_f = liquid fraction

ρ_g = saturated vapor density

ρ_f = saturated liquid density

v_g = vapor velocity

v_f = liquid velocity

C = virtual mass coefficient

ρ = density of mixture

S_g = saturated vapor specific entropy

S_f = saturated liquid specific entropy .

This equation set includes interface force terms due to relative acceleration, since these terms have a significant effect on wave propagation.[7-9] Energy dissipation terms associated with interface mass transfer and relative phase acceleration have been neglected in the mixture entropy equation. Given the assumption of thermal equilibrium, ρ_g, ρ_f, S_g, and S_f are functions of pressure (i.e. saturation values). Using the chain rule and property derivatives for ρ_g, ρ_f, S_g, and S_f,

$$\rho_f^* = \frac{d\rho_f}{dP}^S \quad , \quad \rho_g^* = \frac{d\rho_g}{dP}^S \tag{7-27}$$

$$S_f^* = \frac{dS_f}{dP}^S \quad , \quad S_g^* = \frac{dS_g}{dP}^S \quad . \tag{7-28}$$

Equations (7-23 through 7-26) can be written in terms of α_g, ρ, v_g, and v_f as four quasi-linear, first-order partial differential equations of the form

$$A(\bar{U}) \frac{\partial \bar{U}}{\partial t} + B(\bar{U}) \frac{\partial \bar{U}}{\partial x} + C(\bar{U}) = 0 , \tag{7-29}$$

where A and B are fourth-order square coefficient matrices.

The characteristic velocities of the system of equations defined by Equation (7-29) are the roots[7-16,7-17] (λ_i, $i \leq 4$) of the characteristic polynominal

$$(A\lambda - B) = 0 . \tag{7-30}$$

The real part of any root λ_i gives the velocity of signal propagation along the corresponding path in the space/time plane. If the system of equations defined by Equations (7-29) is considered for a particular region defined by $0 \leq x \leq L$, the number of boundary conditions required at L equals the number of characteristic lines entering the solution region. At $x = L$, as long as any of the λ_i are <0 some information is needed at the boundary to get a solution. If all λ_i are greater than or equal to zero, no boundary conditions are needed at L and the solution on $0 \leq x \leq L$ is not affected by conditions outside the boundary at L. This situation defines the choking criteria, i.e.

$$\lambda_j = 0 \text{ for } j \leq 4 \tag{7-31}$$

$$\lambda_i \geq 0 \text{ for all } i \neq j .$$

Equation (7-30) corresponding to the system defined by Equation (7-29) and the A and B coefficient matrices is

$$\rho C (\lambda - v_f)(\lambda - v_g) + \alpha_f \rho_g (\lambda - v_g)^2 + \alpha_g \rho_f (\lambda - v_f)^2 +$$

$$\left[[\rho_g (\lambda - v_g) - \rho_f (\lambda - v_f)][\alpha_g \rho_g S_g^* (\lambda - v_g) \right.$$

$$+ \alpha_f \rho_f S_f^* (\lambda - v_f)]/(S_g - S_f) - (\alpha_f \rho_g \rho_f^* + \alpha_g \rho_f \rho_g^*)(\lambda - v_f)(\lambda - v_g)\Big]$$

$$\Big[(\lambda - v_f)(\lambda - v_g) + (C\rho\alpha_f/\rho_g)(\lambda - v_f)^2$$

$$+ (C\rho\alpha_g/\rho_f)(\lambda - v_g)^2\Big] = 0 \,. \qquad (7\text{-}32)$$

Equation (7-32) is fourth order in λ, and approximate factorization is possible. Details of the approximate factorization methodology are presented in Reference 7-18. The results for the first two roots are:

$$g_{1,2} = \frac{\Big[\alpha_f \rho_g + \rho C/2 \pm [(\rho C/2)^2 - \alpha_g \alpha_f \rho_g \rho_f]^{1/2}\Big] v_g + \Big[\alpha_g \rho_f + \rho C/2 \pm [(\rho C/2)^2 - \alpha_g \alpha_f \rho_g \rho_f]^{1/2}\Big] v_f}{(\alpha_f \rho_g + \rho C/2) + (\alpha_g \rho_f + \rho C/2)} \,. \qquad (7\text{-}33)$$

These two roots are obtained by neglecting the fourth-order factors relative to the second-order factors in $(\lambda - v_g)$ and $(\lambda - v_f)$. (There are no first- or third-order factors.) Inspection of Equation (7-33) shows that the $\lambda_{1,2}$ have values between v_g and v_f, thus the fourth-order factors $(\lambda - v_g)$ and $(\lambda - v_f)$ are small (i.e., neglecting these terms is justified). The values for $\lambda_{1,2}$ may be real or complex depending on the sign of the quantity $[(\rho C/2)^2 - \alpha_g \alpha_f \rho_g \rho_f]$.

The remaining two roots are obtained by dividing out the quadratic factor containing $\lambda_{1,2}$, neglecting the remainder, and subsequent factorization of the remaining quadratic terms. [This procedure can be shown to be analogous to neglecting the second and higher order terms in the relative velocity, $(v_g - v_f)$.] The remaining roots are:

$$\lambda_{3,4} = v + D\,(v_g - v_f) \pm a \tag{7-34}$$

where

$$v = (\alpha_g \rho_g v_g + \alpha_f \rho_f v_f)/\rho\ , \tag{7-35}$$

$$a = a_{HE}\left[\left[C\rho^2 + \rho(\alpha_g \rho_f + \alpha_f \rho_g)\right]/(C\rho^2 + \rho_g \rho_f)\right]^{1/2}\ , \tag{7-36}$$

and

$$D = 1/2\left[\frac{(\alpha_g \rho_f - \alpha_f \rho_g)}{(\rho C + \alpha_f \rho_g + \alpha_g \rho_f)} + \frac{\rho_g \rho_f (\alpha_f \rho_f - \alpha_g \rho_g)}{\rho(\rho_g \rho_f + C\rho^2)}\right.$$

$$\left. - a_{HE}^2 \frac{\rho(\alpha_g \rho_g^2 S_g^* + \alpha_f \rho_f^2 S_f^*)}{\rho_g \rho_f (S_g - S_f)}\right]\ . \tag{7-37}$$

The quantity a_{HE} is the homogeneous equilibrium speed of sound (see Appendix 7A for development) and is defined as

$$a_{HE} = V\frac{dP^S}{dT} \Big/ \left[X\left(\frac{C_{pg}}{T_g} + V_g \frac{dP^S}{dT}\left(\kappa_g \frac{dP^S}{dT} - 2\beta_g\right)\right) + \right.$$

$$\left. (1 - X)\left(\frac{C_{pf}}{T_f} + V_f \frac{dP^S}{dT}\left(\kappa_f \frac{dP^S}{dT} - 2\beta_f\right)\right)\right]^{1/2}\ , \tag{7-38}$$

where

$$\frac{dP^S}{dT} = \frac{h_g - h_f}{T^S\,(V_g - V_f)}\ \text{(Clapeyron equation)} \tag{7-39}$$

V = specific volume

p^s = saturation pressure

X = mass quality of steam

C_{pg} = saturated vapor specific heat

C_{pf} = saturated liquid specific heat

κ_g = isothermal compressibility for vapor

κ_f = isothermal compressibility for liquid

β_g = isopiestic coefficient of thermal expansion for vapor

β_f = isopiestic coefficient of thermal expansion for liquid.

Since the two roots $\lambda_{1,2}$ are between the phase velocities v_f and v_g, the choking criterion is established from the roots $\lambda_{3,4}$ and Equation (7-31). The choking criterion is

$$v + D(v_g - v_f) = \pm a \tag{7-40}$$

The choking criteria can be rewritten in terms of the mass mean and relative Mach numbers

$$M_v = v/a, \; M_r = (v_g - v_f)/a \tag{7-41}$$

as

$$M_v + DM_r = \pm 1 \; . \tag{7-42}$$

This relation is very similar to the choking criterion for single-phase flow wherein only the mass average Mach number appears and choking also corresponds to a Mach number of unity.

Equation (7-42) forms the basis for the two-phase analytic choking criterion in RELAP5. In the actual implementation, the criterion is considerably simplified as will be discussed in a subsequent section and an approximation to Equation (7-42) is used. From Equation (7-42), it is clear that the choking criterion is a function of the D and a parameters. Trapp and Ransom[7-18] have investigated the impact of the virtual mass coefficient on the sound speed calculated using only Equation (7-36). Results of this calculation are shown in Figure 7-5 (from Reference 7-11) where values of C selected were 0 (stratified flow), 0.5 (dispersed flow), and ∞ (homogeneous flow). As shown in the figure, the value of C has a significant effect on the sound speed. The effects of slip [through the D coefficient, Equation (7-37)] were also calculated. Equation (7-37) is plotted in Figure 7-6 as a function of α_g, with the virtual mass coefficient as a third parameter. The results in Figure 7-6 show that velocity nonequilibrium can have a substantial effect.

As stated in Reference 7-18, the virtual mass coefficient is known for only a fairly narrow range. To preclude problems associated with the selection of C and the evaluation of the choking criteria, simplifications to the criterion are effected. This approximate criterion is

$$\frac{\alpha_g \rho_f v_g + \alpha_f \rho_g v_f}{\alpha_g \rho_f + \alpha_f \rho_g} = a_{HE} \cdot \tag{7-43}$$

Equation (7-43) can be derived from Equation (7-40) as follows. In Equation (7-36), the virtual mass coefficient C is taken to be infinity (the homogeneous equilibrium value). This results in an indeterminant form; and if L'Hopital's rule is used (twice), it can be shown that

$$a\Big|_{C=\infty} = \lim_{C\to\infty} a_{HE}^2 \left[\frac{C\rho^2 + \rho(\alpha_g \rho_f + \alpha_f \rho_g)}{C\rho^2 + \rho_g \rho_f}\right] = a_{HE}^2 \cdot \tag{7-44}$$

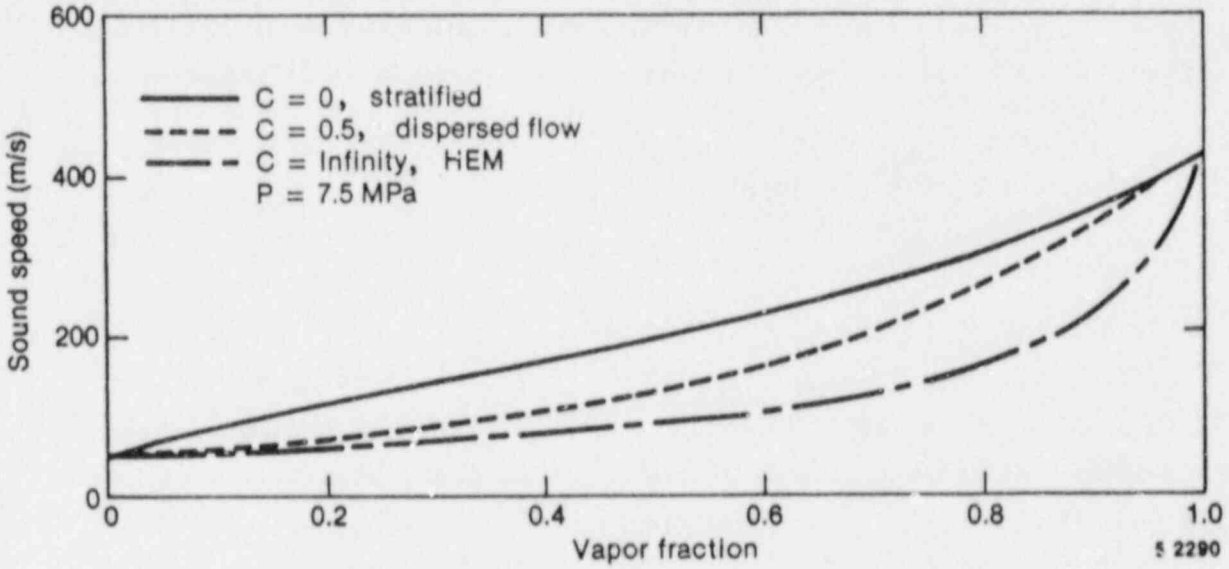

Figure 7-5. Equilibrium sound speed [from Equation (7-36)] as a function of virtual mass coefficient and void fraction.

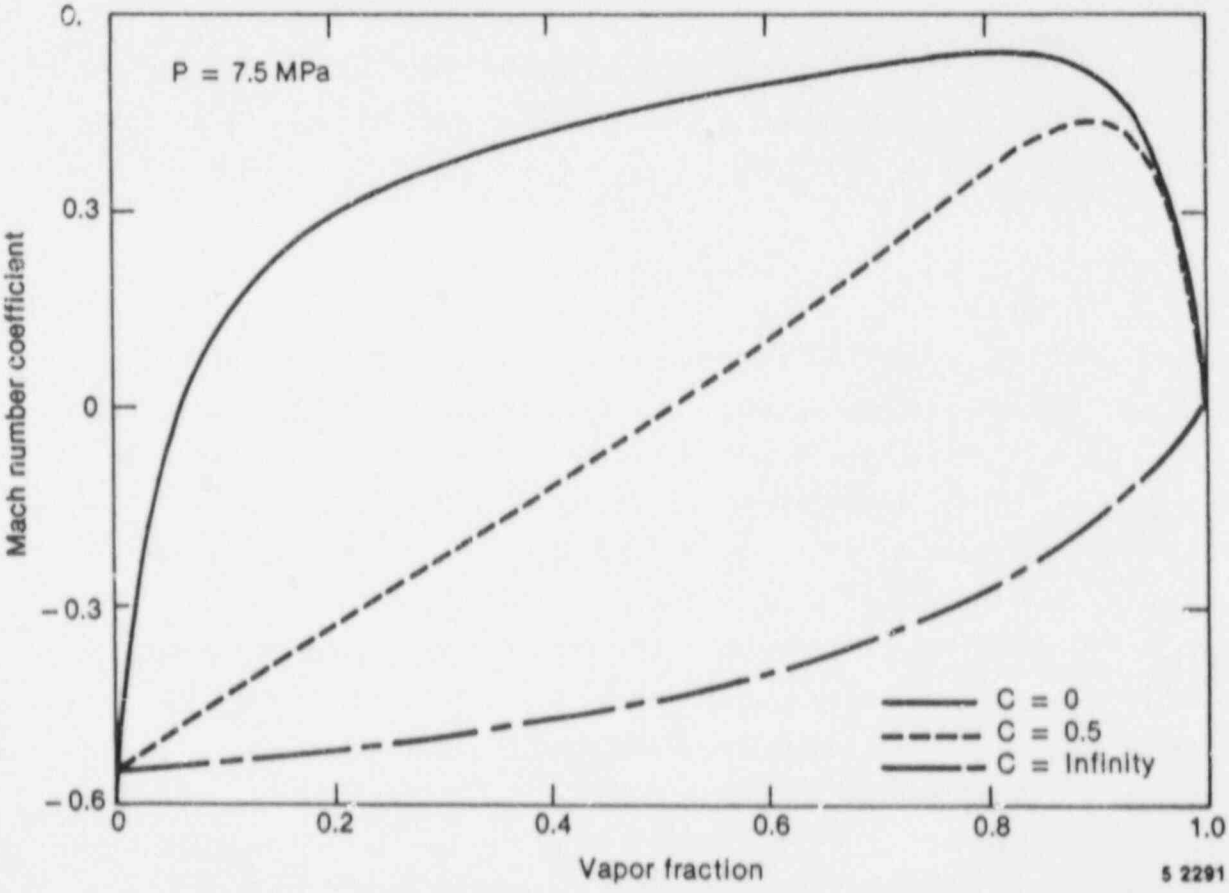

Figure 7-6. Relative Mach number coefficient [Equation (7-37)] as a function of virtual mass coefficient and void fraction.

In Equation (7-37), if the third term is neglected and the virtual mass coefficient is taken as zero (stratified flow), the D coefficient becomes

$$D = \frac{1}{2}\left[\frac{\alpha_g\rho_f - \alpha_f\rho_g}{\alpha_f\rho_g + \alpha_g\rho_f} + \frac{\alpha_f\rho_f - \alpha_g\rho_g}{\rho}\right] . \qquad (7\text{-}45)$$

Substitution of Equations (7-44, 7-45 and 7-35) into Equation (7-10) yields the expression given in Equation (7-43). Although there appears to be little justification for the assumptions regarding C in this derivation, the approximate criterion has been widely used and produces satisfactory results when compared to data.[7-8,11] Additional comparisons to data will be discussed in Section 7.2.7. Note that in the limit as α_g approaches unity, the choking criteria becomes

$$v_g = a_{HE} . \qquad (7\text{-}46)$$

and the choking criterion applies for the vapor phase alone. Furthermore, the expression given in Equation (7-43) retains some effects of velocity nonequilibrium.

7.2.2 Implementation of Choking Criterion in RELAP5

In order to understand the implementation of the choking criterion described in the previous section, it is informative to briefly discuss the overall logic flow for the hydrodynamic advancement in the RELAP5 code. This discussion will help describe the origin of various parameters (frictional parameters, state properties, etc.) that are used in the application of the choked flow criterion. Then the details of the numerical implementation of the choking criterion into the hydrodynamic scheme are described. Included, where appropriate, is a discussion of the calculation of state properties, including the homogeneous sound speed a_{HE} formulations utilized.

7.2.2.1 Hydrodynamic Advancement. The hydrodynamic advancement in RELAP5 is controlled by subroutine HYDRO. HYDRO is the driver that calls other subroutines to effect the calculations necessary to compute wall drag,

interface heat transfer and drag, flow regimes, and intermediate time velocities at cell edges; to apply the choking criterion discussed in Section 7.2.1; to solve for new time pressure, phasic energies, vapor void fraction, new time state properties, and so forth. Table 7-1 depicts this progression, the subroutines called by HYDRO, and a brief verbal description of what each subroutine does. Reference 7-11 describes in detail the overall hydrodynamic numerical implementation. The purpose here is only to indicate how JCHOKE, the subroutine that does the choking computations, fits into the scheme.

As shown in Table 7-1, the subroutine JCHOKE contains the coding for the implementation of the choking criterion. This implementation numerically imposes the choking criterion on the junctions determined to be in a choked state. JCHOKE is self-contained and does not call any other routines except fluid property routines needed to establish thermodynamic conditions. Numerous parameters are passed into JCHOKE through common statement and data blocks for components and junctions.

7.2.2.2 Implementation of Choking Criterion. While the details of the coding for JCHOKE will be discussed in Section 7.2.2.4, it is instructive to illustrate the ultimate use of the choking criterion in the scheme of Table 7-1. Upon entry to JCHOKE, the criterion given in Equation (7-43) is checked using explicit velocities calculated in VEXPLT. If choking is predicted, Equation (7-43) is then written in terms of new-time phasic velocities and solved in conjunction with a difference momentum equation derived from the upstream liquid and vapor momentum equations. The difference momentum equation is derived by subtracting the upstream liquid momentum equation [Equation (6) in Reference 7-12] from the upstream vapor momentum equation [Equation (5) in Reference 7-12], utilizing the definitions of the interface velocity and drag [Equations (8) and (9) from Reference 7-12] and keeping only the time derivative portion of the relative acceleration terms. This subtraction results in elimination of pressure from the differential equation to yield

TABLE 7-1. HYDRODYNAMIC ADVANCEMENT

Subroutine Name	Purpose/Description
HYDRO[a]	Time advancement for hydrodynamics.
VOLVEL	Calculates junction phasic velocities normalized to volume flow area for use in wall friction routine.
VALVE	Computes valve characteristics.
PHAINT	Computes interface drag, interface heat transfer, and some parameters for VEXPLT.
FWDRAG	Calculation of wall drag.
HLOSS	Calculates head loss, throat void fraction, and downstream void fraction for abrupt area change model.
VEXPLT	Computes explicit liquid and vapor velocities for junctions.
JCHOKE	Determines if a junction is choked. If choked applies choking criterion.
JPROP (1)	Recomputes junction properties if the junction velocity has changed sign.
VFINL	Calls PRESEQ to set up matrix elements and source vector for pressure equation by eliminating liquid and vapor specific internal energy, vapor void fraction, and noncondensible quality. Calls SYSSOL (sparse matrix solver) to solve for new-time pressure difference. Computes new-time junction velocities.
EQFINL	Computes new-time pressures and does back substitution to get new-time liquid and vapor specific internal energies, vapor void fraction, noncondensible quality, and boron density. Also computes vapor generation rates and mixture density.
STATE	Controls evaluation of equation of state and calls STATEP to determine thermodynamic properties and property derivatives for all components.
JPROP (0)	Computes junction phasic specific internal energy, liquid and vapor void fraction, and phasic densities.
VLVELA	Calculates average volume velocities.

a. HYDRO calls the subroutines below it in the order listed.

$$\rho_g \left(\frac{\partial v_g}{\partial t} + \frac{1}{2}\frac{\partial v_g^2}{\partial x}\right) - \rho_f\left(\frac{\partial v_f}{\partial t} + \frac{1}{2}\frac{\partial v_f^2}{\partial x}\right) = (\rho_g - \rho_f)\, B_x - FWG\, \rho_g v_g$$

$$+ FWF\, \rho_f v_f + \Gamma_g \frac{(v_I - \alpha_f v_g - \alpha_g v_f)}{\alpha_g \alpha_f} - FI\, \rho_g \rho_f\, (v_g - v_f)$$

$$- C\rho \frac{\partial (v_g - v_f)}{\partial t}\,, \qquad (7\text{-}47)$$

where

B_x	=	body force
FWG	=	wall drag on vapor
FWF	=	wall drag on liquid
Γ_g	=	vapor generation rate per unit volume
FI	=	interface drag term
ρ	=	mixture density .

Equation (7-47) is then integrated from the upstream volume center to the junction to yield the following finite difference equation:

$$\left[(\rho^n_{g,K} + VIRMAS)\frac{\Delta x_K}{2} + [\rho^n_{g,K}\,(FRICGJ + \frac{JCAT^n}{(ATHROT * C_D)^2}(1 + \frac{JCAT^{n+1}}{JCAT^n})\frac{1}{2} v^n_{g,j}\right.$$

$$\left. + FI^n_j - \Gamma^n_{g,j}]\,\Delta t\right] v^{n+1}_{g,j} + \left[-(\rho^n_{f,K} + VIRMAS)\frac{\Delta x_K}{2}\right.$$

$$-[\rho^n_{f,K}\,(FRICFJ + \frac{JCAT^n}{(ATHROT * C_D)^2}(1 + \frac{JCAT^{n+1}}{JCAT^n})\frac{1}{2} v^n_{f,j}) +$$

$$\left. FI^n_j - \Gamma^n_{g,j}]\,\Delta t\right] v^{n+1}_{f,j} = \left[(\rho^n_{g,K} + VIRMAS)\frac{\Delta x_K}{2} v^n_{g,j}\right.$$

$$-(\rho_{f,K} + \text{VIRMAS})\,\frac{\Delta x_K}{2}\,v^n_{f,j} - \Bigg[(\rho^n_{g,K} - \rho^n_{f,K})\,g\,\frac{\Delta z_K}{2} +$$

$$\rho^n_{g,K}\left(-\frac{1}{2}\left[\frac{JCAT^n}{(ATHROT*C_D)^2}\,(v^n_{g,j})^2 + (v^n_{g,K})^2\right]\right) -$$

$$\rho^n_{f,K}\left(-\frac{1}{2}\left[\frac{JCAT^n}{(ATHROT*C_D)^2}\,(v^n_{f,j})^2 + (v^n_{f,K})^2\right]\right)\Delta t\Bigg]\Bigg] . \qquad (7\text{-}48)$$

The finite difference form of Equation (7-43) written in terms of new-time phasic velocities and new-time sound speed is

$$(\dot{\alpha}^n_{g,j}\,\dot{\rho}^n_{f,j})\,v^{n+1}_{g,j} + (\dot{\alpha}^n_{f,j}\,\dot{\rho}^n_{g,j})\,v^{n+1}_{f,j} = (\dot{\alpha}^n_{f,j}\,\dot{\rho}^n_{g,j} +$$

$$\dot{\alpha}^n_{g,j}\,\dot{\rho}^n_{f,j})\left[a^n_j\left(\frac{ATHROT*C_D}{JCAT^{n+1}}\right) + \partial\,\frac{\left(a^n_j\,\frac{ATHROT*C_D}{JCAT^{n+1}}\right)}{\partial P}\,(P^{n+1}_K - P^n_K)\right] . \qquad (7\text{-}49)$$

In these equations, the subscript K refers to the volume upstream of the junction determined to be choked, subscript j denotes the junction under consideration, the dot overscore implies a donored property, n+1 denotes new time, and n denotes current value. The Δx denotes the upwind volume length, and Δz is the volume-elevation change. The velocity terms with subscript K are volume averaged velocities computed using Equations (91) and (92) in Reference (7-12). VIRMAS is the virtual mass coefficient times the mixture average density at the junction, and FRICFJ is a wall friction parameter defined for the liquid as

$$\frac{\Delta x \phi^2 \rho_f\,\frac{\alpha_{f,w}}{\alpha_f}\,\frac{f}{D}\,\left|v^n_{f,j}\right|}{\alpha^n_{f,j}\,\rho^n_{f,j}} \qquad (7\text{-}50)$$

and is similarly defined for the vapor. In this equation, ϕ^2 is a two-phase friction multiplier, the subscript w indicates a wetted wall, f is a Darcy friction factor, and D is the volume hydraulic diameter. C_D is a user-specified discharge coefficient, and the parameters JCAT and ATHROT are density and area ratios that stem from continuity considerations at the choke plane and the manner in which the choke plane area is defined in RELAP5. With reference to Figure 7-7 for the single-phase case, continuity requires

$$\rho_{throat} v_{throat} A_{throat} = \dot{\rho}_j v_j A_j . \tag{7-51}$$

Recalling that $\dot{\rho}_j$ is equal to ρ_K and solving for v_{throat} yields

$$v_{throat} = \frac{\rho_K}{\rho_{throat}} \frac{A_j}{A_{throat}} v_j . \tag{7-52}$$

The density ratio is defined as JCAT, and the area ratio is ATHROT. Specifically, for the two-phase Equations (7-48) and (7-49),

$$JCAT^n = \frac{\dot{\alpha}^n_{f,j} \dot{\rho}^n_{f,j} + \dot{\alpha}^n_{g,j} \dot{\rho}^n_{g,j}}{\rho^n_j} . \tag{7-53}$$

Note that the term in brackets on the right-hand side of Equation (7-49) represents the new-time junction choking velocity approximated as a Taylor expansion in pressure. This approximation is made to increase the degree of the implicitness and numerical stability and to cast the solution in a form consistent for use in VFINL. With respect to Equation (7-48), note that it is written with momentum flux terms in a form recommended by Bryce[7-19] to increase stability. Bryce suggested that the junction momentum flux terms should be kept as implicit as possible Ultimately, one would desire that the flux term be written completely in new-time velocity. Since this is not possible in the present scheme, an approximation is used. Consider the new time velocity squared written as

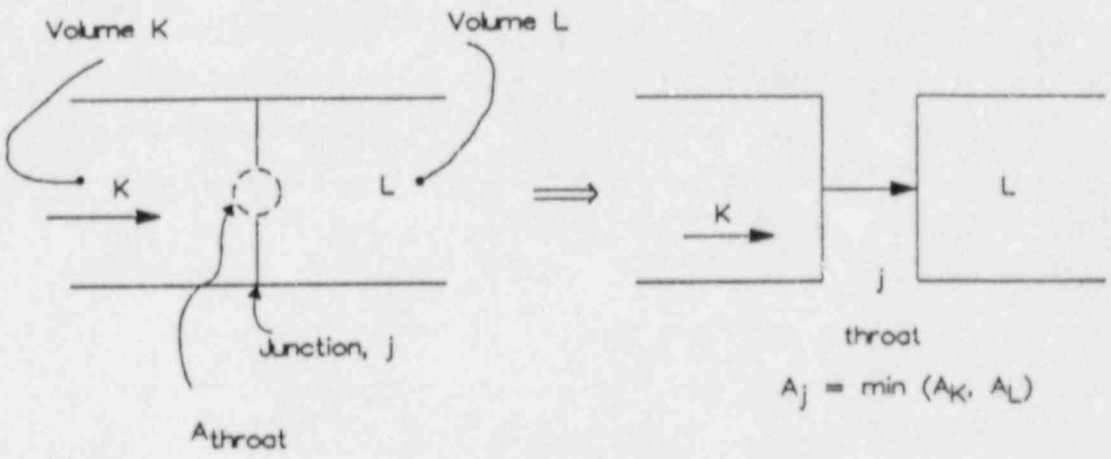

Continuity:

$$\rho_{throat}\ v_{throat}\ A_{throat} = \dot{\rho}_j\ v_j\ A_j$$

$$v_{throat} = \frac{\dot{\rho}_j}{\rho_{throat}}\ \frac{A_j}{A_{throat}}\ v_j = \frac{\rho_k}{\rho_{throat}}\ \frac{A_j}{A_{throat}}\ v_j = \frac{Jcat}{ATHROT}\ v_j$$

Momentum Simplified:

$$P_{throat} = P_k - 1/2\ \rho_{throat}\ v^2_{throat} + 1/2\ \rho_k\ v^2_k$$

$$= P_k - 1/2\ \rho_k \left[\frac{\rho_{throat}}{\rho_k}\ v^2_{throat} - v^2_k \right]$$

$$= P_k - 1/2\ \rho_k \left[\frac{\rho_{throat}}{\rho_k} \left(\frac{Jcat}{ATHROT} \right)^2 v^2_j - v^2_k \right]$$

$$= P_k - 1/2\ \rho_k \left[\frac{Jcat}{(ATHROT)^2}\ v^2_j - v^2_k \right]$$

JEN00435

Figure 7-7. Control volume and junction relationship for subroutine JCHOKE.

$$\frac{1}{2} v_j^{n+1} v_j^{n+1} = \frac{1}{2} (v_j^{n+1} - v_j^n + v_j^n) (v_j^{n+1} - v_j^n + v_j^n) = \frac{1}{2} ((v_j^{n+1} - v_j^n) + v_j^n)^2 . \quad (7\text{-}54)$$

Expanding the right-hand side gives

$$\frac{1}{2} \left[(v_j^{n+1} - v_j^n)^2 + 2 v_j^n (v_j^{n+1} - v_j^n) + (v_j^n)^2 \right] . \quad (7\text{-}55)$$

If the first term in Equation (7-55) is small, then

$$\frac{1}{2} v_j^{n+1} v_j^{n+1} = v_j^n (v_j^{n+1} - v_j^n) + \frac{1}{2} (v_j^n)^2 = v_j^n v_j^{n+1} - (v_j^n)^2 + \frac{1}{2} (v_j^n)^2 . \quad (7\text{-}56)$$

This approximation is used for the junction momentum flux after integration of Equation (7-47) to produce the finite difference form shown in Equation (7-48).

Equation (7-48) and (7-49) form a 2 x 2 set of equations that can be put into the form

$$v_{f,j}^{n+1} = \tilde{v}_{f,j}^n + \frac{\partial \tilde{v}_{f,j}^n}{\partial P} (P_K^{n+1} - P_K^n) \quad (7\text{-}57)$$

$$v_{g,j}^{n+1} = \tilde{v}_{g,j}^n + \frac{\partial \tilde{v}_{g,j}^n}{\partial P} (P_K^{n+1} - P_K^n) .$$

The JCHOKE subroutine in effect computes the quantities

$\tilde{v}_{f,j}^n$, $\tilde{v}_{g,j}^n$, $\partial \tilde{v}_{f,j}^n / \partial P$, and $\partial \tilde{v}_{g,j}^n / \partial P$.

In Equation (7-49), the choking velocity, the homogeneous equilibrium sound speed at the junction, and the derivative of these values are needed. While the upwind volume thermodynamic properties are provided to JCHOKE, values for the junction are calculated in JCHOKE. These parameters are dependent on the thermodynamic state present and will be discussed next.

7.2.2.3 Calculation of Junction Properties. Since the calculation of pressure, void fraction, energy, and density is made at volume centers and thermodynamic properties are needed at the cell edges (junctions), an approximation is made for junction pressure and energy. Upon entry to JCHOKE, Bernoulli's equation [Equation (7-18)] incorporating momentum flux and frictional effects is used to do a half-cell extrapolation to provide an estimate of junction pressure. With reference to Figure 7-7, the Bernoulli balance from the center of volume K to the junction j is

$$P_j^n = P_K^n - (\dot{\alpha}_{f,j}^n \dot{\rho}_{f,j}^n + \dot{\alpha}_{g,j}^n \dot{\rho}_{g,j}^n)\, g\, \frac{\Delta z_K}{2} - \dot{\alpha}_{f,j} \dot{\rho}_{f,j}\, \frac{1}{2} \left[\frac{JCAT^n}{(ATHROT * C_D)^2} (v_{f,j}^n)^2 \right.$$

$$\left. - (v_{f,K}^n)^2 \right] - \dot{\alpha}_{g,j}^n \dot{\rho}_{g,j}^n\, \frac{1}{2} \left[\frac{JCAT^n}{(ATHROT * C_D)^2} (v_{g,j}^n)^2 - (v_{g,K}^n)^2 \right]$$

$$+ \frac{1}{2} \Delta P_{pump} - \dot{\alpha}_{f,j}^n \dot{\rho}_{f,j}^n\, FRICFJ * v_{f,j}^n - \dot{\alpha}_{g,j}^n \dot{\rho}_{g,j}^n\, FRICGJ * v_{g,j}^n . \quad (7\text{-}58)$$

The junction energy is computed from an energy balance approximation.

$$U_j^n = U_K^n + \frac{P_K^n - P_j^n}{\dot{\rho}_{g,j}^n \dot{\rho}_{f,j}^n / (X_{s,K} \dot{\rho}_{f,j}^n + (1 - X_{s,K}) \dot{\rho}_{g,j})} - g\, \frac{\Delta z_K}{2}$$

$$- X_{s,K}\, \frac{1}{2} \left[\frac{JCAT^n}{(ATHROT * C_D)^2} (v_{g,j}^n)^2 - (v_{g,K}^n)^2 \right]$$

$$- (1 - X_{s,K}) \frac{1}{2} \left[\frac{JCAT^n}{(ATHROT * C_D)^2} (v^n_{f,j})^2 - (v^n_{r,K})^2 \right] . \qquad (7\text{-}59)$$

Equation (7-59) has a slight different form if the flow at the previous time step was determined to be stratified flow. These variations will be addressed in Section 7.2.4, describing the actual coding of the model.

As discussed previously, to utilize Equation (7-49), the junction sound speed and the sound speed derivative with pressure are needed. These quantities are calculated in JCHOKE. The method of calculating these parameters depends on whether subcooled choking occured [where Equation (7-21) or Equation (7-22) applies], the flow is two-phase, or is in a transition between the two regions. For example, in the subcooled region, the local homogeneous equilibrium sound speed based on saturation properties at the local temperature is calculated using standard relationships as

$$a_{HE} = \left[\left. \frac{\partial P}{\partial \rho} \right|_S \right]^{1/2} = \frac{V_f \frac{dP}{dT}}{\left[\frac{T_{f,K}}{C_{pf} - T_{f,K} V_f \frac{dP}{dT} (2\beta_f - \kappa_f \frac{dP}{dT})} \right]^{1/2}} , \qquad (7\text{-}60)$$

where V, C_p, β (the isobaric thermal expansion), and κ (the isothermal compressibility) are evaluated using saturated liquid properties at $T_{f,K}$, the upwind volume fluid temperature. The term dP/dT is evaluated using the Clapeyron equation

$$\frac{dP}{dT} = \frac{(h_g - h_f)}{T_{f,K} (V_g - V_f)} , \qquad (7\text{-}61)$$

where h_g (the vapor specific enthalpy) and h_f (the liquid specific enthalpy), V_g, and V_f are saturation values at temperature $T_{f,K}$. If the solution to Equation (7-21) produces a throat velocity (hereafter referred to as SONIC) larger than the value given by Equation (7-60) and the throat pressure is predicted to be less than the local saturation pressure [i.e., if Equation (7-19) yields a value of $\Delta P = P_{sat} - P_t > 0$], the sound speed derivative is calculated by differentiating Equation (7-21), which gives

$$\frac{\partial(v_c)}{\partial P} = \left[\rho_{f,K} v_c - \frac{\partial(\Delta P)}{\partial v_c}\right]^{-1} . \tag{7-62}$$

Note that if the throat pressure is predicted to be saturation pressure, the second term in Equation (7-62) is zero and the derivative is given as the first term. Furthermore, if the homogeneous sound speed is larger than the throat velocity calculated from Equation (7-21), the throat velocity is reset to a_{HE} and a_{HE} replaces v_c in Equation (7-62).

If throat conditions are determined to be saturated liquid, two-phase, or vapor, the steam table routines are accessed with the junction pressure and energy estimates from Equations (7-58) and (7-59) to provide junction thermodynamic properties. If pure vapor is present, the homogeneous equilibrium sound speed is calculated as

$$a_{HE} = V \left[\frac{dP/dT}{V\left(\kappa * \frac{dP}{dT} - \beta\right)}\right]^{1/2} , \tag{7-63}$$

where

$$\frac{dP}{dT} = \frac{C_p}{T_{g,K} V \beta} . \tag{7-64}$$

If the call to the steam tables indicates that two-phase conditions are present at the junction, Equations (7-38) and (7-39) are used to calculate the homogeneous sound speed and dP/dT. T_f and T_g in this case are the saturation temperature and the specific volume, as calculated from the equilibrium quality and saturated vapor and saturated liquid specific volumes. If the junction fluid conditions are determined to be saturated liquid, an additional call to the steam tables is made with saturation temperature (based on junction pressure and specific internal energy) and equilibrium quality set to zero. Equations (7-38) and (7-39) are then used to compute the homogeneous equilibrium sound speed.

If pure vapor conditions exist at the throat, the sound speed derivative is computed by assuming that the vapor behaves as a perfect gas, i.e.

$$\left.\frac{\partial a}{\partial P}\right|_s = k \left.\frac{\partial (PV)}{\partial P}\right|_s = \frac{k-1}{2} \frac{1}{\rho_K \, a_{HE,K}} , \tag{7-65}$$

where k is the specific heat ratio.

If saturated liquid or two-phase conditions are present, the derivative is equilibrium-quality-weighted and has the form

$$\frac{(1 - X_{E,K})}{a_j \rho_{f,K}} + \frac{X_{E,K}}{a_{HE,K} \rho_K} \frac{k-1}{2} . \tag{7-66}$$

Once the junction sound speed and derivative have been computed, these values are multiplied by the ATHROT/JCAT ratio per Equation (7-52).

Any user input discharge coefficient is also factored into the ATHROT parameter, so that the final sound speed expression becomes

$$a_j = a_j \frac{C_D \cdot ATHROT}{JCAT} . \tag{7-67}$$

The derivatives [Equation (7-62) or (7-65)] are likewise multiplied by the C_D . ATHROT/JCAT ratio.

7.2.3 Constants Employed in the RELAP5 Critical Flow Model

The only literature correlation employed in the RELAP5 critical flow model other than the homogeneous sound speed expressions developed in Appendix 7A is the so-called pressure undershoot correlation described in Section 7.2.1.1. The correlation used in the RELAP5 choking model is that described by Jones,[7-14,7-15] which is an extension to the original model proposed by Alamgir and Leinhard.[7-13]

The pressure undershoot model is used to determine the inception of net vaporization in flashing flows. According to Jones,[7-15] the flashing inception can be expressed by two additive effects,; one due to static decompression described by Alamgir and Leinhard[7-13] and one due to turbulent fluctuations in the flowing liquid. As given by Jones, the static depressurization is

$$\Delta P_{static} = \Delta P^{o}_{stat} \left[1 + 13.25\, \Sigma'^{0.8} \right]^{1/2}, \tag{7-68}$$

where Σ' is a depressurization rate and

$$\Delta P^{o}_{stat} = 0.258 \frac{\sigma^{3/2}\, T_R^{13.76}}{\sqrt{k_B T_c}\,(1 - V_f/V_g)} \tag{7-69}$$

and the terms are described in Section 7.2.1.1. Note that Σ' in this equation has units of Matm/s. Jones extended Equation (7-68) by including a turbulence term which, when written with a constant turbulent fluctuation intensity of 0.069984 recommended by Jones, is

$$0.069984 \left(\frac{A_t}{A}\right)^2 v_c^2 \quad . \tag{7-70}$$

For steady flow in a nozzle, the total expansion rate Σ' can be written as

$$\rho \frac{v_c^3}{A_t} \frac{dA_t}{dx} \quad , \tag{7-71}$$

where the area is evaluated at the throat and the area derivative is also evaluated at the throat. When Equation (7-70) is subtracted from Equation (7-68), the result is Equation (7-19), which is the Alamgir-Lienhard-Jones model. Although none of the original constants have been altered, conversion to proper units has been effected so that, as coded, the model is

$$\Delta P_{FI} = \Delta P_{FIOC} \sqrt{1 + \Delta P_{con} \cdot v_c^{2.4}} - K_2 v_c^2 \quad , \tag{7-72}$$

where

$$\Delta P_{FIOC} = \frac{0.258}{\sqrt{k_b T_c}} \left[\frac{T_K}{T_c}\right]^{13.76} (\sigma_k)^{1.5} V_g/(V_g - V_f)$$

$$= (2.72958E9)(T_K * 1.5448787E-3)^{13.76} (\sigma_k)^{1.5} V_g/(V_g - V_f)$$

$$\Delta P_{con} = \left(\rho_{f,K} \frac{1}{A_t} \left(\frac{dA}{dx}\right)_t\right)^{0.8} 13.25 K_1 \text{ a}$$

$$= \left(\rho_{f,K} \frac{1}{A_t} \left(\frac{dA}{dx}\right)_t\right)^{0.8} 2.0778E-8$$

---

a. K_1 is a factor for converting Pa/s to Matm/s raised to the 0.8 power.

$$K_2 = \rho_{f,K}\left(\frac{A_j}{A_K}\right)^2 6.9984E\text{-}2 \ .$$

7.2.4 Model as Coded

The choking criterion described in the previous sections is a complex process. To aid in the understanding of the model and the implementation, a flow chart for subroutine JCHOKE is provided in Figure 7-8. A brief verbal description of the logic flow in the subroutine will help relate the implementation to the previous discussion, identify areas where weighting and averaging are used and where special cases exist.

Upon entry to JCHOKE in the hydrodynamic advancement, a loop over all junctions begins. A logical variable (TRANSR) is set to false for later use in testing whether or not the current conditions indicate transition between choked flow regimes. A user-set flag is then tested to determine if the user desires to apply the choking model at the junction in question. If the choking model is not to be applied, the calculation proceeds to the next junction. Likewise, a flag is tested to see if the junction is connected to an active accumulator and, if it is, the processing proceeds to the next junction. A flag is tested to determine if the junction was choked on the last time step and if the vapor velocity is in the same direction as the last time step. If so, a logical variable (CHOKE) is set to true. Next, the junction vapor and liquid velocities are tested for countercurrent flow and to see if the junction is connected to a time-dependent volume. If countercurrent flow exists or the junction "from volume" is a time-dependent volume, processing for the junction is terminated, since choking is not permitted for those circumstances. If cocurrent flow exists and the "from" volume is not a user-specified time-dependent volume, the logic proceeds to determine upstream and downstream volumes based on the direction of the liquid velocity. Based on the flow direction, geometric properties such as cell half-lengths and volume-to-volume area ratios are set for the upwind

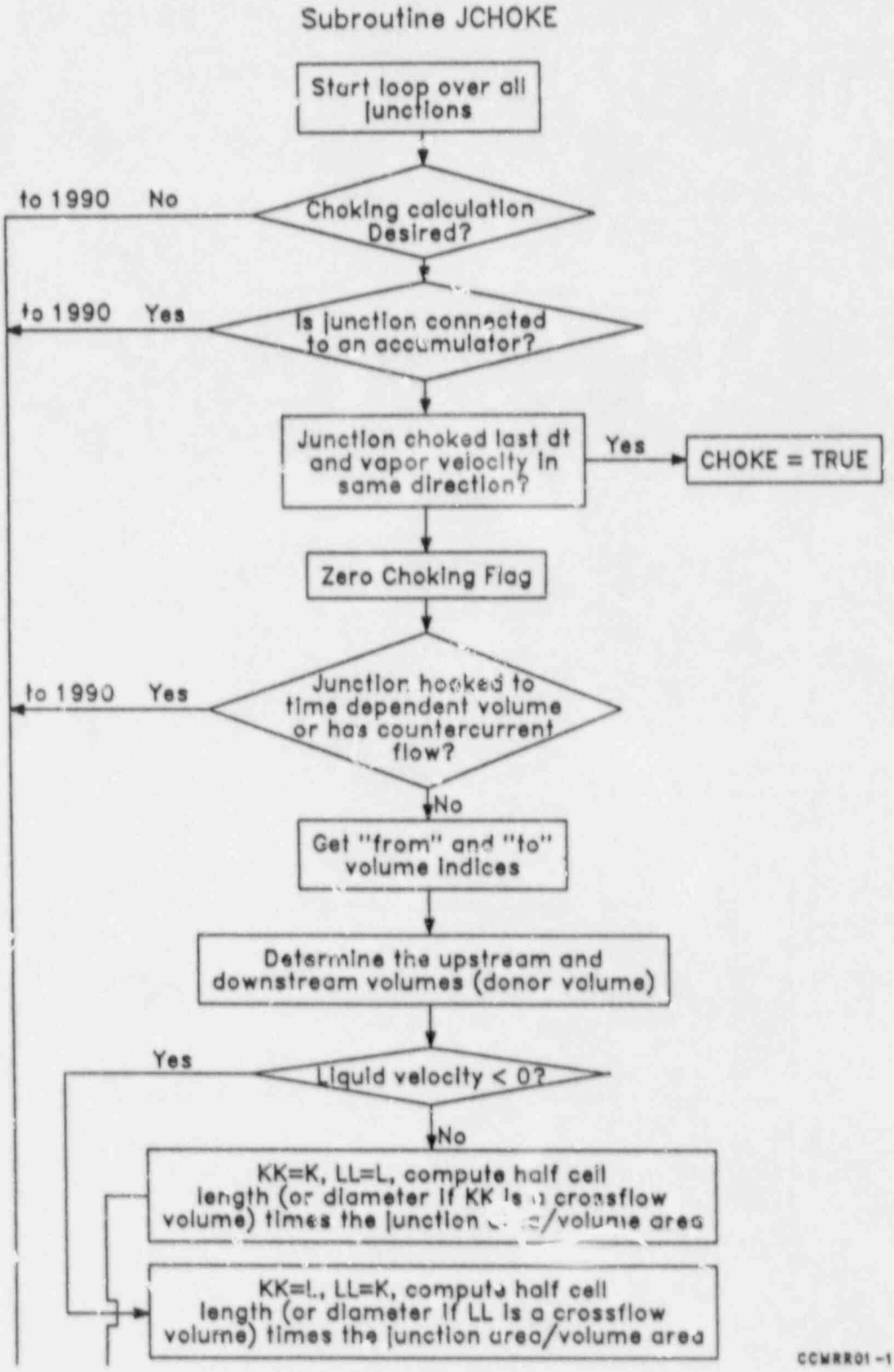

Figure 7-8. Subroutine JCHOKE flow logic.

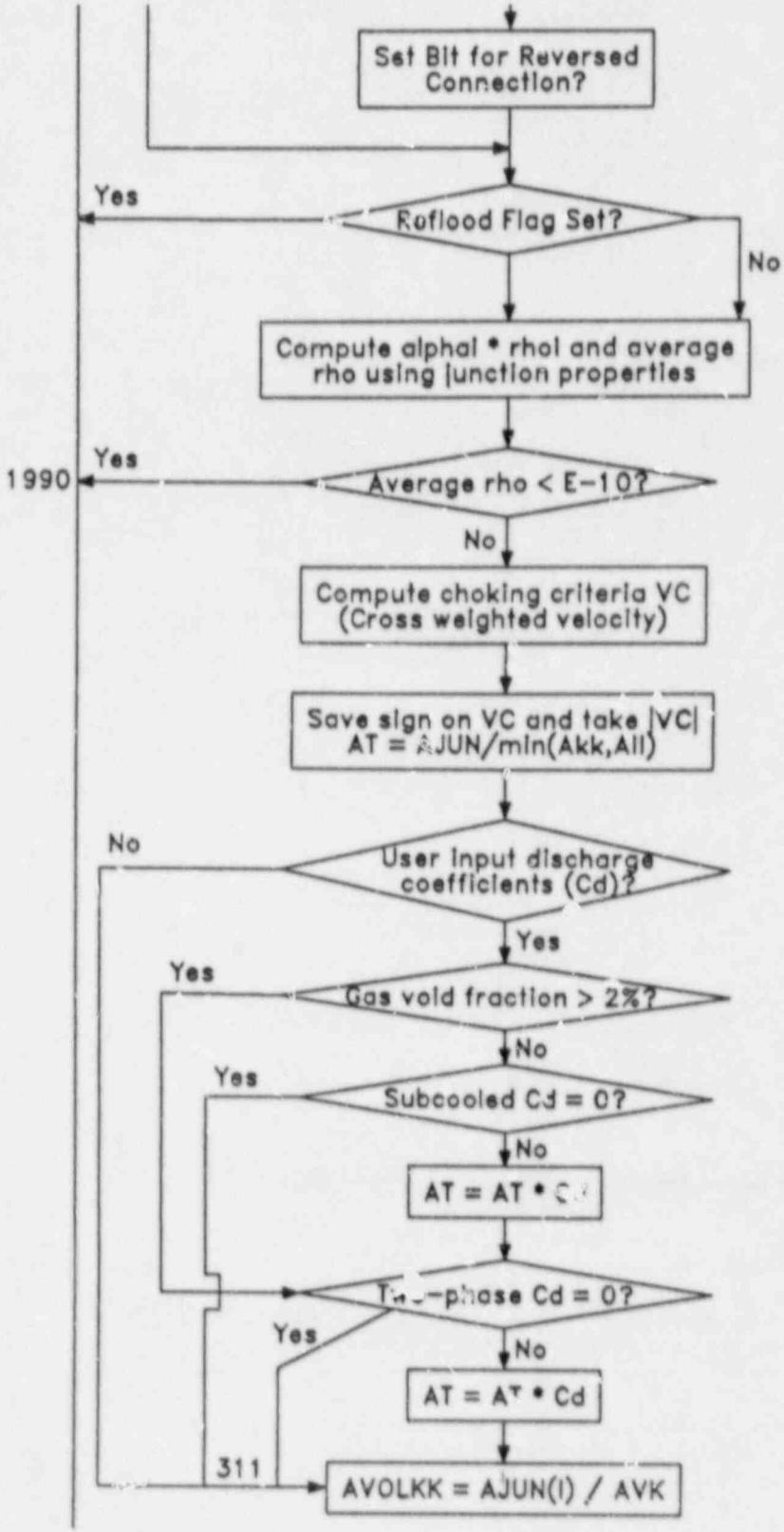

Figure 7-8 (continued).

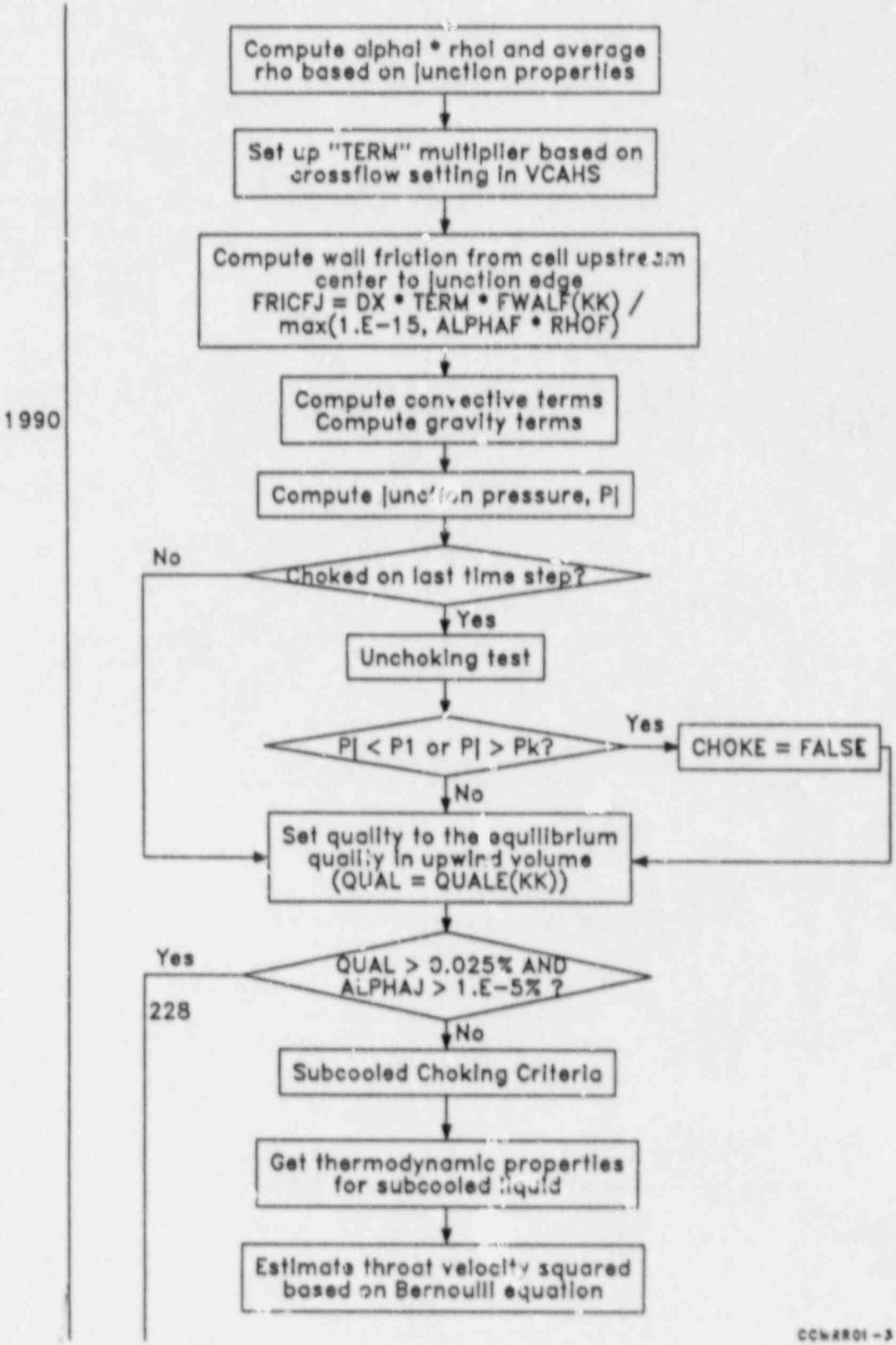

Figure 7-8 (continued).

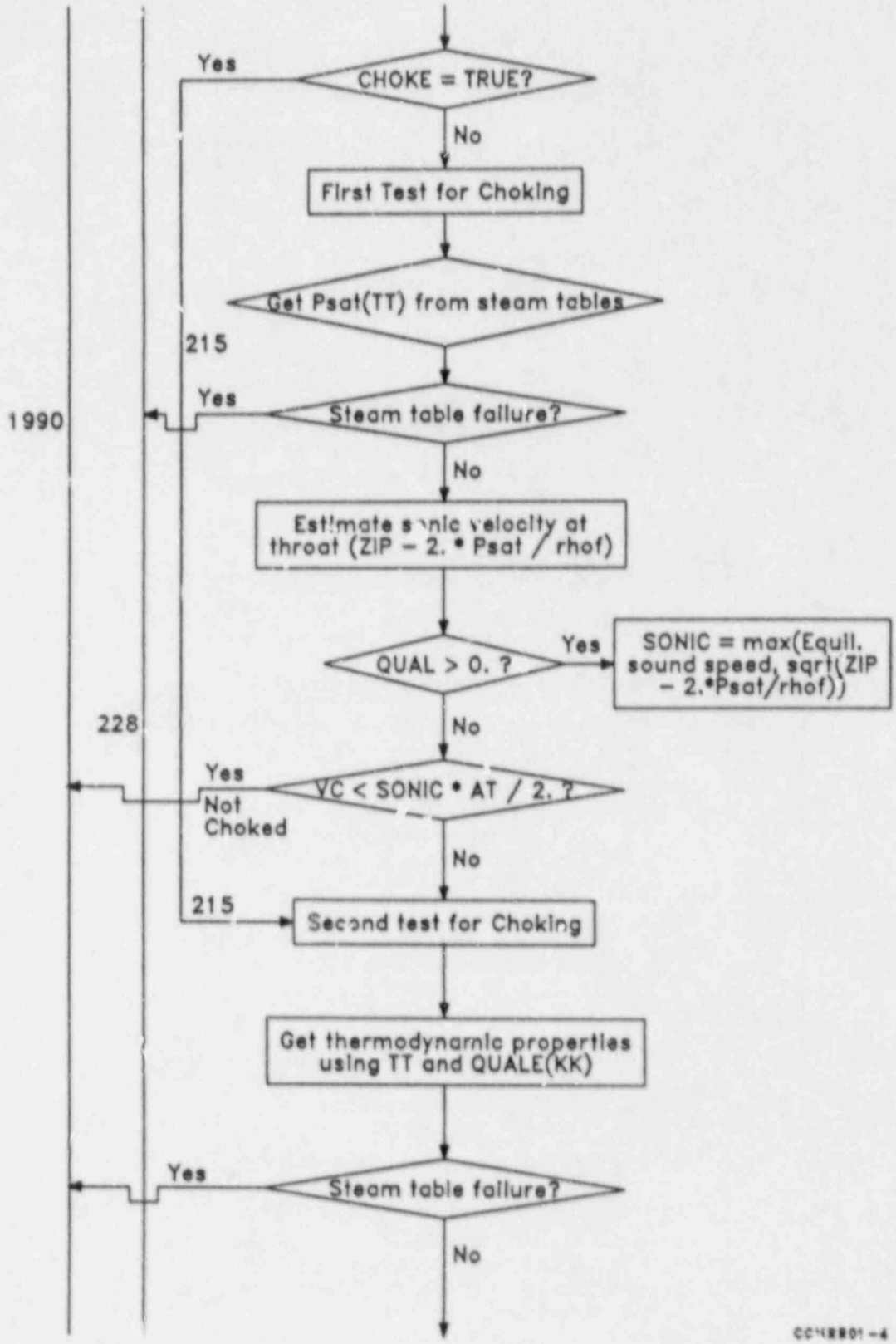

Figure 7-8 (continued).

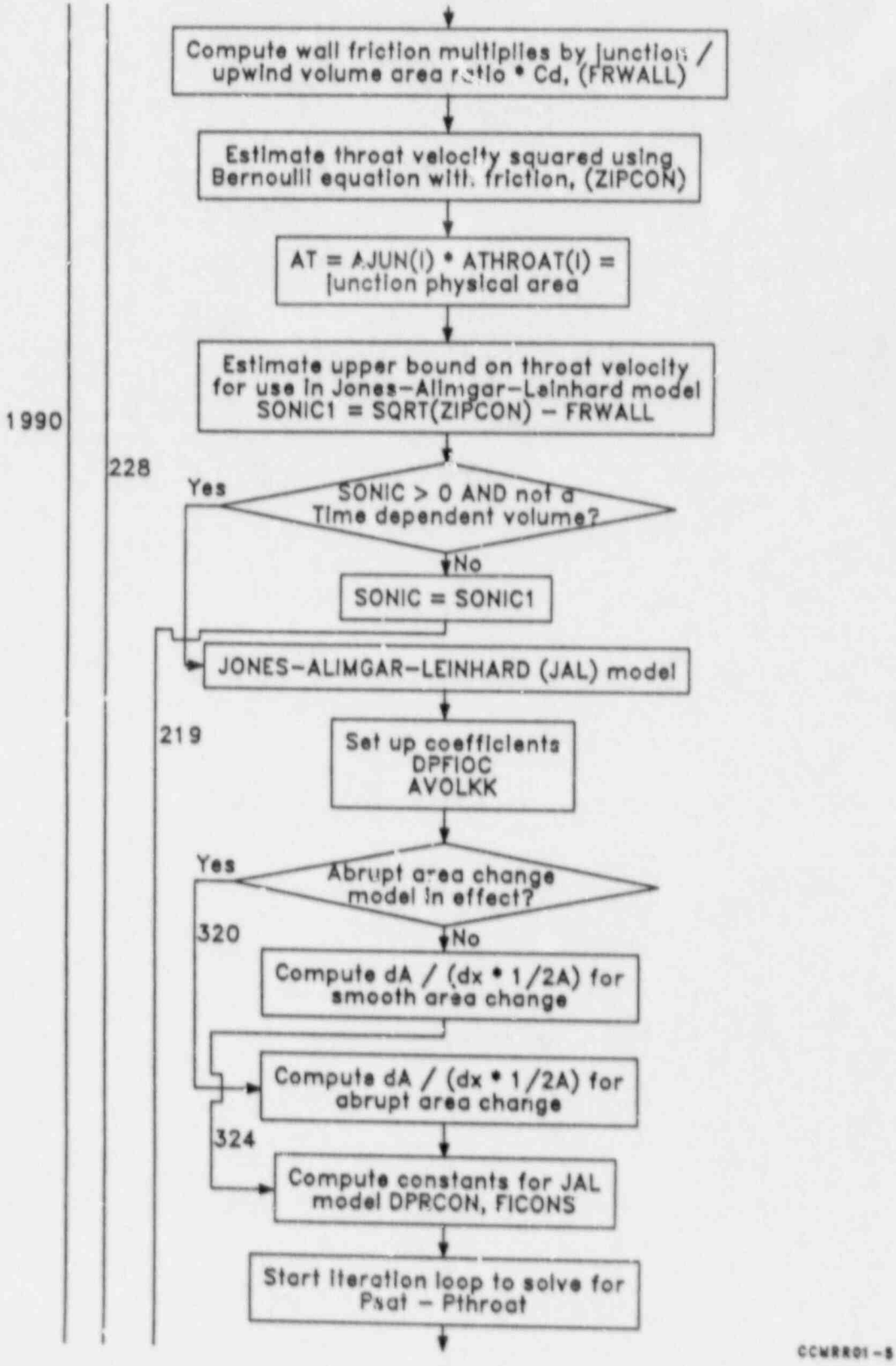

Figure 7-8 (continued).

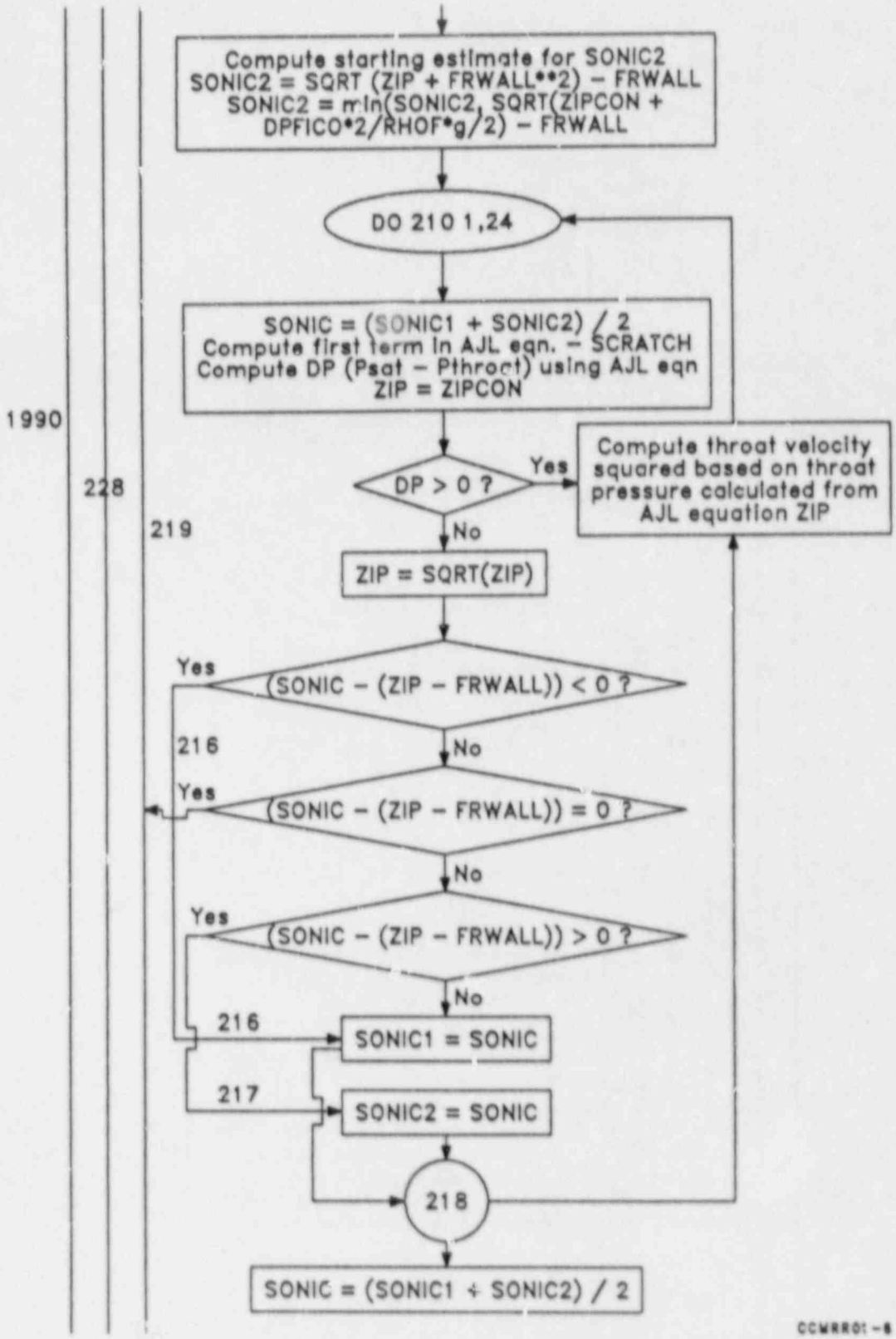

Figure 7-8 (continued).

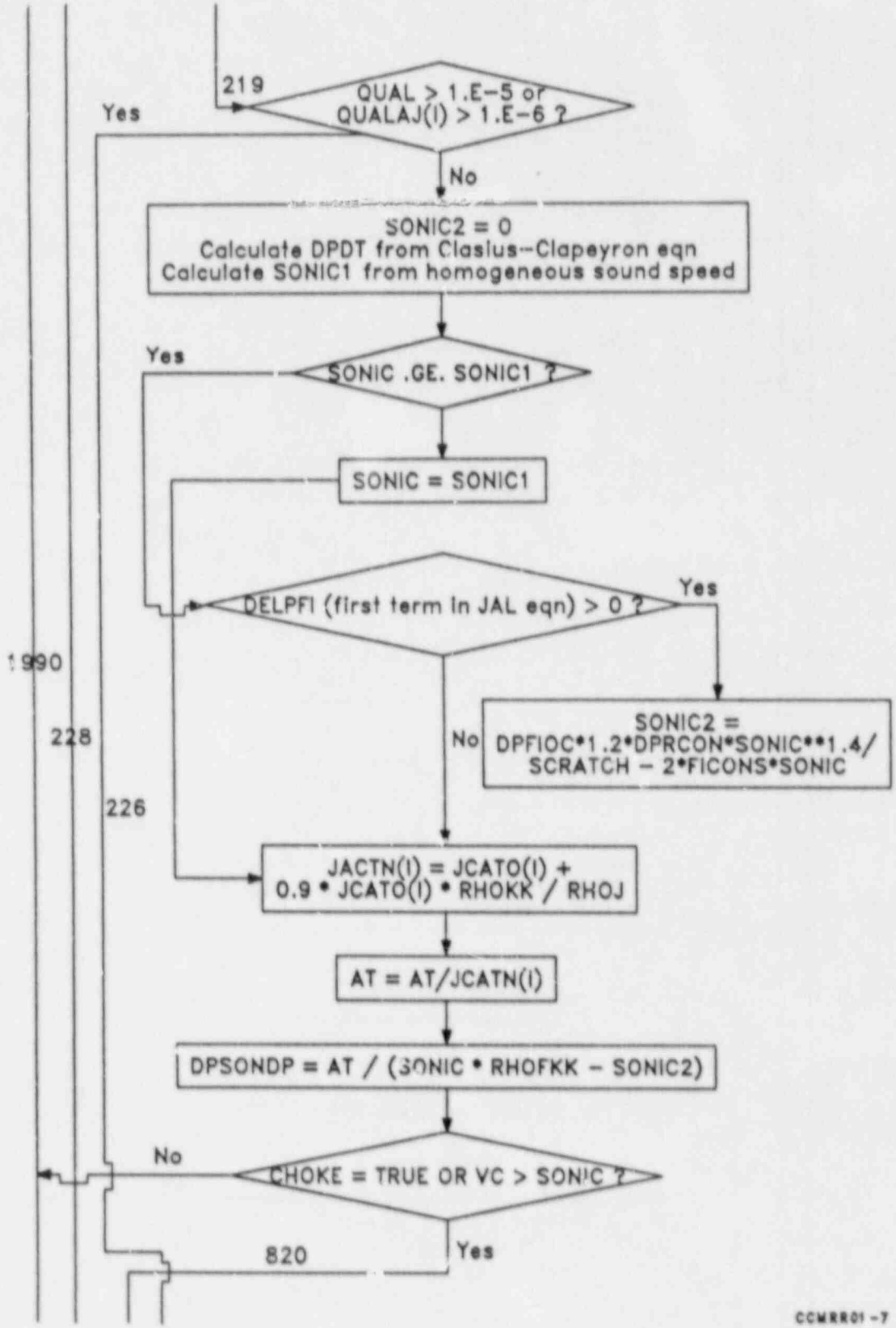

Figure 7-8 (continued).

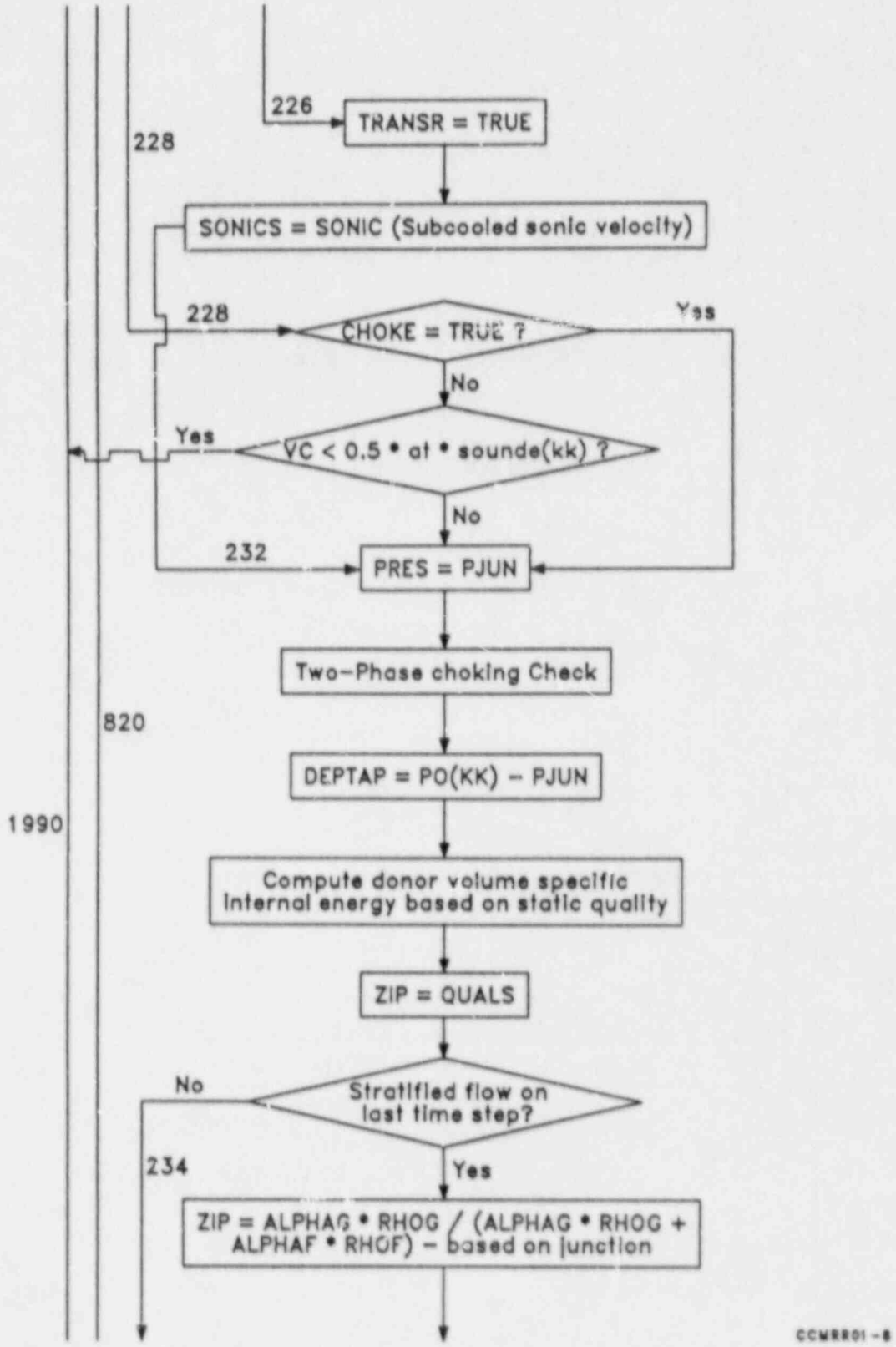

Figure 7-8 (continued).

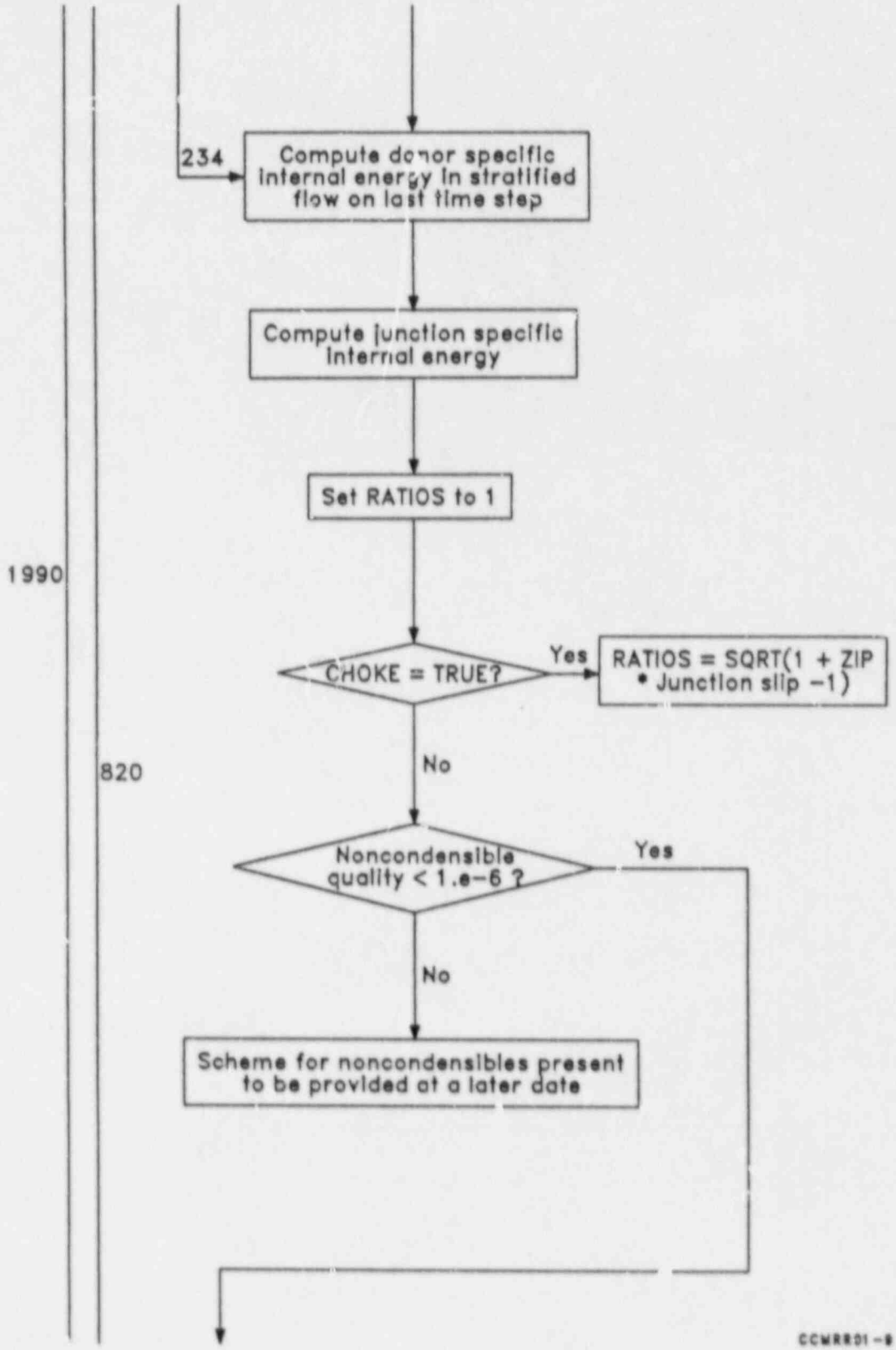

Figure 7-8 (continued).

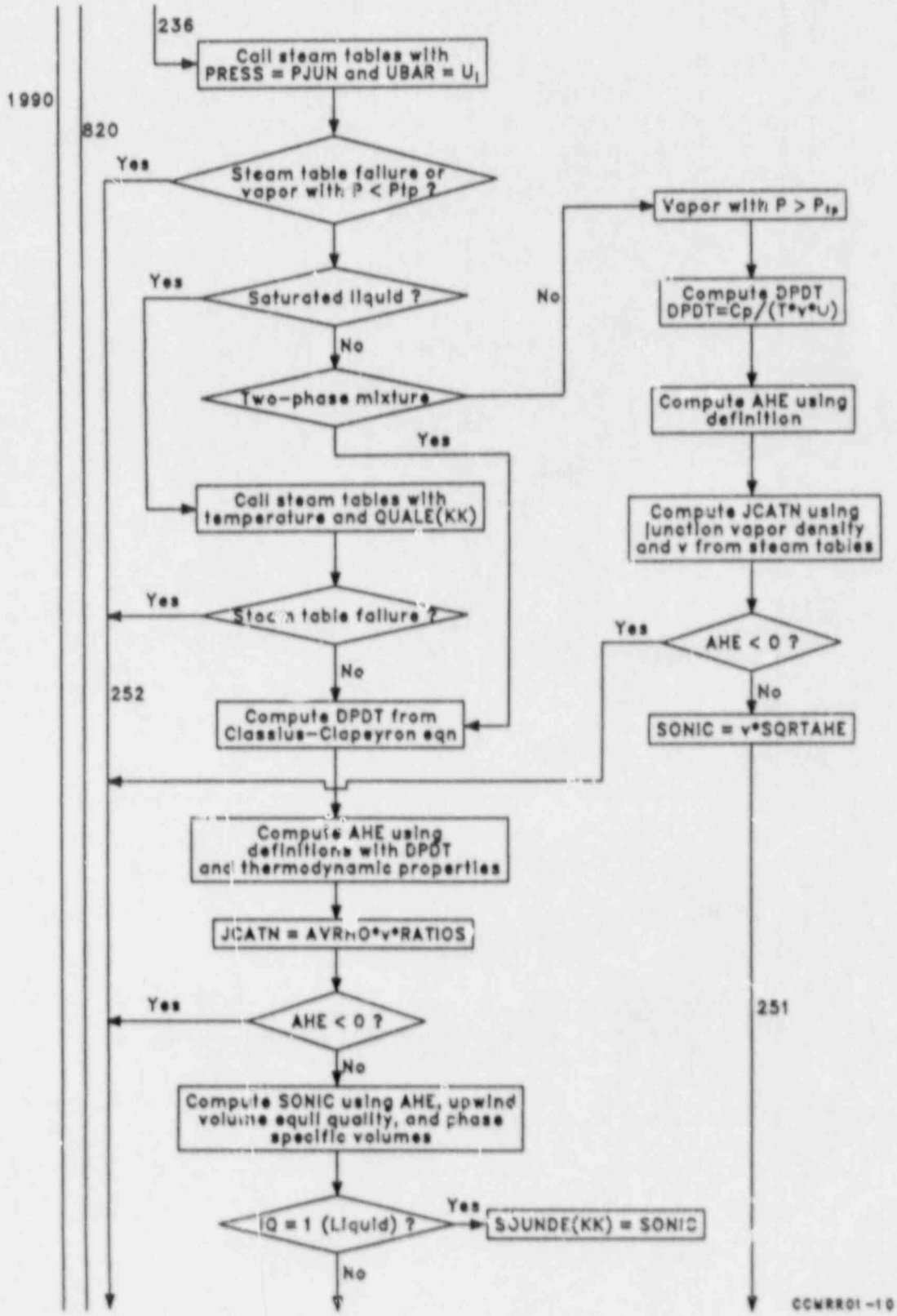

Figure 7-3 (continued).

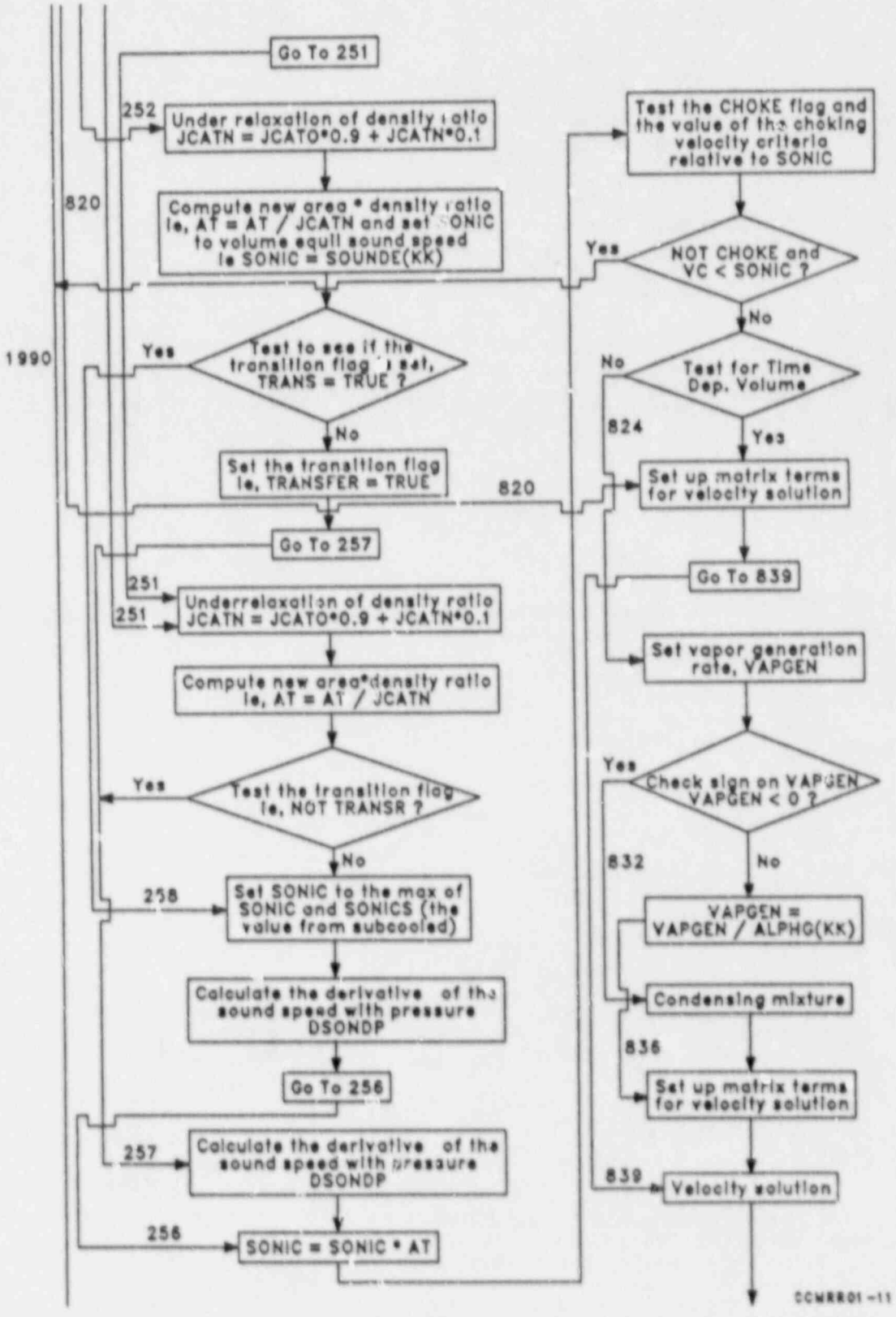

Figure 7-8 (continued).

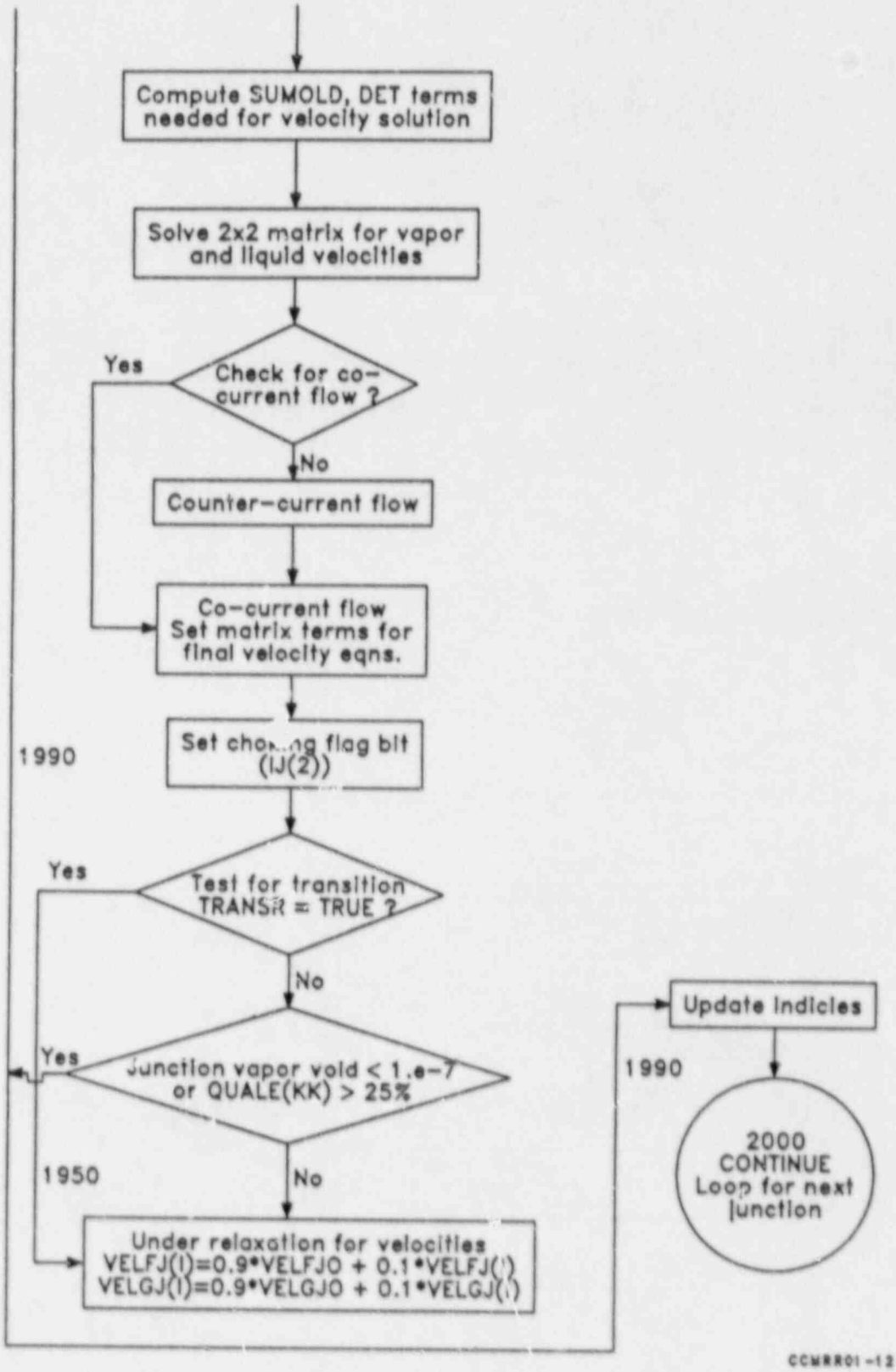

Figure 7-8 (continued).

(donor) volume. The denominator of Equation (7-43) is then calculated. Processing is terminated if the value of $\alpha_{g,j}\rho_{f,j} + \alpha_{f,j}\rho_{g,j}$ is less than 10^{-10}. Otherwise Equation (7-43) is computed for the junction and set to variable VC, e.g.

$$VC = \frac{(\alpha_g\rho_f v_g)_j + (\alpha_f\rho_g v_f)_j}{(\alpha_g\rho_f)_j + (\alpha_f\rho_g)_j} . \qquad (7\text{-}73)$$

The junction physical area-to-volume flow area ratio (ATHROT) is then obtained and multiplied by either a subcooled discharge coefficient or a two-phase discharge coefficient if the user has input values. If the vapor void fraction ($\alpha_{g,j}$) is larger than 2%, the two-phase discharge coefficient is always selected.

The junction average density $[(\alpha_g\rho_g)_j + (\alpha_f\rho_f)_j]$ and frictional, convective, and gravitational terms are then calculated for use in estimating the junction pressure via Equation (7-58). If the cross-flow model is in effect and the "from" volume is a cross-flow volume, a multiplier is set to effectively zero out the frictional and convective terms in the half cell extrapolation. If the junction was choked on the last time step, the newly calculated junction pressure is used in an unchoking test that checks to see if the junction pressure is greater than the upwind pressure or less than the downwind pressure. If the test is true, the logical variable CHOKE is set to false. If the junction was not choked on the last time step, the unchoking test is bypassed.

The equilibrium quality in the upwind volume (X_K) and the junction vapor void fraction ($\alpha_{g,j}$) are then tested to determine whether the subcooled choking or two-phase choking criterion is to be applied. If X_K is greater than 0.025% and $\alpha_{g,j}$ is greater than 10^{-5}%, the flow is considered two-phase and the logic proceeds directly to the two-phase model.

7.2.4.1 Subcooled Criterion. On entry to the subcooled choking criterion subroutine, an estimate of the throat velocity squared is made using the simplified momentum balance shown on Figure 7-7 and assuming the throat pressure is saturation pressure based on the liquid temperature in the upwind volume. A throat velocity (SONIC) is then set to be the square root of the maximum of zero (to prevent errors associated with taking the square root of a negative number) or the value calculated. If the equilibrium quality is greater than zero (but less than 0.025%), the calculated value SONIC is also checked relative to the homogeneous equilibrium sound speed calculated for the upstream volume and the maximum of the two values is taken. The result is multiplied by ATHROT*C_D and compared relative to VC, the value computed from Equation (7-73). If the value of VC is less than 1/2 the calculated throat velocity times the discharge coefficient area ratio product, the junction is considered to be unchoked and processing is terminated. If VC is larger, then a refined calculation is conducted using Equation (7-72) to calculate the throat pressure.

Equation (7-72) must be solved iteratively. To provide throat velocity estimates for use in the iteration, a throat velocity (SONIC1) is calculated by incorporating frictional effects into the Bernoulli balance assuming the throat pressure is P_{sat}. A second estimate of throat velocity, SONIC2, is computed by taking the minimum of a value calculated assuming the throat pressure is zero and a value calculated assuming the throat pressure is determined by $P_{sat} - \Delta P_{FIOC}$ where ΔP_{FIOC} is from Equation (7-72). Wall friction effects are incorporated in both estimates for SONIC2. Equation (7-72) is solved iteratively in conjunction with the Bernoulli equation by starting with an arithmetic average of SONIC1 and SONIC2 and updating either end point of the interval until the assumed throat velocity satisfies the pressure balance.

If the equilibrium quality is greater than 0.001%, the flow conditions are in the defined transition region. The value of the throat velocity computed from the iterative solution is stored in a variable SONICS, the

logical variable TRANSR is set to true, and the calculation proceeds to the two-phase criteria. If the equilibrium quality is less than 0.001%, the value SONIC2 is reset to zero and the homogeneous equilibrium sound speed at the junction is computed using Equations (7-60) and (7-61) and saturated liquid properties. If the throat velocity computed from the Bernoulli equation coupled with the pressure undershoot model is larger than the homogeneous equilibrium sound speed, the density ratio JCAT is updated as

$$JCAT^{n+1} = 0.9\ JCAT^{n} + 0.1\ \frac{(c_g\rho_g)_j + (\alpha_f\rho_f)_j}{\rho_K} \quad . \tag{7-74}$$

Equation (7-62) is used to compute the choking velocity derivative with pressure, and Equation (7-67) is applied to compute the final sonic velocity at the throat.

If the homogeneous equilibrium sound speed is larger than the result of the iterative solution for the throat velocity, the throat velocity is reset to the saturated liquid homogeneous value, $JCAT^{n+1}$ is computed as above, and Equations (7-62) and (7-67) are used for the sound speed derivative and final sonic velocity respectively. For this case, the second term in brackets in Equation (7-62) is set to zero.

At this point, the flow is determined to be subcooled. A final check is made to assert that the flow is choked. If the variable CHOKE is true or the value of VC is greater than or equal to the current value of SONIC where

$$SONIC = MAX\ (v_t,\ a_{HE}) \quad , \tag{7-75}$$

subcooled choked flow is verified and the solution proceeds directly to the calculation of velocities. For the case of subcooled flow, the junction vapor and liquid velocities are set equal to SONIC.

7.2.4.2 Two-Phase Criterion. If on entry to JCHOKE the equilibrium quality is greater than 0.025% and the junction vapor void fraction is greater than 10^{-5}% (two-phase) or if the equilibrium quality is greater than 0.001% (transition region), the two-phase choking criterion will be applied.

If the logic dictates that the two-phase criterion subroutine is entered without first passing through the subcooled criterion, the value VC is tested versus the homogeneous equilibrium sound speed based on the upstream volume conditions. If VC is less than 1/2 of the homogeneous sound speed value, the junction is considered to be unchoked and processing is terminated. If this test is not true or if the choked flow is in the transition regime, the logic proceeds directly to calculate the junction specific internal energy using Equation (7-59). Note that the junction pressure was calculated previously. In Equation (7-59), the parameter $X_{s,K}$ is taken to be the static quality in the upwind volume unless stratified flow exists at the junction, in which case $X_{s,j}$ is defined as $\alpha_{g,j}\rho_{g,j}$ / $(\alpha_{g,j}\rho_{g,j} + \alpha_{f,j}\rho_{f,j})$. Likewise, U_K in Equation (7-59) is defined as

$$X_{s,K}\, U_{g,K} + (1 - X_{s,K})\, U_{f,K} \,. \tag{7-76}$$

unless stratified flow exists in which case U_K is defined as

$$X_{s,j}\, U_{g,j} + (1 - X_{s,j})\, U_{f,j} \,. \tag{7-77}$$

After the junction specific internal energy is calculated, a smoothing function RATIOS is defined. If the flag CHOKE is set to true, RATIOS is given as

$$\left[1 + \max\left(X_s\, (v^n_{g,j}/v^n_{f,j} - 1),\, 0\right)\right]^{1/2} \,, \tag{7-78}$$

otherwise RATIOS is set to unity. The parameter X_s is defined as described above, depending on the existence of stratified flow.

Once the junction energy is computed, the steam tables are entered with junction pressure and energy to establish the fluid state. If pure vapor exists, Equations (7-63) and (7-64) are used to calculate the homogeneous equilibrium sound speed and $(dP/dT)_s$, respectively. The density ratio JCAT is then defined as

$$JCAT^{n+1} = \rho_{g,j} V \ , \tag{7-79}$$

where V is the vapor specific volume. If two-phase conditions are present, Equations (7-38) and (7-39) are used for the sound speed and $(dP/dT)^s$, respectively. Likewise, if liquid conditions are indicated, Equations (7-38) and (7-39) are used. However, an additional call to the steam tables with temperature and quality as input is made to establish saturated liquid properties. In either case (liquid or two-phase), the density ratio JCAT is calculated as

$$JCAT = (\alpha_{g,j}\rho_{g,j} + \alpha_{f,j}\rho_{f,j}) * V * RATIOS \ , \tag{7-80}$$

where V is the specific volume returned from the steam table call.

The value of the density ratio JCAT is then underrelaxed as

$$JCAT^{n+1} = 0.9\ JCAT^{n} + 0.1\ JCAT^{n+1} \ . \tag{7-81}$$

If the choked flow is in the transition regime, the sonic velocity is set to the maximum of the current value and the SONICS value computed in the subcooled flow logic. The sound speed derivative is calculated using Equation (7-66) multiplied by C_D*ATHROT/$JCAT^n$ i.e.,

$$\frac{\partial(SONIC)}{\partial P} = \left[\frac{1 - X_{E,K}}{a_j \rho_{f,K}} + \frac{0.15\ X_{E,K}}{\bar{}_{HE,K}\rho_K}\right] \frac{C_D * ATHROT}{JCAT^n} \ , \tag{7-82}$$

where k = 1.3 (assuming that steam is an ideal gas), and (k - 1)/2 = 0.15. If the flow is not in a transition region, only the second term of this expression with $X_{\ell,K}$ set to unity is used. Finally, Equation (7-67) is used to compute the final junction sonic velocity and the solution proceeds to the velocity computation.

The phasic velocity solution proceeds as outlined in Section 7.2.2.2. Using Equations (7-48) and (7-49), the 2 x 2 system of equations shown as Equations (7-57) can be set up and solved in terms of the old-time and new-time pressures.

If the choked flow calculation is in the transition regime (TRANSR = TRUE), the velocities computed in JCHOKE [$\bar{v}^n_{f,j}$ and $\bar{v}^n_{g,j}$ in Equations (7-57)] are heavily old time weighted or "underrelaxed".

The underrelaxation equations are

$$\bar{v}^n_{f,j} = 0.9\, v^n_{f,j} + 0.1\, \bar{v}^n_{f,j} \,. \qquad (7\text{-}83)$$

and

$$\bar{v}^n_{g,j} = 0.9\, v^n_{g,j} + 0.1\, \bar{v}^n_{g,j}$$

If the junction vapor void fraction is greater than 10^{-5}% or the equilibrium quality in the upwind volume is less than 0.25%, these relaxation equations are also applied before the velocities and velocity derivatives are passed to subroutine VFINL.

7.2.5 Weighting, Magnitude Limits, and Averaging Techniques Used in the RELAP5 Choking Model

Details of the weighting limits and averaging procedures used in JCHOKE were given in Section 7.2.4. The rudiments of these criteria are repeated here for convenience.

As discussed in Section 7.2.4, equilibrium quality is used to determine the regime as follows

$X_K < 0.001\%$ - subcooled

$0.001 \leq X_K \leq 0.025\%$ - transition

$X_K > 0.025\%$

and - two-phase

$\alpha_{g,j} > 10^{-5}\%$

In the transition region or if $\alpha_{g,j}$ is greater than $10^{-5}\%$ or X_K is less than 0.25%, underrelaxation is applied to the calculated junction phasic velocities, i.e.,

$$\bar{v}^n_{i,j} = 0.9\, v^n_{i,j} + 0.1\, \bar{v}^n_{i,j} , \qquad (7\text{-}84)$$

where i is either f or g.

The constants in this relaxation were selected based on comparisons to data in which flow conditions passed through the subcooled to two-phase transition. The heavily old time weighted formulation of Equation (7-83) is used to minimize velocity oscillations and time step reductions caused by large changes in the critical velocity that result during the transition.

The density ratio JCAT is similarly underrelaxed using Equation (7-81).

The expression given in Equation (7-78) represents a static quality weighted slip factor. This expression has no known physical basis and is included basically to help account for the inaccuracies in the approximations used to establish junction properties [i.e., Equations (7-58)

and (7-59)]. In particular, this term represents an additional correction factor for the junction density required for high steam quality conditions to approach homogeneous equilibrium conditions.

In many calculations performed in JCHOKE, great care is exercised to prevent divides by zero or prevent attempts to take the square root of negative numbers. For example, divides by numbers that could possibly be zero (such as the product $\alpha_f \rho_f$). Likewise square roots of value are generally done as SQRT (MAX(0.0, VALUE)).

In computing the sound speed derivative in the transition region, Equation (7-82) is used. The derivative is equilibrium quality weighted as follows. The first term represents the sound speed derivative for the liquid region and is the first term of Equation (7-62) multiplied by $(1 - X_{E,K})$. The second term represents the sound speed derivative for the vapor region multiplied by the equilibrium quality $X_{E,K}$. The factor of 0.15 stems from the assumption that for the purposes of computing the derivative, steam is a perfect gas with a specific heat ratio of 1.3.

7.2.6 Special Cases of Choking Application

The unique situations recognized by JCHOKE were addressed in Section 7.2.4 in the discussion of the model as coded. These special cases are summarized here.

If the junction in question is connected to a user-specified time-dependent volume that is specified as the "from" volume (volume K in Figure 7-7), the choking calculation is bypassed. The "to" volume (volume L in Figure 7-7) may be (and generally is) specified as a time-dependent volume. Also, if the "from" volume is an active accumulator volume, the choking calculation is bypassed until the accumulator has emptied and becomes a normal volume.

As discussed in Section 7.2.4, special considerations in the choking model are given to a junction that is specified to be a cross-flow junction with the "from" volume being the cross-flow volume. In this case, momentum flux based on volume average velocity and frictional pressure drop terms are zeroed out in the calculation of the junction pressure in a manner consistent with the cross-flow mode. If the flow reverses during the course of a calculation and the upwind volume is a cross-flow volume, the choking model recognizes this and zeroes the momentum flux based on volume averaged velocity and frictional pressure drops accordingly.

In the case of horizontal stratified flow, the junction specific internal energy is computed differently than it is for non-stratified flow as was discussed in Section 7.2.4 [see Equations (7-76) and (7-77)]. This difference is made to be consistent with the different donoring scheme used when horizontal stratification exists. The donoring scheme accounts for vapor pull through and liquid entrainment from the stratified volume to the choked junctions, as discussed in Reference 7-12.

If the abrupt area change model is in effect, the area change with spatial distance [Equation (7-72)] for use in the Jones pressure undershoot model is calculated differently than it is for a smooth area change. For a smooth area change,

$$\frac{1}{A_j}\frac{dA}{dx} = \frac{A_K - A_j}{(\Delta x_K/2)A_j} , \qquad (7\text{-}85)$$

where A_K is the flow area in volume K or $50A_j$, whichever is less, Δx_K is the length of volume K, and A_j is the physical area of the junction. If the abrupt area change model is in use, then

$$\frac{1}{A_j}\frac{dA}{dx} = \frac{A'_K - A_j}{D'_K A_j} , \qquad (7\text{-}86)$$

where A'_K is the minimum of $50A_j$ and $A_K Q_j / Q_K$ and Q_j is the junction volumetric flow, Q_K is the mixture volumetric flow rate, and D'_K is the length set to ten times the diameter of volume K. In the limit of increasing volume to junction area, Equation (7-85) goes to $98/\Delta x_K$, whereas Equation (7-86) goes to $4.9/D_K$ where D_K is the volume diameter.

A final special case is worthy of note. If the junction velocity solution computed in JCHOKE indicates that countercurrent flow exists, the liquid and vapor velocities are both set to the sound speed and the junction is flagged as being unchoked.

7.2.7 Assessment of Critical Flow Model

The RELAP5 critical flow model has been assessed using data from standard models used to predict subcooled and saturated critical flow and using data from a number of different thermal-hydraulic facilities. A portion of this assessment is discussed below.

7.2.7.1 Comparison to Homogeneous Equilibrium Model and Henry-Fauske Model. The small model shown in Figure 7-9 was used to drive the RELAP5 critical flow model to provide data for the purpose of comparison to critical flow models in the literature. Data tabulated for the homogeneous equilibrium model (HEM) in Reference 7-20 and data for the Henry-Fauske subcooled critical flow model from Reference 7-21 were used for comparison to the RELAP5 results.

The model consists of a driver time-dependent volume (101) with specified thermodynamic conditions, a pipe component (103) containing four volumes, a time-dependent volume (105) representing atmospheric conditions, and two junctions (components 102 and 104) connecting the driver volume to the pipe and the pipe to the atmosphere, respectively. The choking model with discharge coefficients set to unity was applied at junction 104 and turned off at all other junctions in the model. Wall friction was turned off in all volumes and smooth area changes were used throughout. To compute subcooled choked flow values, the temperature in volume 101 was set to 557.7 K and the pressure was varied from approximately 7 to 18 MPa. For

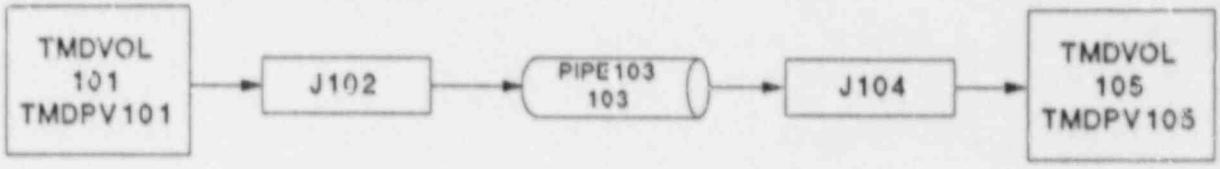

Figure 7-9. RELAP5 nodalization used for subcooled and saturated critical flow investigation.

each pressure, the model was run to a steady state to compute the subcooled choked flow rate at junction 104. To compute saturated critical flow rates, the pressure in volume 101 was set to 8.1 MPa and the equilibrium quality was varied from 0 to 1. For each quality, the model was run to steady state. Computations for the subcooled and saturated cases were run with the equilibrium option and with the nonequilibrium option. In all cases, the mass flux at junction 104 is plotted against the conditions in the volume at the end of pipe 103.

Figure 7-10 compares the subcooled critical mass flux calculated with RELAP5 compared to the Henry-Fauske model. The equilibrium and nonequilibrium options had no impact on the results, since the flow is single-phase. With the exception of pressures near saturation, the RELAP5 results are consistently higher than the Henry-Fauske model. This result is consistent with other applications[7-22] where a discharge coefficient of 0.9 has been applied to bring the RELAP5 results into better agreement with other subcooled choked flow models.

Figure 7-11 compares the RELAP5 calculated critical mass flux for the saturated flow regime with HEM values from Reference 7-20. Both equilibrium and nonequilibrium values are shown for reference. The vapor pull-through and liquid entrainment models were inactivated for these calculations. The results are consistent with applications experience,[a] indicating that the RELAP5 model run with the equilibrium option produces mass fluxes approximately 8% larger than HEM table values. The data in Figure 7-11 show that with the nonequilibrium (two-velocity) option, the RELAP5 results are closer to the HEM values. With respect to the equilibrium (single-velocity) calculated results, the effect of slip for these conditions slightly decreases the mass flux as one would expect. However, one would expect that the single velocity (equilibrium) result would reproduce the HEM result.

---

a. C. B. Davis, INEL, personal communication, December 1987.

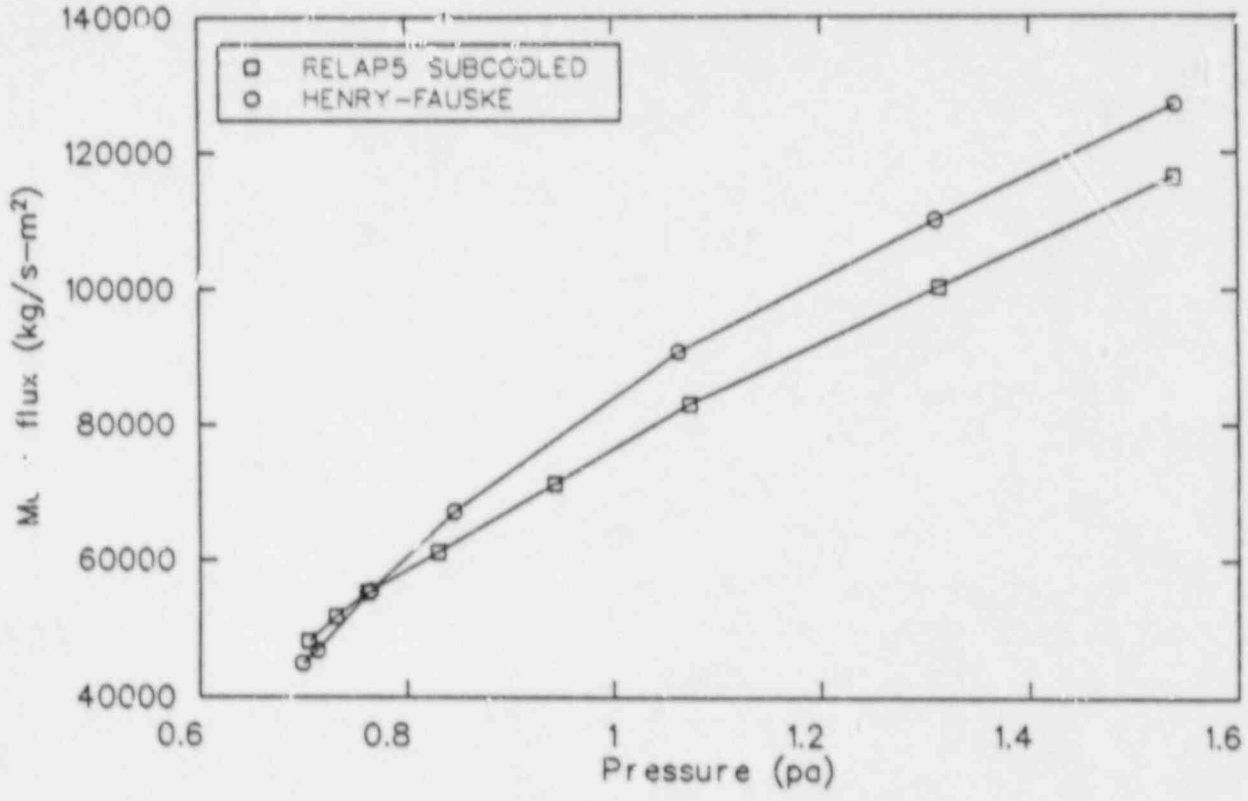

Figure 7-10. RELAP5 subcooled critical flow compared with Henry-Fauske tabulated values (Reference 14) liquid temperature 557.7 K.

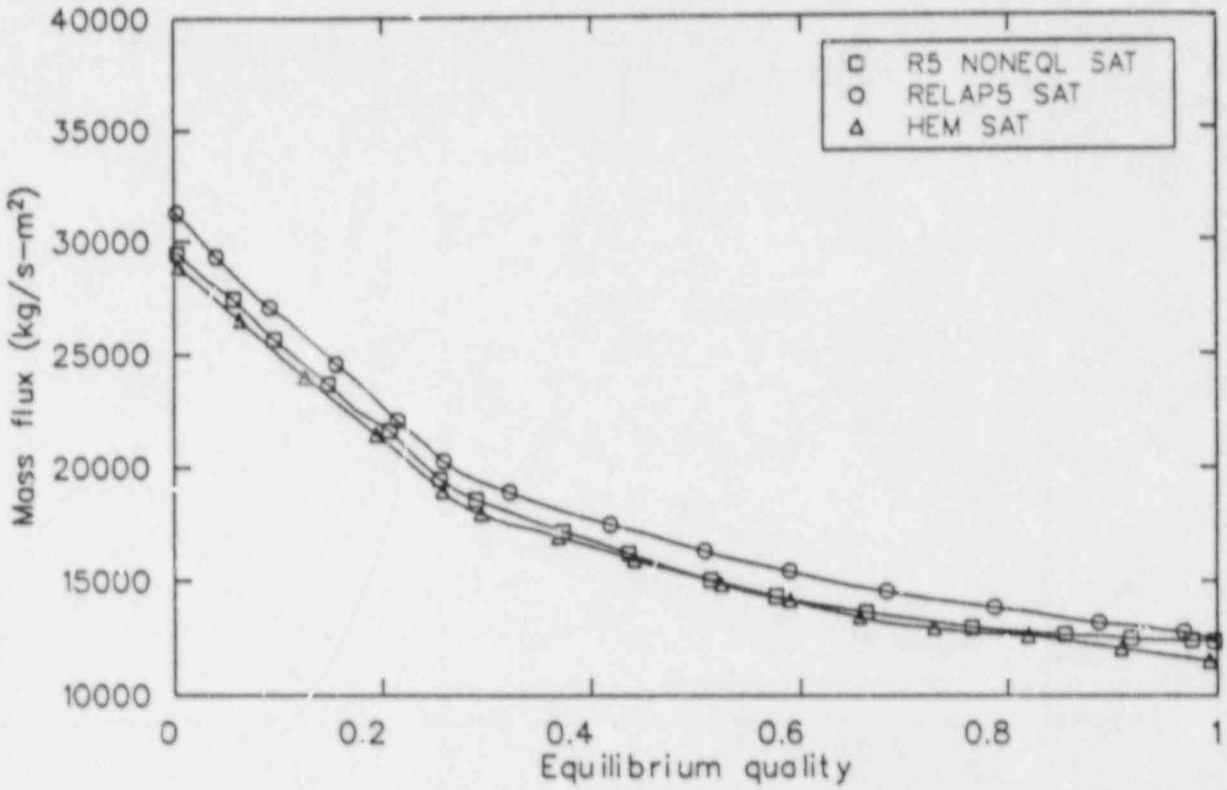

Figure 7-11. RELAP5 calculated two-phase critical mass flux compared with homogeneous equilibrium model values tabulated in Reference CPM-13.

This 8% difference and, of course, the well known vena-contracta effect[7-22,7-23] are reasons why saturated flow discharge coefficients of the range 0.8 to 0.88 are generally applied to the model.

7.2.7.2 Assessment of RELAP5 Critical Flow Model Using Facility Data. Numerous literature citations are available documenting comparisons of RELAP5 critical flow calculations to experimental data. Ransom and Trapp[7-8] used data from the Marviken Power Station Test 4.[7-24] Developmental assessment[7-25] was done using Marviken Tests 24[7-26] and 22.[7-27] Rosdahl and Caraher[7-28] have recently conducted extensive assessment of the model using Marviken Tests JIT-11 and CFT-21 data and various RELAP5 nodalizations. Many other comparisons to integral test data from the LOFT and Semiscale test facilities can be found in Reference 7-25. The discussion below will concentrate on a summary of the comparisons of the RELAP5 model results to Marviken results.

7.2.7.2.1 Marviken Facility Description--The Marviken facility in Sweden was used to conduct large-scale critical flow and jet impingement tests in 1978-1982. The pressure vessel from a full-scale BWR that was never commissioned was used to provide data for the critical discharge of subcooled liquid, low-quality two-phase mixtures, and steam. Figure 7-12 (from Reference 7-28) shows the pressure vessel and associated instrumentation. The vessel ID and height are 5.22 m and 24.55 m, respectively. The total volume is approximately 420 m^3. For experiments producing saturated steam discharge, a standpipe (dotted line) was inserted in the vessel. In the subcooled liquid and two-phase mixture discharge experiments, no standpipe was used and fluid entered the discharge piping directly from the bottom of the vessel. Nozzles of various length-to-diameter ratios (see Figure 7-13) could be attached to the bottom of the vessel. A rupture disk assembly containing two rupture disks was attached to the downstream end of the nozzle. Tests were initiated by overpressurizing the volume between the two disks, which then failed and were discharged from the nozzle region.

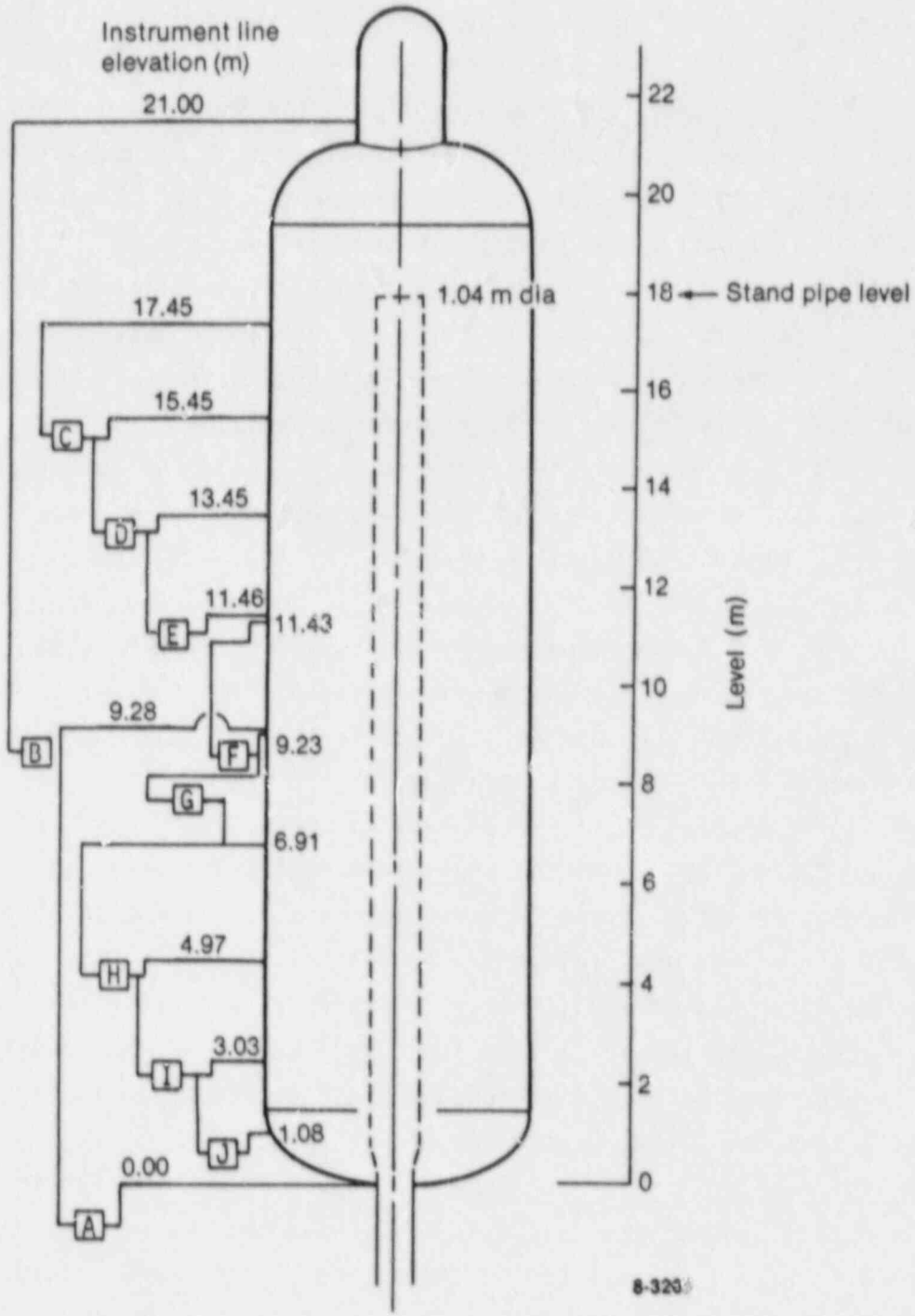

Figure 7-12. Marviken test vessel. Differential pressure transducers A through J.

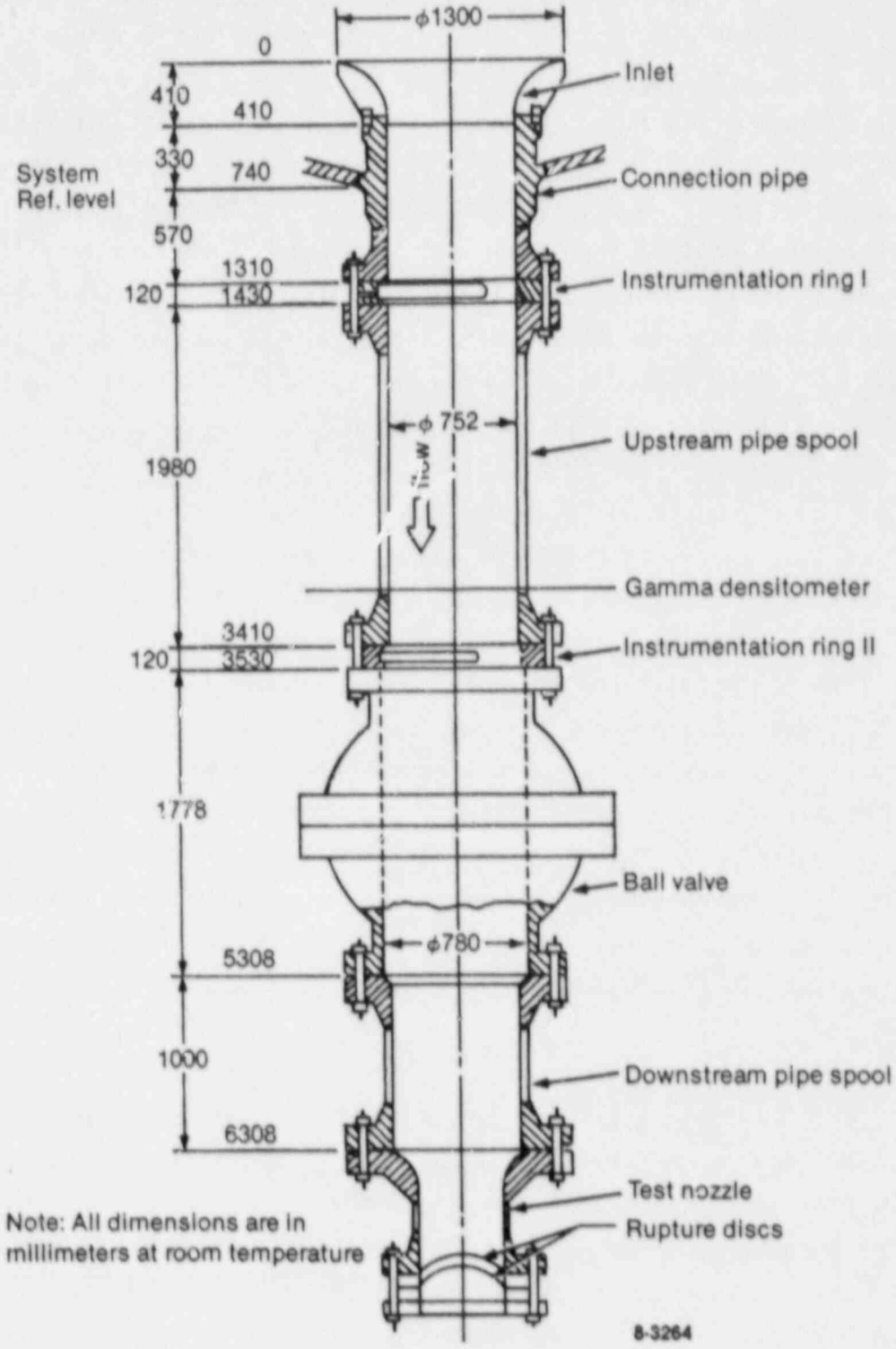

Figure 7-13. Arrangement of components in the discharge pipe for Critical Flow Test 21.

7.2.7.2.2 Calculation of Marviken Test 4 (from Reference 7-9)--Ransom and Trapp[7-8] simulated Marviken Test 4 using RELAP5. The purpose of Test 4 was to establish critical flow rates with subcooled and low-quality fluid at the nozzle inlet. For this experiment, a nozzle with a 0.5-m diameter and a 3.6 length-to-diameter (L/D) ratio was installed in the facility. Figure 7-14 shows the RELAP5 nodalization and initial temperature profile in the vessel. The water level was initially at 16.8 m above the bottom of the vessel, and the steam dome above the water level was saturated at 4.94 MPa. During the test, the subcooling at the nozzle inlet decreased from 60 to 35 K in the first 0.5 s and then decreased gradually until saturated conditions were established at 17 s. Two-phase flow persisted between 17 and 47 s.

Figure 7-15 compares the measured and predicted critical mass fluxes. Measured values were determined from both pitot-static measurements in the discharge pipe and from measurement of the vessel mass rate of change. The transition from subcooled flow to saturated flow at 17 s is clear on Figure 7-15. The good agreement between the prediction and measurements lead to the conclusion that the thermal equilibrium assumption employed in the RELAP5 critical flow model development was appropriate for the conditions encountered in Test 4, since with the large L/D nozzle one would expect conditions approaching equilibrium. It should be noted that the break area in the RELAP5 model was reduced by 5% to account for suspected separation effects.[7-8] In effect, then a discharge coefficient of 0.95 has been applied.

7.2.7.2.3 Calculation of Marviken Tests 22 and 24 (Developmental Assessment from Reference 7-27)--Marviken Tests 22 and 24 were conducted in the same fashion as Test 4 described in the previous section. The major distinguishing features of Tests 22 and 24 relative to Test 4 concern the nozzle L/D ratios. The nozzle L/D ratios for these tests were 1.5 for Test 22 and 0.33 for Test 24. Data from these experiments are valuable for examining the subcooled choking criteria and in particular nonequilibrium effects. The same model as shown in Figure 7-14 was used for the calculations of both tests. Figures 7-16 and 7-17 show pressure and mass flow comparisons obtained for Test 24 (L/D = 0.33). Results for Test 22 are similar.

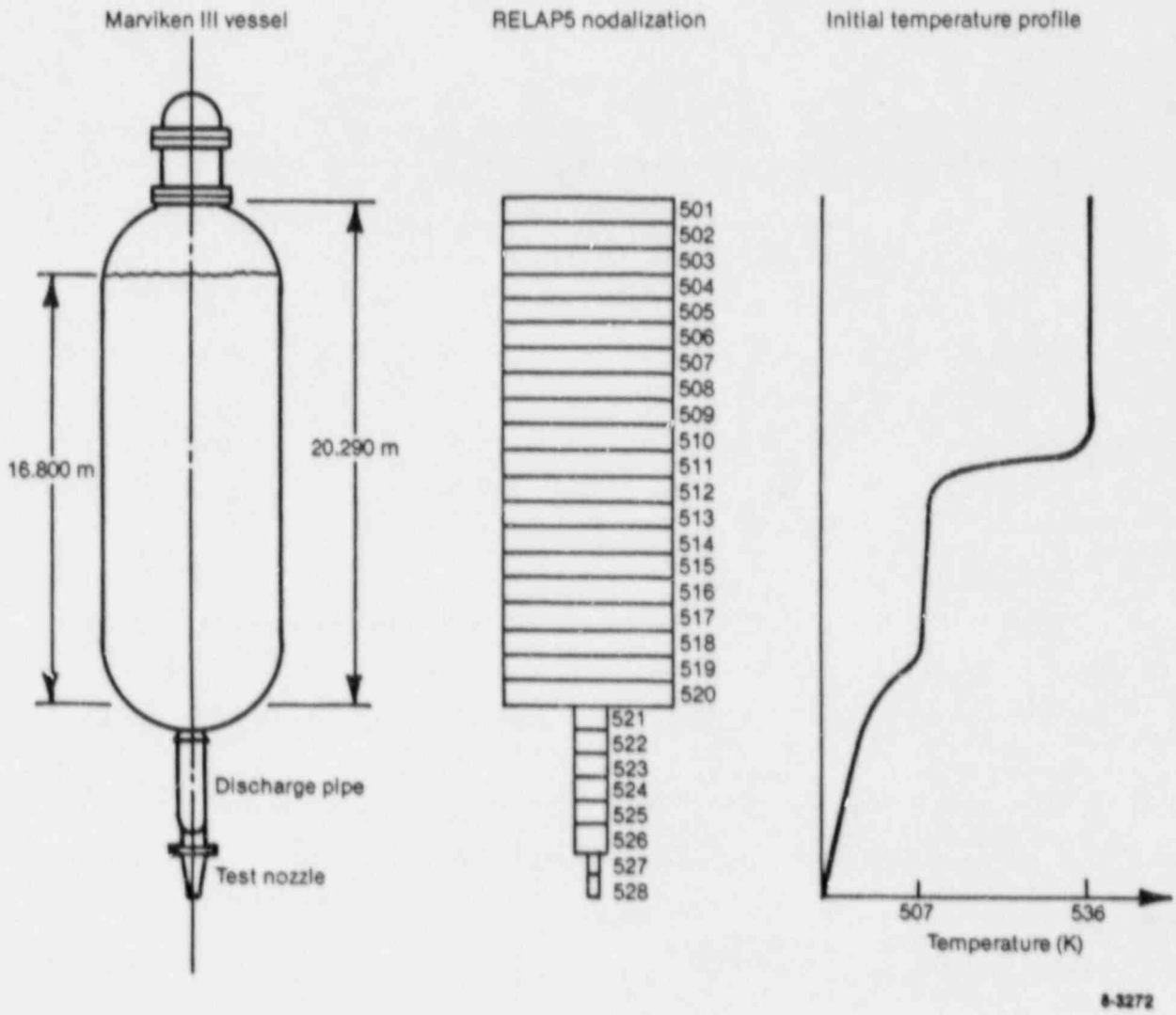

Figure 7-14. Marviken III Test 4 vessel schematic, RELAP5 nodalization, and initial temperature profile.

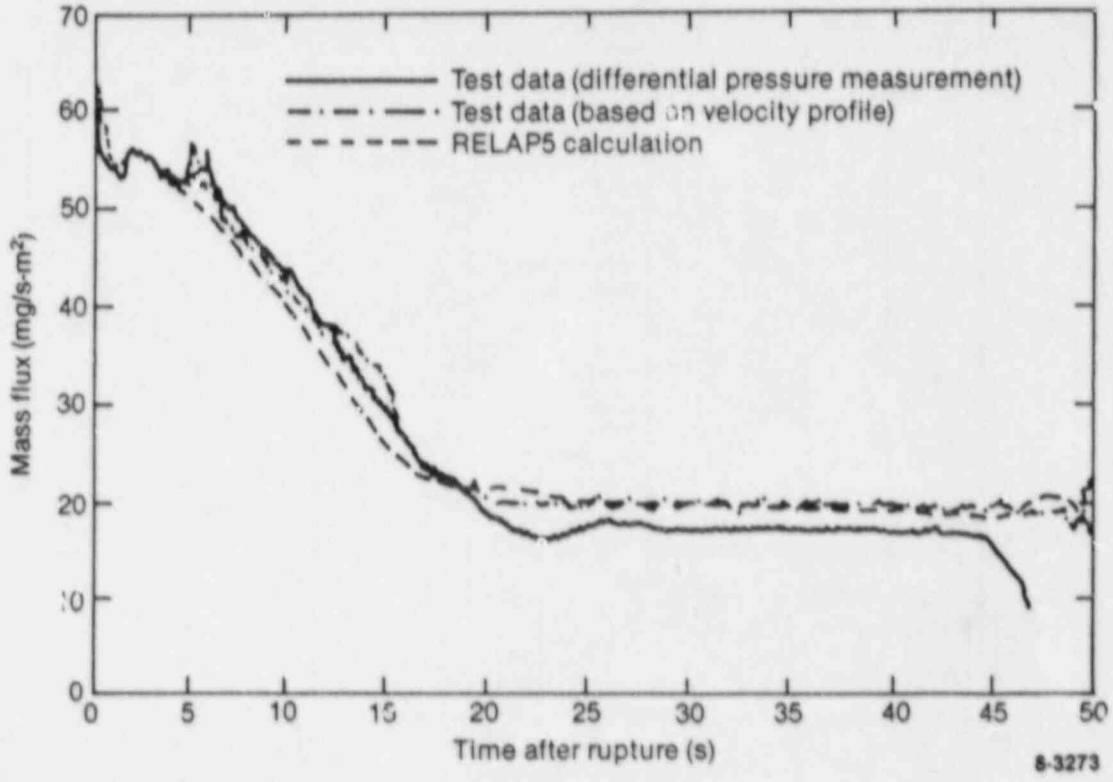

Figure 7-15. Calculated and measured mass flux at nozzle inlet (Cell 526 in RELAP5 nodalization.

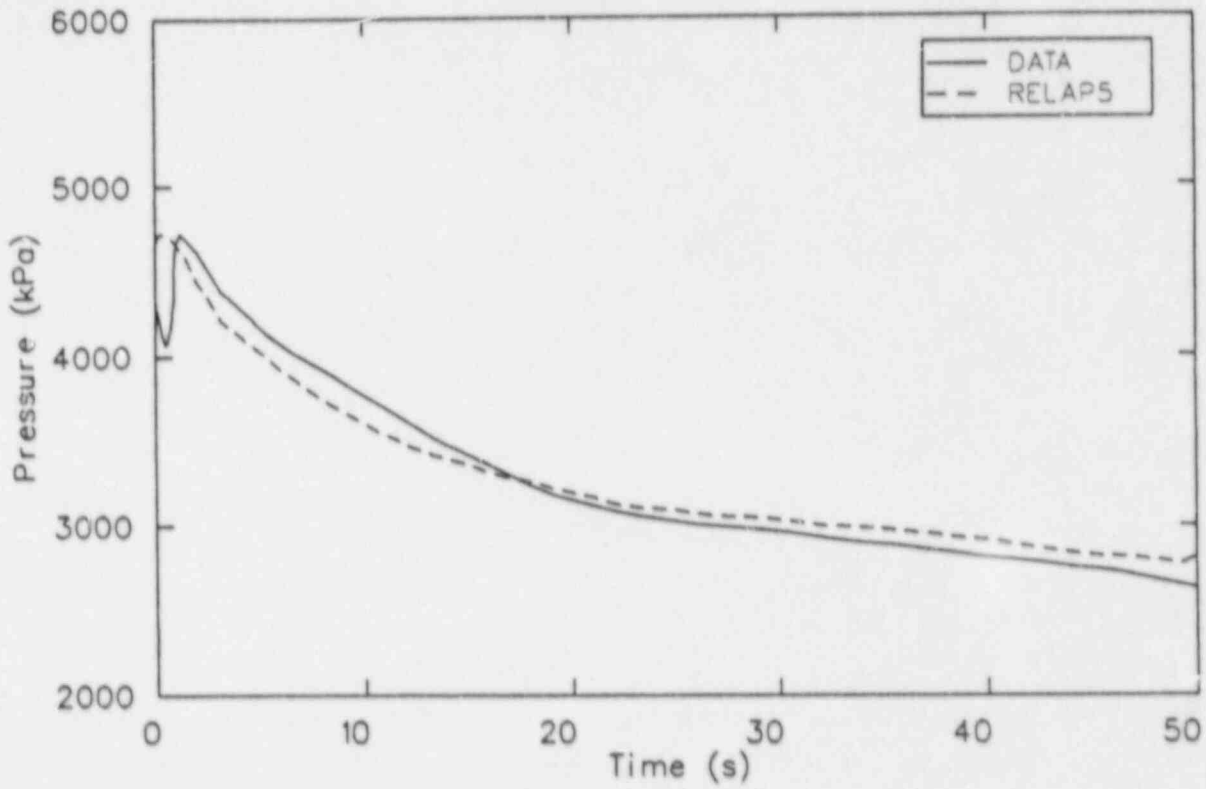

Figure 7-16. Measurement and RELAP5/MOD2 calculation of Marviken Test 24 pressure in the top of the vessel.

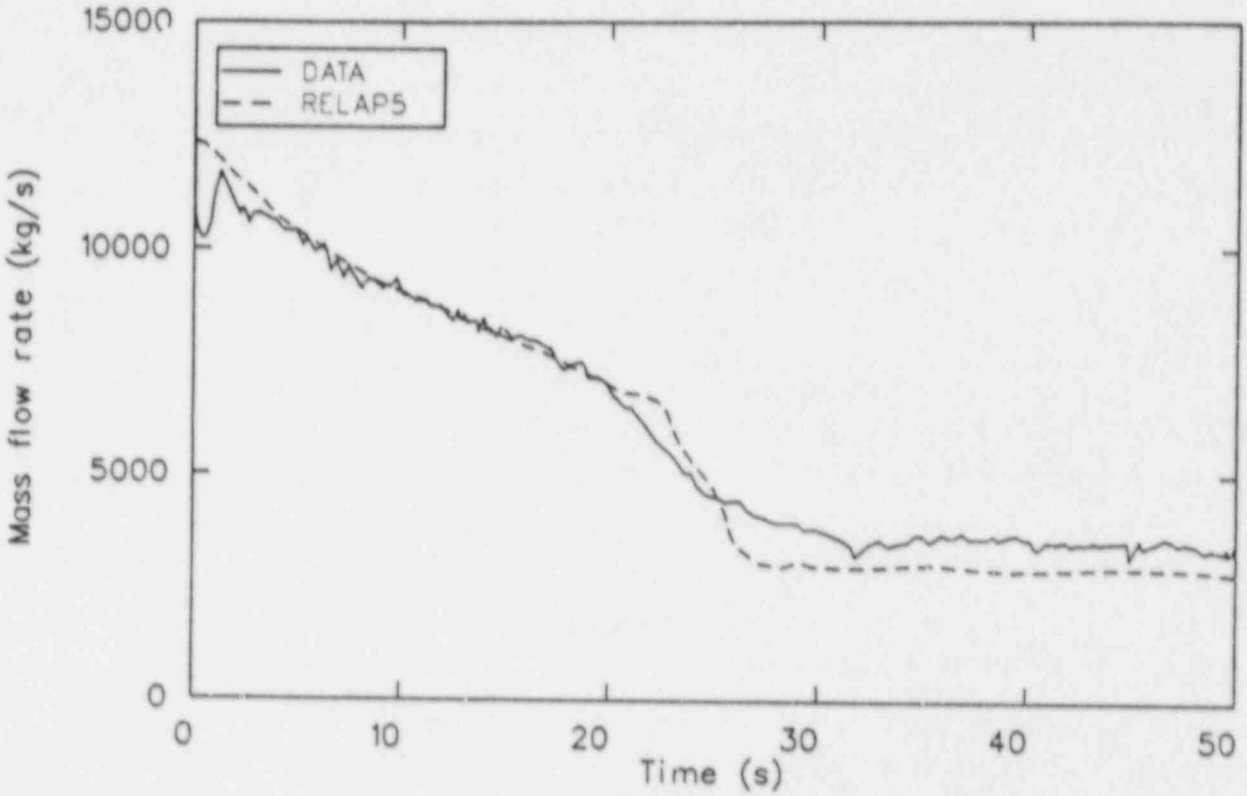

Figure 7-17. Measurement and RELAP5/MOD2 calculation of Marviken Test 24 mass flow rate at the nozzle.

Additional details for both tests can be found in Reference 7-27. For both tests, the vessel pressure was overpredicted for the first second, slightly underpredicted for the majority of the subcooled region, and then slightly overpredicted for the saturated flow region. The initial pressure overprediction has been attributed to the nucleation delay model used in RELAP5. Undoubtedly, this has an effect on the subsequent pressure and critical flow predictions. Given the differences in pressure, it is difficult to make judgments on the subcooled break flow model (the pressure undershoot model implementation), although the comparison for the first 20 s is very good. It was noted for both calculations that the transition to two-phase flow was too abrupt. To eliminate the feedback effect of pressure on the critical flow and vice versa, Rosdahl and Caraher have examined the details of the critical flow model using measured boundary conditions from Marviken experiments to drive the RELAP5 critical flow model. These assessments are discussed next.

7.2.7.2.4 Calculations of Marviken Experiments CFT-21 and JIT-11--Reference 7-28 describes the details of a nodalization study conducted by Rosdahl and Caraher to examine the performance of the RELAP5 critical flow model. Experiment JIT-11[7-29] involved the discharge of saturated steam, and experiment JIT-21[7-30] was similar to those discussed above in that subcooled liquid and low-quality two-phase mixture critical discharge was involved. In the calculations conducted by Rosdahl and Caraher, a time-dependent volume containing thermodynamic conditions derived from vessel measurements was used to drive various representations of the nozzle geometry.

For the saturated steam flow calculations, the pressure history from JIT-11 was used to drive the RELAP5 critical flow model. The various nodalizations examined are listed in Table 7-2. Figure 7-18 shows comparison of the measured flow data and the discharge flow rates from the cases described in Table 7-2. The L/D ratio for the nozzle used in these experiments is 3.9 (length of 1.18 m and diameter of 0.299 m), and the nozzle entrance is well-rounded.

TABLE 7-2. NOZZLE NODALIZATION DESCRIPTION FOR JIT-11 CALCULATIONS (FROM REFERENCE 7-28)

Case	Description
0 node	Vessel modeled as time-dependent volume. Standpipe and discharge pipe not modeled. A single junction component used to represent the discharge area.
7 node	Vessel modeled as time-dependent volume. Standpipe modeled as pipe component (4 cells). Discharge pipe modeled as pipe component (3 cells). Single junction component used to represent the discharge area.
9 node	Same as 7 node model except nozzle included. Nozzle modeled by pipe component (2 cells).
12 node	Same as 9 node model except nozzle now represented with 5 cells.

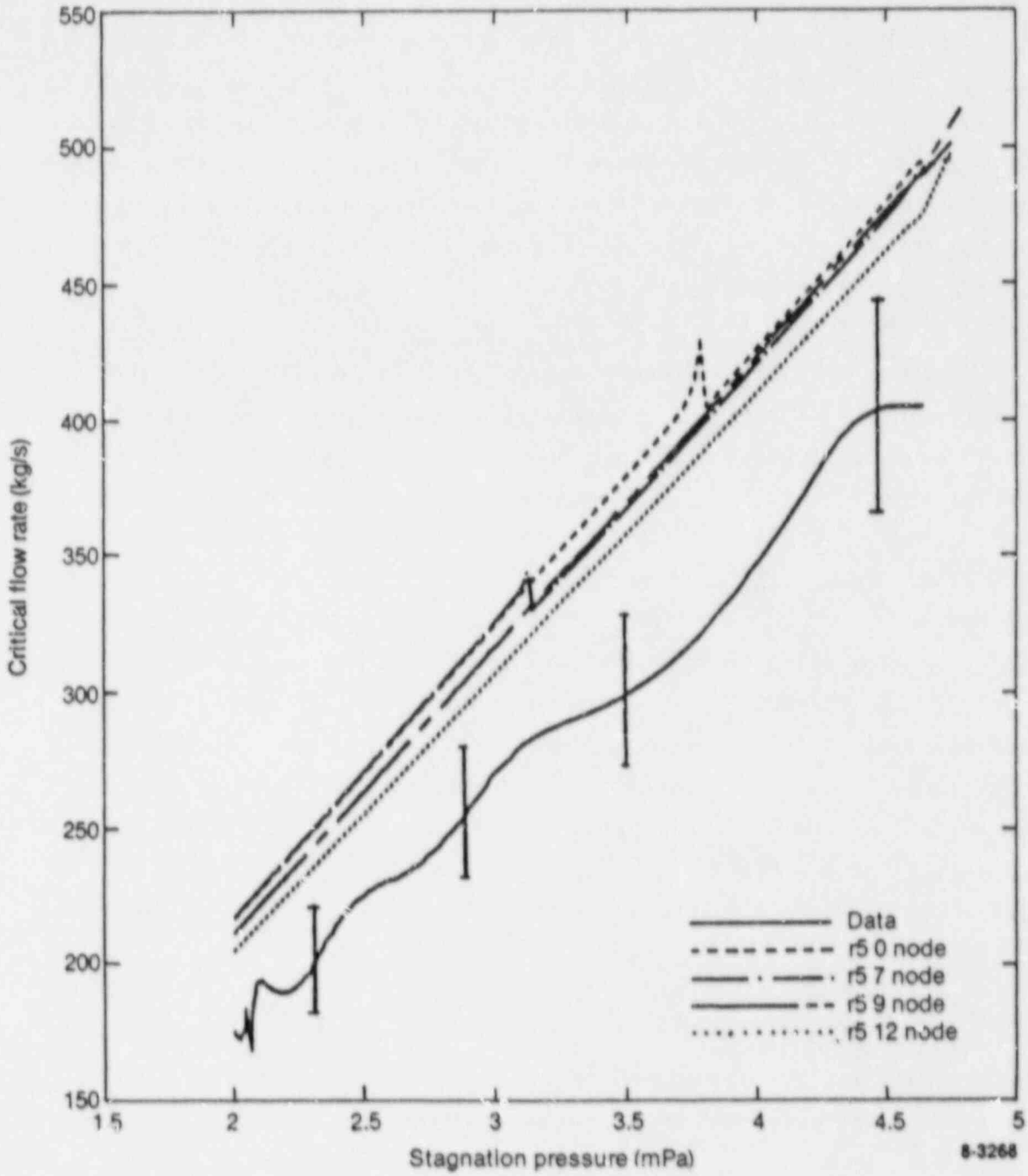

Figure 7-18. Critical flow of saturated steam. RELAP5 simulations and JIT 11 data.

Examination of Figure 7-18 indicates that RELAP5 overpredicts the measured flow rate and that the calculated flow rate is not a strong function of the nodalization. The sudden increases in flow rate in two of the cases have been attributed to the approximation for junction internal energy [i.e., Equation (7-59)]. In Equation (7-59), it is seen that the pressure difference term is divided essentially by ρ_K (rather than dividing P_j by ρ_j). Since there is a small discontinuity in sound speed at the two-phase mixture-vapor boundary, this approximation can lead to discontinuities in the sound speed based on junction pressure and junction internal energy at the boundary.

Rosdahl and Caraher conclude from the data in Figure 7-18 that there is limited incentive to finely nodalize the discharge piping, since the results do not improve substantially and computational costs rise dramatically with increasing nodalization. Furthermore, they recommend using a discharge coefficient of 0.82 to bring the RELAP5 result into agreement with the saturated steam critical flow rate data.

For simulation of subcooled and saturated two-phase flow portions of Test 21, Rosdahl and Caraher used measured vessel pressure and temperature and measured vessel pressure and quality, respectively, for boundary conditions on the RELAP5 critical flow model. The various nozzle nodalization schemes investigated are listed in Table 7-3. As indicated, various discharge coefficients were also examined in the study and the influence of various assumptions regarding boundary conditions were investigated.

The details of the Rosdahl and Caraher analysis is too involved to repeat here and the interested reader is referred to Reference 7-28. Basically, the authors summarized their analysis as follows.

1. RELAP5 critical flow model overpredicts the critical flow of saturated steam. For the JIT-11 simulations, the calculated critical flow could be brought into agreement with the measured flow by applying a discharge coefficient of 0.82.

TABLE 7-3. NOZZLE NODALIZATION DESCRIPTION FOR CFT-21 CALCULATIONS (FROM REFERENCE 7-28)

RELAP5 Case	Description
CFT01	Subcooled boundary conditions. No discharge coefficients. Nozzle not modeled.
CFT02	Subcooled boundary conditions. Subcooled discharge coefficient (C_D) = 0.85. Nozzle not modeled.
CFT03	Subcooled boundary conditions. C_D = 0.85. Boundary condition temperature reduced 2K for t > 18 s. Nozzle not modeled.
CFT04	Saturated boundary conditions. Restarted from CFT03 at 26.5 s. No discharge coefficient for two-phase flow.
CFT05	Saturated boundary conditions. Restarted from CFT03 at 26.5 s. No discharge coefficient. Boundary condition quality limited to upper value of 0.003.
CFT06	Same as CFT05 except C_D = 0.85.
CFT07	Subcooled boundary conditions. No discharge coefficient. Nozzle modeled with one node.
CFT08	Same as CFT07 except C_D = 1.09 for subcooled flow and 1.13 for two-phase flow.

2. Computed results for JIT-11 were not substantially improved by modeling the nozzle. Considering the empirical nature of the RELAP5 choked flow model, it is concluded that there is no benefit in modeling discharge piping having a L/D ratio < 4 when steam is being discharged.

3. An approximation made in the calculation of junction internal energy in subroutine JCHOKE is responsible for nonphysical jumps in computed discharge mass flow rate evident in two of the JIT-11 simulations.

4. RELAP5 overpredicted the subcooled critical mass flow rate for CFT-21 when the nozzle was not explicitly modeled. Calculated mass flow rates could be made to agree with measured ones by using a discharge coefficient of 0.85 in RELAP5.

5. When the nozzle geometry was explicitly modeled in RELAP5, mass flow rates for CFT-21 were underpredicted. Application of discharge coefficients (greater than unity) did not improve computed results; on the contrary, doing so gave rise to a very numerically noisy solution. It is concluded that short-discharge nozzles or pipes (L/D < 2) should not be modeled explicitly in RELAP5.

6. For the saturated blowdown portion of CFT-21, RELAP5 simulated the discharge flow quite accurately when the bounding condition fluid quality was based upon the gamma densitometer measurement. No discharge coefficient was needed to achieve agreement with the experimental data.

7. When the fluid quality boundary condition was lowered (based upon vessel differential pressure measurements), RELAP5 overpredicted the discharge flow rate.

8. The RELAP5 simulation of the discharge of low-quality, two-phase fluid did not respond in a predictable manner when discharge coefficients were applied. It was determined that a feedback exists for low-quality flow such that application of a discharge coefficient may increase the value of the sonic velocity used in the choking criterion, partially offsetting the sonic velocity reduction represented by the discharge coefficient. Application of a discharge coefficient of say, 0.85, will reduce computed flow by only 7 or 8 percent instead of the 15 percent one might expect.

7.2.8 Model Application

Assessment of the RELAP5 critical flow model was discussed in the previous section. As discussed, the recommendation is that short nozzles or discharge pipes ($L/D < 2$) should not be explicitly modeled and that a discharge coefficient of 0.85 should be used for subcooled and two-phase mixture flows. The assessment also showed that there was little benefit in explicitly modeling nozzles discharging saturated steam and the conclusion was that there is little incentive to modeling discharge pipes of $L/D < 4$ when saturated steam is being discharged. Furthermore, a discharge coefficient of 0.82 was necessary to bring saturated steam flows into agreement with Marviken data.

In general, the use of discharge coefficients is required to account for multi-dimensional effects due to the break geometry being modeled. It is the code user's task, then, to determine the necessary discharge coefficient values for the specific geometry.

7.2.9 Scaling Considerations

The RELAP5 break flow model was essentially developed from first principles. One-dimensional approximations are utilized in both the subcooled flow model and the two-phase mixture flow model. Empirical discharge coefficients are used to help account for multi-dimensional effects. One aspect of the model that involves scale considerations is in

the implementation of the pressure undershoot correlation, as discussed in Section 7.2.1.1, and the approximation of the spatial derivatives for the static depressurization term in the correlation described in Section 7.2.6.

As shown in Equations (7-85) and (7-86), the derivative terms depend on nodalization and have different limits depending on the area change option selected. The fact that the model predicts large-scale critical flow data (given appropriate discharge coefficients) as discussed in Section 7.2.7 and small-scale data (see Reference 7-22), given approximately the same discharge coefficients, lends support to the scaling ability of the subcooled critical flow model.

The two-phase critical flow model is analytically developed from a characteristic analysis of a four-equation, one-dimensional, two-fluid model assuming thermal equilibrium. The model development is scale-independent, although simplifications have been made to get a solution for roots in the characteristic analysis. The validity of these assumptions is not expected to be a function of scale. As discussed in the previous sections, the two-phase critical flow model predicts available large-scale critical flow data given the appropriate discharge coefficient.

7.2.10 Summary and Conclusions

The RELAP5 critical flow model represents a first-principle approach to the calculation of subcooled, two-phase mixtures and vapor critical discharge. The model is based on a one-dimensional flow assumption, and discharge coefficients are generally necessary to account for geometry-specific, two-dimensional effects. For the subcooled flow regime, an empirical correlation is used to calculate pressure undershoot (liquid superheat) at the choke point for the estimation of choke plane pressure. Thermal equilibrium assumptions were employed in the development of an analytic choking criterion for two-phase flow.

The model has been assessed against a wide variety of data from experimental facilities and against tabulated critical flow models, such as Henry-Fauske and the HEM. Without application of discharge coefficients, the RELAP5 model overpredicts both Henry-Fauske and HEM tabulated data. Likewise, without the application of discharge coefficients, the RELAP5 model overpredicts available large-scale critical discharge data from the Marviken facility.

Although not discussed in this report, the RELAP5 critical flow model can accommodate a noncondensible gas. Although noncondensible gas is not expected to be present for most PWR LBLOCA analyses, if calculations are run with noncondensible present at the choke plane, critical flow results should be carefully analyzed since this aspect of the model has not had extensive application. Furthermore, if calculations are run that involve extensive derivation from the thermal equilibrium, the results should be carefully analyzed with respect to the choking criterion, since the criterion was based on thermal equilibrium assumptions.

7.3 References

7-1. J. A. Trapp and V. H. Ransom, RELAP5 Hydrodynamic Model Progress Summary--Abrupt Area Changes and Parallel Branching, PG-R-77-92, November 1977.

7-2. J. K. Vennard, Elementary Fluid Mechanics, 4th Edition, New York: John Wiley and Sons, 1965.

7-3. J. Weisman, T. Ake, R. Knott, "Two-Phase Pressure Drop Across Abrupt Area Changes in Oscillatory Flow," Nuclear Science and Engineering, 61, 1976, pp. 297-309.

7-4. J. G. Collier, "Advanced Study Institute on Two-Phase Flows and Heat Transfer," ASI Proceedings, Istanbul, Turkey, August 1976.

7-5. M. M. El-Wakil, Nuclear Heat Transport, Scranton: International Textbook Company, 1971.

7-6. B. Harshe, A. Hussain, J. Weisman, Two-Phase Pressure Drop Across Restrictions and Other Abrupt Area Changes, NUREG-0062, April 1976.

7-7. P. A. Lottes, "Expansion Losses in Two-Phase Flows," Nuclear Science and Energy, 9, 1961, pp. 26-31.

7-8. V. H. Ransom and J. A. Trapp, "The RELAP5 Choked Flow Model and Application to a Large Scale Flow Test," Proceedings of the ANS/ASME/NRC International Topical Meeting on Nuclear Reactor Thermal-Hydraulics, Saratoga Springs, New York, October 5-8, 1980, pp. 799-819.

7-9. J. A. Trapp and V. H. Ransom, "A Choked-Flow Calculation Criterion for Nonhomogeneous, Nonequilibrium, Two-Phase Flows," International Journal of Multiphase Flow, 8, 6, 1982, pp. 669-681.

7-10. J. W. Burnell, "Flow of Boiling Water Through Nozzles, Orifices, and Pipes," Engineering, 1947, pp. 572-576.

7-11. V. H. Ransom, et al., RELAP5/MOD2 Code Manual Volume 1: Code Structure, System Models, and Solution Methods, NUREG/CR-4312, EGG-2396, August 1985.

7-12. F. J. Moody, "Maximum Flow Rate of a Single Component, Two-Phase Mixture," Transactions of the American Society of Mechanical Engineers, February 1965, pp. 136-143.

7-13. M. D. Alamgir and J. H. Lienhard, "Correlation of Pressure Undershoot During Hot Water Depressurization," ASME Journal of Heat Transfer, 103, 1981, pp. 52-73.

7-14. N. Abuaf, O. C. Jones, Jr., and B. J. C. Wu, Critical Flashing Flow in Nozzles with Subcooled Inlet Conditions, BNL-NUREG-27512, 1980.

7-15. O. C. Jones, Jr., "Flashing Inception in Flowing Liquids," ASME Journal of Heat Transfer, 102, 1980, pp. 439-444.

7-16. P. R. Garabedian, Partial Differential Equations, New York: John Wiley and Sons, 1964.

7-17. G. B. Whitham, Linear and Nonlinear Waves, New York: John Wiley and Sons, 1974.

7-18. V. H. Ransom and J. A. Trapp, RELAP5 Progress Summary Analytical Choking Criterion for Two-Phase Flow, CDAP-TR-013, 1978.

7-19. W. M. Bryce, Improvements to the RELAP5/MOD1/014 LOCA Code: The RELAP5/MOD1/WINOO1 Code, AEEW-R-1649, May 1983, pp. 64-65.

7-20. D. G. Hall and L. S. Czapary, Tables of Homogeneous Equilibrium Critical Flow Parameters for Water in SI Units, EGG-2056, September 1980.

7-21. R. E. Henry and H. K. Fauske, "The Two-Phase Critical Flow of One Component Mixtures in Nozzles, Orifices, and Steam Tubes," Journal of Heat Transfer, Trans., 93, pp. 724-737, May 1971.

7-22. M. T. Leonard, Post Test RELAP5 Simulation of the Semiscale S-UT Series of Experiments, EGG-SEMI-5622, October 1982.

7-23. J. R. Travis, C. W. Hirt, and W. C. Rivard, "Multidimensional Effects in Critical Two-Phase Flow," Nuclear Science and Engineering, 68, 1978, pp. 338-348.

7-24. L. Ericson, The Marviken Full-Scale Critical Flow Tests Interim Report: Results from Test 4, A. B. ATOMENERGI SWEDEN, Report MXC-204, May 1979.

7-25. V. H. Ransom et al., RELAP5/MOD2 Code Manual, Volume 3: Developmental Assessment Problems, EGG-TFM-7952, December 1987.

7-26. L. Ericson, et al., The Marviken Full-Scale Critical Flow Tests Interim Report: Results from Test 24, A. B. ATOMENERGI SWEDEN, Report MXC-224, May 1979.

7-27. L. Ericson, et al., The Marviken Full-Scale Critical Flow Tests Interim Report: Results from Test 22, A. B. ATOMENERGI SWEDEN, Report MCX-222, March 1979.

7-28. O. Rosdahl and D. Caraher, Assessment of RELAP5/MOD2 Against Critical Flow Data from Marviken Tests JIT-11 and CFT-21, NUREG/IA-0007, September 1986.

7-29. L. Ericson, et al., The Marviken Full Scale Jet Impingement Tests: Test 11 Results, A. B. ATOMENERGI SWEDEN, Report MXD-211, March 1978.

7-30. L. Ericson, et al., The Marviken Full Scale Critical Flow Tests: Results from Test 21, A. B. ATOMENERGI SWEDEN, Report MXC-221, September 1979.

APPENDIX 7A

DEVELOPMENT OF TWO-PHASE SOUND SPEED EXPRESSIONS

APPENDIX 7A

DEVELOPMENT OF TWO-PHASE SOUND SPEED EXPRESSIONS

The development of the generalized homogenous sound speed formulation presented here is due to V. H. Ransom and is internally documented in RANS-4-77.

The propagation velocity for a small disturbance in a homogenous medium (thermal equilibrium) is

$$a^2 = (\partial P/\partial \rho)_S = -V^2/(\partial V/\partial P)_S \ . \qquad (7A\text{-}1)$$

For a two-phase homogeneous mixture, the specific volume is

$$V = XV_g + (1 - X)V_f \ . \qquad (7A\text{-}2)$$

The partial derivative of specific volume with respect to pressure is

$$(\partial V/\partial P)_S = X(\partial V_g/\partial P)_S + (1 - X)\ (\partial V_f/\partial P)_S + \epsilon(V_g - V_f)(\partial X/\partial P)_S \ , \qquad (7A\text{-}3)$$

where $\epsilon = 0$ for a frozen composition system and $\epsilon = 1$ for equilibrium mass exchange between phases.

The derivatives of specific volume can be expressed in terms of the isothermal compressibility, κ, and the isobaric coefficient of thermal expansion, β, to obtain

$$(\partial V_g/\partial P)_S = V_g[\beta_g(\partial T/\partial P)_S - \kappa_g] \qquad (7A\text{-}4)$$

$$(\partial V_f/\partial P)_S = V_f[\beta_f(\partial T/\partial P)_S - \kappa_f] \qquad (7A\text{-}5)$$

where

$$\beta = (\partial V/\partial T)_P/V \qquad (7A\text{-}6)$$

$$\kappa = -(\partial V/\partial P)_T V \ . \qquad (7A\text{-}7)$$

The quality derivative in Equation (7A-3) is expanded in terms of the individual phase properties by starting with the definition of system entropy.

$$S = XS_g + (1 - X)S_f \ . \qquad (7A\text{-}8)$$

Differentiating Equation (7A-8) with respect to pressure at constant total entropy yields

$$\left(\frac{\partial S}{\partial P}\right)_S = 0 = X\left(\frac{\partial S_g}{\partial P}\right)_S + (1 - X)\left(\frac{\partial S_f}{\partial P}\right)_S + (S_g - S_f)\left(\frac{\partial X}{\partial P}\right)_S \ . \qquad (7A\text{-}9)$$

If S_g and S_f are taken to be functions of P and T then

$$\left(\frac{\partial S_g}{\partial P}\right)_S = \left(\frac{\partial S_g}{\partial P}\right)_T \left(\frac{\partial P}{\partial P}\right)_S + \left(\frac{\partial S_g}{\partial T}\right)_P \left(\frac{\partial T}{\partial P}\right)_S \qquad (7A\text{-}10)$$

$$\left(\frac{\partial S_f}{\partial P}\right)_S = \left(\frac{\partial S_f}{\partial P}\right)_T \left(\frac{\partial P}{\partial P}\right)_S + \left(\frac{\partial S_f}{\partial T}\right)_P \left(\frac{\partial T}{\partial P}\right)_S \ . \qquad (7A\text{-}11)$$

From Maxwell's second relation,

$$\left.\frac{\partial S}{\partial P}\right|_T = -\left.\frac{\partial V}{\partial T}\right|_P \ , \qquad (7A\text{-}12)$$

which, from Equation (7A-6), is $-\beta V$ and, from the definition of specific heat at constant pressure,

$$C_p = T\left(\frac{\partial S}{\partial T}\right)_P \ . \qquad (7A\text{-}13)$$

Using Equations (7A-12) and (7A-13), Equations (7A-10) and (7A-11) become

$$(\partial S_g/\partial P)_S = -V_g\beta_g + (C_{pg}/T)(\partial T/\partial P)_S \qquad (7A\text{-}14)$$

$$(\partial S_f/\partial P)_S = -V_f \beta_f + (C_{pf}/T)(\partial T/\partial P)_S \quad . \tag{7A-15}$$

Substituting Equations (7A-14) and (7A-15) into Equation (7A-9) gives a relation for $(\partial X/\partial P)_S$ in terms of $(\partial T/\partial P)_S$,

$$\left(\frac{\partial X}{\partial P}\right)_S = \frac{-1}{(S_g - S_f)} \left[X \left(\frac{C_{pg}}{T} \left(\frac{\partial T}{\partial P}\right)_S - V_g \beta_g\right) + (1 - X) \left(\frac{C_{pf}}{T} \left(\frac{\partial T}{\partial P}\right)_S - V_f \beta_f\right)\right] . \tag{7A-16}$$

The behavior of the temperature with pressure must be evaluated before the sound speed can be established. For the two-phase system in equilibrium, the temperature is only a function of pressure, and the Clausius-Clayperon relation can be used to obtain the derivative of temperature.

$$(\partial T/\partial P)_S = dT/dP = (V_g - V_f)/(S_g - S_f) \tag{7A-17}$$

or, since $S_g - S_f = (h_g - h_f)/T$,

$$\left(\frac{dP}{dT}\right)_S = \frac{h_g - h_f}{T\,(V_g - V_f)} \quad . \tag{7A-18}$$

If a system having frozen composition is considered, then the behavior of temperature with pressure is obtained from Equation (7A-16) with $(\partial X/\partial P)_S = 0$, i.e.

$$(\partial T/\partial P)_S = T[XV_g\beta_g + (1 - X)\, V_f\beta_f] \,/\, [XC_{pg} + (1 - X)C_{pf}] \quad . \tag{7A-19}$$

If we define P'_ϵ to be Equation (7A-18) for $\epsilon = 1$ (homogeneous equilibrium flow) and

$$P'_\epsilon = \frac{XC_{pg} + (1 - X)C_{pf}}{T(X\beta_g V_g + (1 - X)\beta_f V_f)} \tag{7A-20}$$

for $\epsilon = 0$ (frozen flow), Equations (7A-1), (7A-3), (7A-4), (7A-5), (7A-16), (7A-18), and (7A-20) can be combined to yield a generalized expression for the homogeneous sound speed

$$a^2 = \frac{(XV_g + (1 - X)V_f)^2 \; T \; (P'_\epsilon)^2}{X[\epsilon C_{pg} - TV_g P'_\epsilon \; ((1+\epsilon)\beta_g - \kappa_g P'_\epsilon)] + (1-X) \; [\epsilon C_{pf} - TV_f P'_\epsilon \; ((1+\epsilon)\beta_f - \kappa_f P'_\epsilon)]} \qquad (7A\text{-}21)$$

For $\epsilon = 1$, the homogeneous equilibrium speed of sound is obtained and, for $\epsilon = 0$, the homogeneous frozen speed of sound is obtained. The pure component sound speed (without phase change) is obtained from the expression for the frozen sound speed expression with X = 0 or 1 for liquid and vapor respectively. For example, the pure vapor sound speed is obtained from Equation (7A-21) with X = 1 and $\epsilon = 0$,

$$a^2_{HE,V} = \frac{V_g^2 \left(\frac{dP}{dT}\right)_S^2}{V_g \left(\kappa_g \left(\frac{dP}{dT}\right)_S - \beta_g\right) \left(\frac{dP}{dT}\right)_S} , \qquad (7A\text{-}22)$$

where $(dP/dT)_S$ is from Equation (7A-20) with X = 1 and $\epsilon = 0$

$$\left(\frac{dP}{dT}\right)_S = \frac{C_{pg}}{T\beta_g V_g} . \qquad (7A\text{-}23)$$

With the exception of the vapor state, Equations (7A-18) and (7A-21) with $\epsilon = 1$ are used in RELAP5 to compute the homogeneous equilibrium sound speed. Table 7A-1 summarizes the homogeneous equilibrium sound speed formulas used.

TABLE 7A-1. HOMOGENEOUS EQUILIBRIUM SOUND SPEED FORMULAS USED IN RELAP5

Pure Vapor

$$a_{HE} = V_g \left[\frac{\left(\frac{dP}{dT}\right)_S}{V_g\left(\kappa_g \left(\frac{dP}{dT}\right)_S - \beta_g\right)} \right]^{1/2} \quad ; \left(\frac{dP}{dT}\right)_S = \frac{C_{pg}}{T_g V_g \beta_g}$$

Liquid

$$a_{HE} = V_f \frac{dP}{dT} \left[\frac{T_f}{C_{pf} - T_f V_f \left(\frac{dP}{dT}\right)_S \left[2\beta_f - \kappa_f \left(\frac{dP}{dT}\right)_S\right]} \right]^{1/2} \quad ; \left(\frac{dP}{dT}\right)_S = \frac{h_g - h_f}{T_f (V_g - V_f)}$$

Two-Phase

$$a_{HE} = (XV_g + (1 - X)V_f)\left(\frac{dP}{dT}\right)_S \left[\frac{T}{A + B}\right]^{1/2}$$

$$A = X \left[C_{pg} - TV_g \left(\frac{dP}{dT}\right)_S \left[2\beta_g - \kappa_g \left(\frac{dP}{dT}\right)_S\right] \right]$$

$$B = (1 - X) \left[C_{pf} - TV_f \left(\frac{dP}{dT}\right)_S \left[2\beta_f - \kappa_f \left(\frac{dP}{dT}\right)_S\right] \right]$$

$$\left(\frac{dP}{dT}\right)_S = \frac{h_g - h_f}{T (V_g - V_f)}$$

8. SPECIAL COMPONENT MODELS

8.1 Pump Component

The PUMP component in RELAP5/MOD2 is a special component model composed of a set of functions that alter the way in which the one-dimensional fluid field equations are solved. In particular, the effect of the PUMP component is to add a momentum source term in the form of an additional ΔP included in the momentum equation and treated in a manner similar to that for a body force.

The following discussion of the RELAP5/MOD2 pump model is very similar to that discussed for the TRAC-PF1/MOD1 model[8-1] and, in fact, excerpts from the TRAC discussion are included herein. However, the following discussion will describe the model of the pump source term effecting the one-dimensional fluid field equation, the homogeneous pump model from which these source terms are calculated, the two-phase pump degradation model, and the various pump options allowing simulation of a wide variety of pump drive systems.

In RELAP5/MOD2, the PUMP component refers to an input scheme utilized by the user to define a single hydrodynamic control volume with an inlet and outlet junction and provide the code modeling scheme with the information required to simulate a centrifugal pump. Included in the scheme are options to simulate driving the pump with a motor, turbine, or control system. Details of the input scheme are provided in the RELAP5/MOD2 Code Manual, Volume 2, Appendix A.[8-2]

The pump model is implemented in the one-dimensional fluid field equations by utilizing a dimensionless-homologous pump model to compute the pump head as a function of fluid flow rate and pump speed. Then the head developed by the pump is apportioned equally between the suction and discharge junctions that connect the pump volume to the system. The pump model is interfaced with the two-fluid hydrodynamic model by assuming the head developed by the pump is similar to a body force. Thus, the head term appears in the mixture momentum equation; but, like the gravity body force, it does not appear in the difference of momentum equation.

In RELAP5/MOD2,[8-3] one of two numerical schemes can be used to perform calculations. One is referred to as the semi-implicit scheme, and the other is referred to as the nearly implicit scheme. The pump model is implemented in each scheme in a somewhat different way. In the semi-implicit scheme, the pump head term is included explicitly (i.e., at old-time level); in the nearly implicit scheme, the pump head term is coupled implicitly in terms of its dependence on volumetric fluid flow rate. The equations describing these schemes are Equations (390), (391), and (392) in Ref. 8-3. Fluid energy dissipation in the pump is modeled explicitly in both schemes and is described by Equations (393) and (395) in Ref. 8-3.

The dimensionless-homologous pump model utilized to calculate the pump head term is based on dimensionless similarity principles, and several references have been noted in the TRAC-PF1/MOD1 discussion[8-1] which also apply to the RELAP5/MOD2 model. Reference 8-4 (Chapter 9) provides a good discussion of pump operation, and Section 9.2 of the same reference describes the single-phase homologous curve description of a pump. Reference 8-5 is a general text on pumps and provides much information about pumps and their operating characteristics. Runstadler (Reference 8-6) provides an overview of the state of the art in pump modeling in the mid-1970s. Furuya (Reference 8-7) has also developed an analytical pump model that yields the two-phase performance characteristics based on single-phase characteristics and the details of the pump geometry.

The similarity factor for pumps that is most often discussed is the specific speed ω, defined in the following equation [Reference 8-5, Equation (5.9)]:

$$\omega_s = \frac{\omega Q^{1/2}}{(gH)^{3/4}} \quad , \tag{8-1}$$

where ω is the pump speed, Q the volumetric flow, g the acceleration of gravity, and H the pump head. This specific speed ω_s is dimensionless only if the units of the other parameters are consistent: ω in radians per second (rad-s^{-1}) or revolutions per second (rps), Q in m^3-s^{-1} or ft^3-s^{-1}, H in meters (m) or feet (ft), and g in m-s^{-2} or ft-s^{-2}. Stepanoff (Reference 8-5, p. 27) points out that ω_s is constant for all similar pumps

and ideally does not change with speed for a given pump; however, when it is used as a similarity parameter, ω_s should be calculated at the highest efficiency point of operation. Stepanoff also casts ω_s in another dimensionless form [Reference 8-5, Equation (5.35)], which shows the importance of maintaining certain geometric ratios in similar pumps. All of this discussion really is intended to provide a guide to help the code user determine if a set of homologous curves can be used to describe a particular pump.

In RELAP5/MOD2, the user has the choice of either using the two built-in homologous pump models or inputting the data to define a set of homologous curves. In any case, the following discussion describes the basis of homologous pump modeling.

8.2 Pump Head and Torque From Homologous Curves

A pump is typically described by four quadrant performance curves that describe the pump head and torque response as a function of fluid volumetric flow rate and pump speed. These four quadrant curves can be resolved into homologous curves for which one curve segment represents a family of four quadrant curves. These homologous curves are used in RELAP5 because of their simplicity. The homologous curves describe all operating states of the pump in a dimensionless form by combining positive or negative impeller velocities with positive or negative flow rates. The following discussion outlines the homologous relationship in terms of the following variables:

H = the pump head,

Q = the pump volumetric flow,

ω = the pump impeller angular velocity, and

τ = the pump torque.

The dimensionless terms that allow one set of curves to be used for a variety of similar pumps and relate pump head to flow and speed are:

$$h \equiv \frac{H}{H_R} \quad , \tag{8-2}$$

$$v \equiv \frac{Q}{Q_R} \quad , \tag{8-3}$$

and

$$\alpha \equiv \frac{\omega}{\omega_R} \quad , \tag{8-4}$$

where H_R is the rated pump head, Q_R is the rated pump volumetric flow, and ω_R is the rated pump speed. The pump head similarity relations[8-4] show that

$$\frac{h}{\alpha^2} = f(\frac{v}{\alpha}) \quad . \tag{8-5}$$

However, for small α this correlation is not satisfactory; and the following combination of variables is used:

$$\frac{h}{v^2} = f(\frac{\alpha}{v}) \quad . \tag{8-6}$$

A similar relation expressing pump torque in terms of flow and speed is:

$$\beta \equiv \frac{\tau_{hy}}{\tau_R} \quad , \tag{8-7}$$

where τ_{hy} is the hydraulic torque and τ_R is the rated pump torque. The convention used is that a positive torque acts to retard the pump impeller angular velocity. Thus, the hydraulic torque is in the torque reaction of the fluid upon the pump impeller. The pump torque similarity relations[8-4] show that

$$\frac{\beta}{\alpha^2} = f(\frac{v}{\alpha}) \tag{3-8}$$

and, for small α,

$$\frac{\beta}{v^2} = f\left(\frac{\alpha}{v}\right) \tag{8-9}$$

Figure 8-1 illustrates a typical set of four quadrant pump performance curves. and Figures 8-2 and 8-3 illustrate corresponding pump homologous head and torque curves, respectively. To account for two-phase effects on pump performance, an option is provided to model two-phase degradation effects. To use the model, the user must provide a separate set of two-phase homologous curves in the form of difference curves. These curves were developed from the 1-1/2 loop model Semiscale and Westinghouse Canada Limited (WCL) experiments. Assumptions inherent in the pump model for two-phase flow include:

1. The head multiplier, $M_H(\alpha_g)$, determined empirically for the normal operating region of the pump, is also valid as an interpolating factor in all other operating regions.

2. The relationship of the two-phase to the single-phase behavior of the Semiscale pump is applicable to large reactor pumps. This assumes that the pump model of two-phase flow is independent of pump specific speed.

The single-phase pump head (dimensionless) curve for the Semiscale pump is shown in Figure 8-4, and the fully degraded two-phase pump head curves are shown in Figure 8-5. These represent complete pump characteristics (except for the reverse pump fully degraded region) for the Semiscale pump operating under two-phase conditions with the average of the void fractions of the pump inlet and outlet mixtures between 0.2 and 0.9. The lines drawn through the data were determined by least-square-polynomial fits to the data. Tables of the normalized curves are also provided in the manual.[8-3]

If the two-phase option is selected, the pump head and torque are calculated using a two-phase multiplier approach for which

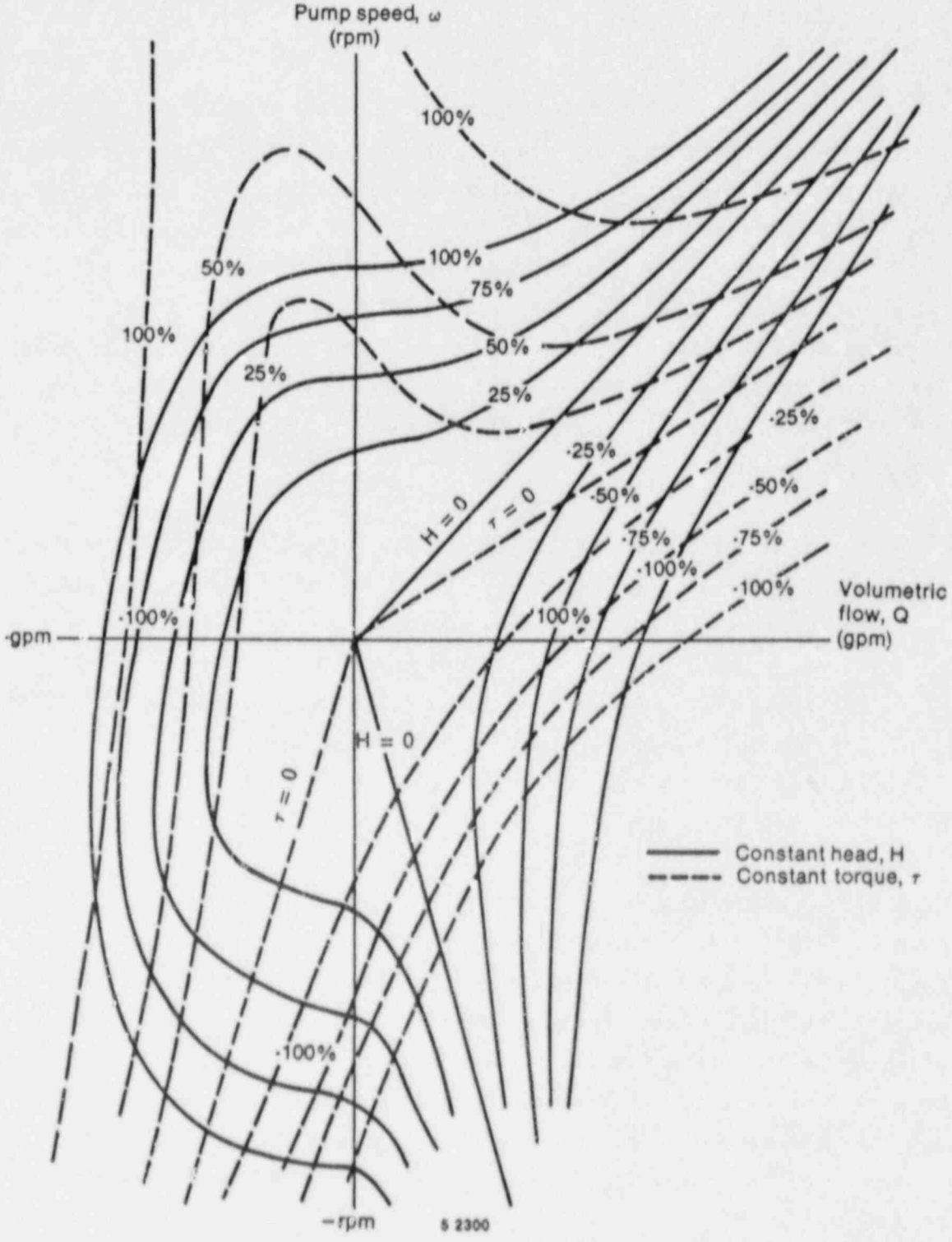

Figure 8-1. Typical pump characteristics four-quadrant curves.

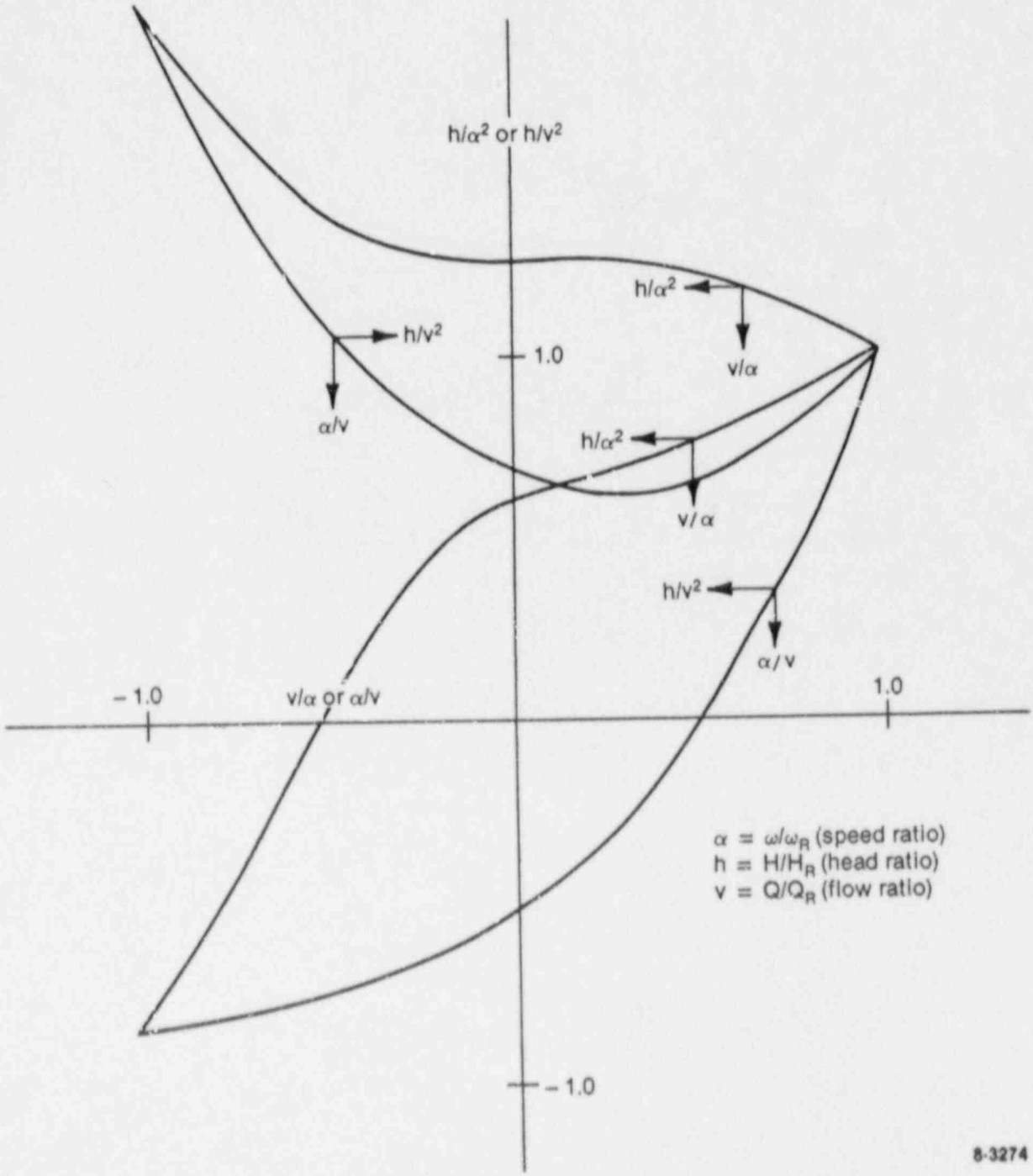

Figure 8-2. Typical pump homologous head curves.

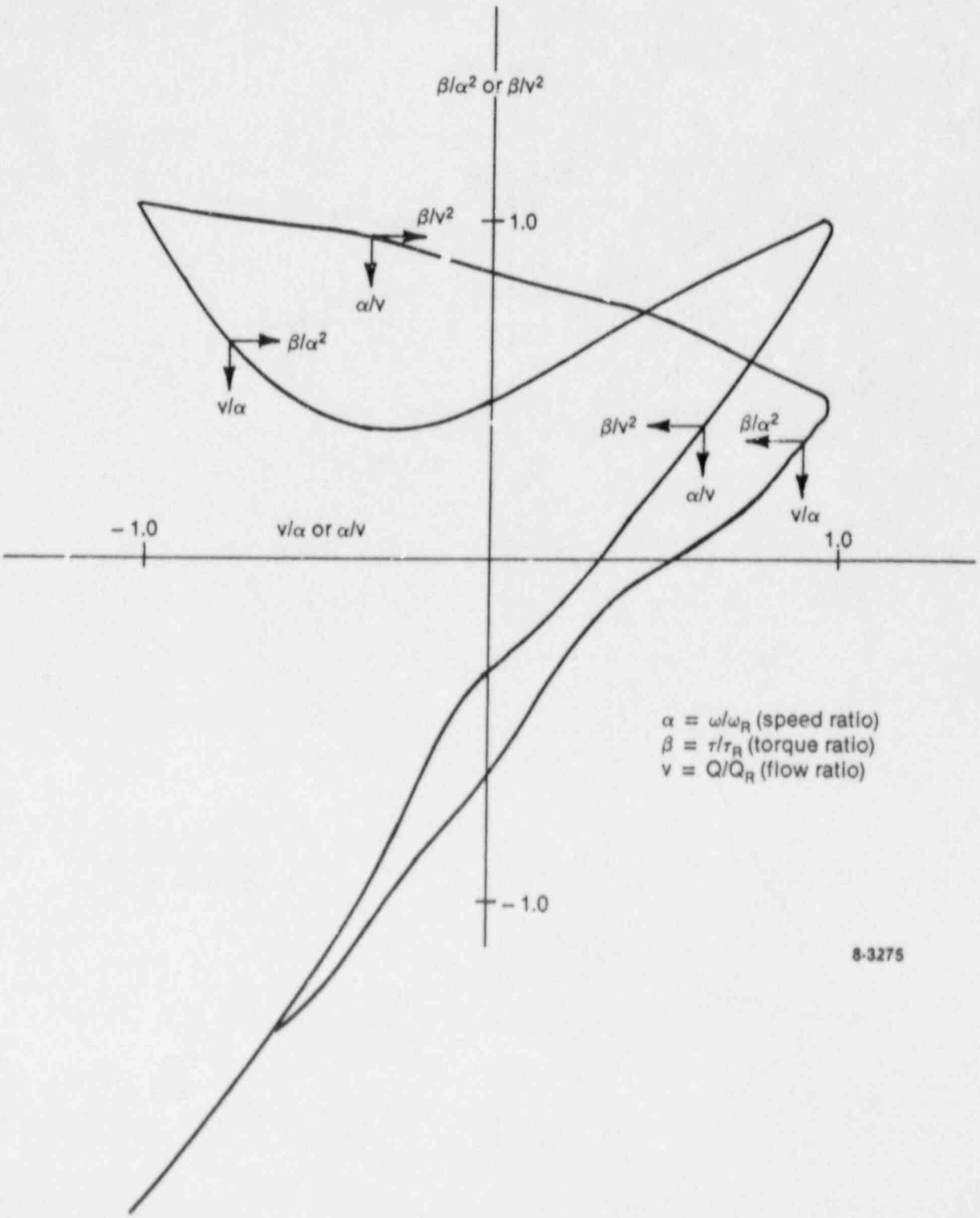

Figure 8-3. Typical pump homologous torque curves.

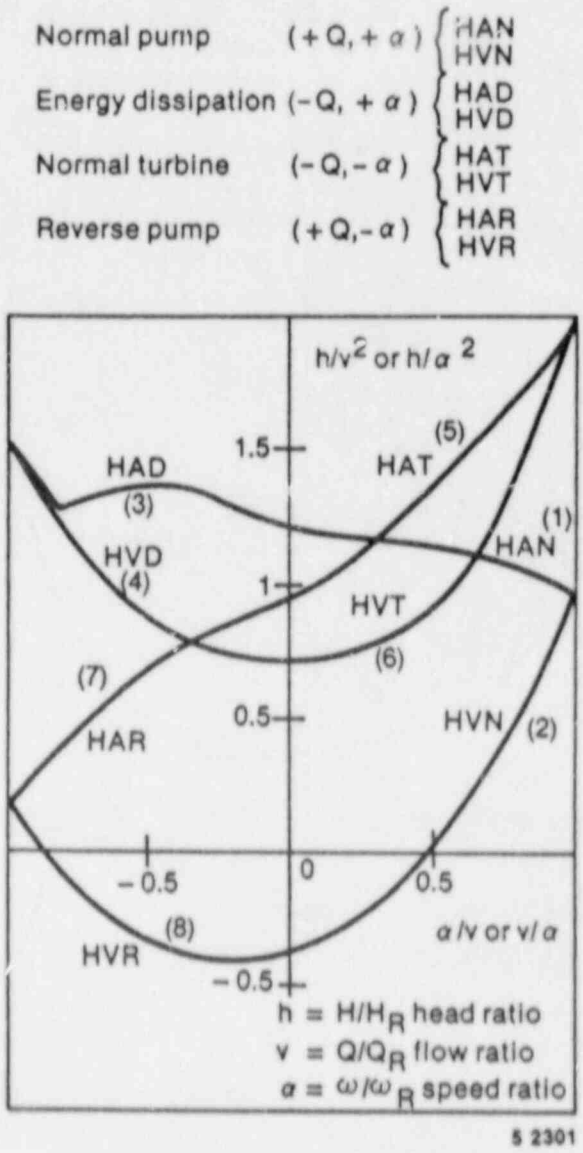

Figure 8-4. Single-phase homologous head curves for 1-1/2 loop MOD1 Semiscale pumps.

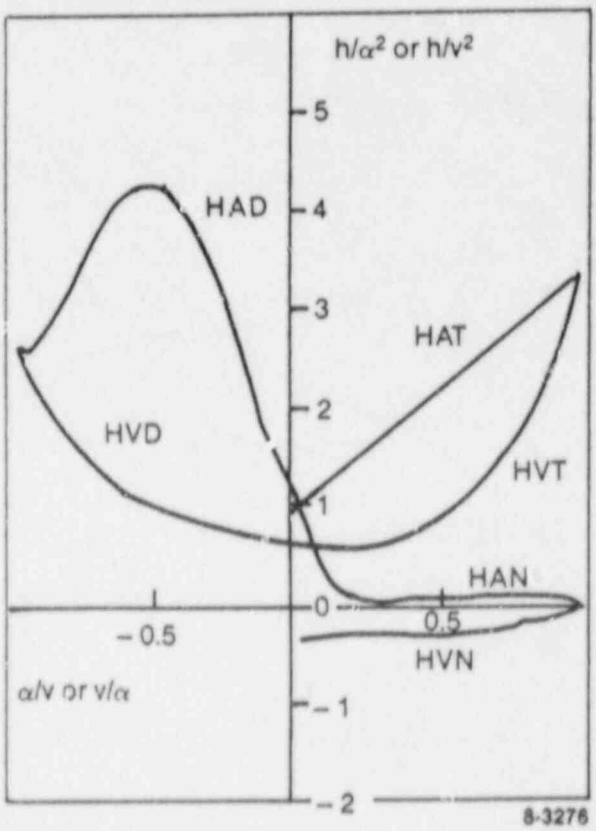

Figure 8-5. Fully degraded two-phase homologous head curves for 1-1/2 loop MOD1 Semiscale pumps.

$$H = H_{1\phi} \quad M_H(\alpha_g)\ (H_{1\phi} - H_{2\phi}) \tag{8-10}$$

$$\tau_{hy} = \tau_{1\phi} - M_\tau(\alpha_g)\ (\tau_{1\phi} - \tau_{2\phi})\ , \tag{8-11}$$

where

1ϕ = single-phase value

2ϕ = two-phase, fully degraded value, $0.2 < \alpha_q < 0.9$

M = multiplier on difference curve

α_g = average volume void fraction.

To this point, no knowledge of density is required to calculate H from the homologous head curves. The average mixture density in the pump control volume is used to convert the total pump head H to the pressure rise through the pump ΔP by the definition $\Delta P = \rho_m H$. The pump ΔP thus determined is applied to the momentum equation by adding 1/2 ΔP to the momentum mixture equation for the pump suction junction and 1/2 ΔP to the momentum mixture equation at the pump outlet junction. To compute the pump hydraulic torque τ_{hy}, the single and two-phase torque components must be computed. The single-phase torque, $\tau_{1\phi}$, is dependent upon the fluid density and is calculated from

$$\tau_{1\phi} = \beta_1 \tau_R \left(\frac{\rho_m}{\rho_R}\right)\ , \tag{8-12}$$

where β_1 is the dimensionless hydraulic torque from the single-phase homologous torque curves, ρ_m is the average pump mixture density, and ρ_R is the rated pump density. The density ratio is needed to correct for the density difference between the pumped fluid and the rated condition. Similarly, the fully degraded torque, $\tau_{2\phi}$, is obtained from

$$\tau_{2\phi} = \beta_2 \tau_R \left(\frac{\rho_m}{\rho_R}\right)\ , \tag{8-13}$$

where β_2 is the dimensionless hydraulic torque from the fully degraded homologous torque curves.

Total pump torque is used for two purposes in the pump model. First, it is used to calculate the pump speed if the electric motor drive or the pump coastdown with trip option are utilized. Second, the product of pump torque and speed is the pump energy dissipation included in the one-dimensional fluid field energy equation. Total pump torque is the sum of the pump hydraulic, frictional, and pump motor drive torques.

If the electric motor drive model is not used, then the total pump torque is calculated by considering the hydraulic torque from the single and two-phase homologous curves and the pump frictional torque.

$$\tau = \tau_{hy} + \tau_{fr} , \tag{8-14}$$

where

τ_{hy} = hydraulic torque

τ_{fr} = frictional torque.

The frictional torque is in the form of a cubic equation, and its value is also dependent on the sign of the pump speed. The user must also input the coefficients for the frictional cubic polynomial.

If the electric motor drive model is used, then the motor torque is included in the total torque as

$$\tau = \tau_{hy} + \tau_{fr} - \tau_{m} , \tag{8-15}$$

where the sign convention for τ_m is such that at steady flow operating conditions total torque is zero.

Utilizing the total torque, then, the pump speed can be calculated from the deceleration equation as

$$\tau = I\frac{d\omega}{dt} , \qquad (8\text{-}16)$$

where I is the rotational moment of inertia of the pump-motor assembly.

It should be noted that the electric motor pump drive model assumes an induction motor. Other drive models can be used, however, depending on the options selected by the user. For example, pump speed tables can be utilized that are governed by user-defined control variables, or the SHAFT component can be used to couple the PUMP component to a TURBINE component or to a GENERATOR component (i.e., the GENERATOR component can be used to simulate a motor). Excellent examples are presented for these cases in the User's Guide section of the RELAP5/MOD2 Code Manual, Volume 2.[8-2]

8.3 Pump Input Option

A versatile set of pump options are provided for the RELAP5/MOD2 pump component. This option can be input using the pump index and option card[8-2] with which up to seven options or combination of options can be specified. In addition to the options card, a pump-shaft connection card is provided that allows the user to utilize the SHAFT component to drive the pump with TURBINE or GENERATOR components.

The following options can be specified using the pump index and options card.

1. Pump table data indicator: Specifies whether user-defined homologous curve data is input or whether one of the built-in pump homologous curve data sets is to be used. Built-in data sets are for either the Bingham or the Westinghouse pumps.

2. Two-phase index: Specifies whether or not the two-phase option is to be used. If the two-phase option is to be used, then the user must provide input for a two-phase multiplier table.

3. Two-phase difference table index: Specifies if a two-phase difference table is needed, if input for a table is provided by the user, or if the built-in Bingham or Westinghouse tables are to be used.

4. Pump motor torque tables index: Specifies whether a table is to be used and whether table input is provided by the user.

5. Time-dependent pump velocity index: Specifies if no time-dependent table is needed or if table data is input by the user. This option cannot be used if a SHAFT component is used to drive the pump. This option can also be used to vary pump speed using a control variable component.

6. Pump trip number: specifies a trip number if non-zero. This trip controls the built-in electric motor model if specified, the pump coastdown model if no drive model is specified, or use of the pump speed table if the speed table option is specified.

7. Pump reverse indicator: Specifies whether or not the pump impeller will be allowed to rotate in reverse (i.e., at negative angular velocity).

If the pump shaft connection card[8-2] is input, then a SHAFT component is assumed to be driving the pump. The user must input the SHAFT component number; and, if the shaft connection is controlled by a trip, then the trip number must be input. Of course, input defining the SHAFT component must also be provided.

A user's guide with two examples of pump modeling is also provided in Section 2 of the RELAP5/M^D2 Code Manual, Volume 2.[8-2]

8.4 Pump Conclusions

The pump model included in the RELAP5/MOD2 code has demonstrated an adequate capability to model reactor pumps under many conditions. Obviously, the quality of the pump simulation is very dependent on the

quality of the homologous curves used to describe the pump, and we recommend that whenever data is available, the user input specific curves for the pump under consideration instead of using the built-in curves. An alternative might be to use the Furuya model[8-7] to generate the fully degraded homologous curves and associated two-phase multiplier curves for the pump geometry and the published single-phase performance curves from the manufacturer. Unless the pump to be modeled is similar to the Bingham or Westinghouse pumps, the least desirable option is to select one of the sets of built-in curves.

From a modeling viewpoint, there are three deficiencies regarding the pump model. First, the assumed treatment of frictional torques in calculating the pump coastdown is limited at best and should be generalized. Secondly, the assumption of churn turbulent flow within the pump, while a reasonably good assumption when the pump is operating at high rotational speed, breaks down as the pump speed approaches zero. At this point, the churn turbulent flow assumption encourages equal phase velocities and, in particular, prevents countercurrent flow. The lack of phase slip can affect the separation of liquid and vapor in the pump suction and discharge and could result in erroneous oscillatory flows. The third deficiency is that no capability is provided to model cavitation induced by phase changes within the pump.

8.5 References

8-1. D. R. Liles et al., TRAC-PF1/MOD1 Correlations and Models, NUREG 5069, LA-11208-MS, August 1988.

8-2. V. H. Ransom, et al., RELAP5/MOD2 Code Manual, Volume 2: Users Guide and Input Requirements, NUREG/CR-4312, EGG-2396, December 1985.

8-3. V. H. Ransom, et al., RELAP5/MOD2 Code Manual, Volume 1: Code Structure, System Models, and Solution Methods, NUREG/CR-4312, EGG-2396, December 1985.

8-4. V. L. Streeter and E. B. Wylie, Hydraulic Transients, New York: McGraw-Hill Book Company, 1967.

8-5. A. J. Stepanoff, Centrifugal and Axial Flow Pumps, 2nd ed., New York: John Wiley & Sons, Inc., 1957.

8-6. P. W. Runstadler, Review and Analysis of State-of-the-Art of Multiphase Pump Technology, EPRI/NP-159, February 1976.

8-7. O. Furuya, Development of an Analytic Model to Determine Pump Performance Under Two-Phase Flow Conditions, EPRI/NP-3519, May 1984.

9. HEAT STRUCTURE PROCESS MODELS

The heat structures in RELAP5/MOD2 permit the calculation of heat across the solid boundaries of the hydrodynamic volumes. Heat transfer from and/or through structures, including fuel pins or plates (with nuclear or electrical heating), steam generator tubes, and pipe and vessel walls, can be modeled. One-dimensional heat conduction in rectangular, cylindrical, and spherical geometry can be represented by the heat structures in RELAP5/MOD2. Surface multipliers are used to convert the unit surface of the one-dimensional calculation to the actual surface of the heat structure. Thermal conductivities and volumetric heat capacities as functions of temperature can be input in tables, or built-in values can be used.

Finite differences are used to advance the heat conduction solutions. Each mesh interval may contain a different mesh spacing, a different material, or both. The spatial dependence of the internal heat source, if any, may vary over each mesh interval. The time-dependence of the heat source can be obtained from the reactor kinetics, a table, or a control system. Boundary conditions can be simulated by using tables of surface temperature versus time, heat transfer rate versus time, heat transfer coefficient versus time, or heat transfer coefficient versus surface temperature. Symmetrical or insulated boundary conditions can also be simulated. For heat structure surfaces connected to hydrodynamic volumes, a heat transfer package containing correlations for convective, nucleate boiling, transition boiling, and film heat transfer from the wall-to-water and reverse transfer from water-to-wall is provided. These correlations were discussed earlier.

9.1 Heat Conduction for Components

One-dimensional heat conduction in rectangular, cylindrical, and spherical geometry can be used to represent the heat structures in any of the components in RELAP5/MOD2. It is assumed in one-dimensional heat conduction that the temperature distribution in the axial or radial

direction is the same throughout the structure being modeled and that the linear heat flow is negligible. The equations governing one-dimensional heat conduction are

$$\rho C_p \frac{\partial T}{\partial t} = \frac{\partial}{\partial x}\left(k \frac{\partial T}{\partial x}\right) + S \qquad \text{for rectangular geometry,} \qquad (9\text{-}1a)$$

$$\rho C_p \frac{\partial T}{\partial t} = \frac{1}{r}\left[\frac{\partial}{\partial r}\left(rk\frac{\partial T}{\partial r}\right)\right] + S \qquad \text{for cylindrical geometry,} \qquad (9\text{-}1b)$$

and

$$\rho C_p \frac{\partial T}{\partial t} = \frac{1}{r^2}\left[\frac{\partial}{\partial r}\left(r^2 k \frac{\partial T}{\partial r}\right)\right] + S \qquad \text{for spherical geometry,} \qquad (9\text{-}1c)$$

where T is the temperature, t is the time, x is the length, r is the radius, S is the internal heat source, ρC_p is the volumetric heat capacity, and k is the thermal conductivity.

In order to model a heat structure in RELAP5/MOD2, a mesh is set up beginning at the left boundary of the structure being modeled and continuing to the right boundary. The mesh point spacing (Figure 9-1) is taken as positive as x or r increases from left to right. Mesh points must be placed on the external boundaries of the structure unless a symmetrical or adiabatic boundary condition is to be used. Mesh points may also be placed at any desired intervals within the structure and should be placed at the interfaces between the different materials. The spacing of the mesh points may vary from material to material and may vary within the material as the user desires. If the structure being modeled is symmetrical, such as a core heater rod, the left boundary must be the center of the rod and the right boundary the outside surface of the rod. This symmetry is simulated by an adiabatic boundary across which no heat may flow (this can also be used to simulate a perfectly insulated boundary). The thermal conductivities (k) and volumetric heat capacities (ρC_p) of the materials between the mesh points are required to complete the description of the heat structure in RELAP5/MOD2. These material properties can be input in tabular form as functions of temperature or the user may choose to use the built-in values.

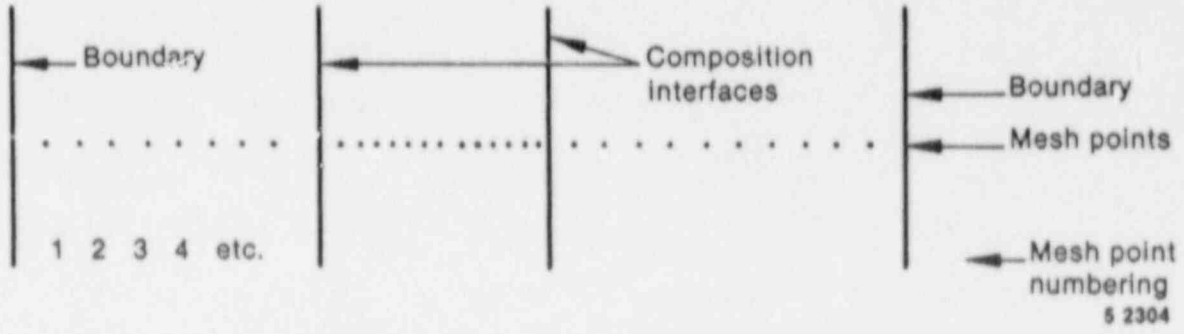

Figure 9-1. Mesh point layout.

Heat may flow across the external heat structure boundaries to either the environment or to the reactor coolant. For heat structure surfaces connected to hydrodynamic volumes containing reactor coolant, a heat transfer package containing correlations for convective, nucleate boiling, transition boiling, and film heat transfer from wall-to-water and reverse heat transfer from water-to-wall is provided. These correlations were discussed earlier and will not be discussed here. Any number of heat structures may be connected to each hydrodynamic volume. These heat structures may vary in geometry type, mesh spacing, internal heat source distribution, etc. This flexibility allows the user to accurately model any type of structure. For heat structure surfaces connected to volumes simulating the environment, tables can be used to simulate the desired boundary conditions. Tables of surface temperature versus time, heat transfer rate versus time, heat transfer coefficient versus time, or heat transfer coefficient versus surface temperature can be used to simulate the boundary conditions. Usually heat losses are modeled using the heat transfer coefficient versus surface temperature boundary condition and combining the radiative and natural convection heat transfer coefficients in the table.

A contact-resistance interface condition cannot be specified directly, since the temperature, instead of being continuous at the interface, is given by $q = h_c \Delta T$ where q is the heat transfer rate across the interface, h_c is the contact conductivity, and ΔT is the temperature change across the interface. This condition can be specified by defining a small mesh interval with thermal properties of $k = h_c$ and $\rho C_p = 0$. The size of the mesh interval is arbitrary except that in the cylindrical and spherical geometries the surface and volume are dependent on the radius. The mesh interval is usually chosen very small with respect to the dimensions of the problem.

Internal heat sources can be placed into any heat structure in RELAP5/MOD2 whether it represents a fuel rod or a pipe wall. The spatial dependence of the heat source can be simulated using weighting factors that partition the heat source to various portions of the heat structure. The time dependence of the heat source can be obtained from the reactor kinetics solution, a table, or a control system.

In RELAP5/MOD2, various subroutines are used in solving the one-dimensional heat conduction equations. HTCOND returns left and right boundary conditions for a heat structure. HTCSOL finds temperature solution by back substitution. HTRC1 computes heat transfer coefficients from correlations. HT1SST solves the one-dimensional steady-state heat problem. HT1TDP advances one heat structure one time step by advancing the transient one-dimensional heat conduction equation. HTADV controls the advancement of heat structures and computes heat added to the hydrodynamic volumes. Subroutines HT1SST and HT1TDP are the same except that HT1SST is used when the heat structure steady-state option is specified by the user. HT1SST differs from HT1TDP in that the time dependence in the difference equations is removed.

The heat conduction equation is not a correlation and can be solved by various numerical techniques. RELAP5/MOD2 uses the Crank-Nicolson[9-1] method for solving this equation. The actual coding will not be shown or discussed here. The discussion in the RELAP5/MOD2 Code Manual[9-2] is representative of what is actually in the code except for the separation of the steady-state and transient solutions into the two subroutines HT1SST and HT1TDP. For the derivation of the finite, difference equations from the one-dimensional heat conduction equations, the reader is referred to the RELAP5/MOD2 Code Manual. Several heat conduction test problems were run to illustrate how well RELAP5/MOD2 calculates heat conduction. All of the cases have closed-form solutions as given in Reference 9-3.

Case 1. Steady-state heat conduction in a composite wall, $0 < x < 1$, with surface temperatures held constant at T_0 and T_1. A 0.24-in. wall consisting of Inconel 718, constantan, stainless steel, and Inconel 600, and with surface temperatures of $T_0 = 80^0F$ and $T_1 = 70^0F$ was modeled. This is the basic and simplest case for heat conduction in rectangular geometry. Figure 9-2 shows a comparison of the RELAP5/MOD2 solution and the textbook solution.

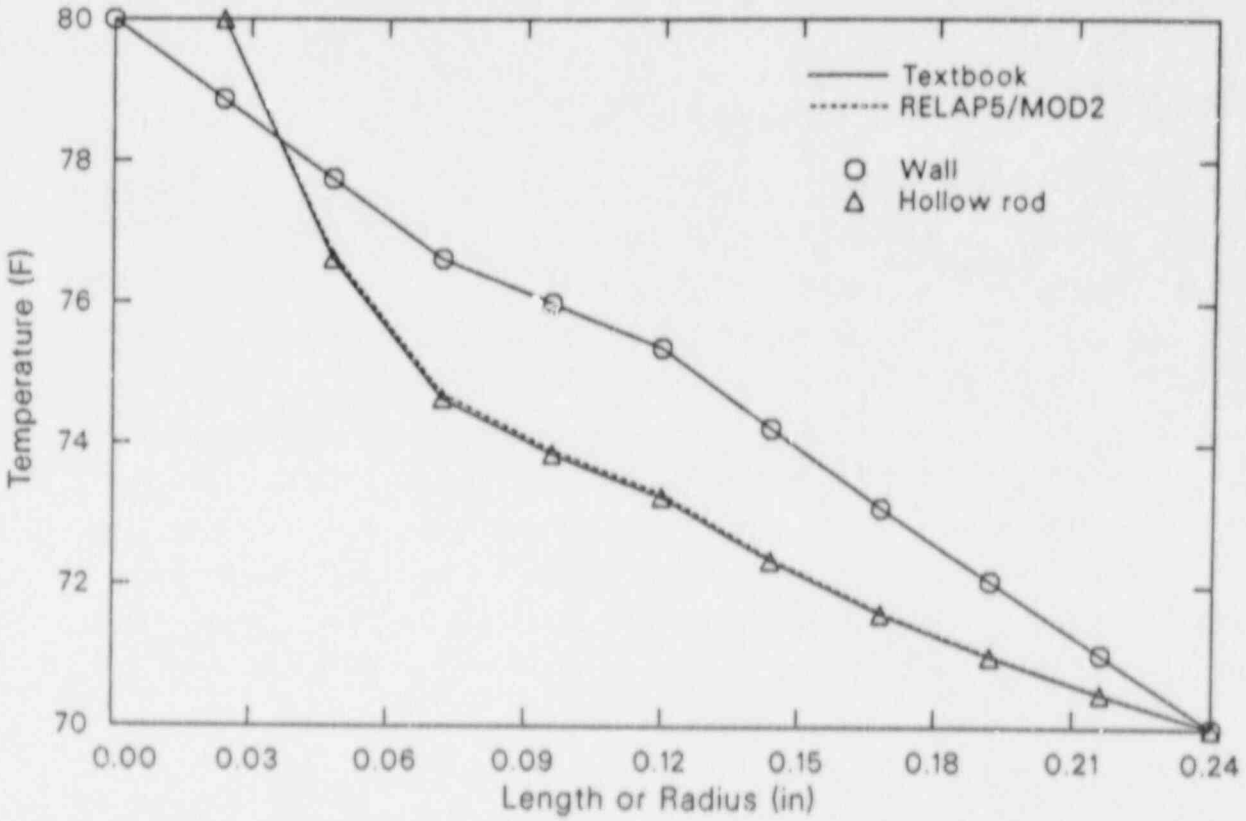

Figure 9-2. Temperature versus length or radius, Cases 1 and 2.

Case 2. Steady-state heat conduction in a composite hollow cylinder, $R_i < r < R_o$, with surface temperatures held constant at T_i and T_o. A hollow cylinder with an inside radius of 0.024 in. and an outside radius of 0.24 in. consisting of Inconel 718, constantan, stainless steel, and Inconel 600, and with surface temperatures of $T_i = 80^oF$ and $T_o = 70^oF$ was modeled. This is the basic and simplest case for heat conduction in cylindrical geometry. Figure 9-2 shows a comparison of the RELAP5/MOD2 solution and the textbook solution.

Case 3. Transient heat conduction in a uniform wall, $-l < x < l$, with an initial temperature distribution of $\Delta T \cos(\pi x/2l) + T_o$ and surface temperatures held constant at T_o. A 0.48-in. wall consisting of stainless steel with a surface temperature of $T_o = 70^oF$ and with $\Delta T = 10^oF$ was modeled. The resulting time dependent temperature distribution is given by

$$T = \Delta T \cdot \cos\left(\frac{\pi x}{2l}\right) \cdot e^{-\kappa\pi^2 t/4l^2} + T_o \quad . \tag{9-2}$$

where κ is $k/\rho C_p$. Figure 9-3 compares the RELAP5/MOD2 solution to the closed-form solution for various times. This problem is run on every new version of RELAP5/MOD2 to test the conduction model before the new version is released.

Case 4. Transient heat conduction in a uniform rod, $0 < r < R_o$, with an initial parabolic temperature distribution of $T_i - ar^2$ and surface temperatures held constant at T_o. A 0.48-in. outside diameter rod consisting of stainless steel with a surface temperature of $T_o = 70^oF$ and with $T_i = 80^oF$ and $a = 25000\ ^oF/ft^2$ was modeled. This gives similar results to Case 3, but for cylindrical geometry. The resulting time-dependent temperature distribution is given by

$$T = \frac{2}{R_o} \cdot \sum_{n=1}^{\infty} \left[e^{-\kappa\alpha_n^2 t} \cdot \frac{J_o(r\alpha_n)}{\alpha_n^2 \cdot J_1^2(R_o\alpha_n)} \cdot (\alpha_n \cdot (T_i - T_o - kR_o^2) \right.$$

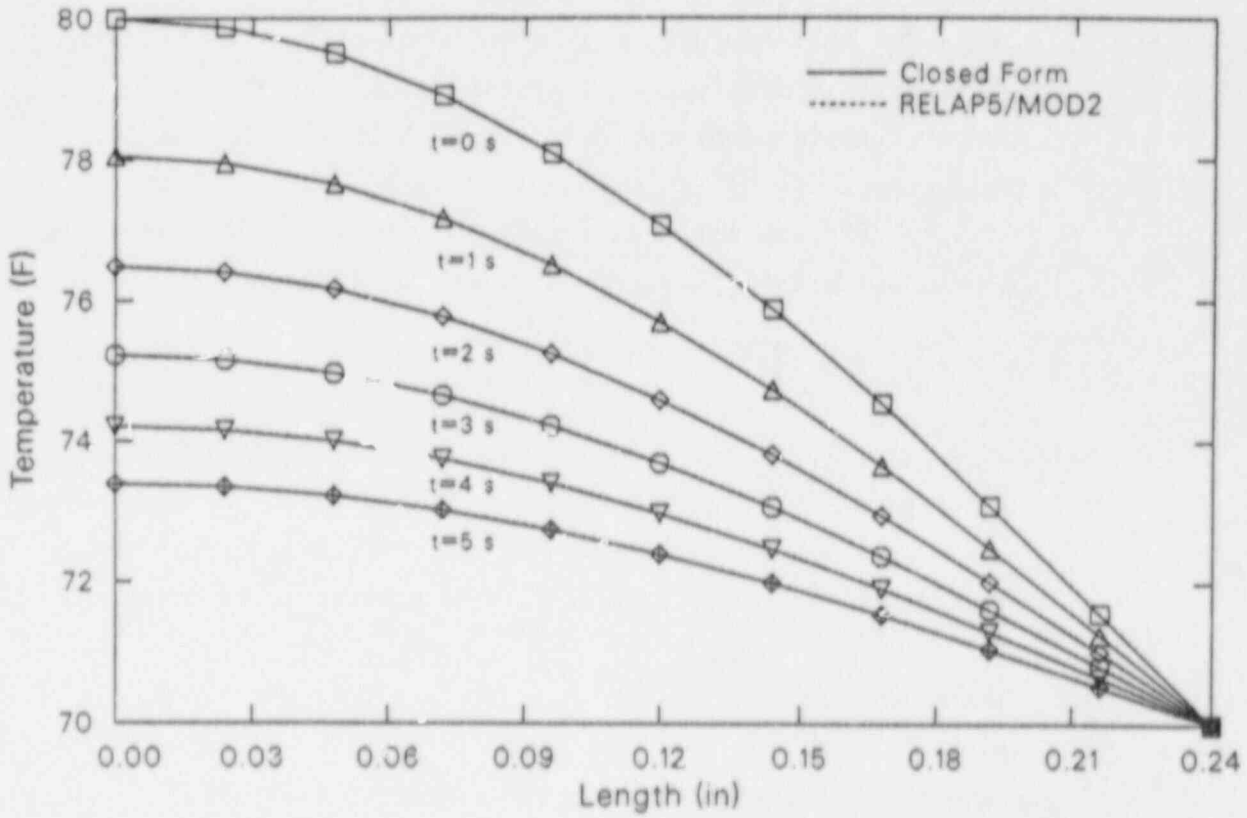

CCMJ501-2

Figure 9-3. Temperature versus length, Case 3.

$$\cdot J_1(R_o\alpha_n) + 2kR_o \cdot J_2(R_o\alpha_n))\Big] + T_o \ , \qquad (9\text{-}3)$$

where κ is $k/\rho C_p$ and α_n are the positive roots of $J_0(\alpha R_o) = 0$. Figure 9-4 compares the RELAP5/MOD2 solution to the closed form solution for various times.

Case 5. Transient heat conduction in a uniform wall, $-1 < x < 1$, with a uniform initial temperature distribution at T_i and surface temperatures maintained at $\Delta T \sin(\omega t) + T_i$ for $t > 0$. A 0.48-in. wall consisting of stainless steel with a uniform initial temperature of $T_i = 75^oF$ and with $\Delta T = 5^oF$ and $\omega = \pi/2\ s^{-1}$ was modeled. The resulting time-dependent temperature distribution is given by

$$T = \Delta T \cdot A \cdot \sin(\omega t + \phi) + T_i$$

$$+ 4\pi\kappa \cdot \sum_{n=0}^{\infty} \left[\frac{(-1)^n (2n+1)(4l^2\omega)}{16l^4\omega^2 + \kappa^2\pi^4 \cdot (2n+1)^4} \right.$$

$$\left. \cdot e^{-\kappa(2n+1)^2\pi^2 t/4\,l^2} \cdot \cos\left[\frac{(2n+1)\pi x}{2l}\right] \right] , \qquad (9\text{-}4)$$

where κ is $k/\rho C_p$ and

$$A = \left| \frac{\cosh(\nu x(1+i))}{\cosh(\nu l(1+i))} \right| = \left[\frac{\cosh(2\nu x) + \cos(2\nu x)}{\cosh(2\nu l) + \cos(2\nu l)}\right]^{1/2}$$

$$\phi = \arg\left[\frac{\cosh(\nu x(1+i))}{\cosh(\nu l(1+i))}\right], \quad \nu = \left(\frac{\omega}{2\kappa}\right)^{1/2} .$$

Figure 9-5 compares the RELAP5/MOD2 solution to the closed form solution for various times.

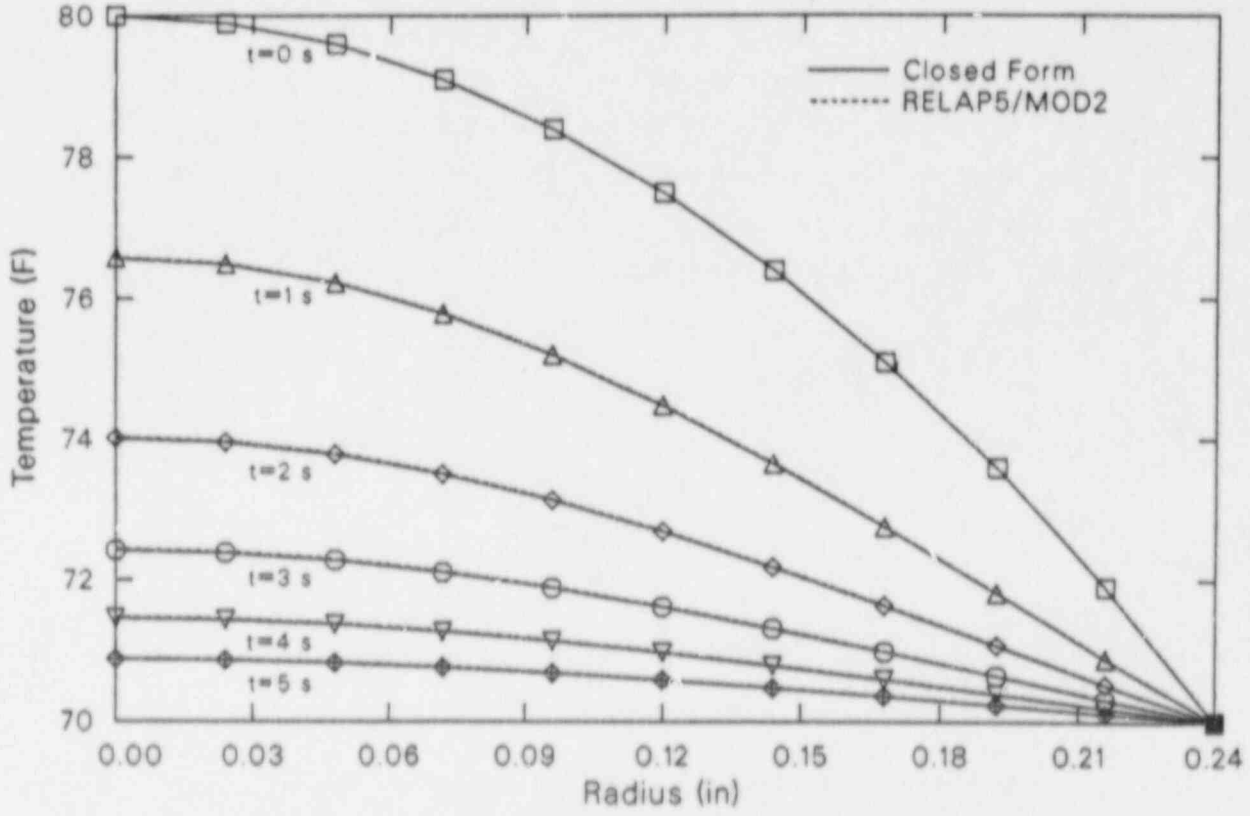

CCM/501-3

Figure 9-4. Temperature versus radius, Case 4.

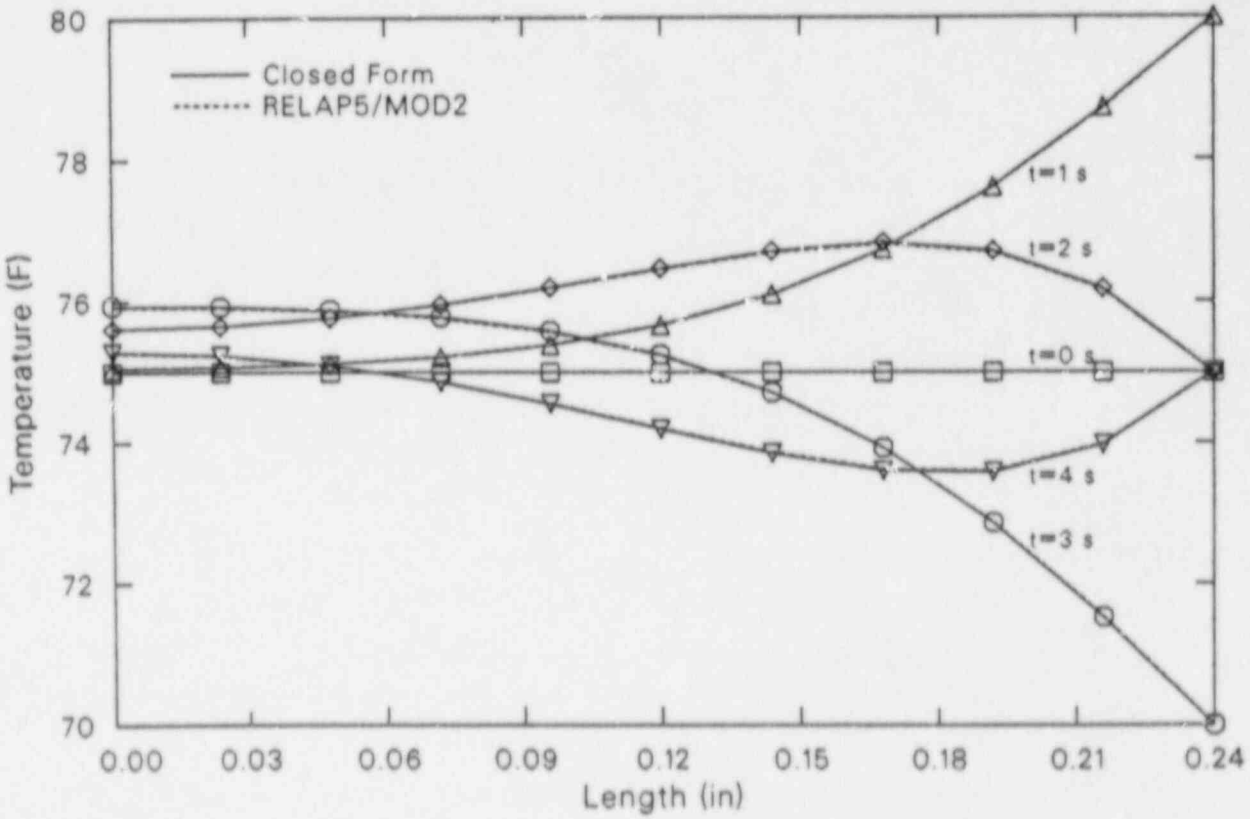

CCMJ501-5

Figure 9-5. Temperature versus length, Case 5.

Case 6. Transient heat conduction in a uniform rod, $0 < r < R_o$, with a uniform initial temperature distribution at T_i and surface temperatures maintained at $\Delta T \sin(\omega t) + T_i$ for $t > 0$. A 0.48-in. outside diameter rod consisting of stainless steel with a uniform initial temperature of $T_i = 75^oF$ and with $\Delta T = 5^oF$ and $\omega = \pi/2\ s^{-1}$ was modeled. The resulting time dependent temperature distribution is given by

$$T = \Delta T \cdot Real\left[\frac{I_o(r \cdot (i\omega/\kappa)^{1/2})}{iI_o(R_o \cdot (i\omega/\kappa)^{1/2})} \cdot e^{i\omega t}\right]$$

$$+ \frac{2\kappa \cdot \Delta I}{R_o} \cdot \sum_{n=1}^{\infty}\left[e^{-\kappa\alpha_n^2 t} \cdot \frac{\alpha_n \cdot \omega \cdot J_o(r\alpha_n)}{(\kappa^2\alpha_n^4 + \omega^2) \cdot J_1(R_o\alpha_n)}\right] + T_i\ , \quad (9\text{-}5)$$

where κ is $k/\rho C_p$ and α_n are the positive roots of $J_0(\alpha R_0) = 0$. Figure 9-6 compares the RELAP5/MOD2 solution to the closed-form solution for various times. This is the same as Case 5 but for cylindrical geometry.

Case 7. Transient heat conduction in a uniform rod, $0 < r < R_o$, with a uniform initial temperature distribution of T_i and with uniform heat production at the rate of $Q_o e^{-\lambda t}$ per unit time per unit volume for $t > 0$. A 0.48-in. outside diameter rod consisting of stainless steel with a uniform initial temperature of $T_i = 70^oF$ and with $Q_o = 709.5$ Btu/s-ft^3 and $\lambda = \ln(2) = 0.693147\ s^{-1}$ was modeled. The resulting time-dependent temperature distribution is given by

$$T = \frac{\kappa Q_o}{kg} \cdot e^{-\lambda t} \cdot \left[\frac{J_o(r \cdot (\lambda/\kappa)^{1/2})}{J_o(R_o \cdot (\lambda/\kappa)^{1/2})} - 1\right]$$

$$- \frac{2Q_o\kappa}{R_o k} \cdot \sum_{n=1}^{\infty}\left[\frac{e^{-\kappa\alpha_n^2 t} \cdot J_o(r\alpha_n)}{\alpha_n \cdot (\kappa\alpha_n^2 - \lambda) \cdot J_1(R_o\alpha_n)}\right] + T_i\ , \quad (9\text{-}6)$$

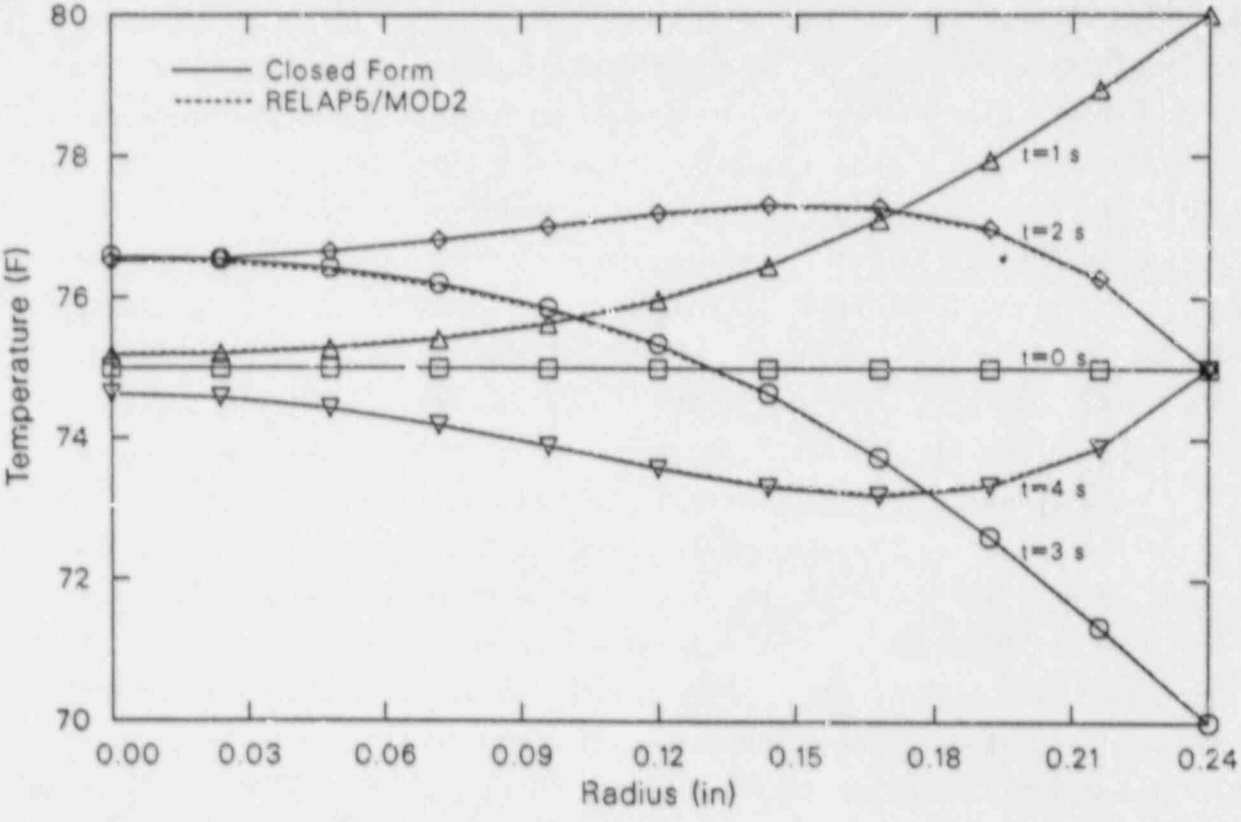

Figure 9-6. Temperature versus radius, Case 6.

where κ is $k/\rho C_p$ and α_n are the positive roots of $J_0(\alpha R_0) = 0$. Figure 9-7 compares the RELAP5/MOD2 solution to the closed form solution for various times. The exponential decay modeled in this case is similar to the decay experienced in a core heater rod.

All seven cases were run with different time step sizes of 0.01, 0.1, 0.5, 1.0, and 2.0 s to test the stability of the RELAP5/MOD2 solution. The Crank-Nicolson method is designed to be stable for all conditions, and the RELAP5/MOD2 solution was stable for all the time steps tested. However, calculational inaccuracies did occur as the time step size was increased. These inaccuracies did not result because of instabilities in the solution technique of the heat conduction equation in RELAP5/MOD2, but resulted from making the time step larger than the time constant for the particular problem and changing the boundary conditions. The time constant for any particular problem is difficult to define, and only in Cases 3 and 4 did the boundary conditions remain constant as the time step size was increased. (For steady-state Cases 1 and 2, the choice of time step size made no difference.) No significant inaccuracies were seen in these two cases until the time step was increased to 1.0 s, and then only in Case 4 with the cylindrical geometry (Figure 9-8.). In these two cases, the temperature variation was fairly benign, but inaccuracies were calculated. The time step size is the choice of the user, and the user should be aware that the larger the time step chosen the greater the possibility that inaccuracies will be calculated. Unless the transient being calculated is at a quasi-steady state, using a time step of 1.0 s is bordering on recklessness and is not recommended. A larger time step size may also change the boundary conditions, because the boundary conditions are assumed to vary linearly between time step values. The boundary conditions input to RELAP5/MOD2 can change only as fast as the time step. If the boundary conditions vary faster than one time step, the change is not input to RELAP5/MOD2. The boundary conditions between the time steps are not actually changed by RELAP5/MOD2; they are never put in. If, for example, a sine wave with a period of 4 s (as in Cases 5 and 6) is used as a boundary condition and a time step of 1 s is used, the resulting boundary condition

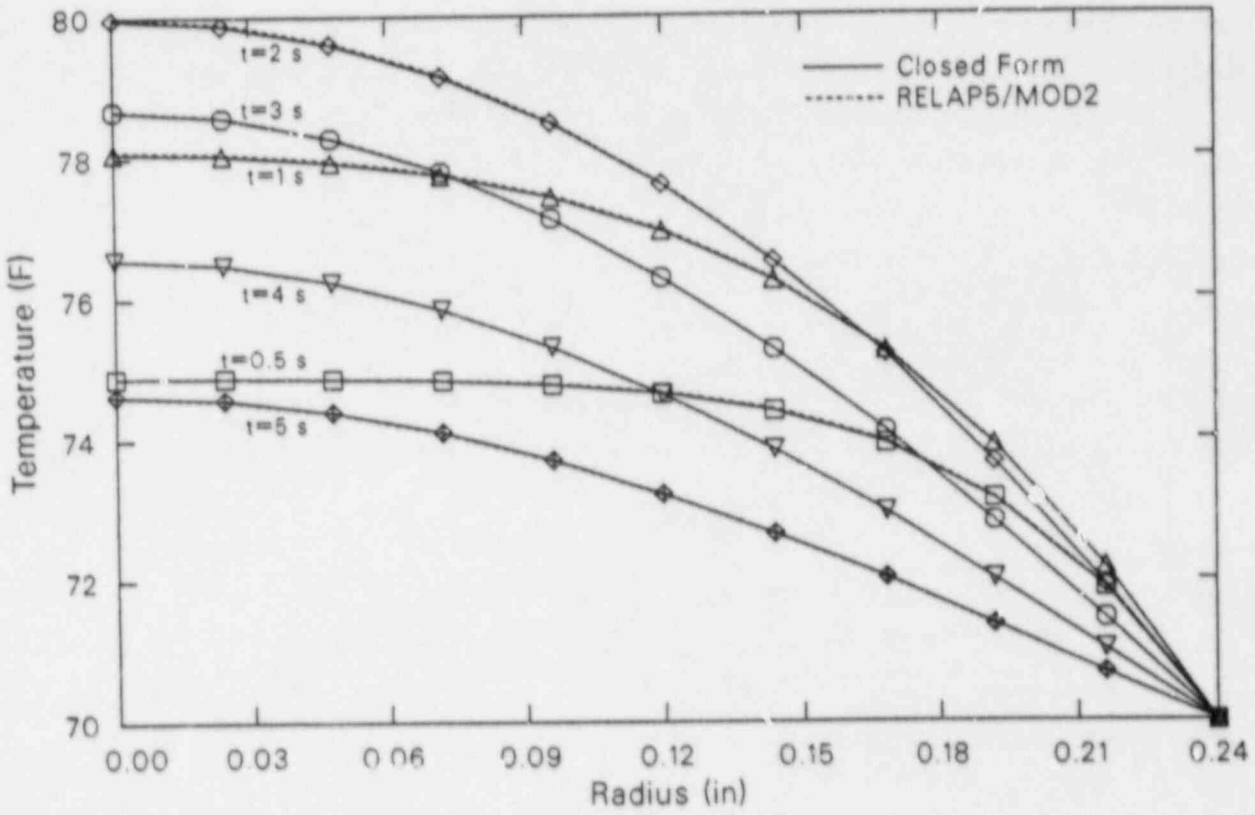

Figure 9-7. Temperature versus radius, Case 7.

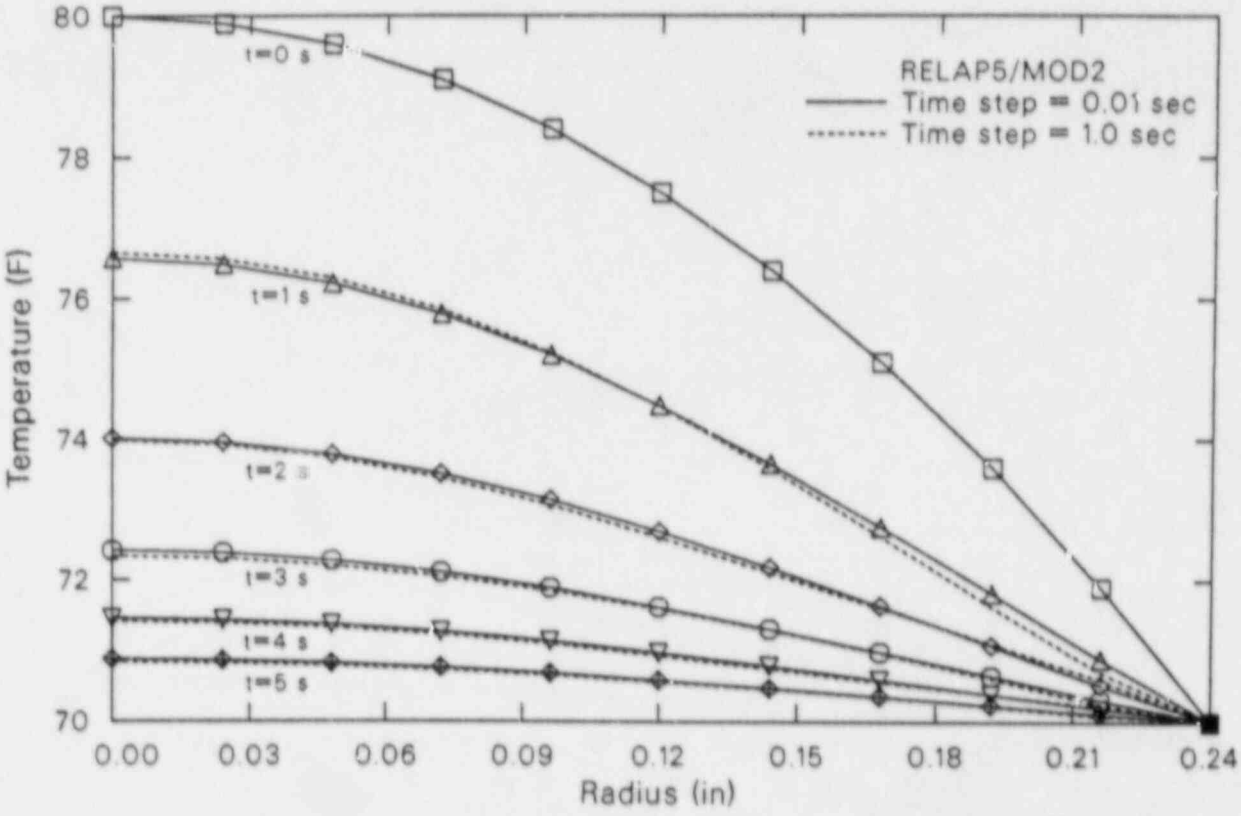

CCMJ501-4

Figure 9-8. Temperature versus radius, varying time steps.

would be a saw tooth curve; if a time step of 2 s is used, the resulting boundary condition would be a straight line. This obviously leads to inaccuracies that are not associated with the RELAP5/MOD2 solution technique.

In all seven cases, when the time step size was 0.01 s the RELAP5/MOD2-calculated temperature distribution agreed very well with the temperature distribution calculated from the closed-form solution. The closed-form solutions involve summations to infinity and had to be approximated. In addition, for cylindrical geometry, the closed-form solutions involve Bessel functions; and approximations were used in calculating these functions. As a result, the closed-form solutions are not exact. No significant differences between RELAP5/MOD2 and the closed-form solutions were found for the small time steps, so the conduction model in RELAP5/MOD2 is judged to work very well.

9.2 Reflood Heat Conduction

A two-dimensional heat conduction scheme is used in the reflood model for cylindrical and rectangular heat structures. This scheme is an extension of the one-dimensional heat conduction scheme and is found in subroutine HT2TDP. Included with the two-dimensional heat conduction scheme is a fine mesh-rezoning scheme. The fine mesh-rezoning scheme is implemented to efficiently use the two-dimensional conduction solution for reflood calculations. The scheme is similar to the one used in COBRA-TF[9-4] and is intended to resolve the large axial variation of wall temperatures and heat fluxes during core reflood. The number of axial nodes in the heat structures is varied in such a way that the fine nodes exist only in the nucleate boiling and transition boiling regions. Detailed discussions of two-dimensional heat conduction solution and the fine mesh-rezoning scheme can be found in the RELAP5/MOD2 Code Manual.[9-2]

Reflood becomes important during a LOCA after the core has been voided and water begins to refill the core as a result of the ECCS. As the core liquid level rises, water contacts the hot core rods and steam is formed. Eventually the rods cool down sufficiently so that they can no longer cause

steam formation. The core rods, however, do not cool down uniformly, and there exists a transition region above which the core rods have not been rewet and below which they have. It is in this transition region that the reflood model and fine mesh rezoning scheme were designed to calculate. In this transition region, there is a large axial variation in wall temperatures and heat fluxes that require a finer noding than is necessary for the normal temperature and heat flux calculations. At the initiation of the reflood model, each heat structure is subdivided into two axial intervals (Figure 9-9). A two-dimensional array of mesh points is thus formed. Thereafter, the number of axial intervals may be doubled, halved, or remain unchanged at each time step as the transition region moves up the core.

The number of axial mesh intervals in a heat structure depends on the heat transfer regimes in the heat structures. At each time step, all heat structures in a heat-structure geometry are searched to find the positions of T_{CHF}, the wall temperature where CHF occurs, of T_Q, the quench or rewetting temperature, and of T_{IB}, the wall temperature at the incipience of boiling. As the transition region moves up through the core, so do the points where T_{CHF}, T_Q, and T_{IB} occur. For heat structures where the transition region has not yet reached (void fraction greater than 0.999), the number of axial mesh points remains subdivided into two. For heat structures where the transition region has past (void fraction equals 0.0), the number of axial mesh points is halved, but not less than two. For heat structures at the beginning and at the end of the transition region (where T_Q and T_{IB} occur), the number of axial mesh points is doubled, but not to more than half the maximum specified by the user. For the heat structures between those containing T_Q and T_{IB} (which includes the heat structure containing T_Q), the number of axial mesh points is doubled up to the maximum specified by the user. This rezoning of the axial mesh points is shown in Figure 9-9. As a result of this rezoning, the largest number of mesh points is always around the transition region as it moves up through the core.

The reflood heat transfer correlations used in the nucleate boiling and transition boiling regions are specialized for the low-pressure and low-flow cases typical of reflood situations. As a result, the reflood model should only be used for pressures less than 1 MPa and mass fluxes less than

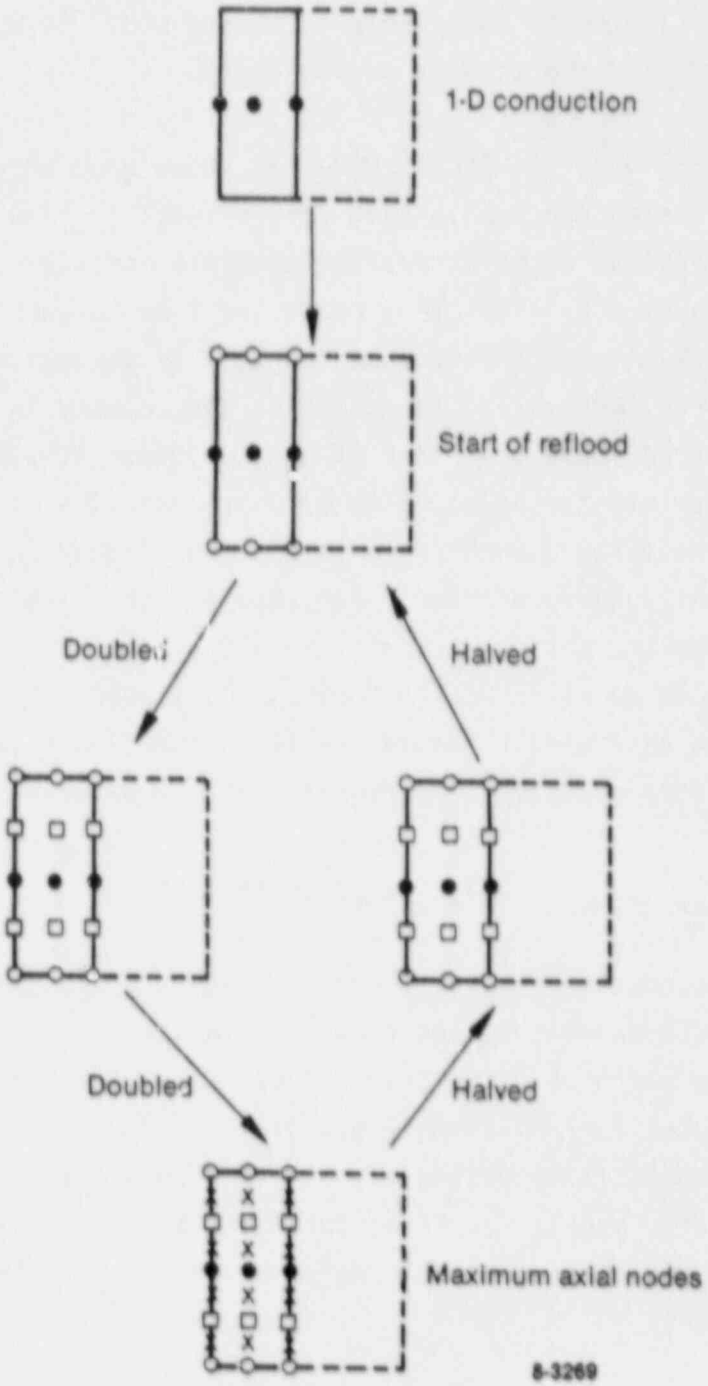

Figure 9-9. An example of fine mesh-rezoning process.

200 kg/s-m^2. In general, the time when the reflood model is activated need not coincide with the time the liquid enters the core. In fact, the most appropriate time to activate the reflood model is when the pressure is less than 1 MPa and the core is nearly empty.

The reflood model in RELAP5/MOD2 has shown good agreement with nonuniformly heated rod bundle data with respect to time to maximum temperature, maximum temperature, and quench temperature, but predicted a longer time to quench.[9-5,6] This predicted time to quench could be larger than the actual time by a factor of 1.1 to 1.5, depending upon the position within the core. Generally, the greatest discrepancy in the time to quench has been observed above the point of maximum power at slow reflood rates. The reason for this is suspected to be overprediction of the liquid entrainment above the quench front so that the liquid inventory in the core is progressively underpredicted. For LBLOCAs, the time to quench may not be as important as the maximum temperature. Comparison to test data has shown that the reflood model in RELAP5/MOD2 yields a good simulation for a high flow rate, but only a fair simulation for a low flow rate. The problem with the low flow rate simulation is probably due to water-packing.

9.3 Gap Conductance Model

The gap conductance between the fuel and the cladding depends strongly on the gap width and has a significant influence on the fuel temperatures. The actual gap width of a LWR fuel rod can be substantially different from the as-fabricated fuel-cladding gap width even during normal reactor operation and especially during a postulated LOCA transient. The change in the fuel-cladding gap is due to differential thermal expansion of the fuel and cladding, elastic and plastic deformation of the fuel and the cladding, and other effects.

The RELAP5/MOD2 gap conductance model accounts for the first-order effects of material deformations under normal reactor operating conditions and most postulated LOCA conditions. The model is based on a simplified material deformation condensed from FRAP-T6[9-7] and is contained in subroutine GAPCON. The material properties are taken from MATPRO-11

(Revision 1).[9-8] The model considers, among other things, the thermal expansion of the fuel and the cladding, and the elastic deformation of cladding under the differential pressure between the gas internal to the gap and the fluid outside the cladding.

The dynamic gap conductance model in subroutine GAPCON defines an effective gap conductivity and employs the following assumptions. First, the fuel-to-cladding radiation heat transfer, which only contributes significantly to the gap conductivity under the conditions of cladding ballooning, is neglected. This is appropriate, since cladding ballooning is not included in this simple model. Second, the minimum gap size is limited such that the maximum effective gap conductivity is about the same order as that of metals. Third, the direct contact of the fuel pellet and the cladding is not explicitly considered. Again, a detailed discussion of the numerical techniques employed in this model is given in the RELAP5/MOD2 Code Manual[9-2] and will not be repeated here.

Steady-state average centerline temperature data from the Power Burst Facility (PBF) Test LOC-11c[9-9] were used to evaluate the dynamic gap conductance model. The test system consists of four nearly identical fuel rods with their own individual flow shroud. Only a single rod along with its flow channel was modeled. The model consists of nine volumes and nine heat structures in the length of the active fuel stack. The top volume has a length of 0.1159 mm and the rest each have a length of 0.1 m. Some other input specifications are listed in Table 9-1. Table 9-2 lists the axial power profile. An earlier cycle of RELAP5/MOD2 was used in these calculations, but the gap conductance model has remained unchanged.

Figure 9-10 shows the comparison of the data and the calculated results. The data are centerline temperatures averaged over four fuel rods. Two RELAP5/MOD2 calculated results are given, one with and one without the gap deformation model. The calculated values using the gap conductance model are about 0 to 100 K higher than the data. However, the calculation without using the gap conductance model yields temperatures much higher than the data. In particular, the differences are about 500 to 700 K in the high-power region. The reduction of centerline temperatures with the gap conductance model is primarily due to thermal expansion of UO_2, which

TABLE 9-1. FUEL ROD GEOMETRY CHARACTERISTICS AND CONDITIONS FOR PBF TEST LOC-11C

Pellet diameter	9.30 mm
Cladding outside diameter	10.72 mm
Cladding inside diameter	9.50 mm
Diametrical gap	0.20 mm
Helium prepressurization	2.41 MPa (Rod 611-3)
Flow channel area	2.257×10^{-4} m^2
Hydraulic diameter	2.68×10^{-2} m
Flow rate	0.643 kg/s
Lower plenum pressure	15.3 MPa
Lower plenum temperature	595.0 K

TABLE 9-2. AXIAL POWER PROFILE OF TEST LOC-11C

Distance from Bottom of Fuel Stack (m)	Normalized Axial Power[a]
0.0	0.163
0.0254	0.326
0.0762	0.620
0.1270	0.862
0.1778	1.047
0.2286	1.184
0.2794	1.285
0.3302	1.355
0.3810	1.396
0.4318	1.400
0.4826	1.368
0.5334	1.304
0.5842	1.221
0.6350	1.128
0.6858	1.028
0.7366	0.910
0.7874	0.754
0.8382	0.548
0.8890	0.290
0.9159	0.256

a. Local power/average power.

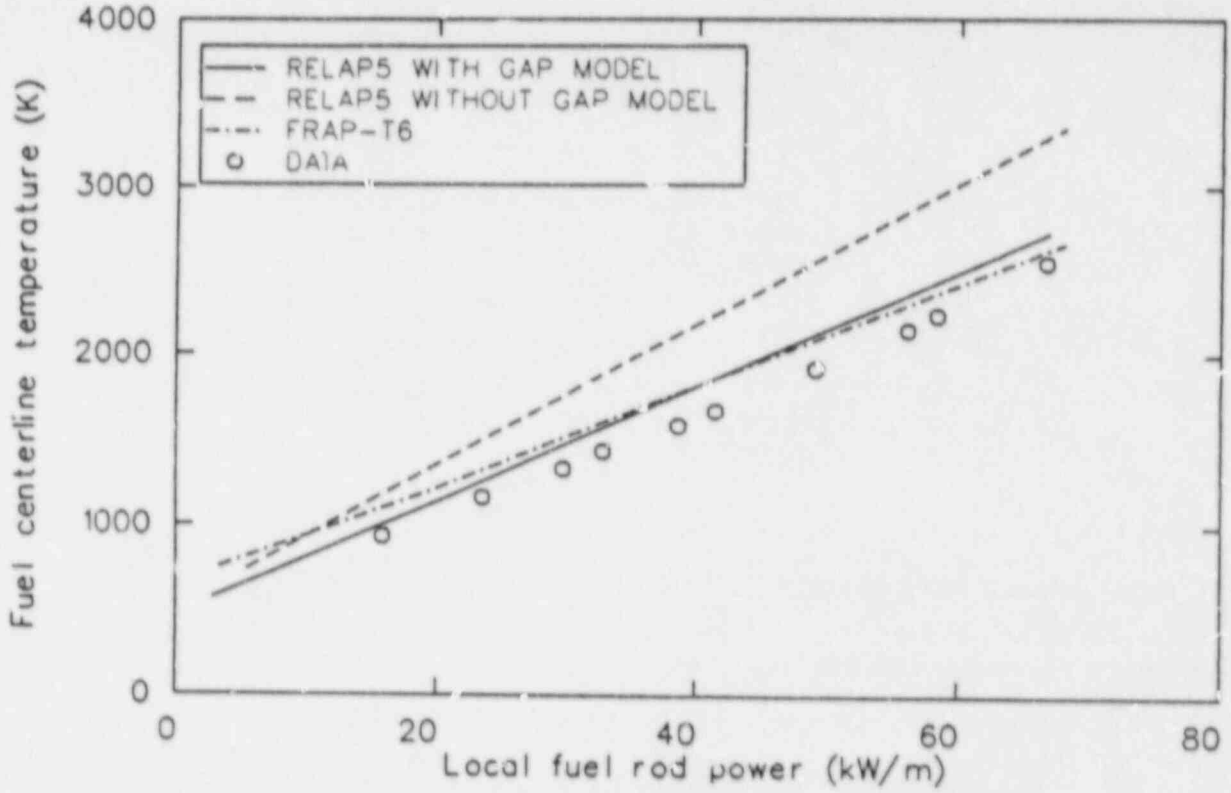

Figure 9-10. Comparison of measured and calculated steady-state fuel centerline temperature for LOFT Test LOC-11C.

reduced the gap size and increased the gap conductance. The dynamic gap conductance model in RELAP5/MOD2 can significantly improve the simulation of nuclear reactor transients where the gap size has a significant effect on the transient.

9.4 Reactor Kinetics

The primary energy source for a nuclear reactor is the reactor core. RELAP5/MOD2 allows the user to model the power generated in the reactor core in several ways: as specified from a table, or as determined by point-reactor kinetics with reactivity feedback. This power is modeled as an internal heat source in user-defined heat structures and can be partitioned by inputting weighting factors to distribute the energy to the various portions of the core as the user desires. The point-reactor or space-independent kinetics approximation is adequate for cases in which the spatial power distribution remains nearly constant.

The point-reactor kinetics model in RELAP5/MOD2 computes both the immediate fission power and the power from decay of fission fragments. The immediate power that is released at the time of fission and includes fission fragment kinetic energy and neutron moderation. Decay power is generated as the fission products undergo radioactive decay. The user can select the decay power model based on either an ANS Standard[9-10] proposed in 1973 or on the 1979 ANS Standard for Decay Heat Power in Light Water Reactors.[9-11] The 1973 proposed standard uses one isotope (^{235}U) for the fission source and 11 groups for fission product decay. The 1979 standard lists data for three isotopes (^{235}U, ^{238}U, ^{239}Pu) and uses 23 groups for each isotope. A user option also allows only the 1979 standard data for ^{235}U to be used. The data for both standards are built into RELAP5/MOD2 as default data, but the user may enter different data. In addition, RELAP5/MOD2 contains an actinide decay model that may be switched on by the user. Two isotopes, ^{239}U and ^{239}Np, are used in the RELAP5/MOD2 model. ^{239}U is produced by neutron capture in ^{238}U and forms ^{239}Np by beta decay. ^{239}Np then forms ^{239}Pu by beta decay. The actinide model gives the result quoted in the 1979 standard.

The point-reactor kinetics equations are

$$\frac{d\phi(t)}{dt} = \frac{[\rho(t) - \beta]\,\phi(t)}{\Lambda} + \sum_{i=1}^{N} \lambda_i\, C_i(t) + S \qquad (9\text{-}7)$$

$$\frac{dC_i(t)}{dt} = \frac{\beta_i}{\Lambda}\,\phi(t) - \lambda_i\, C_i(t) \quad i = 1, 2, \ldots, N \qquad (9\text{-}8)$$

$$\psi(t) = \Sigma_f\, \phi(t) \qquad (9\text{-}9)$$

$$P_f(t) = Q_f\, \psi(t)\ , \qquad (9\text{-}10)$$

where

t	=	time
ϕ	=	neutron flux
C_i	=	number of delayed neutron precursors of group i
β	=	effective delayed neutron fraction
β_i	=	fraction of delayed neutrons of group i
Λ	=	prompt neutron generation time
ρ	=	reactivity -- only the time dependence has been indicated (however, the reactivity is dependent on other variables)
λ_i	=	decay constant of group i
S	=	source
ψ	=	fission rate in #/s
Σ_f	=	fission cross section
P_f	=	immediate fission power in MeV/s
Q_f	=	immediate fission energy per fission in MeV.

After some modifications and variable substitutions, these equations are solved in subroutine RKIN by the modified Runge-Kutta method of Cohen[9-12] used in the AIREK II Reactor Kinetics Code.[9-13] These equations are not correlations, so RELAP5/MOD2 was run to test the point-reactor kinetics model without reactivity feedback against textbook data. The textbook solutions were not programmed into the computer to determine the textbook results, as this would just compare the different

solution techniques. The technique in RELAP5/MOD2 is more complex than any that could be quickly programmed for comparison. Instead, points were scaled from curves in textbooks that showed the results from various reactivity perturbations.

Figure 9-11a shows a comparison for various positive step insertions of reactivity from initial equilibrium in ^{235}U and ^{239}Pu systems with neutron lifetimes of 10^{-4} s. Figure 9-11b shows a comparison for various linear time variations of reactivity from initial equilibrium in ^{235}U systems with neutron lifetimes of 10^{-5} s. Figure 9-11c shows a comparison for various quadratic time variations of reactivity from initial equilibrium in ^{235}U systems with neutron lifetimes of 10^{-4} s. Figure 9-11d shows a comparison for various negative step changes of reactivity from initial equilibrium in ^{235}U systems with neutron lifetimes of 10^{-4} s. The data for Figures 9-11a, b, and c, were obtained from Reference 9-14. Kinetics calculations using the RTS (Reactor Transient Solution) computer code were performed to produce the curves shown in Reference 9-14. The data for Figure 9-11d were obtained from Reference 9-15. Unlike the other figures, only the fission power was normalized in Figure 9-11d and not the total power. Also, a slightly larger delayed neutron fraction (β) was used in determining Figure 9-11d. This slightly larger delayed neutron fraction is typical of ^{235}U reactors with reflectors.

The RELAP5/MOD2 solutions agreed well with the textbook solutions. Differences between the RELAP5/MOD2 solutions and the textbook solutions can be attributed partly to the scaling of a curve from a textbook that may have been distorted as a result of printing or to show a specific trait. The curve from which the data for Figure 9-11d was obtained was one-fourth the size of the curves from which the data for the other figures were obtained. As a result, the data points obtained for Figure 9-11d are not as accurate as those obtained for the other figures. The difference at the larger power levels seen in Figure 9-11a cannot, however, be a result of inaccurate scaling as the difference is too consistent. However, experience with calculations of reactivity-induced accident transients indicates that the power would unlikely go higher than 1000 times the initial power if

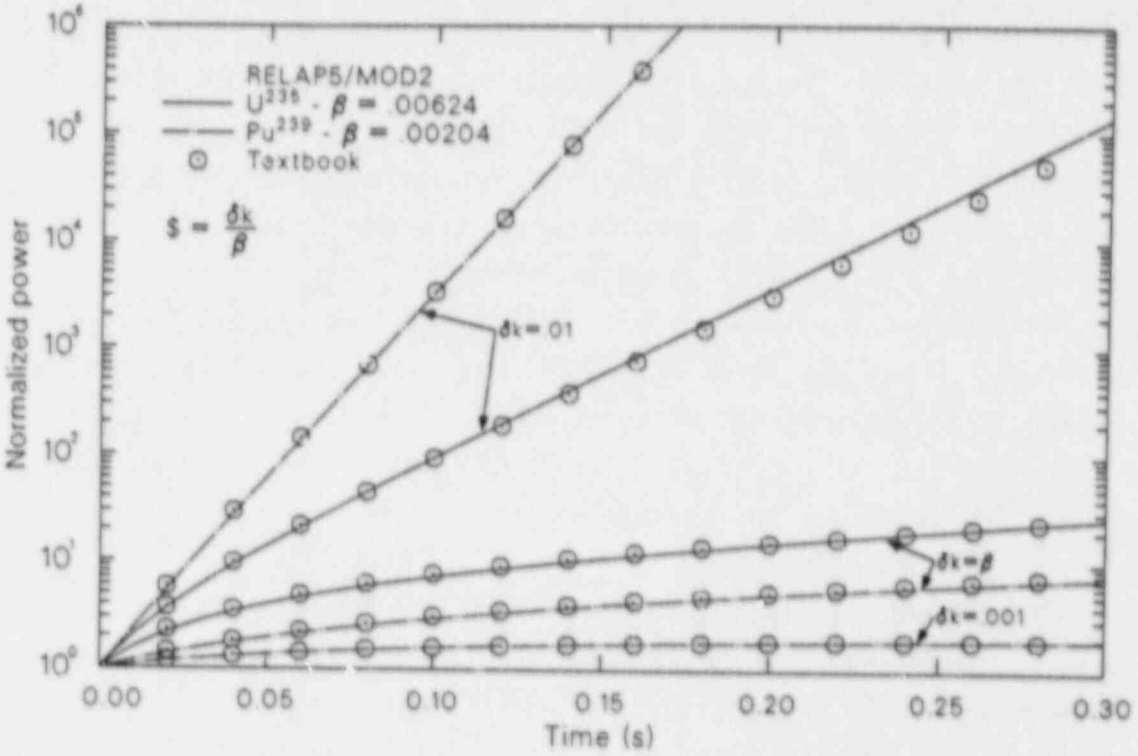

CCM-1201-8

Figure 9-11a. Normalized power versus time.

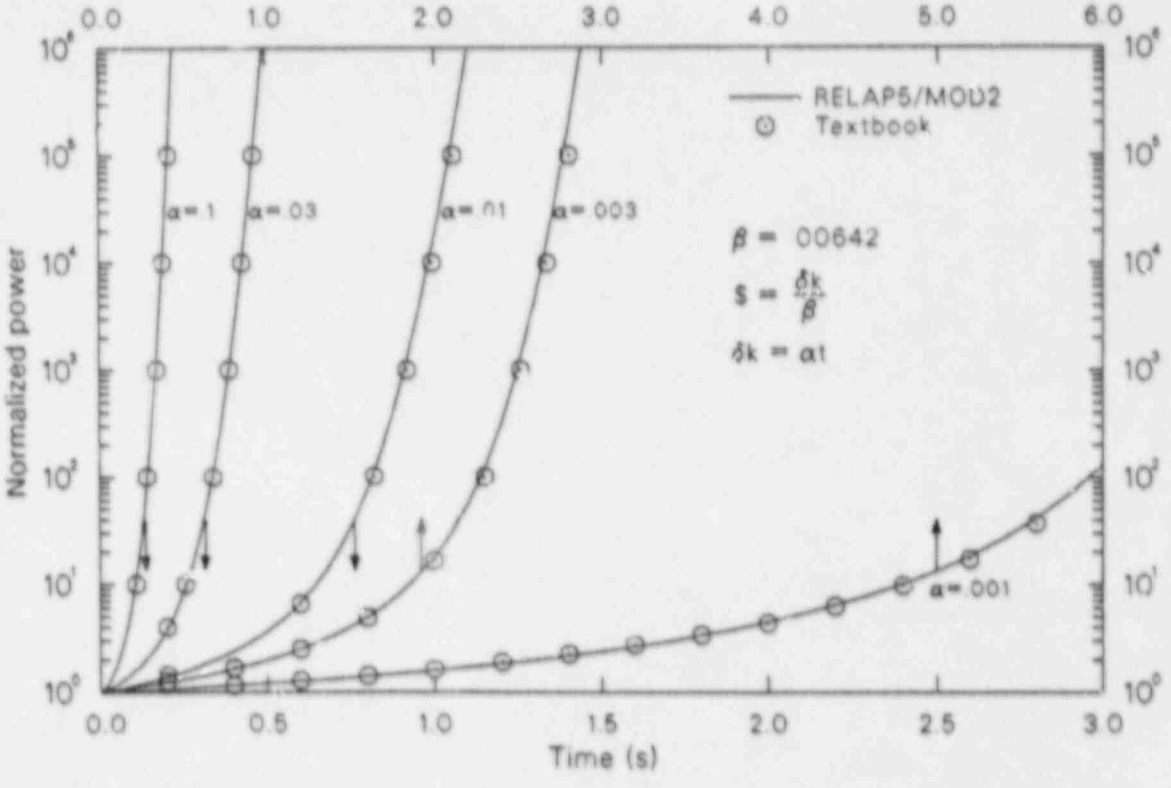

CCM/SD1 -8

Figure 9-11b.

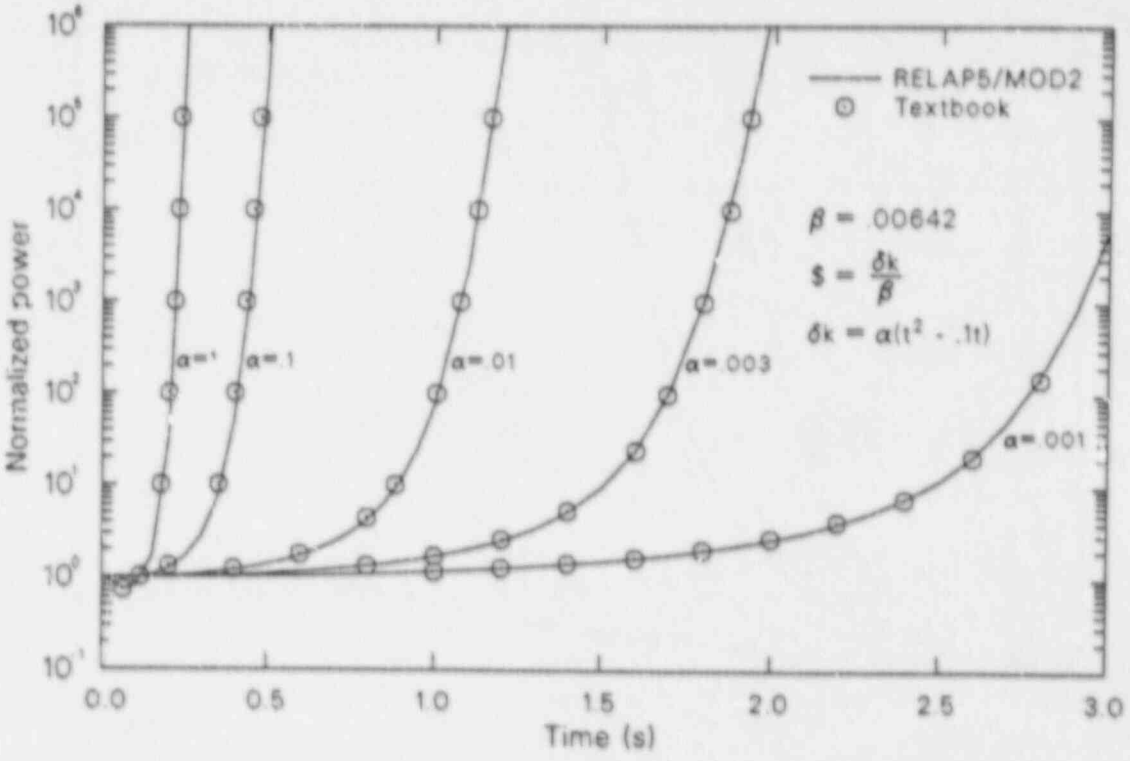

CCMJ501-10

Figure 9-11c.

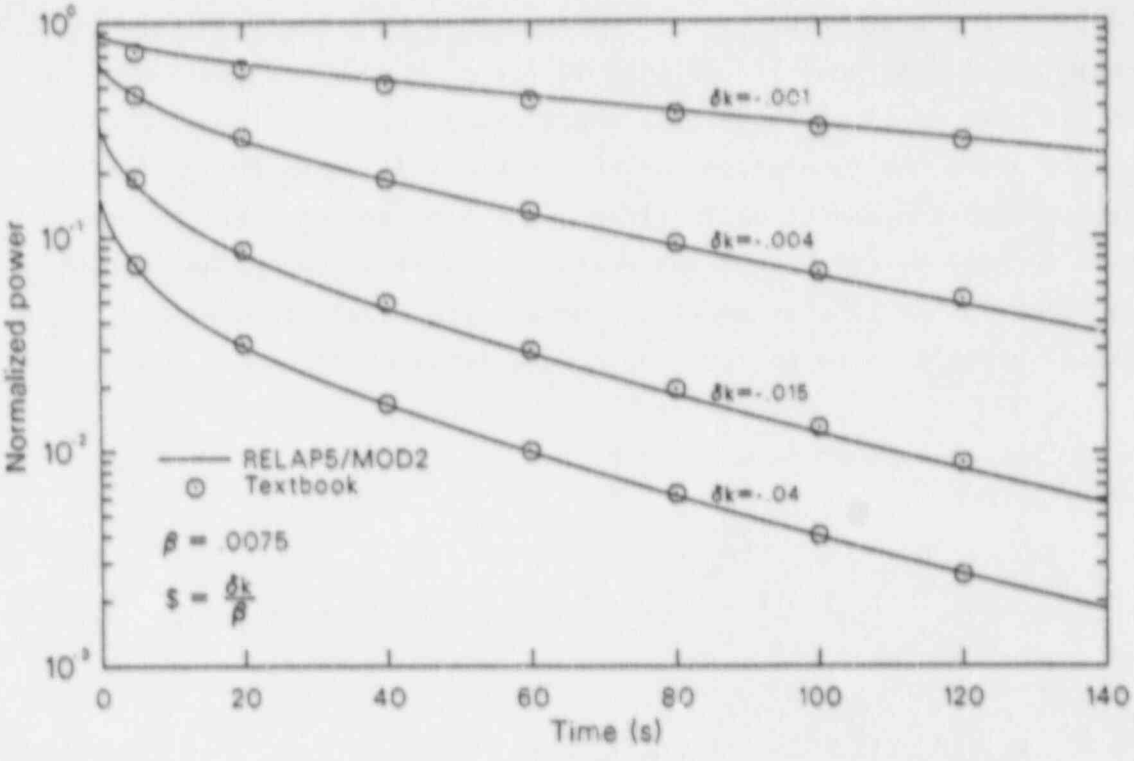
Normalized power
Time (s)
δk=-.001
δk=-.004
δk=-.015
δk=-.04
RELAP5/MOD2
Textbook
β = .0075
$ = δk/β
CCM/S01-11

Figure 9-11d.

reactivity feedback were included in the power determination. In this range, the RELAP5/MOD2 solution and the textbook solution show much better agreement.

Reactivity feedback can be input into RELAP5/MOD2 in one of two models: a separable model and a tabular model. In addition, the tabular model has two options. The separable model is so defined that it assumes that each effect is independent of the other effects. This model also assumes nonlinear feedback effects from moderator density and fuel temperature changes and linear feedback from moderator temperature changes. The separable model does not provide for boron reactivity feedback, although user defined boron feedback can be implemented with a control system. The separable model can, however, be used if boron changes are small and the reactor is near critical about only one state point. For those reactor transients where the assumptions of no interactions among the different feedback mechanisms cannot be justified, the tabular model can be used. All feedback mechanisms can be nonlinear and interactions among the mechanisms are included in the tabular model. However, the expanded modeling capability greatly increases the input data requirements.

The separable model is defined by

$$r(t) = r_0 - r_B + \sum_{i}^{n_s} r_{si}(t) + \sum_{i}^{n_c} V_{ci} + \sum_{i}^{n_\rho} \left[W_{\rho i} \cdot R_\rho (\rho_i(t)) + a_{Wi} \cdot T_{Wi}(t) \right]$$

$$+ \sum_{i}^{n_F} \left[W_{Fi} \cdot R_F (T_{Fi}(t)) + a_{Fi} \cdot T_{Fi}(t) \right] \quad . \qquad (9\text{-}11)$$

The quantity, r_0, is an input quantity and represents the reactivity corresponding to assumed steady-state reactor power at time equal zero. The quantity, r_B, is a bias reactivity calculated during input processing such that the reactivity at time equal zero is r_0. The purpose of the bias reactivity is to ensure that the initial reactivity is equal to the input reactivity after including the feedback effects. Without this quantity, the user would have to manually adjust a scram curve or control variable to obtain the input value of initial reactivity or have a step input of reactivity as the transient starts.

The quantities, r_{si}, are obtained from input tables defining n_s reactivity curves as functions of time. The quantities V_{ci} are n_c control variables that can be user-defined as reactivity contributions. R_ρ is a table defining reactivity as a function of the density of water, $\rho_i(t)$, in the hydrodynamic volume i; $W_{\rho i}$ is the density weighting factor for volume i; T_{Wi} is the temperature of volume i; a_{Wi} is the temperature coefficient (not including density changes) for volume i; and n_ρ is the number of hydrodynamic volumes in the reactor core. The value R_F is a table defining reactivity as a function of the average fuel temperature T_{Fi} in a heat structure; W_{Fi} and a_{Fi} are the fuel temperature weighting factor and the fuel temperature coefficient, respectively. n_F is the number of heat structures in the reactor core.

The tabular model defines reactivity as

$$r(t) = r_o - r_B + \sum_{i}^{n_s} r_{si} + \sum_{i}^{n_c} V_{ci}$$

$$+ R\left[\bar{\rho}(t),\ \bar{T}_W(t),\ \bar{T}_F(t),\ \bar{B}(t)\right] \qquad (9\text{-}12)$$

$$\bar{\rho}(t) = \sum_{i}^{n_\rho} W_{\rho i}\ \rho_i(t) \qquad (9\text{-}13)$$

$$\bar{T}_W(t) = \sum_{i}^{n_\rho} W_{\rho i}\ T_{Wi}(t) \qquad (9\text{-}14)$$

$$\bar{B}(t) = \sum_{i}^{n_\rho} W_{\rho i}\ B_i(t) \qquad (9\text{-}15)$$

$$\bar{T}_F(t) = \sum_{i}^{n_F} W_{Fi}\ T_{Fi}(t)\ , \qquad (9\text{-}16)$$

where B is boron density. The average quantities are obtained with the use of one weighting factor for each hydrodynamic volume and each heat structure

contributing to reactivity feedback. The reactivity function R is defined by a table input by the user. The four-dimensional table lookup and interpolation option computes reactivity as a function of moderator density (ρ), moderator temperature (T_M), volume average fuel temperature (T_F), and boron density (B). The three-dimensional option does not include boron density.

The reactivity function R is evaluated by a direct extension of the one-dimensional table lookup and linear interpolation scheme to multiple dimensions. One-dimensional table lookup and interpolation of the function $V = F(X)$ uses an ordered set of N_X independent variable values X_i, with the corresponding values of the dependent variable V_i, to determine the value of V corresponding to the search argument X. The independent variable is searched such that X_i and X_{i+1} bracket X. An equation for a straight line is fitted to the points X_i, V_i, and X_{i+1}, V_{i+1}, and the straight line equation is evaluated for the given X.

For one dimension, the value of V is bracketed between X_i and X_{i+1}. For two dimensions, the value of V is within the quadrilateral defined by the points X_i, Y_j and X_{i+1}, Y_j and X_i, Y_{j+1} and X_{i+1}, Y_{j+1}. For three dimensions, the value of V lies within the box defined by the points X_i, Y_j, Z_k and X_{i+1}, Y_j, Z_k and X_i, Y_{j+1}, Z_k and X_{i+1}, Y_{j+1}, Z_k and X_i, Y_j, Z_{k+1} and X_{i+1}, Y_j, Z_{k+1} and X_i, Y_{j+1}, Z_{k+1} and X_{i+1}, Y_{j+1}, Z_{k+1}. This process continues for more dimensions. Using the appropriate weighting factors for each dimension, the value of V can be determined by linear interpolation in each dimension, one at a time.

Using N_X, N_Y, N_Z, and N_W as the number of values in the four sets of independent variables, the number of data points for a three-dimensional table is $N_X \cdot N_Y \cdot N_Z$ and is $N_X \cdot N_Y \cdot N_Z \cdot N_W$ for a four-dimensional table. Using only four values for each independent variable, a four-dimensional table requires 256 data points.

9.5 References

9-1. J. Crank and P. Nicolson, "A Practical Method for Numerical Evaluation of Solutions to Partial Differential Equations of the Heat-Conduction Type," Proceedings of the Cambridge Philosophical Society, Vol.43, 1947, pp. 50-67.

9-2. V. H. Ransom et al., RELAP5/MOD2 Code Manual, Volume 1: Code Structure, Systems Models, and Solution Methods, NUREG/CR-4312, EGG-2396, August 1985.

9-3. H. S. Carslaw and J. C. Jeager, Conduction of Heat in Solids, 2nd edition, Oxford: Oxford University Press, 1959.

9-4. J. M. Kelly, "Quench Front Modeling and Reflood Heat Transfer in COBRA-TF," ASME Winter Annual Meeting, 79-WA/HT-63, New York, 1979.

9-5. V. H. Ransom et al., RELAP5/MOD2 Code Manual, Volume 3: Developmental Assessment Problems, EGG-TFM-7952, December, 1987.

9-6. H. Chow and V. H. Ransom, "A Simple Interphase Drag Model for Numerical Two-Fluid Modeling of Two-Phase Flow Systems", ANS Topical Meeting on Nuclear Reactor Thermal Hydraulics, New Orleans, LA, June 1984.

9-7. L. J. Siefken, C. M. Allison, M. P. Bohn, and S. O. Peck, FRAP-T6: A Computer Code for the Transient Analysis of Oxide Fuel Rods, EGG-CDAD-5410, April 1981.

9-8. D. L. Hagrman, G. A. Reymann, and R. F. Mason, MATPRO-Version 11 (Revision 1), NUREG/CR-0479, TREE-1230, Rev. 1, February 1980.

9-9. J. R. Larson, J. M. Broughton, J. W. Spore, L. K. Sepold and R. K. McCardell, PBF-LOCA Test Series Test LOC-11 Test Results Report, NUREG/CR-0618, TREE-1329, April 1979.

9-10. "American Nuclear Society Proposed Standard ANS 5.1, Decay Energy Release Rates Following Shutdown of Uranium-Fueled Thermal Reactors," October 1971, revised October 1973.

9-11. "American National Standard for Decay Heat Power in Light Water Reactors," ANSI/ANS-5.1, 1979.

9-12. E. M. Cohen, "Some Topics in Reactor Kinetics," A/CONF. 15, 1958, p. 629.

9-13. A. Schwartz, Generalized Reactor Kinetics Code AIREK II, NAA-SR-Memo-4980, 1960.

9-14. G. R. Keepin, Physics of Nuclear Reactors, New York: Addison-Wesley Publishing Company Inc., 1965, pp. 287-293.

9-15. M. A. Schultz, Control of Nuclear Reactors and Power Plants, second edition, New York: McGraw-Hill Book Company Inc., 1961, p. 91.

10. CLOSURE RELATIONS REQUIRED BY EXTRA MASS CONSERVATION FIELDS

Noncondensible gas and liquid solute capabilities in RELAP5/MOD2 have not been addressed.

11. STEADY STATE

11.1. Basis for the Model

The model for steady-state analyses using RELAP5/MOD2 was originally implemented in RELAP5/MOD1.5,[11-1] which was a version of RELAP5/MOD1[11-2] extended to provide reflood heat transfer. The steady-state model was subsequently modified for use in RELAP5/MOD2[11-3] and, except for debugging, has remained essentially unchanged since RELAP5/MOD2 was released.

The basic modeling technique used by the steady-state model is that the user must set up the input data base to perform a null transient, so that the problem being simulated will undergo a transient progressing from input initial conditions to the steady-state conditions defined by the user. To achieve this, the algorithm does not solve a set of steady-state formulations of the field equations. Instead, the algorithm utilizes the full transient algorithm and simply provides an automated method of monitoring the calculated results to detect when an average steady-state is achieved and maintained for a reasonable time interval. Upon achievement of steady state, the algorithm automatically stops the calculational process, provides a final "restart/plot" file, and provides the printed and plotted output requested by the user. The user can then examine the results and, if desired, the problem can be either restarted as a continuation of the steady-state problem or restarted as a transient problem.

In performing the transient calculations, the steady-state algorithm utilizes only one special model in the solution of the thermal-hydraulic field equation. The special model utilized ignores the heat structure heat capacity data input by the user and replaces its value with a small value computed to be just large enough to maintain stability for the calculations. This technique reduces the thermal inertia of the bounding heat structures, allowing them to respond quickly and closely to the hydraulic transient as it approaches steady state.

The basis of the algorithm to detect steady state is an original technique utilizing least-squares curve fitting and smoothing methods

to measure the time rates of change in state of the calculational cells and the average linear rate of change of the modeled system. The scheme also considers calculational precision in determining the steady-state convergence criteria. The purpose of the following discussion is to summarize the basic methodology described in the code manual, summarize differences between the manual and the code formulations, and summarize deficiencies noted by users of the technique.

11.2. Summary of the Steady-State Model as Stated in the Manual

In the RELAP5/MOD2 Manual, Volume 1,[11-3] the steady-state model is described in Chapter 4 entitled, "Special Techniques", Section 4.3. Section 4.3 is divided into five subsections discussing the fundamental concepts, the steady-state convergence criteria, the steady-state test time interval control, the heat structure heat conductance scheme and the interrelationship of steady-state and transient restart/plot records.

In the discussion of subsection 4.3.1 concerning fundamental concepts, it is stated that it is only necessary to monitor three terms whose "variation in time include the variations of all the other terms". These three terms are the thermodynamic density, internal energy, and pressure, and these three terms can be combined into the single term, enthalpy. The enthalpy of each volume cell is then formulated as Equation (752).[11-3] Furthermore, it is expressed that an absolute steady state occurs when the time rate of change in enthalpy approaches zero for all of the volume cells in the model, and that this is monitored by fitting the time rate of change in enthalpy to an exponential smoothing function giving a least squares approximation of the root mean square of the time rate of change in enthalpy for the modeled system. A means of monitoring the system average enthalpy is also discussed, for which a straight line is fitted by least-squares to the average system enthalpy results over a time interval. Time average steady state then occurs when the linear average rate of change is zero within a convergence criterion related to the calculational precision.

Section 4.3.2[11-3] discusses the steady-state convergence criterion for time average steady state and its relationship to calculational precision. The formulations presented are statistical equations expressing the difference between the state calculated by the transient numerical algorithm and the state calculated by the thermodynamic equation of state algorithm. This difference in state properties is then shown to be the difference in two-phase mixture densities computed by the two algorithms. This difference has been called the "mass error" in the code manual. A second source of density uncertainty is also discussed. It is the uncertainty of the thermodynamic equation of state itself. Since a steam table computed from the ASME formulation for steam water properties[11-4] is used by RELAP5/MOD2 as the thermodynamic equation of state, and since these tables have five significant figure accuracy, the approximate uncertainty in thermodynamic is ± 5 in the density sixth significant figure. The resultant net uncertainty in the system mean enthalpy is then expressed as the statistical variance, summing the squares of the calculational precision and the steam table standard precision. The uncertainty in the rate of change in state is then written as the net uncertainty divided by the calculational time step.

Section 4.3.3[11-3] discusses the steady-state test time interval control and separates the scheme into two basic tasks, which are:

1. To monitor the behavior of the time smoothed RMS rate of change in system enthalpy, and

2. To monitor the behavior of the linear average rate of change in system enthalpy.

The section also discusses the terms printed in the steady-state printed edit.

In performing a steady-state calculation, the full transient algorithm is solved at each time step; and, after each successful solution, the steady-state monitoring algorithm is entered. Tests for the preceding two tasks are performed as outlined in the following discussion.

In the test time interval control scheme, the first calculations performed are those evaluating the system mean enthalpy, the system mean rate of change in enthalpy, and the system mean square rate of change in enthalpy [i.e., Equations (755), (756), and (767), respectively in Volume 1 of the code manual] at each time step for ten successive successful time steps. At the end of this first time interval, the equation for time smoothed root mean square rate of change in enthalpy [i.e., Equation (758)] is determined using the method of least squares. Equation (758) and its first two derivatives are evaluated at the current time step; and, if the rate of change of Equation (758) is increasing, the progression to steady state is divergent. If the rate of change in Equation (758) is decreasing or zero, the progression to steady state is convergent. If the divergent condition is determined, then the next time at which the test will be performed is estimated by either maintaining, halving, or doubling the current test time interval based on a projected estimate of the current time smoothed convergence function. This test procedure is then successively repeated until a convergent condition is calculated. The discussion of Equations (790), (791) and (792) explain the formulation of this process. If a convergent condition is determined, then testing for linear time average steady state is begun.

After the RMS rate of change test indicates a convergent condition, the linear average rate of change tests are begun. These tests are conducted by curve fitting three overlapping straight line equations to the system mean enthalpy results accumulated over two successive test time intervals. For example, if the two successive test time intervals are over the range in time from t_1 to t_2 to t_3, then three straight lines can be fitted to the results, such that line A is a line fitted from t_1 to t_2, Line B is a line fitted from t_2 to t_3, and Line C is a line fitted from t_1 to t_3. The implication of the manual is that if the slopes of these three straight lines both agree and approach zero within the calculational uncertainty, then the system is approaching a time average steady state. Of course, if the slopes of the three lines disagree and are not approaching zero, then the solution is diverging from steady state.

If the solution is diverging, then the accumulated lines results are discarded and the testing scheme is reset to continue the RMS rate of change scheme until Equation (758) again indicates convergence, at which time the linear time average scheme is reinitiated.

It has been previously noted that the full transient algorithm is solved at each time step for the system being modeled, and that only thermal-hydraulic parameters are monitored to detect steady state, with no mention of how the state of heat structures is monitored as they achieve steady state. In the steady state algorithm, the heat structure response is forced to closely follow the thermal-hydraulic response by ignoring the heat structure heat capacity data input by the user and replacing it with a small value just large enough to assure calculational stability. This technique artificially reduces the thermal inertia of the heat structures, allowing them to rapidly store or reject heat, and thereby closely follow the thermal-hydraulic state as it approaches steady state. The formula used to calculate the minimal heat capacity term is the explicit stability criterion for numerical heat conduction analyses and is given in the manual as Equation (795).

Finally, to allow a high degree of utility in using the steady-state technique, the ability is provided to restart problems as continuations of steady-state problems or as transients using steady-state restart/plot records as initial conditions. Capability is also included to restart steady-state problems utilizing transient restart/plot records as initial conditions. Of course, the fundamental capability of running a new problem as a steady state is also included.

11.3. Summary of the Steady-State Model Implemented in the RELAP5/MOD2 Code

Comparing the steady-state scheme discussed in the manual to the scheme as coded in the subroutine SSTCHK shows that all of the formulations have been implemented as described except two. The first exception is that the standard uncertainty given in Equation (765) is coded as

$$\epsilon^{n+1}_{std,\rho,i} \sim \pm (6 \times 10^{-6})\ \rho_i^{n+1} \quad , \qquad (11\text{-}1)$$

which gives a better approximation to ±5 in the sixth significant figure for density of saturated liquid. The second exception is that upon testing the three straight lines to determine if time average steady state has been achieved, as discussed in the last paragraph, pp. 319 of the manual, if it is determined that steady state has not been achieved, the first test line (i.e., Line A) is not simply reset to the second test line (i.e., Line B). Instead, the straight line results for both Lines A and B are discarded and Line A is replaced by a least-squares fit to the transient algorithm results over the Line B test time interval. The remainder of the time average steady state testing scheme remains as discussed in the manual.

11.4. Deficiencies Reported for the Steady-State Schemes

Very few users have reported deficiencies to the RELAP5/MOD2 code development personnel. However, the deficiencies reported have all been for models simulating full-size power plants or integral test facilities simulating power plants. The deficiencies fall into three categories, which are:

1. The modeled system undergoes a significant transient from user input initial conditions and begins to steady out, but the code terminates the calculation too early with the statement printed that the system has achieved steady state.

2. The modeled system undergoes a significant transient from user input initial conditions to a good steady state, but the algorithm allows calculations to proceed at steady state for too long a time.

3. The modeled system achieved a good steady state in a reasonable simulation time but, for the secondary side, if the steam generator heat transfer conditions are matched, the secondary pressure does not agree with data. If the secondary pressure is matched, then the steam generator heat transfer conditions do not agree with data.

The first deficiency definitely shows a weakness in the time average steady state testing scheme. The deficiency occurs, however, when the user inputs very crude or approximate initial conditions. The transient problem simulated is then quite extreme, resulting in a high calculational uncertainty. This uncertainty is monitored by the code time step control routine as "mass error" and as a result, the time step taken is usually reduced to the minimum value input by the user. Once the minimum time step is reached, the code is then forced to run at that time step and forced to accept the high error. Since this mass error is used by the steady-state algorithm to define the time average steady state convergence criteria, the resultant convergence criterion is large. Hence, since the criterion for time average steady state is that the slope of the time average straight line be zero plus or minus the convergence criterion, the large convergence criterion allows the algorithm to prematurely estimate achievement of time average steady state. The user can generally work around this problem by simply restarting the run as a continuation of the steady-state problem.

The second deficiency is usually a direct function of the steady-state scheme and not really a deficiency. Roughly the first 25% of the total time simulated is the transient approach to steady state. The test time interval for the first achievement of steady state will be of the same approximate duration as this transient time interval. That is, if it takes approximately 100 s simulated time to undergo the transient approach to steady state, then the first test time interval showing the achievement of time average steady state will also be approximately 100 s. The algorithm then repeats the testing scheme for two additional intervals of the same duration, and if this average steady state is successively maintained for

all three time intervals, then the algorithm terminates the calculation with the statement that steady state has been achieved. The time needed to achieve steady-state can usually be shortened by improving the modeled control variables that drive the system to steady state.

The third deficiency noted is also not a deficiency in the steady-state algorithm. It is a heat transfer modeling problem typical of PWR steam generator models. Users should refer to previous sections in this document describing these models for more detailed recommendations (see Section 4.2.3).

It should also be noted that the user can define a plant controller such as a steam generator feedwater control operating between high and low set points that will force the modeled system to a steady oscillating state or an oscillating state with slowly decreasing amplitude. For these circumstances, the steady state algorithm will determine that a time average steady state has been achieved, and within the steady-state edit, the mean RMS amplitude of these oscillations is printed as the term FLUCTUATION. If the user desires to remove these oscillations, a revised controller must be used that will be drive the system to a precise set point.

11.5 Steady-State Conclusions

The steady-state algorithm provides an adequate automated method of performing a null transient solution for steady-state conditions. However, the experienced RELAP5/MOD2 user will undoubtedly have better success than the inexperienced user. RELAP5/MOD2 personnel have recently finished a new modeling capability for self initialization of PWR plant system models.[11-5] Two examples are included that demonstrate how a good steady state can be achieved.

It is also concluded that the steady-state algorithm can be improved by delaying the initiation of testing for steady state until the initial calculational mass error has begun to decrease. This would prevent premature estimates of the achievement of steady state.

11.6 References

11-1. V. H. Ransom, et al., RELAP5/MOD1.5: Models, Developmental Assessment, and User Information, EGG-NSMD-6035, October 1982.

11-2. V. H. Ransom, et al., RELAP5/MOD1 Code Manual, Volume 1: System Models and Numerical Methods, NUREG/CR-1826, EGG-2070, March 1982.

11-3. V. H. Ransom, et al., RELAP5/MOD2 Code Manual, Volume 1: Code Structure, System models, and Solution Methods, NUREG/CR-4312, EGG-2396, August 1985.

11-4. "Thermodynamic and Transport Properties of Steam," American Society of Mechanical Engineers, 1967

11-5. G. W. Johnsen, et al., Self-Initialization Option for RELAP5/MOD2, EGG-RTH-7381, September 1986.

NRC FORM 335 (2 84) NRCM 1102, 3201, 3202

U.S. NUCLEAR REGULATORY COMMISSION

BIBLIOGRAPHIC DATA SHEET

SEE INSTRUCTIONS ON THE REVERSE

1 REPORT NUMBER (Assigned by TIDC and Vol. No., if any)
NUREG/CR-5104
EGG-2531

2 TITLE AND SUBTITLE
RELAP5/MOD2 Models and Correlations

2 LEAVE BLANK

4 DATE REPORT COMPLETED
MONTH: July | YEAR: 1988

5 AUTHOR(S)
Richard A. Dimenna, Thomas K. Larson, Robert G. Hanson, Jay R. Larson, Clayton S. Miller, Dennis M. Kiser, Richard W. Johnson, John E. Streit

6 DATE REPORT ISSUED
MONTH: August | YEAR: 1988

7 PERFORMING ORGANIZATION NAME AND MAILING ADDRESS (Include Zip Code)
EG&G Idaho, Inc.
P. O. Box 1625
Idaho Falls, ID 83415

8 PROJECT/TASK/WORK UNIT NUMBER

9 FIN OR GRANT NUMBER
A6868

10 SPONSORING ORGANIZATION NAME AND MAILING ADDRESS (Include Zip Code)
Division of Reactor and Plant Systems
Office of Nuclear Regulatory Research
U.S.Nuclear Regulatory Commission
Washington, DC 20555

11a TYPE OF REPORT
Research

b PERIOD COVERED (Inclusive dates)

12 SUPPLEMENTARY NOTES

13 ABSTRACT (200 words or less)

A review of the RELAP5/MOD2 computer code has been performed to assess the basis for the models and correlations comprising the code. The review has included verification of the original data base, including thermodynamic, thermal-hydraulic, and geometric conditions; simplifying assumptions in implementation or application; and accuracy of implementation compared to documented descriptions of each of the models. An effort has been made to provide the reader with an understanding of what is in the code and why it is there and to provide enough information that an analyst can assess the impact of the correlation or model on the ability of the code to represent the physics of a reactor transient. Where assessment of the implemented versions of the models or correlations has been accomplished and published, the assessment results have been included.

14 DOCUMENT ANALYSIS - a KEYWORDS/DESCRIPTORS
RELAP5/MOD2 computer code

b IDENTIFIERS/OPEN-ENDED TERMS

15 AVAILABILITY STATEMENT
unlimited

16 SECURITY CLASSIFICATION
(This page) unclassified
(This report) unclassified

17 NUMBER OF PAGES

18 PRICE

UNITED STATES
NUCLEAR REGULATORY COMMISSION
WASHINGTON, D.C. 20555

OFFICIAL BUSINESS
PENALTY FOR PRIVATE USE, $300

SPECIAL FOURTH CLASS RATE
POSTAGE & FEES PAID
USNRC
PERMIT No. G-67

120555139217 1 1AN1R4
US NRC-OARM-ADM
DIV FOIA & PUBLICATIONS SVCS
RRES-PDR NUREG
P-210
WASHINGTON DC 20555